3D LITHOGEOCHEMICAL FOOTPRINT OF THE MILLENNIUM-McARTHUR RIVER UNCONFORMITY-TYPE URANIUM DEPOSITS, SASKATCHEWAN, CANADA

By

© Shannon Dee Guffey

A thesis submitted to the

School of Graduate Studies

in partial fulfillment of the requirements for the degree of

Master of Science

Department of Earth Sciences

Memorial University of Newfoundland

May 2017

St. John's Newfoundland and Labrador

ABSTRACT

The Millennium and McArthur River unconformity-related uranium deposits in the southeastern Athabasca Basin, Saskatchewan, are overlain by hydrothermally altered sandstones of the Manitou Falls Formation. The distal lithogeochemical footprints in these sandstones, from unconformity to subcrop, are useful for vectoring toward mineralization using simple major and trace element analyses. Large first order alteration envelopes are defined by molar element ratios K/Al vs. Mg/Al, which surround smaller, second order trace element haloes. At Millennium, median Mg/K molar ratios >0.2 define a 10-km alteration envelope. Values increase significantly within 2 km of the deposit, coinciding with Mo, Ga, and REE enrichment 100s of metres vertically above the deposit. At McArthur River, K/Al <0.06 and Mg/Al <0.4 (molar), and elevated Ba, Sr, Ga, and Cs, exhibit haloes 4–8 km along strike of the P2 trend, 100s of metres above the McArthur River deposit.

ACKNOWLEDGEMENTS

I have been fortunate during my Master's degree to have had the support of many people. My utmost thanks go to Dr. Stephen J. Piercey, my advisor. His sense of humor and enthusiasm for research is infectious, making his students want to complete the best possible work. He helped design a project that perfectly fit my strengths in data analysis, but that also challenged me daily in every step of the scientific method, and I could not have asked for a better supervisor.

Drs. Kevin Ansdell (University of Saskatchewan) and Kurt Kyser (Queen's University) have combined years of research experience in the world of unconformity-related uranium that was paramount in helping to bring my project to fruition, and they were always the first set of eyes on my work after Dr. Piercey. Gerard Zaluski and Tom Kotzer of Cameco Corporation were incredibly supportive. They reviewed and commented on the quarterly reports for the CMIC-Footprints project in addition to the chapters herein and the amount of time they spent personally on my work impressed me immensely, especially considering their responsibilities to their day jobs. I greatly appreciated their detailed and thoughtful responses to my inquiries, making the scientific discussions engaging and informative. Dave Quirt of AREVA Resources Canada was a tremendous help as well, whose tenacious attention to detail ensured that all information presented was as perfect and as cogent as it could be. Gerard, Tom, and Dave have spent the majority of their careers immersed in unconformity-related uranium deposits and their expertise has been invaluable.

Field work at the McArthur River site, funded in-kind by Cameco, was enormously benefitted by the assistance of Steve, Kevin, Kurt, Gerard, and Tom, who not only guided our work but lifted an impressive amount of core boxes. With me to collect samples and discuss our research objectives were Nicholas Joyce, Mary Devine, and Mohamed Gouiza, all members of the CMIC-Footprints project who made our time there enjoyable. Katelynn Brown, a summer student at Cameco, provided support as well and we thank Cameco for allowing us to utilize her.

My fellow members of the Piercey research group at Memorial University, past and present, have been welcome support. Dr. Jonathan Cloutier, Dr. Stefanie Lode, and Michael Buschette were especially helpful, as excellent editors of my writing drafts and through their tutelage in Target and Illustrator. My writing and figures improved as a direct result of their efforts; the time they spent to help me better my work and their friendship is very much appreciated. Dylan Goudie was a great help with the SEM analysis. Finally, I could not have returned to academia from the working world, and begin a new career at this stage in life, without the love and support of my husband, John Allen. I hope the arduous five-day journey he made with our cat, Buddy, was worth the suffering as my time here in St. John's would not have been as wonderful without them.

Financial support was provided as part of the joint Natural Sciences and Engineering Research Council of Canada (NSERC) and Canadian Mining Innovation Council (CMIC) project “Integrated Multi-Parameter Footprints of Ore Systems: The Next Generation of Ore Deposit Models” through the NSERC Collaborative Research and Development Program, and by the NSERC-Altius Industrial Research Chair to Piercey, funded by NSERC, Altius Resources Inc. and the Research and Development Corporation of Newfoundland and Labrador.

TABLE OF CONTENTS

Chapter 1: Introduction to the Millennium and McArthur River unconformity-related uranium deposits, Athabasca Basin, northern Saskatchewan, Canada

Chapter 2: 3D geochemical footprint of the Millennium unconformity-type uranium deposit, Canada: implications for vectoring

Chapter 4: Summary and Future Work

LIST OF TABLES

LIST OF FIGURES

LIST OF NOMENCLATURE AND ABBREVIATIONS

AAS	Atomic absorption spectrophotometry
APS	Aluminum phosphate-sulfate mineral
B1	B1 conductive trend (Millennium study area)
COMP_S	Whole rock geochemical samples selected as "composite sandstone" (representative) from drill core, collected systematically
DS-K	alkali-deficient dravite/sudoite to kaolin group trend (molar element ratio plots)
EDX	Electron dispersive x-ray spectroscopy
HW	Drill holes in hanging wall (true background) (McArthur River study area)
ICP-OES	Inductively coupled plasma optical emission spectrometry
ICP-MS	Inductively coupled plasma mass spectrometry
I-DS	illite to alkali-deficient dravite/sudoite trend (molar element ratio plots)
IDW	Inverse distance weighting
K-I	kaolin group to illite trend (molar element ratio plots)
LA-ICP-MS	Laser ablation inductively coupled plasma mass spectrometry
LOI	Loss on ignition
M	Drill holes in Main Zone (Millennium deposit)
MFa	Manitou Falls Formation A
MFb	Manitou Falls Formation B
MFc	Manitou Falls Formation C
MFd	Manitou Falls Formation D
MLA	Mineral liberation analysis
N1	Drill holes in North 1 (Millennium study area)
N2	Drill holes in North 2 (Millennium study area)
N3	Drill holes in North 3 (Millennium study area)
N4	Drill holes in North 4 (Millennium study area)
McA	Drill holes surrounding McArthur River deposit, U content 0-5 ppm (McArthur River study area)
McA+	Drill holes surrounding McArthur River deposit, U content 0-10 ppm (McArthur River study area)
McA++	Drill holes in and surrounding McArthur River deposit, U content 0-1000 ppm (McArthur River study area)
P	Drill holes in Proximal Zone (Millennium deposit)

P2	P2 conductive trend (McArthur River deposit); also drill holes in P2 trend (non-mineralized)
P2 Main	Drill holes in P2 Main deposit (subeconomic) (McArthur River study area)
P2SW	Drill holes in southwest end of P2 trend (background) (McArthur River study area)
S	Drill holes in South Zone (Millennium study area)
SEM	Scanning electron microscopy
SPOT_S	Whole rock geochemical samples selected as "spot sandstone" (anomalous, or targeted feature) from drill core
SRC	Saskatchewan Research Council Geoanalytical Laboratories
SWIR	Shortwave infrared spectroscopy
QA	Quality assurance
Q-Q	Quantile-quantile plot
THO	Trans-Hudson Orogeny
UTM	Universal Transverse Mercator
URU	Unconformity-related uranium
WMTZ	Wollaston-Mudjatik Transition Zone

LIST OF APPENDICES

CO-AUTHORSHIP STATEMENT

This thesis consists of four chapters. Chapter One is an introduction to the work plan developed and proposed by the Canadian Mining Innovation Council (CMIC)-Footprints project committee. It includes a literature review and general descriptions of the geology for the two deposits analyzed, and is written by the author with editorial support of Dr. Piercey, supervisor of this thesis.

Chapter Two was written in collaboration with Dr. Piercey, Dr. Kevin Ansdell (University of Saskatchewan), Dr. Kurt Kyser (Queen's University), Dr. Tom Kotzer and Gerard Zaluski (Cameco Corporation), and David Quirt (AREVA Resources Canada, Inc.). All authors contributed significantly in both writing and interpretation of geochemical data. Cameco Corporation provided all data, with laboratory work performed by Saskatchewan Research Council Geoanalytical Laboratories. Additional comments on the manuscript were provided by Dr. Stefanie Lode (Memorial University) and Dr. Jonathan Cloutier (University of St. Andrews). It is intended to be submitted to the journal GEEA after being reviewed by all sponsors of the CMIC-Footprints project per publication guidelines.

Chapter Three was written by the author with the supervision and editorial support of Dr. Piercey. Drs. Piercey, Ansdell, Kyser, Kotzer, and Mr. Zaluski were present for guidance and discussions during field work at the McArthur River deposit site, funded by Cameco Corporation. Additional comments on the manuscript were provided by Dr. Jonathan Cloutier. All data was provided by Cameco Corporation, with laboratory work performed by Saskatchewan Research Council Geoanalytical Laboratories. Written as a stand-alone paper, it is intended to be submitted to a peer-reviewed journal after additional

editorial support and collaboration by the co-authors of Chapter Two, and review by all sponsors of the CMIC-Footprints project per publication guidelines.

Chapter Four is a summary of the thesis, and includes suggestions for future work. It, along with appendices A, B, and C, were written by the author with supervision and editorial support from Dr. Piercey.

CHAPTER 1: INTRODUCTION TO THE MILLENNIUM AND McARTHUR RIVER UNCONFORMITY-RELATED URANIUM DEPOSITS, ATHABASCA BASIN, NORTHERN SASKATCHEWAN, CANADA

1.1 INTRODUCTION

Uranium is a critical resource for nuclear power generation. In nature, U consists of three radiogenic isotopes (^{238}U, ^{235}U, and ^{234}U), only one of which, ^{235}U, is fissionable and necessary for energy production. The ^{235}U has a natural abundance of only 0.7%; therefore, any minable ore is normally enriched as part of the mineral processing (Lehmann, 2008; Kyser, 2014) and any resource must have sufficient grade and tonnage for recovery to be economically feasible. Modern exploration for new prospects that meet these criteria is challenging and often requires a focus on mineralization that is deep and/or hidden below cover.

Unconformity-related U (URU) deposits are known for exceptional grades, making them especially desirable for recovery (Laverret et al., 2006). The preeminent location for these deposits is the Athabasca Basin, northern Saskatchewan and Alberta, Canada, one of the main sources of global uranium (Fig. 1.1; Kyser, 2014). Formation of URU deposits involves extensive hydrothermal fluid flow in a constrained location, and is a result of multiple factors including, but not limited to: timing, fluid chemistry, oxygen fugacity, pH, temperature, and rock composition (Hoeve and Sibbald, 1978; Hoeve and Quirt, 1984: Fayek and Kyser, 1997). Accordingly, lithogeochemistry is particularly useful in

exploration for such deposits because rock chemistry often reflects the above processes and provides vectors towards mineralization (Earle and Sopuck, 1989; Kyser et al., 2009). During the hydrothermal alteration process, hydrothermal fluids leach U from source rocks and transport it, along with mobile elements such as Pb, Cu, Ni, Mo, B, V, and others, until it precipitates from the fluid due to geochemical and structural traps (Hoeve and Sibbald, 1978; Hoeve and Quirt, 1984; Jefferson et al., 2007; Cuney, 2009). Fluid-rock interaction during transport and deposition result in geochemical signatures reflective of ore forming processes. These become particularly enhanced in areas where the processes had been ongoing or occurred repeatedly over extended periods of time, or where fluid volumes were large (Earle and Sopuck, 1989; Kyser et al., 2000; Jackson, 2010). Commonly, clay mineral compositions (via hydrothermal alteration) and pathfinder elements (as redox-sensitive or U-associated arsenides and sulfides) associated with ore forming processes highlight these fluid pathways and can create vectors towards mineralization (Hoeve et al., 1981; Hoeve and Quirt, 1984).

Large-scale alteration haloes consisting of illite, chlorite, and dravite, and anomalous Pb, Ni, Co, Cu, As, Mo, and B, are common vectors towards URU mineralization (Sopuck et al., 1983; Hoeve and Quirt, 1984; Earle and Sopuck, 1989; Fayek and Kyser 1997; Jefferson et al., 2007). Although there are no universal vectors that can be applied to all URU deposits, the fluid-rock interactions associated with mineralization processes result in common mineral and elemental associations (Tremblay, 1982; Earle and Sopuck, 1989). This includes the alteration of the background mineral dickite to illite with K-dominant fluids, with additional alteration forming chlorite and dravite with Mg-dominant fluids (Earle and Sopuck, 1989). These anomalies are no guarantee of URU but

instead are evidence of their potential though hydrothermal processes and the large fluid volumes necessary for deposit formation (Earle and Sopuck, 1989; Cloutier et al., 2010). The later stages are indicative of fluids that can be basinal in origin or that have become enriched in Mg and B through fluid-rock interaction in the basement, the reduced nature of which is also necessary for the precipitation of U (Mercadier et al., 2012; Sheahan et al., 2016). Lead is a decay product of U; therefore, variable ratios of radiogenic Pb isotopes can be indicators of a concentrated source (mineralization), and their mobility in fluid events can leave signatures that can be used as vectors (Holk et al., 2003, Quirt, 2009). Other trace elements (As, Co, Cu, Ni) are pathfinders or indicators as they are found in arsenides and sulfides associated with the formation of complex (polymineralic) U deposits (Hoeve and Sibbald, 1978; Tremblay, 1982). Because redox reactions are responsible for U precipitation, elements that are sensitive to these processes (Mo, V, Se, As, Cu) will be indicators as well (Kyser and Cuney, 2008; Kyser, 2014). Rare earth elements (REE) are also associated with URU deposits because their ionic radii is similar to that of U^{4+}, allowing for substitution in accessory minerals and REE-enrichment in uraninite (Shannon, 1976; Fayek and Kyser, 1997; Kyser, 2014).

The purpose of this thesis is to expand on these common exploration models by creating a detailed characterization of an extensive suite of major and trace elements, and clay mineral distribution, on a regional scale at two well-explored deposits. The Millennium and McArthur River deposits display differing mineralization styles (size, depth, and associated elements) despite their locations being within 50 km of each other and their spatial association with regional illite, chlorite, and dravite anomalies (Fig. 1.2a; Earle and Sopuck, 1989; McGill et al., 1993; Roy et al., 2006). The lithogeochemical

signatures of both deposits, each encompassing tens of kilometres, will be characterized for clay mineralogy and trace element haloes to determine any spatial relationships to mineralization. These features will be used to create scalable mineralogical and geochemical vectors towards mineralization.

1.2 UNCONFORMITY-RELATED URANIUM DEPOSITS

Unconformity-related uranium (URU) deposits are found at or near an unconformity between a Paleo- to Mesoproterozoic sedimentary basin and an Archean to Paleoproterozoic metasedimentary basement (Hoeve and Sibbald, 1978; Tremblay, 1982; Hoeve and Quirt, 1984; Ruzicka, 1996; Cuney 2009; Kyser, 2014). These deposits are found mainly in Canada and Australia, and are often high grade, with several deposits containing greater than 1% U oxides (Ruzicka, 1996; Jefferson et al., 2007). Common elements for URU formation include 1) U-rich source rocks in the basin and basement; 2) an unconformity between basin and basement; 3) fractures or faults across the unconformity; 4) oxidized hydrothermal fluids to transport U interacting with a reductant to reduce the fluid and induce U precipitation at the site of deposition; and 5) forces to drive fluid movement (e.g., tectonics, gravity, density). The evolution in pH, temperature, oxygen fugacity, and salinity of the fluids are also critical to deposit formation (Kyser et al., 2009).

Precipitation of U is a consequence of a redox reaction, as U has two valence states: U^{6+} (uranyl ion) and U^{4+} (uranous ion). The uranyl ion is easily soluble in oxidized, likely basinally-derived hydrothermal fluids, and is transported until reduced and precipitated as the uranous ion, usually as UO_2 (Langmuir, 1978; Romberger, 1985; Alexandre and Kyser

2005; Cuney, 2009). The hydrothermal fluid-rock interaction responsible for mineralization begins with basinal brines extracting U from available detrital heavy minerals in the sandstones of the basin, such as zircon, monazite, and apatite (Hoeve and Sibbald, 1978; Hoeve and Quirt, 1984; Kyser, 2007; Fayek and Kyser, 1997), or from U sources in the basement such as pegmatites, granitoid rocks, and accessory monazite (Annesley et al., 2005; Hecht and Cuney, 2000). The reductant responsible for the precipitation reaction may be reduced fluids from the basement that mix with the oxidized fluids, or the reduced lithology of the basement itself (Hoeve and Sibbald, 1978; Tremblay, 1982; Hoeve and Quirt 1984). The location of the mineralization is dependent on the direction of syn- and post-ore fluid flows that result in precipitation at, above, or below the unconformity between the oxidized basin and reduced basement (Hoeve and Quirt, 1984; Fayek and Kyser, 1997; Ruzicka, 1996; Jefferson et al., 2007).

In addition to oxidized fluids and reductants at the site of deposition, tectonic controls were also critical for converging fluid pathways and driving their movement (e.g., Tremblay, 1982; Ruzicka, 1996). Tectonic stresses created conduits (i.e., fractures and faults) for pathways across the unconformity to focus fluids, and, coupled with gravity, induced fluid flow in and out of the basement and basin (Tremblay, 1982; Cui et al., 2012). Rheological contrast associated with reverse faulting also created necessary voids for fluid transport and deposit formation (Annesley et al., 2005; Kerr and Wallis, 2014). This focussing of fluid flow within a compact network of open fractures controlled both the hydrothermal alteration of country rock and the precipitation of U (Raffensperger and Garven, 1995; Kyser et al., 2000; Alexandre et al., 2009).

Early genetic models for URU formation (Fig. 1.3a–b) were framed as two endmembers — defined by emplacement of mineralization at the unconformity (sandstone-hosted) or below (basement-hosted) — and interpreted to have resulted from fluid flow out of (egress) or into (ingress) the basement, respectively. Mineralization style (poly- or monomineralic) has also been correlated to location above and below the unconformity, respectively (Hoeve and Quirt, 1984; Fayek and Kyser 1997; Jefferson et al., 2007). Subsequent models were based on the source of U: the basin, basement, or both (Ruzicka, 1996; Cuney et al., 2003; Kyser et al., 2000), and whether the reductant was basement-derived fluids or basement lithology (Hoeve and Sibbald, 1978; Hoeve and Quirt 1984; Wilson and Kyser, 1987; Kotzer and Kyser 1995; Komninou and Sverjensky 1995; Fayek and Kyser, 1997). The large diversity of URU deposits with shared characteristics suggests that subtleties exist between model endmembers in terms of their genesis via multiple fluid events (Fig. 1.3c; Mercadier et al., 2012; Sheahan et al., 2016).

The two deposits studied herein are broadly defined as sandstone-hosted (McArthur River) and basement-hosted (Millennium); however, each contain mineralization both at and below the unconformity (McGill et al., 1993; Roy et al., 2006). The majority of the Millennium deposit comprises monomineralic-style mineralization up to 150 m below the unconformity, yet a considerable amount (up to 20%, G. Zaluski, pers. comm. 2015) occurs at the unconformity. McArthur River comprises several mineralized pods, also monomineralic, which occur in multiple ore zones mainly at but also below the unconformity (McGill et al., 1993; Bronkhorst et al., 2012). Both deposits are situated

along major reverse faults that are part of regional fault systems containing abundant graphite (Cloutier et al., 2009; Ng et al., 2013).

1.3 REGIONAL GEOLOGY

1.3.1 Basement

The Rae and Hearne provinces and the Taltson Magmatic Zone of the Canadian Shield Province compose the 2.9–1.8 Ga basement rocks beneath the Athabasca Basin (Fig. 1.1). The Rae and Hearne provinces collided along the Snowbird Tectonic Zone (1.92–1.89 Ga), followed by the accretion of the Paleoproterozoic Reindeer Zone rocks to the eastern margin of the Hearne Province during the Trans-Hudson Orogeny (THO) (Hoffman, 1988; Ansdell, 2005; Corrigan et al., 2009).

The Rae Province underlies the western half of the Athabasca Basin and the Hearne Province the eastern half; URU deposits are associated with both provinces. The Millennium and McArthur River deposits are located in the southeastern part of the basin, where it overlies the Mudjatik and Wollaston domains of the Hearne Province (Lewry and Sibbald 1980; Hoffman, 1988; Ruzicka, 1996; Jefferson et al., 2007). The Mudjatik Domain is to the west of the Wollaston Domain, and consists of mainly Archean granitoid gneisses with scattered Archean and Paleoproterozoic supracrustal rocks; the Wollaston Domain contains Archean granitoid gneisses with overlying Paleoproterozoic metasedimentary rocks (Annesley et al. 2005; Yeo and Delaney, 2007). Unconformity-related U deposits in the southeastern Athabasca Basin are clustered in a region within or near the transition between the Wollaston and Mudjatik domains, an area approximately

20 km wide, known as the Wollaston-Mudjatik Transition Zone (WMTZ) (Fig. 1.2a; Annesley et al., 2005; Jeanneret et al., 2016).

Far-field tectonic activity affected the Rae and Hearne provinces after their amalgamation, reactivating faults and fractures via both extensional and compressional tectonics, which created the space and differential permeability necessary for fluid movement into and out of the basement (Hoeve and Quirt 1984; Alexandre and Kyser, 2005; Boiron et al., 2010; Sheahan et al., 2016). Regional graphite-bearing fault systems are common first order URU exploration targets via electromagnetic techniques. Traditionally, graphite has been an exploration target due to its empirical association with URU deposits after the Key Lake discovery, leading to the hypothesis of the reducing capabilities of the related alteration product, methane; however, current research suggests that U is capable of precipitating with or without its presence (Raffensperger and Garven, 1995; Aghbelagh and Yang, 2014). Instead, the association of graphite with U deposits likely reflects its presence in reactivated faults, creating high permeability conduits for focussing long-term fluid flow between the basin and basement (Aghbelagh and Yang, 2014; Kerr and Wallis, 2014). Other potential reductants for the formation of UO_2 are Fe^{2+} and H_2S from the alteration of pyrite, or Fe^{2+} produced by the chlorite alteration of biotite, both of which are present in the metasedimentary rocks beneath the Athabasca Basin (Yeo and Potter, 2010).

1.3.2 Athabasca Basin

The Athabasca Basin is a basin of quartzose sandstone fill that lies unconformably over the regolith developed atop the Rae and Hearne province basement rocks (Kyser,

2014). Initiation of sedimentation in the Athabasca Basin is suggested to be about 1.75–1.73 Ga based on timing of the Trans-Hudson uplifts (Kyser et al., 2000; Ramaekers and Catuneanu, 2004). An age of 1.74–1.73 Ga has also been proposed by Rainbird et al. (2007), with a 10–20 Ma gap between the end of the THO and the thermal subsidence of the basin, accounting for the difference in orientation between the NE-SW trend of the THO and the E-W geometry of the basin. An age of 1.7–1.65 Ga was suggested by Cumming and Krstic (1992) from U-Pb dating of diagenetic fluorapatite assumed to be representative of the minimum age of deposition.

Three subbasins are found within the Athabasca; from west to east they are the Jackfish (oldest), Mirror (largest and youngest) and Cree. The Cree hosts the Millennium and McArthur River deposits, as well as the majority of URU deposits (Hiatt and Kyser, 2007). The basin contains four sequences comprising a total of eight formations, most of which are interpreted to have been deposited in a fluvial environment (Ramaekers and Catuneanu, 2004). Formations generally exhibit basal, thin, coarsening-upwards beds overlain by a series of fining-upwards sandstones. Ramaekers and Catuneanu (2004) suggested these coarse beds to be a result of a low accommodation systems tract filled in by prograding fluvial deposits; once level, fining up sequences continued deposition as part of a high accommodation systems tract.

The basin is intracratonic with no evidence of rift-related activity (Hiatt and Kyser, 2007). Based on paleomagnetic data, Kotzer et al. (1992) determined that diagenesis within the Athabasca occurred in three distinct time periods: 1.75–1.6 Ga (initial diagenesis), 1.6–1.45 Ga (peak diagenesis), and 0.9 Ga (thermal alteration), concluding that fluid flow was

episodic and basin-wide. After 1.65 Ga, tectonic activity associated with multiple far-field events caused the creation/reactivation of faults and fractures, along with basin tilting, which induced fluid flow along with free thermal convection (Hoeve and Quirt, 1984; Richard et al., 2010; Chi et al., 2013). Uranium-Pb ages on U minerals support the interpretation that punctuated fluid flow events in the Athabasca Basin were responsible for episodes of mineralization; these events coincided with the Wyoming and Mazatzal orogenies (1.6–1.5 Ga), Berthoud Orogeny (1.4 Ga), Mackenzie Dike Swarm (1.3 Ga), Grenville Orogeny (1.1–1.0 Ga), and the breakup of Rodinia (0.8 Ga) (Fayek et al., 2002; Alexandre et al., 2009). During these events, the coincidence of tectonic driven fluid flow, appropriate sedimentary facies with adequate permeability and porosity, structural conduits to focus fluid flow, and suitable physical and chemical traps led to the formation and remobilization of world class U mineralization (Alexandre et al., 2009).

1.4 DEPOSIT GEOLOGY

1.4.1 Wollaston-Mudjatik Transition Zone (Hearne Province)

The Wollaston-Mudjatik Transition Zone (WMTZ), located in the Hearne Province, is a ~20 km wide corridor between the Wollaston and Mudjatik domains that hosts, or is proximal to, many URU deposits in the southeastern Athabasca Basin (Annesley et al., 2005; Jeanneret et al., 2016), including the Millennium and McArthur River deposits (Fig. 1.2a). The rheological contrast and repeated transpressional faulting between the Wollaston and Mudjatik domains resulted in available space for U-bearing intrusions such as leucogranites and pegmatites to form, and pathways for fluid to enter and exit the basement (Annesley et al., 2005). The U-enrichment of the leucogranites and

pegmatites is interpreted to be due to partial melting of the metasedimentary rocks during the end of the THO (1.8 Ga) (Mercadier et al., 2013; Jeanneret et al., 2016). The WMTZ is also located within a high-heat production corridor that may have caused crustal melting, providing unusually high (2–5% by weight) U content in monazites (Annesley et al., 2005). Structural reactivation in the WMTZ, in combination with a U-rich lithologies, created an ideal environment for URU deposit formation (Jeanneret et al., 2016).

1.4.2 B1 and P2 trends

Both the Millennium and the McArthur River deposits are situated on and in major reverse faults near the WMTZ (McGill et al., 1993; Roy et al., 2006). These faults are part of graphitic structural trends that strike NNE, known as the B1 and P2 trends, respectively; they are within 15 km of each other but are not directly connected (Fig. 1.2b).

The B1 basement trend hosts the Millennium deposit, where mineralization is mainly situated between two dominant reverse faults (Fig. 1.4). The lower, footwall fault is known as the 'Mother' fault and the upper, hanging wall fault has no formal name; both probably controlled fluid flow (Roy et al., 2006; Cloutier et al., 2009; Fayek et al., 2010). The basement rocks are deformed and extensively altered, exhibiting distal saussurite and sericite alteration and chlorite, dravite, and argillic alteration proximal to mineralization (Fig. 1.4b). The footwall lithologies have not been fully explored (Roy et al., 2006). The hanging wall lithologies above the Mother fault include calc-silicates, pelitic to semipelitic gneisses and schists, graphitic pelitic schists, pegmatites and leucogranites (Roy et al., 2006; Cloutier et al., 2009). Near the upper reverse fault is the *Marker Unit,* which hosts

ore-grade mineralization and contains graphitic metasedimentary rocks, as well as cordierite porphyroblastic pelitic schist (Roy et al., 2006).

The P2 trend, generally trending 045° in its entirety, hosts the McArthur River deposits (McGill et al., 1993; Ng et al., 2013). The P2 trend reverse fault displaces the hanging wall by 60–80 m, within Wollaston Domain basement rocks rich in graphite, through multiple fault zones dipping 40°–65° SE (McGill et al., 1993; Bronkhorst et al., 2012). These basement rocks consist of metasedimentary units, as in the B1 trend mentioned above. The hanging wall is predominantly pelitic and psammopelitic gneisses containing cordierite and graphite; the footwall is dominantly calc-silicate and quartzite units (McGill et al., 1993). Alteration minerals in the basement rocks include illite, chlorite, and dravite, with chlorite dominant proximal to the orebody, and illite dominant at more distal locations (Alexandre et al., 2005). Mineralization is hosted above, at, and below the unconformity in different zones within the P2 trend. Zones 1–4 South and A–C are collectively considered the McArthur River deposit, formerly known as P2 North (Fig. 1.5; Bronkhorst et al., 2012). There is a currently subeconomic mineralized zone at the southwestern end of the study area, not part of the McArthur River deposit, known as P2 Main (Bronkhorst et al., 2012). Figure 1.2b illustrates the trends and deposit locations for both the Millennium and McArthur River study areas.

1.4.3 Manitou Falls Formation

Fluid inclusion and clay mineralogy studies suggest that the Athabasca Basin was once 5–6 km deep; since its formation, erosion has reduced its overall sediment thickness to 1–2 km (Pagel et al., 1980; Hoeve et al., 1981). In the southeastern area of the basin

hosting the study areas, the depth of sedimentary cover over the Millennium and McArthur River deposits is 500–750 m and 480–560 m, respectively (Roy et al., 2006; McGill et al., 1993).

The Millennium and McArthur River deposits are both overlain by the Manitou Falls Formation (Ramaekers and Catuneanu, 2004). The Manitou Falls Formation comprises sublithic arkose to quartz arenite with 90–95% SiO_2 on average (Quirt 1985; Hiatt and Kyser, 2007), and is unmetamorphosed and generally flat-lying (McGill et al., 1993; Hiatt and Kyser, 2007). It is divided into four lithofacies, the upper three being products of a braided fluvial depositional environment and the stratigraphically lowest sourced from both a braided fluvial and an alluvial fan environment (Hiatt and Kyser, 2007). From oldest to youngest, they are MFa (at the unconformity), overlain by MFb, MFc, and uppermost MFd, which is overlain by up to 100 m of overburden (Campbell, 2007). In some areas, the base of the MFa corresponds to the unconformity itself; in others, the MFa is in contact with a fanglomerate, which is above the unconformable contact (McGill et al., 1993; Quirt, 2000). The fanglomerate is more prevalent at McArthur River than at Millennium, averaging 10 m thick over the hanging wall unconformity and 25 m thick over the footwall unconformity, and consists of clasts of Paleoproterozoic quartzite (McGill et al., 1993). Ramaekers et al. (2007) renamed the Manitou Falls Formation lithofacies; in particular, the MFa to the Read Formation as a method to redefine the basal lithofacies and their relationship to the unconformity. However, as all samples collected for this study are classified as being from one of the A–D Manitou Falls Formation

lithofacies, the original nomenclature is retained in this thesis. These individual lithofacies are described in greater detail in Chapters 2 and 3.

Large-scale alteration halos containing clay-type minerals (illite, chlorite, and dravite) often associated with URU deposits are abundant in the Manitou Falls Formation at all depths (Earle and Sopuck, 1989; Kotzer and Kyser, 1995). They extend for 10s of kilometres and illustrate the extent of diagenetic and hydrothermal processes, accompanied by bleaching (Hoeve and Quirt, 1984; Zhang et al., 2001; Jefferson et al., 2007). The stratigraphy and lithofacies of the Manitou Falls Formation controlled the lateral movement of diagenetic and hydrothermal fluids (Kotzer and Kyser, 1995). This is supported by the interpretation of a diagenetic aquitard in limited locations of the eastern Athabasca between the MFb and MFa lithofacies (Hiatt and Kyser, 2007), and the uranogenic Pb isotope signatures recognized to extend 100s of metres laterally within the MFa (Holk et al., 2003). Consequently, lithostratigraphic variation, along with diagenetic or hydrothermal sealing processes, were important factors in controlling the direction of fluid flow, quartz cementation, and ultimately the location of mineralization (Hoeve and Quirt, 1984; Hiatt and Kyser, 2007; Ng et al., 2013).

1.5 THESIS OBJECTIVES

The main goal of the project was to develop a 3D lithogeochemical footprint of two URU deposits. Both the Millennium and McArthur River deposits are associated with major reverse faults with evidence of past hydrothermal fluid-rock interaction, which left variable mineralogical and geochemical signatures at varying distances from mineralization, at multiple stratigraphic levels. Major elements associated with alteration

minerals (Al, Mg, K) are known to form large-scale (100s of metres) haloes associated with URU deposits (Earle and Sopuck, 1989; Zhang et al., 2001; Laverret et al., 2006; Jefferson et al., 2007). Trace elements related both to U mineralization (e.g., Pb, Co, Ni, As) and other redox active elements (e.g., Mo, V) occur in elevated amounts in and around URU deposits as well, albeit on a smaller scale (Hoeve and Sibbald, 1978; Tremblay, 1982; Ng et al., 2013). The distributions of these traditional pathfinder elements are well documented around the edges of U mineralization; however, less understood are the distal edges of the related alteration haloes and how they can be utilized for vectoring purposes. Abundant legacy data were provided to the author by Cameco Corporation to define the edges of these alteration patterns surrounding the Millennium and McArthur River deposits. Nearly three decades of exploration, including over 10,000 individual sample analyses, facilitated large study areas (~20 km strike length at both locations) that illustrate the alteration footprint on a district scale that has never been fully interrogated before. This results in a more comprehensive footprint than those from smaller or more targeted datasets. By focussing on the distal edges of the sandstone alteration, a set of criteria can be developed to aid in future exploration efforts. In doing so, the following questions were addressed:

1) What elemental concentrations define the distal edges of alteration related to mineralization processes, and what are the halo dimensions?
2) Are there elements or a combination of elements that may be useful as pathfinders to vector toward U mineralization?

The data summarized in this thesis will be integrated with other researchers' work as part of the major data integration initiative in the Canadian Mining Innovation Council

(CMIC)-Footprints project to develop a comprehensive integrated geological, geochemical, mineralogical, and geophysical footprint of the U deposits in the Athabasca Basin.

1.6 METHODS

1.6.1 Whole rock geochemistry: legacy database

The footprint areas for the Millennium and McArthur River deposits have been actively drilled since 1987 and 1984, respectively, creating a legacy database of whole rock geochemical results of over 10,000 samples. These representative (composite) Manitou Falls Formation samples were composed of a series of sandstone chips ~1 cm thick, collected approximately every 1.5 m over intervals of 5, 10, or 20 m, and logged as belonging to a specific lithofacies. Fanglomerate samples were excluded from the data analysis as they are not consistently present throughout the study areas. Early exploration comprised the common pathfinder elements Cu, Ni, Pb, B, and U, which were analyzed using atomic absorption spectrophotometry (AAS) and inductively coupled plasma optical emission spectrometry (ICP-OES) (Quirt, 1985). Later analyses included a greater breadth of major and trace elements, increased accuracy, and lower detection limits with the addition of inductively coupled plasma mass spectrometry (ICP-MS). Saskatchewan Research Council (SRC) Geoanalytical Laboratories performed all whole rock geochemistry, utilizing partial (2-acid) and total (3-acid) digestion methods. Their methodology is described in detail in Chapter 2. Appendix A describes how the data was selected and filtered, for both deposits, with respect to differences in sample collection

and accuracy and precision variations over time. Table A.1 shows the most current analysis suite, including instrumentation used and detection limits for each element.

This database was provided to the author for interpretation. Samples were restricted to those that contained ≤1000 ppm U (total and partial digestion) to focus on the distal geochemical signature not significantly influenced by ore bodies. This legacy data for both the Millennium and McArthur River deposits provide the basis for the bulk of the lithogeochemical and spatial analysis in this thesis, as discussed in Chapters 2, 3, and 4.

1.6.2 Drill core sample collection: new data

New data was also obtained on samples collected from McArthur River deposit drill cores in July–August 2014 to augment the historical data through targeted sample collection related to the McArthur River deposit. A total of 230 sandstone grab samples from 13 cores across four fences (sections) were collected, to include sandstone above and adjacent to areas with high, low, and negligible mineralization, from near surface to the unconformity. Individual samples were split lengthwise at Memorial University, and shared between the author and collaborator Nicholas Joyce (M.Sc. candidate, Queen's University), who focussed on mineralogy, mineral chemistry, and quantitative mineral analysis of the same samples. Adjacent samples were collected for petrophysical analysis by other researchers as part of the data integration initiative of the CMIC-Footprints Project. Of the split samples, the author cut specimens for whole rock geochemistry that were analyzed at SRC Laboratories (ICP-MS1 analysis suite), with the specific addition of SiO_2 and B analyses. Additionally, 58 thin section specimens were cut and prepared by Vancouver Petrographic Laboratories. Sample collection and results are summarized in

Chapter 3. Appendices D and E contain the sample locations and whole rock geochemical (new data only) results.

1.6.3 Short-wave infrared spectroscopy

Short-wave infrared spectroscopy (SWIR) is an instrumental spectral analysis performed directly on drill core without further sample preparation (Russell and Fraser, 1994; Percival et al., 2002). Cameco's portable instrumentation (PIMA II or ASD Terraspec instruments, with MinSpec 4 software) analyzes for 5 minerals: kaolinite, dickite, illite, dravite, and chlorite. The methodology is described in greater detail in Appendix B. As it is inexpensive and can be done immediately upon core retrieval, the analysis for alteration-related mineralogy is a quick and simple way to identify diagenetic and hydrothermal (both K-related (illite); and Mg-related (chlorite, dravite)) alteration for large-scale vectoring. Cameco provided legacy SWIR data to the author, and SWIR determination on the new samples collected in 2014 was completed at Queen's University. Results for both deposits are summarized in Chapter 4 and Appendix B.

1.6.4 Results: 3D analysis and statistics

3D spatial analysis is a visual medium for projecting the lithogeochemical analyses mentioned above in relation to the deposit location. For this thesis, Geosoft® Target version 4.5.5., an add-on to ArcGIS geospatial software, was utilized to add dimensionality to the analysis through the projection of theoretical results between sample locations via inverse-distance weighting algorithms. It was also used to measure the large-scale approximate haloes of geochemical anomalies. All mathematical analysis and graphs utilized SPSS, an IBM-based statistical software program.

1.7 PRESENTATION

This thesis consists of three chapters and four appendices. Chapter 1 is an introduction to unconformity-related U deposits, and the geology associated with the Millennium and McArthur River deposits that are the focus of this study. Chapter 2 is a manuscript presenting the lithogeochemical footprint and the shallow vectoring possibilities of whole rock geochemistry for the Millennium deposit, and is intended for publication in a scientific, peer-reviewed journal. Chapter 3 summarizes the distal lithogeochemical signature of the McArthur deposit and the use of molar element ratios as vectors, and is also intended for eventual publication in a scientific, peer-reviewed journal. Chapter 4 summarizes the similarities and differences between the McArthur and Millennium lithogeochemical footprints. The Appendices include summaries of the data leveling process, SWIR results from the Millennium and McArthur River deposits, preliminary scanning electron microscope work on the thin sections from McArthur River samples collected, and the whole rock geochemical results on the samples collected at the McArthur River deposit.

REFERENCES

Aghbelagh, Y. B., & Yang, J. (2014). Effect of graphite zone in the formation of unconformity-related uranium deposits: Insights from reactive mass transport modeling. *Journal of Geochemical Exploration*, *144*(PA), 12–27. http://doi.org/10.1016/j.gexplo.2014.01.020

Alexandre, P., & Kyser, K. (2005). Effect of cation substitutions and alteration of uraninite. *Canadian Mineralogist*, *45*, 1005–1017. http://doi.org/10.2113/gscanmin.43.3.1005

Alexandre, P., Kyser, K., Polito, P., & Thomas, D. (2005). Alteration mineralogy and stable isotope geochemistry of Paleoproterozoic basement-hosted unconformity-type uranium deposits in the Athabasca Basin, Canada. *Economic Geology*, *100*(8), 1547–1563. http://doi.org/10.2113/gsecongeo.100.8.1547

Alexandre, P., Kyser, K., Thomas, D., Polito, P., & Marlat, J. (2009). Geochronology of unconformity-related uranium deposits in the Athabasca Basin, Saskatchewan, Canada and their integration in the evolution of the basin. *Mineralium Deposita*, *44*(1), 41–59. http://doi.org/10.1007/s00126-007-0153-3

Annesley, I. R., Madore, C., & Portella, P. (2005). Geology and thermotectonic evolution of the western margin of the Trans-Hudson Orogen: evidence from the eastern sub-Athabasca basement, Saskatchewan. *Canadian Journal of Earth Sciences*, *42*(4), 573–597. http://doi.org/10.1139/e05-034

Ansdell, K. M. (2005). Tectonic evolution of the Manitoba-Saskatchewan segment of the Paleoproterozoic Trans-Hudson Orogen, Canada. *Canadian Journal of Earth Sciences*, *42*(4), 741–759. http://doi.org/10.1139/e05-035

Beaufort, D., Cassagnabere, A., Petit, S., Lanson, B., Berger, G., Lacharpagne, J. C., & Johansen, H. (1998). Kaolinite-to-dickite reaction in sandstone reservoirs. *Clay Minerals*, *33*(2), 297–316.

Boiron, M. C., Cathelineau, M., & Richard, A. (2010). Fluid flows and metal deposition near basement/cover unconformity: lessons and analogies from Pb–Zn–F–Ba systems for the understanding of Proterozoic U deposits. *Geofluids*, *10*(1-2), 270–292. http://doi.org/10.1111/j.1468-8123.2010.00289.x

Bronkhorst, D., Edwards, C. R., Mainville, A. G., Murdock, G. M., & Yesnik, L. D. (2012). McArthur River operation, northern Saskatchewan, Canada. *National Instrument 43-101 Technical Report*: Cameco Corporation, 206 p.

Campbell, J. E. (2007). Quaternary geology of the eastern Athabasca Basin, Saskatchewan. *In* Jefferson C. W. & Delaney, G. (eds.), *EXTECH IV: Geology and Uranium EXploration TECHnology of the Proterozoic Athabasca Basin, Saskatchewan and Alberta*: Geological Survey of Canada, Bulletin 588, 211–228.

Card, C. D., Pană, D., Portella, P., Thomas, D. J., & Annesley, I. R. (2007). Basement rocks to the Athabasca basin, Saskatchewan and Alberta. *In* Jefferson C. W. & Delaney, G. (eds.), *EXTECH IV: Geology and Uranium EXploration TECHnology of the Proterozoic Athabasca Basin, Saskatchewan and Alberta*: Geological Survey of Canada, Bulletin 588, 69–87.

Chi, G., Bosman, S., & Card, C. (2013). Numerical modeling of fluid pressure regime in the Athabasca basin and implications for fluid flow models related to the unconformity-type uranium mineralization. *Journal of Geochemical*

Exploration, *125*, 8–19. http://doi.org/10.1016/j.gexplo.2012.10.017

Cloutier, J., Kyser, K., Olivo, G. R., Alexandre, P., & Halaburda, J. (2009). The Millennium uranium deposit, Athabasca Basin, Saskatchewan, Canada: an atypical basement-hosted unconformity-related uranium deposit. *Economic Geology*, *104*(6), 815–840. http://doi.org/10.2113/gsecongeo.104.6.815

Cloutier, J., Kyser, K., Olivo, G. R., & Alexandre, P. (2010). Contrasting patterns of alteration at the Wheeler River area, Athabasca basin, Saskatchewan, Canada: insights into the apparently uranium-barren zone K alteration system. *Economic Geology*, *105*(2), 303–324. http://doi.org/10.2113/gsecongeo.105.2.303

Corrigan, D., Pehrsson, S., Wodicka, N., & de Kemp, E. (2009). The Palaeoproterozoic Trans-Hudson Orogen: a prototype of modern accretionary processes. *Geological Society, London, Special Publications*, *327*(1), 457–479. http://doi.org/10.1144/SP327.19

Cui, T., Yang, J., & Samson, I. M. (2012). Tectonic deformation and fluid flow: implications for the formation of unconformity-related uranium deposits. *Economic Geology*, *107*(1), 147–163. http://doi.org/10.2113/econgeo.107.1.147

Cumming, G. L., & Krstic, D. (1992). The age of unconformity-related uranium mineralization in the Athabasca Basin, northern Saskatchewan. *Canadian Journal of Earth Sciences*, *29*(8), 1623–1639. http://doi.org/10.1139/e92-128

Cuney, M. (2009). The extreme diversity of uranium deposits. *Mineralium Deposita*, *44*(1), 3–9. http://doi.org/10.1007/s00126-008-0223-1

Cuney, M., Brouand, M., Cathelineau, M., Derome, D., Freiberger, R., Hecht, L., Kister, P., Lobaev, V., Lorilleux, G., Peiffert, C., & Bastoul, A. M. (2003). What parameters control the high grade-large tonnage of the Proterozoic unconformity related uranium deposits? *In* Cuney, M. (ed.), *Proceedings of the International Conference on Uranium Geochemistry: Nancy, France,* p. 123–126.

Earle, S. A. M., & Sopuck, V. J. (1989). Regional lithogeochemistry of the eastern part of the Athabasca Basin uranium province, Saskatchewan, Canada. *In* Muller-Kahle, E., (ed.), *Uranium resources and geology of North America: International Atomic Energy Agency,* TECDOC-500, 263–296.

Fayek, M. & Kyser, T. (1997). Characterization of multiple fluid-flow events and rare-earth-element mobility associated with formation of unconformity-type uranium deposits in the Athabasca Basin, Saskatchewan. *The Canadian Mineralogist, 35,* 627–658.

Fayek, M., Kyser, T. K., & Riciputi, L. R. (2002). U and Pb isotope analysis of uranium minerals by ion microprobe and the geochronology of the McArthur River and Sue

Zone uranium deposits, Saskatchewan, Canada. *The Canadian Mineralogist*, *40*(6), 1553–1570.

Fayek, M., Camacho, A., Beshears, C., Jiricka, D., & Halaburda, J. (2010). Two Sources of Uranium at the Millennium Uranium Deposit, Athabasca Basin, Saskatchewan, Canada. In *Geological Association of Canada—Mineralogical Association of Canada 2010 (Calgary) Annual Conference Abstracts Volume,* 4 p.

Hecht, L., & Cuney, M. (2000). Hydrothermal alteration of monazite in the Precambrian crystalline basement of the Athabasca Basin (Saskatchewan, Canada): implications for the formation of unconformity-related uranium deposits. *Mineralium Deposita*, *35*(8), 791–795. http://doi.org/10.1007/s001260050280

Hiatt, E. E., & Kyser, T. K. (2007). Sequence stratigraphy, hydrostratigraphy, and mineralizing fluid flow in the Proterozoic Manitou Falls Formation, eastern Athabasca Basin, Saskatchewan. *In* Jefferson C.W. & Delaney, G. (eds.), *EXTECH IV: Geology and Uranium EXploration TECHnology of the Proterozoic Athabasca Basin, Saskatchewan and Alberta*: Geological Survey of Canada, Bulletin 588, 489–506.

Hoeve, J., & Quirt, D. H. (1984). Mineralization and host rock alteration in relation to clay mineral diagenesis and evolution of the Middle-Proterozoic, Athabasca Basin, northern Saskatchewan, Canada. Saskatchewan Research Council, SRC Technical Report 187, 202 p.

Hoeve, J., & Sibbald, T. I. (1978). On the genesis of Rabbit Lake and other unconformity-type uranium deposits in northern Saskatchewan, Canada. *Economic Geology*, *73*, 1450–1473.

Hoeve, J., Rawsthorn, K., & Quirt, D. (1981). Uranium metallogenetic studies: clay mineral stratigraphy and diagenesis in the Athabasca Group. *In* Summary of Investigations 1981, Saskatchewan Geological Survey, Miscellaneous Report 81-4, p. 76–89.

Hoffman, P. F. (1988). United Plates of America, the birth of a craton: Early Proterozoic assembly and growth of Laurentia. *Annual Review of Earth and Planetary Sciences*, *16*, 543–603.

Holk, G. J., Kyser, T. K., Chipley, D., Hiatt, E. E., & Marlatt, J. (2003). Mobile Pb-isotopes in Proterozoic sedimentary basins as guides for exploration of uranium deposits. *Journal of Geochemical Exploration*, *80*(2), 297–320. http://doi.org/10.1016/S0375-6742(03)00196-1

Jackson, R. G. (2010). Application of 3D geochemistry to mineral exploration. *Geochemistry: Exploration, Environment, Analysis*, *10*(2), 143–156. http://doi.org/10.1144/1467-7873/09-217

Jeanneret, P., Goncalves, P., Durand, C., Trap, P., Marquer, D., Quirt, D., & Ledru, P. (2016). Tectono-metamorphic evolution of the pre-Athabasca basement within the Wollaston–Mudjatik Transition Zone, Saskatchewan. *Canadian Journal of Earth Sciences*, *53*(3), 231–259. http://doi.org/10.1139/cjes-2015-0136

Jefferson, C. W., Thomas, T. J., Gandhi, S. S., Ramaekers, P., Delaney, G., Brisbin, D., Cutts, C., Portella, P., & Olson, R.A. (2007). Unconformity-associated uranium deposits of the Athabasca Basin, Saskatchewan and Alberta. *In* Jefferson C. W. & Delaney, G. (eds.), *EXTECH IV: Geology and Uranium EXploration TECHnology of the Proterozoic Athabasca Basin, Saskatchewan and Alberta*: Geological Survey of Canada, Bulletin 588, 23–67.

Kerr, W. & Wallis, R. (2014). "Real-world" economics of the uranium deposits of the Athabasca Basin, northern Saskatchewan: why grade is not always king! SEG Newsletter, (99) 1, 11–15.

Komninou, A., & Sverjensky, D. A. (1995). Hydrothermal alteration and the chemistry of ore-forming fluids in an unconformity-type uranium deposit. *Geochimica et Cosmochimica Acta*, *59*(13), 2709–2723. http://doi.org/10.1016/0016-7037(95)00167-X

Kotzer, T. G., & Kyser, T. K. (1995). Petrogenesis of the Proterozoic Athabasca Basin, northern Saskatchewan, Canada, and its relation to diagenesis, hydrothermal uranium mineralization and paleohydrogeology. *Chemical Geology*, *120*(1), 45–89. http://doi.org/10.1016/0009-2541(94)00114-N

Kotzer, T. G; Kyser, T. K.; Irving, E. (1992) Paleomagnetism and the evolution of fluids in the Proterozoic Athabasca Basin, northern Saskatchewan, Canada. *Canadian Journal of Earth Sciences* 29(7), 1474–1491. http://doi.org/10.1139/e92-118

Kyser, T. K. (2007). Fluids, basin analysis, and mineral deposits. *Geofluids*, *7*(2), 238–257. http://doi.org/10.1111/j.1468-8123.2007.00178.x

Kyser, K. (2014). Uranium Ore Deposits, *In* Turekian, H. D., Holland, H. D., (eds.), Treatise on Geochemistry (2nd ed.): Oxford, Elsevier, v. 7, p. 489–513. http://doi.org/10.1016/B978-0-08-095975-7.01122-0

Kyser, K., & Cuney, M. (2008). Unconformity-related uranium deposits. *In* Cuney, M. & Kyser, K., (eds.), *Recent and not-so-recent developments in uranium deposits and implications for exploration*. Quebec: Mineralogical Association of Canada Short Course Series Vol. 39, 161–219. ISBN 978-0-921294-48-1

Kyser, K., Hiatt, E., Renac, C., Durocher, K., Holk, G., & Deckart, K. (2000). Diagenetic fluids in Paleo-and Meso-Proterozoic sedimentary basins and their implications for long protracted fluid histories. *In* Kyser, K. (ed.), *Fluids and basin evolution.* Mineralogical Association of Canada Short Course Series 28: 225–262.

http://doi.org/10.13140/2.1.1033.1847

Kyser, K. Alexandre, P. Polito, P., Djouka-Fonkwe, M., Geagea, M., & Uvarova, Y. (2009). Exploration strategies for uranium deposits. *In* Lentz, D. R., Thorne, K. G., & Beal, K-L. (eds.), *Proceedings of the 24th IAGS, Fredericton, Canada*, 439–443. ISBN 978-1-55131-136-4

Langmuir, D. (1978). Uranium solution-mineral equilibria at low temperatures with applications to sedimentary ore deposits. *Geochimica et Cosmochimica Acta*, *42*(6), 547–569. http://doi.org/10.1016/0016-7037(78)90001-7

Laverret, E., Mas, P. P., Beaufort, D., Kister, P., Quirt, D., Bruneton, P., & Clauer, N. (2006). Mineralogy and geochemistry of the host-rock alterations associated with the Shea Creek unconformity-type uranium deposits (Athabasca Basin, Saskatchewan, Canada). Part 1. Spatial variation of illite properties. *Clays and clay minerals*, *54*(3), 275–294. http://doi.org/10.1346/CCMN.2006.0540301

Lehmann, B. (2008). Uranium ore deposits. *Rev. Econ. Geol. AMS Online*, *2008*, 16–26.

Lewry, J. F., & Sibbald, T. I. I. (1980). Thermotectonic evolution of the Churchill Province in northern Saskatchewan. *Tectonophysics*, *68*, 45–82.

McGill, B. D., Marlatt, J. L., Matthews, R. B., Sopuck, V. J., Homeniuk, L. A., & Hubregtse, J. J. (1993). The P2 north uranium deposit, Saskatchewan, Canada. *Exploration and Mining Geology*, *2*(4), 321–331.

Mercadier, J., Richard, A., & Cathelineau, M. (2012). Boron-and magnesium-rich marine brines at the origin of giant unconformity-related uranium deposits: δ11B evidence from Mg-tourmalines. *Geology*, *40*(3), 231–234. http://doi.org/10.1130/G32509.1

Mercadier, J., Annesley, I. R., McKechnie, C. L., Bogdan, T. S., & Creighton, S. (2013). Magmatic and Metamorphic Uraninite Mineralization in the Western Margin of the Trans-Hudson Orogen (Saskatchewan, Canada): A Uranium Source for Unconformity-Related Uranium Deposits? *Economic Geology*, *108*(5), 1037–1065. http://doi.org/10.2113/econgeo.108.5.1037

Ng, R., Alexandre, P., & Kyser, K. (2013). Mineralogical and geochemical evolution of the unconformity-related McArthur River Zone 4 orebody in the Athabasca Basin, Canada: implications of a silicified zone. *Economic Geology*, *108*(7), 1657–1689. http://doi.org/10.2113/econgeo.108.7.1657

Pagel, M., Poty, B., & Sheppard, S. M. F. (1980). Contribution to some Saskatchewan uranium deposits mainly from fluid inclusions and isotopic data. *In* Ferguson, S. & Goleby, A. (eds.), *Uranium in the Pine Creek Geosyncline: Vienna, International Atomic Energy Agency*, p. 639–654.

Percival, J. B., Wasyliuk, K., Reif, T., Bernier, S., Drever, G., & Perkins, C. T. (2002). Mineralogical aspects of three drill cores along the McArthur River transect using a portable infrared spectrometer. *In* Summary of Investigations 2002, Volume 2, Saskatchewan Geological Survey, Saskatchewan Industry Resources, Miscellaneous Report D-14, 15 p.

Quirt, D. H. (1985). Lithogeochemistry of the Athabasca Group: Summary of sandstone data. *In* Summary of Investigations 1985, Saskatchewan Geological Survey, Saskatchewan Energy and Mines, Miscellaneous Report 85-4, p. 128–132.

Quirt, D. (2000). Sub-Athabasca Group fanglomerate in the McArthur River-Read Lake area, Saskatchewan: GeoCanada 2000: The Millennium Geoscience Summit [abs.]: Geological Association of Canada, Mineralogical Association of Canada (GAC-MAC), joint annual meeting, Calgary, Abstract 251.

Quirt, D. (2009). Applying Pb isotopes in unconformity-type uranium exploration. *In* Lentz, D. R., Thorne, K. G., & Beal, K-L. (eds.), *Proceedings of the 24th IAGS, Fredericton, Canada*, 453–456. ISBN 978-1-55131-136-4

Raffensperger, J. P., & Garven, G. (1995). The formation of unconformity-type uranium ore deposits 2, Coupled hydrochemical modeling. *American Journal of Science*, *295*(6), 639–696.

Rainbird, R. H., Stern, R. A., Rayner, N., & Jefferson, C. W. (2007). Age, provenance, and regional correlation of the Athabasca Group, Saskatchewan and Alberta, constrained by igneous and detrital zircon geochronology. *In* Jefferson C. W. & Delaney, G. (eds.), *EXTECH IV: Geology and Uranium EXploration TECHnology of the Proterozoic Athabasca Basin, Saskatchewan and Alberta*: Geological Survey of Canada, Bulletin 588, 193–209.

Ramaekers, P., & Catuneanu, O. (2004). Development and sequences of the Athabasca Basin, early Proterozoic, Saskatchewan and Alberta, Canada. *In* Eriksson P. G., Alterman, W., Nelson, D. R., Mueller, W. U., & Catuneanu, O. (eds.), *The Precambrian Earth: Tempos and Events* (Vol. 12, pp. 705–723). Amsterdam: Elsevier.

Ramaekers, P., Jefferson, C. W., Yeo, G. M., Collier, B., Long, D. G. F., Drever, G., McHardy, S., Jiricka, D., Cutts, C., Wheatley, K., Catuneanu, O., Bernier, S., Kupsch, B., & Post, R. T. (2007). Revised geological map and stratigraphy of the Athabasca Group, Saskatchewan and Alberta. *In* Jefferson C. W. & Delaney, G. (eds.), *EXTECH IV: Geology and Uranium EXploration TECHnology of the Proterozoic Athabasca Basin, Saskatchewan and Alberta*: Geological Survey of Canada, Bulletin 588, 155–187.

Richard, A., Pettke, T., Cathelineau, M., Boiron, M. C., Mercadier, J., Cuney, M., & Derome, D. (2010). Brine–rock interaction in the Athabasca basement (McArthur

River U deposit, Canada): consequences for fluid chemistry and uranium uptake. *Terra Nova*, *22*(4), 303-308. http://doi.org/10.1111/j.1365-3121.2010.00947.x

Romberger, S. B. (1985). Transport and deposition of uranium in hydrothermal systems at temperatures up to 300 degrees C, with genetic implications, *Special Volume - Canadian Institute of Mining and Metallurgy, 32: Canada, Canadian Institute of Mining and Metallurgy*: Montreal, QC, Canada, 12-17.

Roy, C., Halaburda, J., Thomas, D., & Hirsekorn, D. (2006). Millennium deposit-Basement-hosted derivative of the unconformity uranium model. In *Uranium production and raw materials for the nuclear fuel cycle-Supply and demand, economics, the environment and energy security: International Atomic Energy Agency Proceedings Series,* 111-121.

Russell, J. D. & Fraser, A. R. (1994). Infrared methods. *In* Wilson, M. J. (ed.), *Clay Mineralogy: Spectroscopic and Chemical Determinative Methods* (pp. 11–67). Springer Netherlands. ISBN: 978-94-010-4313-7

Ruzicka, V. (1996). Unconformity-associated uranium. *In* Eckstrand, O. R., Sinclair, W. D., & Thorpe, R. I., (eds.), *Geology of Canadian Mineral Deposit Types.* Geological Survey of Canada, Geology of Canada, No. 8, 197–210.

Shannon, R. T. (1976). Revised effective ionic radii and systematic studies of interatomic distances in halides and chalcogenides. *Acta Crystallographica section A: crystal physics, diffraction, theoretical and general crystallography*, *32*, 751–767.

Sheahan, C., Fayek, M., Quirt, D., & Jefferson, C. W. (2016). A Combined Ingress-Egress Model for the Kianna Unconformity-Related Uranium Deposit, Shea Creek Project, Athabasca Basin, Canada. *Economic Geology*, *111*, 225–257.

Sopuck, V. J., De Carle, A., Wray, E. M., & Cooper, B. (1983). Application of lithogeochemistry to the search for unconformity-type uranium deposits in the Athabasca Basin. *In* Cameron, E. M. (ed.), *Uranium Exploration in Athabasca Basin, Saskatchewan, Canada,* Geological Survey of Canada: Paper 82-11, 191–205.

Tremblay, L. (1982). Geology of the uranium deposits related to the sub-Athabasca unconformity, Saskatchewan, Canada. Geological Survey of Canada: Paper 81-20, 56 p.

Wilson, M. R., & Kyser, T. K. (1987). Stable isotope geochemistry of alteration associated with the Key Lake uranium deposit, Canada. *Economic Geology*, *82*(6), 1540–1557. http://doi.org/10.2113/gsecongeo.82.6.1540

Yeo, G. M., & Delaney, G. (2007). The Wollaston supergroup, stratigraphy and metallogeny of a Paleoproterozoic Wilson cycle in the Trans-Hudson Orogen,

Saskatchewan. *In* Jefferson C. W. & Delaney, G. (eds.), *EXTECH IV: Geology and Uranium EXploration TECHnology of the Proterozoic Athabasca Basin, Saskatchewan and Alberta*: Geological Survey of Canada, Bulletin 588, 89-117.

Yeo, G. M., & Potter, E. G. (2010). Review of reducing mechanisms potentially involved in the formation of unconformity-type uranium deposits and their relevance to exploration. *In Summary of Investigations 2010, Volume 2,* Saskatchewan Geological Survey, Sask. Ministry of Energy and Resources, Misc. Report 2010-4.2, Paper A-12, 13 p.

Zhang, G., Wasyliuk, K., & Pan, Y. (2001). The characterization and quantitative analysis of clay minerals in the Athabasca Basin, Saskatchewan: Application of shortwave infrared reflectance spectroscopy. *The Canadian Mineralogist*, *39*(5), 1347-1363. http://doi.org/10.2113/gscanmin.39.5.1347

FIGURES

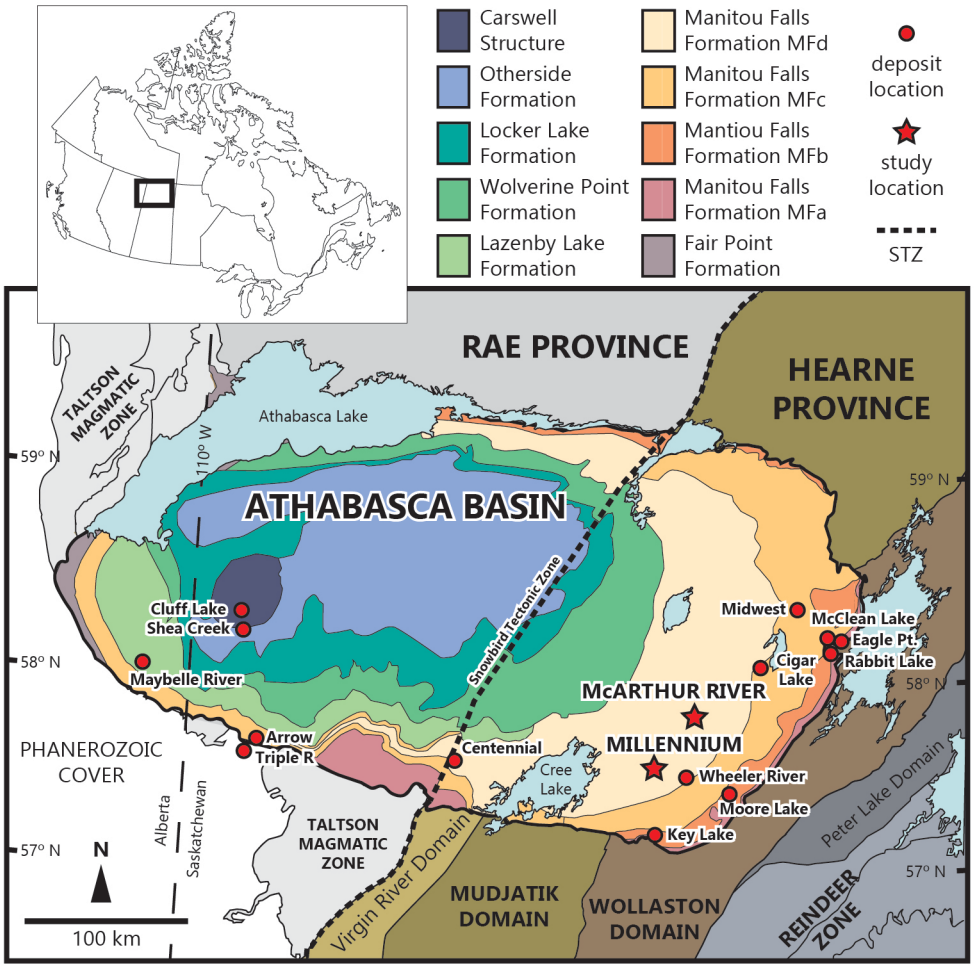

Figure 1.1: Simplified geological map of the Athabasca Basin and underlying Precambrian domains, Saskatchewan and Alberta. STZ: Snowbird Tectonic Zone, responsible for the accretion of the Rae and Hearne provinces. The Trans-Hudson orogen was responsible for the final amalgamation of the basement underlying the Athabasca Basin prior to its formation by accreting the Reindeer Zone to the eastern edge of the Hearne Province (Hoffman, 1988; Ansdell, 2005; Corrigan et al., 2009). Unconformity-related uranium deposits are found throughout the basin, and many, including the Millennium and McArthur River deposits, are located in the eastern portion of the basin, associated with the Wollaston Domain basement rocks. Modified from Card et al. (2007) and Cloutier et al. (2009).

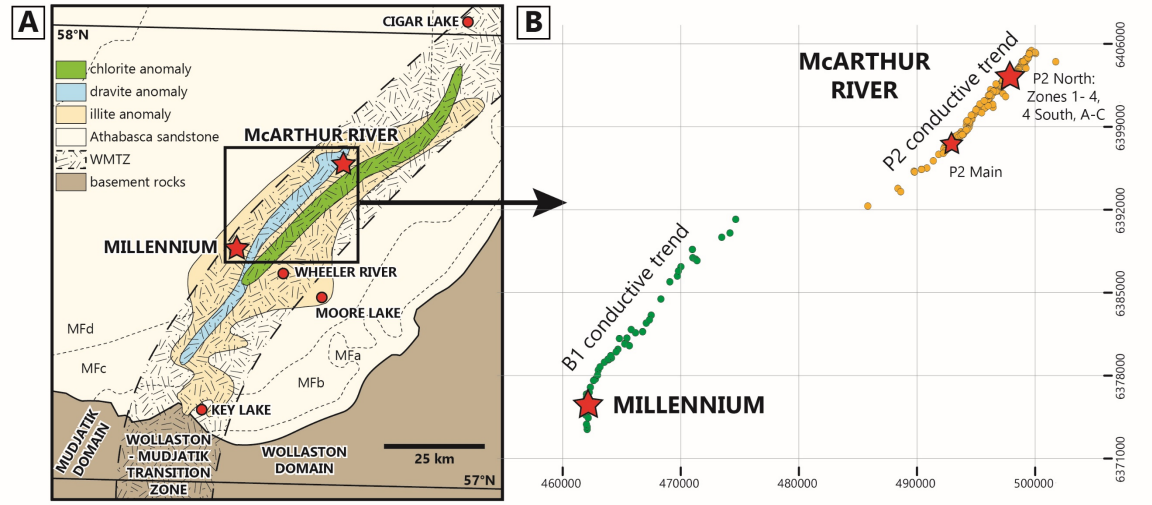

Figure 1.2: Study area of Millennium and McArthur River deposits. (**A**) Southeastern area of Athabasca basin showing the distribution of Manitou Falls lithofacies below the glacial overburden, and clay-type minerals in the Athabasca sandstones. Both deposits are located within a major illite anomaly, and near smaller chlorite and dravite anomalies, all of which are associated with hydrothermal alteration; chlorite and dravite, in particular, have been associated with unconformity-related U deposits. The Wollaston-Mudjatik Transition Zone (WMTZ) is thought to be a particularly fertile environment for URU deposits due to heavy deformation, metamorphism, faulting, and partial melting prior to basin formation. Adapted from Earle and Sopuck (1989), Jefferson et al. (2007), and Jeanneret et al. (2016). (**B**) Inset map of square seen in (**A**). Dots are drill collar locations, from which all samples herein are derived, imported from ArcGIS. Coordinate units are WGS-84 UTM 13N.

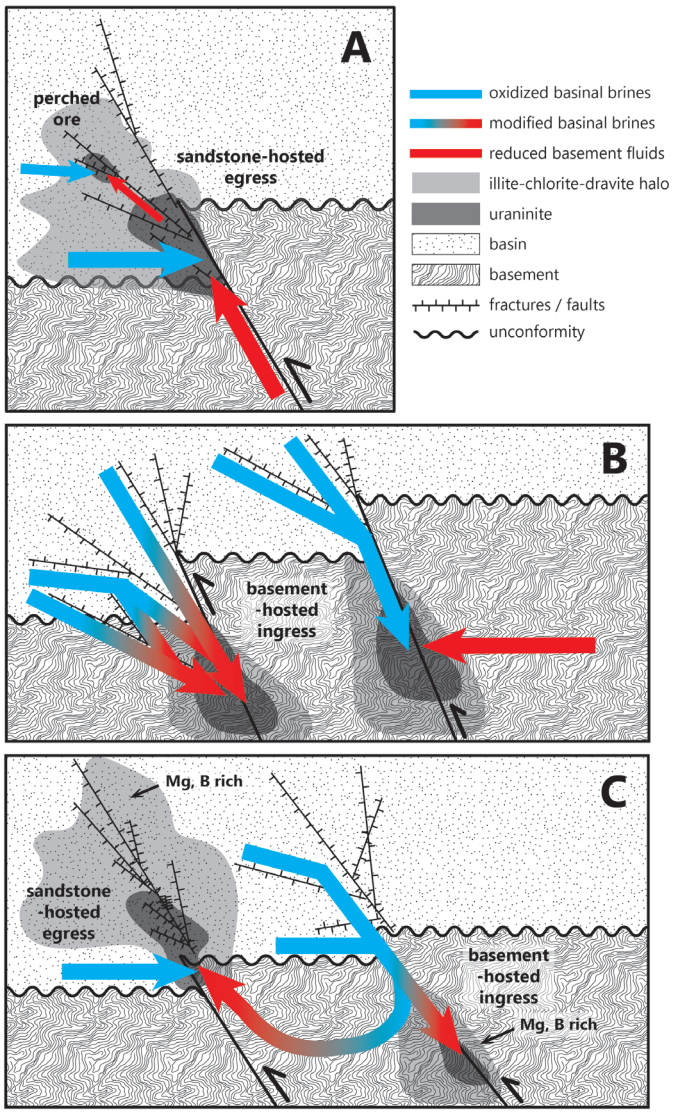

Figure 1.3: Simplified hydrothermal models for unconformity-related uranium (URU) deposits. Endmembers are generally classified as sandstone-hosted and basement-hosted, commonly referred to as egress and ingress models. (**A**) Sandstone-hosted deposits are interpreted to be a result of oxidized, hydrothermal basinal brines that leach U from detrital minerals of the basin sandstones. Reduced fluids derived from the basement enter the sedimentary basin rocks through major reverse faults and mix with the oxidized, U-rich fluids, resulting in U mineralization precipitating at the unconformity. Further upward migration can result in perched ore lenses. (**B**) In the basement-hosted model, the oxidized basinal brines enriched in U enter the basement through reverse faults, where it may also leach U. Mineralization occurs through the interaction with either the reduced lithology (fluid-rock) or the reduced basement fluids (fluid-mixing). (**C**) A single-source genetic model, which proposes that U-rich, oxidized basinal brines are modified by U-rich, reduced basement lithology, and that the placement of mineralization is dependent on the direction and volume of those modified fluids. Modified from Jefferson et al. (2007), Kyser and Cuney (2008), Cloutier et al. (2009), Mercadier et al. (2012), and Sheahan et al. (2016).

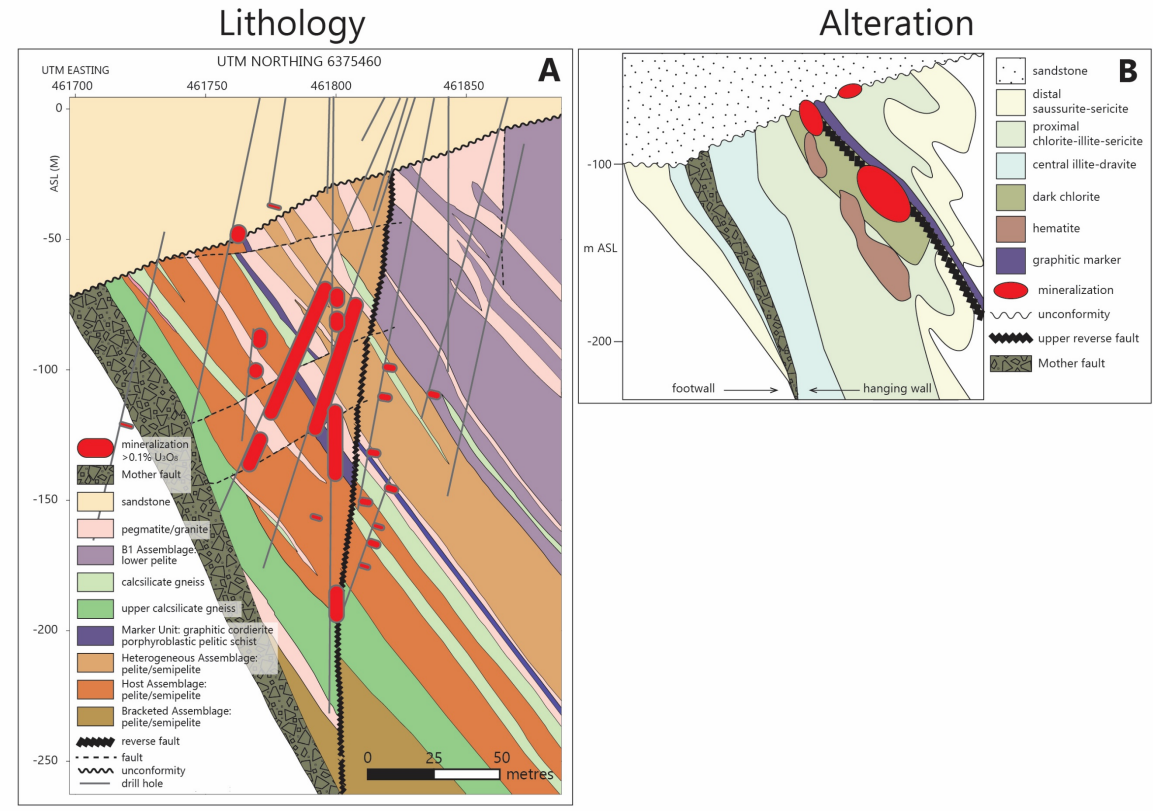

Figure 1.4: Millennium deposit geology of the basement, looking north. Depths are in metres above sea level (ASL); sandstones in the vicinity of the deposit extend to approximately 500 m ASL. (**A**) Cross section at the Millennium deposit discovery hole (CX-040) and surrounding drill holes. The basement hanging wall and footwall are demarcated by the Mother fault; the hanging wall is much more extensively explored. An upper reverse fault in the basement hanging wall is associated both with the graphitic Marker Unit and the majority of mineralization, although up to 20% can be present at the unconformity. Adapted from Cameco Internal Memo, J. Mukwakwami (2013). (**B**) Simplified alteration and mineralization, looking north, adapted from Roy et al. (2006) and Cloutier et al. (2009). Alteration zones of saussurite-sericite (distal) and illite-dravite (central) surround the Mother fault and are present in both hanging and footwalls of the basement rocks; a proximal halo (chlorite-illite-dravite) is associated with the upper reverse fault, graphitic Marker Unit, and mineralization. Hematite and chlorite are also spatially related to mineralization.

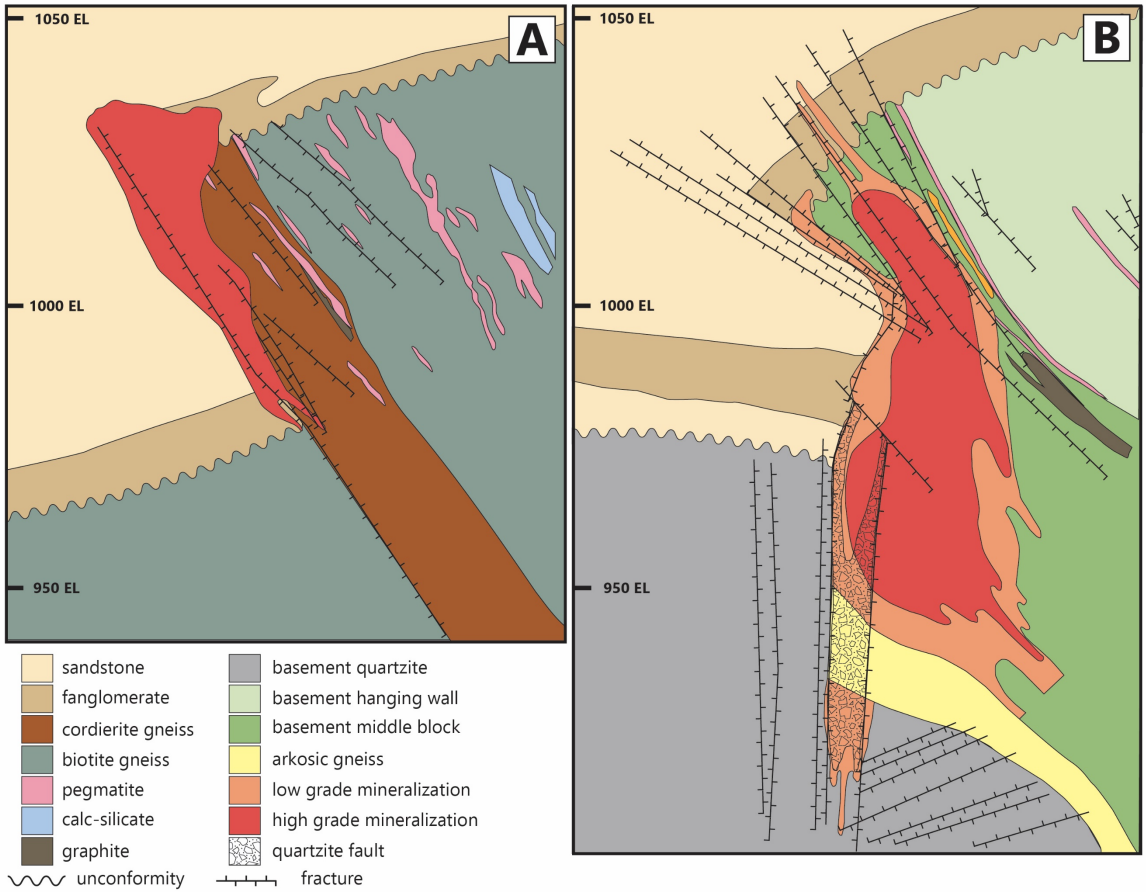

Figure 1.5: Generalized cross section of the McArthur River URU deposit, looking northeast. Composite illustration derived from Bronkhorst et al. (2012). A major graphitic reverse fault and dominant structural control, the P2, offsets the unconformity and hosts the mineralization. "High grade" and "low grade", in the scope of this illustration, is suggested by semi-quantitative radiometric counts in drillholes; "high" being suggestive of 20% or more U_3O_8, and "low" being greater than ~2% (Zaluski, pers. comm. 2017). (**A**) Typical cross section for all zones of the McArthur River deposit, with the exception of Zone 2; mineralization is concentrated within the P2 wedge at the unconformity, where faults and fractures are dominant. (**B**) Typical cross section for Zone 2. Mineralization here is basement-centric, within a middle block displaced by faults.

CHAPTER 2: 3D GEOCHEMICAL FOOTPRINT OF THE MILLENNIUM UNCONFORMITY-TYPE URANIUM DEPOSIT, CANADA: IMPLICATIONS FOR VECTORING

ABSTRACT

The Millennium deposit, a predominantly basement-hosted uranium deposit, is located in the southeastern Athabasca Basin, Saskatchewan, a region containing numerous high-grade unconformity-type U deposits. 3D mapping of the whole-rock lithogeochemistry of sandstones above the deposit shows a distinct footprint with select major and trace elements exhibiting increases towards mineralization. Molar Mg/K ratios increase from background levels 10 km north of the deposit, along strike of the B1 conductive trend, whereas Mo, Co, Rb, and Ga exhibit elevated concentrations immediately above the deposit, extending vertically from the unconformity to surface. Lead, Ag, Bi, Sb, REE, and Y exhibit elevated concentrations up to 650 m above the main mineralized body. Increasing Mg/K values indicate the transition from diagenetic to hydrothermal alteration with shifts from illitic (K-dominant) to chloritic and dravitic (Mg-dominant) alteration, the latter increasing more proximal to mineralization. Trace element enrichment patterns highlight that fractures and faults were conduits for fluid flow from the basement into the basin, both during ore formation and through tectonically driven post-depositional remobilization. Key indicators such as molar element ratios (Mg-K-Al) and trace elements related to redox reactions provide scalable vectors at the Millennium deposit that are likely applicable to similar unconformity-type U deposits elsewhere.

2.1 INTRODUCTION

The Athabasca Basin, located in northern Saskatchewan and Alberta, hosts high-grade unconformity-type U deposits that are important contributors to global U production (Fayek and Kyser, 1997; Cuney, 2005; Hiatt and Kyser, 2007). The Millennium deposit,

located in the southeastern Athabasca Basin, is a basement-hosted deposit containing 75.9 M lbs. U_3O_8, at a grade of 2.4% U_3O_8, (indicated resources); 29.0 M lbs. U_3O_8, at a grade of 3.2% U_3O_8 (inferred resources); and occurs at ~650 m depth (Cameco Corporation, 2015).

Unconformity-type U deposits occur at or near an unconformity between a Paleo- to Mesoproterozoic, redbed sedimentary basin and an Archean to Paleoproterozoic, metasedimentary basement (Tremblay, 1982; Cuney, 2009; Kyser, 2014). Mineralization is a redox reaction product of hydrothermal, oxidized brines carrying dissolved U interacting with a reductant at the site of deposition (diagenetic-hydrothermal metallogenic model: Hoeve and Quirt, 1984; Cuney, 2009; Kyser, 2014). The source of U and the fluids has been interpreted to be the sedimentary basin, the basement, or both (Hoeve and Sibbald, 1978; Fayek and Kyser, 1997; Hecht and Cuney, 2000; Richard et al., 2010). The generalized deposit endmembers are basement-hosted and unconformity-contact, in reference to their location; mineralization is interpreted to be the consequence of dominantly ingress (fluid-rock interaction) or egress (fluid-fluid interaction or mixing) fluid flow, respectively (Hoeve and Quirt, 1984; Fayek and Kyser, 1997). Regardless, most authors agree that the genetic model involves convection- and tectonic-driven hydrothermal fluid transport of oxidized sandstone brine that interacts with reduced basement fluids, or with reduced basement lithologies, leading to deposition of uranium oxides (Hoeve and Sibbald, 1978; Hoeve and Quirt, 1984; Kotzer and Kyser, 1995; Kyser, 2014). Uranium mineralization in the Athabasca Basin typically forms through a coupled

redox reaction involving uranyl (U^{6+}) and ferrous (Fe^{2+}) species (McGill et al., 1993; Alexandre et al., 2005; Ng et al., 2013b).

The hydrothermal processes associated with mineralization affect the basin sandstones to varying degrees, dependent on deposit style, leaving a geochemical signature that changes with proximity to a deposit, and therefore the potential for vectoring (Hoeve and Quirt, 1984; Earle and Sopuck, 1989; Kyser and Cuney, 2008). These alteration haloes in the basinal sandstones are often many times larger than the deposit itself, and are dominated by illite, kaolinite, chlorite, and dravite, and display quartz dissolution and loss of diagenetic hematite ("bleaching") (Hoeve and Quirt, 1984; Zhang et al., 2001). Complex (polymineralic) uranium mineralization associated with the unconformity-contact style of deposit contains varying amounts of sulfides and arsenides that contain pathfinder elements such as Ni, Co, Cu, Mo, Pb, and Zn (Hoeve and Sibbald, 1978; Sopuck et al., 1983; Ng et al., 2013a). Simple (monomineralic) mineralization, such as at Millennium, is usually found in basement-hosted deposits and lacks, or contains only minor amounts of, pathfinder-providing sulfides and arsenides (Fayek and Kyser, 1997; Jefferson et al., 2007). The clean sandstones in the eastern Athabasca Basin are ideal for the characterization of vectoring haloes, as they are unmetamorphosed, and are mainly quartz arenites with monomictic quartz pebble beds and minor siltstone beds (Hiatt and Kyser, 2007; Ramaekers et al., 2007). Against an average rock SiO_2 content of 95% (Quirt, 1985), background values of other major and trace elements in Athabasca Group sandstones are low and uniform; thus, subtle anomalies should be detectable. Therefore, we propose that the hydrothermal influence of monomineralic mineralization is identifiable above the

unconformity, even if weak, and can be mapped in three dimensions as a function of distance to the deposit.

The Millennium deposit is monomineralic and deep, but well explored, and the overlying sandstones can be evaluated for the distal lithogeochemical footprint and its variation with proximity to the deposit. A legacy database of >3000 samples over a 20-km strike length was made available to the author by Cameco Corporation for in-depth data analysis, providing for a comprehensive study capable of capturing subtle variations not seen in a more targeted exploration objective. To avoid undue influence from high-grade mineralization, only samples containing U concentrations <1000 ppm were included in the study. By examining the sandstone geochemistry and host-rock alteration mineralogy of these samples, the footprint of the deposit related to the ore forming processes can be characterized; this will ideally be larger in scale than the footprint related to the mineralization itself, but still provide vectoring capabilities. These characteristics may then be applied to future exploration efforts in the attempt to locate basement-hosted deposits that are often smaller in size than the unconformity-contact variety, but are preferred for extraction due to their simple mineralogy and superior strength and competency of wall-rocks (Alexandre et al., 2005; Roy et al., 2006; Jefferson et al., 2007; Kerr and Wallis, 2014). The aim of this paper is to assess potential vectors toward mineralization through examination of the sandstone lithogeochemical footprint associated with host-rock alteration, variably elevated U contents, and the lithostratigraphy of the sandstone above the deposit.

2.2 REGIONAL GEOLOGY

The Millennium deposit is located in the southeastern Athabasca Basin, a 1.75–1.54 Ga sandstone basin that unconformably overlies the 2.9–1.8 Ga basement of the Rae and Hearne provinces, and the Taltson Magmatic Zone of the Canadian Shield (Fig. 2.1a, Armstrong and Ramaekers, 1985; Kyser et al., 2000; Rainbird et al., 2007; Creaser and Stasiuk, 2007; Alexandre et al., 2009; Jeanneret et al., 2016). The Rae and Hearne provinces were juxtaposed along the Snowbird Tectonic Zone, prior to accretion of Paleoproterozoic rocks of the Reindeer Zone to the eastern margin of the Hearne province during the development of the Trans-Hudson Orogeny (Hoffman, 1988; Ansdell, 2005; Corrigan et al., 2009).

The Hearne Province underlying the eastern Athabasca Basin includes the Mudjatik and Wollaston domains (Lewry and Sibbald, 1980; Hoffman, 1988). The Mudjatik Domain consists of mainly Archean felsic gneisses with lesser Archean and Paleoproterozoic supracrustal rocks, and the Wollaston Domain contains Archean granitoid gneisses and overlying Paleoproterozoic metasedimentary rocks (Annesley et al., 2005; Yeo and Delaney, 2007). Uranium deposits found throughout the eastern Athabasca are generally focussed along the transition between the Mudjatik and Wollaston domains, a 20-km wide corridor known as the Wollaston-Mudjatik Transition Zone (WMTZ) (Fig. 2.1b; Annesley et al., 2005; Jeanneret et al., 2016). The WMTZ represents the transition between differing deformation styles, metamorphism, structure, and lithology in the two domains, defined by the shift in fabric from linear and NE-trending to curvilinear (Lewry and Sibbald, 1980; Annesley et al., 2005; Jeanneret et al., 2016).

The Athabasca Basin contains dominantly quartz arenitic sedimentary fill that formed through rapid tectonic uplift and thermal subsidence (Hiatt and Kyser, 2007; Rainbird et al., 2007). The rocks of the Rae and Hearne provinces were likely weathered before the sandstones were deposited, as an interpreted regolith underlies the basal contact of the basin (Hoeve and Sibbald, 1978; Macdonald, 1985). The Athabasca Group contains four major sedimentary sequences of mainly fluvial, lacustrine, and aeolian material with minor marine detritus in the uppermost units. Generally, the sequences fine upwards; all are sandstone-rich except for the final, marine sequence, which contains shales and carbonates (Ramaekers and Catuneanu, 2004; Hiatt and Kyser, 2007). The Millennium deposit is located below the Manitou Falls Formation, a sandstone-conglomerate formation with high quartz content deposited in an alluvial fan to braided stream environment (Ramaekers et al., 2007; Hiatt and Kyser, 2007). The lack of feldspar and other minerals, along with the presence of clays, suggests that the source rocks were heavily altered through weathering and transport, dominantly east to west, and later diagenesis (Hiatt and Kyser, 2007). Fluid inclusion and clay mineralogy studies suggest that the original depth of the basin was up to 5–6 km, although currently sedimentary cover is 1–2 km thick (Pagel et al., 1980; Hoeve et al., 1981).

Compressional and extensional regimes affected the basement rocks of the Hearne province both prior to and after the development of the Athabasca Basin (Annesley et al., 2005, Jeanneret et al., 2016). These tectonic events were essential for the genesis of uranium mineralization, as they reactivated basement structures that created the faults and fracture zones that served as fluid conduits between the basement and basin rocks, and

were also the driving mechanism for fluid flow across the unconformity (Cui et al., 2012; Chi et al., 2013).

2.3 DEPOSIT GEOLOGY

2.3.1 Basement Geology

The Millennium U deposit is located along the B1 trend, a conductive NNE-trending structural corridor within the WMTZ that contains a number of faults and extensive alteration (Roy et al., 2006). The basement rocks here are complexly folded by two main deformation events (D_1 and D_2) into a series of doubly-plunging, tight, upright to overturned, NE-trending folds with moderately to steeply dipping axial planes. The Wollaston group rocks hosting the Millennium deposit lie in a north-trending D_2 synform (Roy et al., 2006). The Mother fault, a major reverse fault with a northerly strike and moderate easterly dip, demarcates the footwall from the hanging wall of the basement (Fig. 2.2a; Cloutier et al., 2009). It contains pre-ore quartz within an approximately 10 m thick fault breccia hosted in a clay matrix (Roy et al., 2006; Cloutier et al., 2009). The deposit is hosted in the structural hanging wall within a complex fault zone ~10–100 m above the Mother fault.

The basement rocks are a complex assemblage of calc-silicate-bearing rocks, graphitic and non-graphitic pelitic to semi-pelitic gneisses and schists, pegmatites, and leucogranites (Fig. 2.2a; Roy et al., 2006; Cloutier et al., 2009). The hanging wall assemblages above the Mother fault host intensely altered and brecciated graphitic lithologies, which contain uranium mineralization in fracture-filling veins. The elevated permeability of these rocks allowed significant fluid flow into the basement along

associated faults, and this region is interpreted to represent a dilatant portion of the fault system (Roy et al., 2006; Cloutier et al., 2009; Fayek et al., 2010). The footwall assemblage is not well explored, but contains non-graphitic semipelitic and granite gneisses (Roy et al., 2006; Cloutier et al., 2009).

2.3.2 Athabasca Group

The Athabasca Group sandstones immediately overlie the unconformity between basin and basement (Hiatt and Kyser, 2007). In the B1 trend region, the Athabasca Group consists of 500–700 m of the Manitou Falls Formation, being thicker toward the northern end of the B1 trend (Roy et al., 2006). The Manitou Falls Formation is subdivided into four lithofacies (MFa, MFb, MFc, and MFd) having gradational, conformable contacts (Roy et al., 2006; Hiatt and Kyser 2007; Ramaekers et al., 2007). The oldest lithofacies, the MFa, directly overlies the sub-Athabasca unconformity. It is fine- to coarse-grained with disseminated pebbles and rare intercalated siltstones and mudstones, with a maximum thickness of 100 m (Yeo et al., 2002; Roy et al., 2006 Ramaekers et al., 2007). The MFb is medium- to coarse-grained quartz arenite, approximately 150 m thick, with local intercalated siltstone and clast-supported conglomerate beds. The MFa and MFb lithofacies typically contain diagenetic purple specular hematite and heavy mineral bands that are characteristically slightly radioactive due to the presence of Th-bearing aluminum phosphate-sulfate (APS) minerals that have replaced detrital monazite, and are overprinted by pink to red hematite (Hoeve and Quirt, 1984; Roy et al., 2006; Mwenifumbo and Bernius, 2007). The MFc is <100 m thick and consists of medium- to coarse-grained quartz arenite with <1% clay. The MFd is up to 200 m thick and consists of fine- to medium-

grained sandstone with >1% clay intraclasts; in the study area, it lies beneath 0–39 m of glacial overburden (Yeo et al., 2002; Roy et al., 2006; Ramaekers et al., 2007).

2.3.3 Uranium mineralization

The majority of mineralization at Millennium is located in the basement, more than 650 m below the surface and ~100 m below the unconformity; however, ~20% is present at the unconformity (Fig. 2.2b; Roy et al., 2006; Cloutier et al., 2009). It is monomineralic, consisting of mostly uraninite with minor coffinite (Roy et al., 2006; Cloutier et al., 2009; Fayek et al., 2010). Styles of mineralization are diverse and range from massive replacement, which is the dominant style, to matrix replacement in breccia and fracture fills; veins and veinlets; blebs and aggregates; and fine disseminated grains (Roy et al., 2006; Cloutier et al., 2009; Fayek et al., 2010). Mineralization is localized in a 25–55 m thick unit of pelitic-semipelitic gneisses and schists (the *Host Assemblage;* Fig. 2.2a). Ore-grade mineralization is concentrated within a reverse fault in the hanging wall of the basement beneath the *Graphitic Marker* unit (Roy et al., 2006). Weaker mineralization is found both below and above this unit and occurs in various lithologies including calc-silicates, pelitic to semipelitic gneisses and schists, and graphitic metasedimentary rocks (Roy et al., 2006). At the unconformity, massive to semi-massive to densely disseminated pitchblende replaces the sandstone and basement rocks immediately below. Textures here include clasts of pitchblende in a pitchblende matrix, massive replacement, infilling of pore space between sand grains, and thin veinlets (Zaluski, pers. comm. 2016). Mineralization at the unconformity extends downdip into the mineralization located in the basement rocks

along the upper reverse fault system, and grades are similar between these locations (Zaluski, pers. comm. 2016).

Uranium-Pb and Pb-Pb geochronology on uraninite in eastern Athabasca uranium deposits has produced ages that represent fluid events at circa 1.6–1.5 Ga, 1.3 Ga, 1.1 Ga, 0.9 Ga, and 0.3 Ga, corresponding to several far-field orogenic events (Wyoming, Mazatzal, and Grenville orogenies), the 1.27 Ga Mackenzie Dike Swarm, the 1.1 Ga Moore Lakes gabbro-diabase, and the breakup of Rodinia (Fayek and Kyser, 1997; Alexandre et al., 2009; Cloutier et al., 2009; Mercadier et al., 2009; Fayek et al., 2010; among others). Apparent dates on the mineralization at Millennium range from 1.75–0.28 Ga (Cloutier et al., 2009; Mercadier et al., 2009; Fayek et al., 2010). The oldest are model Pb-Pb ages from disseminated uraninite grains, which range from 1.75–1.65 Ga and possibly predate the basin, suggesting that the basement was one of the potential U sources (Fayek et al., 2010). Cloutier et al. (2009) obtained a regressed chemical age for "unaltered" uraninite of 1.59 Ga, which corresponds to an interpreted primary mineralization event observed throughout the Athabasca Basin (Alexandre et al., 2009). As with mineralization elsewhere in the basin, younger ages have also been obtained from Millennium mineralization (circa 1.39–1.35 Ga, 1.28 Ga, and 1.1–0.9 Ga) associated with resetting or Pb-loss events that are temporal with far-field tectonic events (Kotzer and Kyser, 1995; Alexandre et al., 2009; Cloutier et al., 2009; Fayek et al., 2010).

2.3.4 Host-rock alteration

At the Millennium deposit, both diagenetic and hydrothermal alteration are present, with hydrothermal alteration intensifying proximal to mineralization (Roy et al., 2006;

Cloutier et al., 2009; Fayek et al., 2010). Fluid inclusion studies suggest that the dominant fluids responsible for alteration were basinal brines (Cloutier et al., 2009), with late remobilization of materials by meteoric waters (Fayek et al., 2010).

2.3.4.1 Basement alteration

Alteration in the basement is chiefly present above the Mother fault, within the structural hanging wall lithologies, and is characterized by B enrichment and Na_2O and Zn depletion; the footwall lithologies below the Mother fault have not been sufficiently explored to fully characterize the alteration therein (Roy et al., 2006). Cloutier et al. (2009) grouped the alteration into pre-ore, syn-ore, and post-ore phases, correlating with decreasing temperatures. Pre-ore alteration (350–250º C) is a retrograde metamorphic feature of chlorite alteration of biotite (with coincident Fe-Ti oxide exsolution) in the metapelitic assemblages, overprinted by fine- to medium-grained illite ("muscovite" of Cloutier et al. (2009)). The syn-ore alteration includes illite, hematite, and rare fine-grained APS minerals associated with uraninite. Post-ore alteration includes fine-grained dravite in a breccia matrix and quartz-dravite veinlets, with calcite and pyrite veins cross-cutting dravite veins. Later phases of fine-grained chlorite and minor pyrite fill void spaces formed through earlier alteration, with late-stage chlorite alteration (185–175º C) present in the upper reverse fault (Cloutier et al., 2009).

Roy et al. (2006) documented three alteration zones in the basement rocks (Fig. 2.2b): 1) distal alteration in both the hanging wall and footwall characterized by saussurite and sericite of probable retrograde metamorphic origin; 2) a proximal halo in the hanging wall of chlorite and illite with local hematite that surrounds the graphitic Marker Unit; and

3) a central halo of illite-dravite and chlorite alteration, coincident with uranium mineralization, between the proximal halo and the Mother fault. Host-rock argillic alteration of feldspar and mica is only weakly-developed in non-mineralized lithologies; it progressively increases with increasing degrees of mineralization, often with clay minerals species completely replacing the original mineralogy of the rock (Fayek et al., 2010).

2.3.4.2 Sandstone alteration

Manitou Falls Formation sandstones have been diagenetically and hydrothermally altered, producing variable clay mineral species and abundances. Regionally, the Millennium and several other unconformity-type U deposits (e.g., Key Lake, McArthur River), are located within a major semi-regional illite-chlorite-dravite-silicification anomaly within dickite-dominated background sandstones (Fig. 2.1b; Hoeve and Quirt, 1984; Earle and Sopuck, 1989; Quirt and Wasyliuk, 1997; Quirt, 2001). Above the Millennium deposit, the sandstones exhibit strong bleaching and quartz dissolution, and increasing clay mineral contents with increasing depth (Roy et al., 2006). Hydrothermal illite ± chlorite ± kaolinite ± dravite are found in the upper and lower lithofacies, with a middle package of diagenetically altered dickite-dominated sandstones (Roy et al., 2006). The alteration paragenesis at the deposit described here is based primarily on Cloutier et al. (2009), and is similar to that in other areas of the basin (e.g., Hoeve and Quirt, 1984; Fayek and Kyser, 1997): the earliest diagenetic stage consists of hematite rims and quartz overgrowths on detrital quartz, followed by the transformation of matrix kaolinite to dickite (e.g., Beaufort et al., 1998; Quirt, 2001). Early hydrothermal alteration is represented by fine-grained illite and APS minerals (Gaboreau et al., 2007). Later hydrothermal alteration

includes needle-shaped dravite, hematite, pyrite, and fine-grained chlorite. Post-hydrothermal alteration consists of fine-grained kaolinite in microfractures, partially replacing late stage hydrothermal chlorite near the unconformity (Cloutier et al., 2009).

2.4 LITHOGEOCHEMISTRY

The whole-rock geochemical data described herein comes from the Cameco Corporation exploration database for the B1 trend. To reduce the influence of the high-grade mineralization on the geochemical signature of the deposit, the study database was limited to sandstone samples containing <1000 ppm U. This dataset includes 3608 samples (all with partial digestion analyses, 2832 of which also include total digestion). The drill holes included here extend approximately 21 km northeast to southwest along the B1 conductive trend (Fig. 2.3a). The deposit is located at the southern end of the trend, which was the focus of exploration, and therefore contains a greater drill hole density (Roy et al., 2006).

2.4.1 Analytical Methods

All samples were collected by Cameco from 124 drill cores between 1987 and 2014 as part of the Cree Extension project. Sandstone samples consisted of composite samples containing subsample chips ~1 cm in size and collected approximately every 1.5 m over 10 or 20 metre composite intervals. Whole-rock (bulk sample) geochemical analyses were performed by the Saskatchewan Research Council Geoanalytical Laboratories (SRC) using inductively coupled plasma optical emission spectrometry (ICP-OES) and inductively coupled plasma mass spectrometry (ICP-MS) techniques for major and trace element analysis. Samples were dried, and then jaw crushed to 60% at -2 mm. Subsamples of 100–

200 g were obtained using a riffler, and ground to a pulp (90% at -106 microns) in a steel puck-and-ring grinder. Total digestion analyses utilized a mixture of ultra-pure concentrated HF:HNO_3:$HClO_4$ acids for dissolution. The resultant solutions were heated to dryness, dissolved in 5% HNO_3, and brought to volume with deionized water. Partial digestion analyses utilized an 8:1 mixture of ultra-pure concentrated HNO_3:HCl acids for a partial dissolution of the pulps during a one hour hot water bath, followed by decanting and being brought to volume with deionized water. Major elements, Ba, Ce, Cr, La, Li, and Sr were analyzed with total digestion only; Hg, Sb, Se, and Te with partial digestion only; all other elements had both total and partial digestions. Although it is still a fairly aggressive technique, partial digestion results are generally preferred when analyzing footprints related to hydrothermal alteration as this less destructive digestion will preferentially target hydrothermal phases containing the trace elements associated with mineralization as compared to those in the refractory heavy minerals (Jackson, 2010). In this study, both partial and total digestion data were examined as potential vectors to mineralization; partial digestion data gave more discriminating results, with the exception of the major elements, for which only total digestion data are available.

Quality assurance (QA) measures included analysis of blanks and two standards per sample batch, as well as sample replicate analysis of one replicate every 40 analyses. QA failures (deviations outside acceptable parameters) resulted in corrective action and reanalysis as required. Data refinement, to account for instrumental differences between varying instrumentation over several years of analyses, and to ensure robust results, is described in detail in Appendix A.

2.4.2 Defining proximity to mineralization in sandstones

Seven proximity zones were established to determine the extent of the major and trace elemental distributions in the sandstones with respect to distance from mineralization (Fig. 2.3). These zones were defined in the horizontal direction by both U content and distance from the deposit location (described below), and were divided into stratigraphical sub-zones in the vertical direction per the Manitou Falls Formation lithofacies (Fig. 2.3d):

(1) the sandstones with the highest U content (50–1000 ppm, partial digestion) are located directly above U mineralization at the unconformity (Fig. 2.3b) and compose the **Proximal Zone,** a corridor with a length of ~350 m along the B1 structure;

(2) the **Main Zone** is based on the strike length of the main ore body in the basement, plus two additional areas with U >100 ppm (Fig. 2.3c), extending ~1 km to the north and ~0.6 km to the south of the Proximal Zone. The total length is ~2 km. All other zones are based on horizontal distance from this zone and natural breaks in the drill collar distribution (Fig. 2.3a);

(3) the **South Zone** comprises the remainder of drill holes to the south of the Main Zone, ~1.5 km in length;

(4–7) four zones located to the north of the Main Zone, each ~4.5 km in length, and designated **North 1 – North 4**, with North 4 being most distal.

Uranium concentrations within each proximity zone are lowest in the MFd lithofacies and increase with depth.

2.4.3 Statistical and spatial analysis

Statistical and spatial analysis of the data was utilized to define the lithogeochemical signature variations as a function of proximity zones. Analytes with values less than three times the minimum detection limit for an element were removed from the dataset to eliminate noise related to analytical limitations (Jenner, 1996). For the major elements, and many trace elements, including U, background values utilized in the study are from Quirt (1985).

Quantile-quantile (Q-Q) plots and scatterplots were utilized for each element, to determine if concentrations are elevated or anomalous, and in which proximity zone these levels occur (Fig. 2.4) This was done for each element individually, for both partial and total digestion results, to evaluate data variations with respect to distance from the deposit and stratigraphic position (Fig. 2.4). Elevated and anomalous samples were defined using established statistical parameters: *elevated* values are at the high end of the data distribution, whereas *anomalous* values are both elevated and discontinuous from the rest of the population, indicative of additional influences (e.g., a different fluid source; Reimann et al., 2005). Although the data is non-normally distributed, it was not transformed for this study, because normality is not a criterion for *elevated* and *anomalous* as defined here (Reimann et al., 2005). The *elevated* concentrations were generally the 85^{th} percentile or higher, with the *anomalous* values generally found to be the 95^{th} percentile or higher. Results that were *elevated* or *anomalous* approaching, or within, the Proximal and Main zones were considered potential *pathfinder* elements and mapped in Geosoft® Target 4.5.5. for ArcGIS 3D spatial mapping software.

2.4.4 Results

Whole-rock lithogeochemical distributions for this dataset show that two major elements (Mg and K, Figs 2.5–2.7); numerous trace elements (Mo, Co, Ga, Rb, Ag, Bi, Sb, Y, rare earth elements [grouped as heavy rare earth elements Dy, Er, Tb, Yb (HREE), and light rare earth elements Eu, Gd, Nd, Pr, Sm (LREE)] (Figs 2.9–2.12); and select Pb isotope ratios (Fig. 2.13) exhibit quantifiable trends with proximity to elevated U.

2.4.4.1 Major elements

Plots of select major elements are shown in Figures 2.5–2.7. Major elements in the sandstones reflect the varying abundances of quartz, matrix clay minerals, and other detrital and matrix material; the latter two groups being from both detritus and diagenetic/hydrothermal fluid-rock interaction (Quirt, 1985; Beaufort et al., 2005). Normative clay mineral abundances were calculated with major element data using a calculation optimized for the Athabasca Basin (Quirt, 1995). The clay norm results (Fig. 2.5a) illustrate that along the entire 21 km strike of the B1 trend there are similar total clay mineral contents independent of distance from the deposit, with median values ranging from ~3% in the MFd to ~6% in the MFa.

Within the B1 trend, MgO and K_2O are elevated and Fe_2O_3 and Na_2O are depleted in all four lithofacies when compared to background levels for the Manitou Falls Formation sandstones (Quirt, 1985). However, only MgO exhibits any trend with respect to the deposit location. MgO values increase with proximity to mineralization, with median values present above background beginning ~10 km north of the deposit in the MFd, MFc, and MFa lithofacies (North 2 zone), and ~6 km north of the deposit in the MFb lithofacies

(North 1 zone) (Fig. 2.5b-c). This feature is also illustrated in the K/Al vs. Mg/Al molar element ratio diagrams (Fig. 2.6). These diagrams were constructed to evaluate the variations in clay mineral abundances and types, and can be used to delineate data trends between various diagenetic and alteration phases, including 'kaolin group' (dickite and kaolinite), illite, chlorite (Al-Mg-sudoite), and tourmaline (alkali-deficient dravite), all of which are associated with either sandstone diagenesis or syn- to post-hydrothermal alteration (Tremblay, 1982; Hoeve and Quirt, 1984; Earle and Sopuck, 1989; Zhang et al., 2001; among others). In K/Al-Mg/Al molar ratio space, samples that plot on the trend between the kaolin group node and the illite node are dominant >10 km from the deposit (North 3 and North 4) and in all proximity zones within the MFb lithofacies (Fig. 2.6). In the MFd, MFc, and MFa lithofacies, multiple samples display a shift in increasing Mg/Al and decreasing K/Al with proximity to mineralization. This transition from K-dominant to Mg-dominant alteration is recorded as Mg/K molar ratios >2, which are present within 6 km of the deposit in the MFd, MFc, and MFa lithofacies, and represent the 90th percentile in the Proximal zone; median Mg/K molar ratios >0.2 mark the outer, 10-km boundary in the MFd, MFc, and MFa lithofacies (Fig. 2.7).

2.4.4.2 Trace element haloes

For the majority of elements, the partial digestion results delineate alteration haloes and deposit proximity more effectively than total digestion results, particularly in the Proximal and Main zones where they can be divided into three spatial patterns: 1) elevated to anomalous *chimney* patterns that are vertically distributed above the deposit; 2) elevated to anomalous concentrations that form a conical *hump* within 550 m of the deposit; and 3)

bullseye patterns that contain anomalous values horizontally distributed in the MFb/MFa above the deposit (Fig. 2.8 and Table 2.1).

The chimney-type pattern is demonstrated by Mo (Fig. 2.9), Co, Ga, and Rb. Elevated concentrations (partial digestion results) are vertically distributed in the Proximal and Main zones throughout all four lithofacies, forming a halo 1100–1700 m along and 400–650 m across the B1 trend (Table 2.1). Small localized anomalies distal from the deposit are coincident with isolated values of U >1 ppm. As concentrations increase from elevated to anomalous, the haloes become smaller in size but remain centered over the deposit. Molybdenum and Co exhibit the most spatially-dispersed distributions, with anomalous values present even in the near surface lithofacies (MFd).

The elements Dy, Er, Tb, Y and Yb (partial digestion) display the hump-type pattern and exhibit anomalous concentrations within the Proximal and Main zones in the MFa, MFb, and MFc lithofacies (Fig. 2.10). The anomalous values form rounded or conical haloes ranging from 710–1575 m along and 265–490 m across the B1 trend, mainly within 500 m but extending up to 630 m above the unconformity (Table 2.1). In addition to this hump above the deposit, they also have localized enrichments distally, generally corresponding to isolated zones with elevated U content, albeit at a much lower density than in the Proximal and Main zones.

The bullseye-type pattern is demonstrated by the LREE, which are elevated within the MFb lithofacies along the entire study area footprint; this was also observed by Kister et al. (2003) in the Shea Creek region of Saskatchewan. However, Eu, Gd, Nd, Pr, and Sm (partial digestion) exhibit anomalous values in the MFb and MFa lithofacies within the

Proximal and Main zones, occurring as lensoidal shapes ~1130 m along and ~370 m across the B1 trend (Fig. 2.11; Table 2.1). Rare isolated anomalous concentrations appear in locations distal to the deposit.

Silver, Bi, and Sb (partial digestion) also display the chimney-type to hump-type distribution patterns but are elevated almost exclusively in the Proximal or Main zone corridors; up to 650 m above the unconformity for Ag and Sb, and up to 450 m for Bi (Fig. 2.12; Table 2.1). Unlike the trace elements discussed above, these elements are either not detectible, or are at levels less than three times the instrument detection limit, for nearly all samples elsewhere in the footprint.

2.4.4.3 Lead isotope ratios

Radiogenic Pb isotopes (i.e., ^{206}Pb and ^{207}Pb) are decay products of U, and the distribution of co-related or isolated radiogenic Pb isotopes in alteration haloes can act as a geochemical vector toward U mineralization (Holk et al., 2003; Quirt, 2009; Alexandre et al., 2012). Thresholds for Pb isotopic data as indicators of mineralization are defined here as: ≥35 (indicative) or ≥50 and higher (strongly indicative) for $^{206}Pb/^{204}Pb$, and ≤0.4 (indicative) or ≤0.2 (strongly indicative) for $^{207}Pb/^{206}Pb$ (Cloutier et al. 2009; Quirt, 2009).

At Millennium, most samples that are indicative of mineralization are found in the Proximal and Main zones (Fig. 2.13). Of 81 samples containing $^{206}Pb/^{204}Pb$ values ≥35, 51 are present in these zones, mainly within the MFa lithofacies as a contiguous halo up to 65 metres from the unconformity. Twenty samples occur in the North 4 zone. Although most of these samples are not enriched in U, elevated U is present in other samples from the same drill holes. Twenty-six samples contain $^{207}Pb/^{206}Pb$ values of 0.4 to 0.2 and are

present in the Proximal zone, mirroring the $^{206}Pb/^{204}Pb \geq 35$ locations, although with a smaller halo. Only eight other occurrences are noted, in North 2 MFa and North 4 MFa, MFc, and MFd; six of these eight are associated with elevated U contents.

2.5 DISCUSSION

The Millennium deposit is predominantly basement-hosted, with approximately 20% of the mineralization located near the unconformity at ~550 m depth, and the remainder 100–150 m below the unconformity (Fig. 2.2b). There are distinctive geochemical and mineralogical patterns in the Manitou Falls Formation sandstones above the deposit that vary with respect to deposit proximity, from several kilometres distal to within 10s of metres of mineralization. Major elements MgO and K_2O are above background in the study area, and exhibit molar ratio (Mg/Al, K/Al) shifts that delineate the distal envelope of alteration up to 10 km north of the deposit along the B1 trend (Fig. 2.6). In contrast, trace elements behave differently, and comprise three geometric styles: 1) vertical distributions or *chimneys* extending from the unconformity to subcrop; 2) vertical to conical distributions forming rounded *humps* that extend from the unconformity to the MFc; and 3) horizontal distributions that represent lenticular *bullseyes* in the lower to middle lithofacies (Fig. 2.8). All three trace element patterns form haloes up to 1.5 km in size along the B1 trend localized above the deposit.

2.5.1 Geochemical Halo Patterns

Host-rock alteration of the Manitou Falls Formation is present throughout the Millennium study area and can be a compositional and mineralogical record of the same fluid-rock interaction processes that formed U mineralization (Hoeve and Quirt, 1984;

Cuney, 2005; Kerr and Wallis, 2014). Total clay mineral abundances are related to lithostratigraphy, increasing with stratigraphic depth, as demonstrated by the clay mineral norm results throughout the 21-km footprint of the B1 trend (Fig. 2.5a). These total abundances do not display any trend toward mineralization, suggesting that the original clay minerals in each stratigraphic unit were altered without a significant net gain or loss in the total amount of clay minerals in each lithostratigraphic volume. However, K_2O and MgO are present in levels above background, which demonstrate the presence of hydrothermal alteration from fluids enriched in both K and Mg. At Millennium, Cloutier et al. (2009) suggested that K was basinally derived, and that the majority of the Mg was sourced from the basement; the enrichment of both elements implies that the basinal brines responsible for deposit formation had first entered, reacted with, and then exited the basement. This is consistent with the paragenetic sequence described by Cloutier et al. (2009) where illite (K-alteration) comprised the early stages of alteration, and dravite and chlorite (Mg-alteration) were later hydrothermal alteration spatially associated with the unconformity, near mineralization. MgO concentrations are highest proximal to the deposit, and median values above background define the two alteration envelopes at approximately 10 km and 6 km north of the deposit (Fig. 2.5b–c).

The Millennium deposit sits within and near semi-regional illite, dravite, and chlorite anomalies (Fig. 2.1b; Earle and Sopuck, 1989). To better visualize the relationship between K_2O (illite) and MgO (dravite, chlorite) on a district scale, and how their concentrations change with respect to distance to mineralization, molar element ratios (K/Al vs. Mg/Al) were utilized (Fig. 2.6). As total clay abundances are roughly similar

across the study area, and all three minerals are found in variable amounts in all locations, the molar element ratios better demonstrate the transitions or clustering between these endmembers in spatial association to the deposit and therefore have vectoring potential. The distal zones North 3 and North 4, which are 10–20 km north of the deposit, contain samples that plot from the kaolin group (dickite ± kaolinite) node to the illite node almost exclusively (Fig. 2.6). The Al-dominant samples can be either diagenetic (i.e., background), or a consequence of late fracture infilling (Earle and Sopuck, 1989; Beaufort et al., 1998; Cloutier et al., 2009). The K-dominant samples with minor Mg are either diagenetic illite alteration or early hydrothermal illite alteration (Hoeve and Quirt, 1984; Cloutier et al., 2009). All samples within the MFb lithofacies, irrespective of proximity to mineralization, plot on this trend between these two nodes and are weighted toward the Al-dominant mineral. This Al-dominance is likely representative of dickite, as Roy et al. (2006) described the middle lithofacies as dickite-dominated. In contrast, proximity zones within 10 km of the deposit in the MFa, MFc, and MFd lithofacies all contain samples that plot toward the Mg-rich alkali-deficient dravite and sudoite nodes, with the largest displacement within 1 km of the deposit. This geochemical trend is suggestive of later hydrothermal alteration that includes replacement or overprinting of kaolin and illite by alkali-deficient dravite and sudoite via Mg- and B-bearing fluids, originally of basinal origin but highly altered by basement fluid-rock interaction (e.g., Earle and Sopuck, 1989; Cloutier et al., 2009). The mixing between endmembers in the interior of the more proximal plots may be due to an increase in the later stage, hydrothermal kaolinite present in faults and fractures (Cloutier et al., 2009).

To quantify the sample transitions between the illite, sudoite, and alkali-deficient nodes seen in the molar element ratio diagram (i.e., K-dominant to Mg-dominant), the molar ratios of Mg/K were examined. The Mg/K median values in North 3 and North 4 are <0.2, and increase significantly (1.5–2x) inside the 10-km envelope; individual values >2 increase with proximity to the deposit, marking the 6-km envelope in the MFd, MFc, and MFa lithofacies (Fig. 2.7). The MFb has a muted overall trend but contains anomalous Mg/K values >0.6 that mark the 6-km envelope as well. This muted signature suggests original structural and/or lithological differences may have impeded fluid-rock interaction and alteration of the MFb in comparison to the other lithofacies. As in the molar element ratio plots, the proximal signature characterized by the Mg/K ratios is suggestive of greater concentrations of sudoite and alkali-deficient dravite in the Proximal and Main zones. The relative increase in Mg/K may be reflective of overprinting of earlier illite by the Mg-dominant minerals, as Al-Mg-sudoite ± alkali-deficient dravite are paragenetically later (Cloutier et al., 2009), or of replacement of illite by these Mg-bearing phases (e.g., Percival and Kodama, 1989). The largest Mg/K differential is present directly above the deposit and within a 1–2 km strike along the B1 trend, indicative of enhanced fluid-rock interaction, which is potentially related to the greater number of faults and fractures proximal to mineralization. Mg-enriched fluids likely re-entered the basin along these faults and fractures, where both sudoite and alkali-deficient dravite were commonly precipitated (Fayek and Kyser, 1997).

Whereas the major elements display larger haloes representative of host-rock alteration and clay mineral distributions (Hoeve and Quirt, 1984), several trace elements

form distinct patterns (i.e. chimney, hump, and bullseye patterns; Fig. 2.8) of elevated to anomalous concentrations within, or increasing toward, the Proximal or Main zones. This is particularly evident with partial digestion results, which preferentially target the trace elements contained in hydrothermal phases, and provide a better mapping of the fluid flow pathways associated with mineralization (Jackson, 2010). The chimney patterns exhibited by Mo, Co, Rb, and Ga are distributed vertically from the unconformity to surface directly above the deposit, and are interpreted to reflect element transport upwards from the basement along faults or fractures (Fig. 2.9), either during the ore forming event or through subsequent secondary dispersion events. These elements are either redox-sensitive pathfinder elements (e.g., Mo, Co) or coincident with clay alteration in the sandstones and substitution for major elements in clays (e.g., Ga for Al; Rb for K).

The hump-type pattern is transitional from the vertical chimneys to a conical shape above Millennium. Elevated HREE (Fig. 2.10), Y, and $^{206}Pb/^{204}Pb$ and $^{207}Pb/^{206}Pb$ ratios are more restricted than chimney elements; they are concentrated in the middle to lower lithofacies, although present within 500 m vertically of the unconformity. Anomalous concentrations rarely extend above the MFc and, in the case of the Pb isotopes, are mainly restricted to the MFa (Fig. 2.13). This element pattern and grouping is interpreted to reflect HREE-Y-U incorporation into alteration-related xenotime and uraninite associated with deposit formation, and subsequent *in situ* U decay to ^{206}Pb and ^{207}Pb (Quirt et al., 1991; Fayek and Kyser, 1997; Holk et al., 2003).

The bullseye-type pattern is recorded by LREE, which are predominantly stratiform in distribution and concentrated in the MFb-MFa lithofacies, with little discernible

relationship to deposit location. However, anomalous values of some LREE (Eu, Gd, Nd, Pr, Sm) are present within the Proximal and Main zones above the deposit, with small haloes horizontally distributed within the MFb and MFa, 600 m along and 300 m across strike, and up to 400 m above the unconformity (Fig. 2.11, Table 2.1). Detrital heavy minerals are more prevalent in the MFb lithofacies (Roy et al. 2006), and likely account for the stratiform distribution of LREE, whereas the anomalous LREE in the bullseye haloes are likely related to syn-mineralization APS minerals (Gaboreau et al., 2005 and 2007).

In addition to the above trace element patterns, there are enrichments in Ag, Bi, and Sb in the Proximal or Main Zones in all lithofacies (Fig. 2.12). Approximately 90% of all samples with confidently measurable concentrations of these elements are located here, and are below detection limits elsewhere in the study area. This suggests their enrichment was due to an increased fluid-rock interaction, qualifying these elements as indicators of locations that have been affected by the greatest amounts of hydrothermal activity.

2.5.2 Implications for exploration

The clean, mature sandstones of the Manitou Falls Formation surrounding the Millennium deposit have been altered through hydrothermal processes, leaving a weak but identifiable geochemical footprint capable of targeting toward mineralization. This footprint, present several kilometres distal from the deposit, intensifies with proximity to the highest concentrations of U. It is also several times larger than the U halo present in the sandstones directly above the deposit, where the highest U concentrations range from 50 – 1000 ppm (partial digestion). This halo is ~ 350 m along and ~150 m across strike

— roughly the dimensions of the main deposit body in the basement — and present up to 150 m above the unconformity.

There are two main distributions of elemental and mineralogical vectors in the alteration footprint at Millennium. These vectors are greater in dimension than the U halo along strike; dimensions across strike are constrained by drill hole distribution, and the full extent of the vector haloes in that direction are therefore unknown (Figs 2.14–2.15). The vector haloes include: (1) larger scale haloes 6–10 km north along strike of the deposit, along the B1 trend, involving the major elements K and Mg and related normative clay mineralogy; and (2) smaller haloes of several trace elements that extend ~0.6–1.5 km along the B1 trend positioned directly above the deposit. These haloes are present in all lithofacies, up to 600 m above the unconformity.

The first order, larger-scale vector reflects clay mineralogy and the shift from diagenetic to hydrothermal (dickite/kaolinite-illite trend, all zones) to those approaching the sudoite and alkali-deficient dravite nodes (proximal zones) in the molar element ratio plots (Fig. 2.6). This shift is recorded by the changes in Mg/K ratios (Fig. 2.7; Figs 2.14–2.15), and elevated MgO (2–4x background), both of which increase with proximity to the deposit in all four lithofacies (Fig. 2.5b-c). Proximal alteration haloes are more spatially restricted (Figs 2.14–2.15), but still have 2–5 times longer strike lengths than the U halo on the sandstones. These haloes reflect clay mineral formation (Ga, Rb substitution in clays) and redox-related and other elements associated with mineralization (Mo, Co, U, HREE, LREE, radiogenic Pb). The combination of molar element ratios and trace element distribution patterns are representative of both diagenesis and host-rock clay mineral

alteration, and the results herein — specifically where these haloes coincide — illustrate scalable vectors to mineralization and record the mineralizing processes related to unconformity-type U formation and Millennium.

2.6 CONCLUSIONS

The Millennium deposit is a predominantly basement-hosted unconformity-type U deposit with the majority of mineralization located over 650 m below the surface, and approximately 20% at the unconformity ~550 m below the surface. Despite these depths and simple-type mineralization, a unique geochemical signature is present in the Manitou Falls Formation sandstones that extends 100s of metres vertically and horizontally from the deposit that may reflect ore forming processes and associated fluid-rock interaction. Molar element ratios of Mg and K to Al exhibit significant changes within 10 km of the deposit, notably within the upper lithofacies, that signify hydrothermal host-rock alteration consistent with the formation of chlorite (Al-Mg-sudoite) and alkali-deficient dravite, known minerals associated with unconformity-type U deposits. Molar ratios Mg/K increase with proximity to the deposit along the B1 conductive trend. Within 1.5 km of the deposit, several trace elements, including U, REE, and Y, form haloes of elevated to anomalous concentrations that intensify with proximity to the unconformity and the deposit location. These geochemical distributions are likely highlighting primary dispersion along fluid pathways involved in the mineralizing system, in particular, Mo, Co, Rb, and Ga, which form haloes as a vertical plume extending from the unconformity to upper lithofacies. This suggests that vectoring toward a deep, monomineralic U deposit is possible using whole-rock geochemistry from basin sandstones.

REFERENCES

Alexandre, P., Kyser, K., Jiricka, D., & Witt, G. (2012). Formation and evolution of the Centennial unconformity-related uranium deposit in the South-Central Athabasca Basin, Canada. *Economic Geology*, *107*(3), 385–400. http://doi.org/10.2113/econgeo.107.3.385

Alexandre, P., Kyser, K., Polito, P., & Thomas, D. (2005). Alteration mineralogy and stable isotope geochemistry of Paleoproterozoic basement-hosted unconformity-type uranium deposits in the Athabasca Basin, Canada. *Economic Geology*, *100*(8), 1547–1563. http://doi.org/10.2113/gsecongeo.100.8.1547

Alexandre, P., Kyser, K., Thomas, D., Polito, P., & Marlat, J. (2009). Geochronology of unconformity-related uranium deposits in the Athabasca Basin, Saskatchewan, Canada and their integration in the evolution of the basin. *Mineralium Deposita*, *44*(1), 41–59. http://doi.org/10.1007/s00126-007-0153-3

Annesley, I. R., Madore, C., & Portella, P. (2005). Geology and thermotectonic evolution of the western margin of the Trans-Hudson Orogen: evidence from the eastern sub-Athabasca basement, Saskatchewan. *Canadian Journal of Earth Sciences*, *42*(4), 573–597. http://doi.org/10.1139/e05-034

Ansdell, K. M. (2005). Tectonic evolution of the Manitoba-Saskatchewan segment of the Paleoproterozoic Trans-Hudson Orogen, Canada. *Canadian Journal of Earth Sciences*, *42*(4), 741–759. http://doi.org/10.1139/e05-035

Armstrong, R. L., & Ramaekers, P. (1985). Sr isotopic study of Helikian sediment and diabase dikes in the Athabasca Basin, northern Saskatchewan. *Canadian Journal of Earth Sciences*, *22*(3), 399–407.

Beaufort, D., Patrier, P., Laverret, E., Bruneton, P., & Mondy, J. (2005). Clay alteration associated with Proterozoic unconformity-type uranium deposits in the East Alligator Rivers uranium field, Northern Territory, Australia. *Economic Geology*, *100*(3), 515–536. http://doi.org/10.2113/gsecongeo.100.3.515

Beaufort, D., Cassagnabere, A., Petit, S., Lanson, B., Berger, G., Lacharpagne, J. C., & Johansen, H. (1998). Kaolinite-to-dickite reaction in sandstone reservoirs. *Clay Minerals*, *33*(2), 297–316.

Cameco Corporation (2015). *Reserves & Resources - Millennium - Uranium Projects - Businesses - Cameco*. *Cameco.com*. Retrieved 19 September 2016, from https://www.cameco.com/businesses/ uranium-projects/millennium/reserves-resources.

Card, C. D., Pană, D., Portella, P., Thomas, D. J., & Annesley, I. R. (2007). Basement rocks to the Athabasca basin, Saskatchewan and Alberta. *In* Jefferson C.W. & Delaney, G. (eds.), *EXTECH IV: Geology and Uranium EXploration TECHnology*

of the Proterozoic Athabasca Basin, Saskatchewan and Alberta: Geological Survey of Canada, Bulletin 588, 69–87.

Chi, G., Bosman, S., & Card, C. (2013). Numerical modeling of fluid pressure regime in the Athabasca basin and implications for fluid flow models related to the unconformity-type uranium mineralization. *Journal of Geochemical Exploration*, *125*, 8–19. http://doi.org/10.1016/j.gexplo.2012.10.017

Cloutier, J., Kyser, K., Olivo, G. R., Alexandre, P., & Halaburda, J. (2009). The Millennium uranium deposit, Athabasca Basin, Saskatchewan, Canada: an atypical basement-hosted unconformity-related uranium deposit. *Economic Geology*, *104*(6), 815–840. http://doi.org/10.2113/gsecongeo.104.6.815

Corrigan, D., Pehrsson, S., Wodicka, N., & de Kemp, E. (2009). The Palaeoproterozoic Trans-Hudson Orogen: a prototype of modern accretionary processes. *Geological Society, London, Special Publications*, *327*(1), 457–479. http://doi.org/10.1144/SP327.19

Creaser, R. A., & Stasiuk, L. D. (2007). Depositional age of the Douglas Formation, northern Saskatchewan, determined by Re-Os geochronology. *In* Jefferson C.W. & Delaney, G. (eds.), *EXTECH IV: Geology and Uranium EXploration TECHnology of the Proterozoic Athabasca Basin, Saskatchewan and Alberta*: Geological Survey of Canada, Bulletin 588, 341–345.

Cui, T., Yang, J., & Samson, I. M. (2012). Tectonic deformation and fluid flow: implications for the formation of unconformity-related uranium deposits. *Economic Geology*, *107*(1), 147–163. http://doi.org/10.2113/econgeo.107.1.147

Cuney, M. L. (2005). World-class unconformity-related uranium deposits: key factors for their genesis. *In* Mao, J., Bierlein, F. P. (eds.), *Mineral Deposit Research: Meeting the Global Challenge* (pp. 245–248). Springer Berlin Heidelberg. http://doi.org/10.1007/3-540-27946-6_64

Cuney, M. (2009). The extreme diversity of uranium deposits. *Mineralium Deposita*, *44*(1), 3–9. http://doi.org/10.1007/s00126-008-0223-1

Earle, S. A. M., & Sopuck, V. J. (1989). Regional lithogeochemistry of the eastern part of the Athabasca Basin uranium province, Saskatchewan, Canada. *In* Muller-Kahle, E., (ed.), *Uranium resources and geology of North America: International Atomic Energy Agency,* TECDOC-500, 263–296.

Fayek, M. & Kyser, T. (1997). Characterization of multiple fluid-flow events and rare-earth-element mobility associated with formation of unconformity-type uranium deposits in the Athabasca Basin, Saskatchewan. *The Canadian Mineralogist, 35,* 627–658.

Fayek, M., Camacho, A., Beshears, C., Jiricka, D., & Halaburda, J. (2010). Two Sources of Uranium at the Millennium Uranium Deposit, Athabasca Basin, Saskatchewan,

Canada. In *Geological Association of Canada—Mineralogical Association of Canada 2010 (Calgary) Annual Conference Abstracts Volume,* 4 p.

Gaboreau, S., Beaufort, D., Vieillard, P., Patrier, P., & Bruneton, P. (2005). Aluminum phosphate–sulfate minerals associated with Proterozoic unconformity-type uranium deposits in the East Alligator River Uranium Field, Northern Territories, Australia. *The Canadian Mineralogist*, *43*(2), 813–827. http://doi.org/10.2113/gscanmin.43.2.813

Gaboreau, S., Cuney, M., Quirt, D., Beaufort, D., Patrier, P., & Mathieu, R. (2007). Significance of aluminum phosphate-sulfate minerals associated with U unconformity-type deposits: The Athabasca basin, Canada. *American Mineralogist*, *92*(2-3), 267–280. http://doi.org/10.2138/am.2007.2277

Garofalo, P., Audétat, A., Günther, D., Heinrich, C. A., & Ridley, J. (2000). Estimation and testing of standard molar thermodynamic properties of tourmaline end-members using data of natural samples. *American Mineralogist*, *85*(1), 78–88.

Hecht, L., & Cuney, M. (2000). Hydrothermal alteration of monazite in the Precambrian crystalline basement of the Athabasca Basin (Saskatchewan, Canada): implications for the formation of unconformity-related uranium deposits. *Mineralium Deposita*, *35*(8), 791–795. http://doi.org/10.1007/s001260050280

Hiatt, E. E., & Kyser, T. K. (2007). Sequence stratigraphy, hydrostratigraphy, and mineralizing fluid flow in the Proterozoic Manitou Falls Formation, eastern Athabasca Basin, Saskatchewan. *In* Jefferson C.W. & Delaney, G. (eds.), *EXTECH IV: Geology and Uranium EXploration TECHnology of the Proterozoic Athabasca Basin, Saskatchewan and Alberta*: Geological Survey of Canada, Bulletin 588, 489–506.

Hoeve, J., & Quirt, D. H. (1984). Mineralization and host rock alteration in relation to clay mineral diagenesis and evolution of the Middle-Proterozoic, Athabasca Basin, northern Saskatchewan, Canada. Saskatchewan Research Council, SRC Technical Report 187, 202 p.

Hoeve, J., & Sibbald, T. I. (1978). On the genesis of Rabbit Lake and other unconformity-type uranium deposits in northern Saskatchewan, Canada. *Economic Geology*, *73*, 1450–1473.

Hoeve, J., Rawsthorn, K., & Quirt, D. (1981). Uranium metallogenetic studies: clay mineral stratigraphy and diagenesis in the Athabasca Group. *In* Summary of Investigations 1981, Saskatchewan Geological Survey, Miscellaneous Report 81-4, p. 76–89.

Hoffman, P. F. (1988). United Plates of America, the birth of a craton: Early Proterozoic assembly and growth of Laurentia. *Annual Review of Earth and Planetary Sciences*, *16*, 543–603.

Holk, G. J., Kyser, T. K., Chipley, D., Hiatt, E. E., & Marlatt, J. (2003). Mobile Pb-isotopes in Proterozoic sedimentary basins as guides for exploration of uranium deposits. *Journal of Geochemical Exploration*, *80*(2), 297–320. http://doi.org/10.1016/S0375-6742(03)00196-1

Jackson, R. G. (2010). Application of 3D geochemistry to mineral exploration. *Geochemistry: Exploration, Environment, Analysis*, *10*(2), 143–156. http://doi.org/10.1144/1467-7873/09-217

Jeanneret, P., Goncalves, P., Durand, C., Trap, P., Marquer, D., Quirt, D., & Ledru, P. (2016). Tectono-metamorphic evolution of the pre-Athabasca basement within the Wollaston–Mudjatik Transition Zone, Saskatchewan. *Canadian Journal of Earth Sciences*, *53*(3), 231–259. http://doi.org/10.1139/cjes-2015-0136

Jefferson, C. W., Thomas, T. J., Gandhi, S. S., Ramaekers, P., Delaney, G., Brisbin, D., Cutts, C., Portella, P., & Olson, R.A. (2007). Unconformity-associated uranium deposits of the Athabasca Basin, Saskatchewan and Alberta. *In* Jefferson C.W. & Delaney, G. (eds.), *EXTECH IV: Geology and Uranium EXploration TECHnology of the Proterozoic Athabasca Basin, Saskatchewan and Alberta*: Geological Survey of Canada, Bulletin 588, 23–67.

Jenner, G. A. (1996). Trace element geochemistry of igneous rocks: geochemical nomenclature and analytical geochemistry. *In* Wyman, D. A. (ed.), *Trace element geochemistry of volcanic rocks: applications for massive sulphide exploration.* Geological Association of Canada. Short Course Notes, 12, 51–77.

Kerr, W. & Wallis, R. (2014). "Real-world" economics of the uranium deposits of the Athabasca Basin, northern Saskatchewan: why grade is not always king! SEG Newsletter, (99) 1, 11–15.

Kister, P., Laverret, E., Cuney, M., Vieillard, P., & Quirt, D. (2003). 3-D distribution of alteration minerals associated with unconformity-type mineralization: Anne Zone, Shea Creek deposit (Saskatchewan, Canada). *In* Cuney, M. (ed.), *Proceedings of the International Conference on Uranium Geochemistry: Nancy, France,* p. 197–200.

Kotzer, T. G., & Kyser, T. K. (1995). Petrogenesis of the Proterozoic Athabasca Basin, northern Saskatchewan, Canada, and its relation to diagenesis, hydrothermal uranium mineralization and paleohydrogeology. *Chemical Geology*, *120*(1), 45–89. http://doi.org/10.1016/0009-2541(94)00114-N

Kyser, K. (2014). Uranium Ore Deposits, *In* Turekian, H. D., Holland, H. D., (eds.), Treatise on Geochemistry (2nd ed.): Oxford, Elsevier, v. 7, p. 489–513. http://doi.org/10.1016/B978-0-08-095975-7.01122-0

Kyser, K., & Cuney, M. (2008). Unconformity-related uranium deposits. *In* Cuney, M. & Kyser, K., (eds.), *Recent and not-so-recent developments in uranium deposits and implications for exploration*. Quebec: Mineralogical Association of Canada Short

Course Series Vol. 39, 161–219. ISBN 978-0-921294-48-1

Kyser, K., Hiatt, E., Renac, C., Durocher, K., Holk, G., & Deckart, K. (2000). Diagenetic fluids in Paleo-and Meso-Proterozoic sedimentary basins and their implications for long protracted fluid histories. *In* Kyser, K. (ed.), *Fluids and basin evolution.* Mineralogical Association of Canada Short Course Series 28, 225–262. http://doi.org/10.13140/2.1.1033.1847

Lewry, J. F., & Sibbald, T. I. I. (1980). Thermotectonic evolution of the Churchill Province in northern Saskatchewan. *Tectonophysics*, *68*, 45–82.

Macdonald, C. (1985). Mineralogy and geochemistry of the sub-Athabasca regolith near Wollaston Lake. *In* Sibbald, T. I. I. & Petruk, W. (eds.), *Geology of Uranium Deposits: Canadian Institute of Mining and Metallurgy Special Vol. 32*, 155–158.

McGill, B. D., Marlatt, J. L., Matthews, R. B., Sopuck, V. J., Homeniuk, L. A., & Hubregtse, J. J. (1993). The P2 north uranium deposit, Saskatchewan, Canada. *Exploration and Mining Geology*, *2*(4), 321–331.

Mercadier, J., Cuney, M., & Quirt, D. (2009). Basement-hosted uranium oxides from Athabasca Basin: mineralogy, U/Pb dating, major and Rare Earth Element (REE) concentrations: comparison with U-oxides from deposits located in the vicinity of the unconformity. *In* Lentz, D. R., Thorne, K. G., & Beal, K-L. (eds.), *Proceedings of the 24th IAGS, Fredericton, Canada*, 445–448. ISBN 978-1-55131-136-4

Mwenifumbo, C. J. & Bernius, G. R.. (2007). Crandallite-group minerals: host of thorium enrichment in the eastern Athabasca Basin, Saskatchewan. *In* Jefferson C.W. & Delaney, G. (eds.), *EXTECH IV: Geology and Uranium EXploration TECHnology of the Proterozoic Athabasca Basin, Saskatchewan and Alberta*: Geological Survey of Canada, Bulletin 588, 521–532.

Ng, R., Alexandre, P., & Kyser, K. (2013a). Mineralogical and geochemical evolution of the unconformity-related McArthur River Zone 4 orebody in the Athabasca Basin, Canada: implications of a silicified zone. *Economic Geology*, *108*(7), 1657–1689. http://doi.org/10.2113/econgeo.108.7.1657

Ng, R., Alexandre, P., Kyser, K., Cloutier, J., Abdu, Y. A., & Hawthorne, F. C. (2013b). Oxidation state of iron in alteration minerals associated with sandstone-hosted unconformity-related uranium deposits and apparently barren alteration systems in the Athabasca Basin, Canada: Implications for exploration. *Journal of Geochemical Exploration*, *130*, 22–43. http://doi.org/10.1016/j.gexplo.2013.02.009

Pagel, M., Poty, B., & Sheppard, S. M. F. (1980). Contribution to some Saskatchewan uranium deposits mainly from fluid inclusions and isotopic data. *In* Ferguson, S. & Goleby, A. (eds.), *Uranium in the Pine Creek Geosyncline: Vienna, International Atomic Energy Agency*, p. 639–654.

Percival, J. B., & Kodama, H. (1989). Sudoite from Cigar Lake, Saskatchewan. *Canadian Mineralogist*, *27*, 633–641.

Quirt, D. H. (1985). Lithogeochemistry of the Athabasca Group: Summary of sandstone data. *In* Summary of Investigations 1985, Saskatchewan Geological Survey, Saskatchewan Energy and Mines, Miscellaneous Report 85-4, p. 128–132.

Quirt, D. H. (1995). Norm calculation procedure for sandstone clay minerals. Saskatchewan Research Council, Publication No. R-1230-28-E-95, 14 p. plus appendices.

Quirt, D. H. (2001). Kaolinite and dickite in the Athabasca sandstone, northern Saskatchewan, Canada. Saskatchewan Research Council, Publication No. 10400-16D01, 27 p.

Quirt, D. (2009). Applying Pb isotopes in unconformity-type uranium exploration. *In* Lentz, D. R., Thorne, K. G., & Beal, K-L. (eds.), *Proceedings of the 24th IAGS, Fredericton, Canada*, 453–456. ISBN 978-1-55131-136-4

Quirt, D. H., & Wasyliuk, K. (1997). Kaolinite, dickite, and other clay minerals in the Athabasca Group, Canada, and the Kombolgie Formation, Australia: 11th International Clay Conference, Ottawa, Ontario, June 1997. In *Proceedings A* (Vol. 61).

Quirt, D., Kotzer, T., and Kyser, T.K. (1991). Tourmaline, phosphate minerals, zircon and pitchblende in the Athabasca Group: Maw Zone and McArthur River areas. *In* Summary of Investigations 1991: Saskatchewan Geological Survey, Saskatchewan Energy and Mines, Report 91-4, p. 181–191.

Rainbird, R. H., Stern, R. A., Rayner, N., & Jefferson, C. W. (2007). Age, provenance, and regional correlation of the Athabasca Group, Saskatchewan and Alberta, constrained by igneous and detrital zircon geochronology. *In* Jefferson C.W. & Delaney, G. (eds.), *EXTECH IV: Geology and Uranium EXploration TECHnology of the Proterozoic Athabasca Basin, Saskatchewan and Alberta*: Geological Survey of Canada, Bulletin 588, 193–209.

Ramaekers, P., & Catuneanu, O. (2004). Development and sequences of the Athabasca Basin, early Proterozoic, Saskatchewan and Alberta, Canada. *In* Eriksson P. G., Alterman, W., Nelson, D. R., Mueller, W. U., & Catuneanu, O. (eds.), *The Precambrian Earth: Tempos and Events* (Vol. 12, pp. 705–723). Amsterdam: Elsevier.

Ramaekers, P., Jefferson, C. W., Yeo, G. M., Collier, B., Long, D. G. F., Drever, G., McHardy, S., Jiricka, D., Cutts, C., Wheatley, K., Catuneanu, O., Bernier, S., Kupsch, B., & Post, R. T. (2007). Revised geological map and stratigraphy of the Athabasca Group, Saskatchewan and Alberta. *In* Jefferson C.W. & Delaney, G. (eds.), *EXTECH IV: Geology and Uranium EXploration TECHnology of the Proterozoic Athabasca Basin, Saskatchewan and Alberta*: Geological Survey of Canada, Bulletin 588, 155–187.

Reimann, C., Filzmoser, P., & Garrett, R. G. (2005). Background and threshold: critical

comparison of methods of determination. *Science of the Total Environment*, *346*(1), 1–16. http://doi.org/10.1016/j.scitotenv.2004.11.023

Richard, A., Pettke, T., Cathelineau, M., Boiron, M. C., Mercadier, J., Cuney, M., & Derome, D. (2010). Brine–rock interaction in the Athabasca basement (McArthur River U deposit, Canada): consequences for fluid chemistry and uranium uptake. *Terra Nova*, *22*(4), 303-308. http://doi.org/10.1111/j.1365-3121.2010.00947.x

Roy, C., Halaburda, J., Thomas, D., & Hirsekorn, D. (2006). Millennium deposit-Basement-hosted derivative of the unconformity uranium model. In *Uranium production and raw materials for the nuclear fuel cycle-Supply and demand, economics, the environment and energy security: International Atomic Energy Agency Proceedings Series,* 111-121.

Sopuck, V. J., De Carle, A., Wray, E. M., & Cooper, B. (1983). Application of lithogeochemistry to the search for unconformity-type uranium deposits in the Athabasca Basin. *In* Cameron, E. M. (ed.), *Uranium Exploration in Athabasca Basin, Saskatchewan, Canada,* Geological Survey of Canada: Paper 82-11, 191–205.

Tremblay, L. (1982). Geology of the uranium deposits related to the sub-Athabasca unconformity, Saskatchewan, Canada. Geological Survey of Canada: Paper 81-20, 56 p.

Yeo, G. M., & Delaney, G. (2007). The Wollaston supergroup, stratigraphy and metallogeny of a Paleoproterozoic Wilson cycle in the Trans-Hudson Orogen, Saskatchewan. *In* Jefferson C.W. & Delaney, G. (eds.), *EXTECH IV: Geology and Uranium EXploration TECHnology of the Proterozoic Athabasca Basin, Saskatchewan and Alberta*: Geological Survey of Canada, Bulletin 588, 89-117.

Yeo, G., Jefferson, C.W., & Ramaekers, P. (2002). A preliminary comparison of Manitou Falls Formation stratigraphy in four Athabasca Basin deposystems, *In* Summary of Investigations 2002, Volume 2, Saskatchewan Geological Survey, Sask. Industry Resources, Misc. Rep. 2002-4.2 CD-ROM, Paper D-7, 14p.

Zhang, G., Wasyliuk, K., & Pan, Y. (2001). The characterization and quantitative analysis of clay minerals in the Athabasca Basin, Saskatchewan: Application of shortwave infrared reflectance spectroscopy. *The Canadian Mineralogist*, *39*(5), 1347-1363. http://doi.org/10.2113/gscanmin.39.5.1347

FIGURES

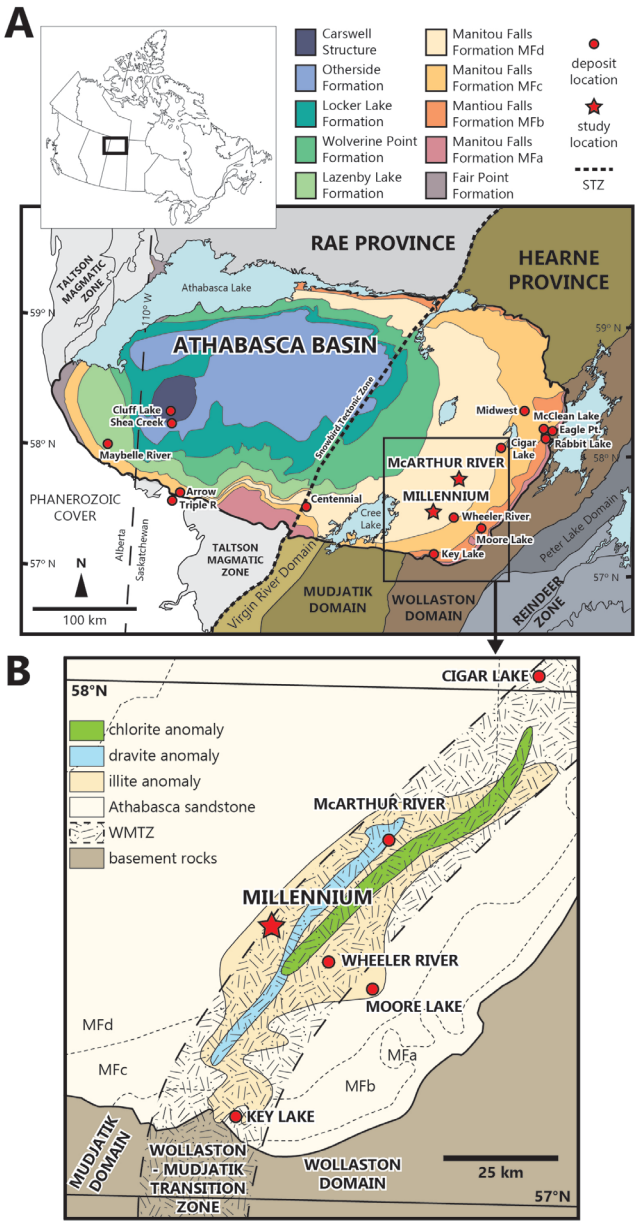

Figure 2.1: (**A**) Simplified geological map of the Athabasca Basin and underlying Precambrian domains in northern Saskatchewan and Alberta. STZ: Snowbird Tectonic Zone, which brought together the Rae and Hearne provinces; the later Trans-Hudson orogen was responsible for the accretion of the Reindeer Zone to the eastern Hearne. A large number of unconformity-type U deposits are found in the eastern basin. Adapted from Card et al. (2007), and Cloutier et al. (2009). (**B**) Geological relationships in the southeastern Athabasca Basin, showing the location of selected uranium deposits relative to the Wollaston-Mudjatik Transition Zone (WMTZ), and regional zones of alteration. Adapted from Earle and Sopuck (1989), Jefferson et al. (2007), and Jeanneret et al. (2016).

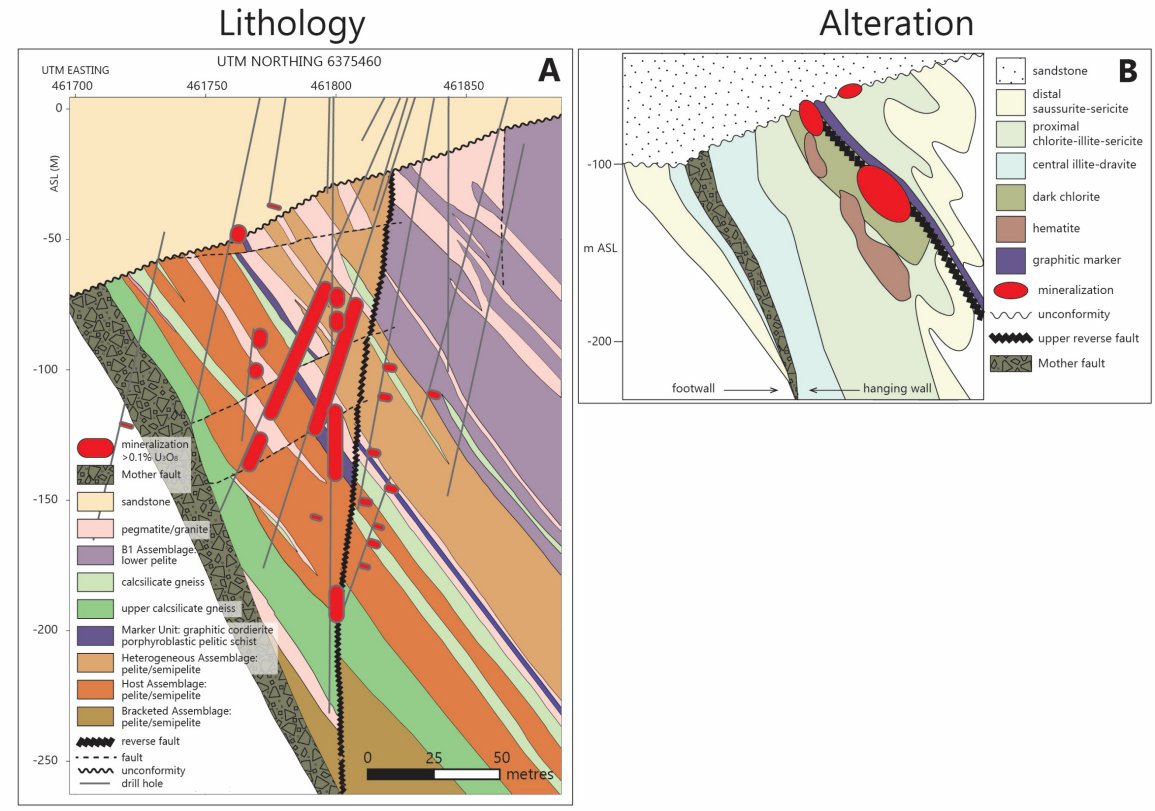

Figure 2.2: Millennium deposit geology of the basement, looking north. Depths are in metres above sea level (ASL); sandstones in the vicinity of the deposit extend to approximately 500 m ASL. (**A**) Cross section at the Millennium deposit discovery hole (CX-040) and surrounding drill holes. The Mother fault demarcates the hanging wall from the footwall of the basement rocks. Mineralization is associated with a reverse fault that cross cuts the graphitic Marker Unit in the basement hanging wall. Although a majority of the mineralization is located in the basement rocks, up to 20% can be found at the unconformity. Adapted from Cameco internal memo, J. Mukwakwami (2013). (**B**) Simplified alteration and mineralization of the basement rocks, looking north, adapted from Roy et al. (2006) and Cloutier et al. (2009). Three alteration zones are described: distal saussurite-sericite alteration found furthest from mineralization in both the hanging and footwalls, a central illite-dravite halo that is crosscut by the Mother fault, and a proximal chlorite-illite-halo associated with mineralization in the hanging wall. Hematite, chlorite, and a graphitic marker unit associated with the upper reverse fault are also found in proximity to mineralization.

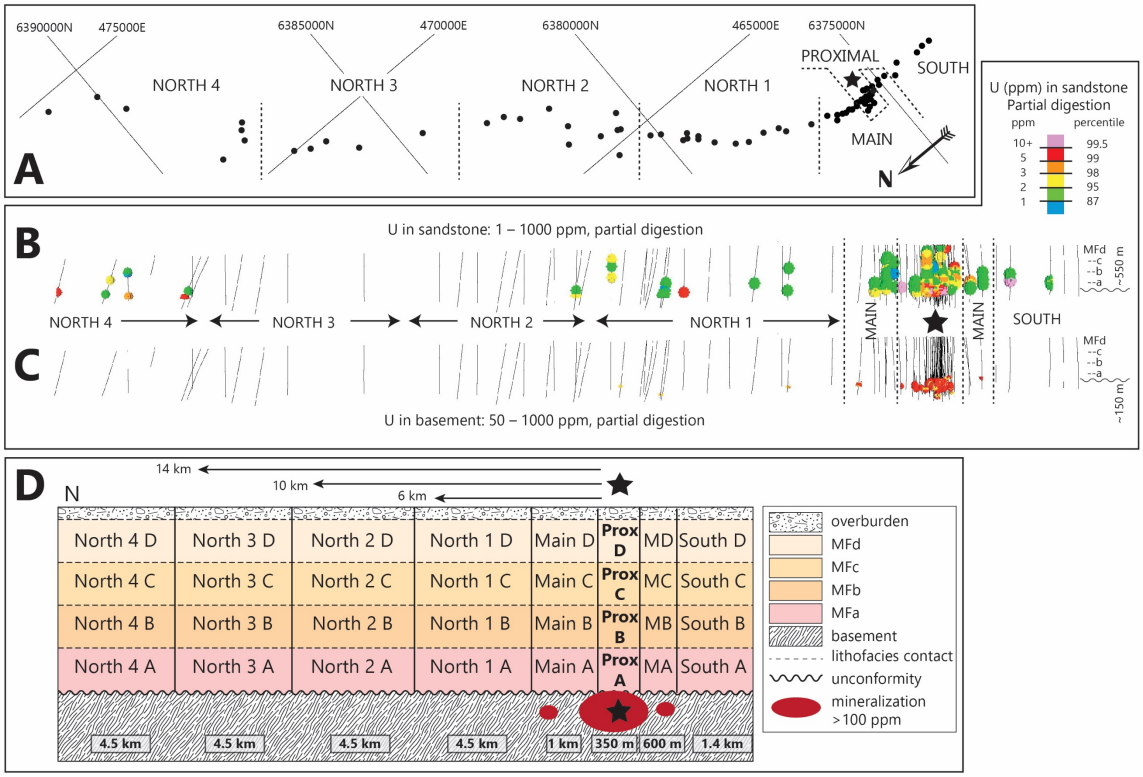

Figure 2.3: The Millennium deposit study area. (**A**) Plan view of the study area. Black dots are drill hole collars. Coordinates are WGS 84 UTM 13N; star is deposit location. (**B**) Longitudinal section along the B1 trend; view of the sandstones with U >1 ppm (partial digestion), looking due east. Vertical lines are drill hole traces. (**C**) As in (**B**) of the basement with U >100 ppm (partial digestion). (**D**) Proximity zones based on the location of U in the sandstones (Prox-A,-B,-C,-D) and basement (Main A,B,C,D on either side). Not to scale. Each lithofacies is considered separately in the quantification of elevated or anomalous results.

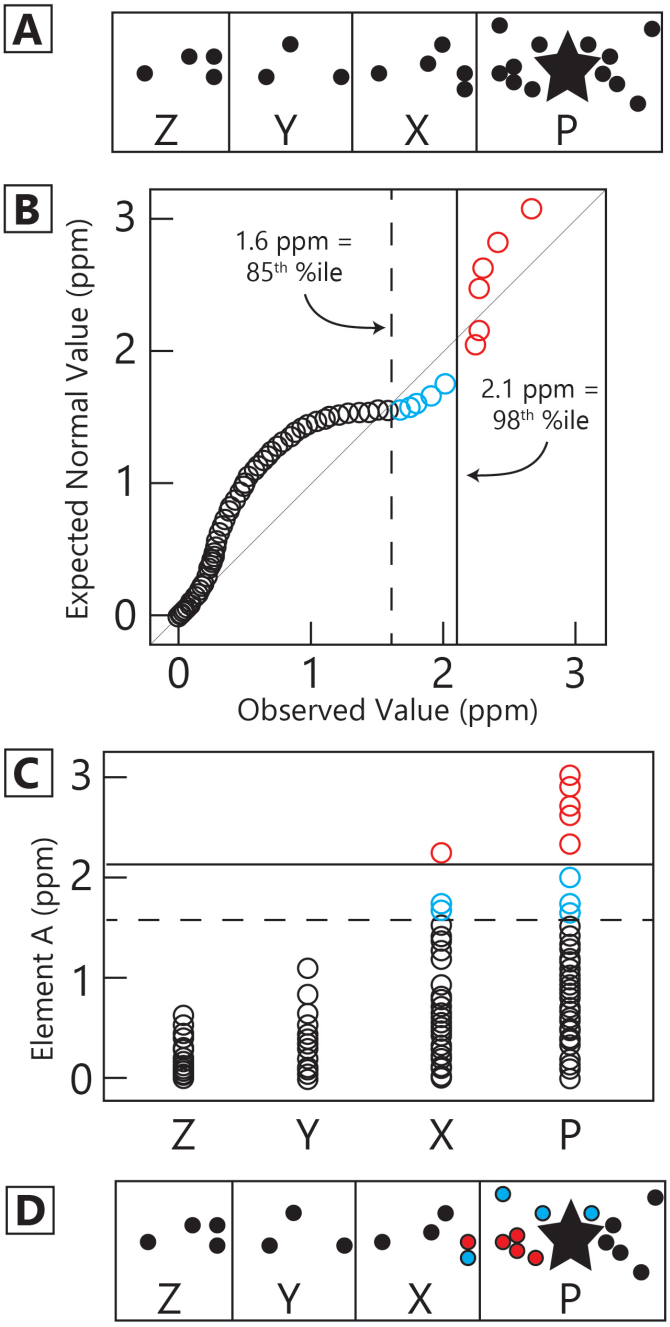

Figure 2.4: Simplified example of how data was examined in this study. (**A**) Footprint was divided into proximity zones determined by horizontal distance of drill collar from deposit location, marked with a star (P = proximal). (**B**) All data from a single element was plotted with a quantile-quantile (Q-Q) plot. Breaks in data distinguish anomalous (red circles) from elevated (blue circles) results. (**C**) Results plotted with regard to proximity zone. If the elevated to anomalous values were found to change with proximity to the deposit location, they were mapped in 3D. (**D**) Plan view of drill holes containing elevated (blue) to anomalous (red) values, showing a spatial relationship to the deposit location.

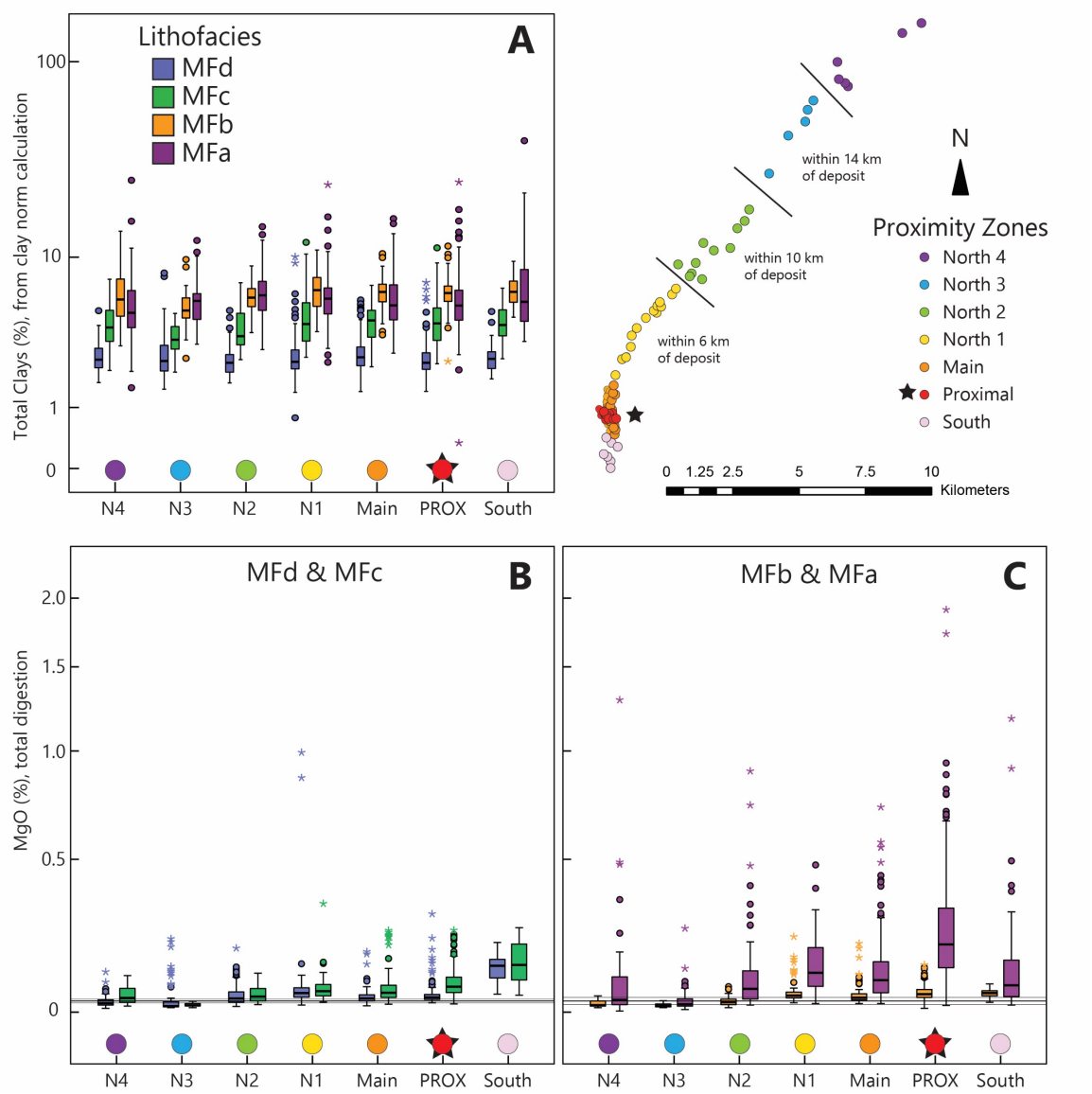

Figure 2.5: (**A**) The total amount of clays present in the study area footprint estimated from a clay norm calculation. The two lower lithofacies (MFb–MFa) contain median values of 6%, the MFc median values of 4%, and the MFd (uppermost) 2.5%. (**B**) MgO concentration in the upper two Manitou Falls Formation lithofacies as compared to background values of Quirt (1985): 0.03 ± 0.005%. Concentrations increase with proximity to the deposit (to the right of the plot, deposit location marked with star). (**C**) MgO concentration in the lower two lithofacies. Background values are 0.03 ± 0.01%. As in the upper two lithofacies, concentrations increase with proximity to the deposit. All results are from total digestion, ICP-OES; n = 2831. N4 = 228, N3 = 209, N2 = 361, N1 = 417, Main = 581, P = 886, S = 149. The star marks the deposit location in all plots.

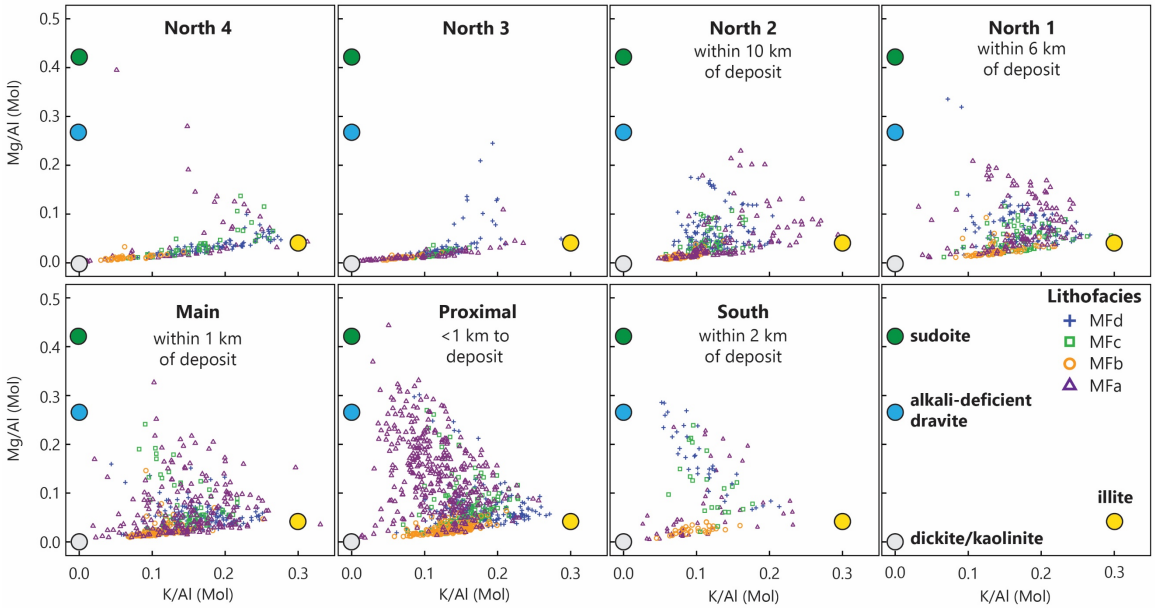

Figure 2.6: Molar element ratio plots demonstrate the varying contents of Mg and K in relation to the deposit location, representative of Al-Mg-sudoite and alkali-deficient dravite alteration. In the least-altered locations, greater than 10 km from the deposit (North 4 and North 3), samples plot on the trend between the kaolin group and illite nodes almost exclusively. Within 10 km of the deposit (North 2), samples shift toward the alkali-deficient dravite and sudoite nodes in the MFd, MFc, and MFa lithofacies. This shift intensifies with proximity to the deposit in all lithofacies but the MFb. Sudoite and illite formulas are from Cloutier et al. (2009); alkali-deficient dravite formula estimated from Garofalo et al. (2000) and Zhang et al. (2001). Total number of samples = 2775. Samples per proximity zone: N4 = 228, N3 = 209, N2 = 361, N1 = 361, Main = 581, Proximal = 886, South = 149.

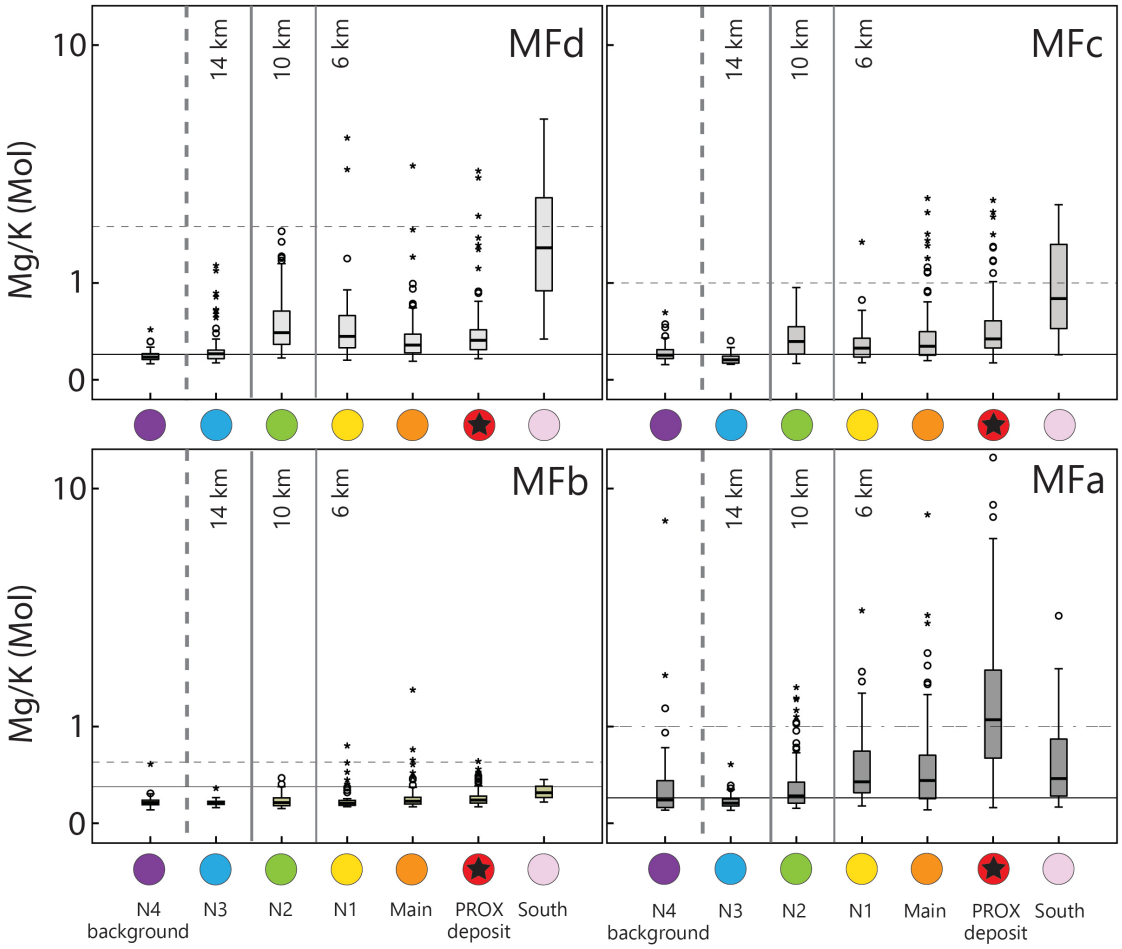

Figure 2.7: The molar ratios of Mg/K increase with proximity to the deposit (to the right of each plot; deposit location marked with star). Median values of MFd, MFc, and MFa lithofacies inside the 10 km halo (solid gray vertical boundary) are >0.2 (solid horizontal line). MFb exhibits values >0.37 (solid horizontal line, 95th percentile for MFb). The following values are present within the 6 km halo: MFd >2.0, MFc >1.0, MFb >0.55 (horizontal dotted lines). MFa shows significant increases with median values >1.0 (dash-dot line) above deposit location.

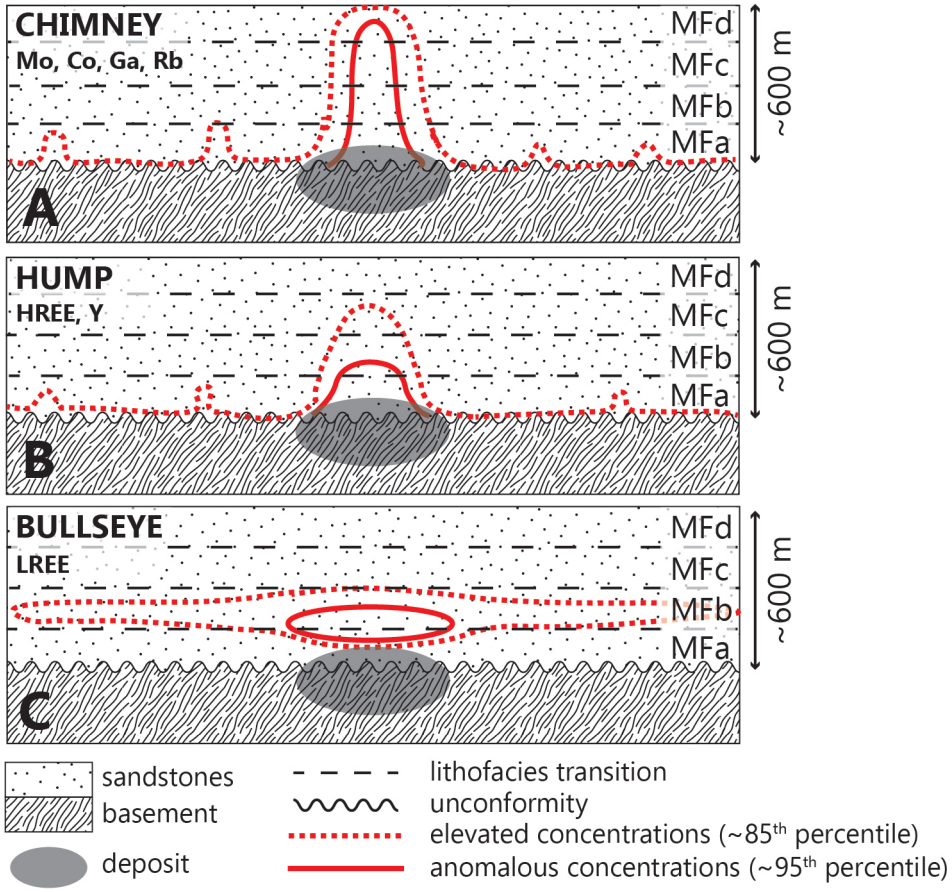

Figure 2.8: Elevated and anomalous concentrations of select elements fit into three broad categories of spatial distribution in relation to the main mineralized body. For all three, halo dimensions diminish as concentration increases. (**A**) The "chimney" elements (Mo, Co, Ga, Rb, partial digestion) appear as vertical plumes directly above the basement deposit, with Mo and Co ascending to the shallowest lithofacies (MFd). Isolated elevated concentrations are also seen distal from the deposit. (**B**) The "hump" elements (HREE, Y; partial digestion) form a more rounded shape which in lesser concentrations does not ascend to the MFd. The halo is centered over the deposit and is non-contiguous. As with the chimney group, there are distal, isolated elevated values, mainly within the MFa. (**C**) The "bullseye" elements (LREE; partial digestion) are concentrated within the lower sandstone (MFb) and appear stratiform throughout the footprint; however, above the deposit body anomalous values are apparent.

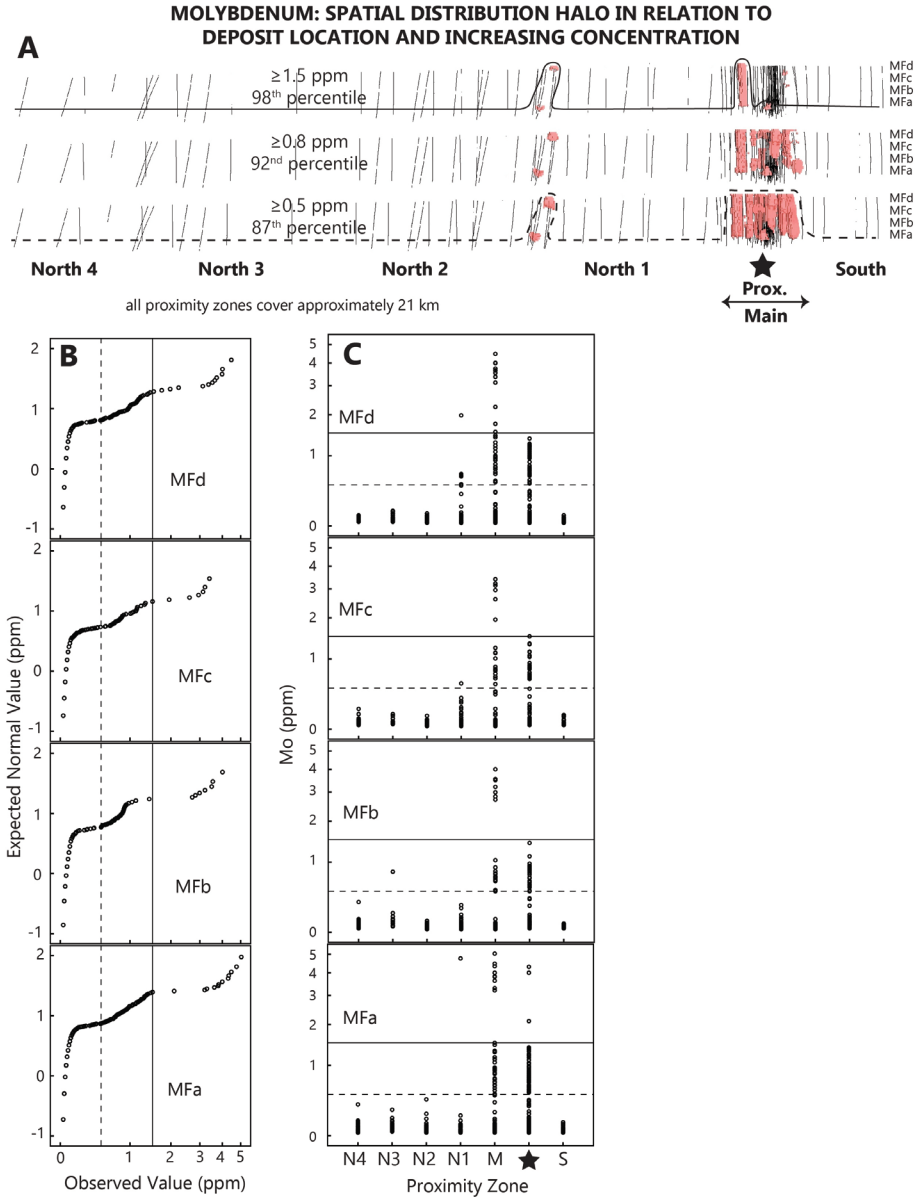

Figure 2.9: Molybdenum (partial digestion) is shown here as an example of the process used to determine spatial relationships of elevated and anomalous concentrations to the deposit location, noted by the star. (**A**) The 3D maps show the "chimney" pattern evident at the 87th percentile (≥ 0.5 ppm) of concentrations grouped above the deposit location and present to the surface in a vertical distribution. The halo becomes less contiguous as the concentrations increase, but remains within the Proximal and Main zones. Vertical lines are drill hole traces. (**B**) Quantile-quantile plots show the data distribution within each lithofacies. Dotted (0.5 ppm) and solid (1.5 ppm) lines represent the cutoff for the upper and lower 3D maps above. The first break in data indicative of anomalies or distinct populations occurs between 0.5–0.6 ppm, with the truly anomalous data >2 ppm in all lithofacies. (**C**) Scatter plots demarcated by proximity show the anomalous data that appears in the North 1 (N1) zone in lithofacies MFa–MFc, which appear in red in the 3D maps. Dotted and solid lines are equivalent to those in (**A**) and (**B**).

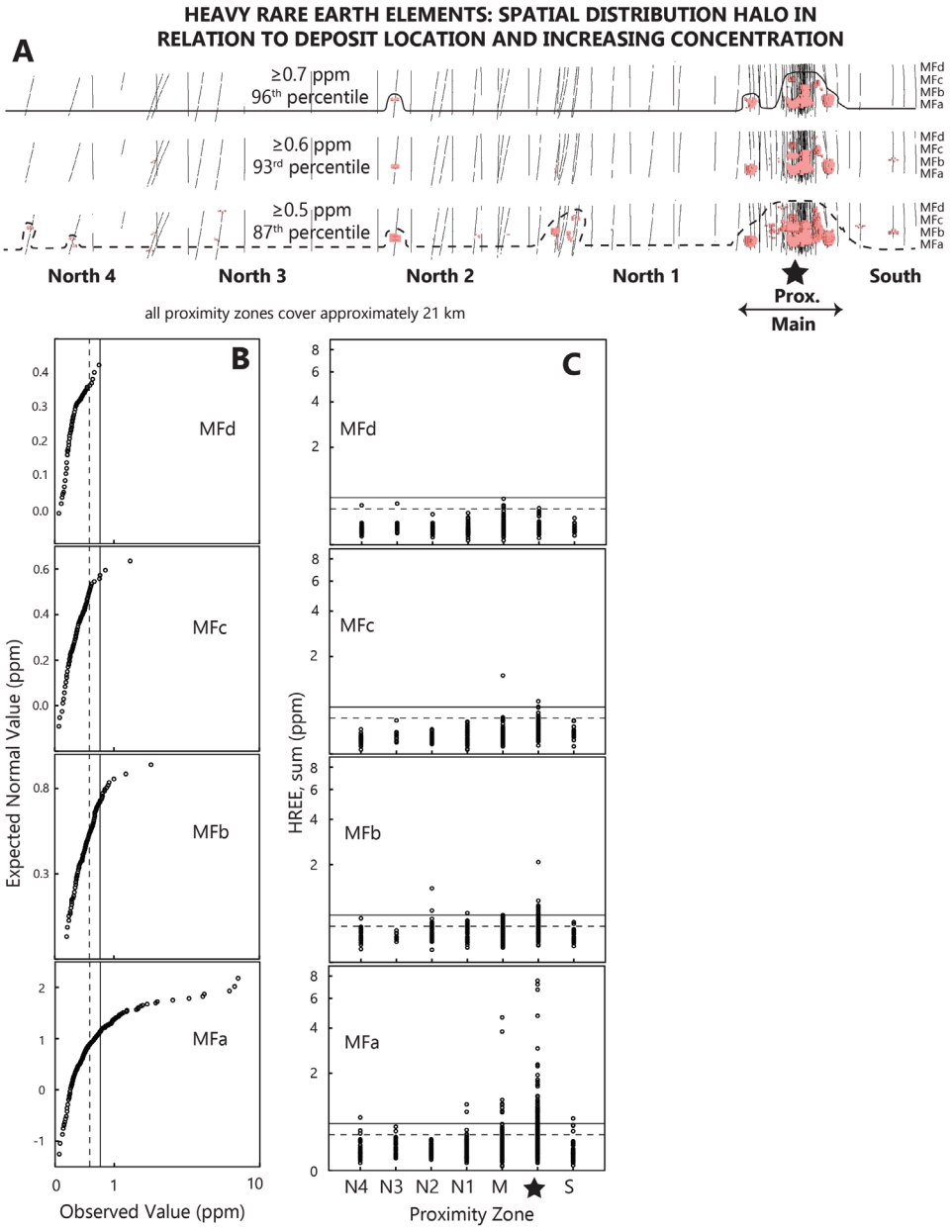

Figure 2.10: The sum of all HREE (partial digestion) is shown as an example of the process used to determine spatial relationships of elevated and anomalous concentrations to the deposit location, noted by the star. (**A**) The 3D maps show the "hump" pattern evident at the 87th percentile (≥ 0.5 ppm) of concentrations grouped above the deposit location as well as areas distal. The halo becomes less contiguous as the concentrations increase, but remains within the Proximal and Main zones. Vertical lines are drill hole traces. (**B**) Quantile-quantile plots show the data distribution within each lithofacies. Dotted and solid black lines shown are at 0.5 and 0.7 ppm, which represent the cutoff for the lower and upper 3D maps above. (**C**) The scatter plots demarcated by proximity show the anomalous data that appears in the North 1 and North 2 (N1, N2) zones in lithofacies MFa–MFb which appear in red in the 3D maps. Dotted and solid lines are equivalent to those in (**A**) and (**B**).

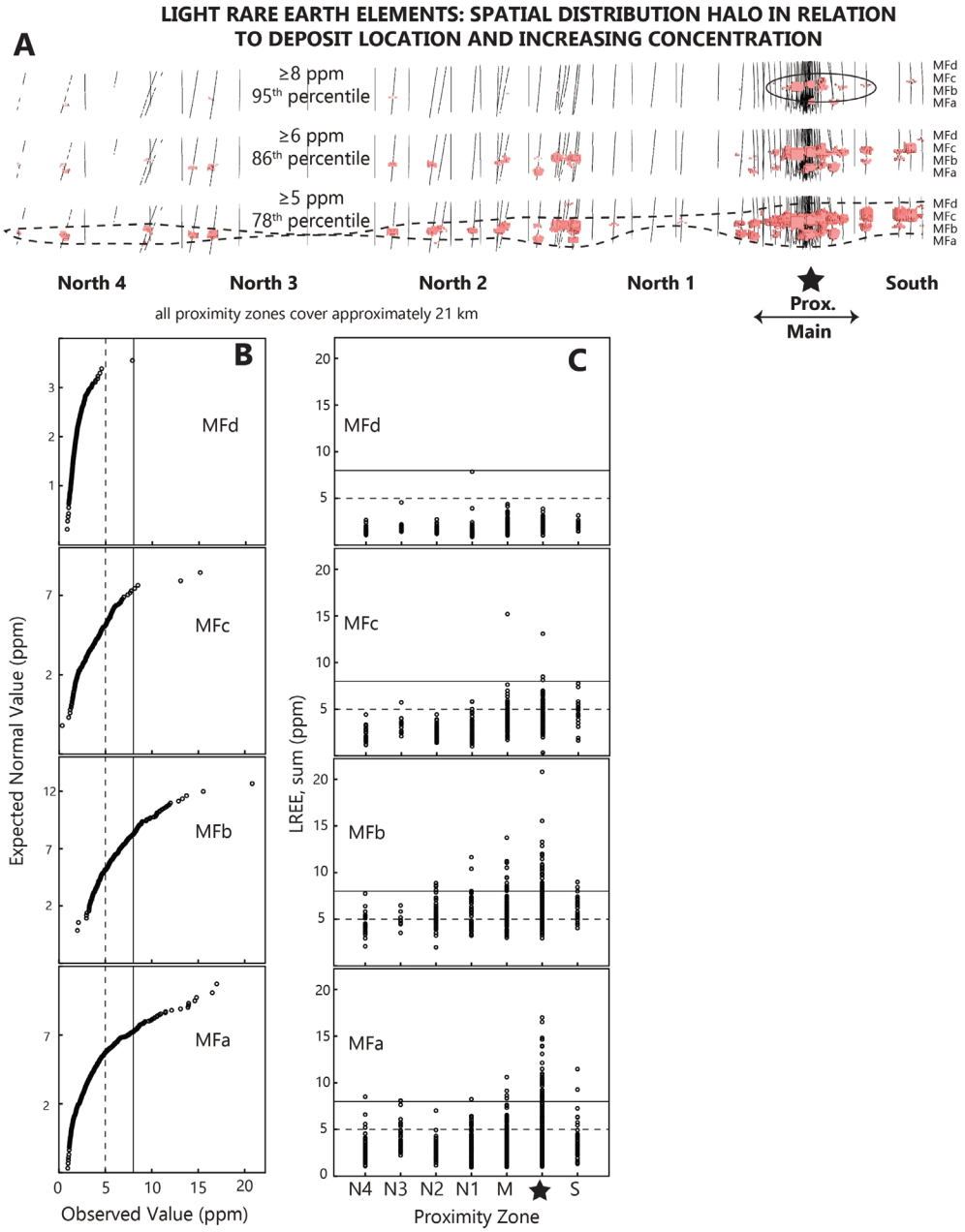

Figure 2.11: The sum of all LREE (partial digestion) is shown as an example of the process used to determine spatial relationships of elevated and anomalous concentrations to the deposit location, noted by the star. (**A**) The 3D maps show the "bullseye" pattern evident at the 78th percentile (≥ 5 ppm) of concentrations grouped above the deposit location as well as areas distal. The halo becomes less contiguous as the concentrations increase, but remains within the Proximal and Main zones. Vertical lines are drill hole traces. (**B**) Quantile-quantile plots show the data distribution within each lithofacies. Dotted and solid black lines shown are at 5 and 8 ppm, which represent the cutoff for the lower and upper 3D maps above. (**C**) The scatter plots demarcated by proximity show the majority of data is located within the MFb. Dotted and solid lines are equivalent to those in (**A**) and (**B**).

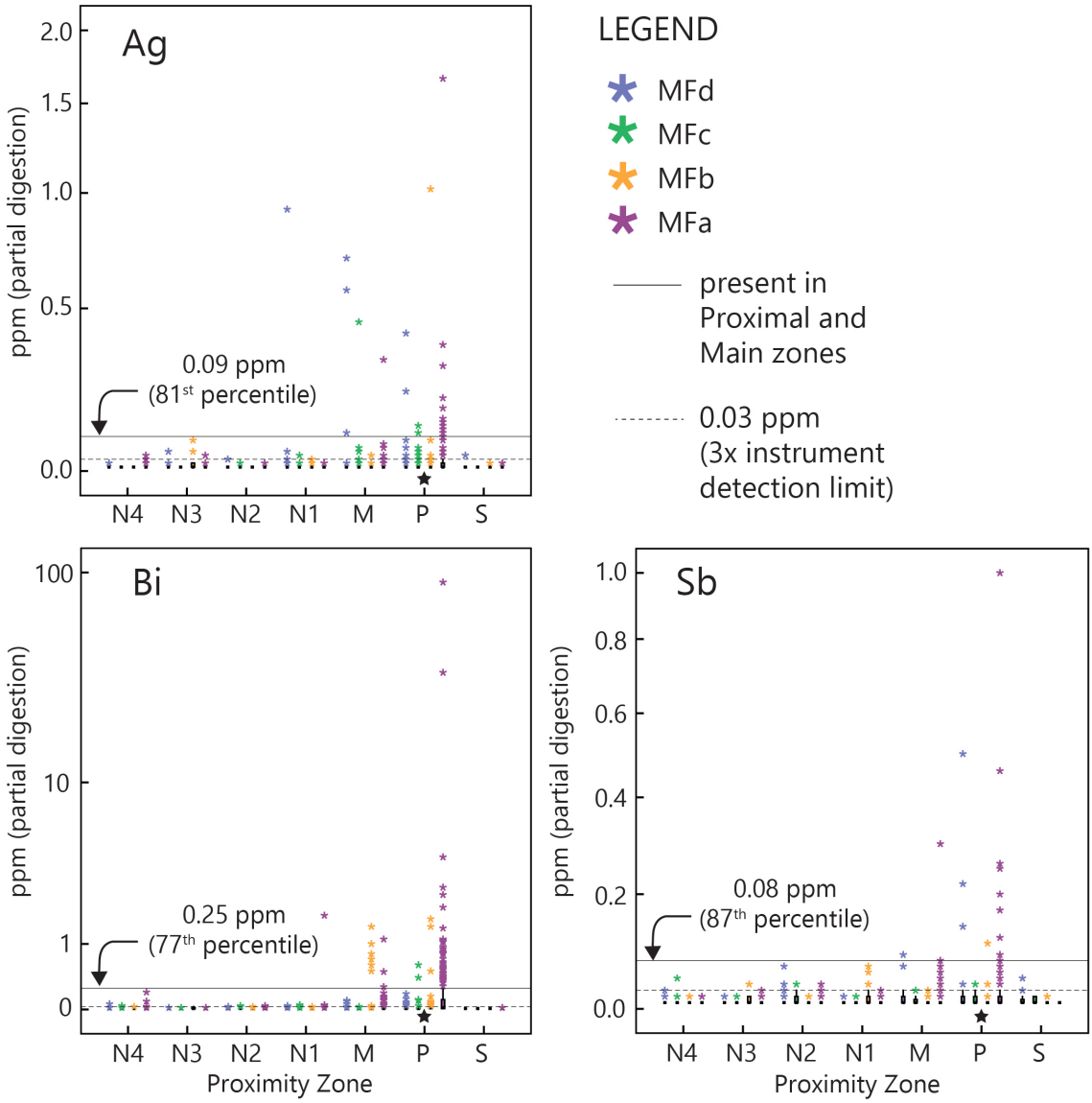

Figure 2.12: Silver, Bi, and Sb concentrations are either below analytical detection limit or less than three times the instrument detection limit (0.03 ppm) throughout most of the footprint, with ~90% of the confidently measurable concentrations present in the Proximal and Main zones. The implication is that the Proximal and Main zones underwent a greater degree of fluid-rock interaction than the other areas; these elements are therefore an indicator of a location in the footprint of increased activity and possible mineralization.

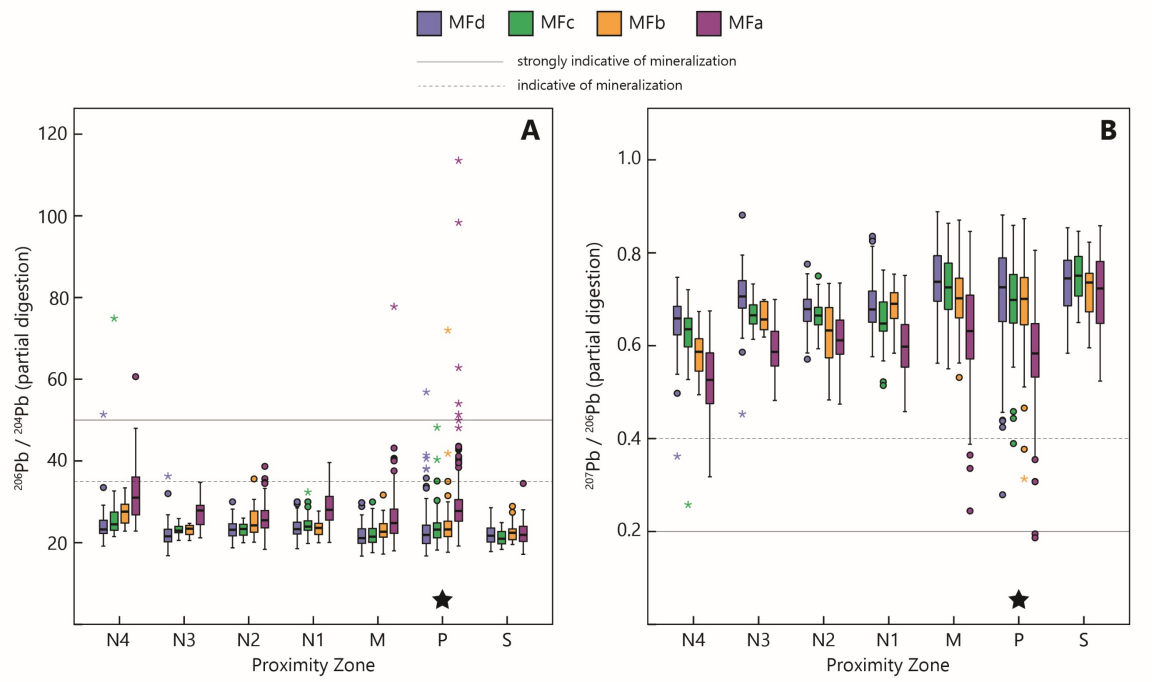

Figure 2.13: Lead isotope results (partial digestion) in the sandstones above the Millennium deposit, separated by lithofacies with regard to proximity to deposit (located with P, star). (**A**) $^{206}Pb/^{204}Pb$ values. Ratios indicative of mineralization are present mainly within the Proximal Zone and in the MFa of the Main Zone. Anomalously indicative ratios in North 4 are located in drill holes with samples containing U >1 ppm. (**B**) As in (**A**), but with $^{207}Pb/^{206}Pb$ values. Sample analyses (n) for each proximity zone: North 4 = 194, North 3 = 102, North 2 = 255, North 1 = 265, Main = 558, Proximal = 762, South = 122.

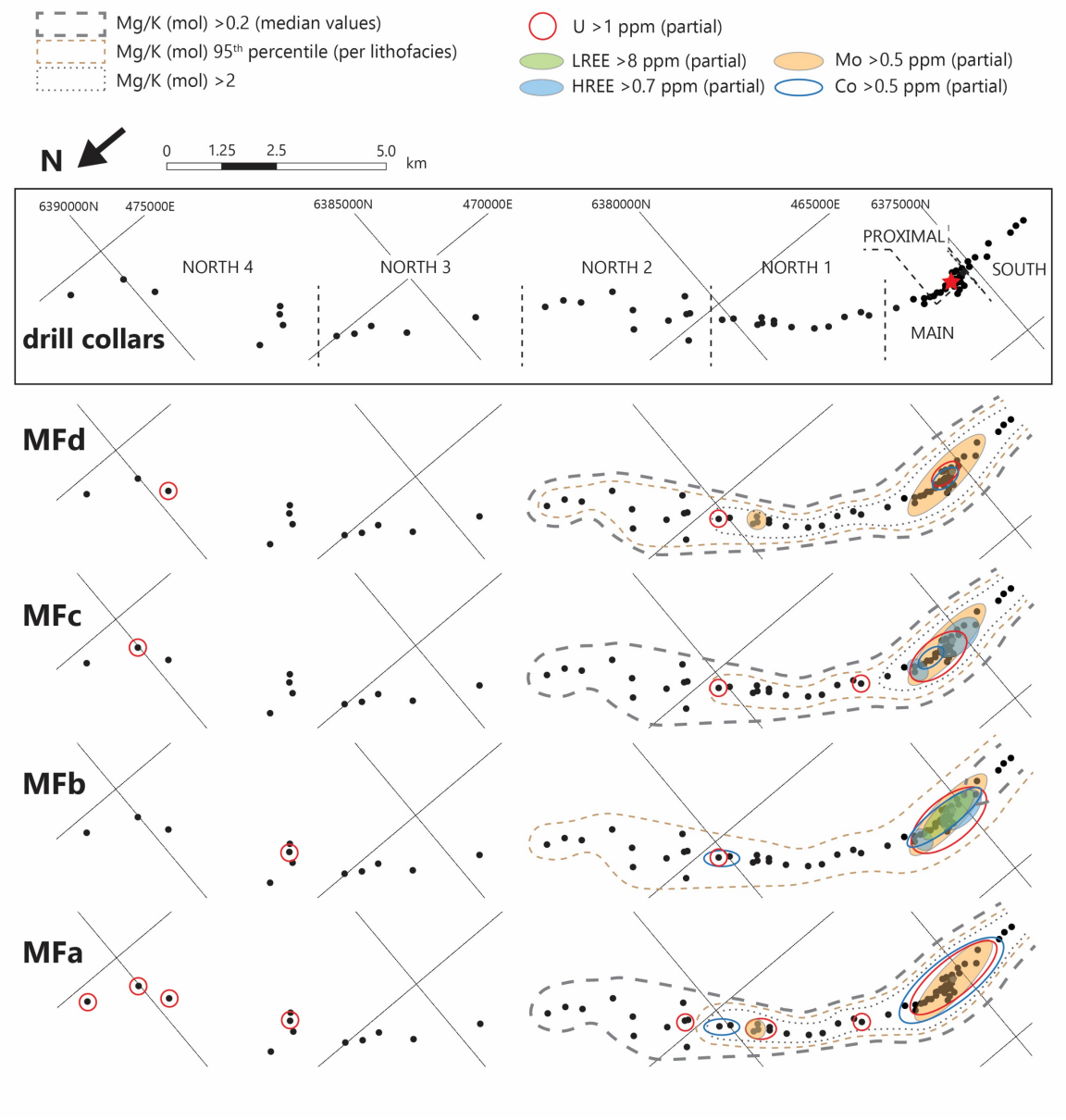

Figure 2.14: Plan view of study footprint, with vectors as defined through whole rock geochemistry. The median values of Mg/K (molar) demonstrate the 10-km envelope as they increase 1.5–2x within these areas, and with proximity to the deposit. Trace elements, including U, are shown highlighting the Main and Proximal corridors through all four lithofacies, which is a 1.9 km strike above the deposit location. Anomalously high values of U, rare and isolated, are found in the north of the study area but are not associated with any deposit. This map demonstrates the validity of utilizing the major and trace element haloes as a vectoring device, which overlap at the location of the deposit (Main, Proximal). Because the area to the south of the deposit is limited by drill hole distribution, it is not fully defined geochemically and the halo boundaries are therefore left open.

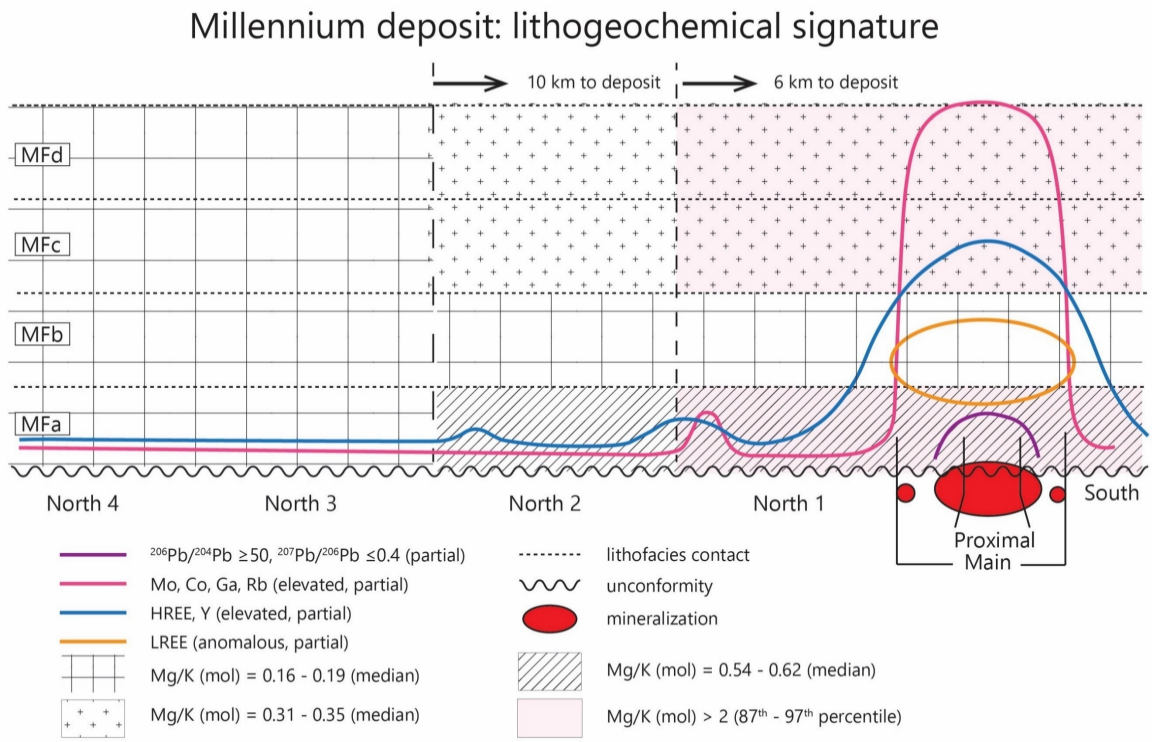

Figure 2.15: Stylized longitudinal section view of study footprint, as in Fig. 2.14, with vectors as defined through whole rock geochemistry. Not to scale. The median values of Mg/K (molar) demonstrate the 10-km envelope as they increase 1.5–2x within these areas, and with proximity to the deposit. The 6-km envelope is defined through anomalous Mg/K molar ratios >2 in the MFd, MFc, and MFa lithofacies. Elevated concentrations of trace elements are vertically distributed within the Main and Proximal corridors, which is a 1.9 km strike above the deposit location.

Table 2.1: ***Trace element haloes measured in the Proximal and Main zones above deposit***

Pattern 1: Chimney (partial digestion) Element	ppm	percentile*	elevated or anom. values†	m‡ along strike	m‡ across strike	m(max)§ above unc.
Mo	≥0.3	86	elevated	1200	440	650
	≥1.0	95	anomalous	975	435	650
	≥1.5	98	anomalous	126	300	650
Co	≥0.4	87	elevated	1110	435	650
	≥0.6	95	anomalous	1030	435	650
	≥1.0	98	anomalous	995	375	160
Ga	≥0.2	83	elevated	1725	510	650
	≥0.3	96	anomalous	1120	480	510
Rb	≥0.25	88	elevated	1725	580	650
	≥0.35	97	anomalous	1110	400	550
Ag	≥0.09	81	elevated	725	400	650
Bi	≥0.25	77	elevated	550	360	510
Sb	≥0.08	87	elevated	600	460	650
Pattern 2: Hump (partial digestion)						
HREE (sum)	≥0.5	87	elevated	1125	510	635
	≥0.7	95	anomalous	850	385	510
Dy	≥0.4	97	anomalous	850	385	510
Er	≥0.13	94	anomalous	850	385	510
Ho	≥0.1	97	anomalous	850	450	610
Tb	≥0.08	97	anomalous	850	360	585
Yb	≥0.1	94	elevated	1525	500	650
	≥0.13	97	anomalous	850	265	435
Y	≥1	90	anomalous	1575	490	630
$^{206}Pb/^{204}Pb$	≥35 (ratio)	97	anomalous	300	230	610
	≥50 (ratio)	99	anomalous	55	35	65
$^{207}Pb/^{206}Pb$	≤0.4 (ratio)	1.2	threshold	175	185	60
	≤0.2 (ratio)	0.1	anomalous	*not enough to measure in Target*		
Pattern 3: Bullseye (partial digestion)						
LREE (sum)	≥6	86	elevated	1400	520	460
	≥8	95	anomalous	1130	370	430
Eu	≥0.1	96	elevated	700	350	435
Gd	≥1	98	anomalous	600	300	400
Nd	≥6	98	anomalous	600	300	410
Pr	≥1.8	98	anomalous	600	300	410
Sm	≥1	98	anomalous	600	300	410

* percentile values do not include data that is less than three times the instrument detection limit.
† anomalous values determined via Q-Q plots, in one or more lithofacies.
‡ halo measurements incorporate 25m cells as displayed by inverse distance weighting in Target for ArcGIS.
§ distance is measured assuming unconformity is up to 650 in depth, utilizing Target for ArcGIS in Z direction.

Table 2.1: Halo dimensions of those elements found with a spatial relationship to the Millennium deposit location. The highest concentrations of U present in the sandstones directly above the deposit (50 – 1000 ppm, partial digestion), provide a halo with strike length along the B1 trend ~350 m, across the B1 trend ~150 m, and up to 150 m above the unconformity. Measurements of these vector haloes are estimated from 3D projections of 25 m cells with an inverse distance weighted algorithm. Not all patterns are contiguous.

CHAPTER 3: THE DISTAL LITHOGEOCHEMICAL FOOTPRINT OF THE McARTHUR RIVER UNCONFORMITY-TYPE URANIUM DEPOSIT: MOLAR ELEMENT RATIOS AND TRACE ELEMENT CONCENTRATIONS AS DISTRICT-SCALE VECTORS

ABSTRACT

The McArthur River deposit is the world's largest and highest grade unconformity-type uranium deposit. Scalable geochemical signatures and mineral assemblages differentiating background, least-altered, and economic zones are present in an extensive distal alteration footprint within the sandstone host rocks, despite intense quartz cementation above the deposit that has suppressed the geochemical signature of most traditional pathfinder elements. Molar element ratios utilizing Mg-K-Al illustrate transitions between the kaolin group, illite, dravite, and chlorite that define the alteration footprint over ~20 km along strike and up to 560 m above the deposit. Samples with molar element ratios K/Al 0–0.06 and Mg/Al 0–0.41 are present ~400–560 m above the deposit and are accompanied by elevated Ga and Cs. Less expansive haloes of elevated P_2O_5, Ba, Sr, and LOI are present up to ~375 m above the deposit and 4–8 km along strike. These results are consistent with significant fluid-rock interaction associated with mineralizing processes at the McArthur River deposit, and are therefore useful distal vectors for high grade U at depth.

3.1 INTRODUCTION

The McArthur River U deposit, located in the southeast Athabasca Basin, is the largest unconformity-type U deposit in the world (Kyser and Cuney, 2008; Kyser, 2014). It is a deposit with multiple ore zones, at depths from 500–640 m below surface, currently

containing 253.3 M lbs. U_3O_8 grading 9.62% (proven reserves), 83.0 M lbs. U_3O_8 grading 18.84% (probable reserves), 5.2 M lbs. U_3O_8 grading 3.83 % (measured resources), and 0.3 M lbs. U_3O_8 grading 3.02% (indicated resources), after 17 years of active mining (Bronkhorst et al., 2012; Cameco Corporation, 2015). Although it has been studied extensively for over twenty years (McGill et al., 1993, Kotzer et al., 1992; Alexandre et al., 2009b; Ng et al., 2013; Adlakha et al., 2015; and many others), the large-scale distal lithogeochemical footprint within the Manitou Falls Formation sandstones has not been fully characterized with respect to the geochemical changes with proximity to mineralization.

Unconformity-type uranium deposits are formed due to redox reactions at or near an unconformity located between an Archean to Paleoproterozoic, metasedimentary basement and a Paleo- to Mesoproterozoic redbed sedimentary basin (Hoeve and Quirt, 1984; Ruzicka et al., 1996; Kyser, 2014). Mineralization occurs when oxidized fluids carrying U interact with a reductant, causing fluid reduction and U precipitation through coupled redox reactions; the reductant can be either basement-derived reduced fluids or the reduced lithologies in the basement itself (Hoeve and Sibbald, 1978; Hoeve and Quirt 1984; Fayek and Kyser, 1997; Hecht and Cuney, 2000). One hallmark of unconformity-type deposits is the extensive alteration of host rock by fluid-rock interaction. McArthur River, a large and multi-lensed deposit, is located at and below the unconformity beneath altered Athabasca Group sandstones (Bronkhorst et al., 2012). These supermature sandstones are unmetamorphosed and extremely clean, containing low concentrations of trace elements

(Hiatt and Kyser, 2007; Wright, 2009) that when altered contain easily identifiable anomalous geochemical signatures.

Geochemical and mineralogical research on unconformity-type U deposits have focussed on two types of pathfinders: 1) clay and other mineral alteration haloes and 2) trace elements, including U itself (Hoeve and Sibbald, 1978; Earle and Sopuck, 1989; Zhang et al., 2001; Ng et al., 2013). Clay-type alteration haloes can be problematic because although their presence is associated with a fertile environment, barren and mineralized areas can have similar mineralogical expressions (Alexandre et al., 2009a; Cloutier et al., 2010). Uranium concentrations themselves are not particularly useful in large-scale or early stage exploration, as they often decrease sharply to background levels proximal to unconformity-type U deposits (Sopuck et al., 1983; Wright, 2009). Trace elements related directly to mineralization processes and associated sulfides (Pb, heavy rare earth elements, As, Cu) or redox reactions (Mo, Ni, V, Co) have been shown to be useful vectors in other unconformity-type U deposits, with elevated distal haloes due to mobilization along structural conduits (Tremblay, 1982; Sopuck et al., 1983; Ruzicka, 1989; Ng et al., 2013). These expressions are suppressed at McArthur River, because the deposit is both monomineralic and located beneath extensive quartz cemented sandstone that has restricted the geochemical signature of most traditional pathfinder elements to within 200 m of the unconformity (Mwenifumbo et al., 2004; Ng et al., 2013). However, the sandstones above this barrier are still altered, and the potential for major and trace elements associated with the footprint related to the mineralization process can be evaluated.

A two-fold approach is utilized to delineate and define the distal halo of mineralization. First, molar element ratios are utilized to characterize clay-type mineral variations proximal and distal to mineralization. Second, individual major and trace elements are examined for elevated or anomalous results in spatial relation to mineralization. Elements with elevated concentrations in strata above the quartz cementation and proximal to mineralization are considered potential pathfinders. Over 10,000 individual geochemical samples were available for modeling, covering nearly three decades of exploration and a strike length of over 20 km, which is the first time that a dataset of this magnitude has been interrogated for a comprehensive study of an unconformity-related uranium deposit.

The aim of this paper is to define the geochemical signature in the sandstones above the McArthur River deposit on a scale approximately 20 km long and 600 m in depth, characterized through both legacy (company) data and new data collected as part of this study. Molar element ratios and anomalous trace elements will be used to demonstrate the transition between diagenetic and hydrothermal alteration, provide vectors toward high grade mineralization, and define boundaries between subeconomic and economic areas of mineralization in the McArthur River area.

3.2 REGIONAL GEOLOGY

The Athabasca Basin unconformably overlies the 2.9–1.8 Ga basement comprising the Rae and Hearne provinces and Taltson Magmatic Zone of the Canadian Shield (Fig. 3.1a; Hoffman, 1988; Ansdell, 2005). The majority of deposits are hosted in the

southeastern rim of the basin in contact with the Hearne Province, although unconformity-type U deposits are located throughout the Athabasca Basin (Jefferson et al., 2007).

The Hearne Province includes the Mudjatik and the Wollaston domains (Lewry and Sibbald, 1980; Hoffman, 1988). The Mudjatik Domain, a northeast trending shear bounded belt, consists of Archean felsic gneisses with localized Archean and Paleoproterozoic supracrustal rocks (Lewry and Sibbald, 1980; Annesley et al., 2005; Jeanneret et al., 2016). The Wollaston Domain also has a northeast trend but is a fold thrust belt, and is dominated by Archean granitoid gneisses overlain by Paleoproterozoic quartzo-feldspathic psammitic to pelititc gneisses (Lewry and Sibbald, 1980; Annesley et al., 2005; Jeanneret et al., 2016). The Wollaston Domain rocks are highly deformed with a complex structural history, and were metamorphosed from mid-upper amphibolite to granulite facies (Annesley et al., 2005; Jeanneret et al., 2016). The McArthur River deposit spans the unconformity between the Wollaston Domain metasedimentary basement rocks and the overlying Athabasca Group sandstone (McGill et al., 1993, Bronkhorst et al., 2012). Multiple unconformity-type U deposits, including McArthur River, are associated with the transition between the Mudjatik and Wollaston domains, a 20-km wide zone known as the Wollaston-Mudjatik Transition Zone (WMTZ) (Fig. 3.1b; Cumming and Krstic, 1992; Annesley et al., 2005; Jeanneret et al., 2016). This area is represented by the transition between deformation styles of the two domains (Lewry and Sibbald, 1980) and alternating rock types strongly deformed during the Trans-Hudson Orogeny (THO) (Annesley et al., 2005; Jeanneret et al., 2016).

The Athabasca Basin is a sedimentary basin that unconformably overlies the Rae and Hearne provinces, formed through rapid uplift and subsidence cycles during its 1.75–1.54 Ga history (Armstrong and Ramaekers, 1985; Kyser et al., 2000; Creaser and Stasiuk, 2007; Alexandre et al., 2009b). The basin consists predominantly of fluvial sandstones capped by an uppermost unit dominated by marine sedimentary rocks, and is currently ~1–2 km deep, eroded from its original burial depth of 5–6 km (Pagel et al., 1980; Ramaekers and Catuneanu, 2004; Alexandre et al., 2009b). It contains three sub-basins, with the McArthur River deposit hosted in the easternmost Cree sub-basin (Cumming and Krstic, 1992; Hiatt and Kyser, 2007). The Manitou Falls Formation in the study area consists of alluvial-fluvial quartzose sandstone-conglomerate with minor siltstones (Ramaekers et al., 2007; Hiatt and Kyser, 2007). These lithofacies contain clays, <15% lithic clasts, lack preserved feldspars, and show evidence of bleaching and hydrothermal alteration, all of which suggest alteration of the source rocks through weathering and transport, coupled with further diagenesis and alteration during and after basin formation (Hiatt and Kyser, 2007).

The Athabasca Basin and basement rocks were affected by numerous tectonic events (Annesley et al., 2005; Jeanneret et al., 2016). Prior to sediment deposition, basement rocks underwent polyphase deformation near the end of the THO, which created complex folds, shears, and numerous faults and fractures (Lewry and Sibbald, 1980; Annesley et al., 2005; Mercadier et al., 2013). After basin formation and sediment deposition, basement faults and fractures were reactivated through compressional and extensional tectonics, resulting in splay faults in the basin (Kotzer and Kyser, 1995;

Alexandre et al., 2009a). These faults, along with overall basin tilting, allowed far-field tectonic forces to drive multiple fluid flow events throughout the basin's history (Kotzer and Kyser, 1995; Hiatt and Kyser, 2007; Cui et al., 2012; Chi et al., 2013).

3.3 DEPOSIT GEOLOGY

The McArthur River deposit study area is approximately 20 km long, trending NE-SW and focussed on the graphite-bearing P2 fault system (Fig. 3.2; McGill et al., 1993; Bronkhorst et al., 2012). A total of 292 drill holes are included in this analysis, encompassing the P2 Main and McArthur River deposits and areas distal to mineralization.

3.3.1 Basement geology

The McArthur River deposit is hosted in the Wollaston Domain basement within the graphite-bearing P2 reverse fault system (McGill et al., 1993; Ng et al., 2013). This fault system consists of two groups of faults: a major reverse fault with 045° strike, dipping 40–65° towards the SE, and two secondary sets of near vertical transcurrent faults, striking 100–110° and 160–170° (Bronkhorst et al., 2012; Ng et al., 2013). The reverse fault (045° strike) offsets the lower Manitou Falls Formation with a vertical displacement of 60–80 m. It is the major structural control for the deposit, and differentiates the basement hanging wall and footwall (McGill et al., 1993; Bronkhorst et al., 2012). The hanging wall rocks to the P2 fault are mainly graphitic pelite to semipelites, whereas the footwall rocks are mainly quartzites and rare pelitic gneisses (McGill et al., 1993; Bronkhorst et al., 2012).

3.3.2 Manitou Falls Formation

The Manitou Falls Formation overlies the McArthur River deposit and consists of unmetamorphosed quartzose sandstones with minor siltstones and pebble beds, with predominantly horizontal stratigraphy (Kotzer and Kyser, 1995; Hiatt and Kyser, 2007; Ramaekers et al., 2007). It comprises 4 lithofacies: MFa, MFb, MFc, and MFd from oldest (deepest) to youngest (beneath overburden). Figure 3.3 shows typical examples of rock types in the MFa through MFd lithofacies.

The MFa lithofacies, nearest the unconformity, ranges in thickness from 85–145 m; its lower unconformable basement contact is offset 60–80 m by the P2 reverse fault (McGill et al., 1993). It comprises medium to coarse grained fluvial sandstones with minor pebble- and microconglomerates (McGill et al., 1993). It is poorly sorted and shows evidence of both alluvial fan and braided stream depositional environments (Hiatt and Kyser, 2007). At many locations the lower MFa lies unconformably above the basement; in other areas the unit is intercalated with a fanglomerate lithofacies which lies in unconformable contact with basement rocks (Quirt, 2000). The fanglomerate consists of well-rounded, poorly-sorted, pebble- to cobble-sized quartz (McGill et al., 1993; Quirt, 2000). The MFb overlies the MFa, and has an average thickness of 125–150 m (McGill et al., 1993). The MFb lithofacies consists of medium- to coarse-grained sandstone with minor (>2%) interbedded clast-supported (micro)conglomerate beds >2 cm thick. The unit contains trough cross-bedding, typical of a high-energy braided stream environment (Hoeve and Sibbald, 1978; Hiatt and Kyser, 2007). Locally, it contains heavy mineral bands that are mildly radioactive due to elevated Th content (Mwenifumbo and Bernius, 2007), and purple, red, and pink

hematitic bands (McGill et al., 1993). The MFc overlies the MFb and averages <100 m in thickness, containing <1% mud intraclasts and pebble beds <2 cm thick (Hiatt and Kyser, 2007). The MFc lithofacies contains planar and trough cross-bedding as well as laminations and is interpreted to represent a braided stream depositional environment (Hiatt and Kyser, 2007). The MFd is the uppermost lithofacies, with an average thickness of 180 m and is covered by up to 100 m of overburden within the study area. The MFd is typically well sorted, containing fine to medium grained quartz arenites with >1% mud intraclasts (Hiatt and Kyser, 2007). Total thickness of the Manitou Falls Formation above the McArthur River deposit averages >500 m, ranging from 480 m above the P2 trend hanging wall and 560 m above the footwall (McGill et al., 1993; Bronkhorst et al., 2012).

3.3.3 Alteration

Basement and basin rocks in the P2 trend have been extensively affected by both diagenetic and hydrothermal alteration throughout the study location (McGill et al., 1993; Adlakha et al., 2014). The P2 fault system is interpreted to have controlled fluid flow and associated fluid-rock interaction above and below the unconformity, as alteration is most intense near faults and mineralization (McGill et al., 1993; Bronkhorst et al., 2012).

3.3.3.1 Basement alteration

The uppermost 15–50 m of Wollaston Domain basement rocks beneath the unconformity have been altered to a regolith (Nash et al., 1981; Macdonald, 1985). At the McArthur River deposit, this well-developed regolith comprises an uppermost, discontinuous bleached zone of kaolin-group minerals and illite at the unconformity, a middle red zone of hematite and kaolinite, and a deeper green zone of chlorite and illite

that transitions into fresh basement rock (Macdonald, 1985; Adlakha et al., 2014). Near the fault, the basement rocks are brecciated with alteration present along the shear zones, splay faults, and fractures above and below the unconformity (Jefferson et al., 2007). Alteration features associated with faulting are intense within the hanging wall, including bleaching, with chlorite and illite dominant near the unconformity and mineralization. Other hanging wall alteration includes illite, sericite, and quartz replacement of biotite and feldspar. Less intense alteration of the footwall includes dravite, apatite, and chlorite (McGill et al., 1993). Nearest the deposit, the alteration profile consists of a metre-scale transition from weak to intense chlorite alteration (Alexandre et al., 2005; Bronkhorst et al., 2012).

3.3.3.2 Manitou Falls Formation alteration

A major regional illite anomaly in the Manitou Falls Formation sandstones covers 10s of kilometres surrounding narrower (100s of metres) chlorite and dravite anomalies ± dickite and kaolinite; all three strike in roughly the same orientation as the WMTZ (Fig. 3.1b; Earle and Sopuck, 1989). The McArthur River deposit sits within the illite anomaly and is proximal to the chlorite and dravite anomalies (Fig. 3.1b). Total clay content is typically <5% in the upper 100–200 m of the Athabasca Basin and increases with depth; in some locations in the basin, the lower Manitou Falls Formation sandstones can contain up to 20% clays, although values typically remain <10% (Earle and Sopuck, 1989). Additional secondary minerals include hematite and limonite, and alteration features include bleaching resulting from the destruction of hematite (McGill et al., 1993). However, in the areas associated with the McArthur River deposit, the sandstones above the deposit exhibit extensive pre-ore quartz cementation (McGill et al., 1993; Bronkhorst et al., 2012; Ng et

al., 2013). This quartz alteration intensifies at depths of 375 m and lower in the sandstones and is concentrated within the lower MFb lithofacies and the finer-grained sandstones, rather than in the MFa or fanglomerate (McGill et al., 1993; Ng et al., 2013).

3.3.4 Mineralization

The McArthur River deposit consists of several economic grade zones (A, B, C, and 1 through 4 South) that are hosted both at and below the unconformity, 500–640 m below surface, and were structurally controlled by the P2 fault system (Fig 3.4; McGill et al., 1993; Bronkhorst et al., 2012). The total strike distance is approximately 1.7 km along the P2 trend (Bronkhorst et al., 2012; Adlakha et al., 2015). Most mineralized zones are located within the basal sandstone or fanglomerate at the basement contact and in the hanging wall wedge. One pod (Zone 2) is found in the basement only, and contains the main mineralization (Fig. 3.4; Bronkhorst et al., 2012; Ng et al., 2013). The ore is high grade, monomineralic, and consists mainly of uraninite with minor galena, pyrite, and chalcopyrite (McGill et al., 1993; Ng et al., 2013). The main mineralization nearest the fault-unconformity contact varies from massive, to blebby/botryoidal, to subhedral aggregates of uraninite. Other mineralization includes disseminated and fracture-hosted uraninite within the sandstones, and disseminated grains and veinlets near the footwall unconformity in narrow chlorite breccia zones that generally border on chlorite- and dravite-altered siltstones. Rare disseminated grains, veinlets, nodules, blebs, and narrow bands of massive uraninite are present in the quartzites in the footwall of the P2 fault (McGill et al., 1993; Bronkhorst et al., 2012). P2 Main is a mineralized zone located

approximately 4.5 km southwest of McArthur River, but is considered subeconomic (Bronkhorst et al., 2012).

Uranium-Pb dating on both basement and sandstone-hosted uraninites have identified two important ages of mineralization: a primary event at 1.51–1.59 Ga and a remobilization event at 1.33–1.38 Ga (Cumming and Krstic, 1992; McGill et al., 1993). Younger ages have also been obtained, which suggest secondary remobilization events at ca. 1.2, 1.1, 0.9, 0.7, and 0.3 Ga (Cumming and Krstic, 1992; Fayek et al., 2002; Alexandre and Kyser, 2005; Alexandre et al., 2009b; Ng et al., 2013). These ages are consistent with other geochronological studies placing primary mineralization at ~1.5 Ga basin-wide with remobilization events correlated to far-field tectonic events (Cumming and Krstic, 1992; Fayek and Kyser, 1997; Fayek et al., 2002; Alexandre et al., 2009b).

3.4 LITHOGEOCHEMISTRY

3.4.1 Methods

Data herein comprises legacy data from the Manitou Falls Formation sandstones, collected by Cameco between 1984–2014, supplemented with drill core samples collected during this study. Legacy samples were approximately 1 cm thick, cut from drill core, and considered representative (composite) of the sandstone within interval distances of 5, 10, and 20 m. They were pulped and analyzed via total (3-acid) and partial (2-acid) digestion for basin sandstones by Saskatchewan Research Council Geoanalytical Laboratories, Saskatoon, Canada; methodology is described in greater detail in Chapter 2. Samples collected from 1984–1985 were analyzed for U, Cu, Ni, Pb, and B; additional elements

were added in years 1985–2007 but not consistently throughout the dataset. Post-2007 samples were analyzed for 54 elements using the SRC ICP-MS1 Sandstone Exploration package (SiO_2 is not included). For the purposes of this study, only samples containing <1000 ppm U were selected from the archival database. This threshold was chosen to avoid undue influence from the ore itself, and to allow for a better understanding of the distal edges and vectoring capabilities on a larger, district scale. Fanglomerate samples are considered lithologically distinct and are not present in all locations, so were removed from the data analysis. Data refinement on this archival database was performed to account for instrumental variation over multiple years of analyses and to ensure robust results; the methodology is explained in detail in Appendix A.

Shortwave infrared (SWIR) spectroscopy was performed directly on drill core with either a PIMA II (pre-2004) or ASD Terraspec portable infrared mineral analyzer and MinSpec 4 software. The analysis targets five minerals: dickite, kaolinite, illite, chlorite (non-specific mineral group), and dravite. SWIR results are in percentage, recalculated by the software to account for only the clay-type minerals identified by the instrument (i.e., 100% clay) within the scanned area.

Supplementary sandstone samples for this study were collected from McArthur River drill core storage to augment the historic data, with the additional analysis of SiO_2, and so that lithogeochemical data could be integrated with microscopy and petrophysical measurements as part of the Canadian Mining Innovation Council (CMIC)-Footprints project. Four fences (sections) of drill holes across the P2 trend were chosen, ranging from areas above little or no mineralization to those directly associated with ore zones (Fig. 3.5).

A total of 229 Manitou Falls Formation sandstone samples were collected from 13 drill holes with an increased sampling frequency nearer to the unconformity. Table 3.1 summarizes the samples collected. The new data generally support the trends observed in the post-2007 legacy data. Appendices D and E contain the locations of samples collected and whole-rock geochemical results.

3.4.2 Statistics

Geochemical data were evaluated statistically using comparisons to standard statistical thresholds and backgrounds for given elements (Quirt, 1985; Jenner, 1996; Matschullat et al., 2000). To eliminate analytical noise, results for a given element were only utilized if concentrations are greater than three times the instrument detection limit. Background values were defined based on U content and spatial relationship to deposit locations in the study area.

Uranium content <1 ppm is considered to be background, as 1 ppm is the average concentration in common sandstones and continental crust (Nash, 1981; Javoy, 1999; Cuney, 2012). In areas of the Athabasca Basin not associated with mineralization, the geometric mean for U content in the Manitou Falls Formation ranges from 0.9-1.1 ppm (total digestion) (Quirt, 1985), confirming U <1 ppm to be a reasonable background value for this study. Three data groups were established to define background values of other elements. The lithogeochemical results from Quirt (1985) were used for background values of major elements (total digestion, AAS and ICP-OES) in regional Manitou Falls Formation sandstones at least 50 kilometres from the study area. Trace elements from the Quirt (1985) study were not used to define background concentrations as there were no

partial digestion results, nor any ICP-MS-based analyses. Consequently, for trace element background values (total and partial digestion, ICP-MS), two groups of drill holes were chosen from the archival database. Four drill holes in the hanging wall (Fig. 3.6b, "HW") were chosen to represent least altered/background sandstones not directly associated with the P2 fault system or mineralized zones, with 130 of 132 samples containing <1 ppm U. Nine holes along strike and within the P2 trend but most distal from mineralization (Fig. 3.6b, "P2SW") were chosen to represent least altered sandstones associated with the P2 fault system, with 293 of 303 samples containing <1 ppm U.

Whole rock geochemical data were examined for concentrations significantly different from the background or least altered samples and that also exhibit trends correlative with proximity to mineralization. Both partial and total digestion data were examined for each element. For spatial evaluations, 3D maps were constructed for all results using Geosoft® Target 4.5.5 for ArcGIS software.

3.4.3 Proximity zones to mineralization

Drill holes were divided into proximity zones determined by location relative to mineralization and U content (partial digestion) in the sandstones (Fig. 3.6a–b, d). Partial digestion was used as the results were more extensive than the total digestion technique, and are ideally more representative of hydrothermal mineralization processes. For each subdivision, especially those with larger amounts of U, the U content categorization is a function of the drill hole intersecting mineralization at depth; not all samples within each proximity zone contain the largest amounts noted below.

HW: background drill holes located above the basement hanging wall, containing the least amount of U in the study with a median value of 0.3 ppm;

P2SW: least altered drill holes within the P2 trend, located at the southwestern limit of the study area, with median U concentrations of 0.3 ppm and rare samples with elevated U concentrations;

P2: non-mineralized drill holes within the P2 trend containing <10 ppm U, with a median value of 0.5 ppm U;

P2 Main: mineralized drill holes associated with the subeconomic P2 Main deposit; the majority of samples contain <1 ppm U, but can contain up to 900 ppm U; the median value overall is 0.4 ppm U;

McA: drill holes in the northeastern 7 km of the study area surrounding the McArthur River deposit; samples can contain up to 5 ppm U, and have a median value of 0.7 ppm U;

McA+: as with McA samples; can contain up to 10 ppm U, and have a median value of 1.2 ppm U;

McA++: as with the McA and McA++ locations, plus those drill holes within the McArthur River deposit economic zones; can contain up to 1000 ppm U, and have a median value of 1.4 ppm U.

The new data (2014) were collected within and near mineralized zones of the McArthur River deposit, across strike of the P2 trend (Figs 3.5 and 3.6c). The Southwest fence is considered to be outside of the mineralized zones due to its location south of Zone 4 South; however, it does contain weak mineralization above the unconformity in MC-336.

Zone 4 is mineralized at the unconformity, as is Zone C. The "Gap" fence lies between Zones 1 and A, with weak mineralization at the unconformity in MAC-208 only. Finally, a single sampled core (MC-434) in line with the three cores in the Gap fence but above the hanging wall, and approximately 800 metres from the P2 trend, is barren.

3.4.4 Results

3.4.4.1 Shortwave infrared spectroscopy

Clay-type minerals identified by SWIR exhibit distinct footprints within the study area (Fig. 3.7). At McArthur River, dickite is concentrated in the mid-lower (MFb) Manitou Falls Formation lithofacies, and is present throughout the study area, but dominant above the deposit and surroundings (Fig. 3.7). Illite is present in all locations, but is dominant in the areas to the south of the deposit in lithofacies MFd–MFb, as well as in the background hanging wall samples. Chlorite and kaolinite are dominant in the upper lithofacies in the northern third of the study area, above mineralization; chlorite is also present in the lower MFa at the unconformity. Dravite is present throughout the study area, with higher concentrations as localized clusters in the MFd–MFb lithofacies, although not obviously associated with mineralization.

3.4.4.2 Major elements

Silica (SiO_2) contents average 96.6% in the new samples collected, ranging from 89.2–99.8%. Manitou Falls Formation sandstones are generally defined as quartz arenites (e.g., Hiatt and Kyser, 2007; Rainbird et al., 2007), and were chemically classified as

sublithic arkose in the Quirt (1985) background study using the Pettijohn et al. (1972) log(SiO_2/Al_2O_3) vs. log (Na_2O/K_2O) discrimination diagram.

In comparison to the background elements as defined in Quirt (1985), MgO, K_2O, and CaO display significantly higher concentrations in all four lithofacies throughout the study area, whereas Fe_2O_3 and Na_2O are significantly lower. Loss on ignition (LOI), MgO, and P_2O_5 increase towards mineralization, particularly in the northeastern portion of the study associated with the deposit, exhibiting anomalous values in all four lithofacies (Fig. 3.8).

3.4.4.3 Molar element ratios

Molar element ratios are useful for discriminating potential hydrothermal minerals using bulk rock geochemical data (Stanley and Madeisky, 1994), and their spatial variations relative to ore mineralization are useful for documenting alteration footprints. Alteration and diagenetic minerals in the Athabasca Basin (e.g., kaolin group, illite, sudoite, and hydrothermal tourmaline (alkali-deficient dravite)) can be spatially related to unconformity-type U deposits (Earle and Sopuck, 1989; Fayek and Kyser, 1997; Jefferson et al., 2007), and are best delineated using K/Al-Mg/Al molar ratios. The rocks throughout the study area contain varying molar element ratios that shift with proximity to mineralization (Fig. 3.9). Samples from the hanging wall (background sandstones) plot exclusively between the kaolin group node and illite node (K-I trend). In contrast, samples from all proximity zones on the P2 trend exhibit both the kaolinite-illite trend and the trend between the illite node and alkali-free dravite and chlorite (Al-Mg-sudoite) nodes (I-DS trend). The samples from the non-mineralized (P2) and subeconomic (P2 Main) drill holes

trend toward the alkali-deficient dravite node in the MFb, MFc, and MFd lithofacies, but demonstrate no association with the sudoite node. The samples from drill holes intersecting elevated U, including those at the McArthur River deposit (McA, McA+, McA++), exhibit both the K-I and I-DS trends, and the I-DS trendline is associated with both the alkali-deficient dravite and sudoite nodes. These samples also exhibit an additional trend, between the alkali-deficient dravite and sudoite nodes and the kaolin group node (DS-K trend), present only in the MFd lithofacies above the deposit and surrounding areas, and in the MFa lithofacies in drill holes with the highest concentrations of U (Fig. 3.9).

3.4.4.4 Trace elements

Several elements in the legacy data exhibit haloes directly related to high U concentrations. Bismuth, Co, Cu, Ni, Mo, Pb, Se, Te, and V (partial digestion) and Be, Bi, Co, Cu, Mo, Ni, Pb, V, and W (total digestion) are concentrated within the MFa lithofacies, forming lateral haloes above the unconformity that are generally restricted to the areas containing drill holes with samples having between 10–1000 ppm U (P2 Main and McA, McA+, McA++ zones) (Fig. 3.10). Smaller, localized areas of high concentrations of Mo and Pb are present in some upper lithofacies, coincident with anomalously high U, but these haloes are very small and isolated.

Barium and Sr (total digestion) are elevated in the MFc–MFa lithofacies within the northeast portion of the trend, forming an 8 km long footprint, in a mostly lateral halo with a hump up to 375 m above the unconformity that overlies the deposit and immediate surroundings (McA, McA+, McA++), but not above P2 Main (Fig. 3.11). Within this halo, Ba is present at the 99th percentile in all four lithofacies. Strontium has significantly higher

median values within the MFb in this area, and exhibits elevated to anomalous values (97th to 99th percentile) in the MFc and MFd.

Gallium and Cs (partial digestion) are present at the 92nd (Ga >0.5 ppm) and 95th (Cs >0.03 ppm) percentiles in the MFd–MFc, and exhibit a lateral halo ~350–560 m above mineralization in the northeastern 3–4 km of the study footprint (Fig. 3.11). Both are also localized in elevated to anomalous amounts above the mineralized zones in the MFa lithofacies. Cesium is only present in extremely low (<0.03 ppm) or non-detectible concentrations throughout the remainder of the study area.

Trace elements (both total and partial digestion results) in the MFd lithofacies were examined for any correlation to the I-DS and DS-K trends shown in the molar element ratio plots. Elements with a correlation are Cs, Ga, Sn, V, Y, and the rare earth elements (partial digestion), and Co, Cu, HREE, V, and Y (total digestion). All are elevated in the samples within the DS-K trend relative to those within the I-DS trend (Fig. 3.12). Uranium (partial and total digestions), along with Rb and Pb (total digestion), are elevated in the samples within the I-DS trend relative to those within the DS-K trend.

3.4.4.5 Lead isotope ratios

Lead isotope results are potentially useful indicators of mineralization, as two radiogenic isotopes, ^{206}Pb and ^{207}Pb, exist solely from the decay of U. These isotopes, along with the non-radiogenic ^{204}Pb, can be used to vector toward mineralization (Holk et al., 2003; Alexandre et al., 2012). Partial digestion results are preferred over total digestion as the weaker method will preferentially target hydrothermally delivered Pb over that originally present in country rock. For vectoring purposes, ratio thresholds were selected

to represent the degree of mineralization based on previous studies at unconformity-type U deposits (e.g., Cloutier et al., 2009; Quirt, 2009). Samples containing ^{207}Pb / ^{206}Pb <0.4 are associated with moderately to strongly radiogenic areas, and <0.2 to be indicative of mineralization. Samples containing ^{206}Pb / ^{204}Pb >30 are considered moderately to strongly radiogenic, and >50 to be indicative of mineralization.

Samples that contain both U levels above 1 ppm and Pb isotope ratios that are at least moderately radiogenic are assumed to be empirical evidence of primary mineralization events, and generally correlate with U content (i.e., *supported* by the U content in the sample). In contrast, samples with moderately radiogenic Pb isotope ratios in samples with <1 ppm U are associated with secondary dispersion, and are considered *unsupported* (Holk et al., 2003). The legacy data shows that unsupported samples do not display any strong vectoring trends, and that supported samples are most frequent in areas associated with mineralization (Fig. 3.13), mainly within the MFa lithofacies. The percentage of supported samples increases from 2% of background samples (HW and PRSW) to 32% of samples associated with the McArthur River mineralization (McA++) in all lithofacies. Although the number of supported samples increases with U content in the MFd, MFc, and MFb lithofacies, they are localized and do not form contiguous haloes. Only samples containing ^{206}Pb / ^{204}Pb ≥150 highlight the McArthur River mineralization at 900 m along and 270 m across strike, and up to 150 m above the unconformity. Although ^{207}Pb / ^{206}Pb <0.4 is found throughout the study area in MFa, only samples containing ratios ≤0.2 highlight the deposit, with a halo in the same location and dimensions as ^{206}Pb / ^{204}Pb ≥150.

3.5 DISCUSSION

The McArthur River U deposit is the highest-grade unconformity-type U deposit in the world (Bronkhorst et al., 2012), and has specific geochemical signatures that vary with stratigraphic height and lateral distance from mineralization along the P2 trend. Elevated concentrations of major and trace elements are present in distributions that range from strong spatial associations with U >10 ppm (Cu, Pb, Co, Mo, and others); to broader haloes several kilometres along strike that reflect both elevated U and the general location of the deposit (Ba, Sr, P_2O_5, LOI); to distal haloes 1000s of metres long, not associated with U content, but that are located directly above the deposit location (select Mg-K-Al molar element ratios, Ga, Cs). The combination of the above geochemical-mineralogical features demonstrate how various elements and mineral assemblages can be used to identify fertile environments and vector toward unconformity-type U mineralization.

3.5.1 Quartz cementation and its effect on trace element distribution (restricted haloes)

In unconformity-type U deposits, traditional pathfinder elements (Cu, Pb, As, Co, Mo, V, and others) reflect proximity to U mineralization, fluid-rock interaction, redox reactions associated with ore formation, and post-ore tectonic remobilization (Ruzicka, 1989; Holk et al., 2003; Wright, 2009; Ng et al., 2013). At McArthur River, there are spatial relationships of elevated Bi, Cu, Mo, Pb, V (partial and total digestion), Co, Cu, Se, Te (partial digestion), and uranogenic Pb isotope signatures with U proximal to the McArthur River and P2 Main deposits. These signatures are concentrated within the MFa, and are lacking in the middle to upper lithofacies (Fig. 3.10; 3.13). Due to their constricted nature,

these haloes are not useful as larger scale vectors, indicating only immediate proximity (10s of metres) to mineralization. Previous studies at McArthur River have documented intense pre-mineralization quartz cementation of the sandstone, as indicated by the preservation of diagenetic dickite in high concentrations (~70%), but only at the deposit site (McGill et al., 1993; Mwenifumbo et al., 2004; Bronkhorst et al., 2012; Ng et al., 2013). These authors interpreted that pre-mineralization quartz cementation suppressed hydrothermal fluid movement, resulting in restricted geochemical signatures for certain elements, generally to within 10s of metres of the unconformity. Our study supports this hypothesis, and SWIR results for dickite ≥70% suggest that the quartz cementation is not only centered over the McArthur River deposit, but also extends several hundred metres to its north and south along the P2 trend (Fig. 3.7).

3.5.2 Trace and major elements with correlations to both U and deposit location (broad haloes)

Barium, Sr, MgO, LOI, and P_2O_5 (total digestion) are elevated in all four lithofacies of the study area relative to background values, suggesting that the bulk of the P2 trend sandstones had greater hydrothermal alteration than background rocks, particularly those associated with the hanging wall. More importantly, Ba, Sr, P_2O_5, and LOI are useful vectors, as they are elevated in the MFb, MFc, and MFd lithofacies above the McArthur River deposit and surrounding areas (McA, McA+, McA++), but not above the subeconomic P2 Main (Fig. 3.11). Loss on ignition is a proxy for clay minerals; Sr and P_2O_5 for aluminum phosphate-sulfate (APS) phases; and MgO for sudoite/dravite, respectively (Earle and Sopuck, 1989; Gaboreau et al., 2007; Wright, 2009), and Ba has

likely modified fluids through interaction with basement rocks (Richard et al., 2010). Despite quartz cementation that occurred pre-mineralization (McGill et al., 1993; Derome et al., 2005), the presence of anomalous concentrations of Ba, Sr, LOI, P_2O_5, and MgO found in strata *above* the cementation reflect intense fluid-rock interaction along the P2 trend. The presence of these anomalies in the upper two lithofacies (Fig. 3.8; Fig. 3.11) suggest that post-cementation fracturing has breached the cementation and allowed substantial fluid movement in volumes sufficient for transport over several hundred metres, either as egress from the basement, or from the MFa sandstones (McGill et al., 1993; Bronkhorst et al., 2012). This group of elements, coupled with molar element ratios (see below) are critical pathfinders to the McArthur River deposit with a halo 4–8 km along strike within the MFb–MFd lithofacies.

The trace elements Ga (>0.5 ppm) and Cs (>0.03 ppm; partial digestion) exhibit large haloes (~4 km) around mineralization within the MFa and in the MFd; these are coincident with molar element ratios that record the transition between alkali-deficient dravite, sudoite, and kaolin group minerals (DS-K trend) (Figs 3.11–3.12). They are hypothesized to reflect clay-type mineral formation, as Ga substitutes for Al, and Cs for K in clay minerals (Oertel, 1961; Rytuba et al., 2003; Brockamp and Clauer, 2005). The presence of Ga and Cs anomalies in the MFd lithofacies above the McArthur River deposit and surrounding areas, but not above P2 Main, suggests that this area has been affected by greater degrees of fluid-rock interaction than elsewhere in the study area (Fig. 3.11); this is supported by the predominance of kaolinite and chlorite as determined by SWIR in the same general location (Fig. 3.7). If Cs is substituting for K, one may expect its distribution

to be similar to illite's. However, at McArthur River, Cs is unique in that its concentrations are minimal throughout most of the study area, mostly within instrumental noise. Therefore, anomalous levels of Cs in the MFd, coincident with elevated MgO, Ga, and the DS-K molar element ratio trend (Figs 3.9, 3.11), do not directly reflect the illite distribution but instead simply suggest that greater volumes of fluids have interacted with the illite present in the location directly above the deposit, increasing Cs concentrations to several times of what is present within the remainder of the footprint.

3.5.3 Clay alteration haloes and molar element ratios as a vectoring method (distal signature)

Clay alteration haloes have long been recognized as large-scale vectors for unconformity-type U deposits. Generally, dickite is associated with diagenetic background sandstones, whereas illite, chlorite and dravite are indicative of K- and Mg-related hydrothermal alteration (Hoeve and Quirt, 1984; Earle and Sopuck, 1989; Zhang et al., 2001). At McArthur River, various assemblages of these clay-type minerals as determined by SWIR can broadly identify regions associated with background or mineralization (Fig. 3.7); however, there are specific data arrays in molar K/Al-Mg/Al space that clearly define areas of the alteration footprint as background, subeconomic, and economic. Background samples (barren profile) plot exclusively between the dickite/kaolinite and illite nodes (K-I trend); this is representative of the transition between diagenetic and hydrothermal alteration (Fig. 3.9), and are within 1 km of the P2 trend to the southeast in the hanging wall. Samples in all other proximity zones exhibit the K-I trend in addition to a trend between the illite and alkali-deficient dravite node (I-DS trend). In the I-DS trend, Mg

increases and K decreases with respect to Al (Fig. 3.9), and is representative of the overprinting or replacement of illite by Mg-bearing minerals via fluids that have transported Mg from the basement into the sandstones (Richard et al., 2010). This demonstrates that the P2 trend, in its entirety, has experienced more advanced alteration than the background, hanging wall samples. The differentiation from least-altered and subeconomic to economic, in the areas of this study, is illustrated by the alkali-deficient dravite and sudoite nodes. The least-altered (P2) and subeconomic (P2 Main) samples in the MFd, MFc, and MFb lithofacies do not exhibit any association with sudoite, whereas the economic (McA, McA+, McA++) samples have an association with both Mg-species (Fig. 3.9). Although both dravite and chlorite can be associated with U mineralization (Earle and Sopuck, 1989; Kotzer and Kyser 1995; Mercadier et al., 2012), the samples at McArthur River suggest that the Mg present in sudoite is more closely associated with ore forming fluids relative to the Mg present in alkali-deficient dravite. This is supported by the SWIR results (Fig. 3.7), which show chlorite to be concentrated above the McArthur River deposit, but not dravite.

Most importantly, the DS-K molar element ratio trend differentiates the economic areas from all other zones, including subeconomic. This trend from sudoite and alkali-deficient dravite to dickite/kaolinite is demonstrated only by samples in the MFd within the northeastern 7 km of the study area (McA, McA+, and McA++ proximity zones), and in the MFa in drill holes that intersect the highest concentrations of U (McA++), which includes the McArthur River deposit (Fig. 3.9). The fact that this trend is not displayed in the MFb and MFc lithofacies may be due to the larger proportion of mud intraclasts in the

MFd or because they were less effective paleoaquifers. Because dickite and kaolinite both lack Mg and K, the molar element ratios used here cannot differentiate between the two; however, SWIR results confirm that the samples in the MFd lithofacies exhibiting the DS-K trend are dominantly kaolinite (Fig. 3.7). Previous studies in other areas of the basin have suggested that late, meteoric waters have circulated throughout the Athabasca Group sandstones (Kotzer and Kyser, 1995; Kyser and Cuney, 2008); this fluid-rock interaction could be responsible for altering the sudoite to produce kaolin-group minerals (e.g., Mercadier et al., 2011). However, within these (DS-K trend) samples, elements Cs, Ga, Sn, V, and Y (partial digestion), along with rare earth elements, and Co, Cu, V, and Y (total digestion) exhibit elevated concentrations (Fig. 3.12). These elements are associated with hydrothermal or redox processes, therefore suggesting that the fluids are related to mineralization. Uranium, Rb, and Pb are more elevated in the MFd in the I-DS trend samples (Fig. 3.12), suggesting that the responsible fluids are related to mineralization as well. Rubidium is likely related to samples in this trend that contain illite, as Rb substitutes readily into the illite structure for K (Brockamp and Clauer, 2005). The elevated presence of U and Pb, however, are likely a consequence of primary mineralization or remobilization, as both sudoite and alkali-deficient dravite are interpreted to be alteration products related to U mineralization processes (Earle and Sopuck, 1989; Kotzer and Kyser, 1995). Regardless of the fluid source, the DS-K trend and elevated trace elements associated with it are evidence that this area of the alteration footprint, which is spatially related to the McArthur River deposit, has undergone more intense fluid-rock interaction than other locations in the study.

Both the I-DS and DS-K trends in the MFd are present within the McA, McA+, and McA++ zones, meaning that individual samples from these proximity zones may fall into either trend category. This suggests that the DS-K trend is related spatially to the presence of increased U on a district scale — the northeastern 7 km of the study area — rather than the McArthur River deposit itself.

3.5.4 Implications for exploration

The McArthur River deposit is located within the expansive southern regional illite anomaly and is proximal to smaller dravite and chlorite anomalies, all of which are indicators that the area has undergone extensive hydrothermal alteration, and are therefore associated with unconformity-type U deposit fertility and are first-order vectors toward mineralization (Fig. 3.1b; Earle and Sopuck, 1989; Zhang et al., 2001). However, using clay-type minerals alone as vectors can be problematic, as all four endmembers as detected by SWIR can be found in varying concentrations throughout the alteration footprint. The use of molar element ratios instead illustrates the transitions between ideal endmember formulae that demonstrate the degree of alteration with respect to different lithofacies and distance from mineralization. The molar element ratios of Mg and K to Al show that on a district scale (~20 km) three distinct alteration trends are evident, acting as a process diagram to represent the transition from background to mineralized areas, and more importantly, the demarcation between economic and subeconomic areas (Fig. 3.9).

Quartz cementation at McArthur River has constrained traditional trace pathfinder elements to within 200 m of the unconformity (Fig. 3.10; Ng et al., 2013). Therefore, the distal expressions of alteration and mineralization are key to defining possible alternative

vectors. This study, which is of much larger dimensions than previous studies, in both number of drill holes and total area, demonstrates that the overlap between Mg-dominant molar element ratio trends and basement-sourced trace element haloes present above quartz cementation is uniquely localized. This localized combination of geochemical signatures includes the molar element ratio trend related to the transition between sudoite, alkali-deficient dravite, and kaolinite (DS-K trend in the MFd and MFa lithofacies); elevated Ga, Cs (MFd–c) and Ba, Sr, and P_2O_5 (MFc–b); and the largest concentrations of U at depth. This comprises the northeast 7 km of the study area, including the <2 km strike of the McArthur River deposit (Fig. 3.14). These distal haloes are significant because they indicate that the area has experienced large volumes of fluid-rock interaction required for high grade mineralization at depth, which have occurred hundreds of metres vertically from the unconformity, resulting in a geochemical signature significantly different than in other areas of the footprint.

This study has highlighted two important vectoring attributes related to the McArthur River deposit: the fact that the alteration halo is highly asymmetrical across strike of the P2 trend, and that a large area (~20 km) was necessary to fully characterize the district-scale differences between background sandstones and minimal, subeconomic, and economic mineralization. For example, background (non-mineralized) holes located above the hanging wall southeast of the P2 trend are less than 1 km from fault system and/or mineralization, yet exhibit a barren profile, illustrating the highly asymmetric nature of the halo. This supports the interpretations from earlier studies that the P2 reverse fault system was the dominant structural control on fluid flow (McGill et al., 1993; Bronkhorst

et al., 2012; Adlakha et al., 2014), and that its dip and strike were key to channeling the fluids associated with mineralization toward the northwest and the hanging wall wedge, away from the hanging wall. The large study area was essential to clearly define the molar element ratio trends, which also may not be obvious without dozens of individual samples in each proximity zone. In addition, the elevated trace element haloes extend several kilometres from the economic grade deposit; therefore, it was necessary to include the most distal samples available from the archival database. By doing so we are able to both define the edges of the alteration footprint and document its variation, from minimal to intense, with proximity to mineralization.

3.6 CONCLUSIONS

Large-scale lithogeochemical studies of sandstones in the McArthur River U deposit area illustrate that there are scalable geochemical signatures and mineralogical assemblages throughout the Manitou Falls Formation that provide spatial vectors towards mineralization from several kilometres distant, despite intense quartz cementation having restricted more traditional pathfinder elements associated with mineralization to within 200 m of the unconformity. Post-cementation fracturing, coupled with intense fluid-rock interaction, resulted in large haloes of Ba, Sr, P_2O_5, and LOI values present in the MFb–MFd lithofacies above the McArthur River deposit, but not the P2 Main. This suggests that the fluid-rock interaction was greatest in the sandstones nearest the economic grade mineralization. Anomalous concentrations of Ga and Cs formed horizontal haloes that are unrelated to U content in the MFc-MFd lithofacies above and to the north of the McArthur River deposit. In this case, the observed enrichment is likely a result of alteration through

greater fluid volumes than elsewhere in the footprint, controlled by the lithostratigraphic variations within the Manitou Falls Formation.

Molar element ratios are a useful way to delineate proximity to mineralization by illustrating the transitions between clay-type minerals. Background samples plot between dickite/kaolinite and illite in K/Al-Mg/Al space. Alteration related to Mg-enriched fluids and the potential for mineralization is shown in samples that transition between illite, alkali-deficient dravite, and sudoite. Least-altered and subeconomic samples above the MFa are associated solely with alkali-deficient dravite, whereas the samples with the highest U concentrations are associated with both alkali-deficient dravite and sudoite. An additional trend, between the Mg-rich species and kaolin (K/Al <0.06, Mg/Al <0.4), is only seen in the uppermost lithofacies above the McArthur River deposit, accompanied by elevated Ga and Cs.

REFERENCES

Adlakha, E. E., Hattori, K., Zaluksi, G., Kotzer, T., and Potter, E. G., (2014). Alteration within the basement rocks associated with the P2 fault and the McArthur River uranium deposit, Athabasca Basin; Geological Survey of Canada Open File Report 7462, 35 p.

Adlakha, E. E., Hattori, K., Zaluski, G., Kotzer, T. G., Davis, W. J., & Potter, E. G. (2015). Mineralogy of a fertile fluid conduit related to unconformity-type uranium deposits in the Athabasca Basin, Saskatchewan. *In* Potter, E.G. & Wright, D. M. (eds.), *Targeted Geoscience Initiative 4: unconformity-related uranium systems*;

Geological Survey of Canada, Open File 7791, 126 p. (pp. 74–82). http://doi.org/10.4095/295776

Alexandre, P., & Kyser, K. (2005). Effect of cation substitutions and alteration of uraninite. *Canadian Mineralogist*, *45*, 1005–1017. http://doi.org/10.2113/gscanmin.43.3.1005

Alexandre, P., Kyser, K., & Jiricka, D. (2009a). Critical geochemical and mineralogical factors for the formation of unconformity-related uranium deposits: comparison between barren and mineralized systems in the Athabasca Basin, Canada. *Economic Geology*, *104*(3), 413–435. http://doi.org/10.2113/gsecongeo.104.3.413

Alexandre, P., Kyser, K., Thomas, D., Polito, P., & Marlat, J. (2009b). Geochronology of unconformity-related uranium deposits in the Athabasca Basin, Saskatchewan, Canada and their integration in the evolution of the basin. *Mineralium Deposita*, *44*(1), 41–59. http://doi.org/10.1007/s00126-007-0153-3

Alexandre, P., Kyser, K., Jiricka, D., & Witt, G. (2012). Formation and evolution of the Centennial unconformity-related uranium deposit in the South-Central Athabasca Basin, Canada. *Economic Geology*, *107*(3), 385-400. http://doi.org/10.2113/econgeo.107.3.385

Alexandre, P., Kyser, K., Polito, P., & Thomas, D. (2005). Alteration mineralogy and stable isotope geochemistry of Paleoproterozoic basement-hosted unconformity-type uranium deposits in the Athabasca Basin, Canada. *Economic Geology*, *100*(8), 1547-1563. http://doi.org/10.2113/gsecongeo.100.8.1547

Annesley, I. R., Madore, C., & Portella, P. (2005). Geology and thermotectonic evolution of the western margin of the Trans-Hudson Orogen: evidence from the eastern sub-Athabasca basement, Saskatchewan. *Canadian Journal of Earth Sciences*, *42*(4), 573-597. http://doi.org/10.1139/e05-034

Ansdell, K. M. (2005). Tectonic evolution of the Manitoba-Saskatchewan segment of the Paleoproterozoic Trans-Hudson Orogen, Canada. *Canadian Journal of Earth Sciences*, *42*(4), 741-759. http://doi.org/10.1139/e05-035

Armstrong, R. L., & Ramaekers, P. (1985). Sr isotopic study of Helikian sediment and diabase dikes in the Athabasca Basin, northern Saskatchewan. *Canadian Journal of Earth Sciences*, *22*(3), 399-407.

Brockamp, O., & Clauer, N. (2005). A km-scale illite alteration zone in sedimentary wall rocks adjacent to a hydrothermal fluorite vein deposit. *Clay Minerals, 40*(2), 245-260. http://doi.org/10.1180/0009855054020170

Bronkhorst, D., Edwards, C. R., Mainville, A. G., Murdock, G. M., & Yesnik, L. D. (2012). McArthur River operation, northern Saskatchewan, Canada. *National Instrument 43-101 Technical Report*: Cameco Corporation, 206 p.

Cameco Corporation (2015). *Reserves & Resources - McArthur/Key Lake - Canada - Uranium Operations - Businesses - Cameco*. *Cameco.com*. Retrieved 19 September 2016, from https://www.cameco.com/businesses/uranium-operations/canada/mcarthur-river-key-lake/reserves-and-resources.

Card, C. D., Pană, D., Portella, P., Thomas, D. J., & Annesley, I. R. (2007). Basement rocks to the Athabasca basin, Saskatchewan and Alberta. *In* Jefferson C. W. & Delaney, G. (eds.), *EXTECH IV: Geology and Uranium EXploration TECHnology of the Proterozoic Athabasca Basin, Saskatchewan and Alberta*: Geological Survey of Canada, Bulletin 588, 69–87.

Chi, G., Bosman, S., & Card, C. (2013). Numerical modeling of fluid pressure regime in the Athabasca basin and implications for fluid flow models related to the unconformity-type uranium mineralization. *Journal of Geochemical Exploration*, *125*, 8–19. http://doi.org/10.1016/j.gexplo.2012.10.017

Cloutier, J., Kyser, K., Olivo, G. R., & Alexandre, P. (2010). Contrasting patterns of alteration at the Wheeler River area, Athabasca basin, Saskatchewan, Canada: insights into the apparently uranium-barren zone K alteration system. *Economic Geology*, *105*(2), 303–324. http://doi.org/10.2113/gsecongeo.105.2.303

Cloutier, J., Kyser, K., Olivo, G. R., Alexandre, P., & Halaburda, J. (2009). The Millennium uranium deposit, Athabasca Basin, Saskatchewan, Canada: an atypical basement-hosted unconformity-related uranium deposit. *Economic Geology*, *104*(6), 815–840. http://doi.org/10.2113/gsecongeo.104.6.815

Creaser, R. A., & Stasiuk, L. D. (2007). Depositional age of the Douglas Formation, northern Saskatchewan, determined by Re-Os geochronology. *In* Jefferson C. W. & Delaney, G. (eds.), *EXTECH IV: Geology and Uranium EXploration TECHnology of the Proterozoic Athabasca Basin, Saskatchewan and Alberta*: Geological Survey of Canada, Bulletin 588, 341–345.

Cui, T., Yang, J., & Samson, I. M. (2012). Tectonic deformation and fluid flow: implications for the formation of unconformity-related uranium deposits. *Economic Geology*, *107*(1), 147–163. http://doi.org/10.2113/econgeo.107.1.147

Cumming, G. L., & Krstic, D. (1992). The age of unconformity-related uranium mineralization in the Athabasca Basin, northern Saskatchewan. *Canadian Journal of Earth Sciences*, *29*(8), 1623–1639. http://doi.org/10.1139/e92-128

Cuney, M. (2012). Uranium and Thorium: The Extreme Diversity of the Resources of the World's Energy Minerals. *In* Sinding-Larsen, R. & Wellmer, F. W. (eds.), *Non-Renewable Resource Issues: Geoscientific and Societal Challenges* (pp. 91–129). http://doi.org/10.1007/978-90-481-8679-2_6

Derome, D., Cathelineau, M., Cuney, M., Fabre, C., Lhomme, T., & Banks, D. A. (2005). Mixing of sodic and calcic brines and uranium deposition at McArthur River, Saskatchewan, Canada: a Raman and laser-induced breakdown spectroscopic study

of fluid inclusions. *Economic Geology*, *100*(8), 1529–1545. http://doi.org/10.2113/gsecongeo.100.8.1529

Earle, S. A. M., & Sopuck, V. J. (1989). Regional lithogeochemistry of the eastern part of the Athabasca Basin uranium province, Saskatchewan, Canada. *In* Muller-Kahle, E., (ed.), *Uranium resources and geology of North America: International Atomic Energy Agency,* TECDOC-500, 263–296.

Fayek, M. & Kyser, T. (1997). Characterization of multiple fluid-flow events and rare-earth-element mobility associated with formation of unconformity-type uranium deposits in the Athabasca Basin, Saskatchewan. *The Canadian Mineralogist, 35,* 627–658.

Fayek, M., Kyser, T. K., & Riciputi, L. R. (2002). U and Pb isotope analysis of uranium minerals by ion microprobe and the geochronology of the McArthur River and Sue Zone uranium deposits, Saskatchewan, Canada. *The Canadian Mineralogist*, *40*(6), 1553–1570.

Gaboreau, S., Cuney, M., Quirt, D., Beaufort, D., Patrier, P., & Mathieu, R. (2007). Significance of aluminum phosphate-sulfate minerals associated with U unconformity-type deposits: The Athabasca basin, Canada. *American Mineralogist*, *92*(2-3), 267–280. http://doi.org/10.2138/am.2007.2277

Hecht, L., & Cuney, M. (2000). Hydrothermal alteration of monazite in the Precambrian crystalline basement of the Athabasca Basin (Saskatchewan, Canada): implications for the formation of unconformity-related uranium deposits. *Mineralium Deposita*, *35*(8), 791–795. http://doi.org/10.1007/s001260050280

Hiatt, E. E., & Kyser, T. K. (2007). Sequence stratigraphy, hydrostratigraphy, and mineralizing fluid flow in the Proterozoic Manitou Falls Formation, eastern Athabasca Basin, Saskatchewan. *In* Jefferson C. W. & Delaney, G. (eds.), *EXTECH IV: Geology and Uranium EXploration TECHnology of the Proterozoic Athabasca Basin, Saskatchewan and Alberta*: Geological Survey of Canada, Bulletin 588, 489–506.

Hoeve, J., & Quirt, D. H. (1984). Mineralization and host rock alteration in relation to clay mineral diagenesis and evolution of the Middle-Proterozoic, Athabasca Basin, northern Saskatchewan, Canada. Saskatchewan Research Council, SRC Technical Report 187, 202 p.

Hoeve, J., & Sibbald, T. I. (1978). On the genesis of Rabbit Lake and other unconformity-type uranium deposits in northern Saskatchewan, Canada. *Economic Geology*, *73*, 1450–1473.

Hoffman, P. F. (1988). United Plates of America, the birth of a craton: Early Proterozoic assembly and growth of Laurentia. *Annual Review of Earth and Planetary Sciences*, *16*, 543–603.

Holk, G. J., Kyser, T. K., Chipley, D., Hiatt, E. E., & Marlatt, J. (2003). Mobile Pb-

isotopes in Proterozoic sedimentary basins as guides for exploration of uranium deposits. *Journal of Geochemical Exploration*, *80*(2), 297–320. http://doi.org/10.1016/S0375-6742(03)00196-1

Javoy, M. (1999). Chemical earth models. *Comptes Rendus de l'Académie des Sciences-Series IIA-Earth and Planetary Science*, *329*(8), 537–555.

Jeanneret, P., Goncalves, P., Durand, C., Trap, P., Marquer, D., Quirt, D., & Ledru, P. (2016). Tectono-metamorphic evolution of the pre-Athabasca basement within the Wollaston–Mudjatik Transition Zone, Saskatchewan. *Canadian Journal of Earth Sciences*, *53*(3), 231–259. http://doi.org/10.1139/cjes-2015-0136

Jefferson, C. W., Thomas, T. J., Gandhi, S. S., Ramaekers, P., Delaney, G., Brisbin, D., Cutts, C., Portella, P., & Olson, R.A. (2007). Unconformity-associated uranium deposits of the Athabasca Basin, Saskatchewan and Alberta. *In* Jefferson C. W. & Delaney, G. (eds.), *EXTECH IV: Geology and Uranium EXploration TECHnology of the Proterozoic Athabasca Basin, Saskatchewan and Alberta*: Geological Survey of Canada, Bulletin 588, 23–67.

Jenner, G. A. (1996). Trace element geochemistry of igneous rocks: geochemical nomenclature and analytical geochemistry. *In* Wyman, D. A. (ed.), *Trace element geochemistry of volcanic rocks: applications for massive sulphide exploration.* Geological Association of Canada. Short Course Notes, 12, 51–77.

Kotzer, T. G., & Kyser, T. K. (1995). Petrogenesis of the Proterozoic Athabasca Basin, northern Saskatchewan, Canada, and its relation to diagenesis, hydrothermal uranium mineralization and paleohydrogeology. *Chemical Geology*, *120*(1), 45–89. http://doi.org/10.1016/0009-2541(94)00114-N

Kotzer, T. G; Kyser, T. K.; Irving, E. (1992) Paleomagnetism and the evolution of fluids in the Proterozoic Athabasca Basin, northern Saskatchewan, Canada. *Canadian Journal of Earth Sciences* 29(7), 1474–1491. http://doi.org/10.1139/e92-118

Kyser, K. (2014). Uranium Ore Deposits, *In* Turekian, H. D., Holland, H. D., (eds.), Treatise on Geochemistry (2nd ed.): Oxford, Elsevier, v. 7, p. 489–513. http://doi.org/10.1016/B978-0-08-095975-7.01122-0

Kyser, K., & Cuney, M. (2008). Unconformity-related uranium deposits. *In* Cuney, M. & Kyser, K., (eds.), *Recent and not-so-recent developments in uranium deposits and implications for exploration*. Quebec: Mineralogical Association of Canada Short Course Series Vol. 39, 161–219. ISBN 978-0-921294-48-1

Kyser, K., Hiatt, E., Renac, C., Durocher, K., Holk, G., & Deckart, K. (2000). Diagenetic fluids in Paleo-and Meso-Proterozoic sedimentary basins and their implications for long protracted fluid histories. *In* Kyser, K. (ed.), *Fluids and basin evolution.* Mineralogical Association of Canada Short Course Series 28, 225–262. http://doi.org/10.13140/2.1.1033.1847

Lewry, J. F., & Sibbald, T. I. I. (1980). Thermotectonic evolution of the Churchill Province in northern Saskatchewan. *Tectonophysics*, *68*, 45–82.

Macdonald, C. (1985). Mineralogy and geochemistry of the sub-Athabasca regolith near Wollaston Lake. *In* Sibbald, T. I. I. & Petruk, W. (eds.), *Geology of Uranium Deposits: Canadian Institute of Mining and Metallurgy Special Vol. 32*, 155–158.

Matschullat, J., Ottenstein, R., & Reimann, C. (2000). Geochemical background–can we calculate it? *Environmental Geology*, *39*(9), 990–1000. doi:10.1007/s002549900084

McGill, B. D., Marlatt, J. L., Matthews, R. B., Sopuck, V. J., Homeniuk, L. A., & Hubregtse, J. J. (1993). The P2 north uranium deposit, Saskatchewan, Canada. *Exploration and Mining Geology*, *2*(4), 321–331.

Mercadier, J., Richard, A., & Cathelineau, M. (2012). Boron-and magnesium-rich marine brines at the origin of giant unconformity-related uranium deposits: δ11B evidence from Mg-tourmalines. *Geology*, *40*(3), 231–234. http://doi.org/10.1130/G32509.1

Mercadier, J., Cuney, M., Cathelineau, M., & Lacorde, M. (2011). U redox fronts and kaolinisation in basement-hosted unconformity-related U ores of the Athabasca Basin (Canada): late U remobilisation by meteoric fluids. *Mineralium Deposita*, *46*(2), 105–135. http://doi.org/10.1007/s00126-010-0314-7

Mercadier, J., Annesley, I. R., McKechnie, C. L., Bogdan, T. S., & Creighton, S. (2013). Magmatic and Metamorphic Uraninite Mineralization in the Western Margin of the Trans-Hudson Orogen (Saskatchewan, Canada): A Uranium Source for Unconformity-Related Uranium Deposits? *Economic Geology*, *108*(5), 1037–1065. http://doi.org/10.2113/econgeo.108.5.1037

Mwenifumbo, C. J. & Bernius, G. R.. (2007). Crandallite-group minerals: host of thorium enrichment in the eastern Athabasca Basin, Saskatchewan. *In* Jefferson C. W. & Delaney, G. (eds.), *EXTECH IV: Geology and Uranium EXploration TECHnology of the Proterozoic Athabasca Basin, Saskatchewan and Alberta*: Geological Survey of Canada, Bulletin 588, 521–532.

Mwenifumbo, C. J., Elliott, B. E., Jefferson, C. W., Bernius, G. R., & Pflug, K. A. (2004). Physical rock properties from the Athabasca Group: designing geophysical exploration models for unconformity uranium deposits. *Journal of Applied Geophysics*, *55*(1), 117–135. http://doi.org/10.1016/j.jappgeo.2003.06.008

Nash, J. T., Granger, H. C., & Adams, S. S. (1981). Geology and concepts of genesis of important types of uranium deposits. *Economic Geology*, *75th Anniv.*, 63–116.

Ng, R., Alexandre, P., & Kyser, K. (2013). Mineralogical and geochemical evolution of the unconformity-related McArthur River Zone 4 orebody in the Athabasca Basin, Canada: implications of a silicified zone. *Economic Geology*, *108*(7), 1657–1689. http://doi.org/10.2113/econgeo.108.7.1657

Oertel, A. C. (1961). Pedogenesis of some red-brown earths based on trace-element profiles. *Journal of Soil Science*, *12*(2), 242–258.

Pagel, M., Poty, B., & Sheppard, S. M. F. (1980). Contribution to some Saskatchewan uranium deposits mainly from fluid inclusions and isotopic data. *In* Ferguson, S. & Goleby, A. (eds.), *Uranium in the Pine Creek Geosyncline: Vienna, International Atomic Energy Agency*, p. 639–654.

Pettijohn, F. J., Potter, P. E., & Siever, R. (1972). Sand and Sandstone, Berlin-Heidelberg-New York: Springer. 618 pp.

Quirt, D. H. (1985). Lithogeochemistry of the Athabasca Group: Summary of sandstone data. *In* Summary of Investigations 1985, Saskatchewan Geological Survey, Saskatchewan Energy and Mines, Miscellaneous Report 85-4, p. 128–132.

Quirt, D. (2000). Sub-Athabasca Group fanglomerate in the McArthur River-Read Lake area, Saskatchewan: GeoCanada 2000: The Millennium Geoscience Summit [abs.]: Geological Association of Canada, Mineralogical Association of Canada (GAC-MAC), joint annual meeting, Calgary, Abstract 251.

Quirt, D. (2009). Applying Pb isotopes in unconformity-type uranium exploration. *In* Lentz, D. R., Thorne, K. G., & Beal, K-L. (eds.), *Proceedings of the 24th IAGS, Fredericton, Canada*, 453–456. ISBN 978-1-55131-136-4

Rainbird, R. H., Stern, R. A., Rayner, N., & Jefferson, C. W. (2007). Age, provenance, and regional correlation of the Athabasca Group, Saskatchewan and Alberta, constrained by igneous and detrital zircon geochronology. *In* Jefferson C. W. & Delaney, G. (eds.), *EXTECH IV: Geology and Uranium EXploration TECHnology of the Proterozoic Athabasca Basin, Saskatchewan and Alberta*: Geological Survey of Canada, Bulletin 588, 193–209.

Ramaekers, P., & Catuneanu, O. (2004). Development and sequences of the Athabasca Basin, early Proterozoic, Saskatchewan and Alberta, Canada. *In* Eriksson P. G., Alterman, W., Nelson, D. R., Mueller, W. U., & Catuneanu, O. (eds.), *The Precambrian Earth: Tempos and Events* (Vol. 12, pp. 705–723). Amsterdam: Elsevier.

Ramaekers, P., Jefferson, C. W., Yeo, G. M., Collier, B., Long, D. G. F., Drever, G., McHardy, S., Jiricka, D., Cutts, C., Wheatley, K., Catuneanu, O., Bernier, S., Kupsch, B., & Post, R. T. (2007). Revised geological map and stratigraphy of the Athabasca Group, Saskatchewan and Alberta. *In* Jefferson C. W. & Delaney, G. (eds.), *EXTECH IV: Geology and Uranium EXploration TECHnology of the Proterozoic Athabasca Basin, Saskatchewan and Alberta*: Geological Survey of Canada, Bulletin 588, 155–187.

Richard, A., Pettke, T., Cathelineau, M., Boiron, M. C., Mercadier, J., Cuney, M., & Derome, D. (2010). Brine–rock interaction in the Athabasca basement (McArthur River U deposit, Canada): consequences for fluid chemistry and uranium uptake.

Terra Nova, *22*(4), 303-308. http://doi.org/10.1111/j.1365-3121.2010.00947.x

Ruzicka, V. (1989). Monometallic and polymetallic deposits associated with the sub-Athabasca unconformity in Saskatchewan. *In Current Research, Part C,* Geological Survey of Canada: Paper 89-1C, 67–79.

Ruzicka, V. (1996). Unconformity-associated uranium. *In* Eckstrand, O. R., Sinclair, W. D., & Thorpe, R. I., (eds.), *Geology of Canadian Mineral Deposit Types.* Geological Survey of Canada, Geology of Canada, No. 8, 197-210.

Rytuba, J. J., Bliss, J. D., Moyle, P. R., & Long, K. R. (2003). Hydrothermal Enrichment of Gallium in Zones of Advanced Argillic Alteration, Examples from the Paradise Peak and McDermitt Ore Deposits, Nevada. *In* Bliss, J., Moyle, R., & Long, K. (eds.), US Department of the Interior, US Geological Survey, Bulletin 2209-C. 20 p.

Sopuck, V. J., De Carle, A., Wray, E. M., & Cooper, B. (1983). Application of lithogeochemistry to the search for unconformity-type uranium deposits in the Athabasca Basin. *In* Cameron, E. M. (ed.), *Uranium Exploration in Athabasca Basin, Saskatchewan, Canada,* Geological Survey of Canada: Paper 82-11, 191–205.

Stanley, C. R., & Madeisky, H. E. (1994). Lithogeochemical exploration for hydrothermal ore deposits using Pearce element ratio analysis. *In* Lentz, D. R. (ed.), *Alteration and Alteration Processes Associated with Ore-forming systems,* Geological Association of Canada, Short Course Notes, (11), 193-211.

Tremblay, L. (1982). Geology of the uranium deposits related to the sub-Athabasca unconformity, Saskatchewan, Canada. Geological Survey of Canada: Paper 81-20, 56 p.

Wright, D. (2009). Vectoring potential of multi-element chemistry in unconformity-associated uranium deposits: major and trace element signatures of the McArthur River Uranium Deposit, Saskatchewan, Canada. *In* Lentz, D. R., Thorne, K. G., & Beal, K-L. (eds.), *Proceedings of the 24th IAGS, Fredericton, Canada*, 493–496. ISBN 978-1-55131-136-4

Zhang, G., Wasyliuk, K., & Pan, Y. (2001). The characterization and quantitative analysis of clay minerals in the Athabasca Basin, Saskatchewan: Application of shortwave infrared reflectance spectroscopy. *The Canadian Mineralogist*, *39*(5), 1347-1363. http://doi.org/10.2113/gscanmin.39.5.1347

FIGURES

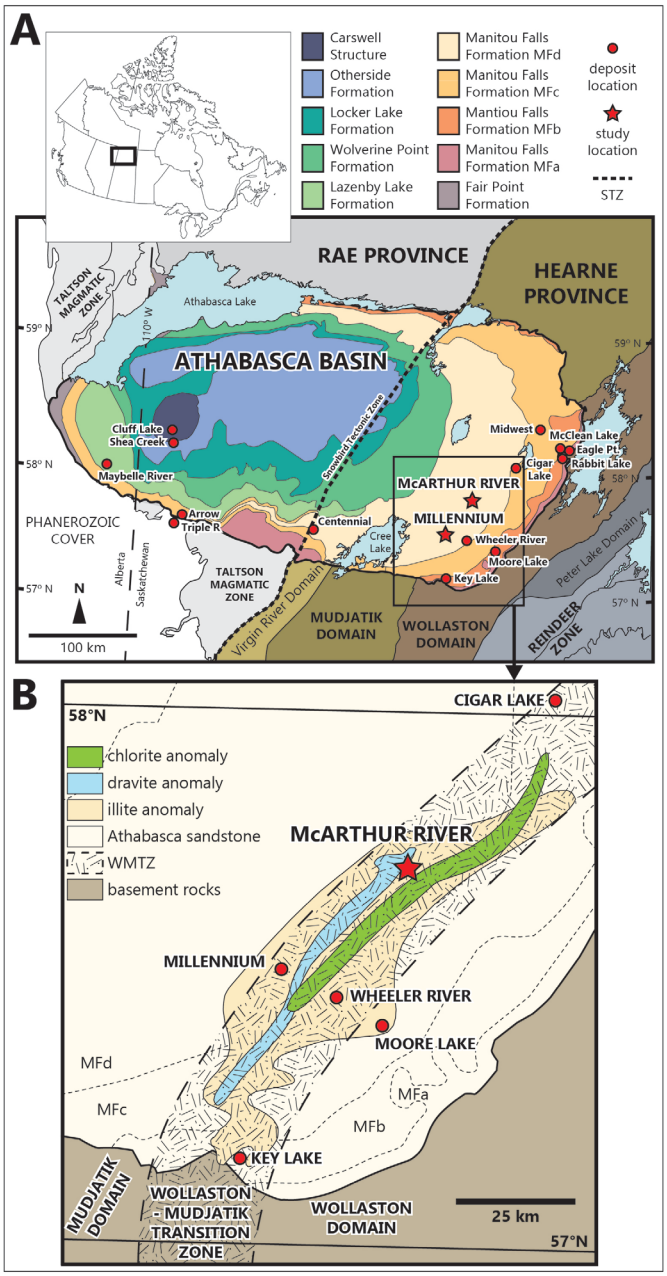

Figure 3.1: (**A**) Simplified geological map of the Athabasca Basin in northern Saskatchewan and Alberta, and underlying Precambrian domains. STZ: Snowbird Tectonic Zone, responsible for the collision of the Rae and Hearne provinces. The later Trans-Hudson was responsible for the final assemlage of the basement rocks below the basin, with the accretion of the Reindeer Zone to the eastern Hearne. Adapted from Card et al. (2007), and Cloutier et al. (2009). (**B**) Southeastern Athabasca Basin illustrating the geological relationships of the Wollaston-Mudjatik Transition Zone (WMTZ) and regional alteration zones to the location of selected uranium deposits. Adapted from Earle and Sopuck (1989), Jefferson et al. (2007), and Jeanneret et al. (2016).

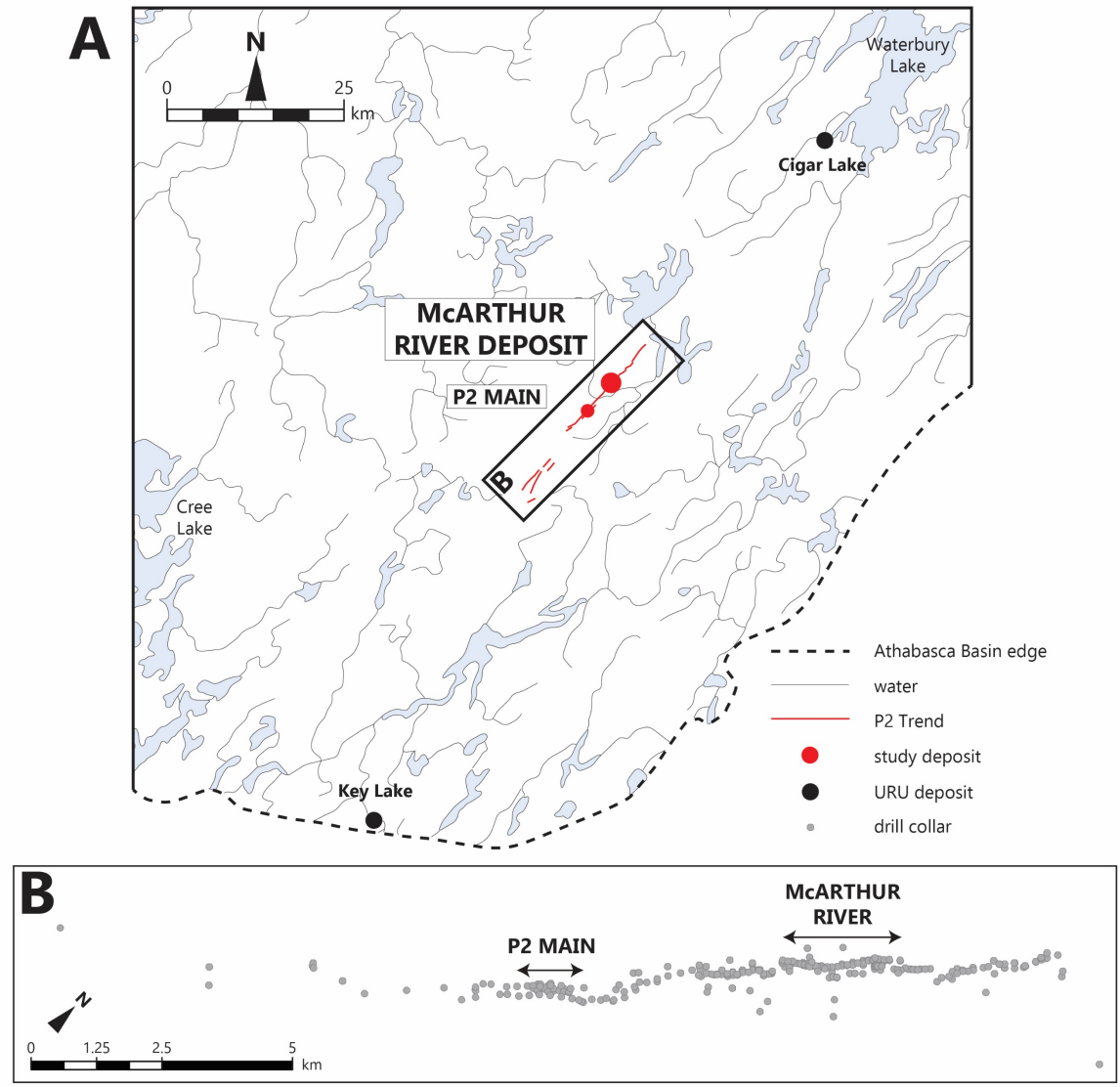

Figure 3.2: Study area in the southeastern Athabasca Basin. (**A**) The McArthur River deposit is economic grade; the P2 Main is currently considered subeconomic. Both are associated with the P2 conductive trend. Whole rock geochemistry herein is derived from this study area (**B**), approximately 20 km in length. Adapted from Cameco internal documents. (**B**) Sample drill holes included in study associated with the P2 conductive trend. Drill hole collar locations mapped from Cameco internal documents.

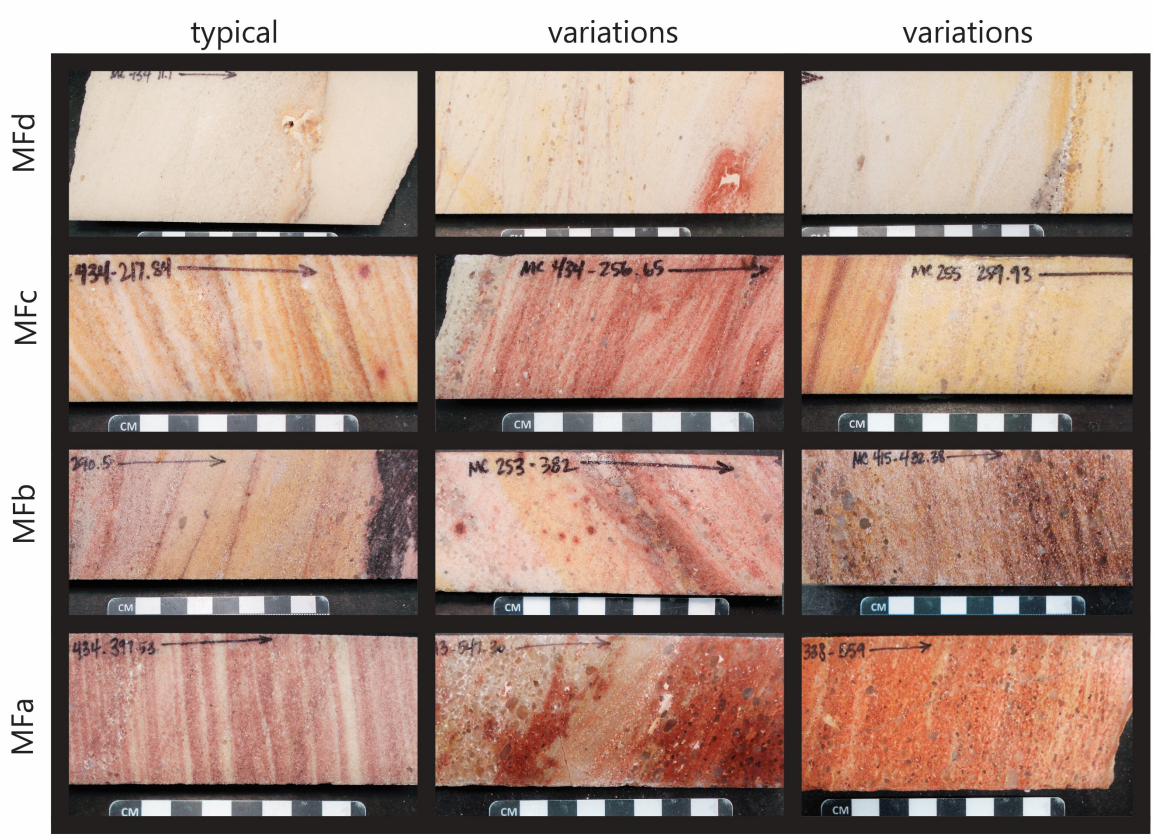

Figure 3.3: Typical Manitou Falls Formation sandstones; arrows indicate down direction. Photographs are from samples collected. Samples in left column are from MC-434, a background drill hole, and represent grain size and alteration features as described in section 3.3.2 that are typical of each lithofacies. Samples in center and right columns are from the Gap Zone, SW Zone, Zone C, and Zone 4 and are selected to show varying grain sizes and alteration features common to each lithofacies: very fine-grain to coarse-grain sizes, cross-bedding, clay clasts, pebble beds and lags, hematite and limonite alteration. Samples from areas proximal to mineralization are not visually distinct from those in non-mineralized locations.

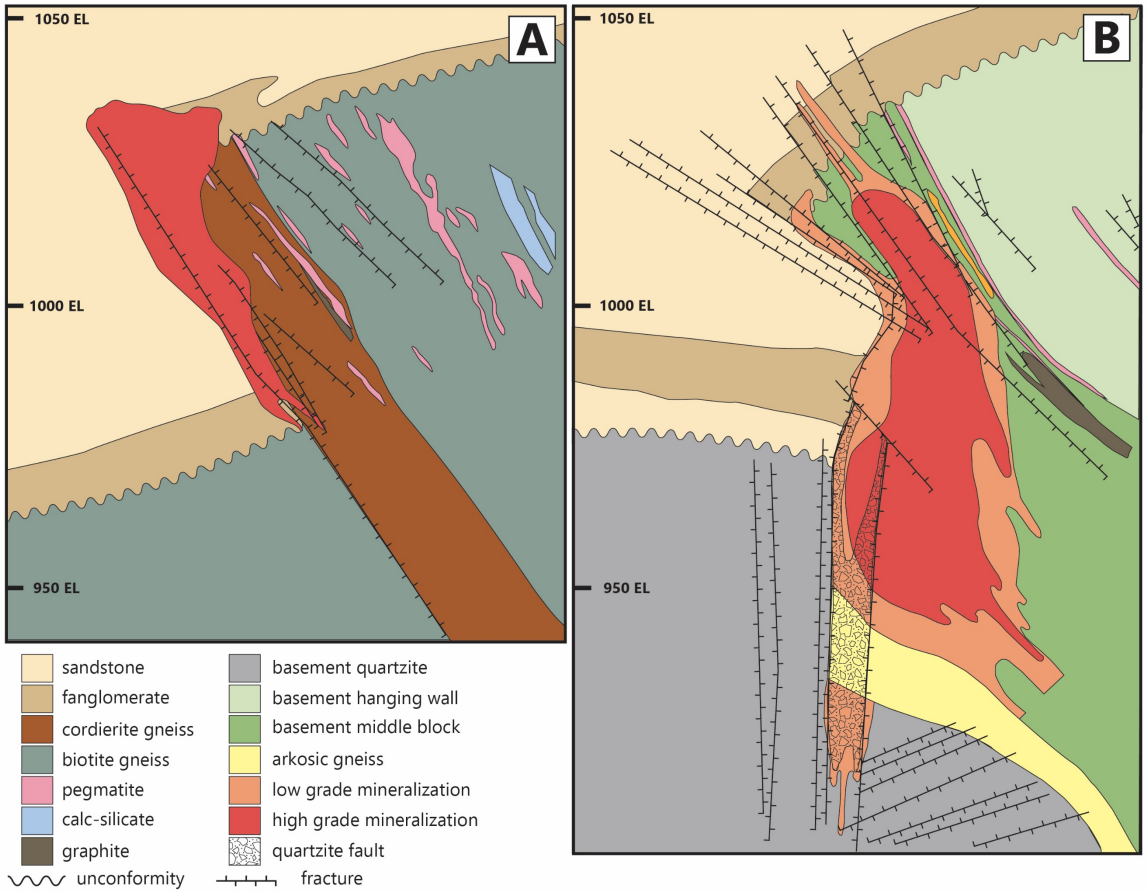

Figure 3.4: Generalized cross section of the McArthur River unconformity-type U deposit, looking northeast. The P2 fault, a graphitic reverse fault, has offset the unconformity and is considered the dominant structural control for the deposit. Composite illustration adapted from Bronkhorst et al. (2012). "High grade" and "low grade", in the scope of this illustration, is suggested by semi-quantitative radiometric counts in drillholes; "high" being suggestive of 20% or more U_3O_8, and "low" being greater than ~2% (Zaluski, pers. comm. 2017). (**A**) Typical cross section for all zones of the McArthur River deposit, with the exception of Zone 2. Mineralization is concentrated where the P2 wedge meets the unconformity. (**B**) Typical cross section for Zone 2. Mineralization here is concentrated both in the P2 wedge and also in the middle basement block displaced by the P2 and quartzite faults.

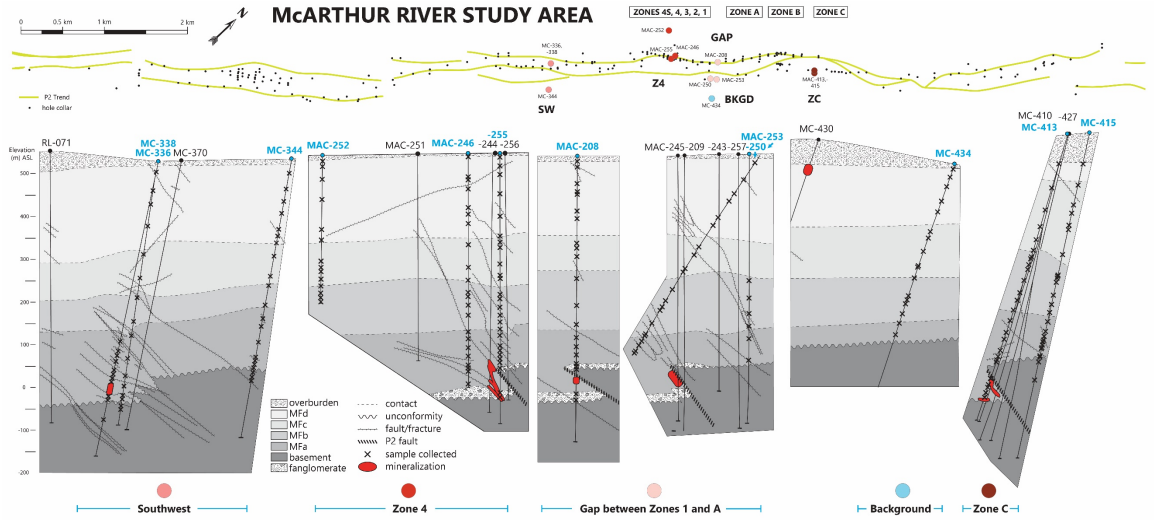

Figure 3.5: Location of fences and samples collected for new data. The approximate E-W location of ore bodies of the McArthur River deposit are noted by their names. Coloured dots in plan view of drill collar map correlate to the cross section fences shown below. Samples were selected from all lithofacies and were composite (representative) of the surrounding sandstones. Map of P2 trend with drill hole locations and cross sections are adapted from Cameco Corporation internal documents.

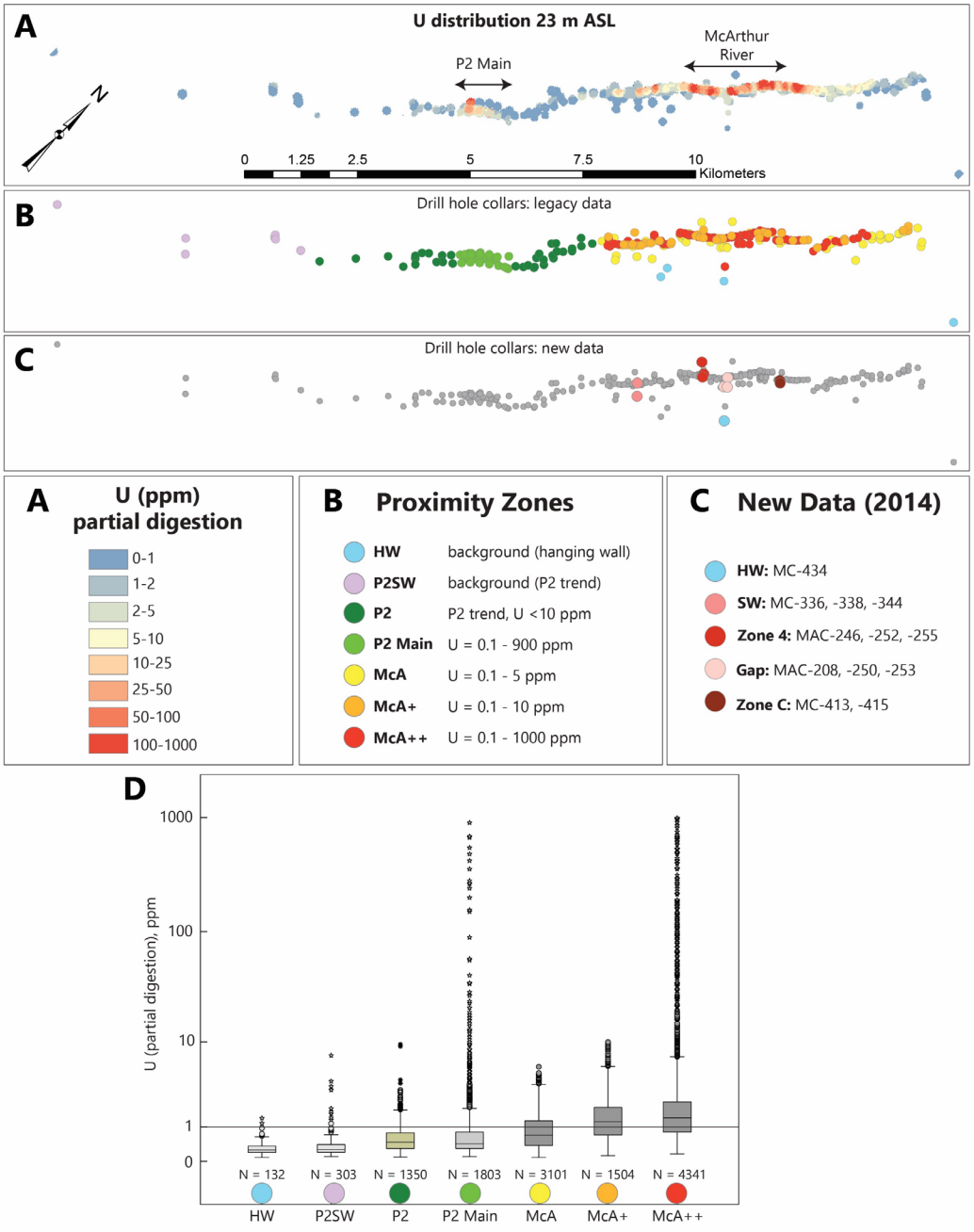

Figure 3.6: Study area surrounding the McArthur River deposit. The proximity zones were determined via both U content (partial digestion) and proximity to mineralization. (**A**) Drill collars in the study area illustrating U content in the MFa lithofacies, at 23 m above sea level (ASL), which shows the McArthur River and P2 Main locations. (**B**) Proximity zones as defined by the highest U content found throughout total drill hole depth. (**C**) Location of samples collected in summer 2014 for additional analyses. (**D**) Uranium distribution within study footprint. Background, defined as <1 ppm (details in text), is shown with horizontal line; McA+ and McA++ have median values above background. Colours refer to (**B**). N = samples analyzed.

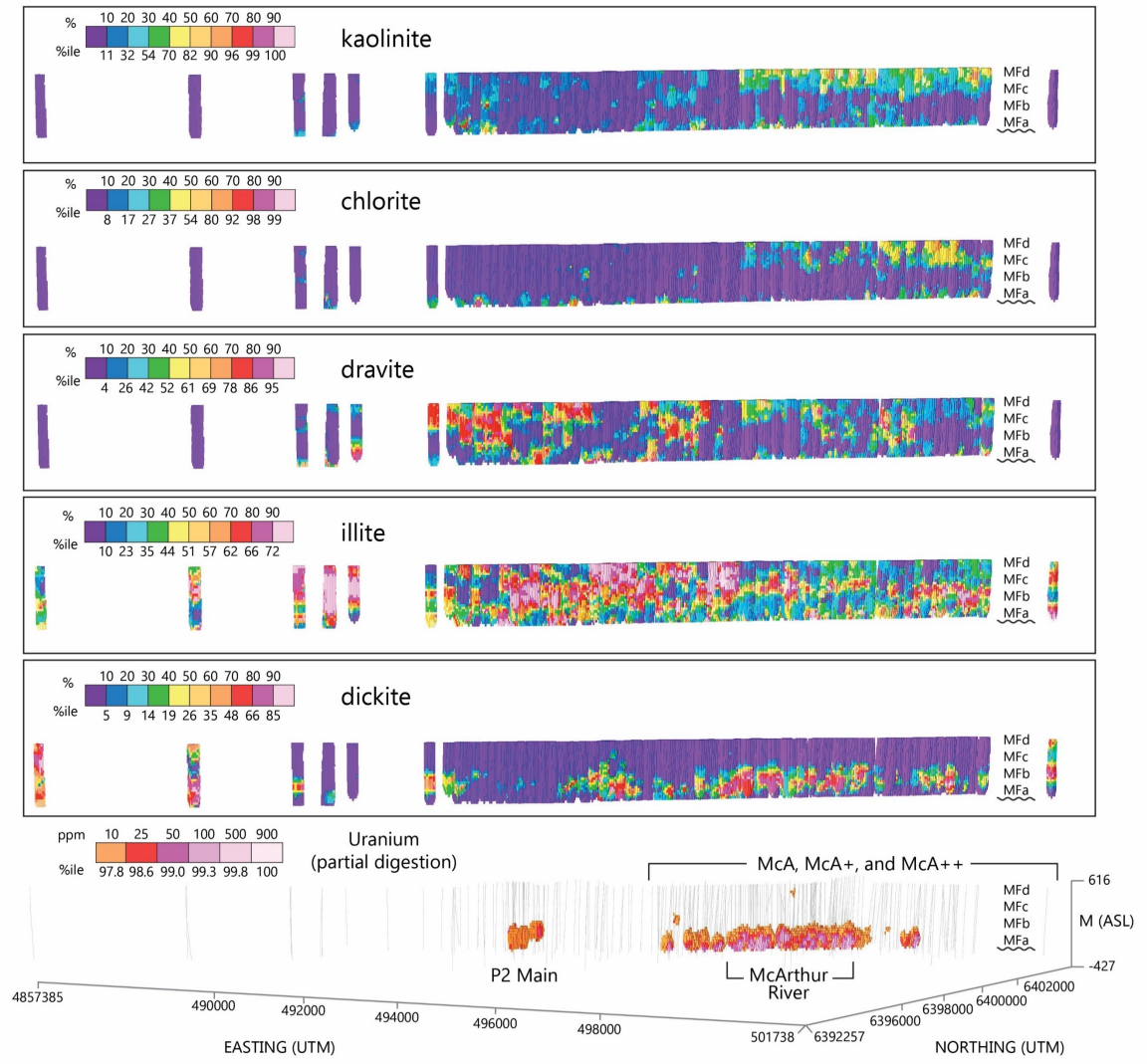

Figure 3.7: Shortwave infrared spectroscopy (SWIR). Three dimensional maps showing distribution of clay-type minerals throughout study area, as compared to the U content of >10 ppm. Looking northwest; vertical exaggeration 2X. Vertical lines are drill core traces. Dickite is assumed to be preserved from alteration through quartz cementation, and its highest concentrations are found above the McArthur River deposit. Illite and dravite show no spatial association at this scale with the McArthur River deposit. Chlorite and kaolinite are concentrated in the upper lithofacies (MFd to MFc) in the northeastern study area, above the McArthur River deposit, but not above P2 Main.

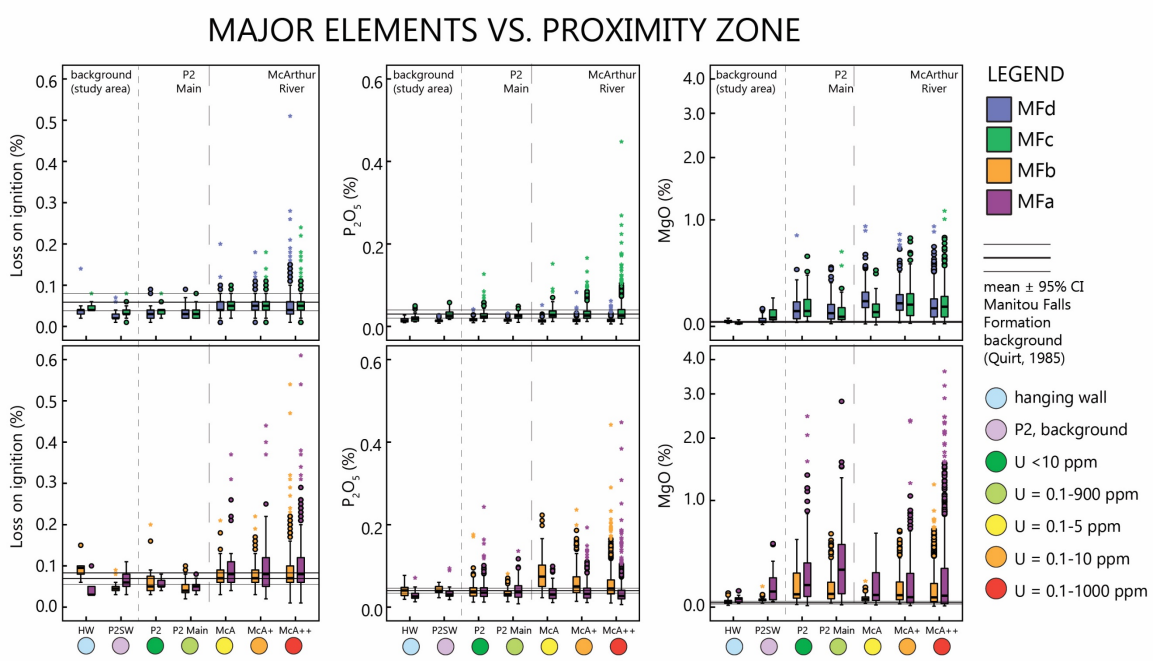

Figure 3.8: Major elements (total digestion) in comparison to Manitou Falls Formation background outside the study location (horizontal solid lines), and in relation to proximity zone as defined in Figure 3.6. Vertical dotted lines separate footprint background from P2 and P2 Main and the mineralized areas surrounding McArthur River; U content increases toward the right in each plot. Loss on ignition (LOI), P2O5, and MgO concentrations all increase with proximity to mineralization. Analyses for the following: HW: LOI n=45, MgO & P_2O_5 n=126; P2SW: LOI n=99 MgO & P_2O_5 n=126; P2: LOI n=65, MgO & P_2O_5 n=874; P2 Main: LOI n=99, MgO & P_2O_5 n=617; McA: LOI n=328, MgO & P_2O_5 n=358 ; McA+: LOI n=686, MgO & P_2O_5 n=1116; McA++: LOI n=2362, MgO & P_2O_5 n=4487.

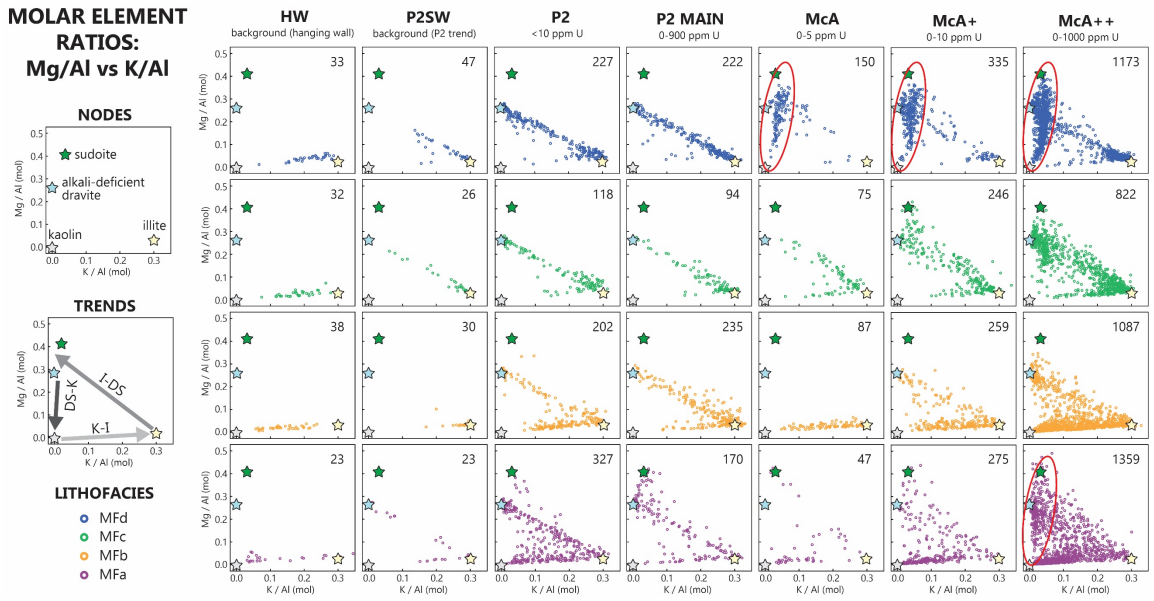

Figure 3.9: Molar element ratios throughout the study footprint, with individual plots per lithofacies within each proximity zone. Number of analyzed samples are noted in the top right corner of each plot. Red ovals show unique DS-K trend that is present only in the economic, mineralized region of the footprint. Notably, the I-DS trend in drill core samples that are in the least-altered to subeconomic areas of the footprint — P2SW to P2 Main — show no association with sudoite (green star = ideal formula). Samples that approach the node for sudoite are found only in those drill cores that appear in the 7 km of the footprint surrounding the McArthur River deposit. The combination of the DS-K trend and an association with sudoite demarcate the economic region of the footprint from the subeconomic region. Mineral formulae calculated from McArthur River samples in previous studies: for illite and sudoite from Ng et al. (2013); for alkali-deficient dravite from Zhang et al. (2001).

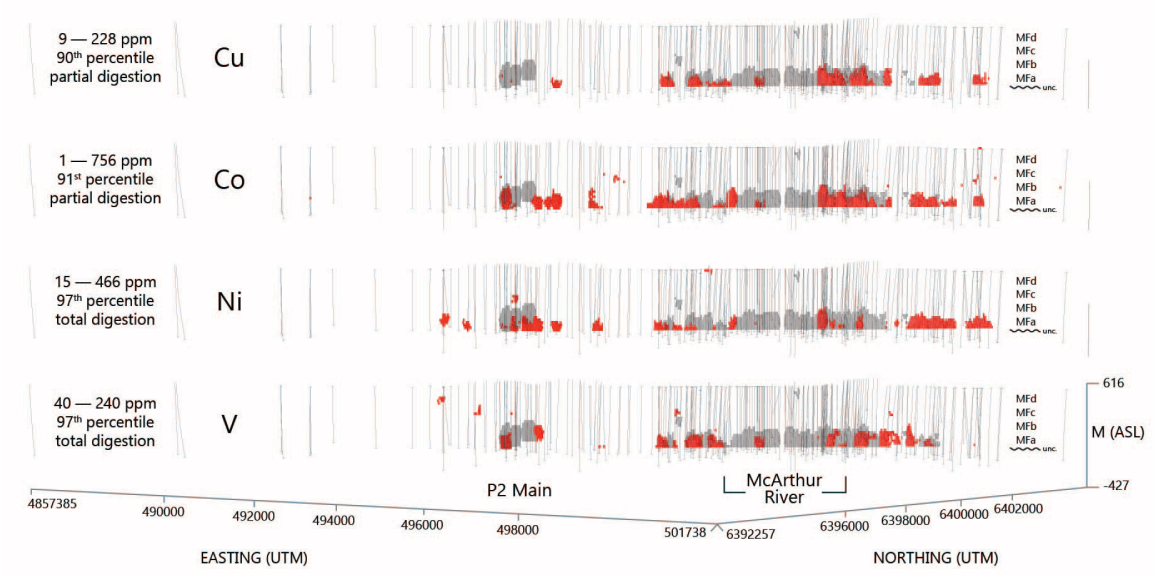

Figure 3.10: Indicator elements at the McArthur River study area, vertical exaggeration 2X, looking northwest. Pathfinder elements traditionally associated with unconformity-type U deposits, along with several others, exhibit elevated concentrations that are coincident with high levels of U, but are so restricted here as to not be useful as large-scale vectors. The elements shown in red have a close spatial relationship with both the economic grade (McArthur River) and subeconomic grade (P2 Main) deposits. Uranium is shown in gray haloes at concentrations of 10 – 1000 ppm (partial digestion). Gray vertical lines are drill hole traces.

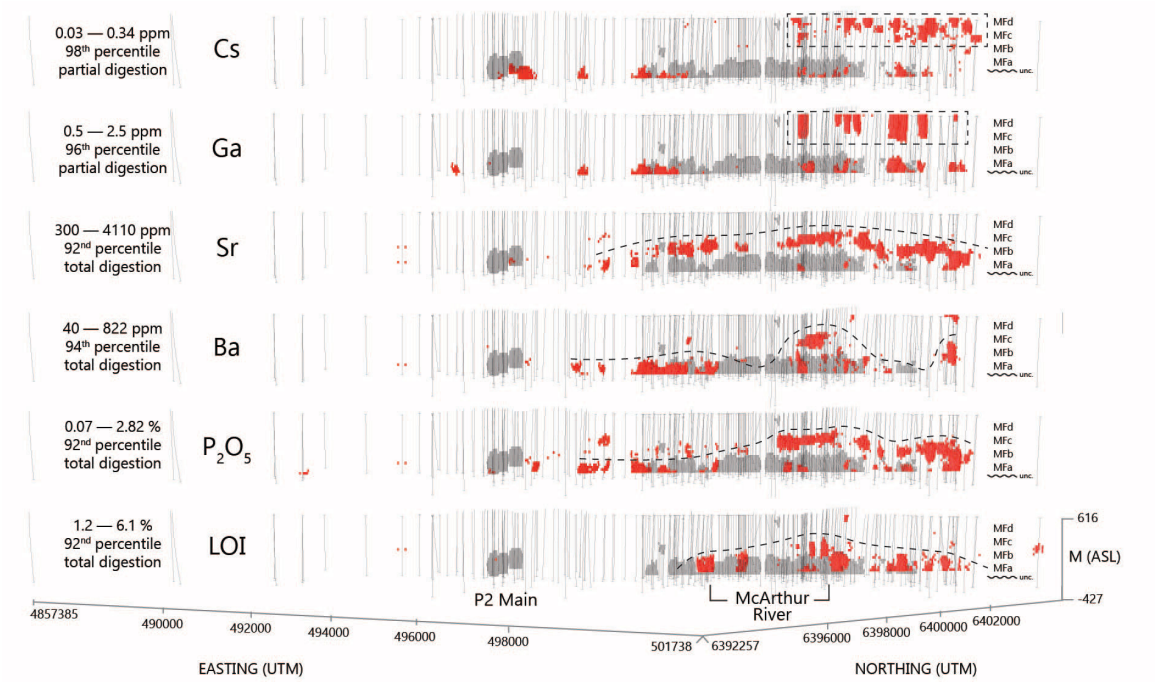

Figure 3.11: Trace elements Cs, Ga, Ba, and Sr plus loss on ignition and P_2O_5 as related to proximity zones display broader, distal haloes that are spatially related to the McArthur River deposit in the middle to upper lithofacies. Notably, these elements are not spatially related to the subeconomic P2 Main deposit. View looking northwest. Vertical exaggeration 2X. Uranium halo is displayed in gray for 10-1000 ppm (partial digestion) in the sandstones. Gray vertical lines are drill hole traces. Pathfinder elements are displayed in red. Cs and Ga (partial digestion) show a distal halo in the uppermost (MFd) lithofacies above mineralization (dashed boxes). Sr, Ba, P_2O_5, and LOI (total digestion) show a broader halo in the middle (MFc–MFb) lithofacies above mineralization (dashed curves).

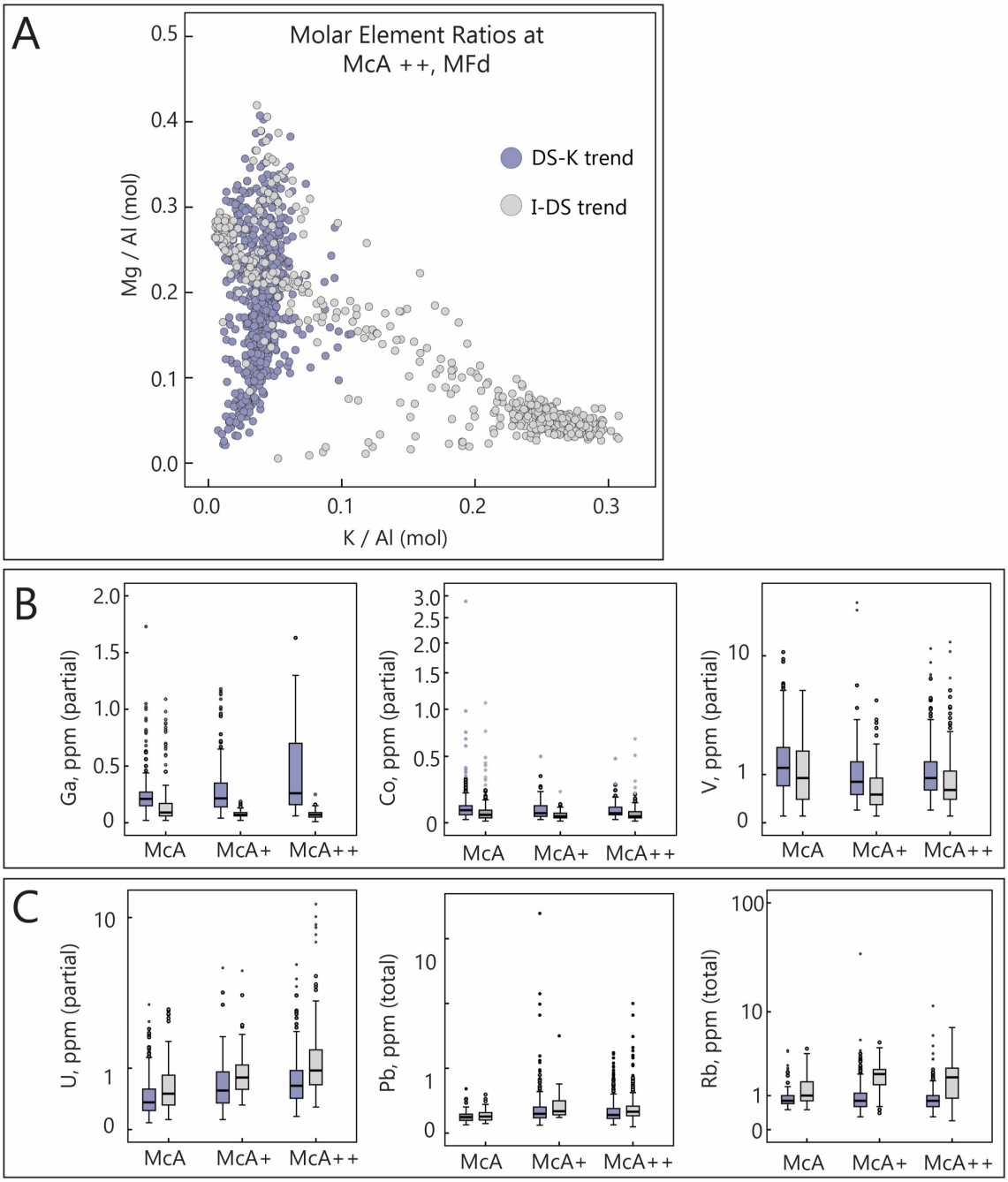

Figure 3.12: Trace elements as related to the molar element ratio trends presented in Figure 3.10. The DS-K trend appears in the MFd above the McArthur River deposit and surroundings, approximately 7 km total strike length. (**A**) Drill holes were separated into either of the I-DS or DS-K trends in MFd lithofacies only. (**B**) Some of the trace elements that are elevated in the DS-K trend relative to the I-DS trend, in the MFd. (**C**) Only U (partial and total digestions), Rb, and Pb (total digestion) show the opposite correlation to (**B**).

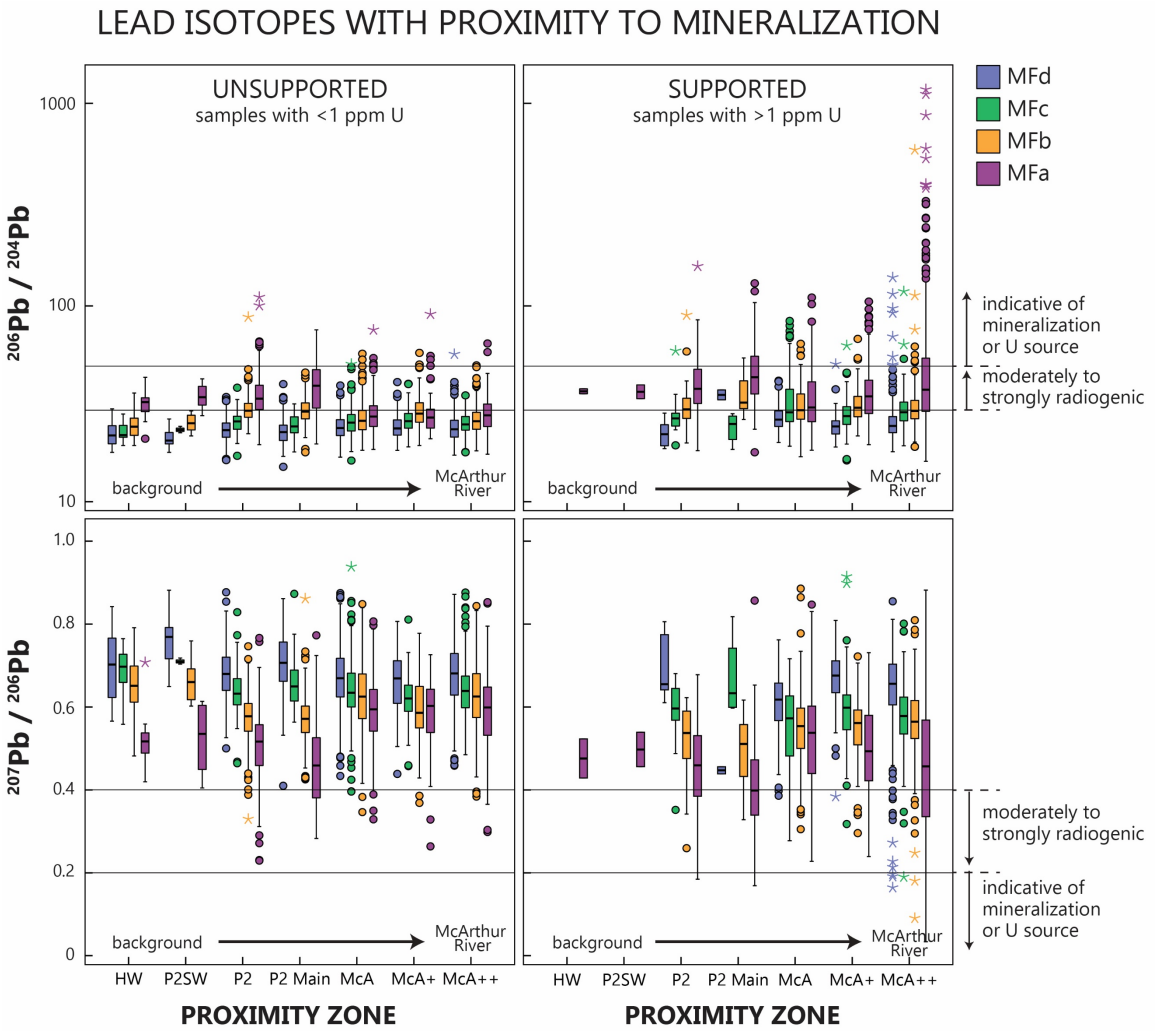

Figure 3.13: Lead isotope distribution throughout the study footprint. Samples that are unsupported and contain <1 ppm U do not exhibit a strong vectoring trend toward mineralization. Samples that are supported and contain >1 ppm U exhibit ratios that are more indicative of mineralization with increasing proximity to the McArthur River deposit, but mainly within the MFa lithofacies. The MFd lithofacies, nearest surface, contains the largest number of samples with ratios indicative of mineralization in drill cores that intersect the McArthur River deposit.

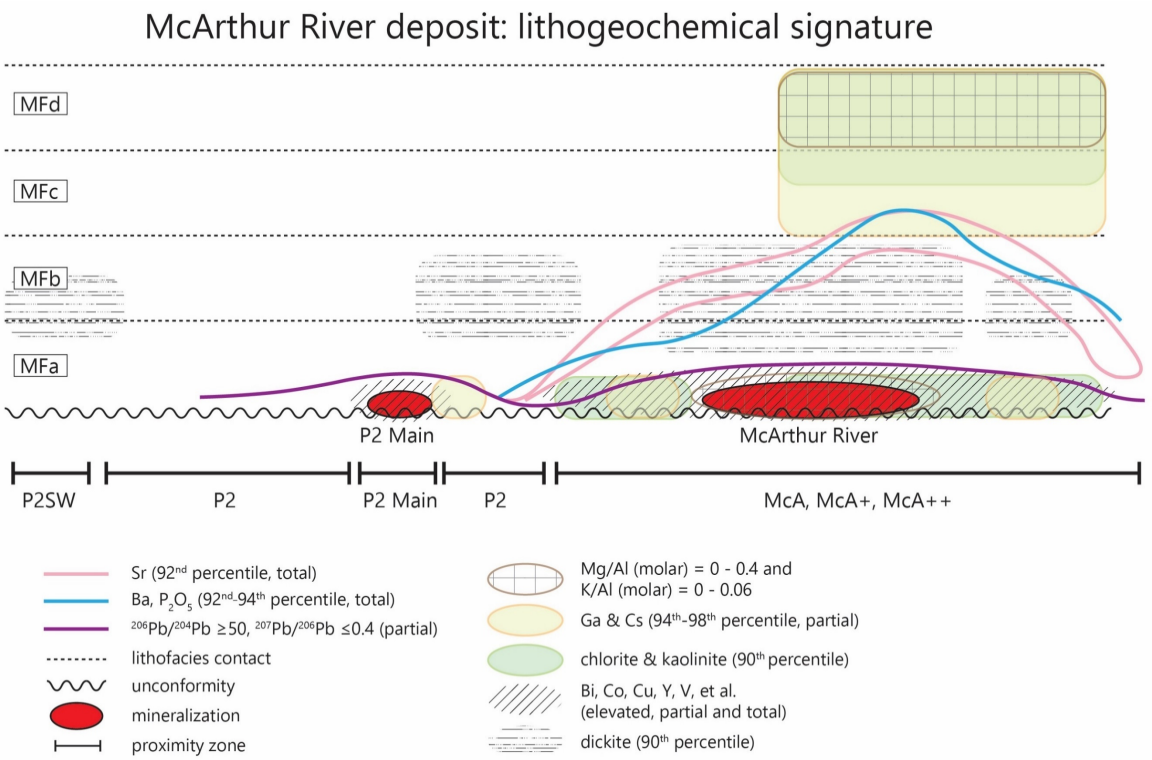

Figure 3.14: Simplified vector map for the suggested pathfinder elements. Trace elements that highlight mineralization as proximal haloes restricted to the MFa lithofacies (indicators) include Bi, Co, Cu, Y, V, and Pb isotopes indicative of mineralization. Trace elements that highlight the location of the McArthur River deposit as distal haloes in the MFb, MFc, and MFd lithofacies (vectors) include Ba, Sr, Ga, and Cs. Molar ratios of Mg/K that trend between ideal sudoite and kaolinite highlight the upper lithofacies above the McArthur River deposit. Chlorite and kaolinite determined from shortwave infrared analysis are concentrated near the McArthur River deposit in the MFa but also highlight its location in the upper lithofacies; dickite is considered a proxy for the intense quartz cementation noted in previous studies. View looking northwest: not to scale.

Fence	Drill Hole	Mineralization drill core depth (m)*	Lithofacies	Depths collected drill core (m)	# samples collected	# with cementation	P2 trend side	Clay species present shortwave infrared spectometry**	Notes
Southwest	MC-336	525-557	MFa	433-571	14	9	FW	Illite > dickite > kaolinite	proximal to P2 wedge
Southwest	MC-338	none	MFd	23-151	4	---	FW	illite > dravite > kaolinite	
Southwest	MC-338	none	MFc	220-272	2	---	FW	illite >> chlorite	
Southwest	MC-338	none	MFb	319-411	3	---	FW	illite >> chlorite > dickite	
Southwest	MC-338	none	MFa	466-559	6	4	FW	illite > kaolinite > dickite > dravite	
Southwest	MC-344	none	MFd	26-199	7	---	HW	dravite > illite > kaolinite	
Southwest	MC-344	none	MFc	230-275	2	---	HW	illite >> dickite	
Southwest	MC-344	none	MFb	299-343	2	---	HW	dickite > illite	
Southwest	MC-344	none	MFa	378-493	8	5	HW	dickite > illite > kaolinite	
Gap	MAC-208	none	MFd	10-149	7	1	HW	kaolinite > dravite > illite > chlorite	
Gap	MAC-208	none	MFc	203-218	2	---	HW	chlorite > illite > dravite > kaolinite	
Gap	MAC-208	none	MFb	237-395	5	1	HW	illite > dickite > chlorite > kaolinite	
Gap	MAC-208	517-530	MFa	425-572	7	5	HW-FW	illite ≥ dickite >> kaolinite	intersects P2 wedge
Gap	MAC-250	none	MFb	298-402	4	---	HW	illite >> dickite > chlorite	
Gap	MAC-250	none	MFa	432-482	2	1	HW	dickite > illite	
Gap	MAC-253	none	MFd	26-205	6	6	HW	kaolinite > dravite > illite	steeply dipping, remains in sandstones
Gap	MAC-253	none	MFc	265-336	4	2	HW	chlorite ≥ illite >> dravite > kaolinite	
Gap	MAC-253	none	MFb	382-550	10	8	HW-FW	dickite > illite > dravite > kaolinite	
Gap	MAC-253	none	MFa	552	1	1	FW	signal:noise ratio < 10	
Zone 4	MAC-246	none	MFd	4-166	7	3	FW	dravite >> kaolinite > illite	
Zone 4	MAC-246	none	MFc	213-298	3	---	FW	illite >> dravite > kaolinite	
Zone 4	MAC-246	none	MFb	324-378	4	1	FW	illite ≥ dickite >> chlorite	
Zone 4	MAC-246	none	MFa	418-543	9	8	FW	dravite >> kaolinite > illite = dickite	proximal to P2 wedge
Zone 4	MAC-252	none	MFd	10-167	5	---	FW	kaolinite = dravite > illite	distal from P2
Zone 4	MAC-252	none	MFc	200-286	5	---	FW	dravite > illite > kaolinite > chlorite	distal from P2
Zone 4	MAC-252	none	MFb	305-343	4	---	FW	dravite > illite > chlorite	distal from P2
Zone 4	MAC-255	none	MFd	6-148	5	---	HW	dravite > illite > kaolinite	
Zone 4	MAC-255	none	MFc	194-379	10	2	HW	illite > dickite > dravite >> kaolinite	
Zone 4	MAC-255	none	MFb	398-426	3	2	HW	dickite >> illite	
Zone 4	MAC-255	~565	MFa	429-503	10	8	HW-FW	dickite > illite > kaolinite > chlorite	intersects P2 wedge
Zone C	MC-413	none	MFd	71-72	1	---	HW	chlorite > kaolinite > dravite	
Zone C	MC-413	none	MFc	130-282	5	---	HW	illite = kaolinite > chlorite ≥ dravite	
Zone C	MC-413	none	MFb	299-404	7	1	HW	illite > dravite ≥ dickite > kaolinite	
Zone C	MC-413	~600, ~615, ~628	MFa	430-649	14	7	HW-FW	dickite >> illite > kaolinite	intersects P2 wedge
Zone C	MC-415	none	MFd	76-77	1	---	HW	chlorite > kaolinite > dravite	
Zone C	MC-415	none	MFc	127-296	6	---	HW	chlorite > illite > kaolinite > dravite	
Zone C	MC-415	none	MFb	341-433	7	1	HW	dravite >> illite > kaolinite	
Zone C	MC-415	none	MFa	456-540	10	7	HW	dravite > illite > kaolinite > chlorite	
Background	MC-434	none	MFd	11-120	5	4	HW	illite > dickite >> dravite	
Background	MC-434	none	MFc	168-282	6	3	HW	dickite > illite	
Background	MC-434	none	MFb	329-371	4	---	HW	dickite >> illite	
Background	MC-434	none	MFa	397-422	2	---	HW	dickite	

* estimated from field notes and data provided by Cameco
** clay species are SWIR results scanned directly onto collected samples, using TerraSpec by Nicholas Joyce, Queen's University

Table 3.1: New core samples collected July-August 2014 from McArthur River core storage, including clay species mineralogy by SWIR.

CHAPTER 4: SUMMARY AND FUTURE WORK

4.1 INTRODUCTION

The Millennium and McArthur River unconformity-related uranium (URU) deposits, located in the southeastern Athabasca Basin, are hosted in similar lithologies within 50 km of each other. They are both situated in and above Wollaston Domain basement rocks and within the Wollaston-Mudjatik Transition Zone (WMTZ) (McGill et al., 1993; Cloutier et al., 2009; Jeanneret et al., 2016), an area rich in URU deposits. They are also partially located in overlying sandstones within a major regional illite anomaly, near chlorite and dravite anomalies, all of which are key indicators of a fertile environment conducive to the formation of URU deposits (Earle and Sopuck 1989; Zhang et al., 2001). However, the two deposits exhibit major differences in their mineralization locations and styles that have resulted in variable expressions of mineralogy and major and trace element geochemistry in the sandstones. By characterizing these deposits for their distal lithogeochemical signatures in the sandstones above deposits, over distances of several kilometres, a set of vectors toward mineralization can be defined that may be utilized in future exploration efforts for all types of URU deposits.

This thesis utilized an archival database of whole rock geochemical data, which included over 10,000 individual samples collected over nearly three decades of exploration. This extensive dataset enabled large areas of study — ~20 km strike lengths for each

deposit — that illustrate comprehensive geochemical variations that are not wholly visible, or are incomplete, using smaller, more scattered, or more tightly targeted lithogeochemical datasets. In addition, the datasets were limited to samples containing < 1000 ppm U, thus avoiding the overt influence of the mineralized bodies. This allows one to understand the extent of the hydrothermal footprint, which is intrinsically more extensive in three dimensions than the mineralization itself, and to evaluate subtle variations in geochemical and mineralogical signatures with proximity to the deposit.

Data evaluation of the McArthur River and Millennium deposits, parameterized stratigraphically and with varying distance to mineralization, has resulted here in the definition of elemental and mineralogical haloes that define the footprint and provide vectors toward mineralization. Manitou Falls Formation sandstones above both locations exhibit large-scale K-Mg alteration haloes that contain smaller-scale trace element enrichments. These scalable mineralogical and geochemical signatures reflect the transition from distal (kilometres) to proximal (10s of metres) sandstones above the deposit. Individual trace element enrichments are not equivalent between the study areas. Therefore, the lithogeochemical signature is likely most dependent on the content of the greatest volumes of fluid flow between the basement and basin rocks, indicative of the potential for deposit formation, irrespective of mineralization style.

4.2 SUMMARY OF KEY RESULTS

Data evaluation of the Manitou Falls Formation sandstones of the Millennium and McArthur River deposits, specifically the spatial relationship of clay-type minerals and

major and trace elements to mineralization, are summarized below. Figure 4.1 shows simplified graphic representations of all patterns described herein.

4.2.1 Shortwave infrared spectroscopy

Shortwave infrared spectroscopy (SWIR) is a quick, non-destructive method used to identify clay-type mineral species *in situ* through semi-quantitative analysis (Russell and Fraser, 1994; Percival et al., 2002). Although it cannot be directly related to individual whole rock geochemical samples, as the from-to intervals of measurements are not equivalent between methods, it is useful for providing a large-scale overview of the five clay-type minerals common to URU deposits: dickite, kaolinite, illite, chlorite, and dravite (Earle and Sopuck, 1989; Zhang et al., 2001). The distribution of these five minerals differs significantly between the McArthur and Millennium deposits, as briefly summarized here. A more detailed description is presented as Appendix B.

The Millennium deposit exhibits a hydrothermal clay alteration envelope with its distal edge approximately 10 km north of the deposit.

- Outside of this envelope, dickite is dominant in all lithofacies, followed by illite, whereas kaolinite, dravite, and chlorite are negligible.
- Within this envelope, dickite remains dominant in the MFb lithofacies, whereas the other minerals increase in the MFd, MFc, and MFa lithofacies.
- Approximately 6 km north of the deposit, illite becomes the dominant mineral in the MFd, MFc, and MFa lithofacies, with increasing kaolinite, chlorite, and dravite.
- Chlorite is concentrated in the Main and Proximal corridors above mineralization.

McArthur River does not exhibit hydrothermal clay alteration envelopes in the same manner as at Millennium; instead, individual minerals target specific areas related to degree of mineralization.

- Dickite is clustered in the MFb lithofacies above the McArthur River deposit and the immediate surroundings due to preservation by quartz cementation, but not above the P2 Main mineralization.
- Illite is the dominant mineral in the background (hanging wall) and least-altered locations of the study area in all lithofacies.
- Dravite is concentrated in small patches throughout the study area in all lithofacies.
- Chlorite and kaolinite are present in concentrations >50% in the MFd above and 7 km north of the McArthur River deposit.

4.2.2 Whole rock geochemistry: major elements

At both deposits, major elements MgO and K_2O are enriched in the Manitou Falls Formation, whereas Fe_2O_3 and Na_2O are depleted, in all four lithofacies when compared to regional background sandstones in the basin (Quirt, 1985). However, only MgO exhibits a spatial relationship with mineralization. Chapters 2 and 3 summarize the major element results at each deposit in greater detail.

- At Millennium, MgO increases with proximity to the deposit in all four lithofacies within the 10-km envelope mentioned above (Fig. 2.5).

- At McArthur River, MgO is present in higher concentrations in all lithofacies in areas associated with mineralization, both subeconomic (P2 Main) and economic (McArthur River) (Fig. 3.9).
- At McArthur River, P_2O_5 and loss on ignition (LOI) also increase with proximity to the deposit; elevated levels are associated with the deposit from the MFa to the MFc (Fig. 3.9).

4.2.3 Whole rock geochemistry: molar element ratios

Molar element ratios of K/Al to Mg/Al are useful vectors within the Athabasca Basin and illustrate the transitions between clay-type species dickite/kaolinite, illite, chlorite (Al-Mg-sudoite), and dravite (alkali-deficient dravite). This allows for the mineralization assemblages to be understood paragenetically as a function of proximity to mineralization. Individual scatter plots of K/Al vs. Mg/Al for each proximity zone per lithofacies were analyzed, with nodes corresponding to the chemical formulae for ideal kaolin, illite, alkali-deficient dravite, and sudoite (Figs 2.6, 3.10).

- Samples that plot between ideal kaolin and ideal illite nodes are dominant in the background or least-altered locations of all lithofacies in both the Millennium and McArthur River study areas. This trend is also dominant in the MFb lithofacies from distal to proximal to mineralization in both deposits.
- Samples shift toward the ideal sudoite and alkali-deficient dravite nodes with proximity to mineralization at both the Millennium and McArthur River study areas in the MFd, MFc, and MFa lithofacies.

- Within the Millennium study area, the shift is gradual on the molar element ratio plots. The displacement between K-dominant to Mg-dominant alteration can be quantified by the ratio of Mg/K.
    - Median Mg/K ratios >0.2 mark the 10-km envelope interior boundary.
    - Displacement toward the sudoite and alkali-deficient dravite nodes increases with proximity to the deposit, and the highest Mg/K ratios occur within 2 km of the deposit.
- Within the McArthur River study area, three trends are evident.
    - Samples associated with the lower U concentrations (P2 trend, nonmineralized; and P2 Main, subeconomic) plot on a linear trend between the illite and alkali-deficient dravite nodes in the MFd and MFc lithofacies, but not the sudoite node.
    - Samples associated with higher U concentrations plot on a generally linear trend between the illite and both alkali-deficient dravite and sudoite nodes. This occurs in the MFa of the P2 trend and P2 Main zones, and in all lithofacies of the McA, McA+, and McA++ zones.
    - A unique trend (DS-K) between the sudoite/alkali-deficient dravite nodes and the kaolin group node in the MFd lithofacies of the McA, McA+, and McA++ zones, and in the MFa of the McA++ zone. These samples have molar ratios of K/Al <0.06 and Mg/Al <0.4.
        - SWIR results for these drill holes confirm that these areas are associated with kaolinite and not dickite (Fig. 3.7).

4.2.4 Whole rock geochemistry: trace elements

Trace element data were evaluated to determine if anomalous concentrations (partial and total digestions) could be used as potential vectors toward mineralization. Trace element signatures were identified at both study areas unique to mineralized locations, but these were not equivalent between deposits.

- At Millennium, the partial digestion results give clearer spatial associations (distribution haloes) to the deposit location than total digestion results, which are generally elevated throughout the study area. Three dimensional maps for these patterns are seen in Chapter 2, Figures 2.9–2.11.
    - Partial digestion results for select trace elements exhibit distribution haloes in three basic patterns, all focussed within a 1–2 km strike above the deposit in middle and upper lithofacies, with increasing values proximal to mineralization.
        - *Chimneys* are vertical distributions of elevated concentrations of Mo, Co, Ga, and Rb that are present in all four lithofacies.
        - *Humps* are heavy rare earth elements (HREE) and Y; those elevated to anomalous concentrations have a more conical distribution and only rarely extend above the MFc.
        - A lensoidal *bullseye* pattern directly above the deposit within the MFb lithofacies is characterized by anomalous light rare earth elements (LREE).

- At McArthur River, trace element distributions also may be categorized into three generalized groupings, but do not have comparable spatial distribution patterns with Millennium's geochemical signature. Three dimensional maps for these patterns are shown in Chapter 3, Figures 3.11–3.12.
    - First, within the MFa and at the unconformity, the majority of trace elements, including traditional pathfinders for URU deposits, are clustered in tight haloes in locations where U >10 ppm. These are considered indicators rather than vectors, as their elevated to anomalous concentrations do not extend beyond the U haloes themselves.
    - Second, elevated Ba and Sr (total digestion) exhibit a similar pattern along with LOI and P_2O_5. This distribution is a dominantly horizontal halo 6–8 km along strike, mainly within the MFa and MFb, with portions in the MFc (~ 400 m) directly above the McArthur River deposit.
    - Third, elevated Ga and Cs (partial digestion) are found in the MFd–MFc as a scattered halo ~460–560 m above and 3-4 km northeast of the McArthur River deposit.

Only one trace element, Ga, can be considered a pathfinder for both deposits in the distal sandstones.

- At Millennium, Ga is one of the chimney elements which highlight the deposit location through a vertical distribution from the unconformity to the MFd.
- At McArthur River, elevated Ga is present in the same locations as the unique molar element ratio trend (DS-K, plotting between the alkali-deficient dravite and kaolin

nodes) mentioned above. It occurs in the MFd lithofacies in the northeastern 7 km of the study area, and is also elevated in the MFc.

Acting in a similar capacity between deposits, but in a proximal manner, are the Pb isotope ratios indicative of mineralization.

- At both Millennium and McArthur River, the contiguous haloes of $^{206}Pb/^{204}Pb$ >35 and $^{207}Pb/^{206}Pb$ <0.4 are present within tens of metres of mineralization in the MFa. Above the MFa, the number of samples with these ratios increases proximal to the deposit, but they are rare and isolated.

Both Millennium and McArthur River study areas contain select trace elements that are only present in confidently measurable levels above instrument noise in areas proximal to the deposit, occurring only at very low concentrations or below background elsewhere.

- At Millennium, Ag, Bi, and Sb (partial digestion) are within the Proximal-Main Zone lithofacies (Fig. 2.12).
- At McArthur River, Cs (partial digestion) is located along the MFa and in the MFd above the deposit and surrounding areas (McA–McA++) (Fig. 3.12).

4.3 DISCUSSION

Chapters 2 and 3 illustrate that the distal lithogeochemical footprints, on a deposit scale, highlight the differences between a deeper and lower grade deposit with the majority of the monomineralic mineralization in the basement (Millennium) versus a larger, high-grade one with the majority of the monomineralic mineralization in the sandstones and at the unconformity (McArthur River). At Millennium, an alteration envelope encompasses

the area of study 10 km to the north and 2 km to the south of the deposit (the southern end being limited by drill core distribution). Inside this envelope there is a gradual increase in Mg-related alteration with proximity to the deposit, and a dominantly vertically expressed halo of chlorite and elevated trace elements spatially related to mineralization and redox processes situated directly above the deposit. At McArthur River, the Mg-related alteration envelope is coincident with the entire strike of the P2 fault system, and trace element haloes highlighting the general location of the deposit within 7 km are dominantly horizontal and either related to clay-type alteration or sourced from the basement lithologies.

Studies have shown that the Millennium and McArthur River deposits share similarities in ages, fluid inclusions, and REE signatures, suggesting that their timing and genesis were similar (Mercadier et al., 2011; Lach et al., 2013; Richard et al., 2015). Similarities in location, lithologies, and mineralization present at both the unconformity and within the basement also suggest that both deposits may be considered hybrids (e.g., Mercadier et al., 2009; 2012; Sheahan et al., 2016) between the ingress and egress models defined by previous researchers (Hoeve and Quirt, 1984; Fayek and Kyser, 1997). Therefore, the differences seen in the lithogeochemical signatures between the deposits are more heavily influenced by the stratigraphic and structural barriers channeling the fluids, and the elemental content through fluid-rock interaction specific to each site, than the precipitation of U itself. We observe this in the contrasting distributions of major and trace elements in the sandstone environment surrounding the two deposits.

Millennium's trace element signature consists of vertically distinct patterns highlighting the probable fluid conduit pathways between the sandstones and basement

directly above the deposit. Conversely, McArthur River's trace element signature is larger, mainly horizontal, and more reflective of the general location of the deposit. These differences can be attributed to variable degrees of quartz cementation within the Manitou Falls sandstones. Quartz cementation is not documented at the Millennium deposit as an alteration feature, although dickite is noted as a preserved package in the middle lithofacies (MFb-MFc; Roy et al., 2006). In contrast, intense quartz cementation is well documented at McArthur River, restricting the majority of the hydrothermal alteration footprint to the MFa lithofacies (McGill et al., 1993; Ng et al., 2013).

At Millennium, hydrothermal fluid flow was not heavily restricted within the study area, as demonstrated by the 10-km envelope representing the transition between diagenetic alteration represented by dickite (diagenetic background) and the K- and Mg-related alteration by later hydrothermal processes. In addition, near-vertical faulting has allowed fluids to travel between the basement deposit location and the sandstones, leaving the trace element signature illustrated by the chimney and hump patterns and chlorite distribution.

At McArthur River, pre-ore quartz cementation is known to be intense at the deposit site, and is characterized by both low porosity and high concentrations of dickite, preserved from later alteration by the quartz cement (McGill et al., 1993; Ng et al., 2013). The distribution of abundant dickite in the SWIR results along the P2 trend on either side of the McArthur River deposit (Appendix B) suggests that quartz cementation extends several kilometres further than has been previously documented, responsible for the trapping and concentration of fluids related to mineralization to depth. This effect explains the tightly

constrained nature of traditional pathfinder haloes, such as Bi, Co, Cu, Mo, V, and others, restricted to the MFa and their correlation with elevated U. However, there are faults associated with intense quartz cementation (Bronkhorst et al., 2012) that allowed select fluid processes to travel into the upper sandstones, resulting in elevated concentrations of MgO, Ba, Sr, P_2O_5, Ga, and Cs in the MFd and MFc lithofacies above the deposit. Probable sources for elemental enrichments include illite (Ga, Cs) and APS minerals (Ba, Sr). The fact that varying groups of elements did or did not transgress cementation may provide clues to the relative timing between fracturing and fluid events. Unlike at Millennium, these elemental distributions extend several kilometres in the horizontal direction, with a concomitantly greater effect from lithostratigraphic control. Elevated Ga and Cs (partial digestion), as well as samples that plot on the molar element ratio trend representative of the transition between kaolin, alkali-deficient dravite, and sudoite, are mainly present in the MFd at McArthur River. The MFd lithofacies contains a greater proportion of mudstone intraclasts available for fluid-rock interaction and alteration processes; these intraclasts are present in smaller amounts or are absent in the MFc and MFb (Hiatt and Kyser, 2007), therefore, the signature would be diminished in these lithofacies in comparison.

4.4 CONCLUSIONS

By studying two similar but unrelated unconformity-related uranium deposits, we have characterized the distal lithogeochemical signature of the surrounding ~20 km of each deposit to present the following conclusions:

1. Lithostratigraphic characteristics of the sandstones, through structure and permeability variations, controlled the geochemical expression in spatial relation to mineralization in patterns unique to each deposit.

Hydrothermal processes, from pre- to post-ore, were responsible for altering the Manitou Falls Formation sandstones in and around the Millennium and McArthur River deposits. The dominant control at Millennium is the concentration of faults and fractures above the deposit location, which allowed fluids to travel from the basement upwards within a narrow corridor. Spatially, this is illustrated as a mainly vertical concentration of chlorite and pathfinder trace elements directly above the deposit. At McArthur River, extensive quartz cementation has restricted major fluid movement to within the lowest lithofacies. Consequently, the majority of the geochemical signature is horizontally extensive, especially for the traditional pathfinders within the MFa. The few trace elements with elevated concentrations that lie above the quartz cementation zone, and the deposit itself, are also mainly horizontal in 3D space and extend for several kilometres along strike. Also stratigraphically constrained is the molar element trend between kaolinite, alkali-deficient dravite, and sudoite, seen only in the MFd, above the areas associated with the McArthur River deposit and to its north.

2. Vectoring toward mineralization is possible using the distal sandstones. By plotting the molar element ratios of K/Al vs. Mg/Al, distal and proximal areas of the alteration footprint can be defined by trends seen between illite (K-altered) and sudoite and alkali-deficient dravite (Mg-altered) ideal formula nodes in 2D molar space. Within the areas of the footprint that plot toward the Mg-rich minerals,

elevated concentrations of trace elements representative of mineralization processes or basement lithology increase with proximity to the deposit, providing additional vectors.

This is true at both deposits, even though the mineralization locations and the smaller trace element haloes, in both distribution pattern and elemental content, differ between them. Molar element ratios are preferred over SWIR or raw data for major element analysis because they best illustrate the transition between clay-type minerals with respect to deposit proximity, as all individual mineral endmembers are detected, to some degree, throughout the study areas. At both study areas, the variations in Mg in relation to K demonstrate a relationship to deposit location. Millennium demonstrates a gradual increase in Mg in relation to K with proximity to mineralization. At McArthur River, distinct linear trends in Mg/K molar space between the endmembers define areas associated with economic and sub-economic mineralization. This is supported by the fact that chlorite in the SWIR results functions as a distal pathfinder for both deposits, present as elevated haloes in the MFd-MFc 400–600 m above the unconformity.

4.5 FUTURE WORK

The McArthur River study area included the collection of 229 samples of drill core. Samples were split and shared with another member of the CMIC-Footprints project, Nicholas Joyce, who carried out microscopy, SWIR, electron microprobe, and LA-ICP-MS work exclusively on the collected samples. In contrast, this thesis focussed on the legacy data and incorporated the whole rock geochemistry that was completed on the collected samples (referred to in Chapter 3 as “new data”). Generally, newly acquired data

either showed no discernible trend between mineralized zones and areas with low or no mineralization, or supported the trends exhibited by the legacy data (e.g., Chapter 3).

Fifty-eight thin sections were cut from the collected samples for use by Memorial University. The new geochemistry data, in agreement with legacy data, exhibited elevated Sr levels in the cores from mineralized fences. Considering the preferential partitioning of Sr by aluminum phosphate-sulfate (APS) minerals, which can act as potential pathfinders for URU deposits (Gaboreau et al. 2005; 2007), a scanning electron microscope (SEM) was utilized to examine the elemental variations in APS minerals with respect to proximity to mineralization. Due to time and fiscal constraints only 12 thin sections were examined by Scanning Electron Microscopy – Energy Dispersive X-Ray (SEM-EDX), and Mineral Liberation Analysis (SEM-MLA). Results showed that samples in closest proximity to mineralization had a larger ratio of the reduced APS endmember (florencite) as compared to the oxidized endmember (svanbergite/goyazite). Appendix C contains details of this study.

Future work would sensibly include microprobe work on the additional thin sections, more extensive examinations of the APS mineral distribution, fluid inclusion studies, SEM-EDX and SEM-MLA for other potential pathfinders, and other research to further characterize the McArthur River URU deposit.

REFERENCES

Bronkhorst, D., Edwards, C. R., Mainville, A. G., Murdock, G. M., & Yesnik, L. D. (2012). McArthur River operation, northern Saskatchewan, Canada. *National Instrument 43-101 Technical Report*: Cameco Corporation, 206 p.

Cloutier, J., Kyser, K., Olivo, G. R., Alexandre, P., & Halaburda, J. (2009). The Millennium uranium deposit, Athabasca Basin, Saskatchewan, Canada: an atypical basement-hosted unconformity-related uranium deposit. *Economic Geology*, *104*(6), 815–840. http://doi.org/10.2113/gsecongeo.104.6.815

Earle, S. A. M., & Sopuck, V. J. (1989). Regional lithogeochemistry of the eastern part of the Athabasca Basin uranium province, Saskatchewan, Canada. *In* Muller-Kahle, E., (ed.), *Uranium resources and geology of North America: International Atomic Energy Agency,* TECDOC-500, 263–296.

Fayek, M. & Kyser, T. (1997). Characterization of multiple fluid-flow events and rare-earth-element mobility associated with formation of unconformity-type uranium deposits in the Athabasca Basin, Saskatchewan. *The Canadian Mineralogist, 35,* 627–658.

Gaboreau, S., Beaufort, D., Vieillard, P., Patrier, P., & Bruneton, P. (2005). Aluminum phosphate–sulfate minerals associated with Proterozoic unconformity-type uranium deposits in the East Alligator River Uranium Field, Northern Territories, Australia. *The Canadian Mineralogist*, *43*(2), 813–827. http://doi.org/10.2113/gscanmin.43.2.813

Gaboreau, S., Cuney, M., Quirt, D., Beaufort, D., Patrier, P., & Mathieu, R. (2007). Significance of aluminum phosphate-sulfate minerals associated with U unconformity-type deposits: The Athabasca basin, Canada. *American Mineralogist*, *92*(2-3), 267–280. http://doi.org/10.2138/am.2007.2277

Hiatt, E. E., & Kyser, T. K. (2007). Sequence stratigraphy, hydrostratigraphy, and mineralizing fluid flow in the Proterozoic Manitou Falls Formation, eastern Athabasca Basin, Saskatchewan. *In* Jefferson C. W. & Delaney, G. (eds.), *EXTECH IV: Geology and Uranium EXploration TECHnology of the Proterozoic Athabasca Basin, Saskatchewan and Alberta*: Geological Survey of Canada, Bulletin 588, 489–506.

Hoeve, J., & Quirt, D. H. (1984). Mineralization and host rock alteration in relation to clay mineral diagenesis and evolution of the Middle-Proterozoic, Athabasca Basin, northern Saskatchewan, Canada. Saskatchewan Research Council, SRC Technical Report 187, 202 p.

Jeanneret, P., Goncalves, P., Durand, C., Trap, P., Marquer, D., Quirt, D., & Ledru, P. (2016). Tectono-metamorphic evolution of the pre-Athabasca basement within the Wollaston–Mudjatik Transition Zone, Saskatchewan. *Canadian Journal of Earth*

Sciences, *53*(3), 231–259. http://doi.org/10.1139/cjes-2015-0136

Lach, P., Mercadier, J., Dubessy, J., Boiron, M. C., & Cuney, M. (2013). In Situ Quantitative Measurement of Rare Earth Elements in Uranium Oxides by Laser Ablation-Inductively Coupled Plasma-Mass Spectrometry. *Geostandards and Geoanalytical Research*, *37*(3), 277–296. http://doi.org/10.1111/j.1751-908X.2012.00161.x

McGill, B. D., Marlatt, J. L., Matthews, R. B., Sopuck, V. J., Homeniuk, L. A., & Hubregtse, J. J. (1993). The P2 north uranium deposit, Saskatchewan, Canada. *Exploration and Mining Geology*, *2*(4), 321–331.

Mercadier, J., Cuney, M., & Quirt, D. (2009). Basement-hosted uranium oxides from Athabasca Basin: mineralogy, U/Pb dating, major and Rare Earth Element (REE) concentrations: comparison with U-oxides from deposits located in the vicinity of the unconformity. *In* Lentz, D. R., Thorne, K. G., & Beal, K-L. (eds.), *Proceedings of the 24th IAGS, Fredericton, Canada*, 445–448. ISBN 978-1-55131-136-4

Mercadier, J., Richard, A., & Cathelineau, M. (2012). Boron-and magnesium-rich marine brines at the origin of giant unconformity-related uranium deposits: δ11B evidence from Mg-tourmalines. *Geology*, *40*(3), 231–234. http://doi.org/10.1130/G32509.1

Mercadier, J., Cuney, M., Lach, P., Boiron, M. C., Bonhoure, J., Richard, A., Leisen, M., & Kister, P. (2011). Origin of uranium deposits revealed by their rare earth element signature. *Terra Nova*, *23*(4), 264–269. http://doi.org/10.1111/j.1365-3121.2011.01008.x

Ng, R., Alexandre, P., & Kyser, K. (2013). Mineralogical and geochemical evolution of the unconformity-related McArthur River Zone 4 orebody in the Athabasca Basin, Canada: implications of a silicified zone. *Economic Geology*, *108*(7), 1657–1689. http://doi.org/10.2113/econgeo.108.7.1657

Percival, J. B., Wasyliuk, K., Reif, T., Bernier, S., Drever, G., & Perkins, C. T. (2002). Mineralogical aspects of three drill cores along the McArthur River transect using a portable infrared spectrometer. *In* Summary of Investigations 2002, Volume 2, Saskatchewan Geological Survey, Saskatchewan Industry Resources, Miscellaneous Report D-14, 15 p.

Quirt, D. H. (1985). Lithogeochemistry of the Athabasca Group: Summary of sandstone data. *In* Summary of Investigations 1985, Saskatchewan Geological Survey, Saskatchewan Energy and Mines, Miscellaneous Report 85-4, p. 128–132.

Richard, A., Cathelineau, M., Boiron, M. C., Mercadier, J., Banks, D. A., & Cuney, M. (2015). Metal-rich fluid inclusions provide new insights into unconformity-related U deposits (Athabasca Basin and Basement, Canada). *Mineralium Deposita*, 1-22. http://doi.org/10.1007/s00126-015-0601-4

Roy, C., Halaburda, J., Thomas, D., & Hirsekorn, D. (2006). Millennium deposit-Basement-hosted derivative of the unconformity uranium model. In *Uranium*

production and raw materials for the nuclear fuel cycle-Supply and demand, economics, the environment and energy security: International Atomic Energy Agency Proceedings Series, 111-121.

Russell, J. D. & Fraser, A. R. (1994). Infrared methods. *In* Wilson, M. J. (ed.), *Clay Mineralogy: Spectroscopic and Chemical Determinative Methods* (pp. 11–67). Springer Netherlands. ISBN: 978-94-010-4313-7

Sheahan, C., Fayek, M., Quirt, D., & Jefferson, C. W. (2016). A Combined Ingress-Egress Model for the Kianna Unconformity-Related Uranium Deposit, Shea Creek Project, Athabasca Basin, Canada. *Economic Geology*, *111*, 225–257.

Zhang, G., Wasyliuk, K., & Pan, Y. (2001). The characterization and quantitative analysis of clay minerals in the Athabasca Basin, Saskatchewan: Application of shortwave infrared reflectance spectroscopy. *The Canadian Mineralogist*, *39*(5), 1347-1363. http://doi.org/10.2113/gscanmin.39.5.1347

FIGURES

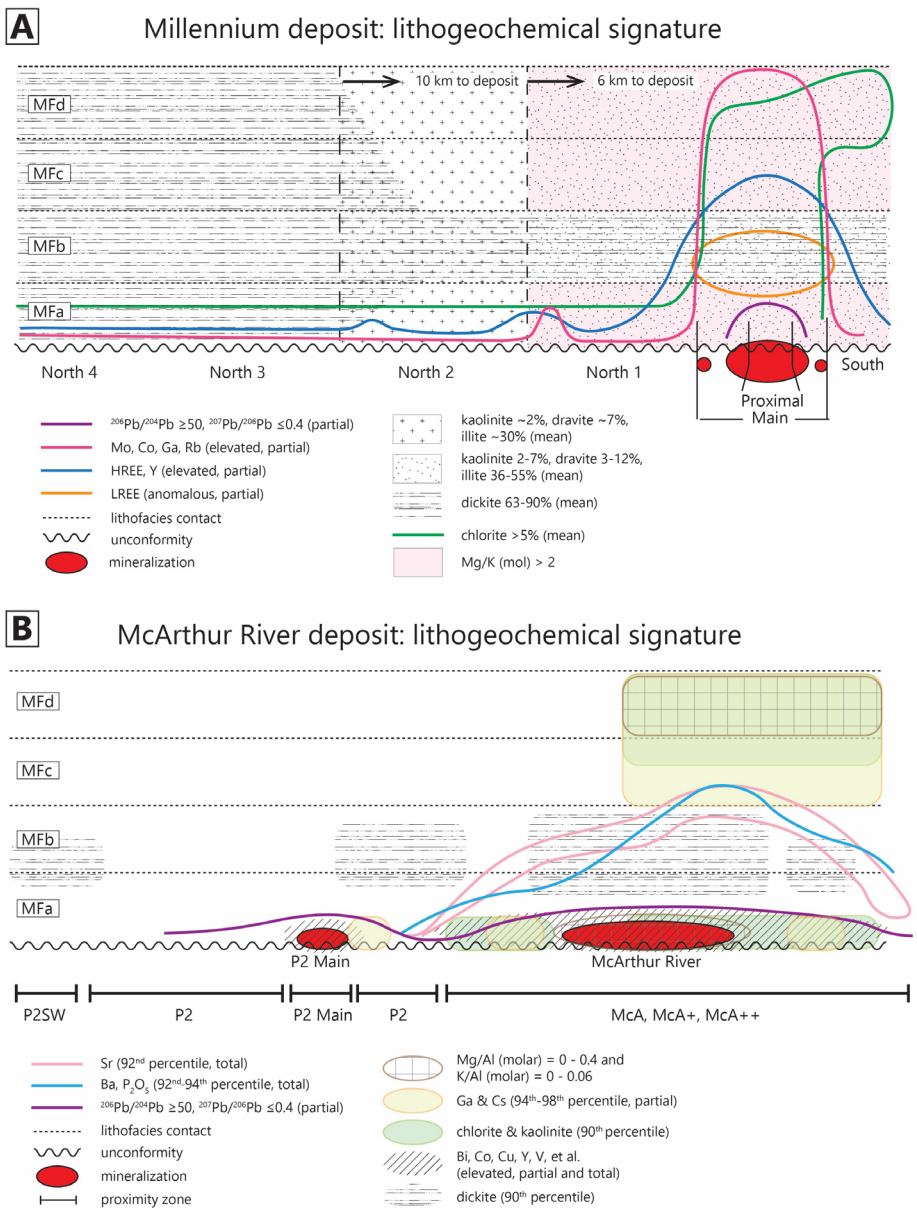

Figure 4.1: Stylized summary of select infrared-active mineral and trace element haloes that highlight the mineralized locations in the Millennium and McArthur River deposits. Not to scale. (**A**) Millennium deposit, looking east. The 10-km alteration envelope is defined by varying concentrations of dickite, kaolinite, and illite; the 6-km envelope is defined by Mg/K (mol) >2. Within 2 km of the deposit, chlorite, and trace elements Mo, Co, Ga, Rb, and REE highlight the deposit location. (**B**) McArthur River study area, looking northwest. Major and trace elements are grouped into restricted, proximal haloes that are indicators of mineralization (Bi, Co, Cu, Y, V, Pb isotopes), broader haloes that act as vectors toward the McArthur River deposit (Ba, Sr, Ga, Cs), and distal indicators for the general location of the deposit (Mg/K molar ratios representative of sudoite to kaolin).

APPENDIX A: LEVELING AND REFINEMENT OF LEGACY WHOLE ROCK GEOCHEMISTRY RESULTS FROM THE CAMECO ARCHIVAL DATABASE FOR USE IN THIS THESIS

A.1 INTRODUCTION

The whole rock geochemical data for this thesis was provided by Cameco Corporation in April 2015 as a contribution from their archival database (1984–2014) to the CMIC-Footprints project for researcher use. The selection and refinement for the Millennium and McArthur River study areas is described below, using exploratory data analysis techniques to ensure a robust, fully characterized dataset for investigation (e.g., Grunsky, 2010; Reimann and Filzmoser, 2000).

A.2 DATA SELECTION AND REFINEMENT

A.2.1 Millennium and McArthur River

For both study areas, the following was completed:

- **Lithofacies:** Only Manitou Falls Formation lithofacies were considered in the analyses; fanglomerate and any other lithology code results were removed.
    - The focus of the thesis was the distal alteration footprint in the Manitou Falls Formation sandstones. Because the fanglomerate lithofacies was not consistently present between deposits and was not part of the distal signature, it was removed for simplification.

- At the contact between lithofacies, samples were coded as a combination of those lithofacies if the transition was >1 m inside the interval measurement. For example, if the sample was collected at a from-to interval of 195–205 m, and the transition between MFd and MFc was at a depth of 200 m, the sample was re-coded as MFdc because the collection point included >1 m from either the MFd or MFc lithofacies.
    - These transition samples were not removed from the dataset and remained for frequency analysis, quantile-quantile (Q-Q) plots, scatter plots, downhole plots, etc.
    - If an analysis was specifically for the differentiation of results among lithofacies, these transition samples were not included to ensure that all data was confidently partitioned within one of the A–D lithofacies.

- **Robust data:** separate data files were created that contained only results that were at least three times the instrument detection limit per element, to ensure that all values were greater than any analytical noise. In all cases results removed are considered null values, not zeroes.
    - These data were used for the following analyses, described in Chapters 2 and 3:
        - Pathfinder element distributions.
        - 3D mapping (Geosoft® Target 4.5.5. for ArcGIS) and halo measurements.
        - Molar element ratios.

- Lead isotope ratios.
- Frequency analyses for percentile determination.

- For samples analyzed in 2007 and later, the detection limits as found on SRC's website for ICP-OES and ICP-MS, total and partial digestions, were used. This information is summarized in Table A.1.
- For samples analyzed prior to 2007, the lowest recorded value was considered the detection limit for that instrument, element, and time period. For most samples, this value was 0.1 ppm but could be as high as 0.2 ppm.
- Samples retained for analysis after the removal are as follows:
  - Millennium, partial digestion: <50% of results were retained for Be, Bi, Ho, Tb; <10% for Ag, Cd, Ge, Hg, Nb, Sb, Sc, Se, Ta, Te, W.
  - Millennium, total digestion: <60% of results were retained for Ag, Be, MnO, W, Zn; <10% for Bi, Cd, Cs.
  - McArthur River, partial digestion: <60% of results were retained for Be, Cu, Ho, Ni, Pb, Tb; <10% for Ag, Bi, Cd, Cs, Ge, Hg, Nb, Sb, Se, Sc, Ta, Te, W.
  - McArthur River, total digestion: 87–88% of results were retained for all elements with the exception of CaO, MnO, and Na_2O, for which <10% were retained.
- For shortwave infrared spectroscopy (SWIR) all samples with a signal to noise ratio of <10 were removed from the data analysis.

- **3D mapping:** All results were mapped with inverse distance weighting (linear) (IDW) algorithms, using 25-m cell projections, with Geosoft® Target for ArcGIS version 4.5.5 software.
    - Because results less than three times the instrument detection limit were null values, inverse distance weighting algorithms for the low end of these 3D projections are less accurate. However, the upper end of results (the 85th percentile or greater) was the focus of the pathfinder haloes.
    - Kriging was not utilized because the data is transformed as part of the kriging process. Visually, inverse distance weighting (IDW) results were nearly identical to kriged maps without the additional smoothing factor, and data results using IDW (ppm or %) were maintained without transformation.
    - Halo dimensions were measured within the Target program by placing the crosshairs on the maximum cells in length and width in plan view, and calculating the difference in UTM coordinates. Distances in the Z direction were similarly measured with elevation depth with a due west or east view. Because the cells are 25-m projections, all halo measurements are approximate.
- Cr (total digestion) was not utilized in any analyses for the legacy data.
    - Chromium levels prior to 2009 (Quirt, 1985; Rob Millar, pers. comm. 2015) were subject to contamination from grinding. This excluded a majority of the samples for both footprints.

For individual deposits, the following data refinement was completed:

A.2.2 Millennium deposit study area

- Drill collars were chosen by name: all had hole IDs with the prefix CX-.
- Analyzed samples had the sample type code of COMP_S (composite sandstone, collected systematically). All other sample type codes were removed from the sandstone data analysis.
    - Uranium content in COMP_B (composite basement, collected systematically) samples (total and partial digestion) were used solely to identify the approximate location of the main deposit body, determining the strike length of the Main Zone as described in Chapter 2.
- CX-051, -052, and -053, and associated wedges, were problematic. Results in these cores had numerous results at a single value that appeared to be a detection limit (e.g., Ag = 0.1) but that were significantly higher than the actual detection limit for several elements (Fig. A.1). These cores are also located in the Main and Proximal zones, which made the data appear artificially high near mineralization. It was suggested that ICP-OES and ICP-MS results were combined; however, this could not be proven. To eliminate any instrumental bias, results that were less than three times these quantized values were eliminated in these drill holes and wedges for the following elements: Ag, As, Bi, Co, Ge, Hg, Mo, Ni, Sb, Te (partial digestion); Ho, Nb, Mo, Sn, Ta, Tb, W (total digestion).
- Samples analyzed post-2006 had the lowest detection limits and highest levels of precision. For the data evaluation process described in Chapter 2, “jumps” in the

Q-Q plots were evidence of analyses that spanned generations of instrumentation with varying levels of detection and precision (Grunsky, 2010). Fortunately, data that is spatially related to the deposit in this study is at the elevated end of the sample population (usually the 85th percentile or higher), meaning that data artifacts attributed to instrumentation should be considered not relevant as they were at the low end of results.

A.2.3 McArthur River deposit study area

- Drill holes were chosen by name and location.
    - All drill holes were included with the prefix MAC- or MC-.
    - Nine drill holes with the prefix REA- and RL- were included as they were located within 400 m of the P2 trend, and were in areas associated with the McArthur River deposit.
    - Nine additional drill holes with the prefix REA- and RL- were included as P2 trend background, as they were situated at the southwest end of the P2 fault system and distal from all mineralization.
- All samples are of sample type code COMP_S (composite sandstone, collected systematically) or SPOT_S (spot sandstone, a targeted location), and sample lengths of 5 m or greater were included, in the interest of retaining as many results as possible for the large-scale characterization of the lithogeochemistry.
    - Sampling methods have changed over the years, and SPOT_S samples were shown to not have significant differences in U content from COMP_S samples for these sample lengths (Fig. A.2).

- No basement samples or other sample codes were used. Proximity zones were determined by U content in the sandstones only, as described in Chapter 3.

- Because the legacy data covered so many years of analysis, there was a significant amount of variation in detection limits and precision as instrumentation varied between elements, analyses, sample type, and year. These were carefully noted, and any anomalous data was verified to be attributed to instrument bias (Fig. A.3).
    - Nickel is shown as an example, as its clear distinction between instruments and sample type was useful in determining how unusual data distributions for other trace elements were attributed to instrument bias. Copper and Pb also gave data distribution patterns that were significantly different over time. In all data analysis, results were grouped into categories established by the population variations of Ni, Cu, and Pb to help determine if and how anomalous values were attributed to instrumentation.
    - All SPOT_S samples, regardless of year, were analyzed with ICP-MS determination methods, for both total and partial digestions.
    - All major elements, in all years, were analysed with ICP-OES determination methods.
    - COMP_S samples were analyzed with ICP-OES determination methods, with varying detection limits and precision levels through 2006. Post-2006, ICP-MS was used for COMP_S samples.
    - Fortunately, the final analyses were focussed on the elevated results (generally the 85th percentile or higher) for the evaluation of pathfinder

status with respect to deposit location. Therefore, the results with mixed detection limits and precision at the lower end of the data populations were considered either insignificant or not relevant to the analysis.

- Only the $^{207}Pb/^{206}Pb$ values and K/Al values decrease in proximity to mineralization. These results were not an issue with instrumentation, as the ^{207}Pb and ^{206}Pb results were all analysed with ICP-MS, and all major elements with ICP-OES exhibiting no significant differences in detection limits or precision.

REFERENCES

Grunsky, E. C. (2010). The interpretation of geochemical survey data. *Geochemistry: Exploration, Environment, Analysis*, *10*, 27–74. http://doi.org/10.1144/1467-7873/09-210

Quirt, D. H. (1985). Lithogeochemistry of the Athabasca Group: Summary of sandstone data. *In* Summary of Investigations 1985, Saskatchewan Geological Survey, Saskatchewan Energy and Mines, Miscellaneous Report 85-4, p. 128–132.

Reimann, C., & Filzmoser, P. (2000). Normal and lognormal data distribution in geochemistry: death of a myth. Consequences for the statistical treatment of geochemical and environmental data. *Environmental geology*, *39*(9), 1001–1014. http://doi.org/10.1007/s002549900081

FIGURES

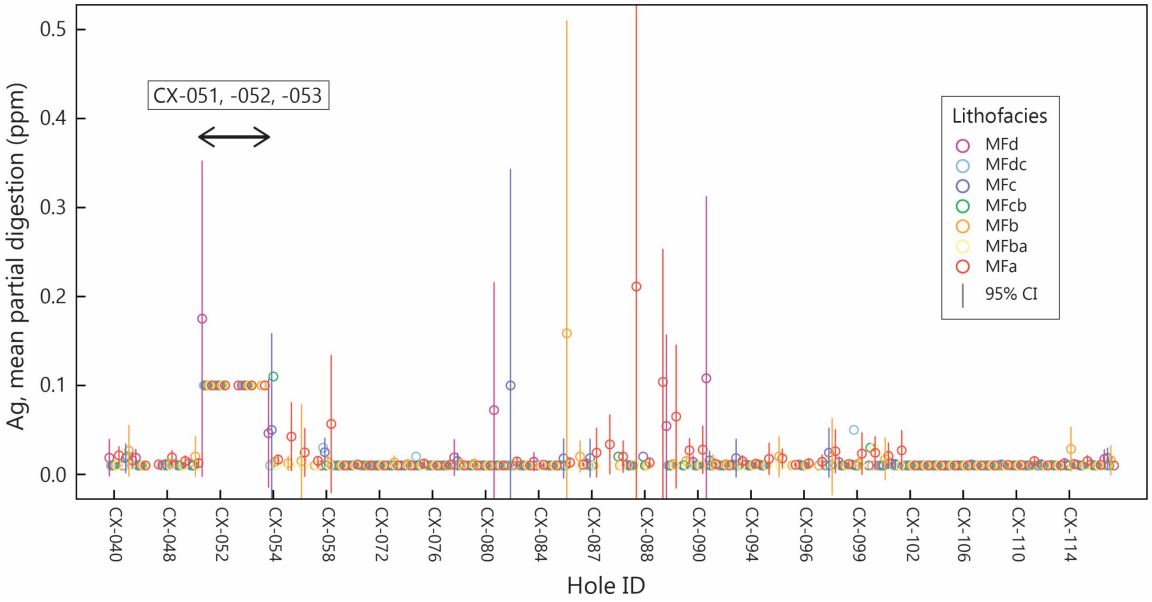

Figure A.1: CX-051, -052, -053 show instrumentation bias in the detection limit; for an unknown reason, several elements had a significantly higher value for its lowest readings that was also an exact number (i.e., 0.1000). Silver is shown as example. These samples were removed from analysis.

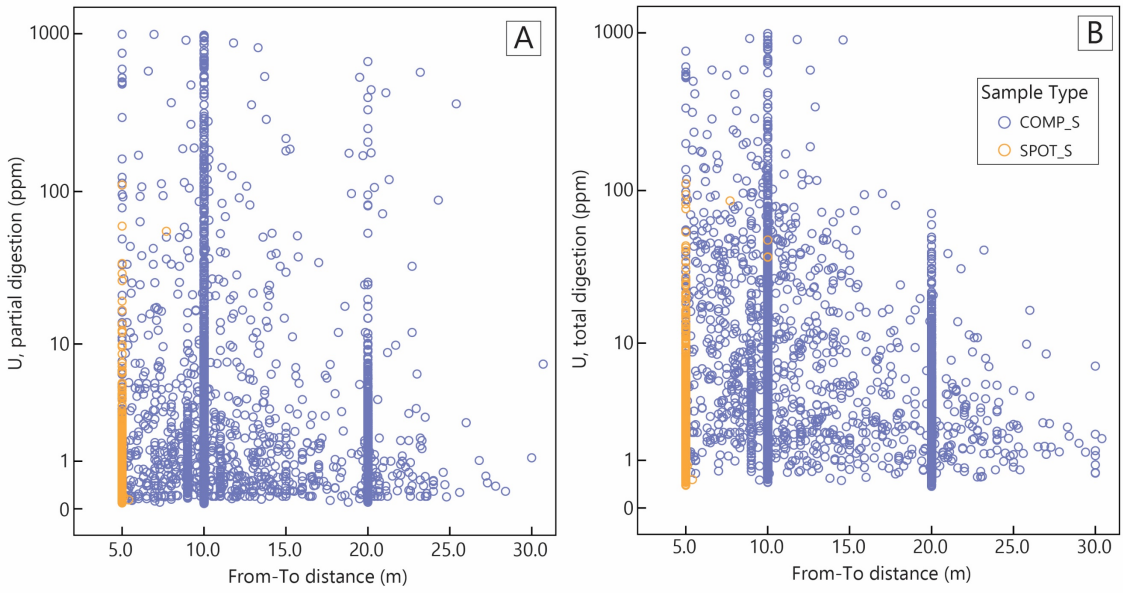

Figure A.2: For the McArthur River study area, all samples logged as either SPOT_S or COMP_S collected with a from-to interval of 5 metres or greater were retained for analysis, as there was no significant difference in U content. (**A**) Partial digestion samples. (**B**) Total digestion samples.

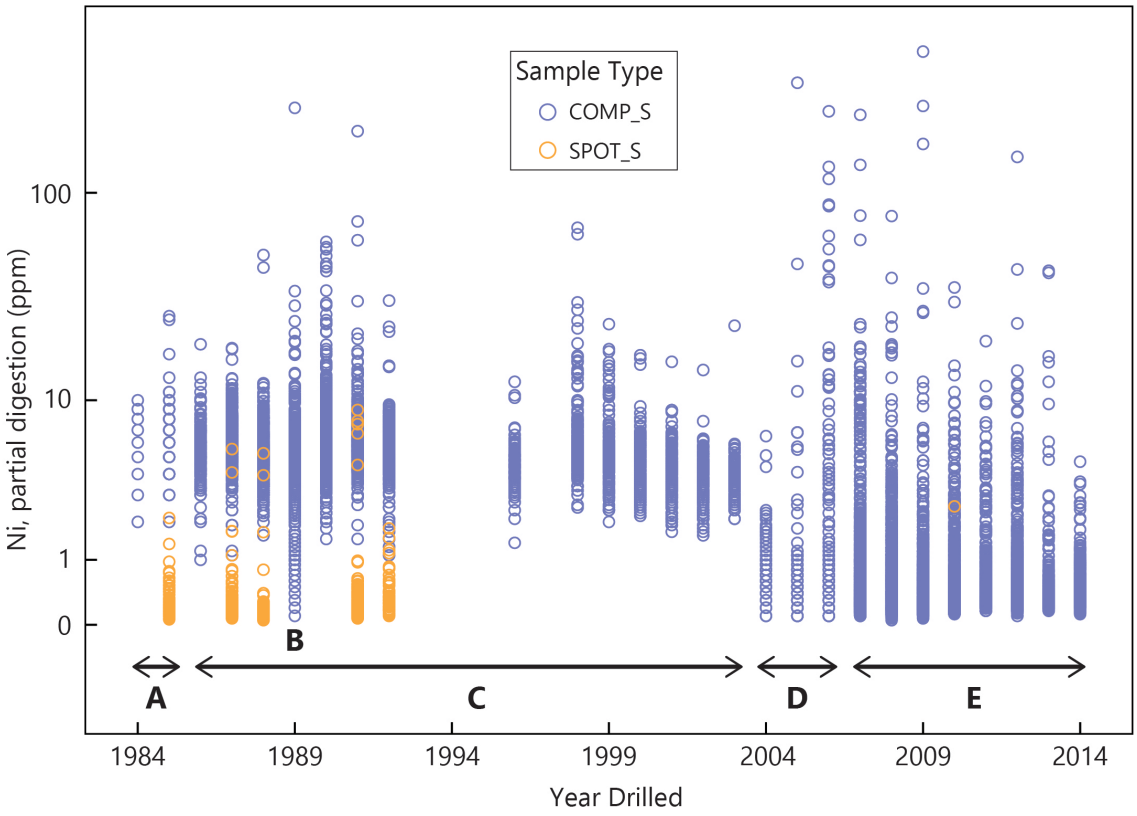

Figure A.3: Nickel analysis at the McArthur River study area over the years 1984–2014, shown here as an illustrative example of the variation in accuracy and precision over decades of analysis. COMP_S samples were analyzed with ICP-OES or ICP-MS dependent on year; SPOT_S samples were analyzed with ICP-MS only. (**A**) 1984–1985 contain ICP-OES results with the highest detection limits and lowest precision values. (**B**) Although the samples in 1989 are all logged as COMP_S, it appears that they may have been analyzed with ICP-MS, as the data distributions are similar to the SPOT_S samples. (**C**) ICP analyses from 1986–2003 had similar detection limits as the oldest results, but higher precision. (**D**) ICP analyses 2004–2006 had the lowest detection limits but similar precision as the previous years'. (**E**) From 2007, all analyses were analyzed with ICP-MS, which gave both the lowest detection limits and the highest precision.

Element	ICP-OES Total DL	Element	ICP-MS Total DL (ppm)	ICP-MS Partial DL (ppm)	Element	ICP-MS Total DL (ppm)	ICP-MS Partial DL (ppm)	Element	ICP-MS Total DL (ppm)	ICP-MS Partial DL (ppm)
TiO_2	0.001%	Ag	0.02	0.01	Hf	0.1	0.01	Sc	0.1	0.1
Al_2O_3	0.01%	As	na	0.01	Hg	na	0.01	Se	na	0.1
Fe_2O_3	0.01%	Be	0.1	0.01	Ho	0.02	0.01	Sm	0.1	0.01
MnO	0.001%	Bi	0.1	0.01	Mo	0.02	0.01	Sn	0.1	0.01
MgO	0.001%	Cd	0.1	0.01	Nb	0.1	0.01	Ta	0.1	0.01
CaO	0.01%	Cs	0.1	0.01	Nd	0.1	0.01	Tb	0.02	0.01
Na_2O	0.01%	Co	0.02	0.01	Ni	0.1	0.01	Te	na	0.01
K_2O	0.002%	Cu	0.1	0.01	Pb	0.02	0.02	Th	0.02	0.01
P_2O_5	0.002%	Dy	0.02	0.01	^{204}Pb	0.01	0.001	U	0.02	0.01
Ba	1 ppm	Er	0.02	0.01	^{206}Pb	0.02	0.02	V	0.1	0.1
Ce	0.1 ppm	Eu	0.02	0.01	^{207}Pb	0.02	0.02	W	0.1	0.1
La	1 ppm	Ga	0.1	0.01	^{208}Pb	0.02	0.02	Y	0.1	0.01
Li	1 ppm	Gd	0.1	0.01	Pr	0.1	0.01	Yb	0.02	0.01
Sr	1 ppm	Ge	na	0.01	Rb	0.1	0.01	Zn	1	0.1
Zr	1 ppm				Sb	na	0.01	Zr	na	0.01

Table A.1: Current analysis capabilities (ICP-MS1 sandstone exploration package) for partial (2-acid) and total (3-acid) digestion whole rock geochemistry methods as performed by Saskatchewan Research Council Geoanalytical Laboratories. ICP-OES = inductively coupled plasma optical emission spectrometry; ICP-MS = inductively coupled plasma mass spectrometry; DL = detection limit; na = not analyzed.

APPENDIX B: SHORTWAVE INFRARED SPECTROSCOPY (SWIR) OF THE MILLENNIUM AND McARTHUR RIVER URANIUM DEPOSITS: VECTORING POSSIBILITIES IN THE ATHABASCA BASIN SANDSTONES

B.1 INTRODUCTION

Unlike whole rock geochemistry, shortwave infrared (SWIR) is a type of spectral analysis performed directly on intact drill core. This type of analysis requires little to no preparation of the core, is quick, inexpensive, and is done *in situ* (Russell and Fraser, 1994; Percival et al., 2002). Cameco generously provided the archival SWIR data for both the Millennium and McArthur River deposits to the author. Results were not included in Chapter 2 in the interest of focussing on whole rock geochemical analyses, but the distribution patterns summarized herein help define the alteration footprint for the Millennium deposit. The results for McArthur River sandstones are included in Chapter 3, and are also briefly summarized here in comparison with the Millennium results to illustrate the differences between sandstone alteration relative to deposit styles.

B.2 METHODS

SWIR analysis was performed by Cameco using the PIMA II (prior to 2004) or ASD Terraspec instrument, both of which are portable infrared mineral analyzers, and MinSpec 4 software (Zaluski, pers. comm. 2016). The instrument is used to scan intact core, and the resultant spectra analyzed to match one of five profiles: kaolinite, dickite, illite, dravite, and chlorite. Content is given in percent, recalculated to account for the clay-type minerals identified by the instrument (i.e., 100% clay) within the scanned area. Results

for spectra that do not match any of the given profiles are returned as 0%. The volume or concentration of those minerals as part of the total bulk sample is not given. Only results for the sandstones are included in this analysis. Samples with a signal to noise ratio of less than 10 were removed to improve the robustness of results.

B.3 RESULTS

At the Millennium deposit, the SWIR results illustrate the presence of a 10-km alteration envelope and a 6-km envelope, whereas at the McArthur River deposit the mineral expressions are defined in a more generalized relation to the deposit location over a span of several kilometres. All five of the clay-type minerals are present to some degree throughout both study areas, so spectra are examined in a large-scale overview (100s of metres to kilometres) to summarize their expressions in spatial relation to mineralization. Figure B.1 summarizes the mean data as bar graphs with respect to lithofacies and proximity zone from data presented in Tables B.1 and B.2. Figures B.2 and B.3 show the three-dimensional expression of each mineral at both locations.

B.3.1 Millennium deposit

The SWIR spectra illustrate the limits of two clay alteration envelopes; a larger one covering approximately half the study area, extending 10 km north of the deposit, and a slightly smaller one extending approximately 6 km north of the deposit (Fig. B.1a). Outside the 10-km envelope, dickite is the dominant mineral, followed by illite. The three other minerals are present at <1% on average (Table B.1). Inside the 10-km envelope, dickite remains the dominant mineral but concentrations decrease slightly; illite concentrations remain similar; and dravite, kaolinite, and chlorite concentrations increase significantly.

Inside the 6-km envelope, dickite is no longer the dominant mineral in the MFd, MFc, or MFa lithofacies, but remains at 63–71% within the MFb. In 3D space, the deposit location at depth is identified by the chlorite distribution at 5% or greater in MFd–MFb. The 6-km envelope is best defined where the dickite concentration remains high within the MFb and drops in the remaining lithofacies, and all other minerals are present in elevated concentrations in the MFd–MFc (Fig. B.2).

Individually, the minerals can be summarized as such:

- The concentration of dickite is highest within the MFb at all locations within the footprint, and is the dominant mineral for background/distal locations in the MFa, MFc, and MFd lithofacies.
- Dravite and kaolinite are present at 10% and greater in the upper lithofacies inside the 10-km envelope.
- Illite is present at 75% and greater in the upper lithofacies inside the 6-km envelope.
- Chlorite highlights a 2 km strike directly above the deposit in the MFd, MFc, and MFb lithofacies at 5% and greater.

Table B.1 summarizes the mean data for each mineral per lithofacies and proximity zone.

B.3.2 McArthur River deposit

The SWIR results at the McArthur River study area also emphasize the locations associated with the highest levels of mineralization (Fig. B.1b). Dickite is the dominant mineral in the MFc–MFb of the hanging wall background, and in the MFa associated with the deposit; elsewhere the dominant mineral is illite. Kaolinite, dravite, and chlorite are

present at less than 2% on average in both the hanging wall background and P2 background cores. Kaolinite and dravite increase significantly in the areas with weak to low mineralization, and remain elevated throughout the P2 trend. Chlorite values remain less than 2% on average until associated with the P2 Main deposit in MFa, where it increases significantly, as well as in the McA, McA+, and McA++ cores in the MFd, MFc, and MFa (Table B.2). In 3D space, dickite is present in high concentrations in the MFa–MFb above the McArthur River deposit. The 90th percentiles of kaolinite and chlorite are observed in the upper lithofacies in the McA, McA+, and McA++ areas of the study footprint (Fig. B.3). The 90th percentile of illite (100%) is mainly in the centre of the footprint, not directly associated with major mineralization, from the unconformity to surface. The 90th percentile of dravite (69%) shows no spatial association with either the P2 Main or McArthur River deposit locations and is present in all lithofacies.

Individually, the minerals' 90th percentile distributions can be summarized as such:

- Dickite highlights the McArthur River deposit site in the lower lithofacies.
- Illite is the dominant mineral throughout the study footprint, and is generally higher in the background (HW, P2SW), P2, and P2 Main locations.
- Kaolinite and chlorite highlight the McA, McA+, and McA++ zones in the MFd and MFc.
- Dravite is present in high concentrations in clusters throughout the central footprint and does not exhibit any spatial association with mineralization.

Table B.2 summarizes the mean data for each mineral per lithofacies and proximity zone.

B.4 DISCUSSION

Unconformity-related U deposit formation commonly results in alteration haloes due to fluid-rock interaction; however, the alteration haloes at barren and mineralized locations can be similar (Alexandre et al., 2009; Cloutier et al., 2010). At both the Millennium and McArthur River deposits, the clay-type mineral haloes outline the hydrothermal footprint around the deposits. The assemblage of five of these clay-type minerals (dickite, kaolinite, illite, chlorite, and dravite) in varying concentrations define areas of the alteration footprint from background to mineralized (Fig. B.1); the enrichment of individual minerals can further serve to highlight the deposit locations (Figs B.2–B.3).

At Millennium, the predominance of dickite in all lithofacies outside the 10-km envelope, and only within the MFb lithofacies closer to the deposit, illustrates the transition between diagenetic (dickite) and hydrothermal alteration haloes at Millennium (Fig. B.2). At McArthur River, dickite is present at the 90^{th} percentile level above the deposit; however, this is likely due to its association with quartz cementation present at McArthur River, which often results in clay minerals being shielded and preserved from breakdown by subsequent hydrothermal events (Fig. B.3; McGill et al., 1993; Ng et al., 2013).

Alkali-deficient dravite and chlorite are often spatially associated with URU deposits, and are interpreted to have their alkali deficient signatures and Mg-enrichment due to interaction with reduced basement fluids (Fayek and Kyser, 1997; Jefferson et al., 2007; de Veslud et al., 2009). At both locations, in the sandstones, dravite acts as an indicator rather than a vector to mineralization, as it is present in high concentrations within several kilometres of mineralization but does not exhibit any change in intensity proximal

to mineralization (Figs B.2–B.3). Alternatively, chlorite is a vector at both deposits. At Millennium, it is present at 5% or greater in all four lithofacies in greater concentrations above the deposit than anywhere else in the footprint (Fig. B.2). At McArthur River, it is present in levels of 40% and greater at the unconformity with the P2 Main deposit, as well as in smaller, localized areas north of the McArthur River deposit (Fig. B.3). More importantly, it and kaolinite are present in high concentrations (90^{th} percentiles) in the MFd–MFc above and to the north of the McArthur River deposit, but does not have any spatial association in the upper lithofacies above the P2 Main, thus, discriminates between economic and subeconomic areas of mineralization at shallower depths (Fig. B.3).

Illite and kaolinite are not spatially associated with mineralization at the Millennium deposit and only define the 6-km extent of the alteration footprint (Fig. B.2). Illite is interpreted to have formed via K-metasomatism associated with early stage, basinal brine-derived fluid-rock interaction (Hoeve and Quirt, 1984; Cloutier et al., 2009). Similarly, at McArthur River, illite is elevated to dominant in the barren, hanging wall background samples and the middle and southern portions of the deposit footprint (Fig. B.3). Kaolinite is spatially associated with mineralization at McArthur River, as it appears in the same location as chlorite, in the MFd 450–560 m above and ~7 km to the northeast of the deposit (Fig. B.3). Kaolinite and chlorite are also coincident with unique molar element ratio and trace element enrichments (see Chapter 3) and are considered pathfinders, likely having formed from syn- to post-ore hydrothermal fluids.

B.5 CONCLUSIONS

Examining the clay-type minerals via shortwave infrared spectroscopy at the Millennium and McArthur River deposits leads us to the following conclusions:

1. **Chlorite is the best pathfinder mineral among SWIR results for both the Millennium and McArthur River deposits.**

Chlorite (Al-Mg-sudoite) has long been associated with URU deposits, due to its Mg content and close spatial relationship to mineralization in alteration haloes. Chlorite as detected by SWIR appears either as a pathfinder associated with faulting or fractures leading to the deposit (Millennium), or as a general location marker in distal sandstones (McArthur River), unlike dravite, which is also rich in Mg but has no spatial relationship to mineralization at either location.

2. **The SWIR results can highlight the transition between diagenetic and hydrothermal alteration processes, or a significant change in the sandstones representative of stages and/or fluid sources of alteration.**

Dickite is representative of background burial diagenesis prior to ore-forming hydrothermal processes. Other significant changes are the increase of K-related alteration (illite), which is often representative of basinal fluids, and the increase of Mg-related alteration (chlorite and dravite), which is often representative of basement fluids.

REFERENCES

Alexandre, P., Kyser, K., & Jiricka, D. (2009). Critical geochemical and mineralogical factors for the formation of unconformity-related uranium deposits: comparison between barren and mineralized systems in the Athabasca Basin, Canada. *Economic Geology*, *104*(3), 413–435. http://doi.org/10.2113/gsecongeo.104.3.413

Cloutier, J., Kyser, K., Olivo, G. R., & Alexandre, P. (2010). Contrasting patterns of alteration at the Wheeler River area, Athabasca basin, Saskatchewan, Canada: insights into the apparently uranium-barren zone K alteration system. *Economic Geology*, *105*(2), 303–324. http://doi.org/10.2113/gsecongeo.105.2.303

Cloutier, J., Kyser, K., Olivo, G. R., Alexandre, P., & Halaburda, J. (2009). The Millennium uranium deposit, Athabasca Basin, Saskatchewan, Canada: an atypical basement-hosted unconformity-related uranium deposit. *Economic Geology*, *104*(6), 815–840. http://doi.org/10.2113/gsecongeo.104.6.815

De Veslud, C. L. C., Cuney, M., Lorilleux, G., Royer, J. J., & Jébrak, M. (2009). 3D modeling of uranium-bearing solution-collapse breccias in Proterozoic sandstones (Athabasca Basin, Canada)—Metallogenic interpretations. *Computers & Geosciences*, *35*(1), 92–107. http://doi.org/10.1016/j.cageo.2007.09.008

Fayek, M. & Kyser, T. (1997). Characterization of multiple fluid-flow events and rare-earth-element mobility associated with formation of unconformity-type uranium deposits in the Athabasca Basin, Saskatchewan. *The Canadian Mineralogist, 35,* 627–658.

Hoeve, J., & Quirt, D. H. (1984). Mineralization and host rock alteration in relation to clay mineral diagenesis and evolution of the Middle-Proterozoic, Athabasca Basin, northern Saskatchewan, Canada. Saskatchewan Research Council, SRC Technical Report 187, 202 p.

Jefferson, C. W., Thomas, T. J., Gandhi, S. S., Ramaekers, P., Delaney, G., Brisbin, D., Cutts, C., Portella, P., & Olson, R.A. (2007). Unconformity-associated uranium deposits of the Athabasca Basin, Saskatchewan and Alberta. *In* Jefferson C. W. & Delaney, G. (eds.), *EXTECH IV: Geology and Uranium EXploration TECHnology of the Proterozoic Athabasca Basin, Saskatchewan and Alberta*: Geological Survey of Canada, Bulletin 588, 23–67.

McGill, B. D., Marlatt, J. L., Matthews, R. B., Sopuck, V. J., Homeniuk, L. A., & Hubregtse, J. J. (1993). The P2 north uranium deposit, Saskatchewan, Canada. *Exploration and Mining Geology*, *2*(4), 321–331.

Ng, R., Alexandre, P., & Kyser, K. (2013). Mineralogical and geochemical evolution of the unconformity-related McArthur River Zone 4 orebody in the Athabasca Basin, Canada: implications of a silicified zone. *Economic Geology*, *108*(7), 1657–1689. http://doi.org/10.2113/econgeo.108.7.1657

Percival, J. B., Wasyliuk, K., Reif, T., Bernier, S., Drever, G., & Perkins, C. T. (2002). Mineralogical aspects of three drill cores along the McArthur River transect using a portable infrared spectrometer. *In* Summary of Investigations 2002, Volume 2, Saskatchewan Geological Survey, Saskatchewan Industry Resources, Miscellaneous Report D-14, 15 p.

Russell, J. D. & Fraser, A. R. (1994). Infrared methods. *In* Wilson, M. J. (ed.), *Clay Mineralogy: Spectroscopic and Chemical Determinative Methods* (pp. 11–67). Springer Netherlands. ISBN: 978-94-010-4313-7

FIGURES

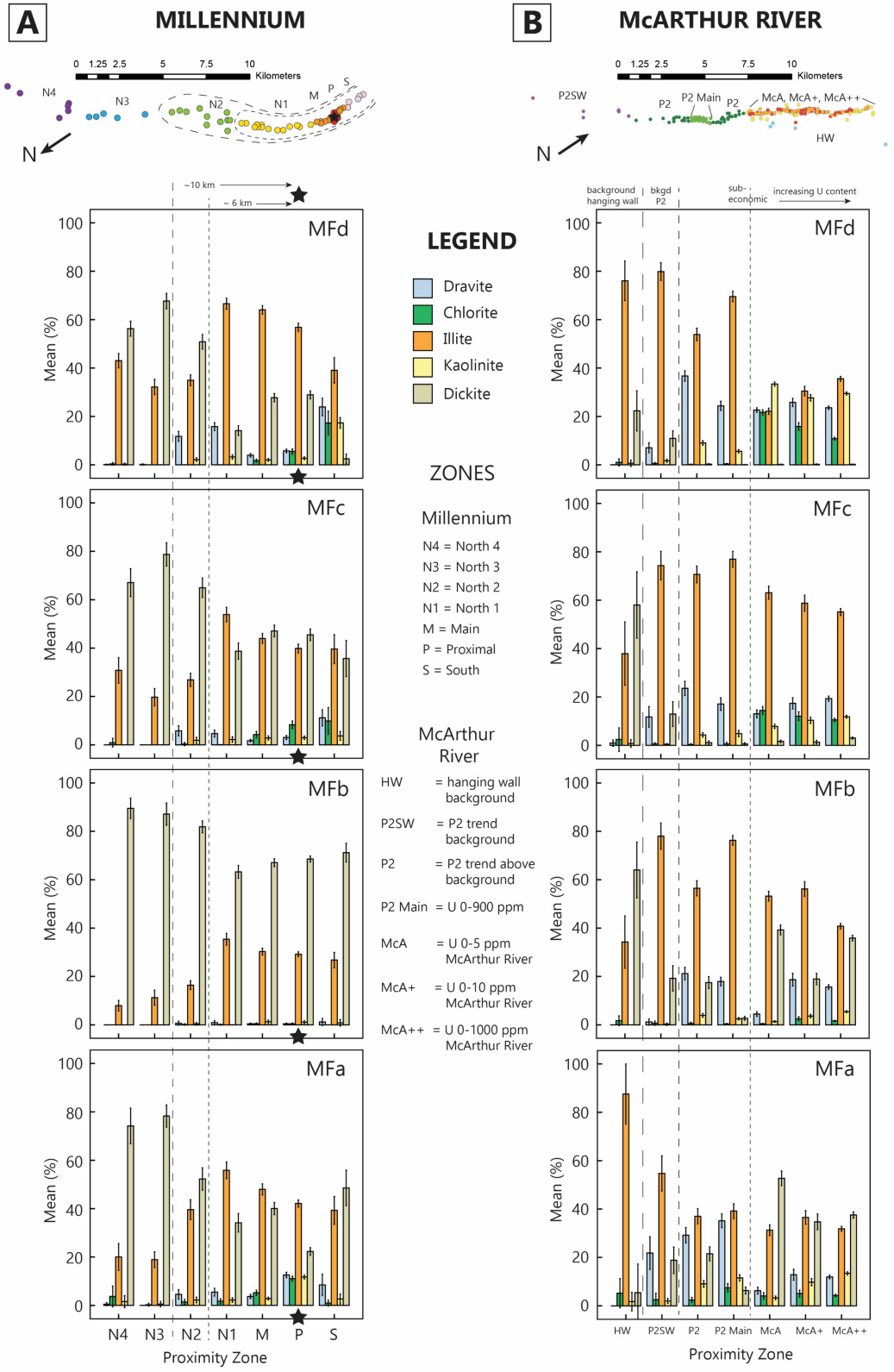
A
MILLENNIUM
0 1.25 2.5 5 7.5 10
Kilometers
N4
N3
N2
N1
M
P
S
N
~10 km
~ 6 km
MFd
MFc
MFb
MFa
Mean (%)
N4 N3 N2 N1 M P S
Proximity Zone
LEGEND
Dravite
Chlorite
Illite
Kaolinite
Dickite
ZONES
Millennium
N4 = North 4
N3 = North 3
N2 = North 2
N1 = North 1
M = Main
P = Proximal
S = South
McArthur River
HW = hanging wall background
P2SW = P2 trend background
P2 = P2 trend above background
P2 Main = U 0-900 ppm
McA = U 0-5 ppm McArthur River
McA+ = U 0-10 ppm McArthur River
McA++ = U 0-1000 ppm McArthur River
B
McARTHUR RIVER
0 1.25 2.5 5 7.5 10
Kilometers
P2SW
P2
P2 Main
P2
McA, McA+, McA++
HW
N
background hanging wall
bkgd P2
sub-economic
increasing U content
MFd
MFc
MFb
MFa
Mean (%)
HW P2SW P2 P2 Main McA McA+ McA++
Proximity Zone

Figure B.1: Mean values for infrared-active minerals detected by shortwave infrared spectroscopy (SWIR) at each study footprint; error bars represent a 95% confidence interval. In both locations, U content increases to the right side of the bar graphs. Data for these plots is presented in Tables B.1 (Millennium) and B.2 (McArthur River). (**A**) Millennium deposit. Location of mineralization depicted by star. The major shift toward mineralization, 10 km north of the deposit, is seen in the marked increase in dravite in the MFa, MFc, and MFd lithofacies; the 6-km envelope is marked by a significant shift in dickite-illite ratios in the MFb. (**B**) McArthur River deposit. Illite concentrations decrease with proximity to the deposit, whereas chlorite and kaolinite increase. Locations of mineralization are P2 Main (subeconomic) and the ~7-km strike surrounding the McArthur River deposit, noted as McA, McA+, and McA++ (economic).

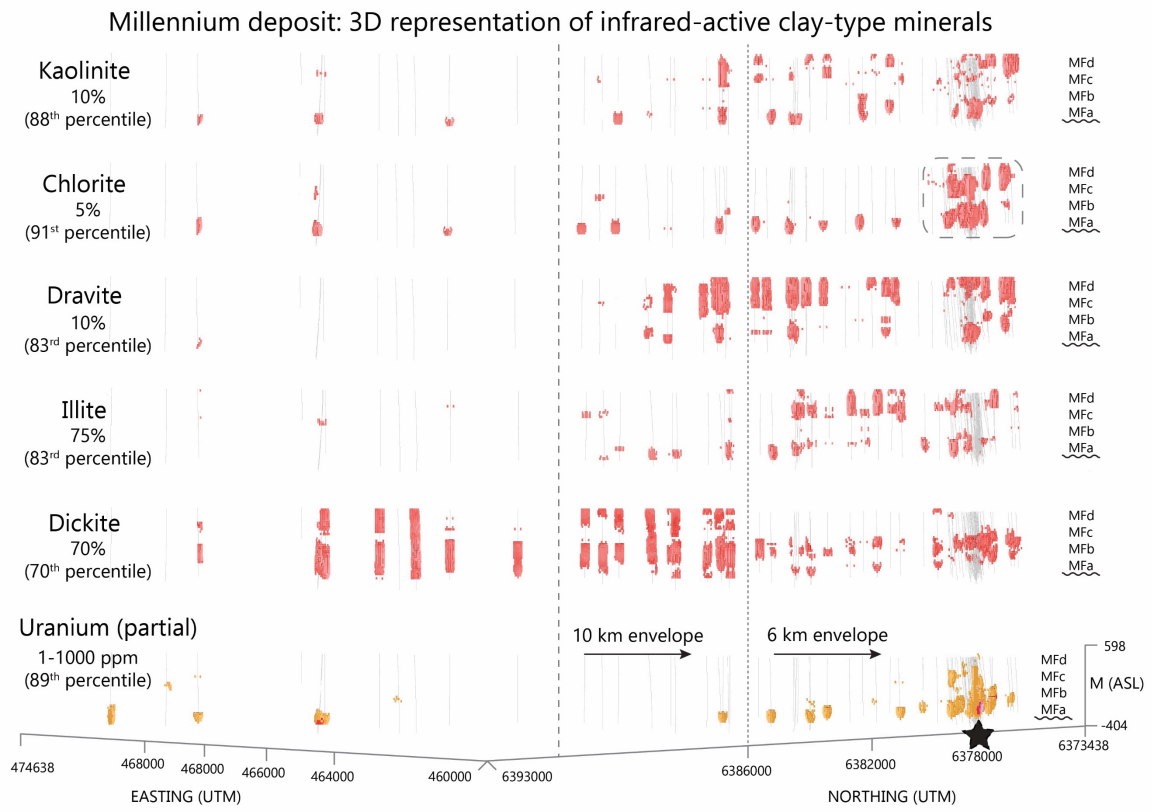

Figure B.2: 3D view of the infrared-active minerals detected by SWIR on drill core samples *in situ* at the Millennium deposit, looking east. Vertical exaggeration is 2X. Chlorite acts as a pathfinder to mineralization (dotted rectangle), whereas the others depict alteration halo envelopes at 6 km and 10 km (dotted vertical lines) north of the deposit, as marked by the star. Mean data shown in Figure B.1, and in Table B.1.

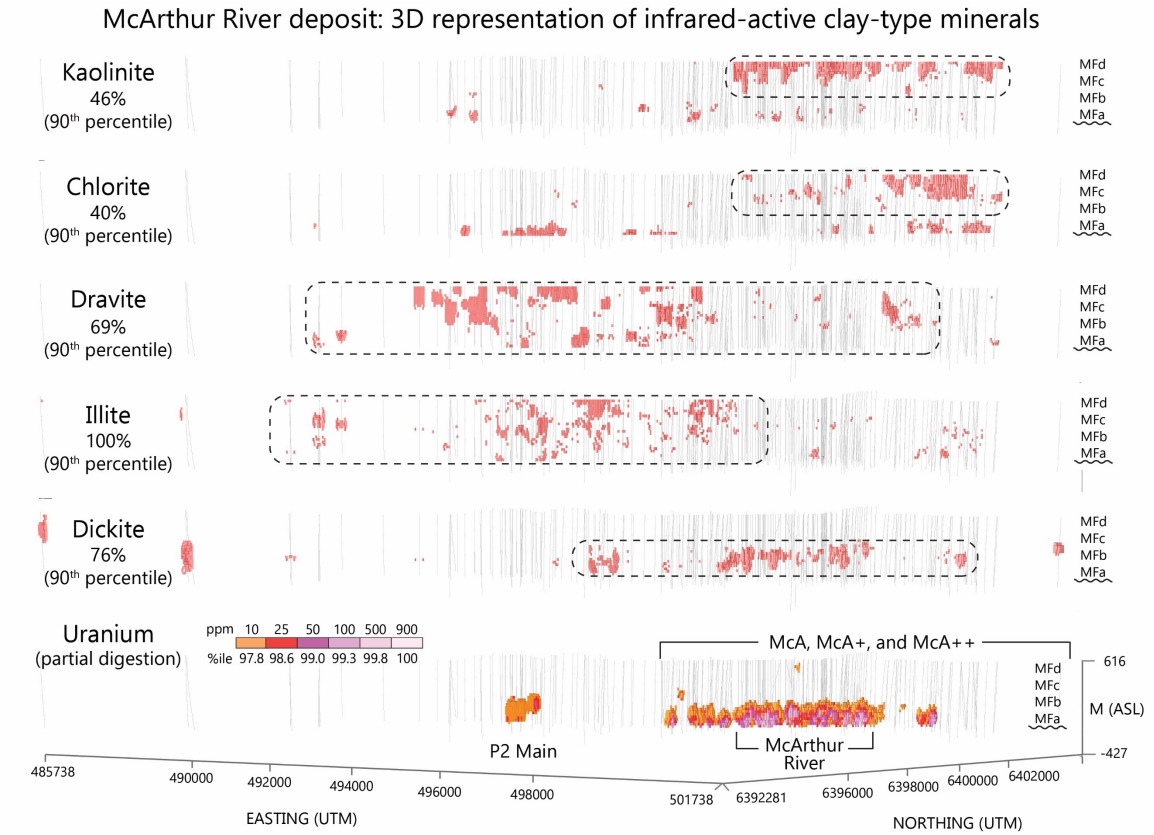

Figure B.3: 3D view of the infrared-active minerals detected by SWIR on drill core samples *in situ* at the McArthur River deposit, looking northwest. Vertical exaggeration is 2X. Chlorite and kaolinite act as a pathfinder to mineralization in the upper lithofacies, whereas dickite is likely representative of intense silicification seen at the McArthur River deposit. Dravite and illite do not exhibit a spatial relationship to mineralization. Mean data shown in Figure B.1, and in Table B.2.

TABLE B.1: Mean values of clay-type minerals in scanned core samples in the Millennium study area (~ 20 km)

Proximity Zone	Lithofacies	Dickite Mean %	*95% CI*	Kaolinite Mean %	*95% CI*	Illite Mean %	*95% CI*	Dravite Mean %	*95% CI*	Chlorite Mean %	*95% CI*
North 4	**All**	**67.7**	***±2.6***	**0.3**	***±0.4***	**30.2**	***±2.3***	**0.1**	***±0.1***	**0.9**	***±0.7***
	MFd	56.3	*±3.1*	0.2	*±0.4*	43.0	*±3.0*	0.1	*±0.2*	0.4	*±0.6*
	MFc	67.1	*±5.8*	--	*na*	30.8	*±5.3*	--	*na*	0.9	*±1.8*
	MFb	89.5	*±4.2*	--	*na*	7.9	*±2.2*	--	*na*	--	*na*
	MFa	74.2	*±7.4*	1.6	*±2.5*	20.0	*±2.8*	0.5	*±0.6*	3.7	*±4.3*
North 3	**All**	**75.0**	***±2.2***	**0.1**	***±0.3***	**23.7**	***±2.0***	**0.1**	***±0.1***	**0.1**	***±0.1***
	MFd	67.7	*±3.2*	--	*na*	32.2	*±3.2*	0.1	*±0.3*	--	*na*
	MFc	78.7	*±4.8*	--	*na*	19.7	*±3.6*	--	*na*	--	*na*
	MFb	87.1	*±4.6*	--	*na*	11.2	*±3.1*	--	*na*	--	*na*
	MFa	78.3	*±4.6*	0.5	*±1.1*	18.9	*±1.6*	--	*na*	0.3	*±0.6*
10 km envelope											
North 2	**All**	**59.6**	***±2.0***	**1.8**	***±0.5***	**30.9**	***±1.5***	**7.0**	***±1.0***	**0.5**	***±0.3***
	MFd	50.8	*±3.0*	2.2	*±0.7*	34.9	*±2.3*	11.8	*±2.0*	0.0	*na*
	MFc	64.9	*±4.0*	1.8	*±1.3*	26.8	*±2.8*	5.8	*±2.1*	0.3	*±0.7*
	MFb	81.9	*±2.4*	0.4	*±0.6*	16.4	*±1.9*	0.7	*±0.8*	0.2	*±0.3*
	MFa	52.3	*±4.7*	2.2	*±1.2*	39.6	*±4.1*	4.5	*±1.0*	1.4	*±1.1*
6 km envelope											
North 1	**All**	**33.7**	***±1.7***	**2.2**	***±0.5***	**55.3**	***±1.5***	**8.0**	***±0.8***	**0.4**	***±0.2***
	MFd	14.1	*±2.0*	3.2	*±0.9*	66.6	*±2.3*	15.8	*±1.7*	0.0	*±0.0*
	MFc	38.7	*±3.3*	2.2	*±1.2*	53.9	*±3.0*	4.7	*±1.4*	0.0	*±0.1*
	MFb	63.3	*±2.7*	0.0	*±0.1*	35.4	*±2.5*	0.9	*±0.9*	0.1	*±0.2*
	MFa	34.2	*±3.8*	2.2	*±0.9*	55.9	*±3.5*	5.5	*±1.6*	0.7	*±1.0*
Main	**All**	**43.5**	***±1.2***	**2.2**	***±0.3***	**48.3**	***±1.1***	**2.7**	***±0.3***	**2.9**	***±0.4***
	MFd	27.7	*±1.7*	2.0	*±0.6*	64.0	*±1.8*	3.9	*±0.7*	1.7	*±0.6*
	MFc	47.1	*±2.4*	2.8	*±0.9*	44.0	*±2.0*	1.7	*±0.5*	4.2	*±1.3*
	MFb	67.1	*±1.6*	1.3	*±0.7*	30.3	*±1.4*	0.4	*±0.3*	0.5	*±0.4*
	MFa	40.0	*±2.5*	2.8	*±0.6*	50.0	*±2.3*	3.7	*±0.9*	5.2	*±1.1*
Proximal	**All**	**36.9**	***±1.0***	**6.1**	***±0.4***	**42.6**	***±0.9***	**7.0**	***±0.5***	**7.2**	***±0.5***
	MFd	28.9	*±1.7*	2.7	*±0.6*	56.8	*±1.7*	5.7	*±0.8*	5.5	*±1.0*
	MFc	45.5	*±2.4*	2.9	*±0.7*	39.8	*±1.9*	3.0	*±0.8*	8.3	*±1.5*
	MFb	68.5	*±1.3*	1.1	*±0.6*	29.2	*±1.0*	0.5	*±0.3*	0.5	*±0.3*
	MFa	22.3	*±1.6*	11.7	*±0.8*	42.1	*±1.5*	12.6	*±1.1*	11.1	*±1.0*
South	**All**	**36.3**	***±3.7***	**7.2**	***±1.2***	**36.3**	***±2.6***	**12.3**	***±1.9***	**7.8**	***±2.1***
	MFd	2.5	*±2.0*	17.3	*±2.2*	39.0	*±5.2*	23.9	*±3.6*	17.2	*±4.9*
	MFc	35.7	*±7.5*	3.7	*±1.8*	39.6	*±6.0*	11.2	*±3.4*	9.9	*±6.6*
	MFb	71.2	*±3.9*	0.8	*±1.4*	26.8	*±3.2*	1.2	*±1.5*	--	*na*
	MFa	48.6	*±7.3*	2.7	*±2.1*	39.3	*±5.7*	8.5	*±4.4*	1.0	*±1.2*

TABLE B.2: Mean values of clay-type minerals in scanned core samples in the McArthur River study area (~ 20 km)

Proximity Zone	Lithofacies	Dickite Mean %	*95% CI*	Kaolinite Mean %	*95% CI*	Illite Mean %	*95% CI*	Dravite Mean %	*95% CI*	Chlorite Mean %	*95% CI*
HW	**All**	**40.2**	***±6.6***	**0.6**	***±0.7***	**57.1**	***±6.4***	**0.2**	***±0.3***	**1.9**	***±1.4***
	MFd	22.3	*±8.3*	0.7	*±1.3*	76.0	*±8.2*	--	*na*	1.0	*±1.5*
hanging wall	MFc	58.0	*±13.7*	0.8	*±1.6*	37.9	*±13.1*	0.9	*±1.3*	2.4	*±4.9*
background	MFb	64.0	*±11.5*	--	*na*	34.3	*±10.8*	--	*na*	1.7	*±2.0*
	MFa	5.4	*±11.8*	1.8	*±3.8*	87.6	*±12.4*	--	*na*	5.2	*±6.0*
P2SW	**All**	**14.6**	***±2.2***	**1.2**	***±0.4***	**74.1**	***±2.6***	**9.1**	***±0.9***	**0.9**	***±0.5***
	MFd	10.9	*±3.2*	1.6	*±0.7*	79.9	*±3.7*	7.0	*±1.0*	0.6	*±0.4*
P2 trend	MFc	12.9	*±5.1*	0.4	*±0.3*	74.3	*±5.9*	11.7	*±4.3*	0.6	*±0.5*
background	MFb	19.2	*±5.2*	0.3	*±0.5*	78.0	*±5.4*	1.2	*±1.3*	0.7	*±0.9*
	MFa	18.8	*±5.5*	2.0	*±1.0*	54.8	*±7.3*	21.8	*±6.8*	2.6	*±2.6*
above background											
P2	**All**	**9.2**	***±1.0***	**7.0**	***±0.5***	**53.9**	***±1.6***	**28.9**	***±1.3***	**0.8**	***±0.1***
	MFd	0.2	*±0.2*	9.0	*±1.0*	53.9	*±2.6*	36.7	*±2.2*	0.1	*±0.1*
no to weak mineralization	MFc	1.1	*±0.8*	4.3	*±0.9*	70.7	*±3.5*	23.5	*±2.9*	0.4	*±0.3*
	MFb	17.5	*±2.5*	3.9	*±0.8*	56.5	*±3.1*	21.2	*±2.6*	0.6	*±0.5*
	MFa	21.5	*±2.9*	9.1	*±1.4*	37.0	*±3.1*	29.2	*±3.2*	2.4	*±1.1*
includes mineralization											
P2 Main	**All**	**2.2**	***±0.4***	**5.7**	***±0.4***	**66.5**	***±1.3***	**23.6**	***±1.1***	**1.8**	***±0.4***
	MFd	0.0	*±0.0*	5.6	*±0.7*	69.6	*±2.2*	24.4	*±1.9*	0.4	*±0.2*
subeconomic	MFc	0.6	*±0.5*	4.8	*±1.3*	76.9	*±3.3*	17.1	*±2.6*	0.6	*±0.7*
	MFb	2.7	*±0.8*	2.5	*±0.5*	76.3	*±2.0*	17.9	*±1.8*	0.4	*±0.2*
	MFa	6.3	*±1.4*	11.5	*±1.3*	39.2	*±3.0*	35.2	*±2.9*	7.5	*±1.7*
McA	**All**	**16.7**	***±0.9***	**17.1**	***±0.6***	**38.2**	***±1.1***	**14.3**	***±0.6***	**12.9**	***±0.7***
	MFd	0.1	*±0.1*	33.4	*±0.9*	22.1	*±1.3*	22.6	*±1.0*	21.7	*±1.1*
U 0-5 ppm	MFc	1.6	*±0.5*	7.8	*±0.9*	63.1	*±2.7*	13.0	*±1.6*	14.4	*±1.6*
McArthur River area	MFb	39.2	*±2.0*	1.4	*±0.4*	53.2	*±2.0*	4.5	*±1.0*	0.4	*±0.2*
	MFa	52.7	*±3.0*	3.3	*±0.8*	31.2	*±2.2*	6.3	*±1.4*	4.1	*±1.3*
McA+	**All**	**11.6**	***±1.0***	**15.3**	***±0.8***	**43.0**	***±1.4***	**20.0**	***±1.1***	**10.0**	***±0.8***
	MFd	0.2	*±0.2*	27.7	*±1.3*	30.5	*±2.0*	25.8	*±1.7*	15.8	*±1.6*
U 0-10 ppm	MFc	1.3	*±0.7*	10.3	*±1.3*	58.7	*±3.4*	17.4	*±2.3*	12.1	*±1.8*
McArthur River area	MFb	19.0	*±2.3*	3.6	*±0.7*	56.2	*±3.1*	18.7	*±2.7*	2.5	*±0.8*
	MFa	34.7	*±3.3*	9.8	*±1.5*	36.5	*±2.8*	12.9	*±2.3*	5.1	*±1.4*
McA++	**All**	**18.3**	***±0.5***	**16.4**	***±0.3***	**39.7**	***±0.6***	**18.1**	***±0.4***	**6.9**	***±0.3***
	MFd	0.2	*±0.1*	29.5	*±0.6*	35.6	*±1.0*	23.6	*±0.7*	10.8	*±0.6*
U 0-1000 ppm	MFc	3.0	*±0.4*	11.8	*±0.6*	55.1	*±1.4*	19.3	*±1.0*	10.5	*±0.7*
McArthur River area	MFb	35.9	*±1.2*	5.5	*±0.4*	40.8	*±1.1*	15.6	*±0.9*	1.6	*±0.3*
	MFa	37.6	*±1.3*	13.4	*±0.7*	31.8	*±1.0*	12.0	*±0.8*	4.3	*±0.5*

APPENDIX C: PRELIMINARY INVESTIGATION OF ALUMINUM PHOSPHATE-SULFATE MINERALS WITH SCANNING ELECTRON MICROSCOPY

C.1 INTRODUCTION

Whole rock geochemical results for both the legacy and new data contain elevated Sr and P_2O_5 proximal to mineralization in the McArthur River study area (Fig. C.1), both of which are present in aluminum phosphate-sulfate (APS) minerals (Gaboreau et al., 2007; Adlakha and Hattori, 2015). Previous studies have indicated that in both basement and sandstone rocks surrounding URU deposits, APS minerals are potential pathfinders to U mineralization, and generally consist of reduced (florencite, LREE-rich) and oxidized (svanbergite and/or goyazite, Sr-rich) APS endmembers (Gaboreau et al., 2005; 2007), and often reflect the oxidized or reduced nature of the ore-forming hydrothermal fluids (Gaboreau et al., 2007; Cloutier et al., 2010). Because APS minerals are minimal in total content, yet contribute significantly to the Sr and REE budget of whole rock analyses, they were investigated using scanning electron microscopy (SEM). Moreover, delineating endmember APS minerals with whole rock geochemistry is difficult, and SEM allows potential discrimination of APS mineral types. As a proof of concept experiment, the aim of this work is to determine if florencite is the dominant endmember proximal to mineralization, with svanbergite/goyazite more prevalent distally, and to quantify potential distances from mineralization of these various phases.

C.2 METHODS

Twelve thin sections were selected, one from each drill hole, to include samples associated with both the hanging wall and footwall, proximal and distal to mineralization. Samples were also chosen to have variable U content based on the whole rock geochemical results (Table C.1).

An FEI™ scanning electron microscope (MLA 650 field electron gun, version 3 software) was used for all analysis using energy dispersive x-ray (EDX) spectroscopy. Each thin section was manually scanned to visually identify the APS minerals by their unique pseudocubic habit, and common association with pore spaces in the sandstones and with illite (Fig. C.2). Spot analyses were taken on <10 individual grains per slide for semi-quantitative elemental contents. For mineral liberation analysis (MLA) of the entire slide, the SEM was calibrated to focus on elements with high atomic numbers (bright phase search), disregarding elements Si and lower, for comparison against a suite of 34 minerals. For the APS minerals, goyazite and florencite were chosen as reference minerals. Crystal structure substitutions result in solid solutions between the endmembers, and the oxidized member may fall between the ideal formulae for goyazite and svanbergite (Riegler et al., 2016); however, only goyazite was available in the MLA reference library.

C.3 RESULTS

All spot analyses on individual APS grains exhibit varying contents of Sr and LREE; in 10 of 12 thin sections, the Sr content is greater than LREE. The 2 thin sections with greater concentrations of LREE are proximal to (<30 m) mineralization.

In the MLA results, florencite is found in greater quantities, in both percent by weight and percent by area, than svanbergite/goyazite in the 4 thin sections that were proximal to (<50 m) mineralization than those distal to (>200 m) mineralization (Fig. C.3, Table C.1).

C.4 DISCUSSION

Preliminary results illustrate that samples with a greater percentage of florencite relative to goyazite are limited to areas <50 m from mineralization, whether the mineralization is minimal/isolated or related to the deposit itself. This supports the findings in previous studies that utilized APS minerals as pathfinders where the reduced endmember was present proximal to mineralization (Gaboreau et al., 2005; 2007; Adlakha and Hattori, 2015). Given the extensive hydrothermal alteration present in the sandstones at McArthur River and the extremely high grade of the deposit, the restricted spatial distribution of florencite was unexpectedly low (e.g., Gaboreau et al., 2007). Instead, quartz cementation may have an effect much like the geochemical signatures observed in Chapter 3: the restriction of the florencite reflects the trapping of reduced fluids within the MFa, close to the unconformity, and is supported by the coincidence of florencite-enrichment with areas below medium to intense quartz cementation.

There is also a discrepancy between the spot analyses and the MLA results. In 4 of 12 samples, MLA results calculate greater florencite content in percent by both weight and area; these samples are <50 m from mineralization. Two of these samples have spot calculations of LREE > Sr in individual APS grain analyses, which confirm the MLA results of higher levels of florencite as compared to goyazite. However, the other two

samples present spot analysis results calculating LREE content to be lower than the Sr in several individual APS grains. The identification of these two samples as being florencite-rich over the entire thin section may be due to the standards used for the mineral identification: the goyazite reference scan did not include an LREE peak, whereas the florencite reference scan included both an LREE and Sr peak. The percent threshold for identification match may also be too low. Spot analyses may also require refinement, with settings adjustments for voltages or a greater number of grains selected for analysis, and possible follow up using quantitative electron microprobe.

C.5. CONCLUSIONS

1. **As identified through MLA, APS minerals identified in terms of florencite and svanbergite/goyazite endmembers are both present throughout all thin sections, irrespective of sample location. However, in those thin sections within 50 m of mineralization, florencite was present in greater concentrations than the oxidized endmember.**
2. **This study illustrates the potential for characterizing APS minerals as pathfinders at a deposit like McArthur River; however, further analysis is required with more robust methods such as LA-ICP-MS or EPMA to more accurately quantify the endmembers.**

REFERENCES

Adlakha, E. E., & Hattori, K. (2015). Compositional variation and timing of aluminum phosphate-sulfate minerals in the basement rocks along the P2 fault and in association with the McArthur River uranium deposit, Athabasca Basin, Saskatchewan, Canada. *American Mineralogist*, *100*(7), 1386–1399. http://doi.org/10.2138/am-2015-5069

Cloutier, J., Kyser, K., Olivo, G. R., & Alexandre, P. (2010). Contrasting patterns of alteration at the Wheeler River area, Athabasca basin, Saskatchewan, Canada: insights into the apparently uranium-barren zone K alteration system. *Economic Geology*, *105*(2), 303–324. http://doi.org/10.2113/gsecongeo.105.2.303

Gaboreau, S., Beaufort, D., Vieillard, P., Patrier, P., & Bruneton, P. (2005). Aluminum phosphate–sulfate minerals associated with Proterozoic unconformity-type uranium deposits in the East Alligator River Uranium Field, Northern Territories, Australia. *The Canadian Mineralogist*, *43*(2), 813–827. http://doi.org/10.2113/gscanmin.43.2.813

Gaboreau, S., Cuney, M., Quirt, D., Beaufort, D., Patrier, P., & Mathieu, R. (2007). Significance of aluminum phosphate-sulfate minerals associated with U unconformity-type deposits: The Athabasca basin, Canada. *American Mineralogist*, *92*(2-3), 267–280. http://doi.org/10.2138/am.2007.2277

Riegler, T., Quirt, D., & Beaufort, D. (2016). Spatial distribution and compositional variation of APS minerals related to uranium deposits in the Kiggavik-Andrew Lake structural trend, Nunavut, Canada. *Mineralium Deposita*, *51*(2), 219-236. http://doi.org/10.1007/s00126-015-0595-y

FIGURES

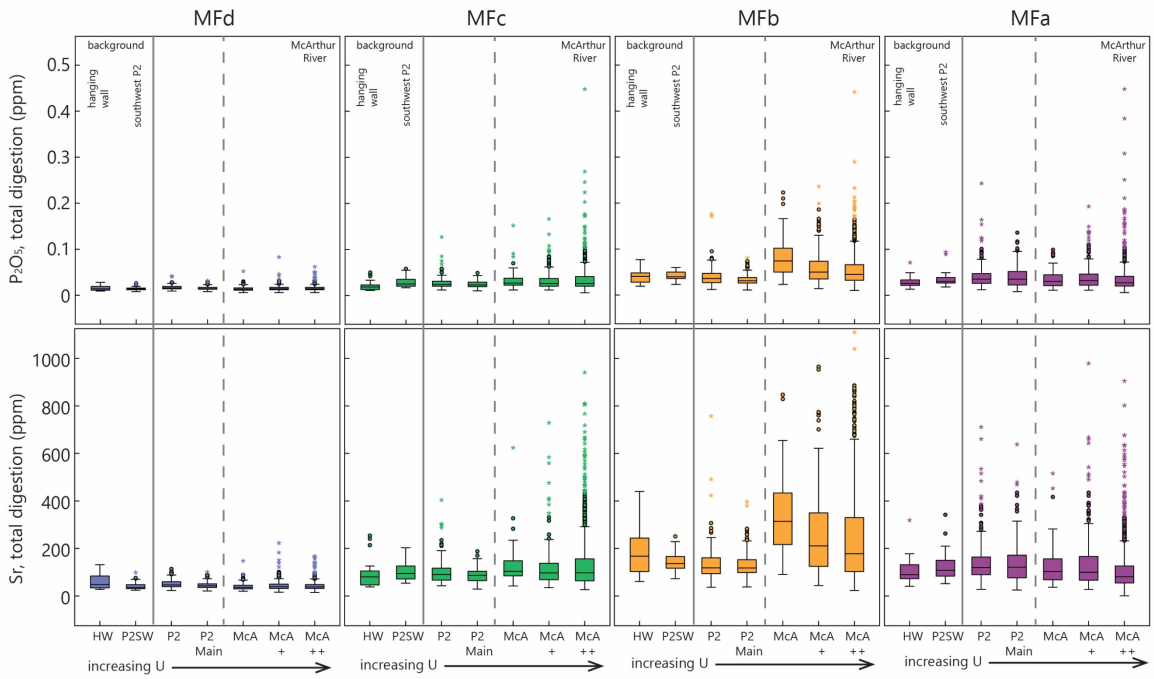

Figure C.1: Whole rock geochemical results indicate that Sr and P_2O_5 increase with proximity to mineralized areas of the McArthur River study area. This is demonstrated by anomalous values in the MFd, MFc, and MFa lithofacies, and by the median values in the MFb. To the left of each chart are the background samples; U content increases toward the right. Total number of analyses for each proximity zone is as follows: HW = 126, P2SW = 126, P2 = 874, P2 Main = 723, McA = 359, McA+ = 1117, McA++ = 4487.

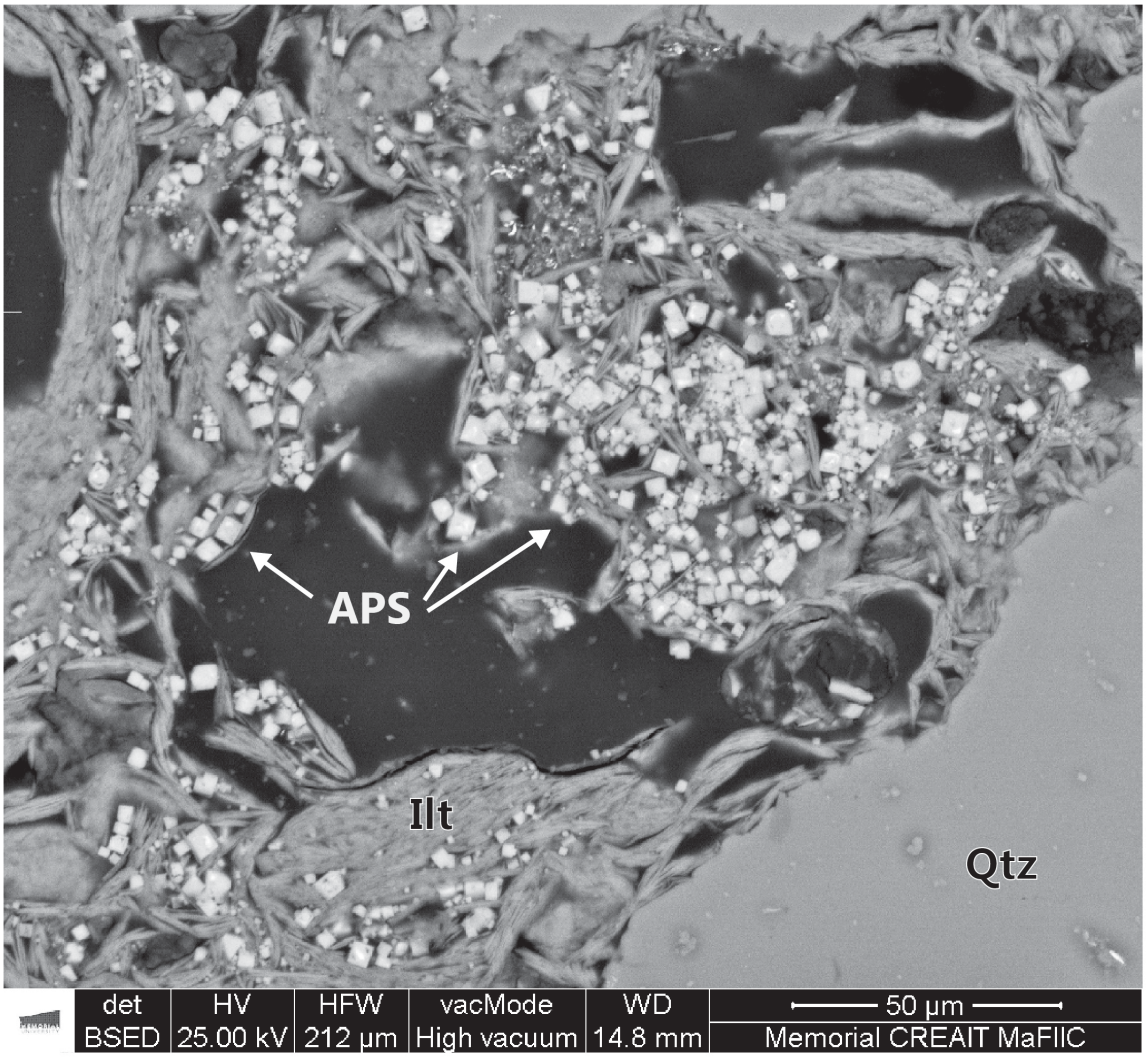

Figure C.2: Pseudocubic aluminum phosphate-sulfate minerals (APS) in thin section. Qtz = quartz; Ilt = illite. Spot samples on individual mineral APS grains were analyzed for LREE and Sr concentrations, and entire thin sections were scanned for mineral liberation analysis (MLA) for mineral concentrations. Results are shown in Table C.1.

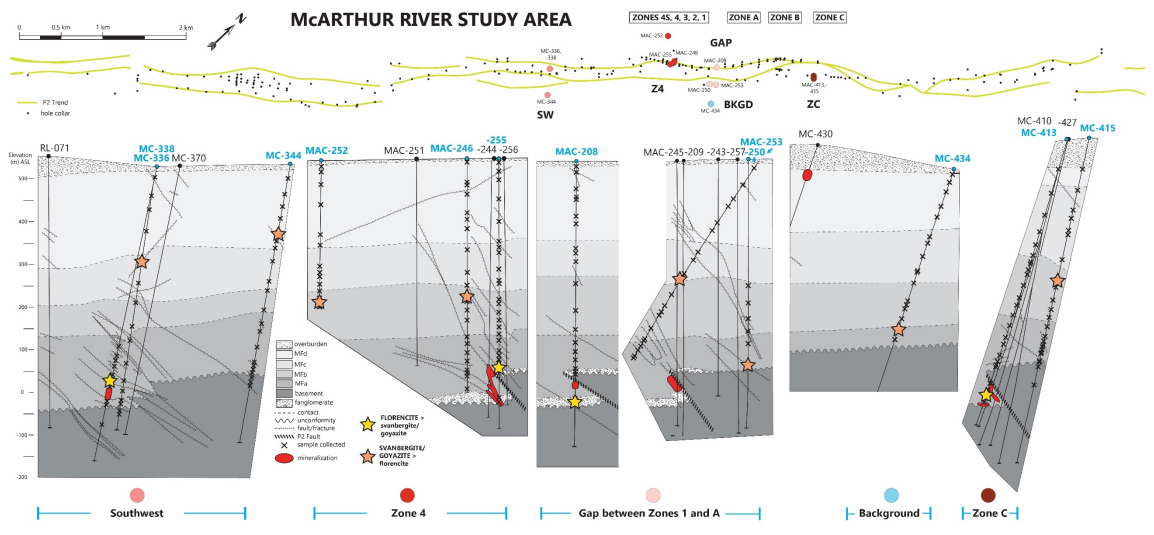

Figure C.3: Fences were chosen to be representative of areas with no, low, and high mineralization. Mineral liberation analysis results show that samples nearest mineralization, regardless of fence location, contain larger volumes (percents in weight and area) of florencite (yellow stars) than svanbergite/goyazite (orange stars). Data are in Table C.1.

TABLE C.1: THIN SECTIONS FROM NEW DATA FOR SEM ANALYSIS

Fence	Hole ID	Depth m	Lithofacies	hanging-/ footwall	P2 trend location	distance from mineralization* m	U in WR sample partial digestion ppm	U in WR sample total digestion ppm	U_3O_8 in thin section wt%	U_3O_8 in thin section area%	svanbergite/ goyazite wt%	florencite wt%	svanbergite/ goyazite area%	florencite area%
Southwest	**336**	**523**	**MFa**	**FW**	**off trend**	**< 40**	**5.31**	**11.30**	**0.01**	**0.01**	**0.26**	**0.48**	**0.34**	**0.57**
Southwest	338	220	MFc	HW	above faulting	300	2.49	5.04	0.08	0.03	0.13	0.00	0.16	0.00
Southwest	344	164	MFd	HW	off trend	550	1.35	6.76	0.00	0.00	0.11	0.02	0.13	0.02
Zone 4	246	324	MFb	FW	off trend	200	1.92	4.62	0.00	0.00	2.45	1.44	3.26	1.72
Zone 4	252	331	MFb	FW	above trend	450	0.90	2.12	0.00	0.00	0.07	0.07	0.09	0.07
Zone 4	**255**	**501**	**MFa**	**HW**	**nose of wedge**	**< 30**	**2.31**	**10.10**	**0.00**	**0.00**	**1.28**	**2.79**	**1.73**	**3.38**
Gap	**208**	**572**	**MFa/fangl.**	**FW**	**below wedge**	**< 50**	**1.97**	**3.12**	**0.00**	**0.00**	**0.37**	**2.38**	**0.48**	**2.76**
Gap	250	432	MFa	HW	off trend	200	5.41	26.10	0.00	0.00	0.61	0.11	0.82	0.13
Gap	253	336	MFc	HW	above trend	250	1.63	4.06	0.01	0.00	0.95	0.26	1.07	0.26
Zone C	**413**	**649**	**MFa**	**FW**	**below wedge**	**< 30**	**0.39**	**1.98**	**0.00**	**0.00**	**0.43**	**1.11**	**0.63**	**1.44**
Zone C	415	345	MFb	HW	off trend	300	0.89	2.84	0.00	0.00	2.51	1.40	2.65	1.32
Background	434	397	MFa	HW	400 m south from P2	400	0.23	0.96	0.00	0.00	0.26	0.16	0.32	0.18

* estimated from cross sections and data logs provided by Cameco

Table C.1: Thin sections chosen for SEM analysis. Drill holes in **bold** are those responding to the yellow stars in Figure C.3.

APPENDIX D: SAMPLE COLLECTION OF McARTHUR RIVER DRILL CORE

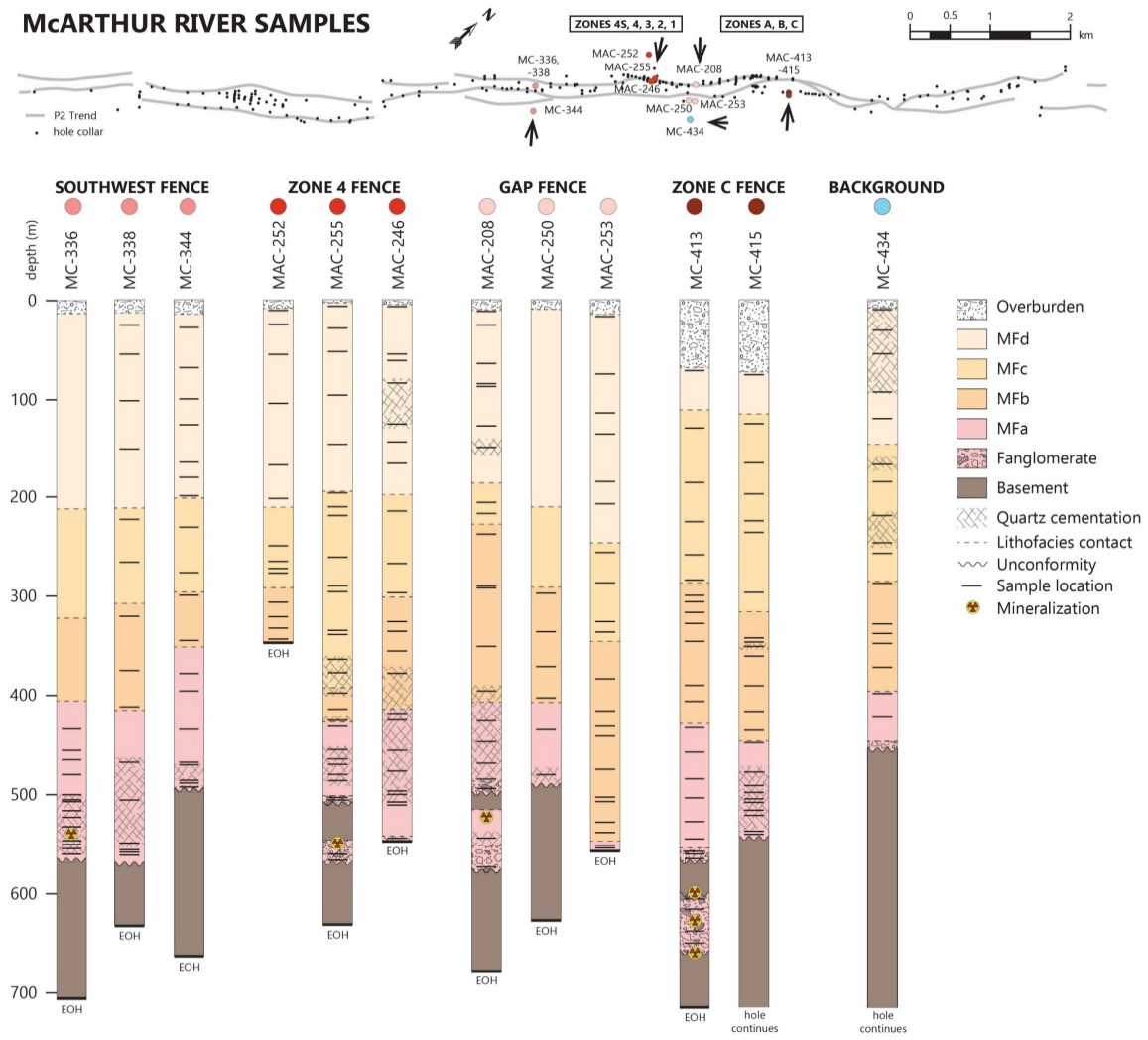

Figure D.1: Drill holes and sample collection locations from the McArthur River deposit. Samples were selected from the Manitou Falls Formation sandstones only, and sampling frequency increased toward the unconformity. The Southwest fence was representative of low mineralization, exhibiting weak mineralization at the base of the MFa lithofacies in one drill hole. The Zone 4 fence was associated with ore, showing mineralization within the P2 wedge of one drill hole, as was Zone C. The Gap fence was representative of the non-mineralized area between ore bodies (Zone 1 and Zone A), however, slight mineralization was located in the P2 wedge of one drill hole. Finally, a single hole (MC-434) was selected as background, which was in line with the Gap fence but located in the hanging wall and presented a barren profile.

APPENDIX E: SAMPLE COLLECTION OF McARTHUR RIVER DRILL CORE: WHOLE ROCK GEOCHEMISTRY

Note: the archival database, containing results for the analyses completed for Chapters 2 and 3, are the confidential property of Cameco Corporation and not included here. The new data, collected in 2014 from McArthur River drill core and analyzed by Saskatchewan Research Council Geoanalytical Laboratories, are shown below.

Group #			G-2014-2129	G-2014-2129	G-2014-2129	G-2014-2129	G-2014-2129	G-2014-2129	G-2014-2129	G-2014-2129	G-2014-2129
Sample #			SG1	SG2	SG3	SG4	SG5	SG6	SG7	SG8	SG9
Fence			Southwest	Southwest	Southwest	Southwest	Southwest	Southwest	Southwest	Southwest	Southwest
Hole ID			MC-336	MC-336	MC-336	MC-336	MC-336	MC-336	MC-336	MC-336	MC-336
From (m)			433.00	455.50	464.87	479.50	500.43	506.55	506.80	517.00	522.86
To (m)			433.22	455.72	465.13	479.75	500.59	506.76	506.99	517.19	523.03
Lithofacies			MFa	MFa	MFa	MFa	MFa	MFa	MFa	MFa	MFa
Date			11-27-2014	11-27-2014	11-27-2014	11-27-2014	11-27-2014	11-27-2014	11-27-2014	11-27-2014	11-27-2014
Sample Type			Sandstone	Sandstone	Sandstone	Sandstone	Sandstone	Sandstone	Sandstone	Sandstone	Sandstone
Ag	ppm	ICP-MS	<0.01	<0.01	<0.01	<0.01	<0.01	<0.01	<0.01	<0.01	<0.01
As	ppm	ICP-MS	0.92	0.41	0.39	0.3	0.17	0.09	1.05	0.15	0.33
Be	ppm	ICP-MS	0.04	0.05	0.03	0.02	0.02	0.02	0.08	0.02	0.07
Bi	ppm	ICP-MS	0.02	0.03	0.02	<0.01	0.02	0.01	<0.01	<0.01	<0.01
Cd	ppm	ICP-MS	0.01	<0.01	<0.01	<0.01	<0.01	<0.01	<0.01	<0.01	<0.01
Co	ppm	ICP-MS	0.07	0.08	0.08	0.04	0.08	0.07	0.17	0.08	0.25
Cs	ppm	ICP-MS	0.01	0.01	0.01	<0.01	0.01	<0.01	0.01	<0.01	0.02
Cu	ppm	ICP-MS	1.47	3.88	1.38	1.37	1.63	1.04	2.22	1.12	2.71
Dy	ppm	ICP-MS	0.19	0.12	0.07	0.05	0.07	0.06	0.08	0.06	0.15
Er	ppm	ICP-MS	0.12	0.06	0.04	0.02	0.04	0.03	0.04	0.03	0.07
Eu	ppm	ICP-MS	0.05	0.06	0.03	0.04	0.03	0.02	0.03	0.02	0.06
Ga	ppm	ICP-MS	0.13	0.17	0.13	0.1	0.12	0.1	0.27	0.11	0.38
Gd	ppm	ICP-MS	0.38	0.37	0.22	0.18	0.17	0.13	0.18	0.11	0.31
Ge	ppm	ICP-MS	<0.01	<0.01	<0.01	<0.01	<0.01	<0.01	<0.01	<0.01	<0.01
Hf	ppm	ICP-MS	0.35	0.15	0.11	0.05	0.11	0.12	0.21	0.16	0.2
Hg	ppm	ICP-MS	<0.01	<0.01	<0.01	<0.01	<0.01	<0.01	<0.01	<0.01	<0.01
Ho	ppm	ICP-MS	0.03	0.02	0.01	<0.01	0.01	<0.01	0.01	0.01	0.02
Mo	ppm	ICP-MS	0.3	0.19	0.23	0.09	0.29	0.15	0.2	0.16	0.1
Nb	ppm	ICP-MS	<0.01	<0.01	<0.01	<0.01	<0.01	<0.01	<0.01	<0.01	<0.01
Nd	ppm	ICP-MS	2.26	2.5	1.54	1.18	1.05	0.76	1.12	0.59	1.89
Ni	ppm	ICP-MS	0.27	0.4	0.54	0.19	0.38	0.46	0.92	0.45	1.58
^{204}Pb	ppm	ICP-MS	0.006	0.006	0.004	0.004	0.005	0.004	0.006	0.005	0.011
^{206}Pb	ppm	ICP-MS	0.282	0.28	0.196	0.148	0.253	0.185	0.254	0.205	0.349
^{207}Pb	ppm	ICP-MS	0.104	0.116	0.065	0.07	0.084	0.079	0.108	0.088	0.183
^{208}Pb	ppm	ICP-MS	0.345	0.391	0.184	0.179	0.198	0.209	0.291	0.224	0.512
Pb	ppm	ICP-MS	0.738	0.794	0.448	0.402	0.54	0.477	0.659	0.522	1.06
$^{206}Pb/^{204}Pb$	--	ICP-MS	47.00	46.67	49.00	37.00	50.60	46.25	42.33	41.00	31.73
$^{207}Pb/^{206}Pb$	--	ICP-MS	0.37	0.41	0.33	0.47	0.33	0.43	0.43	0.43	0.52
$^{207}Pb/^{204}Pb$	--	ICP-MS	17.33	19.33	16.25	17.50	16.80	19.75	18.00	17.60	16.64
$^{208}Pb/^{206}Pb$	--	ICP-MS	1.22	1.40	0.94	1.21	0.78	1.13	1.15	1.09	1.47
$^{208}Pb/^{204}Pb$	--	ICP-MS	57.50	65.17	46.00	44.75	39.60	52.25	48.50	44.80	46.55
Pr	ppm	ICP-MS	0.76	0.83	0.49	0.37	0.32	0.23	0.34	0.19	0.58
Rb	ppm	ICP-MS	0.37	0.29	0.24	0.14	0.36	0.21	0.42	0.22	0.4
Sb	ppm	ICP-MS	<0.01	<0.01	<0.01	<0.01	0.03	<0.01	<0.01	<0.01	<0.01
Sc	ppm	ICP-MS	<0.1	<0.1	<0.1	<0.1	<0.1	<0.1	<0.1	<0.1	0.1
Se	ppm	ICP-MS	<0.1	<0.1	<0.1	<0.1	<0.1	<0.1	<0.1	<0.1	<0.1
Sm	ppm	ICP-MS	0.4	0.44	0.26	0.21	0.2	0.14	0.2	0.12	0.34
Sn	ppm	ICP-MS	0.06	0.07	0.02	0.02	0.04	0.03	0.07	0.03	0.14
Ta	ppm	ICP-MS	<0.01	<0.01	<0.01	<0.01	<0.01	<0.01	<0.01	<0.01	<0.01
Tb	ppm	ICP-MS	0.03	0.02	0.02	0.01	0.01	0.01	0.02	0.01	0.03
Te	ppm	ICP-MS	<0.01	<0.01	<0.01	<0.01	<0.01	<0.01	<0.01	<0.01	<0.01
Th	ppm	ICP-MS	3.13	2.56	1.09	0.5	0.59	0.57	0.75	0.43	1.19
U	ppm	ICP-MS	2.65	2.24	1.85	0.77	0.93	0.88	1.39	0.88	1.64
V	ppm	ICP-MS	1.8	0.9	0.5	0.4	0.4	0.2	1.5	0.4	1.7
W	ppm	ICP-MS	<0.1	<0.1	<0.1	<0.1	<0.1	<0.1	<0.1	<0.1	<0.1
Y	ppm	ICP-MS	1.02	0.5	0.3	0.17	0.32	0.25	0.41	0.31	0.69
Yb	ppm	ICP-MS	0.11	0.04	0.02	0.01	0.03	0.02	0.04	0.03	0.05
Zn	ppm	ICP-MS	0.7	0.9	0.7	3.7	0.8	0.6	1.6	0.7	1.2
Zr	ppm	ICP-MS	13.3	5.05	3.61	1.3	3.57	4.01	6.92	5.96	6.29

Partial Digestion: A 2.00 g pulp is digested with 2.25 ml of 8:1 ultrapure HNO_3:HCl for 1 hour at 95° C.

Group #			G-2014-2129	G-2014-2129	G-2014-2129	G-2014-2129	G-2014-2129	G-2014-2129	G-2014-2129	G-2014-2129	G-2014-2129	G-2014-2129
Sample #			SG10	SG11	SG12	SG13	SG14	SG15	SG16	SG17	SG18	SG19
Fence			Southwest	Southwest	Southwest	Southwest	Southwest	Southwest	Southwest	Southwest	Southwest	Southwest
Hole ID			MC-336	MC-336	MC-336	MC-336	MC-336	MC-338	MC-338	MC-338	MC-338	MC-338
From (m)			532.73	557.00	560.46	564.00	570.50	23.00	65.00	101.00	150.50	220.20
To (m)			532.93	557.13	560.66	564.28	570.79	23.30	65.20	101.37	150.66	220.58
Lithofacies			MFa	MFa	MFa	MFa	MFa	MFd	MFd	MFd	MFd	MFc
Date			11-27-2014	11-27-2014	11-27-2014	11-27-2014	11-27-2014	11-27-2014	11-27-2014	11-27-2014	11-27-2014	11-27-2014
Sample Type			Sandstone	Sandstone	Sandstone	Sandstone	Sandstone	Sandstone	Sandstone	Sandstone	Sandstone	Sandstone
Ag	ppm	ICP-MS	0.06	0.01	<0.01	0.01	<0.01	<0.01	<0.01	<0.01	0.02	<0.01
As	ppm	ICP-MS	0.44	2.23	0.16	1.04	2.9	0.15	0.31	0.3	0.34	0.32
Be	ppm	ICP-MS	0.04	0.05	0.02	0.04	0.1	0.01	0.01	0.01	0.01	0.02
Bi	ppm	ICP-MS	0.13	0.33	0.02	0.02	<0.01	<0.01	<0.01	<0.01	0.01	<0.01
Cd	ppm	ICP-MS	<0.01	0.01	<0.01	0.02	<0.01	<0.01	<0.01	<0.01	<0.01	<0.01
Co	ppm	ICP-MS	0.08	5.25	0.08	0.13	2.28	0.05	0.06	0.03	0.04	0.06
Cs	ppm	ICP-MS	<0.01	0.01	<0.01	<0.01	0.01	<0.01	<0.01	<0.01	<0.01	<0.01
Cu	ppm	ICP-MS	7.36	8.95	0.8	6.7	0.4	0.81	0.63	0.48	0.81	1.48
Dy	ppm	ICP-MS	0.24	0.63	0.05	0.16	0.3	0.2	0.1	0.12	0.1	0.17
Er	ppm	ICP-MS	0.11	0.21	0.02	0.08	0.13	0.1	0.05	0.05	0.06	0.09
Eu	ppm	ICP-MS	0.03	0.05	0.01	0.05	0.07	0.04	0.02	0.03	0.03	0.03
Ga	ppm	ICP-MS	0.16	0.1	0.06	0.03	0.4	0.07	0.07	0.06	0.06	0.09
Gd	ppm	ICP-MS	0.22	0.35	0.09	0.31	0.56	0.28	0.16	0.2	0.17	0.23
Ge	ppm	ICP-MS	<0.01	<0.01	<0.01	<0.01	<0.01	<0.01	<0.01	<0.01	<0.01	<0.01
Hf	ppm	ICP-MS	0.16	0.14	0.05	0.55	0.13	0.2	0.1	0.2	0.13	0.14
Hg	ppm	ICP-MS	<0.01	<0.01	<0.01	<0.01	<0.01	<0.01	<0.01	<0.01	<0.01	<0.01
Ho	ppm	ICP-MS	0.04	0.09	<0.01	0.03	0.04	0.03	0.02	0.02	0.02	0.03
Mo	ppm	ICP-MS	0.37	0.46	0.14	0.16	0.16	0.07	0.11	0.15	0.22	0.25
Nb	ppm	ICP-MS	<0.01	<0.01	<0.01	<0.01	<0.01	<0.01	<0.01	<0.01	<0.01	<0.01
Nd	ppm	ICP-MS	0.65	0.64	0.61	1.76	2.34	1.37	0.8	0.99	0.86	0.88
Ni	ppm	ICP-MS	0.32	3.91	0.31	0.36	1.25	0.19	0.15	0.18	0.22	0.36
^{204}Pb	ppm	ICP-MS	0.027	0.007	0.006	0.024	0.003	0.007	0.005	0.006	0.008	0.006
^{206}Pb	ppm	ICP-MS	2.5	3.66	0.204	0.97	0.205	0.218	0.142	0.156	0.244	0.182
^{207}Pb	ppm	ICP-MS	0.521	0.296	0.101	0.414	0.06	0.118	0.079	0.094	0.131	0.103
^{208}Pb	ppm	ICP-MS	1.34	0.36	0.244	1.42	0.208	0.292	0.198	0.251	0.346	0.304
Pb	ppm	ICP-MS	4.39	4.32	0.555	2.83	0.476	0.635	0.424	0.507	0.729	0.596
$^{206}Pb/^{204}Pb$	--	ICP-MS	92.59	522.86	34.00	40.42	68.33	31.14	28.40	26.00	30.50	30.33
$^{207}Pb/^{206}Pb$	--	ICP-MS	0.21	0.08	0.50	0.43	0.29	0.54	0.56	0.60	0.54	0.57
$^{207}Pb/^{204}Pb$	--	ICP-MS	19.30	42.29	16.83	17.25	20.00	16.86	15.80	15.67	16.38	17.17
$^{208}Pb/^{206}Pb$	--	ICP-MS	0.54	0.10	1.20	1.46	1.01	1.34	1.39	1.61	1.42	1.67
$^{208}Pb/^{204}Pb$	--	ICP-MS	49.63	51.43	40.67	59.17	69.33	41.71	39.60	41.83	43.25	50.67
Pr	ppm	ICP-MS	0.19	0.18	0.2	0.57	0.71	0.44	0.25	0.31	0.27	0.26
Rb	ppm	ICP-MS	0.06	0.23	0.19	0.1	0.26	0.08	0.15	0.16	0.16	0.19
Sb	ppm	ICP-MS	0.02	0.07	<0.01	<0.01	<0.01	<0.01	0.01	<0.01	<0.01	<0.01
Sc	ppm	ICP-MS	<0.1	<0.1	<0.1	<0.1	0.2	0.1	<0.1	<0.1	<0.1	0.2
Se	ppm	ICP-MS	<0.1	<0.1	<0.1	<0.1	<0.1	<0.1	<0.1	<0.1	<0.1	<0.1
Sm	ppm	ICP-MS	0.17	0.23	0.1	0.31	0.49	0.27	0.16	0.2	0.18	0.2
Sn	ppm	ICP-MS	0.05	0.18	0.03	0.06	0.04	0.04	0.04	0.03	0.03	0.09
Ta	ppm	ICP-MS	<0.01	<0.01	<0.01	<0.01	<0.01	<0.01	<0.01	<0.01	<0.01	<0.01
Tb	ppm	ICP-MS	0.04	0.09	<0.01	0.03	0.06	0.03	0.02	0.02	0.02	0.03
Te	ppm	ICP-MS	0.01	<0.01	<0.01	<0.01	<0.01	<0.01	<0.01	<0.01	<0.01	<0.01
Th	ppm	ICP-MS	0.61	0.84	0.5	11.8	1.46	0.83	0.5	1.38	0.61	0.72
U	ppm	ICP-MS	5.31	117	1.57	15.2	0.6	1.04	0.8	0.63	1.23	2.49
V	ppm	ICP-MS	2.1	0.8	0.3	0.5	3.2	0.2	0.4	0.2	0.4	1.6
W	ppm	ICP-MS	<0.1	0.1	<0.1	<0.1	<0.1	<0.1	<0.1	<0.1	<0.1	<0.1
Y	ppm	ICP-MS	1.15	2.02	0.2	0.86	1.05	0.85	0.41	0.43	0.45	0.79
Yb	ppm	ICP-MS	0.07	0.14	0.02	0.08	0.1	0.09	0.04	0.04	0.05	0.07
Zn	ppm	ICP-MS	0.7	1.1	0.6	0.8	1	0.7	0.6	1.7	0.5	0.8
Zr	ppm	ICP-MS	5.6	6.38	1.76	25.1	6.1	7.14	3.98	9.18	5.17	5.3

Partial Digestion: A 2.00 g pulp is digested with 2.25 ml of 8:1 ultrapure HNO_3:HCl for 1 hour at 95° C.

Group #			G-2014-2129	G-2014-2129	G-2014-2129	G-2014-2129	G-2014-2129	G-2014-2129	G-2014-2129	G-2014-2129	G-2014-2129	G-2014-2129
Sample #			SG20	SG21	SG22	SG23	SG24	SG25	SG26	SG27	SG28	SG29
Fence			Southwest	Southwest	Southwest	Southwest	Southwest	Southwest	Southwest	Southwest	Southwest	Southwest
Hole ID			MC-338	MC-338	MC-338	MC-338	MC-338	MC-338	MC-338	MC-338	MC-338	MC-338
From (m)			272.00	318.90	372.17	410.80	466.00	502.37	537.64	554.73	557.50	559.00
To (m)			272.20	319.25	372.50	411.10	466.31	502.60	537.95	555.00	557.71	559.13
Lithofacies			MFc	MFb	MFb	MFb	MFa	MFa	MFa	MFa	MFa	MFa
Date			11-27-2014	11-27-2014	11-27-2014	11-27-2014	11-27-2014	11-27-2014	11-27-2014	11-27-2014	11-27-2014	11-27-2014
Sample Type			Sandstone	Sandstone	Sandstone	Sandstone	Sandstone	Sandstone	Sandstone	Sandstone	Sandstone	Sandstone
Ag	ppm	ICP-MS	<0.01	<0.01	<0.01	<0.01	<0.01	<0.01	0.03	<0.01	<0.01	<0.01
As	ppm	ICP-MS	0.89	0.23	0.61	0.45	0.27	0.1	0.18	0.16	0.85	0.33
Be	ppm	ICP-MS	0.02	0.02	0.01	0.01	0.02	0.01	0.02	0.01	0.07	0.11
Bi	ppm	ICP-MS	<0.01	0.01	0.01	<0.01	<0.01	<0.01	0.02	0.01	<0.01	0.01
Cd	ppm	ICP-MS	<0.01	<0.01	<0.01	<0.01	<0.01	<0.01	<0.01	<0.01	<0.01	<0.01
Co	ppm	ICP-MS	0.05	0.04	0.06	0.05	0.05	0.06	0.09	0.05	0.8	0.61
Cs	ppm	ICP-MS	0.02	<0.01	<0.01	<0.01	<0.01	<0.01	<0.01	<0.01	0.01	0.01
Cu	ppm	ICP-MS	0.77	0.55	1.76	0.4	0.48	0.49	3.03	1.3	10.2	5.17
Dy	ppm	ICP-MS	0.16	0.13	0.09	0.11	0.08	0.06	0.11	0.06	0.13	0.57
Er	ppm	ICP-MS	0.08	0.06	0.04	0.06	0.04	0.03	0.05	0.03	0.07	0.33
Eu	ppm	ICP-MS	0.05	0.04	0.02	0.03	0.03	0.01	0.01	0.01	0.05	0.08
Ga	ppm	ICP-MS	0.18	0.12	0.08	0.09	0.11	0.08	0.1	0.05	0.15	0.19
Gd	ppm	ICP-MS	0.32	0.26	0.2	0.25	0.27	0.1	0.13	0.1	0.29	0.55
Ge	ppm	ICP-MS	<0.01	<0.01	<0.01	<0.01	<0.01	<0.01	<0.01	<0.01	<0.01	<0.01
Hf	ppm	ICP-MS	0.18	0.15	0.09	0.1	0.06	0.04	0.07	0.04	0.24	0.36
Hg	ppm	ICP-MS	<0.01	<0.01	<0.01	<0.01	<0.01	<0.01	<0.01	<0.01	<0.01	<0.01
Ho	ppm	ICP-MS	0.02	0.02	0.01	0.02	0.01	<0.01	0.02	<0.01	0.02	0.1
Mo	ppm	ICP-MS	0.12	0.08	0.1	0.07	0.05	0.13	0.1	0.09	0.14	0.08
Nb	ppm	ICP-MS	<0.01	<0.01	<0.01	<0.01	<0.01	<0.01	<0.01	<0.01	<0.01	<0.01
Nd	ppm	ICP-MS	1.51	1.38	1.23	1.41	1.98	0.54	0.57	0.57	1.92	2.21
Ni	ppm	ICP-MS	0.36	0.16	0.23	0.18	0.2	0.32	0.41	0.24	2.12	1.52
^{204}Pb	ppm	ICP-MS	0.005	0.005	0.002	0.003	0.004	0.003	0.003	0.004	0.01	0.008
^{206}Pb	ppm	ICP-MS	0.152	0.142	0.118	0.093	0.108	0.102	0.248	0.133	0.342	0.349
^{207}Pb	ppm	ICP-MS	0.09	0.084	0.044	0.05	0.06	0.055	0.059	0.066	0.158	0.134
^{208}Pb	ppm	ICP-MS	0.28	0.246	0.138	0.174	0.174	0.146	0.152	0.176	0.45	0.4
Pb	ppm	ICP-MS	0.528	0.476	0.303	0.319	0.346	0.305	0.462	0.379	0.96	0.891
$^{206}Pb/^{204}Pb$	--	ICP-MS	30.40	28.40	59.00	31.00	27.00	34.00	82.67	33.25	34.20	43.63
$^{207}Pb/^{206}Pb$	--	ICP-MS	0.59	0.59	0.37	0.54	0.56	0.54	0.24	0.50	0.46	0.38
$^{207}Pb/^{204}Pb$	--	ICP-MS	18.00	16.80	22.00	16.67	15.00	18.33	19.67	16.50	15.80	16.75
$^{208}Pb/^{206}Pb$	--	ICP-MS	1.84	1.73	1.17	1.87	1.61	1.43	0.61	1.32	1.32	1.15
$^{208}Pb/^{204}Pb$	--	ICP-MS	56.00	49.20	69.00	58.00	43.50	48.67	50.67	44.00	45.00	50.00
Pr	ppm	ICP-MS	0.46	0.42	0.38	0.44	0.6	0.17	0.18	0.19	0.62	0.69
Rb	ppm	ICP-MS	0.26	0.29	0.18	0.21	0.13	0.16	0.06	0.14	0.36	0.68
Sb	ppm	ICP-MS	0.01	<0.01	<0.01	<0.01	<0.01	<0.01	<0.01	<0.01	<0.01	<0.01
Sc	ppm	ICP-MS	<0.1	0.1	<0.1	<0.1	<0.1	<0.1	<0.1	<0.1	0.1	0.2
Se	ppm	ICP-MS	<0.1	<0.1	<0.1	<0.1	<0.1	<0.1	<0.1	<0.1	<0.1	<0.1
Sm	ppm	ICP-MS	0.31	0.27	0.22	0.27	0.35	0.1	0.11	0.1	0.32	0.47
Sn	ppm	ICP-MS	0.15	0.04	0.04	0.03	0.02	0.02	0.04	0.02	0.06	0.05
Ta	ppm	ICP-MS	<0.01	<0.01	<0.01	<0.01	<0.01	<0.01	<0.01	<0.01	<0.01	<0.01
Tb	ppm	ICP-MS	0.03	0.02	0.02	0.02	0.02	<0.01	0.02	0.01	0.02	0.08
Te	ppm	ICP-MS	<0.01	<0.01	<0.01	<0.01	<0.01	<0.01	0.01	<0.01	<0.01	<0.01
Th	ppm	ICP-MS	1.73	1.21	0.96	1.32	0.76	0.45	0.54	0.54	1.31	1.49
U	ppm	ICP-MS	1.18	0.88	0.93	0.51	0.45	0.43	1.45	0.71	6.58	5.69
V	ppm	ICP-MS	1.8	0.7	1.3	0.3	0.2	0.5	0.7	0.4	0.7	0.6
W	ppm	ICP-MS	<0.1	<0.1	<0.1	<0.1	<0.1	<0.1	<0.1	<0.1	<0.1	<0.1
Y	ppm	ICP-MS	0.68	0.55	0.34	0.52	0.28	0.26	0.49	0.3	0.61	3.16
Yb	ppm	ICP-MS	0.05	0.05	0.03	0.05	0.02	0.02	0.03	0.02	0.06	0.27
Zn	ppm	ICP-MS	1.7	0.6	0.7	0.6	0.6	0.7	0.7	0.5	1.2	0.7
Zr	ppm	ICP-MS	7.04	5.55	3.35	3.52	2.08	1.28	2.26	1.65	9.45	14.4

Partial Digestion: A 2.00 g pulp is digested with 2.25 ml of 8:1 ultrapure HNO_3:HCl for 1 hour at 95° C.

Group #			G-2014-2129	G-2014-2129	G-2014-2129	G-2014-2129	G-2014-2129	G-2014-2129	G-2014-2129	G-2014-2129	G-2014-2129	G-2014-2129
Sample #			SG30	SG31	SG32	SG33	SG34	SG35	SG36	SG37	SG33 R	SG38
Fence			Southwest	Southwest	Southwest	Southwest	Southwest	Southwest	Southwest	Southwest	Southwest	Southwest
Hole ID			MC-344	MC-344	MC-344	MC-344	MC-344	MC-344	MC-344	MC-344	MC-344	MC-344
From (m)			26.10	69.00	100.10	128.00	164.00	179.80	199.00	230.00	128.00	275.00
To (m)			26.40	69.40	100.30	128.18	164.30	180.10	199.18	230.27	128.18	275.23
Lithofacies			MFd	MFd	MFd	MFd	MFd	MFd	MFd	MFc	MFd	MFc
Date			11-27-2014	11-27-2014	11-27-2014	11-27-2014	11-27-2014	11-27-2014	11-27-2014	11-27-2014	11-27-2014	11-27-2014
Sample Type			Sandstone	Sandstone	Sandstone	Sandstone	Sandstone	Sandstone	Sandstone	Sandstone	Repeat	Sandstone
Ag	ppm	ICP-MS	<0.01	<0.01	<0.01	<0.01	<0.01	<0.01	<0.01	0.01	<0.01	<0.01
As	ppm	ICP-MS	0.23	0.14	0.14	0.7	0.21	0.11	0.22	0.41	0.73	0.31
Be	ppm	ICP-MS	0.02	0.03	0.02	0.02	0.03	0.02	0.02	0.02	0.02	0.02
Bi	ppm	ICP-MS	0.01	0.08	0.01	<0.01	<0.01	<0.01	<0.01	<0.01	<0.01	<0.01
Cd	ppm	ICP-MS	0.01	<0.01	<0.01	<0.01	<0.01	<0.01	<0.01	<0.01	<0.01	<0.01
Co	ppm	ICP-MS	0.05	0.07	0.06	0.07	0.06	0.05	0.05	0.04	0.07	0.12
Cs	ppm	ICP-MS	<0.01	<0.01	<0.01	<0.01	<0.01	<0.01	<0.01	<0.01	<0.01	<0.01
Cu	ppm	ICP-MS	1.12	1.64	1.59	1.6	0.86	0.6	0.55	1.04	1.62	0.32
Dy	ppm	ICP-MS	0.3	0.29	0.1	0.12	0.21	0.14	0.08	0.08	0.11	0.06
Er	ppm	ICP-MS	0.18	0.16	0.04	0.07	0.11	0.07	0.04	0.04	0.06	0.03
Eu	ppm	ICP-MS	0.04	0.05	0.02	0.03	0.04	0.03	0.02	0.02	0.03	0.02
Ga	ppm	ICP-MS	0.07	0.1	0.06	0.2	0.13	0.07	0.1	0.08	0.2	0.07
Gd	ppm	ICP-MS	0.31	0.36	0.18	0.19	0.26	0.2	0.17	0.18	0.18	0.16
Ge	ppm	ICP-MS	<0.01	<0.01	<0.01	<0.01	<0.01	<0.01	<0.01	<0.01	<0.01	<0.01
Hf	ppm	ICP-MS	0.51	0.35	0.08	0.22	0.44	0.19	0.11	0.14	0.22	0.13
Hg	ppm	ICP-MS	<0.01	<0.01	<0.01	<0.01	<0.01	<0.01	<0.01	<0.01	<0.01	<0.01
Ho	ppm	ICP-MS	0.05	0.05	0.02	0.02	0.04	0.02	0.01	0.01	0.02	<0.01
Mo	ppm	ICP-MS	0.05	0.05	0.1	0.18	0.06	0.08	0.06	0.1	0.18	0.08
Nb	ppm	ICP-MS	<0.01	<0.01	<0.01	<0.01	<0.01	<0.01	<0.01	<0.01	<0.01	<0.01
Nd	ppm	ICP-MS	1.51	1.9	1.01	1.08	1.12	0.97	1.02	0.99	1.04	1.02
Ni	ppm	ICP-MS	0.17	0.18	0.32	0.4	0.2	0.16	0.25	0.59	0.41	0.38
^{204}Pb	ppm	ICP-MS	0.011	0.011	0.006	0.008	0.039	0.007	0.008	0.007	0.008	0.005
^{206}Pb	ppm	ICP-MS	0.316	0.378	0.191	0.221	1.07	0.204	0.2	0.162	0.212	0.135
^{207}Pb	ppm	ICP-MS	0.184	0.184	0.095	0.128	0.626	0.108	0.128	0.113	0.129	0.08
^{208}Pb	ppm	ICP-MS	0.466	0.499	0.229	0.344	2.05	0.302	0.381	0.313	0.343	0.226
Pb	ppm	ICP-MS	0.978	1.07	0.521	0.702	3.79	0.621	0.717	0.595	0.693	0.446
$^{206}Pb/^{204}Pb$	--	ICP-MS	28.73	34.36	31.83	27.63	27.44	29.14	25.00	23.14	26.50	27.00
$^{207}Pb/^{206}Pb$	--	ICP-MS	0.58	0.49	0.50	0.58	0.59	0.53	0.64	0.70	0.61	0.59
$^{207}Pb/^{204}Pb$	--	ICP-MS	16.73	16.73	15.83	16.00	16.05	15.43	16.00	16.14	16.13	16.00
$^{208}Pb/^{206}Pb$	--	ICP-MS	1.47	1.32	1.20	1.56	1.92	1.48	1.91	1.93	1.62	1.67
$^{208}Pb/^{204}Pb$	--	ICP-MS	42.36	45.36	38.17	43.00	52.56	43.14	47.63	44.71	42.88	45.20
Pr	ppm	ICP-MS	0.5	0.63	0.32	0.34	0.34	0.31	0.34	0.32	0.34	0.32
Rb	ppm	ICP-MS	0.05	0.05	0.05	0.11	0.12	0.05	0.2	0.21	0.11	0.19
Sb	ppm	ICP-MS	<0.01	<0.01	<0.01	0.05	<0.01	<0.01	<0.01	<0.01	0.05	<0.01
Sc	ppm	ICP-MS	0.2	0.2	<0.1	<0.1	0.1	<0.1	<0.1	0.1	<0.1	<0.1
Se	ppm	ICP-MS	<0.1	<0.1	<0.1	<0.1	<0.1	<0.1	<0.1	<0.1	<0.1	<0.1
Sm	ppm	ICP-MS	0.29	0.34	0.18	0.2	0.24	0.19	0.19	0.19	0.19	0.18
Sn	ppm	ICP-MS	0.07	0.16	0.04	0.06	0.05	0.03	0.07	0.08	0.06	0.04
Ta	ppm	ICP-MS	<0.01	<0.01	<0.01	<0.01	<0.01	<0.01	<0.01	<0.01	<0.01	<0.01
Tb	ppm	ICP-MS	0.04	0.04	0.02	0.02	0.03	0.02	0.01	0.02	0.02	0.01
Te	ppm	ICP-MS	<0.01	<0.01	<0.01	0.01	<0.01	<0.01	<0.01	<0.01	0.01	<0.01
Th	ppm	ICP-MS	1.46	1.8	0.49	1.36	1.37	0.85	1.31	0.98	1.32	0.83
U	ppm	ICP-MS	1.35	1.22	0.7	1.12	1.35	0.77	0.41	0.32	1.08	0.26
V	ppm	ICP-MS	0.5	0.5	0.5	0.6	0.6	0.2	0.6	0.4	0.6	0.2
W	ppm	ICP-MS	<0.1	<0.1	<0.1	<0.1	<0.1	<0.1	<0.1	<0.1	<0.1	<0.1
Y	ppm	ICP-MS	1.57	1.34	0.38	0.58	1.07	0.61	0.32	0.33	0.59	0.25
Yb	ppm	ICP-MS	0.16	0.13	0.03	0.05	0.09	0.05	0.03	0.03	0.05	0.03
Zn	ppm	ICP-MS	0.7	0.7	0.6	0.9	1	0.6	0.8	0.7	1.1	0.6
Zr	ppm	ICP-MS	19.6	13.8	2.8	9.01	16.2	6.23	4.18	5.52	8.84	5.06

Partial Digestion: A 2.00 g pulp is digested with 2.25 ml of 8:1 ultrapure HNO_3:HCl for 1 hour at 95° C.

Group #			G-2014-2129	G-2014-2129	G-2014-2129	G-2014-2129	G-2014-2129	G-2014-2129	G-2014-2129	G-2014-2129	G-2014-2129	G-2014-2129
Sample #			SG39	SG40	SG41	SG42	SG43	SG44	SG45	SG46	SG47	SG48
Fence			Southwest	Southwest	Southwest	Southwest	Southwest	Southwest	Southwest	Southwest	Southwest	Southwest
Hole ID			MC-344	MC-344	MC-344	MC-344	MC-344	MC-344	MC-344	MC-344	MC-344	MC-344
From (m)			298.82	342.90	378.45	394.34	433.00	467.00	468.80	485.76	488.00	492.93
To (m)			299.00	343.26	378.69	394.59	433.27	467.17	468.99	486.03	488.19	493.13
Lithofacies			MFb	MFb	MFa	MFa	MFa	MFa	MFa	MFa	MFa	MFa
Date			11-27-2014	11-27-2014	11-27-2014	11-27-2014	11-27-2014	11-27-2014	11-27-2014	11-27-2014	11-27-2014	11-27-2014
Sample Type			Sandstone	Sandstone	Sandstone	Sandstone	Sandstone	Sandstone	Sandstone	Sandstone	Sandstone	Sandstone
Ag	ppm	ICP-MS	<0.01	<0.01	<0.01	<0.01	<0.01	<0.01	<0.01	<0.01	<0.01	<0.01
As	ppm	ICP-MS	0.43	0.29	0.5	1.22	0.54	0.21	0.17	0.1	0.07	0.1
Be	ppm	ICP-MS	0.02	<0.01	0.02	0.03	0.02	0.02	<0.01	0.02	0.01	0.03
Bi	ppm	ICP-MS	0.01	<0.01	<0.01	<0.01	<0.01	<0.01	<0.01	<0.01	<0.01	<0.01
Cd	ppm	ICP-MS	0.01	<0.01	<0.01	<0.01	<0.01	<0.01	0.01	<0.01	<0.01	<0.01
Co	ppm	ICP-MS	0.05	0.03	0.04	0.61	0.04	0.06	0.03	0.06	0.04	0.07
Cs	ppm	ICP-MS	<0.01	<0.01	<0.01	<0.01	<0.01	<0.01	<0.01	<0.01	<0.01	<0.01
Cu	ppm	ICP-MS	0.54	0.3	0.42	0.5	0.36	0.46	0.28	0.62	0.31	0.38
Dy	ppm	ICP-MS	0.08	0.05	0.07	0.07	0.06	0.07	0.06	0.06	0.04	0.2
Er	ppm	ICP-MS	0.04	0.02	0.04	0.04	0.03	0.04	0.03	0.03	0.02	0.1
Eu	ppm	ICP-MS	0.03	0.02	0.03	0.03	0.02	0.02	0.02	0.02	0.01	0.04
Ga	ppm	ICP-MS	0.09	0.08	0.12	0.1	0.12	0.13	0.04	0.12	0.18	0.16
Gd	ppm	ICP-MS	0.23	0.14	0.2	0.21	0.14	0.15	0.13	0.12	0.07	0.39
Ge	ppm	ICP-MS	<0.01	<0.01	<0.01	<0.01	<0.01	<0.01	<0.01	<0.01	<0.01	<0.01
Hf	ppm	ICP-MS	0.17	0.05	0.17	0.18	0.12	0.19	0.34	0.09	0.05	0.22
Hg	ppm	ICP-MS	<0.01	<0.01	<0.01	<0.01	<0.01	<0.01	<0.01	<0.01	<0.01	<0.01
Ho	ppm	ICP-MS	0.01	<0.01	0.01	0.01	<0.01	0.01	<0.01	<0.01	<0.01	0.03
Mo	ppm	ICP-MS	0.06	0.04	0.06	0.07	0.07	0.12	0.11	0.13	0.07	0.12
Nb	ppm	ICP-MS	<0.01	<0.01	<0.01	<0.01	<0.01	<0.01	<0.01	<0.01	<0.01	<0.01
Nd	ppm	ICP-MS	1.5	0.92	1.22	1.4	1.03	0.87	0.83	0.79	0.44	2.28
Ni	ppm	ICP-MS	0.19	0.19	0.17	0.82	0.25	0.25	0.18	0.34	0.23	0.35
^{204}Pb	ppm	ICP-MS	0.006	0.004	0.006	0.008	0.005	0.004	0.003	0.005	0.004	0.004
^{206}Pb	ppm	ICP-MS	0.162	0.095	0.143	0.226	0.133	0.14	0.142	0.146	0.099	0.177
^{207}Pb	ppm	ICP-MS	0.11	0.063	0.091	0.135	0.077	0.066	0.057	0.078	0.064	0.078
^{208}Pb	ppm	ICP-MS	0.322	0.178	0.281	0.503	0.228	0.179	0.179	0.196	0.154	0.258
Pb	ppm	ICP-MS	0.6	0.34	0.521	0.873	0.442	0.389	0.38	0.424	0.32	0.518
$^{206}Pb/^{204}Pb$	--	ICP-MS	27.00	23.75	23.83	28.25	26.60	35.00	47.33	29.20	24.75	44.25
$^{207}Pb/^{206}Pb$	--	ICP-MS	0.68	0.66	0.64	0.60	0.58	0.47	0.40	0.53	0.65	0.44
$^{207}Pb/^{204}Pb$	--	ICP-MS	18.33	15.75	15.17	16.88	15.40	16.50	19.00	15.60	16.00	19.50
$^{208}Pb/^{206}Pb$	--	ICP-MS	1.99	1.87	1.97	2.23	1.71	1.28	1.26	1.34	1.56	1.46
$^{208}Pb/^{204}Pb$	--	ICP-MS	53.67	44.50	46.83	62.88	45.60	44.75	59.67	39.20	38.50	64.50
Pr	ppm	ICP-MS	0.47	0.3	0.38	0.47	0.33	0.26	0.26	0.25	0.14	0.71
Rb	ppm	ICP-MS	0.22	0.11	0.16	0.22	0.16	0.06	0.05	0.11	0.13	0.1
Sb	ppm	ICP-MS	<0.01	<0.01	<0.01	<0.01	<0.01	0.06	<0.01	0.05	<0.01	0.02
Sc	ppm	ICP-MS	<0.1	<0.1	<0.1	<0.1	<0.1	<0.1	<0.1	<0.1	<0.1	0.1
Se	ppm	ICP-MS	<0.1	<0.1	<0.1	<0.1	<0.1	<0.1	<0.1	<0.1	<0.1	<0.1
Sm	ppm	ICP-MS	0.29	0.16	0.23	0.24	0.17	0.17	0.15	0.14	0.08	0.44
Sn	ppm	ICP-MS	0.06	0.02	0.02	0.24	0.03	0.08	0.05	0.04	0.04	0.07
Ta	ppm	ICP-MS	<0.01	<0.01	<0.01	<0.01	<0.01	<0.01	<0.01	<0.01	<0.01	<0.01
Tb	ppm	ICP-MS	0.02	0.01	0.02	0.02	0.01	0.01	0.01	0.01	<0.01	0.04
Te	ppm	ICP-MS	<0.01	<0.01	<0.01	<0.01	<0.01	<0.01	<0.01	<0.01	<0.01	<0.01
Th	ppm	ICP-MS	1.55	0.49	1.33	4.42	1.21	0.82	1.08	0.55	0.29	2.41
U	ppm	ICP-MS	0.26	0.25	0.27	0.3	0.3	0.56	0.6	0.41	0.21	0.6
V	ppm	ICP-MS	0.2	0.2	0.3	1.2	0.3	1.1	0.8	0.7	0.9	1.2
W	ppm	ICP-MS	<0.1	<0.1	<0.1	<0.1	<0.1	<0.1	<0.1	<0.1	<0.1	<0.1
Y	ppm	ICP-MS	0.31	0.19	0.3	0.31	0.25	0.32	0.26	0.27	0.15	0.92
Yb	ppm	ICP-MS	0.03	0.02	0.03	0.03	0.03	0.04	0.03	0.02	0.01	0.08
Zn	ppm	ICP-MS	0.7	0.5	1	1.5	1.3	0.6	1.1	0.8	0.5	0.5
Zr	ppm	ICP-MS	6.62	1.84	5.95	6.22	4.3	7.04	15.1	3.68	1.65	8.34

Partial Digestion: A 2.00 g pulp is digested with 2.25 ml of 8:1 ultrapure HNO_3:HCl for 1 hour at 95° C.

Group #			G-2014-2129	G-2014-2129	G-2014-2129	G-2014-2129	G-2014-2129	G-2014-2129	G-2014-2129	G-2014-2129	G-2014-2129	G-2014-2129
Sample #			SG49	SG50	SG51	SG52	SG53	SG54	SG55	SG56	SG57	SG58
Fence			Gap	Gap	Gap	Gap	Gap	Gap	Gap	Gap	Gap	Gap
Hole ID			MAC-208	MAC-208	MAC-208	MAC-208	MAC-208	MAC-208	MAC-208	MAC-208	MAC-208	MAC-208
From (m)			10.20	27.00	63.50	86.50	88.00	128.40	149.00	203.00	217.70	237.00
To (m)			10.61	27.16	63.83	86.76	88.35	128.60	149.24	203.33	217.92	237.32
Lithofacies			MFd	MFd	MFd	MFd	MFd	MFd	MFd	MFc	MFc	MFb
Date			11-27-2014	11-27-2014	11-27-2014	11-27-2014	11-27-2014	11-27-2014	11-27-2014	11-27-2014	11-27-2014	11-27-2014
Sample Type			Sandstone	Sandstone	Sandstone	Sandstone	Sandstone	Sandstone	Sandstone	Sandstone	Sandstone	Sandstone
Ag	ppm	ICP-MS	<0.01	<0.01	<0.01	<0.01	<0.01	<0.01	<0.01	<0.01	<0.01	<0.01
As	ppm	ICP-MS	0.1	0.1	0.31	0.16	0.1	0.09	0.18	0.28	0.73	0.69
Be	ppm	ICP-MS	0.02	0.01	0.02	0.03	0.02	0.02	0.04	0.04	0.06	0.17
Bi	ppm	ICP-MS	0.05	0.01	<0.01	<0.01	<0.01	<0.01	<0.01	<0.01	0.01	<0.01
Cd	ppm	ICP-MS	<0.01	<0.01	<0.01	<0.01	<0.01	<0.01	<0.01	<0.01	0.01	<0.01
Co	ppm	ICP-MS	0.01	0.03	0.04	0.05	0.02	0.06	0.04	0.04	0.04	0.06
Cs	ppm	ICP-MS	<0.01	<0.01	<0.01	<0.01	<0.01	<0.01	<0.01	0.01	0.01	0.02
Cu	ppm	ICP-MS	0.74	0.51	1.28	1.47	0.5	0.82	0.86	1.58	2.55	1.38
Dy	ppm	ICP-MS	0.22	0.16	0.14	0.22	0.16	0.23	0.31	0.19	0.24	0.6
Er	ppm	ICP-MS	0.11	0.08	0.07	0.11	0.07	0.12	0.17	0.08	0.15	0.25
Eu	ppm	ICP-MS	0.05	0.04	0.03	0.04	0.05	0.05	0.08	0.04	0.06	0.15
Ga	ppm	ICP-MS	0.16	0.12	0.23	0.2	0.1	0.15	0.17	0.37	0.32	0.29
Gd	ppm	ICP-MS	0.33	0.25	0.18	0.27	0.27	0.3	0.46	0.32	0.39	0.95
Ge	ppm	ICP-MS	<0.01	<0.01	<0.01	<0.01	<0.01	<0.01	<0.01	<0.01	<0.01	<0.01
Hf	ppm	ICP-MS	0.2	0.12	0.08	0.2	0.1	0.17	0.35	0.16	0.38	0.11
Hg	ppm	ICP-MS	<0.01	<0.01	<0.01	<0.01	<0.01	<0.01	<0.01	<0.01	<0.01	<0.01
Ho	ppm	ICP-MS	0.04	0.02	0.02	0.04	0.02	0.04	0.05	0.03	0.04	0.09
Mo	ppm	ICP-MS	0.03	0.03	0.17	0.06	0.06	0.05	0.05	0.06	0.14	0.09
Nb	ppm	ICP-MS	<0.01	<0.01	<0.01	<0.01	<0.01	<0.01	<0.01	<0.01	<0.01	<0.01
Nd	ppm	ICP-MS	2	1.39	0.72	1.26	1.59	1.38	2.45	1.45	1.89	3.12
Ni	ppm	ICP-MS	0.09	0.16	0.37	0.49	0.23	0.41	0.29	0.87	0.79	0.98
^{204}Pb	ppm	ICP-MS	0.006	0.006	0.002	0.008	0.008	0.006	0.007	0.004	0.327	0.021
^{206}Pb	ppm	ICP-MS	0.166	0.161	0.09	0.198	0.155	0.143	0.162	0.133	9.26	1.09
^{207}Pb	ppm	ICP-MS	0.11	0.104	0.043	0.127	0.119	0.099	0.11	0.073	5.39	0.403
^{208}Pb	ppm	ICP-MS	0.258	0.259	0.118	0.334	0.278	0.252	0.355	0.211	19.3	0.94
Pb	ppm	ICP-MS	0.54	0.53	0.254	0.668	0.56	0.5	0.634	0.422	34.2	2.45
$^{206}Pb/^{204}Pb$	--	ICP-MS	27.67	26.83	45.00	24.75	19.38	23.83	23.14	33.25	28.32	51.90
$^{207}Pb/^{206}Pb$	--	ICP-MS	0.66	0.65	0.48	0.64	0.77	0.69	0.68	0.55	0.58	0.37
$^{207}Pb/^{204}Pb$	--	ICP-MS	18.33	17.33	21.50	15.88	14.88	16.50	15.71	18.25	16.48	19.19
$^{208}Pb/^{206}Pb$	--	ICP-MS	1.55	1.61	1.31	1.69	1.79	1.76	2.19	1.59	2.08	0.86
$^{208}Pb/^{204}Pb$	--	ICP-MS	43.00	43.17	59.00	41.75	34.75	42.00	50.71	52.75	59.02	44.76
Pr	ppm	ICP-MS	0.67	0.46	0.22	0.38	0.49	0.4	0.75	0.45	0.6	0.87
Rb	ppm	ICP-MS	0.06	0.11	0.11	0.09	0.05	0.07	0.07	0.12	0.17	0.26
Sb	ppm	ICP-MS	<0.01	<0.01	0.01	<0.01	<0.01	0.02	<0.01	<0.01	<0.01	<0.01
Sc	ppm	ICP-MS	0.3	0.2	0.1	0.2	<0.1	0.2	0.3	<0.1	0.1	0.2
Se	ppm	ICP-MS	<0.1	<0.1	<0.1	<0.1	<0.1	<0.1	<0.1	<0.1	<0.1	<0.1
Sm	ppm	ICP-MS	0.36	0.26	0.16	0.27	0.3	0.3	0.5	0.29	0.37	0.76
Sn	ppm	ICP-MS	0.1	0.05	0.04	0.15	0.04	0.08	0.09	0.19	0.24	0.12
Ta	ppm	ICP-MS	<0.01	<0.01	<0.01	<0.01	<0.01	<0.01	<0.01	<0.01	<0.01	<0.01
Tb	ppm	ICP-MS	0.04	0.03	0.02	0.03	0.03	0.04	0.05	0.03	0.04	0.11
Te	ppm	ICP-MS	<0.01	<0.01	<0.01	<0.01	<0.01	<0.01	<0.01	<0.01	<0.01	<0.01
Th	ppm	ICP-MS	0.96	0.74	0.5	1.16	0.53	0.93	4.96	1.37	4.69	5.18
U	ppm	ICP-MS	0.55	0.4	1.19	0.84	0.47	0.76	1.29	1.05	2.02	6.44
V	ppm	ICP-MS	0.3	0.3	3.4	0.6	0.1	0.3	0.3	0.2	1.4	0.7
W	ppm	ICP-MS	<0.1	<0.1	<0.1	<0.1	<0.1	<0.1	<0.1	<0.1	<0.1	<0.1
Y	ppm	ICP-MS	0.9	0.67	0.64	0.91	0.6	0.94	1.31	0.72	1.43	2.46
Yb	ppm	ICP-MS	0.09	0.06	0.05	0.09	0.05	0.1	0.14	0.05	0.13	0.13
Zn	ppm	ICP-MS	1.2	1.2	0.8	1.3	0.6	0.9	0.7	1.2	1.3	2.3
Zr	ppm	ICP-MS	7.67	4.6	2.82	7.92	3.75	6.3	14.7	6.22	16.5	5.12

Partial Digestion: A 2.00 g pulp is digested with 2.25 ml of 8:1 ultrapure HNO_3:HCl for 1 hour at 95° C.

Group #			G-2014-2129	G-2014-2129	G-2014-2129	G-2014-2129	G-2014-2129	G-2014-2129	G-2014-2129	G-2014-2129	G-2014-2129
Sample #			SG59	SG60	SG61	SG62	SG63	SG64	SG65	SG66	SG67
Fence			Gap	Gap	Gap	Gap	Gap	Gap	Gap	Gap	Gap
Hole ID			MAC-208	MAC-208	MAC-208	MAC-208	MAC-208	MAC-208	MAC-208	MAC-208	MAC-208
From (m)			289.20	290.50	350.50	395.00	425.10	447.30	468.40	486.60	493.00
To (m)			289.38	290.69	350.80	395.22	425.36	447.52	468.64	486.78	493.24
Lithofacies			MFb	MFb	MFb	MFb	MFa	MFa	MFa	MFa	MFa
Date			11-27-2014	11-27-2014	11-27-2014	11-27-2014	11-27-2014	11-27-2014	11-27-2014	11-27-2014	11-27-2014
Sample Type			Sandstone	Sandstone	Sandstone	Sandstone	Sandstone	Sandstone	Sandstone	Sandstone	Sandstone
Ag	ppm	ICP-MS	<0.01	<0.01	<0.01	<0.01	<0.01	<0.01	<0.01	<0.01	<0.01
As	ppm	ICP-MS	0.71	0.65	0.57	0.37	0.9	0.24	0.31	0.44	1.99
Be	ppm	ICP-MS	0.44	0.18	0.05	0.01	0.02	0.02	0.02	0.03	0.06
Bi	ppm	ICP-MS	<0.01	<0.01	<0.01	<0.01	<0.01	<0.01	<0.01	<0.01	0.05
Cd	ppm	ICP-MS	<0.01	<0.01	<0.01	<0.01	<0.01	<0.01	<0.01	<0.01	<0.01
Co	ppm	ICP-MS	0.02	0.03	0.36	0.04	0.04	0.03	0.05	0.1	0.49
Cs	ppm	ICP-MS	0.01	0.01	<0.01	<0.01	<0.01	<0.01	<0.01	0.02	<0.01
Cu	ppm	ICP-MS	0.92	0.8	0.83	0.45	0.57	0.6	1.41	1.13	5.24
Dy	ppm	ICP-MS	0.97	0.44	0.14	0.08	0.12	0.14	0.12	0.32	0.23
Er	ppm	ICP-MS	0.5	0.2	0.07	0.04	0.07	0.09	0.06	0.15	0.12
Eu	ppm	ICP-MS	0.15	0.09	0.07	0.02	0.03	0.03	0.02	0.09	0.04
Ga	ppm	ICP-MS	0.17	0.12	0.1	0.08	0.14	0.12	0.1	0.31	0.51
Gd	ppm	ICP-MS	0.97	0.58	0.48	0.18	0.22	0.19	0.19	0.57	0.33
Ge	ppm	ICP-MS	<0.01	<0.01	<0.01	<0.01	<0.01	<0.01	<0.01	<0.01	<0.01
Hf	ppm	ICP-MS	0.09	0.14	0.37	0.17	0.24	0.28	0.13	0.14	0.11
Hg	ppm	ICP-MS	<0.01	<0.01	<0.01	<0.01	<0.01	<0.01	<0.01	<0.01	<0.01
Ho	ppm	ICP-MS	0.18	0.07	0.02	0.01	0.02	0.03	0.02	0.05	0.04
Mo	ppm	ICP-MS	0.06	0.06	0.09	0.07	0.15	0.09	0.23	0.27	0.73
Nb	ppm	ICP-MS	<0.01	<0.01	<0.01	<0.01	<0.01	<0.01	<0.01	<0.01	<0.01
Nd	ppm	ICP-MS	2.28	1.86	3.71	1.06	1.31	0.91	0.94	3.16	1.88
Ni	ppm	ICP-MS	0.28	0.24	0.62	0.2	0.18	0.21	0.24	0.76	1.26
^{204}Pb	ppm	ICP-MS	0.019	0.011	0.01	0.005	0.006	0.027	0.007	0.003	0.004
^{206}Pb	ppm	ICP-MS	0.929	0.519	0.259	0.146	0.17	0.686	0.303	0.217	0.678
^{207}Pb	ppm	ICP-MS	0.357	0.19	0.155	0.079	0.099	0.432	0.118	0.067	0.099
^{208}Pb	ppm	ICP-MS	0.859	0.459	0.607	0.213	0.289	1.49	0.335	0.285	0.271
Pb	ppm	ICP-MS	2.16	1.18	1.03	0.443	0.564	2.63	0.763	0.573	1.05
$^{206}Pb/^{204}Pb$	--	ICP-MS	48.89	47.18	25.90	29.20	28.33	25.41	43.29	72.33	169.50
$^{207}Pb/^{206}Pb$	--	ICP-MS	0.38	0.37	0.60	0.54	0.58	0.63	0.39	0.31	0.15
$^{207}Pb/^{204}Pb$	--	ICP-MS	18.79	17.27	15.50	15.80	16.50	16.00	16.86	22.33	24.75
$^{208}Pb/^{206}Pb$	--	ICP-MS	0.92	0.88	2.34	1.46	1.70	2.17	1.11	1.31	0.40
$^{208}Pb/^{204}Pb$	--	ICP-MS	45.21	41.73	60.70	42.60	48.17	55.19	47.86	95.00	67.75
Pr	ppm	ICP-MS	0.66	0.57	1.28	0.33	0.43	0.27	0.28	0.98	0.6
Rb	ppm	ICP-MS	0.3	0.37	0.17	0.06	0.11	0.14	0.21	0.27	0.05
Sb	ppm	ICP-MS	<0.01	<0.01	<0.01	0.01	0.01	<0.01	0.01	0.01	0.15
Sc	ppm	ICP-MS	0.2	0.1	0.1	<0.1	<0.1	0.1	0.1	0.2	0.3
Se	ppm	ICP-MS	<0.1	<0.1	<0.1	<0.1	<0.1	<0.1	<0.1	<0.1	<0.1
Sm	ppm	ICP-MS	0.52	0.4	0.57	0.2	0.23	0.18	0.21	0.62	0.34
Sn	ppm	ICP-MS	0.12	0.12	0.09	0.08	0.14	0.07	0.04	0.17	0.17
Ta	ppm	ICP-MS	<0.01	<0.01	<0.01	<0.01	<0.01	<0.01	<0.01	<0.01	<0.01
Tb	ppm	ICP-MS	0.14	0.07	0.03	0.01	0.02	0.02	0.02	0.06	0.04
Te	ppm	ICP-MS	<0.01	<0.01	<0.01	<0.01	<0.01	<0.01	<0.01	<0.01	0.01
Th	ppm	ICP-MS	1.56	2.28	5.84	0.99	1.75	0.85	0.84	2.33	2
U	ppm	ICP-MS	8.91	4.02	0.39	0.73	1.61	1.62	1.21	1.82	14.8
V	ppm	ICP-MS	0.6	0.5	0.2	1.1	1.7	0.6	1	3.1	7.8
W	ppm	ICP-MS	<0.1	<0.1	<0.1	<0.1	<0.1	<0.1	<0.1	<0.1	<0.1
Y	ppm	ICP-MS	5.15	1.96	0.56	0.33	0.6	0.75	0.55	1.37	1.13
Yb	ppm	ICP-MS	0.24	0.11	0.04	0.03	0.06	0.1	0.05	0.11	0.08
Zn	ppm	ICP-MS	1.3	0.9	0.9	0.7	0.6	0.7	0.8	0.9	1.5
Zr	ppm	ICP-MS	3.25	5.34	14.8	6.21	8.4	11	4.8	5.63	4.94

Partial Digestion: A 2.00 g pulp is digested with 2.25 ml of 8:1 ultrapure HNO_3:HCl for 1 hour at 95° C.

Group #			G-2014-2129	G-2014-2129	G-2014-2129	G-2014-2129	G-2014-2129	G-2014-2129	G-2014-2129	G-2014-2129	G-2014-2129
Sample #			SG71	SG72	SG73	SG74	SG75	SG76	SG77	SG74 R	SG78
Fence			Gap	Gap	Gap	Gap	Gap	Gap	Gap	Gap	Gap
Hole ID			MAC-208	MAC-208	MAC-250	MAC-250	MAC-250	MAC-250	MAC-250	MAC-250	MAC-250
From (m)			553.50	572.00	297.80	335.10	370.80	401.43	431.78	335.10	481.75
To (m)			553.50	572.26	298.05	335.32	371.00	401.56	432.13	335.32	481.95
Lithofacies			MFa	MFa	MFa	MFa	MFa	MFa	MFa	MFa	MFa
Date			11-27-2014	11-27-2014	11-27-2014	11-27-2014	11-27-2014	11-27-2014	11-27-2014	11-27-2014	11-27-2014
Sample Type			Sandstone	Sandstone	Sandstone	Sandstone	Sandstone	Sandstone	Sandstone	Repeat	Sandstone
Ag	ppm	ICP-MS	0.02	<0.01	<0.01	<0.01	<0.01	<0.01	0.01	<0.01	<0.01
As	ppm	ICP-MS	0.22	0.43	0.68	0.37	0.45	0.51	0.55	0.38	0.22
Be	ppm	ICP-MS	0.05	0.09	0.03	0.02	0.08	0.02	0.05	0.03	0.02
Bi	ppm	ICP-MS	0.14	0.04	<0.01	<0.01	0.01	<0.01	<0.01	<0.01	<0.01
Cd	ppm	ICP-MS	<0.01	<0.01	<0.01	<0.01	0.01	<0.01	0.02	<0.01	<0.01
Co	ppm	ICP-MS	0.38	0.75	0.04	0.05	0.72	0.05	0.13	0.05	0.06
Cs	ppm	ICP-MS	<0.01	<0.01	<0.01	<0.01	<0.01	<0.01	0.01	<0.01	<0.01
Cu	ppm	ICP-MS	20.7	21.2	1.51	1.07	1.1	0.86	1.47	1.1	0.63
Dy	ppm	ICP-MS	0.19	0.34	0.12	0.15	0.11	0.1	0.43	0.16	0.2
Er	ppm	ICP-MS	0.09	0.22	0.05	0.06	0.06	0.04	0.29	0.06	0.11
Eu	ppm	ICP-MS	0.08	0.08	0.05	0.07	0.05	0.04	0.09	0.07	0.04
Ga	ppm	ICP-MS	0.08	0.4	0.06	0.09	0.08	0.13	0.12	0.1	0.09
Gd	ppm	ICP-MS	0.45	0.47	0.42	0.5	0.44	0.25	0.59	0.5	0.39
Ge	ppm	ICP-MS	<0.01	<0.01	<0.01	<0.01	<0.01	<0.01	<0.01	<0.01	<0.01
Hf	ppm	ICP-MS	0.11	0.02	0.14	0.16	0.47	0.11	0.73	0.17	0.28
Hg	ppm	ICP-MS	<0.01	<0.01	<0.01	<0.01	<0.01	<0.01	<0.01	<0.01	<0.01
Ho	ppm	ICP-MS	0.03	0.06	0.02	0.02	0.02	0.02	0.08	0.02	0.03
Mo	ppm	ICP-MS	0.12	0.16	0.06	0.07	0.09	0.11	0.13	0.08	0.13
Nb	ppm	ICP-MS	<0.01	<0.01	<0.01	<0.01	<0.01	<0.01	<0.01	<0.01	<0.01
Nd	ppm	ICP-MS	3.05	2.29	2.83	2.92	3.34	1.39	2.37	2.87	2.1
Ni	ppm	ICP-MS	0.69	1.48	0.22	0.3	0.92	0.22	0.33	0.33	0.27
^{204}Pb	ppm	ICP-MS	0.003	0.003	0.005	0.008	0.014	0.007	0.016	0.009	0.005
^{206}Pb	ppm	ICP-MS	0.301	0.477	0.194	0.228	0.341	0.218	0.416	0.231	0.176
^{207}Pb	ppm	ICP-MS	0.059	0.086	0.086	0.136	0.208	0.114	0.258	0.139	0.088
^{208}Pb	ppm	ICP-MS	0.225	0.209	0.28	0.393	0.767	0.36	0.684	0.384	0.29
Pb	ppm	ICP-MS	0.588	0.776	0.565	0.765	1.33	0.7	1.38	0.763	0.559
$^{206}Pb/^{204}Pb$	--	ICP-MS	100.33	159.00	38.80	28.50	24.36	31.14	26.00	25.67	35.20
$^{207}Pb/^{206}Pb$	--	ICP-MS	0.20	0.18	0.44	0.60	0.61	0.52	0.62	0.60	0.50
$^{207}Pb/^{204}Pb$	--	ICP-MS	19.67	28.67	17.20	17.00	14.86	16.29	16.13	15.44	17.60
$^{208}Pb/^{206}Pb$	--	ICP-MS	0.75	0.44	1.44	1.72	2.25	1.65	1.64	1.66	1.65
$^{208}Pb/^{204}Pb$	--	ICP-MS	75.00	69.67	56.00	49.13	54.79	51.43	42.75	42.67	58.00
Pr	ppm	ICP-MS	0.94	0.75	0.86	0.86	1.04	0.42	0.7	0.87	0.66
Rb	ppm	ICP-MS	0.15	0.13	0.27	0.34	0.27	0.35	0.41	0.34	0.15
Sb	ppm	ICP-MS	0.01	<0.01	<0.01	<0.01	0.01	0.01	0.02	<0.01	<0.01
Sc	ppm	ICP-MS	<0.1	0.3	<0.1	<0.1	0.1	0.1	0.4	<0.1	0.1
Se	ppm	ICP-MS	<0.1	<0.1	0.1	<0.1	<0.1	<0.1	<0.1	<0.1	<0.1
Sm	ppm	ICP-MS	0.57	0.43	0.52	0.6	0.55	0.27	0.56	0.6	0.42
Sn	ppm	ICP-MS	0.06	0.12	0.18	0.15	0.14	0.11	0.09	0.15	0.1
Ta	ppm	ICP-MS	<0.01	<0.01	<0.01	<0.01	<0.01	<0.01	<0.01	<0.01	<0.01
Tb	ppm	ICP-MS	0.04	0.06	0.03	0.04	0.03	0.02	0.07	0.04	0.04
Te	ppm	ICP-MS	<0.01	0.03	<0.01	<0.01	<0.01	<0.01	<0.01	<0.01	<0.01
Th	ppm	ICP-MS	1.71	2.5	1.87	1.3	6.76	0.9	2.93	1.36	2.16
U	ppm	ICP-MS	2.67	1.97	0.66	0.76	0.54	1.12	5.41	0.78	1.64
V	ppm	ICP-MS	0.7	1.9	1	0.3	0.9	1.3	0.9	0.3	1.1
W	ppm	ICP-MS	<0.1	<0.1	<0.1	<0.1	<0.1	<0.1	<0.1	<0.1	<0.1
Y	ppm	ICP-MS	1.02	1.97	0.42	0.59	0.51	0.41	2.43	0.59	0.96
Yb	ppm	ICP-MS	0.06	0.18	0.03	0.03	0.05	0.03	0.31	0.03	0.08
Zn	ppm	ICP-MS	0.9	1.2	0.8	0.8	0.9	1.1	2	0.8	0.6
Zr	ppm	ICP-MS	4.34	1.71	4.71	4.77	18.4	4.55	31.8	4.8	10.2

Partial Digestion: A 2.00 g pulp is digested with 2.25 ml of 8:1 ultrapure HNO_3:HCl for 1 hour at 95° C.

Group #			G-2014-2129	G-2014-2129	G-2014-2129	G-2014-2129	G-2014-2129	G-2014-2129	G-2014-2129	G-2014-2129	G-2014-2129
Sample #			SG79	SG80	SG81	SG82	SG83	SG84	SG85	SG86	SG87
Fence			Gap	Gap	Gap	Gap	Gap	Gap	Gap	Gap	Gap
Hole ID			MC-253	MC-253	MC-253	MC-253	MC-253	MC-253	MC-253	MC-253	MC-253
From (m)			26.00	76.00	113.50	136.00	182.80	205.00	265.30	287.50	325.00
To (m)			26.14	76.13	113.63	136.15	182.98	205.20	265.60	287.66	325.30
Lithofacies			MFd	MFd	MFd	MFd	MFd	MFd	MFc	MFc	MFc
Date			11-27-2014	11-27-2014	11-27-2014	11-27-2014	11-27-2014	11-27-2014	11-27-2014	11-27-2014	11-27-2014
Sample Type			Sandstone	Sandstone	Sandstone	Sandstone	Sandstone	Sandstone	Sandstone	Sandstone	Sandstone
Ag	ppm	ICP-MS	<0.01	<0.01	<0.01	<0.01	<0.01	<0.01	<0.01	<0.01	<0.01
As	ppm	ICP-MS	0.09	0.08	0.17	0.06	0.12	0.11	0.22	0.41	0.92
Be	ppm	ICP-MS	0.01	0.02	0.02	0.02	0.01	0.02	0.03	0.04	0.09
Bi	ppm	ICP-MS	<0.01	<0.01	<0.01	<0.01	<0.01	<0.01	<0.01	<0.01	<0.01
Cd	ppm	ICP-MS	<0.01	<0.01	<0.01	<0.01	<0.01	<0.01	<0.01	<0.01	0.03
Co	ppm	ICP-MS	0.03	0.03	0.04	0.03	0.04	0.03	0.05	0.04	0.14
Cs	ppm	ICP-MS	<0.01	0.01	<0.01	<0.01	<0.01	<0.01	<0.01	0.01	0.02
Cu	ppm	ICP-MS	0.67	1.12	0.95	0.38	0.64	0.46	0.78	1.46	1.47
Dy	ppm	ICP-MS	0.18	0.22	0.13	0.15	0.17	0.23	0.16	0.13	0.23
Er	ppm	ICP-MS	0.09	0.11	0.06	0.08	0.08	0.12	0.09	0.06	0.09
Eu	ppm	ICP-MS	0.04	0.04	0.03	0.04	0.04	0.06	0.05	0.05	0.06
Ga	ppm	ICP-MS	0.12	0.27	0.13	0.09	0.12	0.1	0.27	0.15	0.14
Gd	ppm	ICP-MS	0.27	0.29	0.22	0.23	0.27	0.35	0.32	0.33	0.47
Ge	ppm	ICP-MS	<0.01	<0.01	<0.01	<0.01	<0.01	<0.01	<0.01	<0.01	<0.01
Hf	ppm	ICP-MS	0.12	0.15	0.1	0.15	0.1	0.2	0.15	0.11	0.11
Hg	ppm	ICP-MS	<0.01	<0.01	<0.01	<0.01	<0.01	<0.01	<0.01	<0.01	<0.01
Ho	ppm	ICP-MS	0.03	0.04	0.02	0.02	0.03	0.04	0.03	0.02	0.03
Mo	ppm	ICP-MS	0.04	0.05	0.09	0.05	0.05	0.04	0.04	0.05	0.07
Nb	ppm	ICP-MS	<0.01	<0.01	<0.01	<0.01	<0.01	<0.01	<0.01	<0.01	<0.01
Nd	ppm	ICP-MS	1.38	1.25	1.06	1.08	1.35	1.8	1.63	1.88	1.83
Ni	ppm	ICP-MS	0.16	0.26	0.27	0.2	0.28	0.22	0.63	0.6	1.3
^{204}Pb	ppm	ICP-MS	0.006	0.006	0.008	0.007	0.013	0.022	0.1	0.006	0.014
^{206}Pb	ppm	ICP-MS	0.149	0.156	0.174	0.14	0.359	0.564	2.93	0.233	0.79
^{207}Pb	ppm	ICP-MS	0.106	0.103	0.124	0.106	0.217	0.355	1.65	0.11	0.277
^{208}Pb	ppm	ICP-MS	0.27	0.263	0.308	0.266	0.656	1.08	5.53	0.299	0.618
Pb	ppm	ICP-MS	0.532	0.529	0.614	0.519	1.25	2.02	10.2	0.649	1.7
$^{206}Pb/^{204}Pb$	--	ICP-MS	24.83	26.00	21.75	20.00	27.62	25.64	29.30	38.83	56.43
$^{207}Pb/^{206}Pb$	--	ICP-MS	0.71	0.66	0.71	0.76	0.60	0.63	0.56	0.47	0.35
$^{207}Pb/^{204}Pb$	--	ICP-MS	17.67	17.17	15.50	15.14	16.69	16.14	16.50	18.33	19.79
$^{208}Pb/^{206}Pb$	--	ICP-MS	1.81	1.69	1.77	1.90	1.83	1.91	1.89	1.28	0.78
$^{208}Pb/^{204}Pb$	--	ICP-MS	45.00	43.83	38.50	38.00	50.46	49.09	55.30	49.83	44.14
Pr	ppm	ICP-MS	0.46	0.41	0.33	0.34	0.43	0.57	0.52	0.58	0.57
Rb	ppm	ICP-MS	0.07	0.14	0.16	0.1	0.06	0.06	0.15	0.12	0.24
Sb	ppm	ICP-MS	<0.01	<0.01	<0.01	<0.01	<0.01	<0.01	<0.01	<0.01	<0.01
Sc	ppm	ICP-MS	0.2	0.2	<0.1	0.1	<0.1	0.2	0.2	<0.1	0.2
Se	ppm	ICP-MS	<0.1	<0.1	<0.1	<0.1	<0.1	<0.1	<0.1	<0.1	<0.1
Sm	ppm	ICP-MS	0.27	0.26	0.22	0.22	0.28	0.38	0.33	0.39	0.42
Sn	ppm	ICP-MS	0.09	0.15	0.1	0.03	0.04	0.04	0.07	0.25	0.22
Ta	ppm	ICP-MS	<0.01	<0.01	<0.01	<0.01	<0.01	<0.01	<0.01	<0.01	<0.01
Tb	ppm	ICP-MS	0.03	0.03	0.02	0.02	0.03	0.04	0.03	0.03	0.05
Te	ppm	ICP-MS	<0.01	<0.01	<0.01	<0.01	<0.01	<0.01	<0.01	<0.01	<0.01
Th	ppm	ICP-MS	0.73	0.64	0.59	0.78	0.55	0.95	1.71	1.56	1.21
U	ppm	ICP-MS	0.43	0.53	0.6	0.48	0.7	0.88	1.08	0.74	2.67
V	ppm	ICP-MS	0.2	0.9	1	0.1	0.3	0.2	0.2	0.2	1
W	ppm	ICP-MS	<0.1	<0.1	<0.1	<0.1	<0.1	<0.1	<0.1	<0.1	<0.1
Y	ppm	ICP-MS	0.73	1.05	0.59	0.64	0.68	1.01	0.82	0.5	0.88
Yb	ppm	ICP-MS	0.07	0.08	0.04	0.06	0.06	0.09	0.06	0.04	0.06
Zn	ppm	ICP-MS	1	0.8	2.4	0.7	0.8	3.2	1	1	2.6
Zr	ppm	ICP-MS	4.84	5.67	3.72	5.82	3.91	7.84	5.81	4.11	3.82

Partial Digestion: A 2.00 g pulp is digested with 2.25 ml of 8:1 ultrapure HNO_3:HCl for 1 hour at 95° C.

Group #			G-2014-2129	G-2014-2129	G-2014-2129	G-2014-2129	G-2014-2129	G-2014-2129	G-2014-2129	G-2014-2129	G-2014-2129
Sample #			SG88	SG89	SG90	SG91	SG92	SG93	SG94	SG95	SG96
Fence			Gap	Gap	Gap	Gap	Gap	Gap	Gap	Gap	Gap
Hole ID			MC-253	MC-253	MC-253	MC-253	MC-253	MC-253	MC-253	MC-253	MC-253
From (m)			336.20	382.00	416.00	430.10	440.10	472.50	501.00	507.50	528.00
To (m)			336.40	382.18	416.18	430.40	440.28	472.66	501.20	507.80	528.30
Lithofacies			MFc	MFb	MFb	MFb	MFb	MFb	MFb	MFb	MFb
Date			11-27-2014	11-27-2014	11-27-2014	11-27-2014	11-27-2014	11-27-2014	11-27-2014	11-27-2014	11-27-2014
Sample Type			Sandstone	Sandstone	Sandstone	Sandstone	Sandstone	Sandstone	Sandstone	Sandstone	Sandstone
Ag	ppm	ICP-MS	<0.01	<0.01	<0.01	<0.01	<0.01	<0.01	<0.01	<0.01	<0.01
As	ppm	ICP-MS	0.82	0.65	0.7	1.18	0.46	0.24	0.22	0.28	0.31
Be	ppm	ICP-MS	0.08	0.04	0.03	0.06	0.04	0.01	0.01	0.02	0.02
Bi	ppm	ICP-MS	<0.01	<0.01	<0.01	0.01	<0.01	<0.01	<0.01	<0.01	<0.01
Cd	ppm	ICP-MS	<0.01	<0.01	<0.01	<0.01	<0.01	<0.01	<0.01	<0.01	<0.01
Co	ppm	ICP-MS	0.08	0.04	0.04	0.05	0.05	0.03	0.05	0.05	0.05
Cs	ppm	ICP-MS	0.03	<0.01	<0.01	0.02	<0.01	<0.01	<0.01	<0.01	0.01
Cu	ppm	ICP-MS	0.82	0.64	1.19	1.16	0.7	0.49	0.46	0.66	0.59
Dy	ppm	ICP-MS	0.19	0.14	0.14	0.18	0.1	0.06	0.07	0.11	0.16
Er	ppm	ICP-MS	0.09	0.07	0.07	0.1	0.06	0.03	0.04	0.04	0.08
Eu	ppm	ICP-MS	0.08	0.06	0.06	0.08	0.04	0.02	0.02	0.04	0.04
Ga	ppm	ICP-MS	0.18	0.08	0.12	0.19	0.05	0.05	0.08	0.08	0.1
Gd	ppm	ICP-MS	0.52	0.5	0.47	0.52	0.3	0.14	0.16	0.34	0.31
Ge	ppm	ICP-MS	<0.01	<0.01	<0.01	<0.01	<0.01	<0.01	<0.01	<0.01	<0.01
Hf	ppm	ICP-MS	0.16	0.22	0.16	0.31	0.22	0.08	0.11	0.08	0.2
Hg	ppm	ICP-MS	<0.01	<0.01	<0.01	<0.01	<0.01	<0.01	<0.01	<0.01	<0.01
Ho	ppm	ICP-MS	0.03	0.02	0.02	0.03	0.02	<0.01	0.01	0.01	0.03
Mo	ppm	ICP-MS	0.04	0.04	0.03	0.07	0.08	0.06	0.07	0.08	0.14
Nb	ppm	ICP-MS	<0.01	<0.01	<0.01	<0.01	<0.01	<0.01	<0.01	<0.01	<0.01
Nd	ppm	ICP-MS	2.84	3.03	2.99	3.11	1.98	0.9	0.92	2.58	1.46
Ni	ppm	ICP-MS	0.95	0.2	0.2	0.36	0.27	0.21	0.27	0.26	0.21
^{204}Pb	ppm	ICP-MS	0.01	0.007	0.006	0.006	0.006	0.004	0.006	0.004	0.006
^{206}Pb	ppm	ICP-MS	0.361	0.176	0.143	0.17	0.151	0.122	0.135	0.12	0.175
^{207}Pb	ppm	ICP-MS	0.167	0.113	0.098	0.1	0.09	0.071	0.086	0.06	0.095
^{208}Pb	ppm	ICP-MS	0.502	0.415	0.38	0.514	0.341	0.218	0.227	0.18	0.276
Pb	ppm	ICP-MS	1.04	0.711	0.627	0.791	0.588	0.415	0.454	0.364	0.552
^{206}Pb/^{204}Pb	--	ICP-MS	36.10	25.14	23.83	28.33	25.17	30.50	22.50	30.00	29.17
^{207}Pb/^{206}Pb	--	ICP-MS	0.46	0.64	0.69	0.59	0.60	0.58	0.64	0.50	0.54
^{207}Pb/^{204}Pb	--	ICP-MS	16.70	16.14	16.33	16.67	15.00	17.75	14.33	15.00	15.83
^{208}Pb/^{206}Pb	--	ICP-MS	1.39	2.36	2.66	3.02	2.26	1.79	1.68	1.50	1.58
^{208}Pb/^{204}Pb	--	ICP-MS	50.20	59.29	63.33	85.67	56.83	54.50	37.83	45.00	46.00
Pr	ppm	ICP-MS	0.88	0.99	0.95	1	0.68	0.32	0.29	0.7	0.46
Rb	ppm	ICP-MS	0.39	0.23	0.23	0.39	0.06	0.09	0.09	0.12	0.31
Sb	ppm	ICP-MS	<0.01	<0.01	<0.01	<0.01	<0.01	<0.01	<0.01	0.02	<0.01
Sc	ppm	ICP-MS	0.1	0.1	<0.1	0.1	<0.1	<0.1	<0.1	<0.1	<0.1
Se	ppm	ICP-MS	<0.1	<0.1	<0.1	0.1	<0.1	<0.1	<0.1	<0.1	<0.1
Sm	ppm	ICP-MS	0.56	0.56	0.59	0.58	0.35	0.16	0.18	0.52	0.31
Sn	ppm	ICP-MS	0.08	0.1	0.17	0.03	0.02	0.05	0.04	0.1	0.07
Ta	ppm	ICP-MS	<0.01	<0.01	<0.01	<0.01	<0.01	<0.01	<0.01	<0.01	<0.01
Tb	ppm	ICP-MS	0.04	0.04	0.03	0.04	0.02	0.01	0.01	0.02	0.03
Te	ppm	ICP-MS	<0.01	<0.01	<0.01	<0.01	<0.01	<0.01	<0.01	<0.01	<0.01
Th	ppm	ICP-MS	3.49	3.91	4.31	8.44	3.01	1.24	0.68	1.16	1.44
U	ppm	ICP-MS	1.63	0.52	0.68	2.89	0.78	0.49	0.62	0.83	1.39
V	ppm	ICP-MS	0.9	0.5	0.7	0.8	0.5	0.4	0.4	0.8	0.4
W	ppm	ICP-MS	<0.1	<0.1	<0.1	<0.1	<0.1	<0.1	<0.1	<0.1	<0.1
Y	ppm	ICP-MS	0.79	0.54	0.56	0.96	0.46	0.26	0.34	0.37	0.74
Yb	ppm	ICP-MS	0.07	0.04	0.04	0.07	0.04	0.02	0.03	0.03	0.06
Zn	ppm	ICP-MS	2.5	1.3	1.2	1.1	1.1	0.7	0.8	0.7	0.8
Zr	ppm	ICP-MS	5.91	8.84	6.24	13.9	7.22	2.86	4.13	2.65	7.15

Partial Digestion: A 2.00 g pulp is digested with 2.25 ml of 8:1 ultrapure HNO_3:HCl for 1 hour at 95° C.

Group #			G-2014-2129	G-2014-2129	G-2014-2129	G-2014-2129	G-2014-2129	G-2014-2129	G-2014-2129	G-2014-2129	G-2014-2129
Sample #			SG97	SG99	SG100	SG101	SG102	SG103	SG104	SG105	SG106
Fence			Gap	Gap	Gap	Zone 4	Zone 4	Zone 4	Zone 4	Zone 4	Zone 4
Hole ID			MC-253	MC-253	MC-253	MAC-246	MAC-246	MAC-246	MAC-246	MAC-246	MAC-246
From (m)			538.00	550.10	552.00	4.33	54.70	60.60	82.75	126.15	142.86
To (m)			538.15	550.25	552.30	4.48	54.90	60.75	82.93	126.32	143.00
Lithofacies			MFb	MFb	MFa	MFd	MFd	MFd	MFd	MFd	MFd
Date			11-27-2014	11-27-2014	11-27-2014	11-27-2014	11-27-2014	11-27-2014	11-27-2014	11-27-2014	11-27-2014
Sample Type			Sandstone	Sandstone	Sandstone	Sandstone	Sandstone	Sandstone	Sandstone	Sandstone	Sandstone
Ag	ppm	ICP-MS	<0.01	0.02	<0.01	<0.01	<0.01	<0.01	<0.01	<0.01	<0.01
As	ppm	ICP-MS	0.28	0.49	0.3	0.09	0.11	0.09	0.06	0.12	0.27
Be	ppm	ICP-MS	0.01	0.06	0.04	0.02	0.02	0.02	0.01	0.01	0.04
Bi	ppm	ICP-MS	<0.01	0.01	<0.01	<0.01	0.01	<0.01	<0.01	<0.01	<0.01
Cd	ppm	ICP-MS	<0.01	<0.01	<0.01	<0.01	<0.01	<0.01	<0.01	<0.01	<0.01
Co	ppm	ICP-MS	0.05	0.09	0.08	0.02	0.03	0.02	0.03	0.04	0.06
Cs	ppm	ICP-MS	0.01	<0.01	<0.01	<0.01	0.02	<0.01	<0.01	<0.01	<0.01
Cu	ppm	ICP-MS	0.52	2.05	1.09	0.63	2	0.64	0.66	0.66	1.61
Dy	ppm	ICP-MS	0.06	0.16	0.1	0.19	0.27	0.23	0.17	0.13	0.23
Er	ppm	ICP-MS	0.03	0.09	0.05	0.08	0.14	0.11	0.08	0.05	0.12
Eu	ppm	ICP-MS	0.02	0.06	0.04	0.05	0.06	0.06	0.05	0.03	0.06
Ga	ppm	ICP-MS	0.08	0.17	0.05	0.05	0.09	0.08	0.04	0.07	0.13
Gd	ppm	ICP-MS	0.15	0.35	0.27	0.3	0.37	0.34	0.24	0.21	0.31
Ge	ppm	ICP-MS	<0.01	<0.01	<0.01	<0.01	<0.01	<0.01	<0.01	<0.01	<0.01
Hf	ppm	ICP-MS	0.08	0.32	0.28	0.09	0.22	0.2	0.15	0.07	0.24
Hg	ppm	ICP-MS	<0.01	<0.01	<0.01	<0.01	<0.01	<0.01	<0.01	<0.01	<0.01
Ho	ppm	ICP-MS	<0.01	0.02	0.02	0.03	0.04	0.04	0.03	0.02	0.04
Mo	ppm	ICP-MS	0.08	0.1	0.08	0.04	0.03	0.04	0.05	0.06	0.14
Nb	ppm	ICP-MS	<0.01	<0.01	<0.01	<0.01	<0.01	<0.01	<0.01	<0.01	<0.01
Nd	ppm	ICP-MS	0.88	2.35	1.79	1.57	1.88	1.78	1.13	1	1.21
Ni	ppm	ICP-MS	0.26	0.5	0.26	0.12	0.2	0.13	0.18	0.24	0.3
^{204}Pb	ppm	ICP-MS	0.004	0.009	0.007	0.008	0.011	0.008	0.006	0.012	0.023
^{206}Pb	ppm	ICP-MS	0.119	0.333	0.196	0.193	0.214	0.164	0.146	0.31	0.522
^{207}Pb	ppm	ICP-MS	0.066	0.142	0.115	0.128	0.164	0.123	0.097	0.197	0.368
^{208}Pb	ppm	ICP-MS	0.196	0.494	0.332	0.308	0.398	0.315	0.25	0.532	0.962
Pb	ppm	ICP-MS	0.386	0.979	0.651	0.637	0.787	0.61	0.499	1.05	1.88
$^{206}Pb/^{204}Pb$	--	ICP-MS	29.75	37.00	28.00	24.13	19.45	20.50	24.33	25.83	22.70
$^{207}Pb/^{206}Pb$	--	ICP-MS	0.55	0.43	0.59	0.66	0.77	0.75	0.66	0.64	0.70
$^{207}Pb/^{204}Pb$	--	ICP-MS	16.50	15.78	16.43	16.00	14.91	15.38	16.17	16.42	16.00
$^{208}Pb/^{206}Pb$	--	ICP-MS	1.65	1.48	1.69	1.60	1.86	1.92	1.71	1.72	1.84
$^{208}Pb/^{204}Pb$	--	ICP-MS	49.00	54.89	47.43	38.50	36.18	39.38	41.67	44.33	41.83
Pr	ppm	ICP-MS	0.29	0.81	0.59	0.52	0.61	0.59	0.36	0.3	0.36
Rb	ppm	ICP-MS	0.27	0.14	0.06	0.06	0.18	0.08	0.04	0.09	0.11
Sb	ppm	ICP-MS	<0.01	<0.01	<0.01	0.02	<0.01	<0.01	0.01	0.02	0.04
Sc	ppm	ICP-MS	<0.1	0.1	<0.1	0.1	0.4	0.2	0.2	<0.1	0.3
Se	ppm	ICP-MS	<0.1	<0.1	<0.1	<0.1	<0.1	<0.1	<0.1	<0.1	<0.1
Sm	ppm	ICP-MS	0.17	0.4	0.33	0.32	0.38	0.36	0.25	0.21	0.29
Sn	ppm	ICP-MS	0.06	0.05	0.02	0.04	0.33	0.06	0.03	0.03	0.06
Ta	ppm	ICP-MS	<0.01	<0.01	<0.01	<0.01	<0.01	<0.01	<0.01	<0.01	<0.01
Tb	ppm	ICP-MS	0.01	0.03	0.02	0.03	0.04	0.04	0.03	0.02	0.04
Te	ppm	ICP-MS	<0.01	<0.01	<0.01	<0.01	<0.01	<0.01	<0.01	<0.01	<0.01
Th	ppm	ICP-MS	1.28	5.58	1.91	0.56	0.91	1.19	0.7	0.52	1.2
U	ppm	ICP-MS	0.52	1.78	1.7	0.38	0.66	0.59	0.53	0.76	1.88
V	ppm	ICP-MS	0.5	0.8	0.4	0.2	0.8	0.2	0.1	0.3	4.7
W	ppm	ICP-MS	<0.1	<0.1	<0.1	<0.1	<0.1	<0.1	<0.1	<0.1	<0.1
Y	ppm	ICP-MS	0.27	0.78	0.45	0.76	1.11	0.89	0.68	0.46	0.98
Yb	ppm	ICP-MS	0.02	0.07	0.04	0.06	0.11	0.09	0.07	0.04	0.09
Zn	ppm	ICP-MS	1	0.9	0.8	0.8	1.3	0.9	0.7	0.9	2.6
Zr	ppm	ICP-MS	2.69	11.6	9.99	3.64	8.66	7.57	5.63	2.53	9.68

Partial Digestion: A 2.00 g pulp is digested with 2.25 ml of 8:1 ultrapure HNO_3:HCl for 1 hour at 95° C.

Group #			G-2014-2129	G-2014-2129	G-2014-2129	G-2014-2129	G-2014-2129	G-2014-2129	G-2014-2129	G-2014-2129	G-2014-2129
Sample #			SG107	SG108	SG109	SG110	SG111	SG112	SG113	SG114	SG115
Fence			Zone 4	Zone 4	Zone 4	Zone 4	Zone 4	Zone 4	Zone 4	Zone 4	Zone 4
Hole ID			MAC-246	MAC-246	MAC-246	MAC-246	MAC-246	MAC-246	MAC-246	MAC-246	MAC-246
From (m)			165.40	213.43	267.05	297.33	324.50	333.80	354.17	378.25	418.13
To (m)			165.56	213.58	267.25	297.53	324.72	334.00	354.38	378.44	418.30
Lithofacies			MFd	MFc	MFc	MFc	MFb	MFb	MFb	MFb	MFa
Date			11-27-2014	11-27-2014	11-27-2014	11-27-2014	11-27-2014	11-27-2014	11-27-2014	11-27-2014	11-27-2014
Sample Type			Sandstone	Sandstone	Sandstone	Sandstone	Sandstone	Sandstone	Sandstone	Sandstone	Sandstone
Ag	ppm	ICP-MS	<0.01	<0.01	<0.01	<0.01	<0.01	<0.01	<0.01	<0.01	<0.01
As	ppm	ICP-MS	0.11	0.22	0.53	0.54	0.93	0.66	0.51	0.33	0.35
Be	ppm	ICP-MS	0.02	0.02	0.02	0.03	0.07	0.05	0.05	0.02	0.02
Bi	ppm	ICP-MS	<0.01	<0.01	<0.01	0.02	0.01	0.01	<0.01	<0.01	<0.01
Cd	ppm	ICP-MS	<0.01	<0.01	<0.01	<0.01	<0.01	0.01	<0.01	<0.01	<0.01
Co	ppm	ICP-MS	0.04	0.03	0.04	0.03	0.04	0.03	0.04	0.04	0.04
Cs	ppm	ICP-MS	<0.01	<0.01	0.01	<0.01	0.01	<0.01	<0.01	<0.01	<0.01
Cu	ppm	ICP-MS	0.69	0.5	0.96	2.51	1.46	1.14	1.03	0.34	0.4
Dy	ppm	ICP-MS	0.22	0.15	0.13	0.21	0.3	0.21	0.26	0.12	0.07
Er	ppm	ICP-MS	0.11	0.07	0.06	0.11	0.14	0.1	0.13	0.05	0.03
Eu	ppm	ICP-MS	0.06	0.05	0.03	0.05	0.12	0.07	0.08	0.04	0.03
Ga	ppm	ICP-MS	0.09	0.11	0.13	0.12	0.13	0.08	0.13	0.12	0.1
Gd	ppm	ICP-MS	0.34	0.3	0.24	0.43	0.77	0.67	0.64	0.32	0.2
Ge	ppm	ICP-MS	<0.01	<0.01	<0.01	<0.01	<0.01	<0.01	<0.01	<0.01	<0.01
Hf	ppm	ICP-MS	0.17	0.09	0.12	0.34	0.25	0.34	0.35	0.16	0.18
Hg	ppm	ICP-MS	<0.01	<0.01	<0.01	<0.01	<0.01	<0.01	<0.01	<0.01	<0.01
Ho	ppm	ICP-MS	0.04	0.02	0.02	0.04	0.05	0.03	0.04	0.02	<0.01
Mo	ppm	ICP-MS	0.04	0.04	0.07	0.07	0.06	0.05	0.07	0.05	0.06
Nb	ppm	ICP-MS	<0.01	<0.01	<0.01	<0.01	<0.01	0.01	<0.01	<0.01	<0.01
Nd	ppm	ICP-MS	1.66	1.56	1.14	2.05	4.42	4.34	3.05	1.92	1.24
Ni	ppm	ICP-MS	0.21	0.29	0.39	0.4	0.29	0.22	0.28	0.16	0.23
^{204}Pb	ppm	ICP-MS	0.011	0.007	0.009	0.01	0.014	0.029	0.007	0.005	0.006
^{206}Pb	ppm	ICP-MS	0.252	0.162	0.327	0.29	0.403	0.562	0.163	0.138	0.137
^{207}Pb	ppm	ICP-MS	0.178	0.114	0.156	0.157	0.226	0.455	0.11	0.082	0.091
^{208}Pb	ppm	ICP-MS	0.435	0.297	0.381	0.546	0.838	1.38	0.521	0.295	0.301
Pb	ppm	ICP-MS	0.876	0.58	0.873	1	1.48	2.42	0.801	0.52	0.535
$^{206}Pb/^{204}Pb$	--	ICP-MS	22.91	23.14	36.33	29.00	28.79	19.38	23.29	27.60	22.83
$^{207}Pb/^{206}Pb$	--	ICP-MS	0.71	0.70	0.48	0.54	0.56	0.81	0.67	0.59	0.66
$^{207}Pb/^{204}Pb$	--	ICP-MS	16.18	16.29	17.33	15.70	16.14	15.69	15.71	16.40	15.17
$^{208}Pb/^{206}Pb$	--	ICP-MS	1.73	1.83	1.17	1.88	2.08	2.46	3.20	2.14	2.20
$^{208}Pb/^{204}Pb$	--	ICP-MS	39.55	42.43	42.33	54.60	59.86	47.59	74.43	59.00	50.17
Pr	ppm	ICP-MS	0.52	0.48	0.37	0.64	1.44	1.46	0.97	0.64	0.4
Rb	ppm	ICP-MS	0.08	0.1	0.24	0.28	0.33	0.26	0.25	0.07	0.07
Sb	ppm	ICP-MS	0.01	<0.01	<0.01	0.02	<0.01	<0.01	<0.01	<0.01	0.02
Sc	ppm	ICP-MS	0.2	0.1	<0.1	0.1	0.1	<0.1	0.1	<0.1	<0.1
Se	ppm	ICP-MS	<0.1	<0.1	<0.1	<0.1	<0.1	0.1	<0.1	<0.1	<0.1
Sm	ppm	ICP-MS	0.35	0.32	0.23	0.44	0.8	0.76	0.66	0.35	0.22
Sn	ppm	ICP-MS	0.05	0.04	0.17	0.61	0.37	0.28	0.21	0.08	0.07
Ta	ppm	ICP-MS	<0.01	<0.01	<0.01	<0.01	<0.01	<0.01	<0.01	<0.01	<0.01
Tb	ppm	ICP-MS	0.04	0.03	0.02	0.04	0.06	0.05	0.06	0.03	0.02
Te	ppm	ICP-MS	<0.01	<0.01	<0.01	<0.01	<0.01	<0.01	<0.01	<0.01	<0.01
Th	ppm	ICP-MS	1	0.79	1.96	7.46	17.9	11.6	15.3	3.04	2.28
U	ppm	ICP-MS	1.16	0.81	1.21	1.06	1.92	1.23	1	0.67	0.3
V	ppm	ICP-MS	0.3	0.5	0.9	1.2	1.2	0.8	0.7	0.6	1.1
W	ppm	ICP-MS	<0.1	<0.1	<0.1	<0.1	<0.1	<0.1	<0.1	<0.1	<0.1
Y	ppm	ICP-MS	0.9	0.57	0.62	1.03	1.23	0.84	1.15	0.39	0.24
Yb	ppm	ICP-MS	0.08	0.05	0.04	0.09	0.09	0.06	0.1	0.03	0.02
Zn	ppm	ICP-MS	1.2	0.7	0.9	1.2	0.9	2	0.8	0.6	0.9
Zr	ppm	ICP-MS	6.8	3.45	4.8	15.7	12.9	15.6	16.4	5.99	6.81

Partial Digestion: A 2.00 g pulp is digested with 2.25 ml of 8:1 ultrapure HNO_3:HCl for 1 hour at 95° C.

Group #			G-2014-2129	G-2014-2129	G-2014-2129	G-2014-2129	G-2014-2129	G-2014-2129	G-2014-2129	G-2014-2129	G-2014-2129
Sample #			SG113 R	SG116	SG117	SG118	SG119	SG120	SG121	SG122	SG123
Fence			Zone 4	Zone 4	Zone 4	Zone 4	Zone 4	Zone 4	Zone 4	Zone 4	Zone 4
Hole ID			MAC-246	MAC-246	MAC-246	MAC-246	MAC-246	MAC-246	MAC-246	MAC-246	MAC-246
From (m)			354.17	423.80	454.11	475.33	496.42	499.02	508.80	510.20	543.00
To (m)			354.38	423.91	454.34	475.51	496.70	499.24	508.89	510.33	543.26
Lithofacies			MFb	MFa	MFa	MFa	MFa	MFa	MFa	MFa	MFa
Date			11-27-2014	11-27-2014	11-27-2014	11-27-2014	11-27-2014	11-27-2014	11-27-2014	11-27-2014	11-27-2014
Sample Type			Repeat	Sandstone	Sandstone	Sandstone	Sandstone	Sandstone	Sandstone	Sandstone	Sandstone
Ag	ppm	ICP-MS	<0.01	<0.01	<0.01	<0.01	0.01	0.01	0.02	0.01	<0.01
As	ppm	ICP-MS	0.49	0.3	0.66	0.38	0.54	0.66	0.44	0.42	0.12
Be	ppm	ICP-MS	0.04	0.02	0.04	0.02	0.06	0.04	0.06	0.04	0.02
Bi	ppm	ICP-MS	<0.01	<0.01	<0.01	<0.01	0.01	0.01	0.04	<0.01	<0.01
Cd	ppm	ICP-MS	<0.01	<0.01	<0.01	<0.01	<0.01	<0.01	0.01	<0.01	<0.01
Co	ppm	ICP-MS	0.04	0.05	0.07	0.06	0.18	0.19	0.12	0.1	0.08
Cs	ppm	ICP-MS	<0.01	<0.01	<0.01	<0.01	<0.01	<0.01	<0.01	<0.01	<0.01
Cu	ppm	ICP-MS	1.11	0.53	1.16	1.3	5.26	2.77	2.29	4.93	1.52
Dy	ppm	ICP-MS	0.26	0.11	0.11	0.07	0.15	0.23	0.14	0.06	0.09
Er	ppm	ICP-MS	0.13	0.06	0.05	0.04	0.08	0.12	0.07	0.04	0.05
Eu	ppm	ICP-MS	0.07	0.03	0.06	0.02	0.03	0.03	0.04	0.02	0.03
Ga	ppm	ICP-MS	0.13	0.11	0.05	0.04	0.21	0.13	0.12	0.07	0.05
Gd	ppm	ICP-MS	0.61	0.24	0.39	0.13	0.23	0.23	0.22	0.12	0.22
Ge	ppm	ICP-MS	<0.01	<0.01	<0.01	<0.01	<0.01	<0.01	<0.01	<0.01	<0.01
Hf	ppm	ICP-MS	0.37	0.25	0.31	0.21	0.25	0.3	0.47	0.22	0.09
Hg	ppm	ICP-MS	<0.01	<0.01	<0.01	<0.01	<0.01	<0.01	<0.01	<0.01	<0.01
Ho	ppm	ICP-MS	0.04	0.02	0.02	0.01	0.03	0.04	0.02	0.01	0.02
Mo	ppm	ICP-MS	0.07	0.1	0.12	0.14	0.38	0.68	0.3	0.33	0.1
Nb	ppm	ICP-MS	<0.01	<0.01	<0.01	<0.01	<0.01	<0.01	<0.01	<0.01	<0.01
Nd	ppm	ICP-MS	3.01	1.27	2.23	0.65	1.23	1.03	1.04	0.56	1.1
Ni	ppm	ICP-MS	0.28	0.27	0.33	0.28	0.51	0.36	0.3	0.27	0.3
^{204}Pb	ppm	ICP-MS	0.006	0.004	0.008	0.007	0.005	0.011	0.013	0.005	0.005
^{206}Pb	ppm	ICP-MS	0.161	0.133	0.233	0.252	0.385	0.486	0.656	0.261	0.194
^{207}Pb	ppm	ICP-MS	0.107	0.069	0.128	0.124	0.094	0.19	0.222	0.087	0.09
^{208}Pb	ppm	ICP-MS	0.496	0.229	0.474	0.337	0.24	0.452	0.501	0.217	0.258
Pb	ppm	ICP-MS	0.771	0.436	0.843	0.721	0.724	1.14	1.39	0.57	0.547
$^{206}Pb/^{204}Pb$	--	ICP-MS	26.83	33.25	29.13	36.00	77.00	44.18	50.46	52.20	38.80
$^{207}Pb/^{206}Pb$	--	ICP-MS	0.66	0.52	0.55	0.49	0.24	0.39	0.34	0.33	0.46
$^{207}Pb/^{204}Pb$	--	ICP-MS	17.83	17.25	16.00	17.71	18.80	17.27	17.08	17.40	18.00
$^{208}Pb/^{206}Pb$	--	ICP-MS	3.08	1.72	2.03	1.34	0.62	0.93	0.76	0.83	1.33
$^{208}Pb/^{204}Pb$	--	ICP-MS	82.67	57.25	59.25	48.14	48.00	41.09	38.54	43.40	51.60
Pr	ppm	ICP-MS	0.93	0.41	0.71	0.2	0.39	0.33	0.31	0.16	0.34
Rb	ppm	ICP-MS	0.25	0.11	0.05	0.05	0.07	0.05	0.04	0.03	0.11
Sb	ppm	ICP-MS	<0.01	0.01	<0.01	<0.01	<0.01	<0.01	0.02	0.01	0.08
Sc	ppm	ICP-MS	0.2	0.1	<0.1	<0.1	0.2	0.2	0.1	<0.1	<0.1
Se	ppm	ICP-MS	<0.1	<0.1	<0.1	<0.1	<0.1	<0.1	<0.1	<0.1	<0.1
Sm	ppm	ICP-MS	0.64	0.26	0.46	0.13	0.24	0.21	0.23	0.13	0.22
Sn	ppm	ICP-MS	0.23	0.09	0.05	0.03	0.04	0.04	0.08	0.06	0.04
Ta	ppm	ICP-MS	<0.01	<0.01	<0.01	<0.01	<0.01	<0.01	<0.01	<0.01	<0.01
Tb	ppm	ICP-MS	0.06	0.02	0.03	0.01	0.02	0.03	0.02	0.01	0.02
Te	ppm	ICP-MS	<0.01	<0.01	<0.01	<0.01	<0.01	<0.01	<0.01	<0.01	<0.01
Th	ppm	ICP-MS	14.9	1.74	3.54	0.77	0.9	0.81	0.78	0.32	1.24
U	ppm	ICP-MS	1.02	1.52	2.08	2.41	5.62	5.55	4.31	5.35	0.66
V	ppm	ICP-MS	0.6	0.9	1.2	0.7	2	1.5	4.8	1.8	0.5
W	ppm	ICP-MS	<0.1	<0.1	<0.1	<0.1	<0.1	<0.1	<0.1	0.2	<0.1
Y	ppm	ICP-MS	1.13	0.51	0.47	0.39	0.82	1.19	0.94	0.44	0.42
Yb	ppm	ICP-MS	0.1	0.06	0.04	0.04	0.07	0.1	0.06	0.03	0.05
Zn	ppm	ICP-MS	0.8	0.6	0.8	0.6	1.2	1.2	1.1	1	0.7
Zr	ppm	ICP-MS	16.8	9.43	10.7	7.84	9.04	11.6	18.9	8.87	3.56

Partial Digestion: A 2.00 g pulp is digested with 2.25 ml of 8:1 ultrapure HNO_3:HCl for 1 hour at 95° C.

Group #			G-2014-2129	G-2014-2129	G-2014-2129	G-2014-2129	G-2014-2129	G-2014-2129	G-2014-2129	G-2014-2129	G-2014-2129
Sample #			SG124	SG125	SG126	SG127	SG128	SG129	SG130	SG131	SG132
Fence			Zone 4	Zone 4	Zone 4	Zone 4	Zone 4	Zone 4	Zone 4	Zone 4	Zone 4
Hole ID			MAC-252	MAC-252	MAC-252	MAC-252	MAC-252	MAC-252	MAC-252	MAC-252	MAC-252
From (m)			10.15	25.70	55.65	102.48	167.20	199.86	249.43	261.91	271.20
To (m)			10.30	25.85	55.80	102.70	167.42	200.11	249.56	262.07	271.35
Lithofacies			MFd	MFd	MFd	MFd	MFd	MFc	MFc	MFc	MFc
Date			11-27-2014	11-27-2014	11-27-2014	11-27-2014	11-27-2014	11-27-2014	11-27-2014	11-27-2014	11-27-2014
Sample Type			Sandstone	Sandstone	Sandstone	Sandstone	Sandstone	Sandstone	Sandstone	Sandstone	Sandstone
Ag	ppm	ICP-MS	<0.01	<0.01	<0.01	<0.01	<0.01	<0.01	<0.01	<0.01	<0.01
As	ppm	ICP-MS	0.11	0.1	0.1	0.2	0.2	0.3	0.54	0.23	0.99
Be	ppm	ICP-MS	0.02	0.02	0.03	0.02	0.04	0.05	0.05	0.04	0.2
Bi	ppm	ICP-MS	<0.01	<0.01	<0.01	<0.01	<0.01	<0.01	0.02	<0.01	<0.01
Cd	ppm	ICP-MS	<0.01	<0.01	<0.01	<0.01	<0.01	<0.01	<0.01	<0.01	<0.01
Co	ppm	ICP-MS	0.03	0.03	0.07	0.06	0.03	0.06	0.06	0.04	0.2
Cs	ppm	ICP-MS	<0.01	<0.01	<0.01	<0.01	<0.01	0.01	<0.01	<0.01	0.02
Cu	ppm	ICP-MS	1.06	0.76	1.76	1.15	0.78	3.08	1.1	0.94	0.47
Dy	ppm	ICP-MS	0.2	0.23	0.2	0.15	0.2	0.22	0.16	0.17	0.22
Er	ppm	ICP-MS	0.1	0.12	0.1	0.07	0.11	0.12	0.08	0.08	0.1
Eu	ppm	ICP-MS	0.05	0.05	0.04	0.03	0.06	0.05	0.06	0.05	0.12
Ga	ppm	ICP-MS	0.1	0.17	0.26	0.16	0.12	0.21	0.19	0.11	0.18
Gd	ppm	ICP-MS	0.32	0.28	0.24	0.21	0.38	0.37	0.41	0.35	0.82
Ge	ppm	ICP-MS	<0.01	<0.01	<0.01	<0.01	<0.01	<0.01	<0.01	<0.01	<0.01
Hf	ppm	ICP-MS	0.11	0.18	0.15	0.1	0.25	0.36	0.22	0.29	0.12
Hg	ppm	ICP-MS	<0.01	<0.01	<0.01	<0.01	<0.01	<0.01	<0.01	<0.01	<0.01
Ho	ppm	ICP-MS	0.03	0.04	0.03	0.02	0.03	0.04	0.02	0.03	0.03
Mo	ppm	ICP-MS	0.03	0.04	0.02	0.09	0.04	0.04	0.05	0.05	0.05
Nb	ppm	ICP-MS	<0.01	<0.01	<0.01	<0.01	<0.01	0.01	<0.01	<0.01	<0.01
Nd	ppm	ICP-MS	1.86	1.36	0.99	1.02	2.31	2.29	2.89	2.18	5.18
Ni	ppm	ICP-MS	0.14	0.21	0.38	0.38	0.22	0.53	0.48	0.3	1.3
^{204}Pb	ppm	ICP-MS	0.01	0.013	0.005	0.008	0.011	0.076	0.014	0.019	0.022
^{206}Pb	ppm	ICP-MS	0.214	0.265	0.138	0.202	0.223	2.02	0.294	0.472	0.474
^{207}Pb	ppm	ICP-MS	0.155	0.203	0.086	0.135	0.166	1.22	0.217	0.308	0.348
^{208}Pb	ppm	ICP-MS	0.378	0.488	0.223	0.336	0.427	4.09	0.582	0.906	1.23
Pb	ppm	ICP-MS	0.757	0.969	0.453	0.682	0.828	7.4	1.11	1.7	2.07
$^{206}Pb/^{204}Pb$	--	ICP-MS	21.40	20.38	27.60	25.25	20.27	26.58	21.00	24.84	21.55
$^{207}Pb/^{206}Pb$	--	ICP-MS	0.72	0.77	0.62	0.67	0.74	0.60	0.74	0.65	0.73
$^{207}Pb/^{204}Pb$	--	ICP-MS	15.50	15.62	17.20	16.88	15.09	16.05	15.50	16.21	15.82
$^{208}Pb/^{206}Pb$	--	ICP-MS	1.77	1.84	1.62	1.66	1.91	2.02	1.98	1.92	2.59
$^{208}Pb/^{204}Pb$	--	ICP-MS	37.80	37.54	44.60	42.00	38.82	53.82	41.57	47.68	55.91
Pr	ppm	ICP-MS	0.6	0.44	0.32	0.32	0.77	0.74	0.94	0.72	1.76
Rb	ppm	ICP-MS	0.07	0.12	0.1	0.09	0.07	0.09	0.08	0.1	0.22
Sb	ppm	ICP-MS	<0.01	0.01	<0.01	0.06	<0.01	<0.01	<0.01	<0.01	<0.01
Sc	ppm	ICP-MS	0.2	0.2	0.1	<0.1	0.1	0.1	0.1	<0.1	<0.1
Se	ppm	ICP-MS	<0.1	<0.1	<0.1	<0.1	<0.1	<0.1	<0.1	<0.1	<0.1
Sm	ppm	ICP-MS	0.35	0.28	0.21	0.22	0.4	0.42	0.5	0.38	0.94
Sn	ppm	ICP-MS	0.16	0.06	0.2	0.07	0.11	0.58	0.16	0.18	0.14
Ta	ppm	ICP-MS	<0.01	<0.01	<0.01	<0.01	<0.01	<0.01	<0.01	<0.01	<0.01
Tb	ppm	ICP-MS	0.03	0.03	0.03	0.02	0.03	0.04	0.03	0.03	0.05
Te	ppm	ICP-MS	<0.01	<0.01	<0.01	<0.01	<0.01	<0.01	<0.01	<0.01	<0.01
Th	ppm	ICP-MS	0.74	0.8	0.5	0.68	2.25	2.6	2.34	3.5	18.5
U	ppm	ICP-MS	0.35	0.45	0.42	0.66	0.7	1.36	0.82	0.92	0.55
V	ppm	ICP-MS	0.2	0.3	0.4	0.6	0.2	0.4	0.6	0.4	1.1
W	ppm	ICP-MS	<0.1	<0.1	<0.1	<0.1	<0.1	<0.1	<0.1	<0.1	<0.1
Y	ppm	ICP-MS	0.85	1.01	0.87	0.66	1.01	1	0.71	0.76	0.84
Yb	ppm	ICP-MS	0.08	0.1	0.07	0.05	0.09	0.08	0.06	0.07	0.06
Zn	ppm	ICP-MS	0.7	1.3	0.8	1	0.9	0.9	1	1	1.2
Zr	ppm	ICP-MS	4.42	7.27	5.14	4.3	9.8	15.7	8.51	11.4	5.98

Partial Digestion: A 2.00 g pulp is digested with 2.25 ml of 8:1 ultrapure HNO_3:HCl for 1 hour at 95° C.

Group #			G-2014-2129	G-2014-2129	G-2014-2129	G-2014-2129	G-2014-2129	G-2014-2129	G-2014-2129	G-2014-2129	G-2014-2129
Sample #			SG133	SG134	SG135	SG136	SG137	SG138	SG139	SG140	SG141
Fence			Zone 4	Zone 4	Zone 4	Zone 4	Zone 4	Zone 4	Zone 4	Zone 4	Zone 4
Hole ID			MAC-252	MAC-252	MAC-252	MAC-252	MAC-252	MAC-255	MAC-255	MAC-255	MAC-255
From (m)			286.20	305.30	319.44	331.70	342.50	6.13	29.21	51.63	95.00
To (m)			286.37	305.50	319.60	331.95	342.66	6.31	29.40	51.85	95.22
Lithofacies			MFc	MFb	MFb	MFb	MFb	MFd	MFd	MFd	MFd
Date			11-27-2014	11-27-2014	11-27-2014	11-27-2014	11-27-2014	11-27-2014	11-27-2014	11-27-2014	11-27-2014
Sample Type			Sandstone	Sandstone	Sandstone	Sandstone	Sandstone	Sandstone	Sandstone	Sandstone	Sandstone
Ag	ppm	ICP-MS	<0.01	<0.01	<0.01	<0.01	<0.01	<0.01	<0.01	<0.01	<0.01
As	ppm	ICP-MS	0.39	0.42	0.62	0.76	0.31	0.16	0.61	0.2	0.24
Be	ppm	ICP-MS	0.06	0.04	0.07	0.1	0.03	0.03	0.04	0.02	0.02
Bi	ppm	ICP-MS	<0.01	<0.01	<0.01	<0.01	<0.01	0.01	0.01	<0.01	<0.01
Cd	ppm	ICP-MS	<0.01	<0.01	0.01	<0.01	<0.01	<0.01	<0.01	<0.01	<0.01
Co	ppm	ICP-MS	0.06	0.04	0.31	0.21	0.04	0.04	0.16	0.04	0.03
Cs	ppm	ICP-MS	<0.01	<0.01	<0.01	0.01	<0.01	<0.01	0.08	<0.01	<0.01
Cu	ppm	ICP-MS	1.6	0.6	0.98	3.11	0.72	0.94	5.65	1.93	2.02
Dy	ppm	ICP-MS	0.12	0.08	0.47	0.08	0.08	0.35	0.27	0.38	0.19
Er	ppm	ICP-MS	0.05	0.03	0.21	0.04	0.04	0.17	0.13	0.2	0.1
Eu	ppm	ICP-MS	0.06	0.04	0.08	0.05	0.05	0.09	0.06	0.08	0.05
Ga	ppm	ICP-MS	0.06	0.03	0.09	0.16	0.07	0.07	0.27	0.09	0.11
Gd	ppm	ICP-MS	0.46	0.25	0.62	0.33	0.33	0.54	0.32	0.45	0.3
Ge	ppm	ICP-MS	<0.01	<0.01	<0.01	<0.01	<0.01	<0.01	<0.01	<0.01	<0.01
Hf	ppm	ICP-MS	0.14	0.15	0.25	0.15	0.07	0.33	0.11	0.37	0.16
Hg	ppm	ICP-MS	<0.01	<0.01	<0.01	<0.01	<0.01	<0.01	<0.01	<0.01	<0.01
Ho	ppm	ICP-MS	0.02	0.01	0.07	0.01	0.01	0.06	0.04	0.06	0.03
Mo	ppm	ICP-MS	0.04	0.1	0.06	0.05	0.04	0.04	0.15	0.04	0.06
Nb	ppm	ICP-MS	<0.01	<0.01	<0.01	<0.01	<0.01	<0.01	<0.01	<0.01	<0.01
Nd	ppm	ICP-MS	2.92	1.66	3.23	2.12	2.12	2.89	1	1.76	1.5
Ni	ppm	ICP-MS	0.36	0.24	0.73	1.49	0.22	0.19	0.79	0.2	0.21
^{204}Pb	ppm	ICP-MS	0.007	0.007	0.008	0.014	0.008	0.01	0.01	0.007	0.009
^{206}Pb	ppm	ICP-MS	0.188	0.145	0.207	0.324	0.182	0.229	0.259	0.171	0.208
^{207}Pb	ppm	ICP-MS	0.109	0.108	0.139	0.227	0.131	0.166	0.166	0.113	0.141
^{208}Pb	ppm	ICP-MS	0.456	0.286	0.462	0.768	0.356	0.406	0.43	0.291	0.351
Pb	ppm	ICP-MS	0.76	0.545	0.816	1.33	0.676	0.813	0.865	0.581	0.709
$^{206}Pb/^{204}Pb$	--	ICP-MS	26.86	20.71	25.88	23.14	22.75	22.90	25.90	24.43	23.11
$^{207}Pb/^{206}Pb$	--	ICP-MS	0.58	0.74	0.67	0.70	0.72	0.72	0.64	0.66	0.68
$^{207}Pb/^{204}Pb$	--	ICP-MS	15.57	15.43	17.38	16.21	16.38	16.60	16.60	16.14	15.67
$^{208}Pb/^{206}Pb$	--	ICP-MS	2.43	1.97	2.23	2.37	1.96	1.77	1.66	1.70	1.69
$^{208}Pb/^{204}Pb$	--	ICP-MS	65.14	40.86	57.75	54.86	44.50	40.60	43.00	41.57	39.00
Pr	ppm	ICP-MS	0.92	0.54	1.01	0.7	0.66	0.95	0.3	0.52	0.49
Rb	ppm	ICP-MS	0.15	0.05	0.28	0.21	0.18	0.08	0.78	0.09	0.09
Sb	ppm	ICP-MS	<0.01	<0.01	<0.01	<0.01	<0.01	<0.01	0.02	<0.01	<0.01
Sc	ppm	ICP-MS	<0.1	<0.1	0.1	<0.1	<0.1	0.3	0.8	0.4	<0.1
Se	ppm	ICP-MS	<0.1	<0.1	<0.1	<0.1	<0.1	<0.1	<0.1	<0.1	<0.1
Sm	ppm	ICP-MS	0.56	0.3	0.68	0.39	0.41	0.56	0.28	0.43	0.3
Sn	ppm	ICP-MS	0.31	0.08	0.23	0.28	0.12	0.08	0.58	0.27	0.18
Ta	ppm	ICP-MS	<0.01	<0.01	<0.01	<0.01	<0.01	<0.01	<0.01	<0.01	<0.01
Tb	ppm	ICP-MS	0.03	0.02	0.07	0.02	0.02	0.06	0.04	0.06	0.03
Te	ppm	ICP-MS	<0.01	<0.01	<0.01	<0.01	<0.01	<0.01	<0.01	<0.01	<0.01
Th	ppm	ICP-MS	5.49	1.29	3.72	6.35	1.11	1.36	0.8	1.06	0.89
U	ppm	ICP-MS	0.26	0.29	0.26	0.9	0.18	0.8	3.47	1.43	2.06
V	ppm	ICP-MS	0.9	0.8	0.8	1.9	0.4	0.2	11.4	1	0.5
W	ppm	ICP-MS	<0.1	<0.1	<0.1	<0.1	<0.1	<0.1	<0.1	<0.1	<0.1
Y	ppm	ICP-MS	0.44	0.3	2.27	0.33	0.3	1.49	1.09	1.66	0.81
Yb	ppm	ICP-MS	0.03	0.02	0.13	0.02	0.02	0.14	0.09	0.18	0.08
Zn	ppm	ICP-MS	1.8	1.2	2.3	2.7	2.1	1.1	2.1	1.1	1.1
Zr	ppm	ICP-MS	5.33	6.11	10.3	6.72	2.55	12.9	4.48	14.9	6.58

Partial Digestion: A 2.00 g pulp is digested with 2.25 ml of 8:1 ultrapure HNO_3:HCl for 1 hour at 95° C.

Group #			G-2014-2129	G-2014-2155	G-2014-2155	G-2014-2155	G-2014-2155	G-2014-2155	G-2014-2155	G-2014-2155	G-2014-2155
Sample #			SG141 R	SG143	SG144	SG145	SG146	SG147	SG148	SG149	SG150
Fence			Zone 4	Zone 4	Zone 4	Zone 4	Zone 4	Zone 4	Zone 4	Zone 4	Zone 4
Hole ID			MAC-255	MAC-255	MAC-255	MAC-255	MAC-255	MAC-255	MAC-255	MAC-255	MAC-255
From (m)			95.00	148.00	194.47	209.83	217.68	259.93	288.82	293.40	332.33
To (m)			95.22	149.19	194.69	210.06	218.00	260.03	289.03	293.51	332.55
Lithofacies			MFd	MFd	MFc	MFc	MFc	MFc	MFc	MFc	MFc
Date			11-27-2014	11-28-2014	11-28-2014	11-28-2014	11-28-2014	11-28-2014	11-28-2014	11-28-2014	11-28-2014
Sample Type			Repeat	Sandstone	Sandstone	Sandstone	Sandstone	Sandstone	Sandstone	Sandstone	Sandstone
Ag	ppm	ICP-MS	<0.01	<0.01	<0.01	<0.01	<0.01	<0.01	0.01	<0.01	<0.01
As	ppm	ICP-MS	0.24	0.12	0.12	0.09	0.82	0.5	0.75	0.34	0.36
Be	ppm	ICP-MS	0.02	0.02	0.02	0.02	0.04	0.02	0.02	0.02	0.02
Bi	ppm	ICP-MS	<0.01	0.02	0.01	<0.01	<0.01	<0.01	<0.01	<0.01	<0.01
Cd	ppm	ICP-MS	<0.01	<0.01	<0.01	<0.01	<0.01	<0.01	<0.01	<0.01	<0.01
Co	ppm	ICP-MS	0.03	0.06	0.03	0.04	0.07	0.02	0.02	0.03	0.03
Cs	ppm	ICP-MS	<0.01	<0.01	<0.01	0.01	<0.01	<0.01	<0.01	0.02	<0.01
Cu	ppm	ICP-MS	1.99	1.61	1.28	1.89	1.89	1.33	1.8	1.49	0.78
Dy	ppm	ICP-MS	0.19	0.2	0.2	0.15	0.15	0.14	0.14	0.25	0.11
Er	ppm	ICP-MS	0.1	0.11	0.1	0.08	0.07	0.06	0.07	0.1	0.05
Eu	ppm	ICP-MS	0.05	0.04	0.05	0.04	0.04	0.03	0.03	0.07	0.04
Ga	ppm	ICP-MS	0.11	0.09	0.07	0.16	0.15	0.08	0.12	0.13	0.08
Gd	ppm	ICP-MS	0.3	0.24	0.32	0.26	0.25	0.25	0.26	0.5	0.24
Ge	ppm	ICP-MS	<0.01	<0.01	<0.01	<0.01	<0.01	<0.01	<0.01	<0.01	<0.01
Hf	ppm	ICP-MS	0.16	0.16	0.22	0.14	0.08	0.16	0.12	0.15	0.06
Hg	ppm	ICP-MS	<0.01	<0.01	<0.01	<0.01	<0.01	<0.01	<0.01	<0.01	<0.01
Ho	ppm	ICP-MS	0.03	0.03	0.03	0.02	0.02	0.02	0.02	0.04	0.02
Mo	ppm	ICP-MS	0.06	0.36	0.13	0.04	0.22	0.07	0.11	0.06	0.1
Nb	ppm	ICP-MS	<0.01	<0.01	<0.01	<0.01	<0.01	<0.01	<0.01	<0.01	<0.01
Nd	ppm	ICP-MS	1.45	0.95	1.59	1.3	1.03	1.08	1.39	1.88	1.22
Ni	ppm	ICP-MS	0.2	0.26	0.21	0.29	0.57	0.25	0.31	0.4	0.29
^{204}Pb	ppm	ICP-MS	0.008	0.005	0.026	0.007	0.007	0.006	0.024	0.004	0.026
^{206}Pb	ppm	ICP-MS	0.211	0.298	0.577	0.175	0.192	0.314	0.635	0.128	0.449
^{207}Pb	ppm	ICP-MS	0.142	0.104	0.411	0.118	0.121	0.109	0.393	0.067	0.39
^{208}Pb	ppm	ICP-MS	0.341	0.248	1.05	0.328	0.35	0.256	1.33	0.219	0.922
Pb	ppm	ICP-MS	0.702	0.656	2.06	0.628	0.67	0.684	2.38	0.419	1.79
$^{206}Pb/^{204}Pb$	--	ICP-MS	26.38	59.60	22.19	25.00	27.43	52.33	26.46	32.00	17.27
$^{207}Pb/^{206}Pb$	--	ICP-MS	0.67	0.35	0.71	0.67	0.63	0.35	0.62	0.52	0.87
$^{207}Pb/^{204}Pb$	--	ICP-MS	17.75	20.80	15.81	16.86	17.29	18.17	16.38	16.75	15.00
$^{208}Pb/^{206}Pb$	--	ICP-MS	1.62	0.83	1.82	1.87	1.82	0.82	2.09	1.71	2.05
$^{208}Pb/^{204}Pb$	--	ICP-MS	42.63	49.60	40.38	46.86	50.00	42.67	55.42	54.75	35.46
Pr	ppm	ICP-MS	0.47	0.27	0.48	0.39	0.31	0.33	0.43	0.55	0.37
Rb	ppm	ICP-MS	0.09	0.14	0.08	0.19	0.16	0.18	0.28	0.29	0.15
Sb	ppm	ICP-MS	<0.01	0.02	<0.01	<0.01	0.04	<0.01	<0.01	<0.01	<0.01
Sc	ppm	ICP-MS	<0.1	0.2	0.2	0.2	0.2	<0.1	<0.1	<0.1	<0.1
Se	ppm	ICP-MS	<0.1	<0.1	<0.1	<0.1	<0.1	<0.1	<0.1	<0.1	<0.1
Sm	ppm	ICP-MS	0.29	0.24	0.34	0.27	0.24	0.24	0.28	0.44	0.25
Sn	ppm	ICP-MS	0.1	0.09	0.91	0.38	0.12	0.22	0.23	0.26	1.32
Ta	ppm	ICP-MS	<0.01	<0.01	<0.01	<0.01	<0.01	<0.01	<0.01	<0.01	<0.01
Tb	ppm	ICP-MS	0.03	0.03	0.03	0.03	0.02	0.03	0.02	0.05	0.02
Te	ppm	ICP-MS	<0.01	<0.01	<0.01	<0.01	0.01	<0.01	<0.01	<0.01	<0.01
Th	ppm	ICP-MS	0.89	0.68	1.4	1.35	0.74	1.19	1.99	1.88	0.73
U	ppm	ICP-MS	2.1	1.92	1.57	0.89	2.24	0.7	1.2	1.64	0.96
V	ppm	ICP-MS	0.5	1	0.4	0.4	8.4	0.8	1.1	0.4	1
W	ppm	ICP-MS	0.1	<0.1	<0.1	<0.1	<0.1	<0.1	<0.1	<0.1	<0.1
Y	ppm	ICP-MS	0.81	0.92	0.86	0.67	0.65	0.51	0.66	0.84	0.45
Yb	ppm	ICP-MS	0.08	0.1	0.08	0.06	0.05	0.04	0.05	0.06	0.03
Zn	ppm	ICP-MS	1.1	1	0.8	1	2.4	2.3	1.3	1.4	1.2
Zr	ppm	ICP-MS	6.64	5.78	8	5.4	3.17	6.62	4.88	4.91	2.58

Partial Digestion: A 2.00 g pulp is digested with 2.25 ml of 8:1 ultrapure HNO_3:HCl for 1 hour at 95° C.

Group #			G-2014-2155	G-2014-2155	G-2014-2155	G-2014-2155	G-2014-2155	G-2014-2155	G-2014-2155	G-2014-2155	G-2014-2155	G-2014-2155
Sample #			SG151	SG152	SG153	SG154	SG155	SG156	SG157	SG158	SG159	SG160
Fence			Zone 4	Zone 4	Zone 4	Zone 4	Zone 4	Zone 4	Zone 4	Zone 4	Zone 4	Zone 4
Hole ID			MAC-255	MAC-255	MAC-255	MAC-255	MAC-255	MAC-255	MAC-255	MAC-255	MAC-255	MAC-255
From (m)			338.00	362.46	378.33	397.78	412.58	426.30	429.50	451.78	462.07	469.36
To (m)			338.20	362.67	378.59	398.00	412.85	426.60	429.63	451.96	462.24	469.63
Lithofacies			MFc	MFc	MFc	MFb	MFb	MFb	MFa	MFa	MFa	MFa
Date			11-28-2014	11-28-2014	11-28-2014	11-28-2014	11-28-2014	11-28-2014	11-28-2014	11-28-2014	11-28-2014	11-28-2014
Sample Type			Sandstone	Sandstone	Sandstone	Sandstone	Sandstone	Sandstone	Sandstone	Sandstone	Sandstone	Sandstone
Ag	ppm	ICP-MS	<0.01	<0.01	<0.01	<0.01	<0.01	<0.01	<0.01	<0.01	<0.01	<0.01
As	ppm	ICP-MS	0.83	0.24	0.62	0.38	0.63	0.34	0.32	0.22	0.37	0.4
Be	ppm	ICP-MS	0.02	0.01	0.01	0.01	0.02	0.02	0.01	0.02	0.02	0.01
Bi	ppm	ICP-MS	<0.01	0.05	<0.01	<0.01	<0.01	<0.01	<0.01	<0.01	<0.01	<0.01
Cd	ppm	ICP-MS	<0.01	<0.01	<0.01	<0.01	<0.01	<0.01	<0.01	<0.01	<0.01	<0.01
Co	ppm	ICP-MS	0.02	0.08	0.03	0.03	0.05	0.04	0.04	0.05	0.06	0.04
Cs	ppm	ICP-MS	<0.01	<0.01	<0.01	<0.01	<0.01	<0.01	<0.01	<0.01	<0.01	<0.01
Cu	ppm	ICP-MS	1.09	0.57	0.38	0.36	0.38	0.42	0.38	0.39	0.39	0.32
Dy	ppm	ICP-MS	0.13	0.1	0.1	0.06	0.13	0.12	0.08	0.09	0.1	0.08
Er	ppm	ICP-MS	0.06	0.05	0.06	0.03	0.08	0.07	0.04	0.05	0.06	0.05
Eu	ppm	ICP-MS	0.04	0.03	0.03	0.02	0.03	0.04	0.03	0.03	0.03	0.02
Ga	ppm	ICP-MS	0.13	0.08	0.12	0.14	0.12	0.13	0.11	0.14	0.11	0.05
Gd	ppm	ICP-MS	0.28	0.23	0.2	0.13	0.24	0.22	0.18	0.17	0.18	0.11
Ge	ppm	ICP-MS	<0.01	<0.01	<0.01	<0.01	<0.01	<0.01	<0.01	<0.01	<0.01	<0.01
Hf	ppm	ICP-MS	0.19	0.11	0.2	0.1	0.28	0.21	0.11	0.19	0.39	0.17
Hg	ppm	ICP-MS	<0.01	<0.01	<0.01	<0.01	<0.01	<0.01	<0.01	<0.01	<0.01	<0.01
Ho	ppm	ICP-MS	0.02	0.02	0.02	<0.01	0.02	0.02	0.01	0.02	0.02	0.01
Mo	ppm	ICP-MS	0.04	0.08	0.07	0.08	0.07	0.06	0.07	0.07	0.08	0.12
Nb	ppm	ICP-MS	<0.01	<0.01	<0.01	<0.01	<0.01	<0.01	<0.01	<0.01	<0.01	<0.01
Nd	ppm	ICP-MS	1.49	1.12	1.36	0.85	1.48	1.44	1.21	0.83	0.96	0.52
Ni	ppm	ICP-MS	0.16	0.2	0.18	0.18	0.2	0.23	0.18	0.2	0.19	0.23
^{204}Pb	ppm	ICP-MS	0.01	0.004	0.006	0.005	0.004	0.005	0.005	0.006	0.006	0.003
^{206}Pb	ppm	ICP-MS	0.232	0.105	0.138	0.122	0.122	0.137	0.126	0.144	0.18	0.124
^{207}Pb	ppm	ICP-MS	0.157	0.066	0.091	0.086	0.07	0.089	0.077	0.086	0.096	0.057
^{208}Pb	ppm	ICP-MS	0.522	0.199	0.289	0.23	0.248	0.274	0.224	0.219	0.266	0.149
Pb	ppm	ICP-MS	0.92	0.374	0.523	0.443	0.444	0.506	0.432	0.455	0.548	0.334
$^{206}Pb/^{204}Pb$	--	ICP-MS	23.20	26.25	23.00	24.40	30.50	27.40	25.20	24.00	30.00	41.33
$^{207}Pb/^{206}Pb$	--	ICP-MS	0.68	0.63	0.66	0.70	0.57	0.65	0.61	0.60	0.53	0.46
$^{207}Pb/^{204}Pb$	--	ICP-MS	15.70	16.50	15.17	17.20	17.50	17.80	15.40	14.33	16.00	19.00
$^{208}Pb/^{206}Pb$	--	ICP-MS	2.25	1.90	2.09	1.89	2.03	2.00	1.78	1.52	1.48	1.20
$^{208}Pb/^{204}Pb$	--	ICP-MS	52.20	49.75	48.17	46.00	62.00	54.80	44.80	36.50	44.33	49.67
Pr	ppm	ICP-MS	0.45	0.33	0.44	0.27	0.51	0.48	0.4	0.25	0.3	0.16
Rb	ppm	ICP-MS	0.19	0.12	0.11	0.09	0.09	0.1	0.06	0.15	0.07	0.05
Sb	ppm	ICP-MS	0.01	<0.01	<0.01	<0.01	<0.01	<0.01	0.02	<0.01	0.04	0.01
Sc	ppm	ICP-MS	<0.1	<0.1	<0.1	<0.1	<0.1	0.2	0.1	<0.1	0.1	<0.1
Se	ppm	ICP-MS	<0.1	<0.1	<0.1	<0.1	<0.1	<0.1	<0.1	<0.1	<0.1	<0.1
Sm	ppm	ICP-MS	0.3	0.24	0.22	0.15	0.25	0.26	0.2	0.18	0.19	0.11
Sn	ppm	ICP-MS	0.16	0.09	0.08	0.08	0.05	0.1	0.05	0.1	0.07	0.04
Ta	ppm	ICP-MS	<0.01	<0.01	<0.01	<0.01	<0.01	<0.01	<0.01	<0.01	<0.01	<0.01
Tb	ppm	ICP-MS	0.02	0.02	0.02	0.01	0.02	0.02	0.02	0.02	0.02	0.01
Te	ppm	ICP-MS	<0.01	<0.01	<0.01	<0.01	<0.01	<0.01	<0.01	<0.01	<0.01	<0.01
Th	ppm	ICP-MS	1.83	1.14	1.54	0.74	2.12	1.56	0.91	0.52	1.07	0.72
U	ppm	ICP-MS	0.89	0.62	0.64	0.63	0.89	0.9	0.97	0.97	1.8	1.22
V	ppm	ICP-MS	1.2	0.6	0.5	0.9	0.6	0.5	0.4	0.5	0.6	0.6
W	ppm	ICP-MS	<0.1	<0.1	<0.1	<0.1	<0.1	<0.1	<0.1	<0.1	<0.1	<0.1
Y	ppm	ICP-MS	0.56	0.46	0.47	0.24	0.64	0.52	0.35	0.46	0.54	0.42
Yb	ppm	ICP-MS	0.05	0.04	0.04	0.02	0.08	0.06	0.04	0.04	0.06	0.04
Zn	ppm	ICP-MS	1.3	1.1	0.9	1.1	2.9	1.2	0.9	1.1	0.9	0.8
Zr	ppm	ICP-MS	7.14	4.14	6.9	3.42	9.23	6.84	3.71	6.98	15.2	6.26

Partial Digestion: A 2.00 g pulp is digested with 2.25 ml of 8:1 ultrapure HNO_3:HCl for 1 hour at 95° C.

Group #			G-2014-2155	G-2014-2155	G-2014-2155	G-2014-2155	G-2014-2155	G-2014-2155	G-2014-2155	G-2014-2155	G-2014-2155	G-2014-2155
Sample #			SG161	SG162	SG163	SG164	SG165	SG166	SG167	SG168	SG169	SG170
Fence			Zone 4	Zone 4	Zone 4	Zone 4	Zone 4	Zone 4	Zone C	Zone C	Zone C	Zone C
Hole ID			MAC-255	MAC-255	MAC-255	MAC-255	MAC-255	MAC-255	MC-413	MC-413	MC-413	MC-413
From (m)			479.27	483.68	501.32	503.26	559.00	564.36	71.64	130.00	183.26	224.00
To (m)			479.31	483.93	501.50	503.49	559.10	564.50	71.80	130.22	183.43	224.32
Lithofacies			MFa	MFa	MFa	MFa	MFa	MFa	MFd	MFc	MFc	MFc
Date			11-28-2014	11-28-2014	11-28-2014	11-28-2014	11-28-2014	11-28-2014	11-28-2014	11-28-2014	11-28-2014	11-28-2014
Sample Type			Sandstone	Sandstone	Sandstone	Sandstone	Sandstone	Sandstone	Sandstone	Sandstone	Sandstone	Sandstone
Ag	ppm	ICP-MS	<0.01	<0.01	0.01	<0.01	0.02	0.08	<0.01	<0.01	<0.01	<0.01
As	ppm	ICP-MS	0.32	1.56	3.99	0.77	0.67	1.89	0.12	0.13	0.3	0.49
Be	ppm	ICP-MS	0.02	0.01	0.04	0.05	1.12	0.78	0.02	0.02	0.03	0.04
Bi	ppm	ICP-MS	0.02	<0.01	0.01	0.02	0.11	0.1	<0.01	<0.01	0.01	<0.01
Cd	ppm	ICP-MS	<0.01	<0.01	<0.01	<0.01	<0.01	<0.01	<0.01	<0.01	<0.01	<0.01
Co	ppm	ICP-MS	0.07	0.04	0.44	0.34	3.25	3.53	0.05	0.03	0.05	0.03
Cs	ppm	ICP-MS	<0.01	<0.01	<0.01	<0.01	0.02	0.03	0.03	0.01	0.03	0.01
Cu	ppm	ICP-MS	0.49	0.66	3.34	2.35	14.2	4.44	0.9	0.59	1.39	2.12
Dy	ppm	ICP-MS	0.14	0.06	0.21	0.12	0.41	1.12	0.19	0.15	0.2	0.16
Er	ppm	ICP-MS	0.08	0.04	0.12	0.06	0.22	0.56	0.1	0.07	0.11	0.09
Eu	ppm	ICP-MS	0.03	0.01	0.04	0.03	0.06	0.16	0.04	0.04	0.04	0.03
Ga	ppm	ICP-MS	0.1	0.06	0.1	0.37	2.54	1.82	0.21	0.19	0.41	0.3
Gd	ppm	ICP-MS	0.2	0.09	0.32	0.22	0.64	1.22	0.24	0.22	0.27	0.21
Ge	ppm	ICP-MS	<0.01	<0.01	<0.01	<0.01	0.04	<0.01	<0.01	<0.01	<0.01	<0.01
Hf	ppm	ICP-MS	0.25	0.08	0.1	0.03	0.11	0.04	0.16	0.09	0.12	0.1
Hg	ppm	ICP-MS	<0.01	<0.01	<0.01	<0.01	<0.01	<0.01	<0.01	<0.01	<0.01	<0.01
Ho	ppm	ICP-MS	0.02	0.01	0.04	0.02	0.07	0.19	0.03	0.02	0.04	0.03
Mo	ppm	ICP-MS	0.14	0.53	0.91	0.98	0.27	0.43	0.02	0.02	0.06	0.13
Nb	ppm	ICP-MS	<0.01	<0.01	<0.01	<0.01	0.02	<0.01	<0.01	<0.01	<0.01	<0.01
Nd	ppm	ICP-MS	0.9	0.42	1.44	1.24	3.58	3.92	1.13	1.16	0.97	0.83
Ni	ppm	ICP-MS	0.22	0.24	1.2	2.27	10.1	16.9	0.34	0.33	0.77	0.42
^{204}Pb	ppm	ICP-MS	0.006	0.004	0.024	0.003	0.005	0.016	0.006	0.006	0.008	0.004
^{206}Pb	ppm	ICP-MS	0.221	0.154	0.922	0.443	7.07	2.98	0.157	0.126	0.17	0.094
^{207}Pb	ppm	ICP-MS	0.099	0.071	0.408	0.06	0.123	0.338	0.095	0.089	0.12	0.058
^{208}Pb	ppm	ICP-MS	0.26	0.182	1.34	0.197	0.595	0.997	0.246	0.233	0.335	0.158
Pb	ppm	ICP-MS	0.586	0.411	2.7	0.703	7.79	4.33	0.503	0.454	0.633	0.313
$^{206}Pb/^{204}Pb$	--	ICP-MS	36.83	38.50	38.42	147.67	1414.00	186.25	26.17	21.00	21.25	23.50
$^{207}Pb/^{206}Pb$	--	ICP-MS	0.45	0.46	0.44	0.14	0.02	0.11	0.61	0.71	0.71	0.62
$^{207}Pb/^{204}Pb$	--	ICP-MS	16.50	17.75	17.00	20.00	24.60	21.13	15.83	14.83	15.00	14.50
$^{208}Pb/^{206}Pb$	--	ICP-MS	1.18	1.18	1.45	0.44	0.08	0.33	1.57	1.85	1.97	1.68
$^{208}Pb/^{204}Pb$	--	ICP-MS	43.33	45.50	55.83	65.67	119.00	62.31	41.00	38.83	41.88	39.50
Pr	ppm	ICP-MS	0.28	0.13	0.43	0.38	1.17	1.2	0.36	0.36	0.27	0.25
Rb	ppm	ICP-MS	0.11	0.08	0.32	0.13	0.16	0.19	0.12	0.07	0.17	0.1
Sb	ppm	ICP-MS	0.01	0.02	0.02	0.01	<0.01	0.01	<0.01	<0.01	<0.01	<0.01
Sc	ppm	ICP-MS	0.2	<0.1	0.1	0.2	1	1.3	0.1	0.1	<0.1	0.3
Se	ppm	ICP-MS	<0.1	<0.1	0.3	<0.1	<0.1	0.1	<0.1	<0.1	<0.1	<0.1
Sm	ppm	ICP-MS	0.19	0.09	0.31	0.24	0.65	1	0.23	0.23	0.24	0.19
Sn	ppm	ICP-MS	0.06	0.05	0.09	0.1	0.17	0.32	0.19	0.06	0.13	0.09
Ta	ppm	ICP-MS	<0.01	<0.01	<0.01	<0.01	<0.01	<0.01	<0.01	<0.01	<0.01	<0.01
Tb	ppm	ICP-MS	0.02	<0.01	0.03	0.02	0.07	0.18	0.03	0.02	0.03	0.02
Te	ppm	ICP-MS	<0.01	<0.01	0.03	0.02	<0.01	<0.01	<0.01	<0.01	<0.01	<0.01
Th	ppm	ICP-MS	0.73	0.5	1.94	0.83	16.9	7.37	0.81	0.76	1.03	0.72
U	ppm	ICP-MS	2.05	1.28	2.31	1.11	2.72	9.75	0.42	0.24	0.53	1.42
V	ppm	ICP-MS	0.6	1	1.3	4.2	12.3	13.3	0.4	0.3	0.7	4
W	ppm	ICP-MS	<0.1	<0.1	<0.1	<0.1	<0.1	<0.1	<0.1	<0.1	<0.1	<0.1
Y	ppm	ICP-MS	0.77	0.31	1.59	0.59	1.96	5.78	0.88	0.66	1.12	0.86
Yb	ppm	ICP-MS	0.08	0.03	0.08	0.04	0.19	0.42	0.07	0.05	0.08	0.07
Zn	ppm	ICP-MS	1	1	2	2.2	4.1	2.7	0.8	0.9	0.8	1.3
Zr	ppm	ICP-MS	9.34	2.91	3.91	1.42	3.51	1.92	6.07	3.22	4.74	4.06

Partial Digestion: A 2.00 g pulp is digested with 2.25 ml of 8:1 ultrapure HNO_3:HCl for 1 hour at 95° C.

Group #			G-2014-2155	G-2014-2155	G-2014-2155	G-2014-2155	G-2014-2155	G-2014-2155	G-2014-2155	G-2014-2155	G-2014-2155	G-2014-2155
Sample #			SG171	SG172	SG173	SG174	SG175	SG176	SG177	SG178	SG179	SG175 R
Fence			Zone C	Zone C	Zone C	Zone C	Zone C	Zone C	Zone C	Zone C	Zone C	Zone C
Hole ID			MC-413	MC-413	MC-413	MC-413	MC-413	MC-413	MC-413	MC-413	MC-413	MC-413
From (m)			258.26	282.17	299.00	303.50	317.96	328.54	354.67	388.82	404.00	317.96
To (m)			258.50	282.40	299.16	303.80	318.16	328.57	354.90	389.00	404.25	318.16
Lithofacies			MFc	MFc	MFb	MFb	MFb	MFb	MFb	MFb	MFb	MFb
Date			11-28-2014	11-28-2014	11-28-2014	11-28-2014	11-28-2014	11-28-2014	11-28-2014	11-28-2014	11-28-2014	11-28-2014
Sample Type			Sandstone	Sandstone	Sandstone	Sandstone	Sandstone	Sandstone	Sandstone	Sandstone	Sandstone	Repeat
Ag	ppm	ICP-MS	<0.01	<0.01	<0.01	<0.01	<0.01	<0.01	<0.01	0.16	0.01	<0.01
As	ppm	ICP-MS	0.29	0.34	1.47	0.5	0.44	0.54	0.29	0.53	0.33	0.42
Be	ppm	ICP-MS	0.04	0.03	0.11	0.05	0.03	0.03	0.01	0.07	0.04	0.03
Bi	ppm	ICP-MS	<0.01	<0.01	0.01	<0.01	0.01	<0.01	<0.01	<0.01	<0.01	<0.01
Cd	ppm	ICP-MS	<0.01	<0.01	<0.01	<0.01	<0.01	<0.01	<0.01	<0.01	0.02	<0.01
Co	ppm	ICP-MS	0.03	0.03	0.05	0.02	0.05	0.01	0.02	0.03	0.05	0.03
Cs	ppm	ICP-MS	0.01	<0.01	<0.01	<0.01	<0.01	<0.01	<0.01	<0.01	<0.01	<0.01
Cu	ppm	ICP-MS	1.16	0.96	4.08	0.58	0.68	0.8	0.46	1.12	0.79	0.71
Dy	ppm	ICP-MS	0.17	0.16	0.19	0.26	0.17	0.28	0.12	0.63	0.27	0.17
Er	ppm	ICP-MS	0.09	0.07	0.11	0.12	0.08	0.09	0.06	0.37	0.17	0.08
Eu	ppm	ICP-MS	0.04	0.04	0.05	0.08	0.04	0.09	0.05	0.18	0.07	0.04
Ga	ppm	ICP-MS	0.26	0.11	0.15	0.1	0.05	0.06	0.09	0.11	0.08	0.05
Gd	ppm	ICP-MS	0.29	0.31	0.31	0.56	0.37	0.61	0.34	1.54	0.47	0.38
Ge	ppm	ICP-MS	<0.01	<0.01	<0.01	<0.01	<0.01	<0.01	<0.01	<0.01	<0.01	<0.01
Hf	ppm	ICP-MS	0.16	0.1	0.16	0.19	0.22	0.07	0.12	0.14	0.98	0.24
Hg	ppm	ICP-MS	<0.01	<0.01	<0.01	<0.01	<0.01	<0.01	<0.01	<0.01	<0.01	<0.01
Ho	ppm	ICP-MS	0.03	0.02	0.03	0.04	0.03	0.04	0.02	0.1	0.05	0.03
Mo	ppm	ICP-MS	0.06	0.05	0.18	0.06	0.07	0.04	0.05	0.11	0.06	0.08
Nb	ppm	ICP-MS	<0.01	<0.01	<0.01	<0.01	<0.01	<0.01	<0.01	<0.01	<0.01	<0.01
Nd	ppm	ICP-MS	1.56	1.57	1.56	2.69	2.07	2.37	1.93	9.38	2.62	2.1
Ni	ppm	ICP-MS	0.35	0.32	0.55	0.27	0.29	0.15	0.2	0.37	0.28	0.27
^{204}Pb	ppm	ICP-MS	0.007	0.004	0.004	0.005	0.006	0.007	0.006	0.005	0.005	0.005
^{206}Pb	ppm	ICP-MS	0.178	0.133	0.149	0.171	0.17	0.169	0.127	0.164	0.165	0.169
^{207}Pb	ppm	ICP-MS	0.122	0.074	0.075	0.092	0.091	0.108	0.089	0.08	0.086	0.091
^{208}Pb	ppm	ICP-MS	0.344	0.232	0.239	0.366	0.371	0.291	0.265	0.554	0.422	0.369
Pb	ppm	ICP-MS	0.651	0.444	0.467	0.634	0.638	0.575	0.487	0.803	0.678	0.634
$^{206}Pb/^{204}Pb$	--	ICP-MS	25.43	33.25	37.25	34.20	28.33	24.14	21.17	32.80	33.00	33.80
$^{207}Pb/^{206}Pb$	--	ICP-MS	0.69	0.56	0.50	0.54	0.54	0.64	0.70	0.49	0.52	0.54
$^{207}Pb/^{204}Pb$	--	ICP-MS	17.43	18.50	18.75	18.40	15.17	15.43	14.83	16.00	17.20	18.20
$^{208}Pb/^{206}Pb$	--	ICP-MS	1.93	1.74	1.60	2.14	2.18	1.72	2.09	3.38	2.56	2.18
$^{208}Pb/^{204}Pb$	--	ICP-MS	49.14	58.00	59.75	73.20	61.83	41.57	44.17	110.80	84.40	73.80
Pr	ppm	ICP-MS	0.49	0.49	0.46	0.83	0.66	0.7	0.61	2.46	0.85	0.67
Rb	ppm	ICP-MS	0.14	0.12	0.26	0.2	0.05	0.17	0.19	0.1	0.12	0.05
Sb	ppm	ICP-MS	<0.01	<0.01	<0.01	<0.01	<0.01	<0.01	<0.01	<0.01	<0.01	<0.01
Sc	ppm	ICP-MS	<0.1	<0.1	0.4	<0.1	<0.1	<0.1	<0.1	0.7	0.4	<0.1
Se	ppm	ICP-MS	<0.1	<0.1	<0.1	<0.1	<0.1	<0.1	<0.1	0.1	<0.1	<0.1
Sm	ppm	ICP-MS	0.3	0.33	0.32	0.56	0.39	0.53	0.37	2.36	0.52	0.38
Sn	ppm	ICP-MS	0.13	0.08	0.11	0.05	0.03	0.07	0.05	0.12	0.16	0.03
Ta	ppm	ICP-MS	<0.01	<0.01	<0.01	<0.01	<0.01	<0.01	<0.01	<0.01	<0.01	<0.01
Tb	ppm	ICP-MS	0.03	0.03	0.03	0.05	0.03	0.06	0.03	0.12	0.04	0.03
Te	ppm	ICP-MS	<0.01	<0.01	<0.01	<0.01	<0.01	<0.01	<0.01	<0.01	<0.01	<0.01
Th	ppm	ICP-MS	1.7	2.58	1.75	4.99	5.61	1.35	1.27	14.4	7.3	5.69
U	ppm	ICP-MS	0.73	0.69	3.98	0.92	0.66	1.06	0.5	3.85	1.81	0.68
V	ppm	ICP-MS	0.6	0.3	4.6	0.5	0.2	0.2	0.2	0.7	0.6	0.2
W	ppm	ICP-MS	<0.1	<0.1	<0.1	<0.1	<0.1	<0.1	<0.1	<0.1	<0.1	<0.1
Y	ppm	ICP-MS	0.84	0.63	1.01	1.03	0.66	0.71	0.46	2.74	1.43	0.66
Yb	ppm	ICP-MS	0.06	0.05	0.08	0.08	0.06	0.04	0.04	0.32	0.18	0.06
Zn	ppm	ICP-MS	1.2	0.8	1.2	0.6	0.8	1.1	0.7	0.9	1	1.3
Zr	ppm	ICP-MS	6.08	3.65	5.67	7.06	7.49	2.38	4.62	9.64	38.1	7.63

Partial Digestion: A 2.00 g pulp is digested with 2.25 ml of 8:1 ultrapure HNO_3:HCl for 1 hour at 95° C.

Group #			G-2014-2155	G-2014-2155	G-2014-2155	G-2014-2155	G-2014-2155	G-2014-2155	G-2014-2155	G-2014-2155	G-2014-2155	G-2014-2155
Sample #			SG180	SG181	SG182	SG183	SG184	SG185	SG186	SG187	SG188	SG189
Fence			Zone C	Zone C	Zone C	Zone C	Zone C	Zone C	Zone C	Zone C	Zone C	Zone C
Hole ID			MC-413	MC-413	MC-413	MC-413	MC-413	MC-413	MC-413	MC-413	MC-413	MC-413
From (m)			430.57	456.68	482.25	501.66	527.67	547.30	557.44	559.73	566.28	603.83
To (m)			430.79	456.95	482.43	501.85	527.92	547.51	557.57	559.91	566.52	604.11
Lithofacies			MFa	MFa	MFa	MFa	MFa	MFa	MFa	MFa	MFa	MFa
Date			11-28-2014	11-28-2014	11-28-2014	11-28-2014	11-28-2014	11-28-2014	11-28-2014	11-28-2014	11-28-2014	11-28-2014
Sample Type			Sandstone	Sandstone	Sandstone	Sandstone	Sandstone	Sandstone	Sandstone	Sandstone	Sandstone	Sandstone
Ag	ppm	ICP-MS	<0.01	<0.01	<0.01	<0.01	<0.01	<0.01	0.01	<0.01	0.03	0.02
As	ppm	ICP-MS	0.35	0.16	0.3	0.21	0.03	0.16	0.22	5.1	2.15	15.1
Be	ppm	ICP-MS	0.02	0.01	0.03	0.01	<0.01	0.01	0.02	0.08	0.05	0.26
Bi	ppm	ICP-MS	<0.01	<0.01	<0.01	<0.01	<0.01	<0.01	<0.01	0.01	<0.01	0.03
Cd	ppm	ICP-MS	<0.01	<0.01	0.02	<0.01	<0.01	<0.01	<0.01	<0.01	<0.01	0.02
Co	ppm	ICP-MS	0.03	0.04	0.03	0.04	0.03	0.03	0.11	0.2	0.08	10.4
Cs	ppm	ICP-MS	<0.01	<0.01	<0.01	<0.01	<0.01	<0.01	<0.01	<0.01	0.03	0.04
Cu	ppm	ICP-MS	0.43	0.48	0.43	0.45	0.28	0.43	0.64	4.57	1.14	3
Dy	ppm	ICP-MS	0.12	0.06	0.21	0.07	0.05	0.16	0.19	0.48	0.22	0.27
Er	ppm	ICP-MS	0.07	0.03	0.14	0.04	0.03	0.1	0.11	0.17	0.11	0.15
Eu	ppm	ICP-MS	0.04	0.03	0.06	0.02	0.01	0.04	0.06	0.06	0.05	0.15
Ga	ppm	ICP-MS	0.1	0.05	0.1	0.07	0.07	0.12	0.11	0.43	0.21	0.38
Gd	ppm	ICP-MS	0.28	0.18	0.46	0.14	0.1	0.22	0.48	1.06	0.35	0.82
Ge	ppm	ICP-MS	<0.01	<0.01	<0.01	<0.01	<0.01	<0.01	<0.01	<0.01	<0.01	<0.01
Hf	ppm	ICP-MS	0.32	0.08	0.76	0.13	0.13	0.3	0.22	0.15	0.2	0.47
Hg	ppm	ICP-MS	<0.01	<0.01	<0.01	<0.01	<0.01	<0.01	<0.01	<0.01	<0.01	<0.01
Ho	ppm	ICP-MS	0.02	<0.01	0.04	0.01	<0.01	0.03	0.03	0.06	0.04	0.04
Mo	ppm	ICP-MS	0.08	0.06	0.06	0.08	0.04	0.06	0.09	0.36	0.14	1.66
Nb	ppm	ICP-MS	<0.01	<0.01	<0.01	<0.01	<0.01	<0.01	<0.01	<0.01	<0.01	<0.01
Nd	ppm	ICP-MS	2.07	1.27	3.11	0.82	0.6	1.1	3.21	6.22	1.92	7.32
Ni	ppm	ICP-MS	0.23	0.28	0.2	0.28	0.16	0.24	0.47	1.13	0.28	16.9
^{204}Pb	ppm	ICP-MS	0.01	0.003	0.007	0.004	0.003	0.005	0.004	0.003	0.012	0.013
^{206}Pb	ppm	ICP-MS	0.235	0.087	0.209	0.13	0.088	0.17	0.185	0.782	0.351	1.45
^{207}Pb	ppm	ICP-MS	0.168	0.054	0.118	0.069	0.052	0.082	0.076	0.093	0.199	0.265
^{208}Pb	ppm	ICP-MS	0.548	0.175	0.554	0.188	0.143	0.216	0.286	0.625	0.604	1.59
Pb	ppm	ICP-MS	0.962	0.32	0.887	0.392	0.286	0.474	0.552	1.5	1.17	3.32
$^{206}Pb/^{204}Pb$	--	ICP-MS	23.50	29.00	29.86	32.50	29.33	34.00	46.25	260.67	29.25	111.54
$^{207}Pb/^{206}Pb$	--	ICP-MS	0.71	0.62	0.56	0.53	0.59	0.48	0.41	0.12	0.57	0.18
$^{207}Pb/^{204}Pb$	--	ICP-MS	16.80	18.00	16.86	17.25	17.33	16.40	19.00	31.00	16.58	20.38
$^{208}Pb/^{206}Pb$	--	ICP-MS	2.33	2.01	2.65	1.45	1.63	1.27	1.55	0.80	1.72	1.10
$^{208}Pb/^{204}Pb$	--	ICP-MS	54.80	58.33	79.14	47.00	47.67	43.20	71.50	208.33	50.33	122.31
Pr	ppm	ICP-MS	0.71	0.39	1	0.24	0.19	0.33	0.9	1.97	0.64	2.51
Rb	ppm	ICP-MS	0.1	0.05	0.1	0.06	0.07	0.06	0.17	0.04	0.76	0.45
Sb	ppm	ICP-MS	<0.01	<0.01	0.01	<0.01	<0.01	<0.01	0.01	<0.01	0.02	<0.01
Sc	ppm	ICP-MS	<0.1	<0.1	0.1	<0.1	<0.1	0.2	0.2	0.4	0.2	0.4
Se	ppm	ICP-MS	<0.1	<0.1	<0.1	<0.1	<0.1	<0.1	<0.1	<0.1	<0.1	<0.1
Sm	ppm	ICP-MS	0.33	0.23	0.56	0.16	0.12	0.22	0.7	1.28	0.35	1.07
Sn	ppm	ICP-MS	0.16	0.06	0.16	0.07	0.04	0.08	0.19	0.24	0.26	0.14
Ta	ppm	ICP-MS	<0.01	<0.01	<0.01	<0.01	<0.01	<0.01	<0.01	<0.01	<0.01	<0.01
Tb	ppm	ICP-MS	0.02	0.01	0.04	0.01	<0.01	0.02	0.04	0.1	0.03	0.05
Te	ppm	ICP-MS	<0.01	<0.01	<0.01	<0.01	<0.01	<0.01	<0.01	<0.01	<0.01	<0.01
Th	ppm	ICP-MS	3.25	0.78	7.22	0.9	0.44	0.84	2.77	8.18	1.67	60.8
U	ppm	ICP-MS	0.78	0.36	1.46	0.79	0.3	2.11	1.91	12.8	2.99	15
V	ppm	ICP-MS	0.4	0.4	0.8	0.8	0.2	0.8	1.6	7.5	2.8	3.3
W	ppm	ICP-MS	<0.1	<0.1	<0.1	<0.1	<0.1	<0.1	<0.1	<0.1	<0.1	<0.1
Y	ppm	ICP-MS	0.56	0.25	1.18	0.31	0.27	0.84	0.92	1.74	0.99	1.3
Yb	ppm	ICP-MS	0.06	0.02	0.13	0.03	0.02	0.1	0.09	0.08	0.1	0.11
Zn	ppm	ICP-MS	0.6	0.6	1	1.1	0.5	0.7	0.8	3.9	2	2
Zr	ppm	ICP-MS	11.6	2.86	30.1	4.76	4.8	10.9	8.23	5.01	7.2	19.4

Partial Digestion: A 2.00 g pulp is digested with 2.25 ml of 8:1 ultrapure HNO_3:HCl for 1 hour at 95° C.

Group #			G-2014-2155	G-2014-2155	G-2014-2155	G-2014-2155	G-2014-2155	G-2014-2155	G-2014-2155	G-2014-2155	G-2014-2155	G-2014-2155
Sample #			SG190	SG191	SG192	SG193	SG194	SG195	SG196	SG197	SG198	SG199
Fence			Zone C	Zone C	Zone C	Zone C	Zone C	Zone C	Zone C	Zone C	Zone C	Zone C
Hole ID			MC-413	MC-413	MC-413	MC-413	MC-415	MC-415	MC-415	MC-415	MC-415	MC-415
From (m)			614.83	623.78	638.86	649.00	76.73	127.56	173.74	197.00	222.34	232.50
To (m)			615.05	624.09	639.19	649.20	76.92	127.73	173.90	197.22	222.44	232.70
Lithofacies			MFa	MFa	MFa	MFa	MFd	MFc	MFc	MFc	MFc	MFc
Date			11-28-2014	11-28-2014	11-28-2014	11-28-2014	11-28-2014	11-28-2014	11-28-2014	11-28-2014	11-28-2014	11-28-2014
Sample Type			Sandstone	Sandstone	Sandstone	Sandstone	Sandstone	Sandstone	Sandstone	Sandstone	Sandstone	Sandstone
Ag	ppm	ICP-MS	0.03	0.01	<0.01	<0.01	<0.01	<0.01	<0.01	<0.01	<0.01	<0.01
As	ppm	ICP-MS	3.17	0.39	0.38	0.51	0.12	0.12	0.41	0.29	0.1	0.28
Be	ppm	ICP-MS	0.23	0.03	0.04	0.04	0.01	0.02	0.02	0.02	0.02	0.03
Bi	ppm	ICP-MS	0.4	0.02	<0.01	<0.01	<0.01	<0.01	0.02	<0.01	<0.01	<0.01
Cd	ppm	ICP-MS	0.04	<0.01	<0.01	0.01	<0.01	<0.01	<0.01	<0.01	<0.01	<0.01
Co	ppm	ICP-MS	5.12	0.31	0.15	0.24	0.04	0.03	0.05	0.18	0.14	0.03
Cs	ppm	ICP-MS	<0.01	<0.01	0.01	<0.01	0.02	0.01	0.02	0.02	0.02	0.01
Cu	ppm	ICP-MS	13.6	0.37	0.43	0.23	0.41	0.43	2.27	2.02	0.84	0.74
Dy	ppm	ICP-MS	0.32	0.06	0.38	0.2	0.14	0.17	0.14	0.12	0.12	0.17
Er	ppm	ICP-MS	0.18	0.03	0.34	0.12	0.06	0.08	0.07	0.06	0.06	0.08
Eu	ppm	ICP-MS	0.08	0.02	0.07	0.05	0.03	0.04	0.04	0.03	0.03	0.05
Ga	ppm	ICP-MS	0.31	0.05	0.14	0.1	0.16	0.35	0.36	0.2	0.22	0.24
Gd	ppm	ICP-MS	0.69	0.13	0.44	0.46	0.21	0.24	0.22	0.18	0.2	0.31
Ge	ppm	ICP-MS	<0.01	0.01	<0.01	<0.01	<0.01	<0.01	<0.01	<0.01	<0.01	<0.01
Hf	ppm	ICP-MS	0.47	0.28	0.13	0.45	0.1	0.14	0.07	0.06	0.06	0.16
Hg	ppm	ICP-MS	<0.01	<0.01	<0.01	<0.01	<0.01	<0.01	<0.01	<0.01	<0.01	<0.01
Ho	ppm	ICP-MS	0.05	0.01	0.08	0.03	0.02	0.03	0.02	0.02	0.02	0.03
Mo	ppm	ICP-MS	0.38	0.3	0.34	0.41	0.07	0.03	0.08	0.14	0.06	0.07
Nb	ppm	ICP-MS	<0.01	<0.01	<0.01	<0.01	<0.01	<0.01	<0.01	<0.01	<0.01	<0.01
Nd	ppm	ICP-MS	4.97	0.9	3.05	4.3	1.06	1.26	1.02	0.98	1	1.56
Ni	ppm	ICP-MS	7.21	1.18	0.66	0.44	0.41	0.53	0.8	0.57	0.43	0.45
^{204}Pb	ppm	ICP-MS	0.031	0.004	0.002	0.006	0.005	0.005	0.009	0.004	0.004	0.006
^{206}Pb	ppm	ICP-MS	3.3	0.494	0.13	0.256	0.12	0.13	0.187	0.135	0.115	0.139
^{207}Pb	ppm	ICP-MS	0.637	0.078	0.043	0.112	0.078	0.089	0.131	0.068	0.062	0.106
^{208}Pb	ppm	ICP-MS	1.93	0.227	0.212	0.515	0.196	0.229	0.342	0.181	0.165	0.304
Pb	ppm	ICP-MS	5.9	0.802	0.387	0.888	0.398	0.453	0.668	0.388	0.346	0.556
$^{206}Pb/^{204}Pb$	--	ICP-MS	106.45	123.50	65.00	42.67	24.00	26.00	20.78	33.75	28.75	23.17
$^{207}Pb/^{206}Pb$	--	ICP-MS	0.19	0.16	0.33	0.44	0.65	0.68	0.70	0.50	0.54	0.76
$^{207}Pb/^{204}Pb$	--	ICP-MS	20.55	19.50	21.50	18.67	15.60	17.80	14.56	17.00	15.50	17.67
$^{208}Pb/^{206}Pb$	--	ICP-MS	0.58	0.46	1.63	2.01	1.63	1.76	1.83	1.34	1.43	2.19
$^{208}Pb/^{204}Pb$	--	ICP-MS	62.26	56.75	106.00	85.83	39.20	45.80	38.00	45.25	41.25	50.67
Pr	ppm	ICP-MS	1.64	0.29	0.93	1.54	0.34	0.38	0.3	0.32	0.32	0.48
Rb	ppm	ICP-MS	0.05	0.07	0.29	0.23	0.11	0.11	0.15	0.12	0.12	0.1
Sb	ppm	ICP-MS	<0.01	<0.01	<0.01	<0.01	<0.01	<0.01	<0.01	0.02	<0.01	<0.01
Sc	ppm	ICP-MS	0.2	<0.1	<0.1	0.2	<0.1	0.1	0.1	<0.1	<0.1	<0.1
Se	ppm	ICP-MS	<0.1	<0.1	<0.1	<0.1	<0.1	<0.1	<0.1	<0.1	<0.1	<0.1
Sm	ppm	ICP-MS	0.88	0.15	0.55	0.57	0.21	0.26	0.22	0.19	0.2	0.31
Sn	ppm	ICP-MS	0.11	0.04	0.06	0.1	0.04	0.04	0.34	0.28	0.1	0.09
Ta	ppm	ICP-MS	<0.01	<0.01	<0.01	<0.01	<0.01	<0.01	<0.01	<0.01	<0.01	<0.01
Tb	ppm	ICP-MS	0.06	0.01	0.05	0.03	0.02	0.03	0.02	0.02	0.02	0.03
Te	ppm	ICP-MS	<0.01	<0.01	<0.01	<0.01	<0.01	<0.01	<0.01	<0.01	<0.01	<0.01
Th	ppm	ICP-MS	13.2	2.3	2.34	11.2	0.73	0.68	0.55	0.72	0.62	2.53
U	ppm	ICP-MS	17.6	1.78	0.4	0.39	0.29	0.4	0.48	0.77	0.38	0.4
V	ppm	ICP-MS	8.4	0.6	3.6	2	0.2	0.8	0.7	0.2	0.5	0.9
W	ppm	ICP-MS	<0.1	<0.1	<0.1	<0.1	<0.1	<0.1	<0.1	<0.1	<0.1	<0.1
Y	ppm	ICP-MS	1.51	0.28	2.29	0.81	0.57	0.76	0.72	0.51	0.58	0.78
Yb	ppm	ICP-MS	0.15	0.03	0.36	0.1	0.04	0.06	0.05	0.04	0.04	0.06
Zn	ppm	ICP-MS	18.5	0.7	1.4	0.6	0.8	0.6	0.9	0.6	0.8	0.7
Zr	ppm	ICP-MS	22.8	11.6	4.85	17.9	3.34	5.29	2.83	1.99	2.37	6.13

Partial Digestion: A 2.00 g pulp is digested with 2.25 ml of 8:1 ultrapure HNO_3:HCl for 1 hour at 95° C.

Group #			G-2014-2155	G-2014-2155	G-2014-2155	G-2014-2155	G-2014-2155	G-2014-2155	G-2014-2155	G-2014-2155	G-2014-2155	G-2014-2155
Sample #			SG200	SG201	SG202	SG203	SG204	SG205	SG206	SG207	SG208	SG209
Fence			Zone C	Zone C	Zone C	Zone C	Zone C	Zone C	Zone C	Zone C	Zone C	Zone C
Hole ID			MC-415	MC-415	MC-415	MC-415	MC-415	MC-415	MC-415	MC-415	MC-415	MC-415
From (m)			295.67	341.40	345.80	350.35	359.10	389.00	416.08	432.38	455.72	477.00
To (m)			295.86	341.50	345.90	350.52	360.20	389.24	416.28	432.61	455.92	477.20
Lithofacies			MFc	MFb	MFb	MFb	MFb	MFb	MFb	MFb	MFa	MFa
Date			11-28-2014	11-28-2014	11-28-2014	11-28-2014	11-28-2014	11-28-2014	11-28-2014	11-28-2014	11-28-2014	11-28-2014
Sample Type			Sandstone	Sandstone	Sandstone	Sandstone	Sandstone	Sandstone	Sandstone	Sandstone	Sandstone	Sandstone
Ag	ppm	ICP-MS	<0.01	<0.01	<0.01	<0.01	<0.01	<0.01	<0.01	<0.01	<0.01	<0.01
As	ppm	ICP-MS	0.3	0.49	0.42	0.45	0.28	0.51	0.39	0.3	0.21	0.16
Be	ppm	ICP-MS	0.04	0.04	0.04	0.04	0.03	0.08	0.02	0.03	0.02	0.03
Bi	ppm	ICP-MS	<0.01	0.01	0.03	<0.01	<0.01	<0.01	<0.01	<0.01	<0.01	<0.01
Cd	ppm	ICP-MS	<0.01	<0.01	<0.01	<0.01	<0.01	0.01	<0.01	<0.01	<0.01	<0.01
Co	ppm	ICP-MS	0.02	0.03	0.04	0.04	0.04	0.06	0.04	0.04	0.05	0.05
Cs	ppm	ICP-MS	<0.01	<0.01	<0.01	<0.01	<0.01	<0.01	<0.01	<0.01	<0.01	<0.01
Cu	ppm	ICP-MS	0.46	0.6	0.99	0.77	0.82	1.18	0.86	0.83	0.71	0.71
Dy	ppm	ICP-MS	0.15	0.3	0.15	0.12	0.1	0.21	0.06	0.09	0.08	0.12
Er	ppm	ICP-MS	0.07	0.12	0.06	0.05	0.05	0.12	0.03	0.05	0.04	0.07
Eu	ppm	ICP-MS	0.05	0.08	0.06	0.08	0.05	0.1	0.02	0.04	0.03	0.04
Ga	ppm	ICP-MS	0.09	0.11	0.14	0.04	0.07	0.06	0.09	0.07	0.05	0.06
Gd	ppm	ICP-MS	0.33	0.58	0.39	0.5	0.31	0.71	0.14	0.23	0.24	0.25
Ge	ppm	ICP-MS	<0.01	<0.01	<0.01	<0.01	<0.01	<0.01	<0.01	<0.01	<0.01	<0.01
Hf	ppm	ICP-MS	0.1	0.24	0.16	0.32	0.2	0.44	0.12	0.19	0.17	0.28
Hg	ppm	ICP-MS	<0.01	<0.01	<0.01	<0.01	<0.01	<0.01	<0.01	<0.01	<0.01	<0.01
Ho	ppm	ICP-MS	0.02	0.04	0.02	0.02	0.02	0.03	<0.01	0.01	0.01	0.02
Mo	ppm	ICP-MS	0.04	0.1	0.06	0.09	0.06	0.11	0.05	0.07	0.07	0.06
Nb	ppm	ICP-MS	<0.01	<0.01	<0.01	<0.01	<0.01	<0.01	<0.01	<0.01	<0.01	<0.01
Nd	ppm	ICP-MS	1.97	2.45	2.31	3.39	1.67	4.49	1.05	1.6	1.6	1.65
Ni	ppm	ICP-MS	0.23	0.21	0.23	0.28	0.3	0.29	0.21	0.24	0.3	0.31
^{204}Pb	ppm	ICP-MS	0.006	0.008	0.006	0.006	0.006	0.006	0.015	0.005	0.004	0.004
^{206}Pb	ppm	ICP-MS	0.143	0.203	0.145	0.162	0.145	0.174	0.283	0.102	0.105	0.114
^{207}Pb	ppm	ICP-MS	0.094	0.127	0.097	0.102	0.098	0.103	0.232	0.072	0.061	0.068
^{208}Pb	ppm	ICP-MS	0.294	0.398	0.316	0.459	0.316	0.734	0.587	0.22	0.181	0.222
Pb	ppm	ICP-MS	0.537	0.736	0.565	0.729	0.566	1.02	1.12	0.398	0.351	0.408
$^{206}Pb/^{204}Pb$	--	ICP-MS	23.83	25.38	24.17	27.00	24.17	29.00	18.87	20.40	26.25	28.50
$^{207}Pb/^{206}Pb$	--	ICP-MS	0.66	0.63	0.67	0.63	0.68	0.59	0.82	0.71	0.58	0.60
$^{207}Pb/^{204}Pb$	--	ICP-MS	15.67	15.88	16.17	17.00	16.33	17.17	15.47	14.40	15.25	17.00
$^{208}Pb/^{206}Pb$	--	ICP-MS	2.06	1.96	2.18	2.83	2.18	4.22	2.07	2.16	1.72	1.95
$^{208}Pb/^{204}Pb$	--	ICP-MS	49.00	49.75	52.67	76.50	52.67	122.33	39.13	44.00	45.25	55.50
Pr	ppm	ICP-MS	0.64	0.72	0.72	1.04	0.51	1.53	0.36	0.48	0.45	0.56
Rb	ppm	ICP-MS	0.19	0.23	0.25	0.04	0.06	0.04	0.13	0.05	0.04	0.04
Sb	ppm	ICP-MS	<0.01	<0.01	<0.01	0.01	<0.01	0.01	<0.01	<0.01	<0.01	<0.01
Sc	ppm	ICP-MS	<0.1	0.1	<0.1	<0.1	<0.1	0.1	<0.1	<0.1	<0.1	0.1
Se	ppm	ICP-MS	<0.1	<0.1	<0.1	<0.1	<0.1	<0.1	<0.1	<0.1	<0.1	<0.1
Sm	ppm	ICP-MS	0.36	0.54	0.44	0.67	0.36	0.82	0.16	0.29	0.36	0.28
Sn	ppm	ICP-MS	0.04	0.16	0.08	0.05	0.04	0.22	0.22	0.06	0.06	0.04
Ta	ppm	ICP-MS	<0.01	<0.01	<0.01	<0.01	<0.01	<0.01	<0.01	<0.01	<0.01	<0.01
Tb	ppm	ICP-MS	0.03	0.06	0.03	0.03	0.02	0.05	0.01	0.02	0.02	0.02
Te	ppm	ICP-MS	<0.01	<0.01	<0.01	<0.01	<0.01	<0.01	<0.01	<0.01	<0.01	<0.01
Th	ppm	ICP-MS	1.86	2.98	1.72	6.09	1.83	20.7	1.59	1.42	0.97	1.52
U	ppm	ICP-MS	0.43	0.98	0.89	0.93	0.44	1.98	0.71	0.84	0.7	0.95
V	ppm	ICP-MS	0.2	0.3	0.7	0.5	0.2	0.7	1	0.8	0.3	0.3
W	ppm	ICP-MS	<0.1	<0.1	<0.1	<0.1	<0.1	<0.1	<0.1	<0.1	<0.1	<0.1
Y	ppm	ICP-MS	0.62	1.13	0.58	0.44	0.43	1.04	0.29	0.41	0.35	0.59
Yb	ppm	ICP-MS	0.04	0.08	0.04	0.03	0.04	0.11	0.02	0.04	0.03	0.06
Zn	ppm	ICP-MS	0.5	0.6	0.9	0.7	0.7	0.8	0.8	0.7	0.6	0.7
Zr	ppm	ICP-MS	3.47	9.48	4.71	17.1	6.56	22.9	3.84	5.63	5.81	8.93

Partial Digestion: A 2.00 g pulp is digested with 2.25 ml of 8:1 ultrapure HNO_3:HCl for 1 hour at 95° C.

Group #			G-2014-2155	G-2014-2155	G-2014-2155	G-2014-2155	G-2014-2155	G-2014-2155	G-2014-2155	G-2014-2155	G-2014-2155	G-2014-2155
Sample #			SG210	SG211	SG212	SG213	SG214	SG215	SG216	SG213 R	SG217	SG218
Fence			Zone C	Zone C	Zone C	Zone C	Zone C	Zone C	Zone C	Zone C	Zone C	Background
Hole ID			MC-415	MC-415	MC-415	MC-415	MC-415	MC-415	MC-415	MC-415	MC-415	MC-434
From (m)			490.78	497.62	503.32	508.60	513.34	520.15	537.00	508.60	539.69	11.10
To (m)			490.91	497.86	503.54	508.75	513.45	520.35	537.15	508.75	539.84	11.22
Lithofacies			MFa	MFa	MFa	MFa	MFa	MFa	MFa	MFa	MFa	MFd
Date			11-28-2014	11-28-2014	11-28-2014	11-28-2014	11-28-2014	11-28-2014	11-28-2014	11-28-2014	11-28-2014	11-28-2014
Sample Type			Sandstone	Sandstone	Sandstone	Sandstone	Sandstone	Sandstone	Sandstone	Repeat	Sandstone	Sandstone
Ag	ppm	ICP-MS	<0.01	<0.01	<0.01	<0.01	<0.01	<0.01	<0.01	<0.01	<0.01	<0.01
As	ppm	ICP-MS	0.07	0.1	0.12	0.23	0.69	0.65	1.25	0.24	0.88	0.27
Be	ppm	ICP-MS	<0.01	0.02	0.01	0.02	0.04	0.04	0.1	0.02	0.04	0.01
Bi	ppm	ICP-MS	<0.01	<0.01	<0.01	<0.01	<0.01	<0.01	<0.01	<0.01	<0.01	<0.01
Cd	ppm	ICP-MS	<0.01	<0.01	<0.01	<0.01	<0.01	<0.01	<0.01	<0.01	<0.01	<0.01
Co	ppm	ICP-MS	0.02	0.04	0.04	0.06	0.05	0.08	0.08	0.06	0.07	0.05
Cs	ppm	ICP-MS	<0.01	<0.01	<0.01	0.01	<0.01	<0.01	<0.01	0.01	<0.01	<0.01
Cu	ppm	ICP-MS	0.29	0.73	0.54	1.2	8.1	2.27	0.97	1.18	1.26	0.99
Dy	ppm	ICP-MS	0.05	0.11	0.11	0.07	0.09	0.08	0.38	0.07	0.14	0.09
Er	ppm	ICP-MS	0.02	0.06	0.07	0.04	0.05	0.05	0.2	0.04	0.07	0.06
Eu	ppm	ICP-MS	0.02	0.03	0.02	0.02	0.02	0.02	0.14	0.02	0.11	0.02
Ga	ppm	ICP-MS	0.03	0.05	0.03	0.12	0.07	0.09	0.19	0.12	0.34	0.06
Gd	ppm	ICP-MS	0.1	0.18	0.16	0.11	0.15	0.14	1.1	0.11	0.86	0.15
Ge	ppm	ICP-MS	<0.01	<0.01	<0.01	<0.01	<0.01	<0.01	<0.01	<0.01	<0.01	<0.01
Hf	ppm	ICP-MS	0.05	0.25	0.3	0.09	0.15	0.16	0.28	0.09	0.06	0.23
Hg	ppm	ICP-MS	<0.01	<0.01	<0.01	<0.01	<0.01	<0.01	<0.01	<0.01	<0.01	<0.01
Ho	ppm	ICP-MS	<0.01	0.02	0.02	0.01	0.02	0.01	0.06	0.01	0.02	0.02
Mo	ppm	ICP-MS	0.05	0.05	0.05	0.08	0.16	0.17	0.13	0.09	0.13	0.1
Nb	ppm	ICP-MS	<0.01	<0.01	<0.01	<0.01	<0.01	<0.01	<0.01	<0.01	<0.01	<0.01
Nd	ppm	ICP-MS	0.58	0.94	0.82	0.58	0.87	0.68	6.75	0.6	9.68	1
Ni	ppm	ICP-MS	0.17	0.29	0.27	0.38	0.67	0.36	0.45	0.36	0.55	0.28
^{204}Pb	ppm	ICP-MS	0.003	0.005	0.004	0.004	0.004	0.003	0.005	0.005	0.005	0.011
^{206}Pb	ppm	ICP-MS	0.086	0.131	0.153	0.103	0.125	0.128	0.194	0.114	0.132	0.315
^{207}Pb	ppm	ICP-MS	0.055	0.088	0.075	0.065	0.073	0.059	0.091	0.076	0.078	0.176
^{208}Pb	ppm	ICP-MS	0.139	0.222	0.192	0.167	0.19	0.162	0.857	0.193	0.253	0.533
Pb	ppm	ICP-MS	0.284	0.446	0.424	0.338	0.392	0.352	1.15	0.388	0.469	1.04
$^{206}Pb/^{204}Pb$	--	ICP-MS	28.67	26.20	38.25	25.75	31.25	42.67	38.80	22.80	26.40	28.64
$^{207}Pb/^{206}Pb$	--	ICP-MS	0.64	0.67	0.49	0.63	0.58	0.46	0.47	0.67	0.59	0.56
$^{207}Pb/^{204}Pb$	--	ICP-MS	18.33	17.60	18.75	16.25	18.25	19.67	18.20	15.20	15.60	16.00
$^{208}Pb/^{206}Pb$	--	ICP-MS	1.62	1.69	1.25	1.62	1.52	1.27	4.42	1.69	1.92	1.69
$^{208}Pb/^{204}Pb$	--	ICP-MS	46.33	44.40	48.00	41.75	47.50	54.00	171.40	38.60	50.60	48.45
Pr	ppm	ICP-MS	0.17	0.29	0.26	0.18	0.28	0.22	2.17	0.19	2.72	0.33
Rb	ppm	ICP-MS	0.05	0.07	0.05	0.22	0.13	0.19	0.17	0.22	0.2	0.16
Sb	ppm	ICP-MS	<0.01	<0.01	<0.01	<0.01	<0.01	0.01	0.01	<0.01	<0.01	0.12
Sc	ppm	ICP-MS	<0.1	0.1	<0.1	<0.1	<0.1	<0.1	0.2	<0.1	0.3	0.1
Se	ppm	ICP-MS	<0.1	<0.1	<0.1	<0.1	<0.1	<0.1	<0.1	<0.1	<0.1	<0.1
Sm	ppm	ICP-MS	0.11	0.19	0.17	0.11	0.16	0.14	1.33	0.12	1.55	0.17
Sn	ppm	ICP-MS	0.04	0.1	0.07	0.06	1.51	0.08	0.48	0.11	0.28	0.13
Ta	ppm	ICP-MS	<0.01	<0.01	<0.01	<0.01	<0.01	<0.01	<0.01	<0.01	<0.01	<0.01
Tb	ppm	ICP-MS	<0.01	0.02	0.02	0.01	0.02	0.01	0.08	0.01	0.04	0.01
Te	ppm	ICP-MS	<0.01	<0.01	<0.01	<0.01	<0.01	<0.01	0.03	<0.01	<0.01	<0.01
Th	ppm	ICP-MS	0.35	0.66	0.7	0.42	0.56	0.55	51.4	1.16	1.31	1.26
U	ppm	ICP-MS	0.33	0.93	0.99	1.12	1.77	2.86	2.66	1.08	0.99	0.52
V	ppm	ICP-MS	0.1	0.2	0.3	1.6	2.9	3.6	3.4	1.6	2.2	0.2
W	ppm	ICP-MS	<0.1	<0.1	<0.1	<0.1	<0.1	<0.1	<0.1	<0.1	<0.1	<0.1
Y	ppm	ICP-MS	0.22	0.56	0.62	0.32	0.46	0.43	1.68	0.33	0.41	0.44
Yb	ppm	ICP-MS	0.02	0.06	0.07	0.02	0.04	0.04	0.16	0.02	0.02	0.05
Zn	ppm	ICP-MS	0.6	1.4	0.7	0.8	0.8	1.2	0.9	0.8	0.8	1.1
Zr	ppm	ICP-MS	2.08	8.58	11.2	2.39	5.16	5.8	12.4	2.42	2.14	8.46

Partial Digestion: A 2.00 g pulp is digested with 2.25 ml of 8:1 ultrapure HNO_3:HCl for 1 hour at 95° C.

Group #			G-2014-2155	G-2014-2155	G-2014-2155	G-2014-2155	G-2014-2155	G-2014-2155	G-2014-2155	G-2014-2155	G-2014-2155	G-2014-2155
Sample #			SG219	SG220	SG221	SG222	SG223	SG224	SG225	SG226	SG227	SG228
Fence			Background	Background	Background	Background	Background	Background	Background	Background	Background	Background
Hole ID			MC-434	MC-434	MC-434	MC-434	MC-434	MC-434	MC-434	MC-434	MC-434	MC-434
From (m)			31.63	54.07	93.9	119.66	168.25	183.4	217.84	253.64	256.65	282.2
To (m)			31.78	54.12	94.10	119.88	168.38	183.54	218.00	253.78	256.78	282.36
Lithofacies			MFd	MFd	MFd	MFd	MFc	MFc	MFc	MFc	MFc	MFc
Date			11-28-2014	11-28-2014	11-28-2014	11-28-2014	11-28-2014	11-28-2014	11-28-2014	11-28-2014	11-28-2014	11-28-2014
Sample Type			Sandstone	Sandstone	Sandstone	Sandstone	Sandstone	Sandstone	Sandstone	Sandstone	Sandstone	Sandstone
Ag	ppm	ICP-MS	<0.01	<0.01	<0.01	0.02	<0.01	<0.01	<0.01	<0.01	<0.01	<0.01
As	ppm	ICP-MS	0.27	0.14	0.07	0.5	0.13	0.12	0.4	0.29	0.44	0.28
Be	ppm	ICP-MS	0.01	<0.01	<0.01	0.01	0.01	0.01	0.02	0.01	0.02	0.01
Bi	ppm	ICP-MS	<0.01	<0.01	<0.01	<0.01	<0.01	<0.01	<0.01	<0.01	0.01	<0.01
Cd	ppm	ICP-MS	0.01	0.01	<0.01	<0.01	<0.01	<0.01	<0.01	<0.01	<0.01	<0.01
Co	ppm	ICP-MS	0.03	0.02	0.02	0.04	0.04	0.02	0.04	0.02	0.05	0.02
Cs	ppm	ICP-MS	<0.01	<0.01	<0.01	<0.01	<0.01	<0.01	<0.01	<0.01	<0.01	<0.01
Cu	ppm	ICP-MS	0.4	0.4	0.28	0.96	0.33	0.35	0.7	0.45	0.53	0.54
Dy	ppm	ICP-MS	0.09	0.07	0.06	0.08	0.06	0.06	0.1	0.07	0.08	0.09
Er	ppm	ICP-MS	0.06	0.05	0.03	0.04	0.04	0.03	0.06	0.03	0.04	0.04
Eu	ppm	ICP-MS	0.02	0.02	0.02	0.03	0.02	0.02	0.04	0.03	0.03	0.03
Ga	ppm	ICP-MS	0.07	0.08	0.05	0.12	0.08	0.07	0.09	0.08	0.1	0.1
Gd	ppm	ICP-MS	0.15	0.14	0.13	0.14	0.14	0.15	0.28	0.22	0.26	0.23
Ge	ppm	ICP-MS	<0.01	<0.01	<0.01	<0.01	<0.01	<0.01	<0.01	<0.01	<0.01	<0.01
Hf	ppm	ICP-MS	0.43	0.39	0.08	0.15	0.22	0.18	0.2	0.12	0.23	0.21
Hg	ppm	ICP-MS	<0.01	<0.01	<0.01	<0.01	<0.01	<0.01	<0.01	<0.01	<0.01	<0.01
Ho	ppm	ICP-MS	0.02	0.01	<0.01	0.01	0.01	<0.01	0.02	0.01	0.01	0.01
Mo	ppm	ICP-MS	0.04	0.04	0.03	0.12	0.04	0.03	0.05	0.03	0.22	0.03
Nb	ppm	ICP-MS	<0.01	<0.01	<0.01	<0.01	<0.01	<0.01	<0.01	<0.01	<0.01	<0.01
Nd	ppm	ICP-MS	0.98	1.01	0.88	0.67	0.99	1.09	1.81	1.35	1.68	1.46
Ni	ppm	ICP-MS	0.19	0.16	0.17	0.58	0.14	0.12	0.19	0.16	0.13	0.12
^{204}Pb	ppm	ICP-MS	0.005	0.005	0.005	0.014	0.005	0.015	0.025	0.006	0.006	0.005
^{206}Pb	ppm	ICP-MS	0.128	0.14	0.111	0.365	0.151	0.277	0.59	0.114	0.161	0.201
^{207}Pb	ppm	ICP-MS	0.082	0.087	0.082	0.236	0.091	0.222	0.405	0.087	0.096	0.093
^{208}Pb	ppm	ICP-MS	0.231	0.254	0.199	0.719	0.26	0.564	1.31	0.246	0.366	0.254
Pb	ppm	ICP-MS	0.445	0.486	0.397	1.34	0.508	1.08	2.33	0.452	0.629	0.553
$^{206}Pb/^{204}Pb$	--	ICP-MS	25.60	28.00	22.20	26.07	30.20	18.47	23.60	19.00	26.83	40.20
$^{207}Pb/^{206}Pb$	--	ICP-MS	0.64	0.62	0.74	0.65	0.60	0.80	0.69	0.76	0.60	0.46
$^{207}Pb/^{204}Pb$	--	ICP-MS	16.40	17.40	16.40	16.86	18.20	14.80	16.20	14.50	16.00	18.60
$^{208}Pb/^{206}Pb$	--	ICP-MS	1.80	1.81	1.79	1.97	1.72	2.04	2.22	2.16	2.27	1.26
$^{208}Pb/^{204}Pb$	--	ICP-MS	46.20	50.80	39.80	51.36	52.00	37.60	52.40	41.00	61.00	50.80
Pr	ppm	ICP-MS	0.35	0.37	0.31	0.2	0.35	0.37	0.58	0.44	0.55	0.47
Rb	ppm	ICP-MS	0.17	0.15	0.09	0.19	0.14	0.14	0.15	0.14	0.17	0.17
Sb	ppm	ICP-MS	<0.01	<0.01	<0.01	<0.01	<0.01	<0.01	<0.01	<0.01	<0.01	<0.01
Sc	ppm	ICP-MS	0.1	0.1	<0.1	0.1	<0.1	<0.1	<0.1	<0.1	<0.1	<0.1
Se	ppm	ICP-MS	<0.1	<0.1	<0.1	<0.1	<0.1	<0.1	<0.1	<0.1	<0.1	<0.1
Sm	ppm	ICP-MS	0.17	0.15	0.15	0.15	0.17	0.17	0.32	0.24	0.29	0.25
Sn	ppm	ICP-MS	0.04	0.07	0.03	0.08	0.09	0.04	0.17	0.11	0.14	0.08
Ta	ppm	ICP-MS	<0.01	<0.01	<0.01	<0.01	<0.01	<0.01	<0.01	<0.01	<0.01	<0.01
Tb	ppm	ICP-MS	0.01	0.01	0.01	0.01	0.01	0.01	0.02	0.02	0.02	0.02
Te	ppm	ICP-MS	<0.01	<0.01	<0.01	<0.01	<0.01	<0.01	<0.01	<0.01	<0.01	<0.01
Th	ppm	ICP-MS	1.34	1.68	0.5	0.56	1.44	1.19	1.72	0.88	2.97	1.29
U	ppm	ICP-MS	0.32	0.32	0.24	0.85	0.26	0.24	0.64	0.14	0.3	0.43
V	ppm	ICP-MS	0.2	0.2	0.1	1.2	0.7	0.8	0.6	0.2	0.8	0.3
W	ppm	ICP-MS	<0.1	<0.1	<0.1	<0.1	<0.1	<0.1	<0.1	<0.1	<0.1	<0.1
Y	ppm	ICP-MS	0.42	0.34	0.23	0.35	0.26	0.24	0.41	0.26	0.33	0.32
Yb	ppm	ICP-MS	0.06	0.06	0.02	0.04	0.03	0.03	0.05	0.03	0.04	0.04
Zn	ppm	ICP-MS	1	0.6	0.8	0.9	0.8	0.8	1.4	0.9	1.2	1
Zr	ppm	ICP-MS	19.1	15.6	2.92	4.97	9.42	7.1	6.73	4.09	9.08	7.6

Partial Digestion: A 2.00 g pulp is digested with 2.25 ml of 8:1 ultrapure HNO_3:HCl for 1 hour at 95° C.

Group #			G-2014-2155	G-2014-2155	G-2014-2155	G-2014-2155	G-2014-2155	G-2014-2155	G-2014-2155
Sample #			SG229	SG230	SG231	SG232	SG233	SG234	SG234 R
Fence			Background	Background	Background	Background	Background	Background	Background
Hole ID			MC-434	MC-434	MC-434	MC-434	MC-434	MC-434	MC-434
From (m)			328.83	338.05	348.28	370.63	397.53	421.67	421.67
To (m)			329.00	338.20	348.45	370.75	397.67	421.83	421.83
Lithofacies			MFb	MFb	MFb	MFb	MFa	MFa	MFa
Date			11-28-2014	11-28-2014	11-28-2014	11-28-2014	11-28-2014	11-28-2014	11-28-2014
Sample Type			Sandstone	Sandstone	Sandstone	Sandstone	Sandstone	Sandstone	Repeat
Ag	ppm	ICP-MS	<0.01	<0.01	<0.01	<0.01	<0.01	<0.01	<0.01
As	ppm	ICP-MS	0.41	0.56	0.28	0.45	0.32	0.32	0.34
Be	ppm	ICP-MS	0.02	0.02	0.02	0.02	0.02	0.02	0.02
Bi	ppm	ICP-MS	<0.01	<0.01	0.01	<0.01	<0.01	<0.01	<0.01
Cd	ppm	ICP-MS	<0.01	<0.01	<0.01	<0.01	<0.01	<0.01	<0.01
Co	ppm	ICP-MS	0.02	0.04	0.02	0.07	0.05	0.03	0.03
Cs	ppm	ICP-MS	<0.01	<0.01	<0.01	<0.01	<0.01	<0.01	<0.01
Cu	ppm	ICP-MS	0.36	1.06	0.5	0.48	0.32	0.44	0.48
Dy	ppm	ICP-MS	0.09	0.05	0.06	0.07	0.08	0.07	0.07
Er	ppm	ICP-MS	0.04	0.03	0.04	0.04	0.04	0.03	0.03
Eu	ppm	ICP-MS	0.03	0.02	0.03	0.03	0.05	0.04	0.03
Ga	ppm	ICP-MS	0.1	0.11	0.11	0.1	0.12	0.08	0.08
Gd	ppm	ICP-MS	0.29	0.14	0.18	0.21	0.33	0.25	0.27
Ge	ppm	ICP-MS	<0.01	<0.01	<0.01	<0.01	<0.01	<0.01	<0.01
Hf	ppm	ICP-MS	0.16	0.11	0.36	0.25	0.25	0.17	0.16
Hg	ppm	ICP-MS	<0.01	<0.01	<0.01	<0.01	<0.01	<0.01	<0.01
Ho	ppm	ICP-MS	0.01	<0.01	0.01	0.01	0.01	<0.01	0.01
Mo	ppm	ICP-MS	0.03	0.07	0.03	0.04	0.04	0.04	0.04
Nb	ppm	ICP-MS	<0.01	<0.01	<0.01	<0.01	<0.01	<0.01	<0.01
Nd	ppm	ICP-MS	1.91	0.87	1.24	1.53	2.59	1.78	1.79
Ni	ppm	ICP-MS	0.12	0.3	0.13	0.21	0.17	0.15	0.17
^{204}Pb	ppm	ICP-MS	0.005	0.003	0.004	0.004	0.005	0.005	0.005
^{206}Pb	ppm	ICP-MS	0.122	0.084	0.142	0.142	0.131	0.158	0.155
^{207}Pb	ppm	ICP-MS	0.08	0.053	0.078	0.074	0.083	0.083	0.081
^{208}Pb	ppm	ICP-MS	0.269	0.156	0.3	0.362	0.255	0.283	0.278
Pb	ppm	ICP-MS	0.476	0.296	0.525	0.583	0.475	0.529	0.519
$^{206}Pb/^{204}Pb$	--	ICP-MS	24.40	28.00	35.50	35.50	26.20	31.60	31.00
$^{207}Pb/^{206}Pb$	--	ICP-MS	0.66	0.63	0.55	0.52	0.63	0.53	0.52
$^{207}Pb/^{204}Pb$	--	ICP-MS	16.00	17.67	19.50	18.50	16.60	16.60	16.20
$^{208}Pb/^{206}Pb$	--	ICP-MS	2.20	1.86	2.11	2.55	1.95	1.79	1.79
$^{208}Pb/^{204}Pb$	--	ICP-MS	53.80	52.00	75.00	90.50	51.00	56.60	55.60
Pr	ppm	ICP-MS	0.6	0.27	0.42	0.52	0.77	0.55	0.55
Rb	ppm	ICP-MS	0.13	0.15	0.16	0.16	0.09	0.09	0.09
Sb	ppm	ICP-MS	<0.01	<0.01	0.01	<0.01	<0.01	<0.01	<0.01
Sc	ppm	ICP-MS	<0.1	<0.1	<0.1	<0.1	<0.1	<0.1	<0.1
Se	ppm	ICP-MS	<0.1	<0.1	<0.1	<0.1	<0.1	<0.1	<0.1
Sm	ppm	ICP-MS	0.36	0.16	0.22	0.25	0.5	0.32	0.32
Sn	ppm	ICP-MS	0.05	0.05	0.04	0.07	0.1	0.28	0.12
Ta	ppm	ICP-MS	<0.01	<0.01	<0.01	<0.01	<0.01	<0.01	<0.01
Tb	ppm	ICP-MS	0.02	0.01	0.01	0.01	0.02	0.02	0.02
Te	ppm	ICP-MS	<0.01	<0.01	<0.01	<0.01	<0.01	<0.01	<0.01
Th	ppm	ICP-MS	1.67	0.6	2.4	4.77	1.58	2.13	2.15
U	ppm	ICP-MS	0.26	0.95	0.38	0.25	0.23	0.25	0.27
V	ppm	ICP-MS	0.3	0.5	0.3	0.7	0.4	0.5	0.5
W	ppm	ICP-MS	<0.1	<0.1	<0.1	<0.1	<0.1	<0.1	<0.1
Y	ppm	ICP-MS	0.33	0.23	0.27	0.3	0.3	0.26	0.27
Yb	ppm	ICP-MS	0.03	0.02	0.03	0.03	0.03	0.02	0.02
Zn	ppm	ICP-MS	0.7	1	0.6	0.7	0.6	0.8	0.8
Zr	ppm	ICP-MS	5.28	3.25	13.4	9.28	8.52	5.83	5.68

Partial Digestion: A 2.00 g pulp is digested with 2.25 ml of 8:1 ultrapure HNO_3:HCl for 1 hour at 95° C.

Group #			G-2014-2129	G-2014-2129	G-2014-2129	G-2014-2129	G-2014-2129	G-2014-2129	G-2014-2129	G-2014-2129	G-2014-2129
Description			SG1	SG2	SG3	SG4	SG5	SG6	SG7	SG8	SG9
Fence			Southwest	Southwest	Southwest	Southwest	Southwest	Southwest	Southwest	Southwest	Southwest
HoleID			MC-336	MC-336	MC-336	MC-336	MC-336	MC-336	MC-336	MC-336	MC-336
From			433.00	455.50	464.87	479.50	500.43	506.55	506.80	517.00	522.86
To			433.22	455.72	465.13	479.75	500.59	506.76	506.99	517.19	523.03
Lithofacies			MFa	MFa	MFa	MFa	MFa	MFa	MFa	MFa	MFa
Date			11-27-2014	11-27-2014	11-27-2014	11-27-2014	11-27-2014	11-27-2014	11-27-2014	11-27-2014	11-27-2014
Sample Type			Sandstone	Sandstone	Sandstone	Sandstone	Sandstone	Sandstone	Sandstone	Sandstone	Sandstone
C	%	LECO	0.08	0.08	0.18	0.11	0.17	0.05	0.1	0.08	0.08
S	%	LECO	0.01	0.01	0.01	0.01	0.01	0.01	0.01	0.01	0.01
B	ppm	fusion	48	166	428	102	143	394	1490	219	629
LOI	%	1000°C	0.5	2	0.9	1.8	0.5	0.6	1.2	0.7	1.8
Al_2O_3	%	ICP-OES	2.39	6.04	3.05	5.01	2.27	2.26	5.78	2.03	6.1
CaO	%	ICP-OES	0.01	0.02	0.02	0.01	0.01	0.02	0.02	0.02	0.02
Fe_2O_3	%	ICP-OES	0.42	0.17	0.15	0.08	0.14	0.09	0.72	0.1	0.28
K_2O	%	ICP-OES	0.688	0.514	0.364	0.197	0.543	0.374	0.832	0.39	0.531
MgO	%	ICP-OES	0.064	0.154	0.364	0.055	0.145	0.216	0.659	0.152	0.671
MnO	%	ICP-OES	<0.001	<0.001	<0.001	<0.001	<0.001	<0.001	<0.001	<0.001	<0.001
Na_2O	%	ICP-OES	<0.01	0.01	0.02	<0.01	0.01	0.02	0.06	0.02	0.03
P_2O_5	%	ICP-OES	0.036	0.046	0.026	0.022	0.019	0.021	0.049	0.02	0.053
SiO_2	%	ICP-OES	95.4	90.5	95.1	93	96	96.1	91.2	96.4	90.3
TiO_2	%	ICP-OES	0.234	0.323	0.087	0.035	0.058	0.042	0.174	0.048	0.241
Ag	ppm	ICP-MS	0.07	0.13	0.04	0.03	0.03	0.03	0.05	0.03	0.07
Ba	ppm	ICP-OES	14	27	11	11	17	28	44	40	60
Be	ppm	ICP-MS	0.2	0.4	0.4	0.2	0.2	0.3	0.9	0.3	0.9
Bi	ppm	ICP-MS	<0.1	0.1	<0.1	<0.1	<0.1	<0.1	<0.1	<0.1	<0.1
Cd	ppm	ICP-MS	0.3	0.2	<0.1	<0.1	<0.1	<0.1	0.2	0.1	0.2
Ce	ppm	ICP-OES	46	75	36	29	24	22	43	20	55
Co	ppm	ICP-MS	0.15	0.22	0.39	0.19	0.34	0.28	0.92	0.24	1.14
Cr	ppm	ICP-OES	4	15	5	6	7	8	19	12	16
Cs	ppm	ICP-MS	<0.1	<0.1	<0.1	<0.1	<0.1	<0.1	<0.1	<0.1	<0.1
Cu	ppm	ICP-MS	2.4	5.4	2.3	2	3	1.7	4.6	2.5	8.7
Dy	ppm	ICP-MS	1.12	0.91	0.44	0.33	0.47	0.45	0.98	0.52	1.35
Er	ppm	ICP-MS	0.88	0.62	0.3	0.18	0.27	0.25	0.61	0.32	0.75
Eu	ppm	ICP-MS	0.39	0.52	0.25	0.29	0.25	0.25	0.5	0.23	0.63
Ga	ppm	ICP-MS	3	6.2	3.2	3.5	2.1	2.3	5.8	2.3	6.8
Gd	ppm	ICP-MS	2.8	3.6	1.8	1.4	1.4	1.3	2.8	1.2	3.4
Hf	ppm	ICP-MS	13.3	9.2	4.7	1.6	2.8	3.7	10.2	5.4	8.1
Ho	ppm	ICP-MS	0.28	0.21	0.1	0.06	0.1	0.09	0.21	0.11	0.28
La	ppm	ICP-OES	28	39	19	14	11	11	23	10	30
Li	ppm	ICP-OES	5	20	7	11	5	14	16	18	23
Mo	ppm	ICP-MS	0.46	0.33	0.32	0.14	0.36	0.18	0.33	0.19	0.2
Nb	ppm	ICP-MS	4.8	7.4	2.2	0.9	1.2	1	3.8	1.1	4.9
Nd	ppm	ICP-MS	19.4	27.2	14.6	11.1	9.4	9	18.4	8	23.4
Ni	ppm	ICP-MS	0.9	2.2	4.1	0.8	2.1	2.1	5.9	1.8	11.5
^{204}Pb	ppm	ICP-MS	0.032	0.056	0.025	0.035	0.03	0.042	0.063	0.048	0.102
^{206}Pb	ppm	ICP-MS	0.974	1.39	0.664	0.673	0.725	0.843	1.39	0.991	2.36
^{207}Pb	ppm	ICP-MS	0.519	0.914	0.409	0.521	0.5	0.644	0.999	0.708	1.57
^{208}Pb	ppm	ICP-MS	2.04	3.52	1.3	1.42	1.31	1.73	2.8	1.84	4.38
Pb	ppm	ICP-MS	3.56	5.88	2.4	2.65	2.57	3.26	5.25	3.58	8.41
$^{206}Pb/^{204}Pb$	--	ICP-MS	30.44	24.82	26.56	19.23	24.17	20.07	22.06	20.65	23.14
$^{207}Pb/^{206}Pb$	--	ICP-MS	0.53	0.66	0.62	0.77	0.69	0.76	0.72	0.71	0.67
$^{207}Pb/^{204}Pb$	--	ICP-MS	16.22	16.32	16.36	14.89	16.67	15.33	15.86	14.75	15.39
$^{208}Pb/^{206}Pb$	--	ICP-MS	2.09	2.53	1.96	2.11	1.81	2.05	2.01	1.86	1.86
$^{208}Pb/^{204}Pb$	--	ICP-MS	63.75	62.86	52.00	40.57	43.67	41.19	44.44	38.33	42.94
Pr	ppm	ICP-MS	6.3	8.6	4.4	3.3	2.7	2.7	5.5	2.5	7
Rb	ppm	ICP-MS	6.9	6	4.1	2.2	6.1	3.3	7.5	3.4	6.6
Sc	ppm	ICP-MS	1.1	1.4	0.7	0.4	0.4	0.4	1.1	0.5	1.8
Sm	ppm	ICP-MS	3.3	4.3	2.1	1.8	1.7	1.6	3.2	1.4	4.1
Sn	ppm	ICP-MS	0.45	0.6	0.26	0.17	0.22	0.2	0.57	0.21	0.9
Sr	ppm	ICP-OES	96	136	84	59	55	56	127	58	142
Ta	ppm	ICP-MS	0.51	0.71	0.23	0.09	0.1	0.1	0.32	0.1	0.4
Tb	ppm	ICP-MS	0.22	0.2	0.1	0.08	0.1	0.1	0.2	0.1	0.27
Th	ppm	ICP-MS	20.6	21.3	7	3.8	3.24	3.95	7.79	2.94	10.2
U	ppm	ICP-MS	6.35	4.67	3.46	1.46	1.81	1.87	3.95	2.62	6.64
V	ppm	ICP-MS	6.3	8.6	3.1	1.5	2	2	6	2.7	8.2
W	ppm	ICP-MS	0.2	0.2	<0.1	<0.1	<0.1	<0.1	<0.1	<0.1	0.1
Y	ppm	ICP-MS	7.6	5.1	2.5	1.4	2.4	2.3	5.8	3.1	7.1
Yb	ppm	ICP-MS	1.18	0.73	0.36	0.16	0.29	0.26	0.7	0.38	0.76
Zn	ppm	ICP-MS	4	5	4	8	3	4	5	3	5
Zr	ppm	ICP-OES	466	306	157	46	96	126	367	183	290

Carbon and Sulfur: a 0.2 g pulp is analyzed in a Leco SC144DR C/S analyzer for Carbon and Sulfur.

SiO_2 Analysis: A 0.1 gram pulp is fused at 1000 C with lithium metaborate then dissolved in dilute HNO_3.

LOI: A 1.00 gram pulp is heated at 1000 C overnight and the weight loss determined.

Boron: A 0.1 gram pulp is fused at 650 C in a mixture of Na_2O_2/Na_2CO_3.

Total Digestion: A 0.250 g pulp is gently heated in a mixture of ultrapure $HF/HNO_3/HClO_4$ until dry and the residue dissolved in dilute ultrapure HNO_3.

Group #			G-2014-2129	G-2014-2129	G-2014-2129	G-2014-2129	G-2014-2129	G-2014-2129	G-2014-2129	G-2014-2129	G-2014-2129
Description			SG10	SG11	SG12	SG13	SG14	SG15	SG16	SG17	SG18
Fence			Southwest	Southwest	Southwest	Southwest	Southwest	Southwest	Southwest	Southwest	Southwest
HoleID			MC-336	MC-336	MC-336	MC-336	MC-336	MC-338	MC-338	MC-338	MC-338
From			532.73	557.00	560.46	564.00	570.50	23.00	65.00	101.00	150.50
To			532.93	557.13	560.66	564.28	570.79	23.30	65.20	101.37	150.66
Lithofacies			MFa	MFa	MFa	MFa	MFa	MFd	MFd	MFd	MFd
Date			11-27-2014	11-27-2014	11-27-2014	11-27-2014	11-27-2014	11-27-2014	11-27-2014	11-27-2014	11-27-2014
Sample Type			Sandstone	Sandstone	Sandstone	Sandstone	Sandstone	Sandstone	Sandstone	Sandstone	Sandstone
C	%	LECO	0.08	0.19	0.2	0.07	0.28	0.06	0.04	0.08	0.06
S	%	LECO	0.01	0.03	0.01	0.01	0.01	0.01	0.01	0.01	0.01
B	ppm	fusion	393	18	17	9	152	351	20	20	20
LOI	%	1000°C	0.5	0.4	0.6	0.3	1.6	0.2	0.2	0.3	0.2
Al_2O_3	%	ICP-OES	1.1	0.75	1.79	0.45	2.76	0.58	0.72	0.91	0.75
CaO	%	ICP-OES	0.02	0.02	0.02	0.02	0.12	<0.01	<0.01	<0.01	<0.01
Fe_2O_3	%	ICP-OES	0.07	0.09	0.06	0.08	3.16	0.04	0.06	0.06	0.07
K_2O	%	ICP-OES	0.037	0.162	0.362	0.087	0.287	0.03	0.192	0.252	0.206
MgO	%	ICP-OES	0.114	0.031	0.043	0.015	0.691	0.109	0.022	0.028	0.026
MnO	%	ICP-OES	<0.001	<0.001	<0.001	<0.001	0.018	<0.001	<0.001	<0.001	<0.001
Na_2O	%	ICP-OES	0.02	0.01	<0.01	<0.01	0.01	0.01	<0.01	<0.01	<0.01
P_2O_5	%	ICP-OES	0.012	0.008	0.013	0.027	0.114	0.011	0.01	0.016	0.015
SiO_2	%	ICP-OES	98	98.4	96.7	99	92.5	98.5	98.4	98.1	98.3
TiO_2	%	ICP-OES	0.031	0.024	0.026	0.184	0.126	0.034	0.037	0.072	0.069
Ag	ppm	ICP-MS	0.14	0.04	0.03	0.06	0.03	0.03	0.02	0.03	0.05
Ba	ppm	ICP-OES	32	24	25	21	35	9	7	13	13
Be	ppm	ICP-MS	0.4	0.3	0.2	0.2	0.7	0.2	<0.1	<0.1	<0.1
Bi	ppm	ICP-MS	0.5	0.4	<0.1	<0.1	<0.1	0.2	<0.1	<0.1	<0.1
Cd	ppm	ICP-MS	<0.1	<0.1	<0.1	0.2	0.2	<0.1	<0.1	0.1	0.1
Ce	ppm	ICP-OES	13	11	17	32	83	17	16	22	24
Co	ppm	ICP-MS	0.22	6.35	0.2	0.24	3.33	0.18	0.06	0.05	0.07
Cr	ppm	ICP-OES	16	10	16	22	18	6	3	9	8
Cs	ppm	ICP-MS	<0.1	<0.1	<0.1	<0.1	<0.1	<0.1	<0.1	<0.1	<0.1
Cu	ppm	ICP-MS	18.4	14.2	1.6	9.5	0.8	1.4	1	0.9	1.2
Dy	ppm	ICP-MS	0.98	0.98	0.29	0.61	1.31	0.6	0.39	0.62	0.56
Er	ppm	ICP-MS	0.46	0.4	0.19	0.38	0.87	0.34	0.22	0.37	0.36
Eu	ppm	ICP-MS	0.21	0.13	0.14	0.25	0.65	0.16	0.14	0.22	0.21
Ga	ppm	ICP-MS	1.7	0.9	1.8	0.4	5.3	1.1	0.8	0.9	0.7
Gd	ppm	ICP-MS	1.3	0.9	0.8	1.6	4.7	1.1	0.9	1.4	1.3
Hf	ppm	ICP-MS	3.4	1.4	1.6	8.6	10.8	2.2	2.2	5.3	4.4
Ho	ppm	ICP-MS	0.2	0.19	0.06	0.14	0.29	0.13	0.08	0.14	0.13
La	ppm	ICP-OES	7	6	9	16	43	9	8	9	10
Li	ppm	ICP-OES	9	15	11	7	20	2	4	4	3
Mo	ppm	ICP-MS	0.57	0.53	0.16	0.31	0.68	0.1	0.14	0.18	0.27
Nb	ppm	ICP-MS	0.8	0.7	0.7	3.4	2.4	0.8	0.8	1.6	1.7
Nd	ppm	ICP-MS	5.8	4.3	6.3	10.8	34.2	6.7	6	8.2	8.3
Ni	ppm	ICP-MS	1.3	5	0.6	0.7	6.7	1.1	0.4	0.4	0.4
^{204}Pb	ppm	ICP-MS	0.09	0.026	0.037	0.076	0.035	0.03	0.031	0.041	0.056
^{206}Pb	ppm	ICP-MS	6.42	5.96	0.778	2.44	0.935	0.65	0.621	0.793	1.12
^{207}Pb	ppm	ICP-MS	1.63	0.636	0.562	1.22	0.58	0.492	0.468	0.642	0.886
^{208}Pb	ppm	ICP-MS	4.48	1.11	1.41	4.79	2.02	1.27	1.25	1.82	2.47
Pb	ppm	ICP-MS	12.6	7.74	2.78	8.54	3.57	2.45	2.37	3.3	4.53
$^{206}Pb/^{204}Pb$	--	ICP-MS	71.33	229.23	21.03	32.11	26.71	21.67	20.03	19.34	20.00
$^{207}Pb/^{206}Pb$	--	ICP-MS	0.25	0.11	0.72	0.50	0.62	0.76	0.75	0.81	0.79
$^{207}Pb/^{204}Pb$	--	ICP-MS	18.11	24.46	15.19	16.05	16.57	16.40	15.10	15.66	15.82
$^{208}Pb/^{206}Pb$	--	ICP-MS	0.70	0.19	1.81	1.96	2.16	1.95	2.01	2.30	2.21
$^{208}Pb/^{204}Pb$	--	ICP-MS	49.78	42.69	38.11	63.03	57.71	42.33	40.32	44.39	44.11
Pr	ppm	ICP-MS	1.7	1.3	1.9	3.6	10	2.1	1.9	2.5	2.5
Rb	ppm	ICP-MS	0.6	2	3.8	1.1	4.8	0.6	1.8	2.3	1.9
Sc	ppm	ICP-MS	0.6	0.2	0.3	0.5	2.6	0.5	0.3	0.3	0.4
Sm	ppm	ICP-MS	1.3	0.8	1	1.7	6.2	1.2	1	1.5	1.6
Sn	ppm	ICP-MS	0.15	0.24	0.12	0.8	0.52	0.19	0.22	0.21	0.14
Sr	ppm	ICP-OES	32	22	34	101	336	28	27	46	42
Ta	ppm	ICP-MS	0.08	0.08	0.06	0.41	0.24	0.08	0.08	0.15	0.15
Tb	ppm	ICP-MS	0.17	0.16	0.06	0.13	0.3	0.1	0.07	0.12	0.11
Th	ppm	ICP-MS	2.76	2.16	2.41	34.8	15.6	3.27	3.1	11	4.37
U	ppm	ICP-MS	11.3	124	4.02	27.3	2.36	2	1.8	2.03	2.6
V	ppm	ICP-MS	7.4	3.9	5.3	3.8	24	1.9	1.5	1.5	1.6
W	ppm	ICP-MS	<0.1	0.1	<0.1	0.1	0.9	<0.1	<0.1	<0.1	<0.1
Y	ppm	ICP-MS	5.3	4.2	1.5	3.8	6.8	3.2	2	3.3	3.2
Yb	ppm	ICP-MS	0.45	0.35	0.18	0.49	1.13	0.38	0.25	0.43	0.42
Zn	ppm	ICP-MS	6	4	4	3	4	3	4	3	3
Zr	ppm	ICP-OES	111	45	49	320	404	69	68	182	155

Carbon and Sulfur: a 0.2 g pulp is analyzed in a Leco SC144DR C/S analyzer for Carbon and Sulfur.

SiO_2 Analysis: A 0.1 gram pulp is fused at 1000 C with lithium metaborate then dissolved in dilute HNO_3.

LOI: A 1.00 gram pulp is heated at 1000 C overnight and the weight loss determined.

Boron: A 0.1 gram pulp is fused at 650 C in a mixture of Na_2O_2/Na_2CO_3.

Total Digestion: A 0.250 g pulp is gently heated in a mixture of ultrapure $HF/HNO_3/HClO_4$ until dry and the residue dissolved in dilute ultrapure HNO_3.

Group #			G-2014-2129	G-2014-2129	G-2014-2129	G-2014-2129	G-2014-2129	G-2014-2129	G-2014-2129	G-2014-2129	G-2014-2129
Description			SG19	SG20	SG21	SG22	SG23	SG24	SG25	SG26	SG27
Fence			Southwest	Southwest	Southwest	Southwest	Southwest	Southwest	Southwest	Southwest	Southwest
HoleID			MC-338	MC-338	MC-338	MC-338	MC-338	MC-338	MC-338	MC-338	MC-338
From			220.20	272.00	318.90	372.17	410.80	466.00	502.37	537.64	554.73
To			220.58	272.20	319.25	372.50	411.10	466.31	502.60	537.95	555.00
Lithofacies			MFc	MFc	MFb	MFb	MFb	MFa	MFa	MFa	MFa
Date			11-27-2014	11-27-2014	11-27-2014	11-27-2014	11-27-2014	11-27-2014	11-27-2014	11-27-2014	11-27-2014
Sample Type			Sandstone	Sandstone	Sandstone	Sandstone	Sandstone	Sandstone	Sandstone	Sandstone	Sandstone
C	%	LECO	0.07	0.01	0.06	0.02	0.02	0.06	0.1	0.04	0.01
S	%	LECO	0.01	0.01	0.01	0.02	0.01	0.01	0.01	0.01	0.01
B	ppm	fusion	67	47	46	20	23	61	39	374	15
LOI	%	1000°C	0.4	0.7	0.5	0.4	0.4	1.6	0.4	0.4	0.3
Al_2O_3	%	ICP-OES	1.44	2.35	2.09	1.23	1.23	4.43	1.17	0.96	0.82
CaO	%	ICP-OES	0.01	0.02	0.01	0.02	0.01	0.01	0.01	0.01	0.01
Fe_2O_3	%	ICP-OES	0.13	0.18	0.12	0.11	0.07	0.08	0.1	0.07	0.06
K_2O	%	ICP-OES	0.357	0.519	0.594	0.324	0.327	0.174	0.228	0.037	0.201
MgO	%	ICP-OES	0.057	0.142	0.067	0.03	0.036	0.039	0.052	0.124	0.028
MnO	%	ICP-OES	<0.001	0.001	<0.001	<0.001	<0.001	<0.001	<0.001	<0.001	<0.001
Na_2O	%	ICP-OES	<0.01	<0.01	<0.01	<0.01	<0.01	<0.01	<0.01	0.02	0.01
P_2O_5	%	ICP-OES	0.022	0.036	0.026	0.072	0.026	0.042	0.01	0.01	0.01
SiO_2	%	ICP-OES	97.2	95.5	96.8	97.2	97.6	93.6	98.1	98.2	98.1
TiO_2	%	ICP-OES	0.116	0.191	0.139	0.051	0.084	0.063	0.02	0.022	0.025
Ag	ppm	ICP-MS	0.05	0.08	0.06	0.04	0.04	0.04	0.02	0.07	0.03
Ba	ppm	ICP-OES	15	19	13	8	7	12	21	23	21
Be	ppm	ICP-MS	0.2	0.2	0.2	0.1	0.1	0.2	0.1	0.4	0.1
Bi	ppm	ICP-MS	<0.1	<0.1	<0.1	<0.1	<0.1	<0.1	<0.1	<0.1	<0.1
Cd	ppm	ICP-MS	0.1	0.2	0.1	<0.1	<0.1	<0.1	<0.1	<0.1	<0.1
Ce	ppm	ICP-OES	31	45	34	27	24	76	11	13	15
Co	ppm	ICP-MS	0.12	0.18	0.11	0.1	0.15	0.17	0.19	0.36	0.11
Cr	ppm	ICP-OES	10	9	3	9	4	8	21	13	9
Cs	ppm	ICP-MS	<0.1	<0.1	<0.1	<0.1	<0.1	<0.1	<0.1	<0.1	<0.1
Cu	ppm	ICP-MS	2.1	1.5	0.9	2.5	0.8	1	1	8.3	2
Dy	ppm	ICP-MS	1.24	1.23	0.84	0.72	0.5	0.82	0.3	0.56	0.3
Er	ppm	ICP-MS	0.76	0.69	0.49	0.28	0.29	0.34	0.17	0.24	0.17
Eu	ppm	ICP-MS	0.3	0.41	0.3	0.18	0.21	0.38	0.13	0.12	0.12
Ga	ppm	ICP-MS	1.8	3.1	2.6	1.5	1.7	3.5	1.6	1.5	0.9
Gd	ppm	ICP-MS	2.1	2.9	2	1.7	1.5	4.6	0.8	0.8	0.7
Hf	ppm	ICP-MS	6	7	5.2	2.1	2.6	2.3	1.2	1.4	1.4
Ho	ppm	ICP-MS	0.28	0.26	0.19	0.11	0.11	0.11	0.06	0.1	0.06
La	ppm	ICP-OES	14	20	15	12	11	34	5	7	7
Li	ppm	ICP-OES	6	7	5	3	4	11	10	9	12
Mo	ppm	ICP-MS	0.28	0.23	0.17	0.12	0.11	0.08	0.18	0.14	0.13
Nb	ppm	ICP-MS	2.7	4.8	3.5	1.5	2.3	1.7	0.5	0.6	0.7
Nd	ppm	ICP-MS	11.3	16.3	12.8	10.6	9.6	39.6	5.3	4.6	5.4
Ni	ppm	ICP-MS	0.8	2.3	0.6	0.5	0.6	0.7	1	1.4	0.5
^{204}Pb	ppm	ICP-MS	0.054	0.044	0.044	0.015	0.018	0.034	0.031	0.031	0.03
^{206}Pb	ppm	ICP-MS	1.14	0.924	0.849	0.441	0.415	0.63	0.57	1.24	0.586
^{207}Pb	ppm	ICP-MS	0.829	0.7	0.665	0.25	0.278	0.504	0.469	0.516	0.446
^{208}Pb	ppm	ICP-MS	2.64	2.21	1.95	0.893	1	1.52	1.22	1.23	1.16
Pb	ppm	ICP-MS	4.67	3.88	3.51	1.6	1.71	2.68	2.29	3.02	2.22
$^{206}Pb/^{204}Pb$	--	ICP-MS	21.11	21.00	19.30	29.40	23.06	18.53	18.39	40.00	19.53
$^{207}Pb/^{206}Pb$	--	ICP-MS	0.73	0.76	0.78	0.57	0.67	0.80	0.82	0.42	0.76
$^{207}Pb/^{204}Pb$	--	ICP-MS	15.35	15.91	15.11	16.67	15.44	14.82	15.13	16.65	14.87
$^{208}Pb/^{206}Pb$	--	ICP-MS	2.32	2.39	2.30	2.02	2.41	2.41	2.14	0.99	1.98
$^{208}Pb/^{204}Pb$	--	ICP-MS	48.89	50.23	44.32	59.53	55.56	44.71	39.35	39.68	38.67
Pr	ppm	ICP-MS	3.4	4.8	3.8	3.2	2.8	10.7	1.6	1.5	1.7
Rb	ppm	ICP-MS	3.3	5.8	5.5	3.1	3.1	1.8	2.3	0.6	2.1
Sc	ppm	ICP-MS	1.1	0.7	0.8	0.4	0.4	0.5	0.4	0.3	0.2
Sm	ppm	ICP-MS	2.2	3.1	2.4	1.8	1.7	7	0.9	0.8	0.8
Sn	ppm	ICP-MS	0.29	0.52	0.24	0.16	0.3	0.16	0.14	0.14	0.16
Sr	ppm	ICP-OES	60	131	90	449	122	93	23	21	28
Ta	ppm	ICP-MS	0.26	0.45	0.3	0.15	0.23	0.16	0.04	0.06	0.06
Tb	ppm	ICP-MS	0.22	0.24	0.16	0.19	0.12	0.24	0.06	0.1	0.06
Th	ppm	ICP-MS	7.27	13.4	9.65	6.57	7.54	6.12	1.76	2.28	2.28
U	ppm	ICP-MS	5.04	2.98	2.64	2.01	1.3	1.26	1.05	3.69	2.16
V	ppm	ICP-MS	6.3	13.2	5	3.9	2.7	2.4	2.2	9	4.8
W	ppm	ICP-MS	<0.1	0.2	<0.1	<0.1	<0.1	<0.1	<0.1	<0.1	<0.1
Y	ppm	ICP-MS	7.4	7.3	4.8	2.7	2.8	2.4	1.5	2.6	1.7
Yb	ppm	ICP-MS	0.7	0.72	0.54	0.28	0.35	0.24	0.17	0.23	0.16
Zn	ppm	ICP-MS	4	5	4	3	3	3	3	4	3
Zr	ppm	ICP-OES	205	231	174	64	78	75	40	45	44

Carbon and Sulfur: a 0.2 g pulp is analyzed in a Leco SC144DR C/S analyzer for Carbon and Sulfur.

SiO_2 Analysis: A 0.1 gram pulp is fused at 1000 C with lithium metaborate then dissolved in dilute HNO_3.

LOI: A 1.00 gram pulp is heated at 1000 C overnight and the weight loss determined.

Boron: A 0.1 gram pulp is fused at 650 C in a mixture of Na_2O_2/Na_2CO_3.

Total Digestion: A 0.250 g pulp is gently heated in a mixture of ultrapure $HF/HNO_3/HClO_4$ until dry and the residue dissolved in dilute ultrapure HNO_3.

Group #			G-2014-2129	G-2014-2129	G-2014-2129	G-2014-2129	G-2014-2129	G-2014-2129	G-2014-2129	G-2014-2129	G-2014-2129
Description			SG28	SG29	SG30	SG31	SG32	SG33	SG34	SG35	SG36
Fence			Southwest	Southwest	Southwest	Southwest	Southwest	Southwest	Southwest	Southwest	Southwest
HoleID			MC-338	MC-338	MC-344	MC-344	MC-344	MC-344	MC-344	MC-344	MC-344
From			557.50	559.00	26.10	69.00	100.10	128.00	164.00	179.80	199.00
To			557.71	559.13	26.40	69.40	100.30	128.18	164.30	180.10	199.18
Lithofacies			MFa	MFa	MFd	MFd	MFd	MFd	MFd	MFd	MFd
Date			11-27-2014	11-27-2014	11-27-2014	11-27-2014	11-27-2014	11-27-2014	11-27-2014	11-27-2014	11-27-2014
Sample Type			Sandstone	Sandstone	Sandstone	Sandstone	Sandstone	Sandstone	Sandstone	Sandstone	Sandstone
C	%	LECO	0.06	0.08	0.04	0.02	0.01	0.08	0.09	0.06	0.1
S	%	LECO	0.01	0.01	0.01	0.01	0.01	0.01	0.01	0.01	0.01
B	ppm	fusion	38	425	469	861	741	268	2160	1110	72
LOI	%	1000°C	0.7	0.9	0.2	0.3	0.3	0.4	0.5	0.4	0.3
Al_2O_3	%	ICP-OES	2.49	5.16	0.62	1.03	1.03	0.98	2.89	1.48	1.14
CaO	%	ICP-OES	0.02	0.02	<0.01	<0.01	<0.01	<0.01	0.01	<0.01	<0.01
Fe_2O_3	%	ICP-OES	0.15	0.34	0.03	0.02	0.04	0.12	0.17	0.08	0.12
K_2O	%	ICP-OES	0.484	1.32	0.01	0.012	0.013	0.076	0.093	0.026	0.287
MgO	%	ICP-OES	0.19	0.26	0.122	0.21	0.203	0.185	0.556	0.299	0.05
MnO	%	ICP-OES	<0.001	<0.001	<0.001	<0.001	<0.001	<0.001	<0.001	<0.001	<0.001
Na_2O	%	ICP-OES	0.01	0.02	0.01	0.02	0.02	<0.01	0.06	0.04	<0.01
P_2O_5	%	ICP-OES	0.039	0.057	0.012	0.014	0.014	0.016	0.024	0.018	0.019
SiO_2	%	ICP-OES	96	91.9	99.2	97.8	98.2	97.7	95.2	97.4	97.7
TiO_2	%	ICP-OES	0.14	0.198	0.05	0.052	0.027	0.092	0.179	0.053	0.082
Ag	ppm	ICP-MS	0.06	0.07	0.02	0.03	0.03	0.04	0.07	0.02	0.05
Ba	ppm	ICP-OES	56	48	8	8	9	11	14	10	12
Be	ppm	ICP-MS	0.5	0.8	0.3	0.5	0.4	0.3	0.8	0.6	0.1
Bi	ppm	ICP-MS	<0.1	<0.1	<0.1	0.2	<0.1	<0.1	<0.1	<0.1	<0.1
Cd	ppm	ICP-MS	0.2	0.2	0.1	<0.1	<0.1	0.1	0.2	<0.1	<0.1
Ce	ppm	ICP-OES	50	62	15	21	24	22	26	24	29
Co	ppm	ICP-MS	1.47	1.16	0.19	0.29	0.21	0.14	0.42	0.28	0.12
Cr	ppm	ICP-OES	13	11	6	3	15	6	6	9	7
Cs	ppm	ICP-MS	<0.1	0.1	<0.1	<0.1	<0.1	<0.1	<0.1	<0.1	<0.1
Cu	ppm	ICP-MS	14	9.1	3	3.8	3.8	2.7	2.6	1.6	1.2
Dy	ppm	ICP-MS	1.11	3.39	1.06	0.86	0.47	0.65	1.48	0.74	0.62
Er	ppm	ICP-MS	0.64	2.03	0.66	0.52	0.24	0.4	0.83	0.39	0.34
Eu	ppm	ICP-MS	0.5	0.7	0.17	0.19	0.18	0.19	0.3	0.2	0.22
Ga	ppm	ICP-MS	2.7	6.7	1.7	2.9	2.4	2.1	4.9	3.2	1.5
Gd	ppm	ICP-MS	2.7	4.8	1.3	1.4	1.2	1.3	2	1.4	1.6
Hf	ppm	ICP-MS	7.5	10.8	6.4	3.8	1.3	5.6	10.5	2.8	3.4
Ho	ppm	ICP-MS	0.24	0.8	0.26	0.19	0.09	0.15	0.34	0.16	0.13
La	ppm	ICP-OES	26	32	7	10	10	9	12	10	12
Li	ppm	ICP-OES	23	17	1	1	2	3	2	1	4
Mo	ppm	ICP-MS	0.22	0.13	0.1	0.08	0.16	0.23	0.13	0.14	0.11
Nb	ppm	ICP-MS	3.1	4.3	1.3	1.3	0.6	2.5	4.4	1.2	2.1
Nd	ppm	ICP-MS	19.5	25.4	6.4	7.8	8.2	8.1	10	8.7	10.3
Ni	ppm	ICP-MS	5.9	4	1.3	1.7	1.7	2.1	3.9	1.8	0.9
^{204}Pb	ppm	ICP-MS	0.076	0.068	0.029	0.035	0.038	0.048	0.179	0.047	0.063
^{206}Pb	ppm	ICP-MS	1.81	1.93	0.824	1.2	0.928	0.892	4.26	1.03	1.22
^{207}Pb	ppm	ICP-MS	1.22	1.1	0.458	0.59	0.599	0.714	2.76	0.717	0.97
^{208}Pb	ppm	ICP-MS	3.4	3.34	1.28	1.58	1.45	2	9.28	2.05	2.76
Pb	ppm	ICP-MS	6.51	6.44	2.59	3.4	3.02	3.66	16.5	3.84	5.01
$^{206}Pb/^{204}Pb$	--	ICP-MS	23.82	28.38	28.41	34.29	24.42	18.58	23.80	21.91	19.37
$^{207}Pb/^{206}Pb$	--	ICP-MS	0.67	0.57	0.56	0.49	0.65	0.80	0.65	0.70	0.80
$^{207}Pb/^{204}Pb$	--	ICP-MS	16.05	16.18	15.79	16.86	15.76	14.88	15.42	15.26	15.40
$^{208}Pb/^{206}Pb$	--	ICP-MS	1.88	1.73	1.55	1.32	1.56	2.24	2.18	1.99	2.26
$^{208}Pb/^{204}Pb$	--	ICP-MS	44.74	49.12	44.14	45.14	38.16	41.67	51.84	43.62	43.81
Pr	ppm	ICP-MS	6	7.8	2	2.5	2.5	2.5	3	2.7	3.1
Rb	ppm	ICP-MS	6.7	16.1	0.5	0.4	0.4	1.1	1.3	0.5	2.8
Sc	ppm	ICP-MS	1.3	2.4	0.9	0.8	0.4	0.4	1	0.5	0.4
Sm	ppm	ICP-MS	3.2	4.6	1.2	1.3	1.4	1.5	2	1.5	1.8
Sn	ppm	ICP-MS	0.6	1.34	0.24	0.29	0.12	0.27	0.55	0.27	0.26
Sr	ppm	ICP-OES	123	157	29	39	41	42	54	49	63
Ta	ppm	ICP-MS	0.28	0.38	0.11	0.2	0.07	0.23	0.42	0.1	0.19
Tb	ppm	ICP-MS	0.21	0.61	0.17	0.14	0.1	0.12	0.25	0.13	0.13
Th	ppm	ICP-MS	8.99	12.3	5.23	5.9	2.38	9.32	11.5	6.23	8.58
U	ppm	ICP-MS	16.2	17	4.03	3.85	2.33	2.89	6.76	3	1.76
V	ppm	ICP-MS	10.4	13.8	8.8	17.6	22	3	7.4	4.8	3.7
W	ppm	ICP-MS	<0.1	0.5	<0.1	<0.1	<0.1	<0.1	<0.1	<0.1	<0.1
Y	ppm	ICP-MS	5.9	21.4	6.9	5	2.2	4.1	9	3.9	3.2
Yb	ppm	ICP-MS	0.67	2.1	0.73	0.5	0.21	0.48	0.85	0.36	0.35
Zn	ppm	ICP-MS	11	4	4	4	3	4	5	4	4
Zr	ppm	ICP-OES	273	389	199	114	40	198	347	89	106

Carbon and Sulfur: a 0.2 g pulp is analyzed in a Leco SC144DR C/S analyzer for Carbon and Sulfur.

SiO_2 Analysis: A 0.1 gram pulp is fused at 1000 C with lithium metaborate then dissolved in dilute HNO_3.

LOI: A 1.00 gram pulp is heated at 1000 C overnight and the weight loss determined.

Boron: A 0.1 gram pulp is fused at 650 C in a mixture of Na_2O_2/Na_2CO_3.

Total Digestion: A 0.250 g pulp is gently heated in a mixture of ultrapure $HF/HNO_3/HClO_4$ until dry and the residue dissolved in dilute ultrapure HNO_3.

Group #			G-2014-2129	G-2014-2129	G-2014-2129	G-2014-2129	G-2014-2129	G-2014-2129	G-2014-2129	G-2014-2129	G-2014-2129
Description			SG37	SG33 R	SG38	SG39	SG40	SG41	SG42	SG43	SG44
Fence			Southwest	Southwest	Southwest	Southwest	Southwest	Southwest	Southwest	Southwest	Southwest
HoleID			MC-344	MC-344	MC-344	MC-344	MC-344	MC-344	MC-344	MC-344	MC-344
From			230.00	128.00	275.00	298.82	342.90	378.45	394.34	433.00	467.00
To			230.27	128.18	275.23	299.00	343.26	378.69	394.59	433.27	467.17
Lithofacies			MFc	MFd	MFc	MFb	MFb	MFa	MFa	MFa	MFa
Date			11-27-2014	11-27-2014	11-27-2014	11-27-2014	11-27-2014	11-27-2014	11-27-2014	11-27-2014	11-27-2014
Sample Type			Sandstone	Repeat	Sandstone	Sandstone	Sandstone	Sandstone	Sandstone	Sandstone	Sandstone
C	%	LECO	0.06	0.08	0.08	0.08	0.07	0.08	0.09	0.06	0.08
S	%	LECO	0.01	0.01	0.01	0.01	0.01	0.01	0.01	0.01	0.01
B	ppm	fusion	58	261	52	83	20	33	64	36	19
LOI	%	1000°C	0.3	0.4	0.3	0.5	0.7	1	0.7	0.7	0.9
Al_2O_3	%	ICP-OES	0.93	1.01	1.03	1.68	1.78	2.74	2.05	2.08	2.28
CaO	%	ICP-OES	0.01	<0.01	<0.01	0.01	<0.01	0.01	0.01	0.01	<0.01
Fe_2O_3	%	ICP-OES	0.08	0.13	0.09	0.23	0.05	0.1	0.61	0.27	0.53
K_2O	%	ICP-OES	0.24	0.078	0.237	0.328	0.111	0.2	0.336	0.255	0.036
MgO	%	ICP-OES	0.032	0.189	0.028	0.038	0.014	0.023	0.04	0.028	0.011
MnO	%	ICP-OES	<0.001	<0.001	<0.001	<0.001	<0.001	<0.001	0.003	<0.001	0.002
Na_2O	%	ICP-OES	<0.01	0.01	<0.01	<0.01	<0.01	<0.01	<0.01	<0.01	<0.01
P_2O_5	%	ICP-OES	0.019	0.017	0.018	0.026	0.015	0.02	0.021	0.02	0.023
SiO_2	%	ICP-OES	98	97.6	98	96.7	96.7	95.5	96.2	96.3	95.9
TiO_2	%	ICP-OES	0.162	0.104	0.071	0.182	0.032	0.15	0.15	0.114	0.068
Ag	ppm	ICP-MS	0.07	0.06	0.03	0.07	0.03	0.08	0.06	0.05	0.06
Ba	ppm	ICP-OES	11	12	9	12	10	13	14	13	25
Be	ppm	ICP-MS	0.2	0.2	0.1	0.2	0.1	0.2	0.2	0.1	0.4
Bi	ppm	ICP-MS	<0.1	<0.1	<0.1	<0.1	<0.1	<0.1	<0.1	<0.1	0.2
Cd	ppm	ICP-MS	0.1	0.1	<0.1	<0.1	<0.1	<0.1	<0.1	0.1	0.2
Ce	ppm	ICP-OES	28	24	24	38	23	29	32	31	23
Co	ppm	ICP-MS	0.1	0.16	0.21	0.12	0.08	0.12	0.9	0.12	0.39
Cr	ppm	ICP-OES	8	6	17	14	13	7	12	7	12
Cs	ppm	ICP-MS	<0.1	<0.1	<0.1	<0.1	<0.1	<0.1	<0.1	<0.1	<0.1
Cu	ppm	ICP-MS	1.1	2.8	0.7	1	0.5	0.8	1	0.7	1.2
Dy	ppm	ICP-MS	0.76	0.67	0.43	0.56	0.29	0.5	0.41	0.4	0.61
Er	ppm	ICP-MS	0.43	0.43	0.28	0.34	0.16	0.34	0.25	0.29	0.46
Eu	ppm	ICP-MS	0.23	0.2	0.16	0.28	0.19	0.29	0.24	0.22	0.28
Ga	ppm	ICP-MS	1.3	2.1	1.2	1.8	1.8	3	2.4	2.7	2.8
Gd	ppm	ICP-MS	1.8	1.3	1.2	2	1.1	1.6	1.4	1.5	1.6
Hf	ppm	ICP-MS	4.8	6.2	3.3	4.6	1.4	4.9	4.2	4.9	5.8
Ho	ppm	ICP-MS	0.16	0.16	0.1	0.12	0.05	0.11	0.08	0.09	0.15
La	ppm	ICP-OES	12	10	10	16	10	13	15	15	10
Li	ppm	ICP-OES	2	4	3	5	7	9	7	10	11
Mo	ppm	ICP-MS	0.11	0.22	0.25	0.14	0.09	0.11	0.12	0.09	0.23
Nb	ppm	ICP-MS	4.1	2.7	1.8	4.5	1	3.4	3.8	2.9	1.6
Nd	ppm	ICP-MS	9.8	8.2	8.3	14.4	8.2	11	10.7	12.4	9.9
Ni	ppm	ICP-MS	0.6	2.1	1.2	0.7	0.5	0.5	1.5	0.6	1
^{204}Pb	ppm	ICP-MS	0.046	0.05	0.044	0.049	0.034	0.039	0.045	0.032	0.044
^{206}Pb	ppm	ICP-MS	0.842	0.922	0.852	0.857	0.574	0.809	0.969	0.679	0.982
^{207}Pb	ppm	ICP-MS	0.717	0.722	0.68	0.734	0.496	0.635	0.726	0.488	0.719
^{208}Pb	ppm	ICP-MS	1.96	2.03	1.86	2.16	1.31	1.89	2.67	1.46	1.9
Pb	ppm	ICP-MS	3.57	3.72	3.44	3.8	2.42	3.37	4.41	2.66	3.64
$^{206}Pb/^{204}Pb$	--	ICP-MS	18.30	18.44	19.36	17.49	16.88	20.74	21.53	21.22	22.32
$^{207}Pb/^{206}Pb$	--	ICP-MS	0.85	0.78	0.80	0.86	0.86	0.78	0.75	0.72	0.73
$^{207}Pb/^{204}Pb$	--	ICP-MS	15.59	14.44	15.45	14.98	14.59	16.28	16.13	15.25	16.34
$^{208}Pb/^{206}Pb$	--	ICP-MS	2.33	2.20	2.18	2.52	2.28	2.34	2.76	2.15	1.93
$^{208}Pb/^{204}Pb$	--	ICP-MS	42.61	40.60	42.27	44.08	38.53	48.46	59.33	45.63	43.18
Pr	ppm	ICP-MS	3	2.5	2.5	4.3	2.6	3.4	3.5	3.8	2.9
Rb	ppm	ICP-MS	2.4	1.1	2.3	2.9	1.2	2	3	2.3	0.7
Sc	ppm	ICP-MS	0.5	0.5	0.4	0.6	0.3	0.7	0.6	0.7	0.8
Sm	ppm	ICP-MS	1.9	1.4	1.4	2.7	1.3	2	1.8	1.9	1.9
Sn	ppm	ICP-MS	0.28	0.27	0.27	0.38	0.2	0.35	0.68	0.33	0.34
Sr	ppm	ICP-OES	74	45	83	112	54	65	74	64	78
Ta	ppm	ICP-MS	0.32	0.24	0.16	0.37	0.1	0.34	0.55	0.29	0.18
Tb	ppm	ICP-MS	0.15	0.12	0.09	0.12	0.06	0.11	0.09	0.09	0.14
Th	ppm	ICP-MS	6.98	9.24	5.44	10.5	3.28	9.55	24.2	6.51	5.27
U	ppm	ICP-MS	1.36	2.94	1.26	1.03	0.76	1.44	1.01	1.2	2.58
V	ppm	ICP-MS	3.9	3.4	1.9	3	2.2	3.9	4.9	3.3	3.3
W	ppm	ICP-MS	<0.1	<0.1	<0.1	<0.1	<0.1	<0.1	<0.1	<0.1	<0.1
Y	ppm	ICP-MS	3.9	4.2	2.3	2.7	1.3	2.6	2.1	2.3	3.5
Yb	ppm	ICP-MS	0.46	0.49	0.33	0.38	0.19	0.43	0.29	0.38	0.65
Zn	ppm	ICP-MS	4	5	4	4	4	4	5	4	4
Zr	ppm	ICP-OES	151	201	111	151	41	156	136	164	189

Carbon and Sulfur: a 0.2 g pulp is analyzed in a Leco SC144DR C/S analyzer for Carbon and Sulfur.

SiO_2 Analysis: A 0.1 gram pulp is fused at 1000 C with lithium metaborate then dissolved in dilute HNO_3.

LOI: A 1.00 gram pulp is heated at 1000 C overnight and the weight loss determined.

Boron: A 0.1 gram pulp is fused at 650 C in a mixture of Na_2O_2/Na_2CO_3.

Total Digestion: A 0.250 g pulp is gently heated in a mixture of ultrapure $HF/HNO_3/HClO_4$ until dry and the residue dissolved in dilute ultrapure HNO_3.

Group #			G-2014-2129	G-2014-2129	G-2014-2129	G-2014-2129	G-2014-2129	G-2014-2129	G-2014-2129	G-2014-2129	G-2014-2129
Description			SG45	SG46	SG47	SG48	SG49	SG50	SG51	SG52	SG53
Fence			Southwest	Southwest	Southwest	Southwest	IB1A	Gap	Gap	Gap	Gap
HoleID			MC-344	MC-344	MC-344	MC-344	MAC-208	MAC-208	MAC-208	MAC-208	MAC-208
From			468.80	485.76	488.00	492.93	10.20	27.00	63.50	86.50	88.00
To			468.99	486.03	488.19	493.13	10.61	27.16	63.83	86.76	88.35
Lithofacies			MFa	MFa	MFa	MFa	MFd	MFd	MFd	MFd	MFd
Date			11-27-2014	11-27-2014	11-27-2014	11-27-2014	11-27-2014	11-27-2014	11-27-2014	11-27-2014	11-27-2014
Sample Type			Sandstone	Sandstone	Sandstone	Sandstone	Sandstone	Sandstone	Sandstone	Sandstone	Sandstone
C	%	LECO	0.09	0.08	0.07	0.11	0.09	0.07	0.11	0.08	0.28
S	%	LECO	0.01	0.01	0.01	0.01	0.01	0.01	0.01	0.01	0.01
B	ppm	fusion	<2	5	7	7	75	171	257	677	233
LOI	%	1000°C	0.4	0.4	0.9	0.7	0.4	0.3	0.5	0.7	0.2
Al_2O_3	%	ICP-OES	0.6	0.9	2.55	1.54	0.64	0.57	1.21	1.9	0.52
CaO	%	ICP-OES	0.01	0.01	<0.01	<0.01	<0.01	<0.01	<0.01	0.01	<0.01
Fe_2O_3	%	ICP-OES	0.49	0.08	0.1	0.44	0.02	0.03	0.15	0.07	0.03
K_2O	%	ICP-OES	0.011	0.053	0.116	0.046	0.011	0.023	0.04	0.032	0.01
MgO	%	ICP-OES	0.008	0.012	0.011	0.02	0.024	0.062	0.131	0.352	0.123
MnO	%	ICP-OES	<0.001	<0.001	<0.001	0.001	<0.001	<0.001	<0.001	<0.001	<0.001
Na_2O	%	ICP-OES	<0.01	<0.01	<0.01	<0.01	<0.01	<0.01	0.01	0.02	<0.01
P_2O_5	%	ICP-OES	0.012	0.01	0.013	0.023	0.011	0.01	0.015	0.021	0.013
SiO_2	%	ICP-OES	98.1	98.2	96.1	96.9	98.6	98.8	97.6	96.2	98
TiO_2	%	ICP-OES	0.073	0.032	0.026	0.09	0.037	0.026	0.04	0.107	0.031
Ag	ppm	ICP-MS	<0.02	0.03	0.03	0.03	0.03	0.02	0.02	0.05	0.02
Ba	ppm	ICP-OES	11	26	39	33	14	13	10	19	12
Be	ppm	ICP-MS	0.1	0.4	0.4	0.4	0.1	0.1	0.2	0.4	0.2
Bi	ppm	ICP-MS	<0.1	<0.1	<0.1	<0.1	<0.1	<0.1	<0.1	<0.1	<0.1
Cd	ppm	ICP-MS	0.2	<0.1	<0.1	0.2	<0.1	<0.1	<0.1	0.1	<0.1
Ce	ppm	ICP-OES	15	14	16	33	21	20	20	30	27
Co	ppm	ICP-MS	0.06	0.16	0.12	0.22	0.06	0.08	0.13	0.19	0.07
Cr	ppm	ICP-OES	12	13	14	11	2	4	8	13	9
Cs	ppm	ICP-MS	<0.1	<0.1	<0.1	<0.1	<0.1	<0.1	<0.1	<0.1	<0.1
Cu	ppm	ICP-MS	0.5	0.7	0.6	0.9	1.6	1.5	2.6	3	1.4
Dy	ppm	ICP-MS	0.33	0.27	0.3	1.15	0.64	0.58	0.69	1.22	0.6
Er	ppm	ICP-MS	0.27	0.16	0.18	0.79	0.37	0.32	0.4	0.66	0.31
Eu	ppm	ICP-MS	0.12	0.12	0.15	0.31	0.16	0.15	0.18	0.3	0.22
Ga	ppm	ICP-MS	0.6	1.5	3.8	2.3	1.1	1.2	2.6	3.6	1.1
Gd	ppm	ICP-MS	0.9	0.7	0.8	2.2	1.1	1.1	1.2	1.9	1.4
Hf	ppm	ICP-MS	8.8	2.2	1.3	7.7	2	1.5	2.6	5.6	1.3
Ho	ppm	ICP-MS	0.09	0.06	0.06	0.28	0.13	0.12	0.16	0.26	0.12
La	ppm	ICP-OES	7	6	8	16	10	9	9	13	11
Li	ppm	ICP-OES	3	10	19	12	3	2	4	5	2
Mo	ppm	ICP-MS	0.23	0.14	0.12	0.22	0.04	0.04	0.21	0.1	0.08
Nb	ppm	ICP-MS	1.4	0.8	0.8	1.8	0.9	0.7	0.9	2.4	0.7
Nd	ppm	ICP-MS	6.5	5.2	6	13.8	7.6	7.2	7.5	11.2	9.3
Ni	ppm	ICP-MS	0.4	0.6	1.9	1.4	0.5	0.7	1.5	3.4	1.2
^{204}Pb	ppm	ICP-MS	0.023	0.032	0.059	0.044	0.028	0.03	0.024	0.059	0.038
^{206}Pb	ppm	ICP-MS	0.655	0.621	0.912	1.09	0.61	0.652	0.576	1.21	0.651
^{207}Pb	ppm	ICP-MS	0.369	0.488	0.85	0.704	0.432	0.494	0.39	0.91	0.588
^{208}Pb	ppm	ICP-MS	1.08	1.23	2.07	1.97	1.1	1.26	1.06	2.49	1.45
Pb	ppm	ICP-MS	2.13	2.38	3.89	3.8	2.17	2.44	2.05	4.67	2.72
$^{206}Pb/^{204}Pb$	--	ICP-MS	28.48	19.41	15.46	24.77	21.79	21.73	24.00	20.51	17.13
$^{207}Pb/^{206}Pb$	--	ICP-MS	0.56	0.79	0.93	0.65	0.71	0.76	0.68	0.75	0.90
$^{207}Pb/^{204}Pb$	--	ICP-MS	16.04	15.25	14.41	16.00	15.43	16.47	16.25	15.42	15.47
$^{208}Pb/^{206}Pb$	--	ICP-MS	1.65	1.98	2.27	1.81	1.80	1.93	1.84	2.06	2.23
$^{208}Pb/^{204}Pb$	--	ICP-MS	46.96	38.44	35.08	44.77	39.29	42.00	44.17	42.20	38.16
Pr	ppm	ICP-MS	1.9	1.6	1.9	4	2.5	2.4	2.3	3.3	2.9
Rb	ppm	ICP-MS	0.2	1.1	2	1.2	0.4	0.6	0.8	0.7	0.2
Sc	ppm	ICP-MS	0.4	0.2	0.4	0.8	0.7	0.5	0.6	1	0.3
Sm	ppm	ICP-MS	1.1	0.8	0.9	2.5	1.3	1.2	1.3	2.1	1.6
Sn	ppm	ICP-MS	0.21	0.15	0.21	0.4	0.32	0.3	0.3	0.63	0.21
Sr	ppm	ICP-OES	42	27	26	51	25	25	26	52	34
Ta	ppm	ICP-MS	0.16	0.07	0.06	0.17	0.08	0.06	0.09	0.2	0.07
Tb	ppm	ICP-MS	0.06	0.05	0.06	0.2	0.11	0.1	0.12	0.21	0.11
Th	ppm	ICP-MS	5.5	2	2.1	10.2	3.18	2.91	3.89	8.45	2.31
U	ppm	ICP-MS	2.28	1.01	0.9	2.73	1.67	1.32	2.65	3.4	1.28
V	ppm	ICP-MS	2.5	1.6	2.2	5.2	1.6	2.4	7.2	6.2	1.8
W	ppm	ICP-MS	<0.1	<0.1	<0.1	<0.1	<0.1	<0.1	<0.1	<0.1	<0.1
Y	ppm	ICP-MS	2.2	1.5	1.6	6.8	3.4	3	4.1	7	3
Yb	ppm	ICP-MS	0.42	0.21	0.18	0.91	0.35	0.29	0.4	0.67	0.27
Zn	ppm	ICP-MS	4	3	3	8	4	4	4	4	3
Zr	ppm	ICP-OES	319	71	43	269	63	47	83	191	40

Carbon and Sulfur: a 0.2 g pulp is analyzed in a Leco SC144DR C/S analyzer for Carbon and Sulfur.

SiO_2 Analysis: A 0.1 gram pulp is fused at 1000 C with lithium metaborate then dissolved in dilute HNO_3.

LOI: A 1.00 gram pulp is heated at 1000 C overnight and the weight loss determined.

Boron: A 0.1 gram pulp is fused at 650 C in a mixture of Na_2O_2/Na_2CO_3.

Total Digestion: A 0.250 g pulp is gently heated in a mixture of ultrapure $HF/HNO_3/HClO_4$ until dry and the residue dissolved in dilute ultrapure HNO_3.

Group #			G-2014-2129	G-2014-2129	G-2014-2129	G-2014-2129	G-2014-2129	G-2014-2129	G-2014-2129	G-2014-2129	G-2014-2129
Description			SG54	SG55	SG56	SG57	SG58	SG59	SG60	SG61	SG62
Fence			Gap	Gap	Gap	Gap	Gap	Gap	Gap	Gap	Gap
HoleID			MAC-208	MAC-208	MAC-208	MAC-208	MAC-208	MAC-208	MAC-208	MAC-208	MAC-208
From			128.40	149.00	203.00	217.70	237.00	289.20	290.50	350.50	395.00
To			128.60	149.24	203.33	217.92	237.32	289.38	290.69	350.80	395.22
Lithofacies			MFd	MFd	MFc	MFc	MFb	MFb	MFb	MFb	MFb
Date			11-27-2014	11-27-2014	11-27-2014	11-27-2014	11-27-2014	11-27-2014	11-27-2014	11-27-2014	11-27-2014
Sample Type			Sandstone	Sandstone	Sandstone	Sandstone	Sandstone	Sandstone	Sandstone	Sandstone	Sandstone
C	%	LECO	0.16	0.01	0.09	0.08	0.07	0.08	0.09	0.16	0.38
S	%	LECO	0.01	0.01	0.01	0.01	0.01	0.01	0.04	0.01	0.01
B	ppm	fusion	636	493	143	584	27	22	46	180	9
LOI	%	1000°C	0.4	0.3	0.5	0.6	0.6	0.4	0.6	1.1	0.7
Al_2O_3	%	ICP-OES	1.31	0.89	1.25	2	1.64	1.46	2.7	2.81	1.36
CaO	%	ICP-OES	<0.01	<0.01	0.01	0.02	0.02	0.02	0.02	<0.01	0.01
Fe_2O_3	%	ICP-OES	0.04	0.05	0.06	0.15	0.11	0.11	0.28	0.21	0.08
K_2O	%	ICP-OES	0.029	0.016	0.057	0.138	0.18	0.331	0.747	0.159	0.021
MgO	%	ICP-OES	0.307	0.19	0.322	0.424	0.368	0.063	0.061	0.066	0.012
MnO	%	ICP-OES	<0.001	<0.001	<0.001	<0.001	<0.001	<0.001	<0.001	<0.001	<0.001
Na_2O	%	ICP-OES	0.02	0.02	<0.01	0.02	<0.01	<0.01	<0.01	0.01	<0.01
P_2O_5	%	ICP-OES	0.017	0.021	0.028	0.039	0.073	0.231	0.079	0.032	0.017
SiO_2	%	ICP-OES	97.4	98.3	98.2	95.8	97.1	96.8	95.5	96	97.5
TiO_2	%	ICP-OES	0.086	0.075	0.104	0.3	0.265	0.074	0.177	0.168	0.06
Ag	ppm	ICP-MS	0.04	0.03	0.04	0.11	0.1	0.04	0.07	0.06	0.03
Ba	ppm	ICP-OES	18	21	12	15	94	227	103	11	14
Be	ppm	ICP-MS	0.4	0.3	0.2	0.5	0.4	0.7	0.4	0.2	0.1
Bi	ppm	ICP-MS	<0.1	<0.1	<0.1	<0.1	<0.1	<0.1	<0.1	<0.1	<0.1
Cd	ppm	ICP-MS	<0.1	0.1	0.1	0.3	0.2	<0.1	<0.1	0.2	<0.1
Ce	ppm	ICP-OES	27	29	27	36	30	29	34	51	21
Co	ppm	ICP-MS	0.15	0.14	0.18	0.19	0.26	0.06	0.07	0.46	0.08
Cr	ppm	ICP-OES	7	7	7	8	10	6	10	8	9
Cs	ppm	ICP-MS	<0.1	<0.1	<0.1	<0.1	<0.1	<0.1	<0.1	<0.1	<0.1
Cu	ppm	ICP-MS	2.5	2	3	4.2	2.4	1.3	1.2	1.3	0.9
Dy	ppm	ICP-MS	0.93	0.97	0.77	1.26	1.17	1.3	1.05	0.58	0.34
Er	ppm	ICP-MS	0.57	0.54	0.47	0.84	0.64	0.71	0.59	0.36	0.2
Eu	ppm	ICP-MS	0.27	0.27	0.25	0.34	0.33	0.3	0.31	0.3	0.19
Ga	ppm	ICP-MS	2.5	2	3	3.5	3	1.8	3.1	2.5	1.3
Gd	ppm	ICP-MS	1.7	1.7	1.7	2.4	2.4	2.2	2.1	2.2	1.1
Hf	ppm	ICP-MS	3.9	5.4	5.3	12.4	7.2	2.5	5.3	8.3	2.9
Ho	ppm	ICP-MS	0.21	0.21	0.17	0.31	0.26	0.32	0.23	0.12	0.07
La	ppm	ICP-OES	11	13	12	16	14	12	15	27	9
Li	ppm	ICP-OES	3	2	5	5	7	3	3	5	5
Mo	ppm	ICP-MS	0.08	0.07	0.09	0.25	0.14	0.08	0.09	0.12	0.13
Nb	ppm	ICP-MS	2.2	1.9	2.4	7.1	6.7	2	4.3	3.9	1.5
Nd	ppm	ICP-MS	10.5	11.1	10	12.9	11.8	10.2	12.1	17.8	8.3
Ni	ppm	ICP-MS	2.6	1.8	5	4.7	5.9	1	0.7	1.4	0.5
^{204}Pb	ppm	ICP-MS	0.047	0.033	0.027	0.436	0.05	0.035	0.028	0.032	0.027
^{206}Pb	ppm	ICP-MS	0.814	0.648	0.622	11.4	1.78	1.21	0.954	0.702	0.612
^{207}Pb	ppm	ICP-MS	0.707	0.495	0.428	7.08	0.827	0.594	0.468	0.49	0.432
^{208}Pb	ppm	ICP-MS	1.84	1.62	1.25	25.7	2.33	1.64	1.43	2.05	1.23
Pb	ppm	ICP-MS	3.41	2.8	2.32	44.6	4.98	3.48	2.88	3.27	2.3
$^{206}Pb/^{204}Pb$	--	ICP-MS	17.32	19.64	23.04	26.15	35.60	34.57	34.07	21.94	22.67
$^{207}Pb/^{206}Pb$	--	ICP-MS	0.87	0.76	0.69	0.62	0.46	0.49	0.49	0.70	0.71
$^{207}Pb/^{204}Pb$	--	ICP-MS	15.04	15.00	15.85	16.24	16.54	16.97	16.71	15.31	16.00
$^{208}Pb/^{206}Pb$	--	ICP-MS	2.26	2.50	2.01	2.25	1.31	1.36	1.50	2.92	2.01
$^{208}Pb/^{204}Pb$	--	ICP-MS	39.15	49.09	46.30	58.94	46.60	46.86	51.07	64.06	45.56
Pr	ppm	ICP-MS	3.1	3.3	3	3.9	3.5	3.1	3.7	5.9	2.5
Rb	ppm	ICP-MS	0.6	0.5	1	1.7	2.2	3.5	7.4	1.8	0.4
Sc	ppm	ICP-MS	1	0.9	0.5	0.9	0.7	0.4	0.7	1	0.3
Sm	ppm	ICP-MS	2	2.1	1.8	2.5	2.4	1.9	2.2	2.6	1.4
Sn	ppm	ICP-MS	0.36	0.43	0.54	0.85	0.75	0.3	0.5	0.42	0.24
Sr	ppm	ICP-OES	43	61	72	102	187	370	204	113	70
Ta	ppm	ICP-MS	0.16	0.19	0.21	0.64	0.76	0.19	0.38	0.41	0.16
Tb	ppm	ICP-MS	0.16	0.17	0.15	0.22	0.23	0.24	0.19	0.13	0.08
Th	ppm	ICP-MS	5.68	17.4	7.58	23	15	5.38	10.6	20.3	5.09
U	ppm	ICP-MS	2.99	3.61	2.74	6.64	9.36	10.3	5.64	1.4	2.35
V	ppm	ICP-MS	3.1	3	2.3	5.6	4.1	2.8	4.7	2	2.4
W	ppm	ICP-MS	<0.1	<0.1	<0.1	<0.1	<0.1	<0.1	<0.1	<0.1	<0.1
Y	ppm	ICP-MS	5.1	5	4.6	8.5	6.6	7.8	5.6	3	1.8
Yb	ppm	ICP-MS	0.64	0.6	0.49	0.97	0.71	0.57	0.58	0.42	0.24
Zn	ppm	ICP-MS	3	32	5	5	6	4	4	4	4
Zr	ppm	ICP-OES	133	186	179	429	240	77	169	285	91

Carbon and Sulfur: a 0.2 g pulp is analyzed in a Leco SC144DR C/S analyzer for Carbon and Sulfur.

SiO_2 Analysis: A 0.1 gram pulp is fused at 1000 C with lithium metaborate then dissolved in dilute HNO_3.

LOI: A 1.00 gram pulp is heated at 1000 C overnight and the weight loss determined.

Boron: A 0.1 gram pulp is fused at 650 C in a mixture of Na_2O_2/Na_2CO_3.

Total Digestion: A 0.250 g pulp is gently heated in a mixture of ultrapure $HF/HNO_3/HClO_4$ until dry and the residue dissolved in dilute ultrapure HNO_3.

Group #			G-2014-2129	G-2014-2129	G-2014-2129	G-2014-2129	G-2014-2129	G-2014-2129	G-2014-2129	G-2014-2129	G-2014-2129
Description			SG63	SG64	SG65	SG66	SG67	SG71	SG72	SG73	SG74
Fence			Gap	Gap	Gap	Gap	Gap	Gap	Gap	Gap	Gap
HoleID			MAC-208	MAC-208	MAC-208	MAC-208	MAC-208	MAC-208	MAC-208	MAC-250	MAC-250
From			425.10	447.30	468.40	486.60	493.00	553.50	572.00	297.80	335.10
To			425.36	447.52	468.64	486.78	493.24	553.50	572.26	298.05	335.32
Lithofacies			MFa	MFa	MFa	MFa	MFa	MFa	MFa	MFa	MFa
Date			11-27-2014	11-27-2014	11-27-2014	11-27-2014	11-27-2014	11-27-2014	11-27-2014	11-27-2014	11-27-2014
Sample Type			Sandstone	Sandstone	Sandstone	Sandstone	Sandstone	Sandstone	Sandstone	Sandstone	Sandstone
C	%	LECO	0.12	0.07	0.08	0.07	0.09	0.08	0.09	0.1	0.13
S	%	LECO	0.01	0.01	0.01	0.01	0.01	0.01	0.01	0.01	0.01
B	ppm	fusion	8	13	25	18	5	866	1240	25	29
LOI	%	1000°C	1.1	0.5	0.4	1	0.9	0.5	0.9	0.4	0.6
Al_2O_3	%	ICP-OES	2.61	1.56	1.18	3.38	1.97	1.8	2.86	1.67	2.49
CaO	%	ICP-OES	<0.01	0.01	0.02	0.02	0.02	0.01	0.22	0.01	0.02
Fe_2O_3	%	ICP-OES	0.16	0.09	0.09	0.32	0.33	0.15	0.22	0.14	0.08
K_2O	%	ICP-OES	0.088	0.23	0.281	0.472	0.024	0.103	0.072	0.468	0.686
MgO	%	ICP-OES	0.01	0.032	0.046	0.396	0.024	0.317	0.776	0.063	0.126
MnO	%	ICP-OES	<0.001	<0.001	<0.001	0.001	<0.001	<0.001	<0.001	<0.001	<0.001
Na_2O	%	ICP-OES	<0.01	<0.01	0.01	0.02	0.01	0.05	0.06	<0.01	<0.01
P_2O_5	%	ICP-OES	0.022	0.021	0.012	0.033	0.017	0.018	0.181	0.047	0.052
SiO_2	%	ICP-OES	95.8	97	97.2	94.4	96.1	96.5	95.2	97.1	95.8
TiO_2	%	ICP-OES	0.117	0.072	0.034	0.194	0.064	0.054	0.088	0.065	0.065
Ag	ppm	ICP-MS	0.05	0.03	0.02	0.07	0.05	0.05	0.05	0.03	0.04
Ba	ppm	ICP-OES	22	26	22	60	39	64	10	13	10
Be	ppm	ICP-MS	0.1	0.2	0.1	0.4	0.5	0.8	0.6	0.2	0.1
Bi	ppm	ICP-MS	<0.1	<0.1	<0.1	<0.1	0.1	0.4	<0.1	<0.1	<0.1
Cd	ppm	ICP-MS	0.1	0.1	<0.1	0.1	<0.1	<0.1	<0.1	<0.1	<0.1
Ce	ppm	ICP-OES	31	27	15	52	24	38	41	34	46
Co	ppm	ICP-MS	0.09	0.16	0.14	0.7	1.53	1.21	1.34	0.1	0.17
Cr	ppm	ICP-OES	8	7	11	26	16	15	12	10	8
Cs	ppm	ICP-MS	<0.1	<0.1	<0.1	0.1	<0.1	0.3	<0.1	<0.1	<0.1
Cu	ppm	ICP-MS	1.1	1.7	4	4	11.1	38.1	29.8	2.6	1.6
Dy	ppm	ICP-MS	0.73	0.82	0.56	1.53	0.86	0.5	0.66	0.53	1.06
Er	ppm	ICP-MS	0.48	0.54	0.33	0.87	0.51	0.31	0.42	0.28	0.51
Eu	ppm	ICP-MS	0.28	0.27	0.19	0.5	0.17	0.29	0.32	0.2	0.38
Ga	ppm	ICP-MS	2.5	2.2	1.4	4.6	4.6	2.8	4.3	1.8	2.8
Gd	ppm	ICP-MS	1.6	1.6	1.1	3.5	1.4	1.7	1.8	1.9	3.2
Hf	ppm	ICP-MS	6	6.4	2.8	4.5	1.7	1.9	1.6	2.5	3.1
Ho	ppm	ICP-MS	0.16	0.19	0.12	0.33	0.2	0.11	0.15	0.1	0.2
La	ppm	ICP-OES	16	13	7	27	12	20	22	15	21
Li	ppm	ICP-OES	10	12	11	24	16	18	36	2	6
Mo	ppm	ICP-MS	0.22	0.14	0.28	0.61	1.03	0.22	0.21	0.08	0.12
Nb	ppm	ICP-MS	3.4	1.6	0.9	2.5	1.1	0.9	2.2	1.6	1.6
Nd	ppm	ICP-MS	11.2	11.1	6.6	21	9.2	14.4	14.5	13.2	19.8
Ni	ppm	ICP-MS	0.5	0.7	0.6	5.8	7.4	3.1	6.7	0.6	1.8
^{204}Pb	ppm	ICP-MS	0.057	0.122	0.036	0.028	0.017	0.014	0.016	0.017	0.035
^{206}Pb	ppm	ICP-MS	1.09	2.78	1.07	1.4	2.55	1.24	1.11	0.585	0.852
^{207}Pb	ppm	ICP-MS	0.859	1.9	0.601	0.52	0.422	0.24	0.299	0.289	0.557
^{208}Pb	ppm	ICP-MS	2.48	6.79	1.68	1.7	1.01	0.854	0.9	0.964	1.73
Pb	ppm	ICP-MS	4.49	11.6	3.39	3.65	3.99	2.35	2.33	1.86	3.18
$^{206}Pb/^{204}Pb$	--	ICP-MS	19.12	22.79	29.72	50.00	150.00	88.57	69.38	34.41	24.34
$^{207}Pb/^{206}Pb$	--	ICP-MS	0.79	0.68	0.56	0.37	0.17	0.19	0.27	0.49	0.65
$^{207}Pb/^{204}Pb$	--	ICP-MS	15.07	15.57	16.69	18.57	24.82	17.14	18.69	17.00	15.91
$^{208}Pb/^{206}Pb$	--	ICP-MS	2.28	2.44	1.57	1.21	0.40	0.69	0.81	1.65	2.03
$^{208}Pb/^{204}Pb$	--	ICP-MS	43.51	55.66	46.67	60.71	59.41	61.00	56.25	56.71	49.43
Pr	ppm	ICP-MS	3.6	3.3	1.9	6.3	2.9	4.5	4.7	3.9	5.8
Rb	ppm	ICP-MS	1	2	2.8	6.7	0.5	4.1	1.5	4.7	7.4
Sc	ppm	ICP-MS	0.8	0.7	0.5	1.9	1.1	1.1	1.4	0.4	0.7
Sm	ppm	ICP-MS	1.8	1.9	1.4	4.1	1.5	2.3	2.2	2.4	3.7
Sn	ppm	ICP-MS	0.33	0.23	0.16	0.88	0.45	0.74	0.82	0.35	0.36
Sr	ppm	ICP-OES	52	52	29	90	24	48	58	197	257
Ta	ppm	ICP-MS	0.37	0.18	0.13	0.28	0.12	0.1	0.3	0.16	0.17
Tb	ppm	ICP-MS	0.13	0.15	0.1	0.29	0.15	0.1	0.13	0.14	0.24
Th	ppm	ICP-MS	11.2	4.78	2.94	13.4	6.78	5.54	8.07	6.17	5.09
U	ppm	ICP-MS	4.79	5.74	3.63	8.43	23.2	5.18	3.12	1.8	3.42
V	ppm	ICP-MS	3.6	2.7	2.4	18.7	31.2	7.4	12.4	4.1	3.5
W	ppm	ICP-MS	<0.1	<0.1	<0.1	0.2	0.1	<0.1	0.7	<0.1	<0.1
Y	ppm	ICP-MS	4.2	5	3.4	8.9	5.4	3.4	4.2	2.5	5.2
Yb	ppm	ICP-MS	0.55	0.73	0.36	0.92	0.54	0.3	0.4	0.26	0.44
Zn	ppm	ICP-MS	3	4	4	5	5	4	4	4	4
Zr	ppm	ICP-OES	196	222	93	151	58	66	52	77	112

Carbon and Sulfur: a 0.2 g pulp is analyzed in a Leco SC144DR C/S analyzer for Carbon and Sulfur.

SiO_2 Analysis: A 0.1 gram pulp is fused at 1000 C with lithium metaborate then dissolved in dilute HNO_3.

LOI: A 1.00 gram pulp is heated at 1000 C overnight and the weight loss determined.

Boron: A 0.1 gram pulp is fused at 650 C in a mixture of Na_2O_2/Na_2CO_3.

Total Digestion: A 0.250 g pulp is gently heated in a mixture of ultrapure $HF/HNO_3/HClO_4$ until dry and the residue dissolved in dilute ultrapure HNO_3.

Group #			G-2014-2129	G-2014-2129	G-2014-2129	G-2014-2129	G-2014-2129	G-2014-2129	G-2014-2129	G-2014-2129	G-2014-2129
Description			SG75	SG76	SG77	SG74 R	SG78	SG79	SG80	SG81	SG82
Fence			Gap	Gap	Gap	Gap	Gap	Gap	Gap	Gap	Gap
HoleID			MAC-250	MAC-250	MAC-250	MAC-250	MAC-250	MC-253	MC-253	MC-253	MC-253
From			370.80	401.43	431.78	335.10	481.75	26.00	76.00	113.50	136.00
To			371.00	401.56	432.13	335.32	481.95	26.14	76.13	113.63	136.15
Lithofacies			MFa	MFa	MFa	MFa	MFa	MFd	MFd	MFd	MFd
Date			11-27-2014	11-27-2014	11-27-2014	11-27-2014	11-27-2014	11-27-2014	11-27-2014	11-27-2014	11-27-2014
Sample Type			Sandstone	Sandstone	Sandstone	Repeat	Sandstone	Sandstone	Sandstone	Sandstone	Sandstone
C	%	LECO	0.08	0.06	0.07	0.1	0.07	0.08	0.11	0.01	0.14
S	%	LECO	0.01	0.01	0.01	0.01	0.01	0.01	0.01	0.01	0.01
B	ppm	fusion	27	28	469	32	11	149	161	173	377
LOI	%	1000°C	0.9	0.6	1.1	0.6	0.4	0.4	0.5	0.4	0.3
Al_2O_3	%	ICP-OES	2.76	2.23	4.03	2.5	0.91	0.73	0.83	0.98	0.81
CaO	%	ICP-OES	0.01	0.02	0.02	0.02	<0.01	<0.01	0.01	<0.01	<0.01
Fe_2O_3	%	ICP-OES	0.56	0.15	0.23	0.08	0.18	0.03	0.04	0.05	0.03
K_2O	%	ICP-OES	0.459	0.612	0.799	0.695	0.104	0.019	0.043	0.136	0.06
MgO	%	ICP-OES	0.069	0.076	0.194	0.125	0.013	0.049	0.1	0.1	0.12
MnO	%	ICP-OES	<0.001	<0.001	<0.001	<0.001	<0.001	<0.001	<0.001	<0.001	<0.001
Na_2O	%	ICP-OES	<0.01	<0.01	0.02	<0.01	<0.01	<0.01	<0.01	0.01	0.01
P_2O_5	%	ICP-OES	0.042	0.034	0.062	0.051	0.018	0.01	0.013	0.014	0.012
SiO_2	%	ICP-OES	94.9	96.3	93.4	96.2	97.7	98.4	98.2	98	98.3
TiO_2	%	ICP-OES	0.288	0.052	0.226	0.064	0.068	0.033	0.066	0.05	0.056
Ag	ppm	ICP-MS	0.07	0.04	0.06	0.03	0.03	0.03	0.04	0.03	0.03
Ba	ppm	ICP-OES	15	20	41	10	25	15	12	12	13
Be	ppm	ICP-MS	0.3	0.2	0.5	0.2	0.2	0.1	0.2	0.1	0.2
Bi	ppm	ICP-MS	<0.1	<0.1	<0.1	<0.1	<0.1	<0.1	<0.1	<0.1	<0.1
Cd	ppm	ICP-MS	0.3	<0.1	0.4	<0.1	0.2	<0.1	<0.1	<0.1	<0.1
Ce	ppm	ICP-OES	73	30	67	46	26	19	22	22	19
Co	ppm	ICP-MS	1.08	0.22	0.76	0.18	0.22	0.11	0.14	0.1	0.1
Cr	ppm	ICP-OES	15	14	19	8	15	6	4	5	7
Cs	ppm	ICP-MS	<0.1	<0.1	<0.1	<0.1	<0.1	<0.1	<0.1	<0.1	<0.1
Cu	ppm	ICP-MS	1.8	2.1	3.3	1.5	1.3	1.6	2	1.6	1
Dy	ppm	ICP-MS	0.79	0.86	2.03	1.08	0.95	0.64	0.96	0.61	0.56
Er	ppm	ICP-MS	0.6	0.41	1.38	0.52	0.61	0.34	0.53	0.35	0.33
Eu	ppm	ICP-MS	0.34	0.27	0.72	0.37	0.24	0.16	0.21	0.21	0.18
Ga	ppm	ICP-MS	2.6	2.7	3.8	2.7	1.4	1.5	2.1	1.4	1.2
Gd	ppm	ICP-MS	3.6	2.1	4.8	3.1	1.7	1.1	1.4	1.3	1.1
Hf	ppm	ICP-MS	15.2	2.4	17.4	3.6	7.2	1.8	3.4	3.3	2.9
Ho	ppm	ICP-MS	0.19	0.16	0.48	0.21	0.22	0.14	0.22	0.14	0.13
La	ppm	ICP-OES	36	14	35	22	12	9	10	9	8
Li	ppm	ICP-OES	6	6	10	6	8	3	2	4	2
Mo	ppm	ICP-MS	0.14	0.26	0.24	0.09	0.27	0.09	0.1	0.13	0.11
Nb	ppm	ICP-MS	6.7	1.4	4.7	1.6	1.6	0.8	1.7	1.1	1.3
Nd	ppm	ICP-MS	27.9	12.3	27.3	19.3	10.3	6.7	7.6	8.3	7
Ni	ppm	ICP-MS	1.4	0.7	1.7	1.7	0.9	0.9	1.3	1.2	1
^{204}Pb	ppm	ICP-MS	0.036	0.042	0.065	0.033	0.034	0.028	0.032	0.048	0.034
^{206}Pb	ppm	ICP-MS	0.892	1.16	1.92	0.844	0.875	0.549	0.626	0.844	0.632
^{207}Pb	ppm	ICP-MS	0.565	0.678	1.05	0.547	0.529	0.414	0.458	0.735	0.528
^{208}Pb	ppm	ICP-MS	2.85	2.19	3.52	1.7	1.46	1.08	1.22	1.82	1.39
Pb	ppm	ICP-MS	4.34	4.07	6.55	3.13	2.9	2.08	2.34	3.44	2.58
$^{206}Pb/^{204}Pb$	--	ICP-MS	24.78	27.62	29.54	25.58	25.74	19.61	19.56	17.58	18.59
$^{207}Pb/^{206}Pb$	--	ICP-MS	0.63	0.58	0.55	0.65	0.60	0.75	0.73	0.87	0.84
$^{207}Pb/^{204}Pb$	--	ICP-MS	15.69	16.14	16.15	16.58	15.56	14.79	14.31	15.31	15.53
$^{208}Pb/^{206}Pb$	--	ICP-MS	3.20	1.89	1.83	2.01	1.67	1.97	1.95	2.16	2.20
$^{208}Pb/^{204}Pb$	--	ICP-MS	79.17	52.14	54.15	51.52	42.94	38.57	38.13	37.92	40.88
Pr	ppm	ICP-MS	8.6	3.7	8.2	5.6	3	2.2	2.4	2.5	2.1
Rb	ppm	ICP-MS	5.5	6.7	8.7	7.1	2.3	0.6	1.1	1.6	0.9
Sc	ppm	ICP-MS	1.2	0.6	2.2	0.7	1	0.6	0.8	0.4	0.5
Sm	ppm	ICP-MS	4.6	2.3	5.3	3.7	1.9	1.1	1.4	1.4	1.3
Sn	ppm	ICP-MS	0.71	0.41	0.54	0.33	0.33	0.26	0.4	0.22	0.22
Sr	ppm	ICP-OES	127	126	187	251	45	26	28	28	32
Ta	ppm	ICP-MS	0.66	0.13	0.5	0.17	0.17	0.08	0.16	0.1	0.11
Tb	ppm	ICP-MS	0.18	0.19	0.41	0.25	0.17	0.11	0.17	0.12	0.11
Th	ppm	ICP-MS	36.8	4.71	24	5.23	7.12	3.32	3.89	3.04	4.82
U	ppm	ICP-MS	2.3	3.1	26.1	3.47	6.75	1.51	2.03	2.06	1.93
V	ppm	ICP-MS	4.5	4	6.3	3.4	3.4	1.2	3	2.2	1.4
W	ppm	ICP-MS	0.1	<0.1	<0.1	<0.1	0.5	0.2	0.3	0.2	0.3
Y	ppm	ICP-MS	4.9	4.2	12.7	5.4	5.9	3.5	6.1	3.5	3.2
Yb	ppm	ICP-MS	0.82	0.36	1.78	0.47	0.71	0.34	0.52	0.34	0.35
Zn	ppm	ICP-MS	4	4	6	4	3	4	3	4	4
Zr	ppm	ICP-OES	532	70	629	115	237	57	111	107	94

Carbon and Sulfur: a 0.2 g pulp is analyzed in a Leco SC144DR C/S analyzer for Carbon and Sulfur.

SiO_2 Analysis: A 0.1 gram pulp is fused at 1000 C with lithium metaborate then dissolved in dilute HNO_3.

LOI: A 1.00 gram pulp is heated at 1000 C overnight and the weight loss determined.

Boron: A 0.1 gram pulp is fused at 650 C in a mixture of Na_2O_2/Na_2CO_3.

Total Digestion: A 0.250 g pulp is gently heated in a mixture of ultrapure $HF/HNO_3/HClO_4$ until dry and the residue dissolved in dilute ultrapure HNO_3.

Group #			G-2014-2129	G-2014-2129	G-2014-2129	G-2014-2129	G-2014-2129	G-2014-2129	G-2014-2129	G-2014-2129	G-2014-2129
Description			SG83	SG84	SG85	SG86	SG87	SG88	SG89	SG90	SG91
Fence			Gap	Gap	Gap	Gap	Gap	Gap	Gap	Gap	Gap
HoleID			MC-253	MC-253	MC-253	MC-253	MC-253	MC-253	MC-253	MC-253	MC-253
From			182.80	205.00	265.30	287.50	325.00	336.20	382.00	416.00	430.10
To			182.98	205.20	265.60	287.66	325.30	336.40	382.18	416.18	430.40
Lithofacies			MFd	MFd	MFc	MFc	MFc	MFc	MFb	MFb	MFb
Date			11-27-2014	11-27-2014	11-27-2014	11-27-2014	11-27-2014	11-27-2014	11-27-2014	11-27-2014	11-27-2014
Sample Type			Sandstone	Sandstone	Sandstone	Sandstone	Sandstone	Sandstone	Sandstone	Sandstone	Sandstone
C	%	LECO	0.09	0.09	0.08	0.1	0.09	0.24	0.62	0.08	0.07
S	%	LECO	0.01	0.01	0.01	0.01	0.01	0.03	0.06	0.01	0.01
B	ppm	fusion	326	332	517	222	43	168	25	20	137
LOI	%	1000°C	0.3	0.3	0.8	0.5	0.6	0.9	0.6	0.9	1.6
Al_2O_3	%	ICP-OES	0.66	0.58	2.34	1.11	1.42	3.26	2.03	2.91	6.15
CaO	%	ICP-OES	0.01	<0.01	0.01	0.01	0.02	0.02	0.01	0.01	0.02
Fe_2O_3	%	ICP-OES	0.03	0.03	0.04	0.05	0.21	0.19	0.1	0.14	0.25
K_2O	%	ICP-OES	0.015	0.011	0.101	0.066	0.229	0.61	0.353	0.354	0.874
MgO	%	ICP-OES	0.15	0.126	0.484	0.287	0.248	0.38	0.041	0.03	0.112
MnO	%	ICP-OES	<0.001	<0.001	<0.001	<0.001	<0.001	<0.001	<0.001	<0.001	<0.001
Na_2O	%	ICP-OES	0.01	0.01	0.02	0.01	<0.01	0.01	<0.01	<0.01	0.01
P_2O_5	%	ICP-OES	0.016	0.013	0.029	0.036	0.046	0.042	0.067	0.049	0.059
SiO_2	%	ICP-OES	98.8	98.9	95.8	97.8	96.9	94.5	96.7	95.6	91.1
TiO_2	%	ICP-OES	0.031	0.05	0.096	0.057	0.07	0.118	0.135	0.126	0.411
Ag	ppm	ICP-MS	0.03	0.02	0.05	0.03	0.04	0.06	0.05	0.05	0.12
Ba	ppm	ICP-OES	11	10	12	8	20	12	16	13	25
Be	ppm	ICP-MS	0.2	0.2	0.4	0.2	0.2	0.3	0.2	0.2	0.4
Bi	ppm	ICP-MS	<0.1	<0.1	<0.1	<0.1	<0.1	<0.1	<0.1	<0.1	<0.1
Cd	ppm	ICP-MS	<0.1	<0.1	<0.1	<0.1	<0.1	<0.1	0.1	0.1	0.4
Ce	ppm	ICP-OES	23	23	28	29	28	33	39	46	68
Co	ppm	ICP-MS	0.09	0.09	0.26	0.14	0.31	0.36	0.09	0.08	0.16
Cr	ppm	ICP-OES	7	6	7	4	5	7	5	4	9
Cs	ppm	ICP-MS	<0.1	<0.1	<0.1	<0.1	<0.1	0.1	<0.1	<0.1	<0.1
Cu	ppm	ICP-MS	1.5	1.2	1.7	1.9	2.2	1.6	1	1.6	2.5
Dy	ppm	ICP-MS	0.62	0.84	0.7	0.49	0.49	0.73	0.89	1.03	1.18
Er	ppm	ICP-MS	0.32	0.44	0.4	0.26	0.26	0.42	0.51	0.56	0.86
Eu	ppm	ICP-MS	0.18	0.2	0.23	0.2	0.18	0.29	0.29	0.3	0.56
Ga	ppm	ICP-MS	1.4	1.2	4.1	1.9	2.2	4.5	2.1	2.9	6.9
Gd	ppm	ICP-MS	1.2	1.3	1.6	1.4	1.5	1.9	2.4	2.9	4
Hf	ppm	ICP-MS	1.8	3	4.5	2.4	2.2	4.7	6.4	4.9	18.5
Ho	ppm	ICP-MS	0.13	0.18	0.16	0.1	0.1	0.15	0.18	0.21	0.28
La	ppm	ICP-OES	10	9	12	12	12	14	18	22	35
Li	ppm	ICP-OES	2	1	6	4	6	10	6	7	18
Mo	ppm	ICP-MS	0.09	0.08	0.15	0.08	0.13	0.09	0.08	0.06	0.21
Nb	ppm	ICP-MS	0.8	1.2	2.3	1.5	1.9	2.8	3.4	3.2	9.3
Nd	ppm	ICP-MS	7.8	7.8	9.8	10	9.4	12	14.8	18.9	27.4
Ni	ppm	ICP-MS	1.5	1.5	5.2	3.6	5	6.4	0.7	0.6	1.5
^{204}Pb	ppm	ICP-MS	0.059	0.069	0.221	0.026	0.034	0.032	0.029	0.028	0.052
^{206}Pb	ppm	ICP-MS	1.27	1.57	5.79	0.69	1.21	0.987	0.655	0.589	1.32
^{207}Pb	ppm	ICP-MS	0.871	1.06	3.44	0.431	0.569	0.524	0.444	0.415	0.816
^{208}Pb	ppm	ICP-MS	2.62	3.3	11.8	1.27	1.43	1.59	1.7	1.66	4.17
Pb	ppm	ICP-MS	4.82	6	21.3	2.42	3.24	3.13	2.83	2.69	6.36
$^{206}Pb/^{204}Pb$	--	ICP-MS	21.53	22.75	26.20	26.54	35.59	30.84	22.59	21.04	25.38
$^{207}Pb/^{206}Pb$	--	ICP-MS	0.69	0.68	0.59	0.62	0.47	0.53	0.68	0.70	0.62
$^{207}Pb/^{204}Pb$	--	ICP-MS	14.76	15.36	15.57	16.58	16.74	16.38	15.31	14.82	15.69
$^{208}Pb/^{206}Pb$	--	ICP-MS	2.06	2.10	2.04	1.84	1.18	1.61	2.60	2.82	3.16
$^{208}Pb/^{204}Pb$	--	ICP-MS	44.41	47.83	53.39	48.85	42.06	49.69	58.62	59.29	80.19
Pr	ppm	ICP-MS	2.5	2.4	2.9	3	2.9	3.6	4.4	5.5	8.3
Rb	ppm	ICP-MS	0.4	0.4	1.6	1.1	2.7	6.8	3.7	3.5	8.3
Sc	ppm	ICP-MS	0.4	0.6	0.8	0.3	0.4	0.8	0.7	0.7	2.4
Sm	ppm	ICP-MS	1.3	1.4	1.8	1.8	1.6	2.2	2.8	3.4	4.8
Sn	ppm	ICP-MS	0.18	0.18	0.4	0.42	0.44	0.36	0.33	0.42	0.91
Sr	ppm	ICP-OES	33	33	110	125	83	104	342	219	172
Ta	ppm	ICP-MS	0.07	0.12	0.2	0.16	0.17	0.25	0.33	0.32	0.95
Tb	ppm	ICP-MS	0.12	0.14	0.14	0.1	0.12	0.15	0.2	0.23	0.27
Th	ppm	ICP-MS	2.94	3.72	8.77	6.11	4.66	8.17	13.7	14.7	49.7
U	ppm	ICP-MS	2.12	2.73	3.87	1.7	4.7	4.06	1.64	1.81	7.6
V	ppm	ICP-MS	2.8	3	4.5	1.6	3.3	7	4	3.5	6.7
W	ppm	ICP-MS	<0.1	0.2	0.3	0.3	0.2	0.3	0.3	0.3	0.7
Y	ppm	ICP-MS	3.4	4.7	4.1	2.5	2.5	3.9	4.5	5.4	7.9
Yb	ppm	ICP-MS	0.31	0.44	0.42	0.29	0.28	0.49	0.58	0.58	1.11
Zn	ppm	ICP-MS	4	4	4	4	6	7	4	5	4
Zr	ppm	ICP-OES	55	97	143	72	71	155	207	159	658

Carbon and Sulfur: a 0.2 g pulp is analyzed in a Leco SC144DR C/S analyzer for Carbon and Sulfur.

SiO_2 Analysis: A 0.1 gram pulp is fused at 1000 C with lithium metaborate then dissolved in dilute HNO_3.

LOI: A 1.00 gram pulp is heated at 1000 C overnight and the weight loss determined.

Boron: A 0.1 gram pulp is fused at 650 C in a mixture of Na_2O_2/Na_2CO_3.

Total Digestion: A 0.250 g pulp is gently heated in a mixture of ultrapure $HF/HNO_3/HClO_4$ until dry and the residue dissolved in dilute ultrapure HNO_3.

Group #			G-2014-2129	G-2014-2129	G-2014-2129	G-2014-2129	G-2014-2129	G-2014-2129	G-2014-2129	G-2014-2129	G-2014-2129
Description			SG92	SG93	SG94	SG95	SG96	SG97	SG99	SG100	SG101
Fence			Gap	Gap	Gap	Gap	Gap	Gap	Gap	Gap	Zone 4
HoleID			MC-253	MC-253	MC-253	MC-253	MC-253	MC-253	MC-253	MC-253	MAC-246
From			440.10	472.50	501.00	507.50	528.00	538.00	550.10	552.00	4.33
To			440.28	472.66	501.20	507.80	528.30	538.15	550.25	552.30	4.48
Lithofacies			MFb	MFb	MFb	MFb	MFb	MFb	MFb	MFa	MFd
Date			11-27-2014	11-27-2014	11-27-2014	11-27-2014	11-27-2014	11-27-2014	11-27-2014	11-27-2014	11-27-2014
Sample Type			Sandstone	Sandstone	Sandstone	Sandstone	Sandstone	Sandstone	Sandstone	Sandstone	Sandstone
C	%	LECO	0.01	0.07	0.09	0.09	0.08	0.06	0.07	0.09	0.14
S	%	LECO	0.01	0.01	0.01	0.01	0.01	0.01	0.01	0.01	0.01
B	ppm	fusion	2000	43	9	160	195	39	746	1540	658
LOI	%	1000°C	0.5	0.5	0.6	0.4	0.6	0.5	0.6	0.5	0.3
Al_2O_3	%	ICP-OES	2.63	1.15	1.08	1	2.52	1.66	2	2.32	0.77
CaO	%	ICP-OES	0.02	0.01	0.01	0.02	0.02	0.01	0.02	0.02	<0.01
Fe_2O_3	%	ICP-OES	0.12	0.08	0.07	0.09	0.19	0.18	0.2	0.08	0.02
K_2O	%	ICP-OES	0.021	0.095	0.048	0.174	0.543	0.366	0.124	0.016	0.008
MgO	%	ICP-OES	0.523	0.026	0.012	0.074	0.103	0.054	0.35	0.457	0.164
MnO	%	ICP-OES	<0.001	<0.001	<0.001	<0.001	<0.001	<0.001	<0.001	<0.001	<0.001
Na_2O	%	ICP-OES	0.06	<0.01	<0.01	0.01	0.02	<0.01	0.03	0.05	0.02
P_2O_5	%	ICP-OES	0.026	0.011	0.011	0.052	0.034	0.013	0.028	0.023	0.012
SiO_2	%	ICP-OES	95.7	97.2	97.8	97.2	95.6	96.8	96.5	96.3	98.7
TiO_2	%	ICP-OES	0.122	0.066	0.045	0.043	0.113	0.048	0.168	0.109	0.035
Ag	ppm	ICP-MS	0.04	0.04	0.03	0.03	0.05	0.03	0.1	0.06	0.03
Ba	ppm	ICP-OES	13	13	20	27	26	18	27	18	12
Be	ppm	ICP-MS	1	0.1	0.1	0.3	0.3	0.2	0.6	0.9	0.4
Bi	ppm	ICP-MS	<0.1	<0.1	<0.1	<0.1	<0.1	<0.1	<0.1	<0.1	<0.1
Cd	ppm	ICP-MS	0.1	<0.1	<0.1	<0.1	0.1	<0.1	0.2	<0.1	<0.1
Ce	ppm	ICP-OES	35	21	17	86	29	19	39	33	21
Co	ppm	ICP-MS	0.21	0.09	0.08	0.14	0.15	0.18	0.53	0.57	0.12
Cr	ppm	ICP-OES	13	11	8	11	8	11	10	9	5
Cs	ppm	ICP-MS	<0.1	<0.1	<0.1	<0.1	<0.1	<0.1	<0.1	<0.1	<0.1
Cu	ppm	ICP-MS	1.5	0.9	0.7	1	1.4	1.3	6.1	2.7	1.9
Dy	ppm	ICP-MS	0.48	0.31	0.28	1.13	1.31	0.38	0.82	0.53	0.67
Er	ppm	ICP-MS	0.33	0.18	0.17	0.45	0.66	0.22	0.54	0.32	0.35
Eu	ppm	ICP-MS	0.26	0.13	0.14	0.46	0.31	0.18	0.3	0.25	0.19
Ga	ppm	ICP-MS	3.2	1.3	1.1	1.6	2.6	1.6	2.6	2.4	1.9
Gd	ppm	ICP-MS	1.6	0.9	0.8	6.3	2.3	1	1.8	1.6	1.2
Hf	ppm	ICP-MS	6.2	2.4	2.1	2.1	5.1	2.6	8.4	5.1	1.3
Ho	ppm	ICP-MS	0.11	0.06	0.06	0.14	0.28	0.08	0.19	0.12	0.14
La	ppm	ICP-OES	17	10	7	28	14	9	21	17	10
Li	ppm	ICP-OES	2	7	10	11	12	9	9	3	1
Mo	ppm	ICP-MS	0.12	0.11	0.1	0.14	0.14	0.21	0.18	0.13	0.09
Nb	ppm	ICP-MS	3.1	1.7	1.2	1.2	2.7	1.4	4.1	2.8	0.8
Nd	ppm	ICP-MS	12.4	7.1	6	72.1	11.9	7.1	12.8	12.1	8
Ni	ppm	ICP-MS	2.9	0.5	0.4	0.8	0.9	1	2.7	2	1.2
^{204}Pb	ppm	ICP-MS	0.029	0.029	0.028	0.021	0.048	0.036	0.044	0.042	0.031
^{206}Pb	ppm	ICP-MS	0.647	0.593	0.56	0.489	0.978	0.725	1.61	0.964	0.712
^{207}Pb	ppm	ICP-MS	0.459	0.448	0.437	0.332	0.694	0.554	0.726	0.624	0.466
^{208}Pb	ppm	ICP-MS	1.74	1.34	1.13	0.966	1.99	1.48	2.45	1.85	1.2
Pb	ppm	ICP-MS	2.88	2.41	2.16	1.81	3.71	2.79	4.83	3.48	2.41
$^{206}Pb/^{204}Pb$	--	ICP-MS	22.31	20.45	20.00	23.29	20.38	20.14	36.59	22.95	22.97
$^{207}Pb/^{206}Pb$	--	ICP-MS	0.71	0.76	0.78	0.68	0.71	0.76	0.45	0.65	0.65
$^{207}Pb/^{204}Pb$	--	ICP-MS	15.83	15.45	15.61	15.81	14.46	15.39	16.50	14.86	15.03
$^{208}Pb/^{206}Pb$	--	ICP-MS	2.69	2.26	2.02	1.98	2.03	2.04	1.52	1.92	1.69
$^{208}Pb/^{204}Pb$	--	ICP-MS	60.00	46.21	40.36	46.00	41.46	41.11	55.68	44.05	38.71
Pr	ppm	ICP-MS	4	2.4	1.8	15.6	3.5	2.2	4.2	3.8	2.4
Rb	ppm	ICP-MS	0.6	1.2	0.6	1.8	5.4	4.4	1.6	0.4	0.3
Sc	ppm	ICP-MS	0.9	0.3	0.2	0.4	0.8	0.4	0.9	0.7	0.7
Sm	ppm	ICP-MS	2	1	1	13.4	2.3	1.2	2	1.9	1.3
Sn	ppm	ICP-MS	0.27	0.21	0.14	0.24	0.33	0.21	0.54	0.47	0.16
Sr	ppm	ICP-OES	60	25	35	136	128	32	66	52	34
Ta	ppm	ICP-MS	0.28	0.15	0.08	0.13	0.26	0.14	0.64	0.27	0.06
Tb	ppm	ICP-MS	0.1	0.06	0.06	0.32	0.25	0.08	0.16	0.11	0.12
Th	ppm	ICP-MS	15.3	6.71	2.87	5.15	8.21	5.3	24.3	9.86	2.92
U	ppm	ICP-MS	2.41	1.58	1.9	1.97	6.46	1.63	6.22	5.97	1.5
V	ppm	ICP-MS	2.7	2.2	1.7	6.5	3.5	2	7.5	7	2.1
W	ppm	ICP-MS	0.4	0.2	0.1	0.2	0.3	0.2	1.3	0.8	0.1
Y	ppm	ICP-MS	2.9	1.6	1.5	2.7	7.3	2.1	5.3	2.9	3.6
Yb	ppm	ICP-MS	0.41	0.2	0.2	0.28	0.69	0.26	0.61	0.37	0.32
Zn	ppm	ICP-MS	4	4	3	3	4	5	4	5	4
Zr	ppm	ICP-OES	193	71	69	67	183	79	286	167	39

Carbon and Sulfur: a 0.2 g pulp is analyzed in a Leco SC144DR C/S analyzer for Carbon and Sulfur.

SiO_2 Analysis: A 0.1 gram pulp is fused at 1000 C with lithium metaborate then dissolved in dilute HNO_3.

LOI: A 1.00 gram pulp is heated at 1000 C overnight and the weight loss determined.

Boron: A 0.1 gram pulp is fused at 650 C in a mixture of Na_2O_2/Na_2CO_3.

Total Digestion: A 0.250 g pulp is gently heated in a mixture of ultrapure $HF/HNO_3/HClO_4$ until dry and the residue dissolved in dilute ultrapure HNO_3.

Group #			G-2014-2129	G-2014-2129	G-2014-2129	G-2014-2129	G-2014-2129	G-2014-2129	G-2014-2129	G-2014-2129	G-2014-2129
Description			SG102	SG103	SG104	SG105	SG106	SG107	SG108	SG109	SG110
Fence			Zone 4	Zone 4	Zone 4	Zone 4	Zone 4	Zone 4	Zone 4	Zone 4	Zone 4
HoleID			MAC-246	MAC-246	MAC-246	MAC-246	MAC-246	MAC-246	MAC-246	MAC-246	MAC-246
From			54.70	60.60	82.75	126.15	142.86	165.40	213.43	267.05	297.33
To			54.90	60.75	82.93	126.32	143.00	165.56	213.58	267.25	297.53
Lithofacies			MFd	MFd	MFd	MFd	MFd	MFd	MFc	MFc	MFc
Date			11-27-2014	11-27-2014	11-27-2014	11-27-2014	11-27-2014	11-27-2014	11-27-2014	11-27-2014	11-27-2014
Sample Type			Sandstone	Sandstone	Sandstone	Sandstone	Sandstone	Sandstone	Sandstone	Sandstone	Sandstone
C	%	LECO	0.07	0.41	0.13	0.13	0.07	0.07	0.07	0.06	0.1
S	%	LECO	0.01	0.01	0.01	0.01	0.01	0.01	0.01	0.01	0.01
B	ppm	fusion	377	307	799	226	1180	485	163	32	25
LOI	%	1000°C	0.3	0.3	0.4	0.3	0.5	0.3	0.3	0.5	0.4
Al_2O_3	%	ICP-OES	0.68	0.65	0.99	0.63	1.92	0.8	0.57	2.1	1.75
CaO	%	ICP-OES	<0.01	<0.01	<0.01	<0.01	0.01	<0.01	<0.01	0.01	0.01
Fe_2O_3	%	ICP-OES	0.03	0.02	0.04	0.04	0.11	0.04	0.04	0.14	0.12
K_2O	%	ICP-OES	0.015	0.016	0.012	0.052	0.044	0.025	0.034	0.532	0.466
MgO	%	ICP-OES	0.12	0.092	0.214	0.094	0.348	0.162	0.119	0.136	0.067
MnO	%	ICP-OES	<0.001	<0.001	<0.001	<0.001	<0.001	<0.001	<0.001	<0.001	<0.001
Na_2O	%	ICP-OES	0.01	0.01	0.03	0.01	0.04	0.02	<0.01	<0.01	<0.01
P_2O_5	%	ICP-OES	0.012	0.012	0.015	0.013	0.026	0.014	0.017	0.029	0.044
SiO_2	%	ICP-OES	98.7	98.7	98.1	98.7	96.8	98	98.8	96.6	96.7
TiO_2	%	ICP-OES	0.044	0.043	0.073	0.03	0.13	0.042	0.05	0.146	0.308
Ag	ppm	ICP-MS	0.03	0.03	0.04	0.03	0.05	0.03	0.03	0.07	0.12
Ba	ppm	ICP-OES	18	14	28	20	36	16	15	13	15
Be	ppm	ICP-MS	0.3	0.2	0.5	0.2	0.6	0.2	0.2	0.2	0.2
Bi	ppm	ICP-MS	<0.1	<0.1	<0.1	<0.1	<0.1	<0.1	<0.1	<0.1	<0.1
Cd	ppm	ICP-MS	<0.1	<0.1	<0.1	<0.1	0.2	<0.1	<0.1	<0.1	0.2
Ce	ppm	ICP-OES	18	21	24	23	30	23	29	33	42
Co	ppm	ICP-MS	0.1	0.08	0.12	0.11	0.21	0.12	0.08	0.11	0.09
Cr	ppm	ICP-OES	4	3	11	8	9	6	5	5	6
Cs	ppm	ICP-MS	<0.1	<0.1	<0.1	<0.1	<0.1	<0.1	<0.1	<0.1	<0.1
Cu	ppm	ICP-MS	2.9	1.7	2	1.5	3.9	1.7	0.9	1.5	3.2
Dy	ppm	ICP-MS	0.85	0.74	0.84	0.51	1.1	0.74	0.51	0.64	1.33
Er	ppm	ICP-MS	0.5	0.4	0.47	0.26	0.66	0.37	0.26	0.36	0.8
Eu	ppm	ICP-MS	0.19	0.18	0.21	0.19	0.31	0.22	0.21	0.22	0.35
Ga	ppm	ICP-MS	1.5	1.4	2.4	0.9	3	1.6	1	3	2.5
Gd	ppm	ICP-MS	1.2	1.2	1.3	1.2	1.9	1.3	1.5	1.6	2.7
Hf	ppm	ICP-MS	3.8	3	3.6	1.8	7.4	2.7	1.9	4.6	10
Ho	ppm	ICP-MS	0.2	0.16	0.18	0.1	0.25	0.15	0.1	0.14	0.3
La	ppm	ICP-OES	9	9	10	9	13	10	11	15	19
Li	ppm	ICP-OES	2	2	1	2	3	2	1	5	4
Mo	ppm	ICP-MS	0.09	0.1	0.1	0.09	0.21	0.08	0.08	0.12	0.16
Nb	ppm	ICP-MS	1.2	1	1.9	0.8	3.2	1.1	1.3	3.5	7.4
Nd	ppm	ICP-MS	6.9	7.2	8.2	8	10.8	8.3	10	11	15.9
Ni	ppm	ICP-MS	1.2	1	1.3	0.9	2.6	1.6	1.3	2.2	1.3
^{204}Pb	ppm	ICP-MS	0.027	0.027	0.037	0.062	0.109	0.048	0.042	0.037	0.039
^{206}Pb	ppm	ICP-MS	0.56	0.533	0.751	1.32	2.45	0.879	0.747	1.3	1.1
^{207}Pb	ppm	ICP-MS	0.412	0.397	0.562	0.961	1.67	0.669	0.627	0.621	0.602
^{208}Pb	ppm	ICP-MS	1.08	1.07	1.47	2.67	5	1.78	1.61	1.71	2.5
Pb	ppm	ICP-MS	2.08	2.03	2.82	5.02	9.23	3.37	3.03	3.68	4.24
$^{206}Pb/^{204}Pb$	--	ICP-MS	20.74	19.74	20.30	21.29	22.48	18.31	17.79	35.14	28.21
$^{207}Pb/^{206}Pb$	--	ICP-MS	0.74	0.74	0.75	0.73	0.68	0.76	0.84	0.48	0.55
$^{207}Pb/^{204}Pb$	--	ICP-MS	15.26	14.70	15.19	15.50	15.32	13.94	14.93	16.78	15.44
$^{208}Pb/^{206}Pb$	--	ICP-MS	1.93	2.01	1.96	2.02	2.04	2.03	2.16	1.32	2.27
$^{208}Pb/^{204}Pb$	--	ICP-MS	40.00	39.63	39.73	43.06	45.87	37.08	38.33	46.22	64.10
Pr	ppm	ICP-MS	2.2	2.2	2.6	2.3	3.2	2.6	3	3.4	4.7
Rb	ppm	ICP-MS	0.7	0.5	0.4	0.8	0.9	0.5	0.7	5.4	5
Sc	ppm	ICP-MS	1.1	0.8	1.1	0.3	1.4	0.6	0.4	0.7	0.9
Sm	ppm	ICP-MS	1.2	1.3	1.4	1.4	2	1.5	1.7	1.9	3
Sn	ppm	ICP-MS	0.45	0.29	0.26	0.15	0.36	0.21	0.17	0.48	1
Sr	ppm	ICP-OES	28	32	37	34	58	37	49	90	174
Ta	ppm	ICP-MS	0.13	0.1	0.17	0.08	0.29	0.09	0.1	0.37	0.67
Tb	ppm	ICP-MS	0.14	0.13	0.14	0.1	0.19	0.14	0.11	0.13	0.26
Th	ppm	ICP-MS	3.6	5.01	4.9	3.04	10.4	4.35	4.17	13.9	33.4
U	ppm	ICP-MS	2.16	1.98	2.41	2.18	6.5	3.18	2.21	3.19	3.51
V	ppm	ICP-MS	2.5	1.6	2.5	1.2	9.4	2	1.7	4.2	6.2
W	ppm	ICP-MS	0.2	0.2	0.3	<0.1	0.3	0.1	<0.1	0.5	0.7
Y	ppm	ICP-MS	4.9	3.9	4.7	2.4	6.6	3.9	2.4	3.6	8
Yb	ppm	ICP-MS	0.52	0.44	0.52	0.24	0.71	0.37	0.26	0.4	0.93
Zn	ppm	ICP-MS	4	4	4	3	6	4	3	5	5
Zr	ppm	ICP-OES	127	101	113	56	255	84	58	150	335

Carbon and Sulfur: a 0.2 g pulp is analyzed in a Leco SC144DR C/S analyzer for Carbon and Sulfur.

SiO_2 Analysis: A 0.1 gram pulp is fused at 1000 C with lithium metaborate then dissolved in dilute HNO_3.

LOI: A 1.00 gram pulp is heated at 1000 C overnight and the weight loss determined.

Boron: A 0.1 gram pulp is fused at 650 C in a mixture of Na_2O_2/Na_2CO_3.

Total Digestion: A 0.250 g pulp is gently heated in a mixture of ultrapure $HF/HNO_3/HClO_4$ until dry and the residue dissolved in dilute ultrapure HNO_3.

Group #			G-2014-2129	G-2014-2129	G-2014-2129	G-2014-2129	G-2014-2129	G-2014-2129	G-2014-2129	G-2014-2129	G-2014-2129
Description			SG111	SG112	SG113	SG114	SG115	SG113 R	SG116	SG117	SG118
Fence			Zone 4	Zone 4	Zone 4	Zone 4	Zone 4	Zone 4	Zone 4	Zone 4	Zone 4
HoleID			MAC-246	MAC-246	MAC-246	MAC-246	MAC-246	MAC-246	MAC-246	MAC-246	MAC-246
From			324.50	333.80	354.17	378.25	418.13	354.17	423.80	454.11	475.33
To			324.72	334.00	354.38	378.44	418.30	354.38	423.91	454.34	475.51
Lithofacies			MFb	MFb	MFb	MFb	MFa	MFb	MFa	MFa	MFa
Date			11-27-2014	11-27-2014	11-27-2014	11-27-2014	11-27-2014	11-27-2014	11-27-2014	11-27-2014	11-27-2014
Sample Type			Sandstone	Sandstone	Sandstone	Sandstone	Sandstone	Repeat	Sandstone	Sandstone	Sandstone
C	%	LECO	0.07	0.07	0.06	0.04	0.05	0.05	0.07	0.08	0.01
S	%	LECO	0.01	0.01	0.01	0.01	0.01	0.01	0.01	0.01	0.01
B	ppm	fusion	45	32	44	11	10	42	24	2340	710
LOI	%	1000°C	0.8	0.6	0.6	0.8	0.8	0.6	0.8	0.5	0.4
Al_2O_3	%	ICP-OES	2.83	1.96	2.29	1.87	1.75	2.33	2.18	3	1.19
CaO	%	ICP-OES	0.02	0.02	0.02	0.01	0.01	0.02	0.01	0.02	0.02
Fe_2O_3	%	ICP-OES	0.17	0.53	0.18	0.1	0.48	0.18	0.08	0.37	0.07
K_2O	%	ICP-OES	0.63	0.437	0.598	0.044	0.077	0.612	0.122	0.011	0.03
MgO	%	ICP-OES	0.076	0.05	0.047	0.012	0.012	0.047	0.018	0.592	0.215
MnO	%	ICP-OES	<0.001	<0.001	<0.001	<0.001	0.002	<0.001	<0.001	<0.001	<0.001
Na_2O	%	ICP-OES	<0.01	<0.01	0.01	<0.01	<0.01	0.01	<0.01	0.06	0.03
P_2O_5	%	ICP-OES	0.098	0.073	0.063	0.046	0.028	0.064	0.026	0.036	0.016
SiO_2	%	ICP-OES	95.2	96	96.2	97	96.1	96.1	96.4	95.3	97.6
TiO_2	%	ICP-OES	0.263	0.298	0.272	0.086	0.102	0.265	0.116	0.163	0.052
Ag	ppm	ICP-MS	0.09	0.12	0.09	0.04	0.04	0.1	0.06	0.06	0.04
Ba	ppm	ICP-OES	38	18	22	17	18	22	38	14	24
Be	ppm	ICP-MS	0.3	0.2	0.3	0.2	0.2	0.3	0.2	1.1	0.5
Bi	ppm	ICP-MS	<0.1	<0.1	<0.1	<0.1	<0.1	<0.1	<0.1	<0.1	<0.1
Cd	ppm	ICP-MS	0.2	0.2	0.3	<0.1	0.1	0.3	0.1	0.2	0.1
Ce	ppm	ICP-OES	52	53	60	40	26	59	29	45	18
Co	ppm	ICP-MS	0.16	0.1	0.12	0.1	0.18	0.12	0.12	0.3	0.33
Cr	ppm	ICP-OES	8	5	17	9	9	14	10	15	10
Cs	ppm	ICP-MS	<0.1	<0.1	<0.1	<0.1	<0.1	<0.1	<0.1	<0.1	<0.1
Cu	ppm	ICP-MS	2.6	1.4	2	0.9	0.8	1.8	1.4	2.8	2.5
Dy	ppm	ICP-MS	1.3	1.24	2	0.72	0.45	1.91	0.63	0.62	0.43
Er	ppm	ICP-MS	0.73	0.72	1.21	0.28	0.22	1.13	0.37	0.38	0.26
Eu	ppm	ICP-MS	0.43	0.31	0.44	0.25	0.2	0.44	0.28	0.39	0.2
Ga	ppm	ICP-MS	3.2	2.1	3.3	2.3	2	3.3	2.2	2.8	1.2
Gd	ppm	ICP-MS	3.2	3.1	4.3	2.3	1.5	4.2	1.7	2.6	1.1
Hf	ppm	ICP-MS	10.3	10.6	11.9	3.8	4.3	12.5	6.3	8	4.6
Ho	ppm	ICP-MS	0.28	0.26	0.45	0.11	0.08	0.41	0.13	0.12	0.09
La	ppm	ICP-OES	24	25	29	19	12	28	14	22	9
Li	ppm	ICP-OES	11	6	8	5	9	8	12	2	7
Mo	ppm	ICP-MS	0.13	0.13	0.45	0.13	0.13	0.17	0.24	0.24	0.25
Nb	ppm	ICP-MS	6.3	7.6	6.4	2.2	2.5	6.2	2.8	3.9	1.3
Nd	ppm	ICP-MS	19.7	20	23.7	15.2	9.7	23.7	11	17.3	7.2
Ni	ppm	ICP-MS	1.1	0.7	0.6	0.4	0.8	0.6	0.8	2.9	1.5
^{204}Pb	ppm	ICP-MS	0.044	0.055	0.033	0.029	0.052	0.032	0.037	0.044	0.027
^{206}Pb	ppm	ICP-MS	1.19	1.15	0.863	0.637	0.994	0.848	0.889	1.14	0.906
^{207}Pb	ppm	ICP-MS	0.691	0.826	0.514	0.441	0.808	0.517	0.579	0.654	0.472
^{208}Pb	ppm	ICP-MS	2.96	3.27	2.77	1.69	2.45	2.74	1.83	2.56	1.35
Pb	ppm	ICP-MS	4.89	5.3	4.18	2.8	4.3	4.13	3.33	4.4	2.75
$^{206}Pb/^{204}Pb$	--	ICP-MS	27.05	20.91	26.15	21.97	19.12	26.50	24.03	25.91	33.56
$^{207}Pb/^{206}Pb$	--	ICP-MS	0.58	0.72	0.60	0.69	0.81	0.61	0.65	0.57	0.52
$^{207}Pb/^{204}Pb$	--	ICP-MS	15.70	15.02	15.58	15.21	15.54	16.16	15.65	14.86	17.48
$^{208}Pb/^{206}Pb$	--	ICP-MS	2.49	2.84	3.21	2.65	2.46	3.23	2.06	2.25	1.49
$^{208}Pb/^{204}Pb$	--	ICP-MS	67.27	59.45	83.94	58.28	47.12	85.63	49.46	58.18	50.00
Pr	ppm	ICP-MS	5.8	6.1	7.1	4.6	2.9	6.8	3.3	5.3	2.1
Rb	ppm	ICP-MS	6.3	4.4	5.2	0.7	0.8	5.2	1.3	0.3	0.4
Sc	ppm	ICP-MS	1.1	1	1.9	0.5	0.6	2	0.8	0.9	0.6
Sm	ppm	ICP-MS	3.5	3.4	4.4	2.5	1.6	4.4	2	3.2	1.3
Sn	ppm	ICP-MS	1.16	0.68	1.12	0.26	0.32	1.09	0.33	0.91	0.21
Sr	ppm	ICP-OES	505	353	261	221	116	256	84	105	41
Ta	ppm	ICP-MS	0.67	0.7	0.73	0.23	0.26	0.72	0.31	0.54	0.14
Tb	ppm	ICP-MS	0.28	0.27	0.41	0.2	0.12	0.39	0.14	0.16	0.09
Th	ppm	ICP-MS	46.6	30.3	49.3	13.6	11.7	48.3	11.7	19.1	5.01
U	ppm	ICP-MS	4.62	3.65	3.42	2.45	1.24	3.39	8.01	8.34	9.23
V	ppm	ICP-MS	8.3	4.6	6.7	2.7	5.2	6.6	3.8	5.2	2.6
W	ppm	ICP-MS	1	0.6	0.8	0.2	0.2	0.7	0.3	1.5	0.4
Y	ppm	ICP-MS	7.1	7	11.9	2.6	1.9	10.6	3.4	3.3	2.6
Yb	ppm	ICP-MS	0.83	0.8	1.37	0.36	0.3	1.34	0.49	0.44	0.33
Zn	ppm	ICP-MS	4	5	4	5	5	4	4	4	3
Zr	ppm	ICP-OES	339	363	432	121	141	435	206	263	149

Carbon and Sulfur: a 0.2 g pulp is analyzed in a Leco SC144DR C/S analyzer for Carbon and Sulfur.

SiO_2 Analysis: A 0.1 gram pulp is fused at 1000 C with lithium metaborate then dissolved in dilute HNO_3.

LOI: A 1.00 gram pulp is heated at 1000 C overnight and the weight loss determined.

Boron: A 0.1 gram pulp is fused at 650 C in a mixture of Na_2O_2/Na_2CO_3.

Total Digestion: A 0.250 g pulp is gently heated in a mixture of ultrapure $HF/HNO_3/HClO_4$ until dry and the residue dissolved in dilute ultrapure HNO_3.

Group #			G-2014-2129	G-2014-2129	G-2014-2129	G-2014-2129	G-2014-2129	G-2014-2129	G-2014-2129	G-2014-2129	G-2014-2129
Description			SG119	SG120	SG121	SG122	SG123	SG124	SG125	SG126	SG127
Fence			Zone 4	Zone 4	Zone 4	Zone 4	Zone 4	Zone 4	Zone 4	Zone 4	Zone 4
HoleID			MAC-246	MAC-246	MAC-246	MAC-246	MAC-246	MAC-252	MAC-252	MAC-252	MAC-252
From			496.42	499.02	508.80	510.20	543.00	10.15	25.70	55.65	102.48
To			496.70	499.24	508.89	510.33	543.26	10.30	25.85	55.80	102.70
Lithofacies			MFa	MFa	MFa	MFa	MFa	MFd	MFd	MFd	MFd
Date			11-27-2014	11-27-2014	11-27-2014	11-27-2014	11-27-2014	11-27-2014	11-27-2014	11-27-2014	11-27-2014
Sample Type			Sandstone	Sandstone	Sandstone	Sandstone	Sandstone	Sandstone	Sandstone	Sandstone	Sandstone
C	%	LECO	0.1	0.06	0.08	0.08	0.06	0.09	0.09	0.07	0.07
S	%	LECO	0.01	0.01	0.01	0.01	0.01	0.01	0.01	0.01	0.01
B	ppm	fusion	1930	1110	1930	2930	153	309	154	2600	567
LOI	%	1000°C	0.8	0.6	0.6	0.7	0.4	0.2	0.3	0.8	0.5
Al_2O_3	%	ICP-OES	3.12	1.78	2.36	3.61	0.9	0.62	0.58	3.76	1.48
CaO	%	ICP-OES	0.02	0.02	0.02	0.03	0.02	<0.01	<0.01	0.02	<0.01
Fe_2O_3	%	ICP-OES	0.17	0.11	0.09	0.09	0.31	0.02	0.04	0.06	0.05
K_2O	%	ICP-OES	0.027	0.014	0.013	0.011	0.139	0.014	0.028	0.052	0.026
MgO	%	ICP-OES	0.672	0.369	0.47	0.762	0.061	0.092	0.066	0.835	0.224
MnO	%	ICP-OES	<0.001	<0.001	<0.001	<0.001	<0.001	<0.001	<0.001	0.001	0.008
Na_2O	%	ICP-OES	0.06	0.04	0.05	0.07	0.02	0.01	<0.01	0.09	0.02
P_2O_5	%	ICP-OES	0.022	0.017	0.02	0.017	0.014	0.011	0.012	0.022	0.016
SiO_2	%	ICP-OES	95.1	96.8	96.2	94.8	97.6	99.8	99.2	94.2	97.5
TiO_2	%	ICP-OES	0.117	0.071	0.086	0.041	0.047	0.031	0.056	0.105	0.058
Ag	ppm	ICP-MS	0.07	0.06	0.07	0.06	0.04	0.03	0.03	0.04	0.03
Ba	ppm	ICP-OES	35	32	17	18	20	13	15	14	19
Be	ppm	ICP-MS	2	1.2	1.6	2.2	0.2	0.2	0.2	1.3	0.4
Bi	ppm	ICP-MS	<0.1	<0.1	0.1	<0.1	<0.1	<0.1	<0.1	<0.1	<0.1
Cd	ppm	ICP-MS	<0.1	<0.1	0.1	<0.1	<0.1	<0.1	0.1	<0.1	<0.1
Ce	ppm	ICP-OES	29	25	22	18	19	19	21	26	23
Co	ppm	ICP-MS	1.07	0.9	0.92	0.84	0.27	0.1	0.1	0.32	0.16
Cr	ppm	ICP-OES	12	14	12	11	15	1	4	4	10
Cs	ppm	ICP-MS	<0.1	<0.1	<0.1	<0.1	<0.1	<0.1	<0.1	<0.1	<0.1
Cu	ppm	ICP-MS	10.3	6.6	6.5	8.2	2.3	2.8	2	5.5	2.5
Dy	ppm	ICP-MS	0.73	0.88	0.63	0.38	0.62	0.61	1.07	1.11	0.66
Er	ppm	ICP-MS	0.43	0.49	0.34	0.23	0.46	0.34	0.61	0.66	0.38
Eu	ppm	ICP-MS	0.26	0.22	0.23	0.18	0.28	0.18	0.23	0.25	0.21
Ga	ppm	ICP-MS	6.1	3.5	5.6	8.3	1.4	1.4	1.5	9.9	2.7
Gd	ppm	ICP-MS	1.6	1.4	1.4	1.1	1.5	1.1	1.4	1.6	1.3
Hf	ppm	ICP-MS	3.4	3.8	5.6	3.1	3.1	1.5	4.7	4	3.6
Ho	ppm	ICP-MS	0.17	0.2	0.14	0.09	0.15	0.14	0.24	0.26	0.15
La	ppm	ICP-OES	15	13	11	9	9	9	10	13	10
Li	ppm	ICP-OES	12	9	7	11	6	3	1	3	2
Mo	ppm	ICP-MS	0.6	1.02	0.47	0.53	0.18	0.07	0.1	0.06	0.12
Nb	ppm	ICP-MS	2.4	1.5	1.9	1	1.1	0.7	1.4	2.1	1.2
Nd	ppm	ICP-MS	11.3	8.9	9.3	7	8.3	7.7	8.4	10.1	8.6
Ni	ppm	ICP-MS	3.2	2	2.6	3.3	1	0.9	1	5.1	2.2
^{204}Pb	ppm	ICP-MS	0.035	0.035	0.038	0.042	0.035	0.032	0.035	0.034	0.047
^{206}Pb	ppm	ICP-MS	1.86	1.85	2.45	2.07	0.8	0.619	0.755	0.857	0.864
^{207}Pb	ppm	ICP-MS	0.536	0.551	0.654	0.677	0.547	0.475	0.55	0.56	0.712
^{208}Pb	ppm	ICP-MS	1.38	1.42	1.59	1.65	1.48	1.15	1.42	1.44	1.8
Pb	ppm	ICP-MS	3.8	3.86	4.73	4.44	2.86	2.28	2.76	2.89	3.42
$^{206}Pb/^{204}Pb$	--	ICP-MS	53.14	52.86	64.47	49.29	22.86	19.34	21.57	25.21	18.38
$^{207}Pb/^{206}Pb$	--	ICP-MS	0.29	0.30	0.27	0.33	0.68	0.77	0.73	0.65	0.82
$^{207}Pb/^{204}Pb$	--	ICP-MS	15.31	15.74	17.21	16.12	15.63	14.84	15.71	16.47	15.15
$^{208}Pb/^{206}Pb$	--	ICP-MS	0.74	0.77	0.65	0.80	1.85	1.86	1.88	1.68	2.08
$^{208}Pb/^{204}Pb$	--	ICP-MS	39.43	40.57	41.84	39.29	42.29	35.94	40.57	42.35	38.30
Pr	ppm	ICP-MS	3.4	2.8	2.7	2	2.2	2.4	2.5	3.1	2.6
Rb	ppm	ICP-MS	0.5	0.3	0.2	0.2	1.7	0.4	0.7	1.1	0.5
Sc	ppm	ICP-MS	1.6	1.3	1.1	1.5	0.6	0.6	1.2	1.5	0.5
Sm	ppm	ICP-MS	1.9	1.4	1.7	1.2	1.7	1.3	1.5	1.7	1.5
Sn	ppm	ICP-MS	0.2	0.13	0.24	0.15	0.19	0.34	0.21	0.61	0.23
Sr	ppm	ICP-OES	44	35	41	27	40	27	31	41	36
Ta	ppm	ICP-MS	0.21	0.14	0.17	0.1	0.11	0.06	0.12	0.18	0.1
Tb	ppm	ICP-MS	0.14	0.15	0.12	0.08	0.12	0.11	0.17	0.19	0.11
Th	ppm	ICP-MS	4.64	4.14	4.08	2.81	6.25	2.71	4.49	5.29	4.83
U	ppm	ICP-MS	15.5	16.2	14.8	14.2	2.23	1.16	2.21	2.39	2.32
V	ppm	ICP-MS	25.6	29.4	147	82.2	5.4	2.8	2.7	15.9	3.1
W	ppm	ICP-MS	0.3	0.3	0.7	0.4	0.2	0.1	0.3	0.2	0.3
Y	ppm	ICP-MS	4.4	5.5	4.6	2.7	3.3	3.4	6.1	7.5	3.9
Yb	ppm	ICP-MS	0.46	0.5	0.39	0.26	0.56	0.32	0.62	0.69	0.38
Zn	ppm	ICP-MS	5	4	5	4	4	3	4	2	4
Zr	ppm	ICP-OES	110	126	191	104	103	45	151	130	122

Carbon and Sulfur: a 0.2 g pulp is analyzed in a Leco SC144DR C/S analyzer for Carbon and Sulfur.

SiO_2 Analysis: A 0.1 gram pulp is fused at 1000 C with lithium metaborate then dissolved in dilute HNO_3.

LOI: A 1.00 gram pulp is heated at 1000 C overnight and the weight loss determined.

Boron: A 0.1 gram pulp is fused at 650 C in a mixture of Na_2O_2/Na_2CO_3.

Total Digestion: A 0.250 g pulp is gently heated in a mixture of ultrapure $HF/HNO_3/HClO_4$ until dry and the residue dissolved in dilute ultrapure HNO_3.

Group #			G-2014-2129	G-2014-2129	G-2014-2129	G-2014-2129	G-2014-2129	G-2014-2129	G-2014-2129	G-2014-2129	G-2014-2129
Description			SG128	SG129	SG130	SG131	SG132	SG133	SG134	SG135	SG136
Fence			Zone 4	Zone 4	Zone 4	Zone 4	Zone 4	Zone 4	Zone 4	Zone 4	Zone 4
HoleID			MAC-252	MAC-252	MAC-252	MAC-252	MAC-252	MAC-252	MAC-252	MAC-252	MAC-252
From			167.20	199.86	249.43	261.91	271.20	286.20	305.30	319.44	331.70
To			167.42	200.11	249.56	262.07	271.35	286.37	305.50	319.60	331.95
Lithofacies			MFd	MFc	MFc	MFc	MFc	MFc	MFb	MFb	MFb
Date			11-27-2014	11-27-2014	11-27-2014	11-27-2014	11-27-2014	11-27-2014	11-27-2014	11-27-2014	11-27-2014
Sample Type			Sandstone	Sandstone	Sandstone	Sandstone	Sandstone	Sandstone	Sandstone	Sandstone	Sandstone
C	%	LECO	0.04	0.08	0.26	0.2	0.32	0.11	0.08	0.02	0.03
S	%	LECO	0.01	0.01	0.01	0.01	0.03	0.01	0.01	0.02	0.01
B	ppm	fusion	439	219	455	696	101	626	1410	163	256
LOI	%	1000°C	0.2	0.3	0.3	0.3	0.6	0.5	0.3	0.5	0.7
Al_2O_3	%	ICP-OES	0.68	0.74	0.98	1.02	2.05	1.64	1.7	2.11	2.26
CaO	%	ICP-OES	<0.01	0.01	<0.01	<0.01	0.02	0.02	0.01	0.01	0.01
Fe_2O_3	%	ICP-OES	0.02	0.03	0.03	0.04	0.14	0.23	0.14	0.4	0.85
K_2O	%	ICP-OES	0.014	0.023	0.015	0.017	0.36	0.193	0.01	0.538	0.327
MgO	%	ICP-OES	0.142	0.159	0.268	0.234	0.302	0.232	0.338	0.072	0.375
MnO	%	ICP-OES	<0.001	<0.001	<0.001	<0.001	<0.001	0.001	<0.001	0.001	0.001
Na_2O	%	ICP-OES	0.01	0.01	0.01	0.02	<0.01	0.03	0.04	<0.01	0.02
P_2O_5	%	ICP-OES	0.014	0.023	0.02	0.022	0.071	0.041	0.024	0.062	0.052
SiO_2	%	ICP-OES	99.1	98.7	98.4	98	93.6	97	97.5	96	95.1
TiO_2	%	ICP-OES	0.062	0.172	0.054	0.111	0.275	0.166	0.125	0.203	0.245
Ag	ppm	ICP-MS	0.03	0.06	0.03	0.05	0.1	0.06	0.06	0.08	0.1
Ba	ppm	ICP-OES	10	10	9	9	22	10	8	12	14
Be	ppm	ICP-MS	0.3	0.3	0.4	0.4	0.5	0.4	0.6	0.3	0.4
Bi	ppm	ICP-MS	<0.1	<0.1	<0.1	<0.1	<0.1	<0.1	<0.1	<0.1	<0.1
Cd	ppm	ICP-MS	<0.1	0.2	<0.1	0.1	0.3	0.1	<0.1	0.2	0.1
Ce	ppm	ICP-OES	23	32	32	29	49	43	32	44	41
Co	ppm	ICP-MS	0.11	0.14	0.16	0.14	0.47	0.16	0.18	0.45	0.47
Cr	ppm	ICP-OES	4	3	4	5	8	4	8	6	10
Cs	ppm	ICP-MS	<0.1	<0.1	<0.1	<0.1	0.1	<0.1	<0.1	<0.1	<0.1
Cu	ppm	ICP-MS	1.8	4.2	1.2	1.7	1.1	2	1.1	2.4	4.4
Dy	ppm	ICP-MS	0.64	1.05	0.54	0.78	1.07	0.76	0.41	5.36	0.77
Er	ppm	ICP-MS	0.37	0.59	0.28	0.42	0.66	0.4	0.23	2.42	0.42
Eu	ppm	ICP-MS	0.2	0.24	0.22	0.2	0.36	0.31	0.23	0.52	0.32
Ga	ppm	ICP-MS	1.3	1.5	2.1	2.2	3.2	2.1	1.6	2.2	3.5
Gd	ppm	ICP-MS	1.3	1.8	1.5	1.5	2.8	2.4	1.5	4.4	2.3
Hf	ppm	ICP-MS	3.7	8.1	2.8	4.5	11.9	6.1	3.6	7	6.5
Ho	ppm	ICP-MS	0.15	0.23	0.11	0.18	0.25	0.15	0.09	1.17	0.16
La	ppm	ICP-OES	10	13	13	13	23	19	13	19	18
Li	ppm	ICP-OES	1	2	4	1	6	2	<1	2	8
Mo	ppm	ICP-MS	0.07	0.07	0.06	0.07	0.12	0.07	0.16	0.15	0.14
Nb	ppm	ICP-MS	1.6	4	1.6	2.9	7.2	4.2	3.2	4.8	5.8
Nd	ppm	ICP-MS	8.2	11	12.3	10.2	16.7	15.1	10.7	18	14.5
Ni	ppm	ICP-MS	1.4	2.3	2.2	1.9	7.2	1.8	1.7	1.4	5.8
^{204}Pb	ppm	ICP-MS	0.031	0.156	0.039	0.07	0.045	0.025	0.034	0.031	0.051
^{206}Pb	ppm	ICP-MS	0.626	3.72	0.767	1.53	0.952	0.564	0.627	0.748	1.02
^{207}Pb	ppm	ICP-MS	0.473	2.45	0.575	1.06	0.674	0.394	0.508	0.498	0.773
^{208}Pb	ppm	ICP-MS	1.31	8.16	1.61	3.23	2.92	1.6	1.42	1.77	2.68
Pb	ppm	ICP-MS	2.44	14.5	2.99	5.88	4.59	2.58	2.59	3.04	4.53
$^{206}Pb/^{204}Pb$	--	ICP-MS	20.19	23.85	19.67	21.86	21.16	22.56	18.44	24.13	20.00
$^{207}Pb/^{206}Pb$	--	ICP-MS	0.76	0.66	0.75	0.69	0.71	0.70	0.81	0.67	0.76
$^{207}Pb/^{204}Pb$	--	ICP-MS	15.26	15.71	14.74	15.14	14.98	15.76	14.94	16.06	15.16
$^{208}Pb/^{206}Pb$	--	ICP-MS	2.09	2.19	2.10	2.11	3.07	2.84	2.26	2.37	2.63
$^{208}Pb/^{204}Pb$	--	ICP-MS	42.26	52.31	41.28	46.14	64.89	64.00	41.76	57.10	52.55
Pr	ppm	ICP-MS	2.5	3.3	3.6	3.1	5.2	4.6	3.2	5	4.3
Rb	ppm	ICP-MS	0.4	0.6	0.5	0.5	4	2	0.3	4.8	3.7
Sc	ppm	ICP-MS	0.4	0.6	0.6	0.7	0.9	0.7	0.7	1.2	0.9
Sm	ppm	ICP-MS	1.4	2	1.9	1.6	3	2.8	1.8	4	2.6
Sn	ppm	ICP-MS	0.23	0.8	0.19	0.66	0.74	0.5	0.35	0.6	0.74
Sr	ppm	ICP-OES	39	60	64	61	184	146	65	318	262
Ta	ppm	ICP-MS	0.14	0.3	0.15	0.28	0.74	0.39	0.24	0.43	0.53
Tb	ppm	ICP-MS	0.12	0.18	0.1	0.14	0.23	0.17	0.1	0.82	0.17
Th	ppm	ICP-MS	7.37	11.2	8.04	13.1	46	18.5	6.71	14.6	21.2
U	ppm	ICP-MS	2.47	4.98	2.5	3	2.04	1.07	0.99	1.31	2.12
V	ppm	ICP-MS	1.7	3.9	6.4	9.4	5.8	3.9	2.3	4.6	5.5
W	ppm	ICP-MS	0.1	0.6	0.1	0.4	0.6	0.3	0.3	0.4	0.9
Y	ppm	ICP-MS	4	6.1	2.9	4.7	6.6	4.3	2.3	33	5.4
Yb	ppm	ICP-MS	0.4	0.6	0.28	0.42	0.76	0.43	0.26	1.9	0.5
Zn	ppm	ICP-MS	3	3	4	4	5	5	4	5	6
Zr	ppm	ICP-OES	117	256	85	145	394	200	116	237	221

Carbon and Sulfur: a 0.2 g pulp is analyzed in a Leco SC144DR C/S analyzer for Carbon and Sulfur.

SiO_2 Analysis: A 0.1 gram pulp is fused at 1000 C with lithium metaborate then dissolved in dilute HNO_3.

LOI: A 1.00 gram pulp is heated at 1000 C overnight and the weight loss determined.

Boron: A 0.1 gram pulp is fused at 650 C in a mixture of Na_2O_2/Na_2CO_3.

Total Digestion: A 0.250 g pulp is gently heated in a mixture of ultrapure $HF/HNO_3/HClO_4$ until dry and the residue dissolved in dilute ultrapure HNO_3.

Group #			G-2014-2129	G-2014-2129	G-2014-2129	G-2014-2129	G-2014-2129	G-2014-2129	G-2014-2155	G-2014-2155	G-2014-2155
Description			SG137	SG138	SG139	SG140	SG141	SG141 R	SG143	SG144	SG145
Fence			Zone 4	Zone 4	Zone 4	Zone 4	Zone 4	Zone 4	Zone 4	Zone 4	Zone 4
HoleID			MAC-252	MAC-255	MAC-255	MAC-255	MAC-255	MAC-255	MAC-255	MAC-255	MAC-255
From			342.50	6.13	29.21	51.63	95.00	95.00	148.00	194.47	209.83
To			342.66	6.31	29.40	51.85	95.22	95.22	149.19	194.69	210.06
Lithofacies			MFb	MFd	MFd	MFd	MFd	MFd	MFd	MFc	MFc
Date			11-27-2014	11-27-2014	11-27-2014	11-27-2014	11-27-2014	11-27-2014	11-28-2014	11-28-2014	11-28-2014
Sample Type			Sandstone	Sandstone	Sandstone	Sandstone	Sandstone	Repeat	Sandstone	Sandstone	Sandstone
C	%	LECO	0.09	0.07	0.07	0.09	0.06	0.06	0.06	0.05	0.06
S	%	LECO	0.01	0.01	0.02	0.01	0.01	0.01	0.01	0.01	0.01
B	ppm	fusion	941	527	315	1220	278	273	301	268	53
LOI	%	1000°C	0.4	0.2	0.6	0.5	0.2	0.2	0.5	0.3	0.4
Al_2O_3	%	ICP-OES	1.68	0.66	1.01	1.99	0.59	0.59	1.19	0.52	0.65
CaO	%	ICP-OES	<0.01	<0.01	0.02	0.01	<0.01	<0.01	<0.01	<0.01	0.01
Fe_2O_3	%	ICP-OES	0.13	0.03	0.3	0.08	0.04	0.03	0.06	0.04	0.04
K_2O	%	ICP-OES	0.126	0.011	0.036	0.028	0.043	0.042	0.141	0.026	0.089
MgO	%	ICP-OES	0.272	0.139	0.122	0.353	0.098	0.096	0.132	0.104	0.087
MnO	%	ICP-OES	<0.001	<0.001	0.001	<0.001	<0.001	<0.001	<0.001	<0.001	<0.001
Na_2O	%	ICP-OES	0.04	0.02	0.02	0.04	0.01	0.01	0.02	0.01	<0.01
P_2O_5	%	ICP-OES	0.024	0.014	0.02	0.022	0.012	0.012	0.015	0.019	0.016
SiO_2	%	ICP-OES	97.2	98.6	97.6	96.7	98.9	98.8	97.3	98.5	98.2
TiO_2	%	ICP-OES	0.079	0.051	0.045	0.117	0.03	0.033	0.081	0.079	0.076
Ag	ppm	ICP-MS	0.05	0.03	0.04	0.05	0.02	0.02	0.03	0.04	0.03
Ba	ppm	ICP-OES	6	13	35	17	11	10	19	21	18
Be	ppm	ICP-MS	0.4	0.4	0.3	0.7	0.2	0.2	0.3	0.2	0.1
Bi	ppm	ICP-MS	<0.1	<0.1	<0.1	<0.1	<0.1	<0.1	<0.1	<0.1	<0.1
Cd	ppm	ICP-MS	<0.1	<0.1	<0.1	0.1	<0.1	<0.1	0.1	<0.1	<0.1
Ce	ppm	ICP-OES	32	22	25	27	23	22	21	29	23
Co	ppm	ICP-MS	0.17	0.11	0.34	0.29	0.09	0.1	0.16	0.11	0.1
Cr	ppm	ICP-OES	5	4	9	4	5	5	7	7	3
Cs	ppm	ICP-MS	<0.1	<0.1	0.3	<0.1	<0.1	<0.1	<0.1	<0.1	<0.1
Cu	ppm	ICP-MS	1.2	1.9	9.7	5.4	3.3	3.4	2.8	2.1	2.7
Dy	ppm	ICP-MS	0.43	0.93	1.05	1.68	0.57	0.56	0.81	0.73	0.59
Er	ppm	ICP-MS	0.24	0.51	0.56	0.98	0.32	0.31	0.51	0.43	0.36
Eu	ppm	ICP-MS	0.24	0.21	0.24	0.32	0.2	0.19	0.22	0.23	0.2
Ga	ppm	ICP-MS	2.2	1.7	2	4	1	1	1.6	1	1.3
Gd	ppm	ICP-MS	1.6	1.4	1.5	2.1	1.2	1.2	1.5	1.6	1.3
Hf	ppm	ICP-MS	2.1	3.7	3.6	6.8	2	2	4.1	4.2	3.8
Ho	ppm	ICP-MS	0.09	0.2	0.23	0.38	0.13	0.12	0.19	0.16	0.13
La	ppm	ICP-OES	13	10	12	13	9	9	10	12	10
Li	ppm	ICP-OES	1	1	4	2	2	2	3	1	2
Mo	ppm	ICP-MS	0.06	0.07	0.27	0.11	0.08	0.12	0.45	0.18	0.09
Nb	ppm	ICP-MS	2.6	1.1	1.2	2.5	0.7	0.7	1.7	1.8	2.1
Nd	ppm	ICP-MS	11.7	8.4	8.9	11	8.1	8	8.6	10.2	9.1
Ni	ppm	ICP-MS	1.5	1.2	2.1	2.6	0.9	0.8	1.4	1	1.2
^{204}Pb	ppm	ICP-MS	0.028	0.03	0.073	0.042	0.045	0.043	0.032	0.073	0.044
^{206}Pb	ppm	ICP-MS	0.537	0.627	1.77	0.978	0.758	0.763	0.932	1.76	0.933
^{207}Pb	ppm	ICP-MS	0.414	0.448	1.11	0.65	0.617	0.629	0.518	1.2	0.698
^{208}Pb	ppm	ICP-MS	1.21	1.16	3.12	1.76	1.58	1.6	1.3	3.52	1.98
Pb	ppm	ICP-MS	2.19	2.26	6.07	3.43	3	3.03	2.78	6.56	3.66
$^{206}Pb/^{204}Pb$	--	ICP-MS	19.18	20.90	24.25	23.29	16.84	17.74	29.13	24.11	21.20
$^{207}Pb/^{206}Pb$	--	ICP-MS	0.77	0.71	0.63	0.66	0.81	0.82	0.56	0.68	0.75
$^{207}Pb/^{204}Pb$	--	ICP-MS	14.79	14.93	15.21	15.48	13.71	14.63	16.19	16.44	15.86
$^{208}Pb/^{206}Pb$	--	ICP-MS	2.25	1.85	1.76	1.80	2.08	2.10	1.39	2.00	2.12
$^{208}Pb/^{204}Pb$	--	ICP-MS	43.21	38.67	42.74	41.90	35.11	37.21	40.63	48.22	45.00
Pr	ppm	ICP-MS	3.4	2.6	2.8	3.3	2.4	2.4	2.6	3	2.7
Rb	ppm	ICP-MS	1.4	0.4	2.6	1	0.7	0.6	2	0.6	1.5
Sc	ppm	ICP-MS	0.5	0.8	1.8	2.1	0.3	0.3	1.1	0.7	0.7
Sm	ppm	ICP-MS	2	1.5	1.6	2.2	1.4	1.4	1.6	1.8	1.6
Sn	ppm	ICP-MS	0.32	0.25	0.98	0.67	0.24	0.24	0.35	0.95	0.58
Sr	ppm	ICP-OES	89	38	33	49	32	32	37	55	51
Ta	ppm	ICP-MS	0.25	0.09	0.1	0.2	0.06	0.06	0.13	0.15	0.15
Tb	ppm	ICP-MS	0.1	0.16	0.18	0.28	0.11	0.1	0.15	0.14	0.11
Th	ppm	ICP-MS	5.09	3.81	4.34	6.78	3.86	3.71	5.26	7.88	8.82
U	ppm	ICP-MS	0.74	2.16	5.82	5.18	3.64	3.72	5.24	4.9	3.48
V	ppm	ICP-MS	1.7	2.2	17.8	5.4	1.5	1.3	3.6	2	2
W	ppm	ICP-MS	0.2	0.2	0.3	0.4	<0.1	0.1	0.3	0.3	0.2
Y	ppm	ICP-MS	2.2	5.4	5.6	9.5	3.1	2.9	5.1	4	3.3
Yb	ppm	ICP-MS	0.25	0.52	0.56	1.07	0.32	0.3	0.58	0.42	0.38
Zn	ppm	ICP-MS	5	4	6	5	4	4	6	4	4
Zr	ppm	ICP-OES	63	121	115	231	63	65	138	138	116

Carbon and Sulfur: a 0.2 g pulp is analyzed in a Leco SC144DR C/S analyzer for Carbon and Sulfur.

SiO_2 Analysis: A 0.1 gram pulp is fused at 1000 C with lithium metaborate then dissolved in dilute HNO_3.

LOI: A 1.00 gram pulp is heated at 1000 C overnight and the weight loss determined.

Boron: A 0.1 gram pulp is fused at 650 C in a mixture of Na_2O_2/Na_2CO_3.

Total Digestion: A 0.250 g pulp is gently heated in a mixture of ultrapure $HF/HNO_3/HClO_4$ until dry and the residue dissolved in dilute ultrapure HNO_3.

Group #			G-2014-2155	G-2014-2155	G-2014-2155	G-2014-2155	G-2014-2155	G-2014-2155	G-2014-2155	G-2014-2155	G-2014-2155	G-2014-2155
Description			SG146	SG147	SG148	SG149	SG150	SG151	SG152	SG153	SG154	SG155
Fence			Zone 4	Zone 4	Zone 4	Zone 4	Zone 4	Zone 4	Zone 4	Zone 4	Zone 4	Zone 4
HoleID			MAC-255	MAC-255	MAC-255	MAC-255	MAC-255	MAC-255	MAC-255	MAC-255	MAC-255	MAC-255
From			217.68	259.93	288.82	293.40	332.33	338.00	362.46	378.33	397.78	412.58
To			218.00	260.03	289.03	293.51	332.55	338.20	362.67	378.59	398.00	412.85
Lithofacies			MFc	MFc	MFc	MFc	MFc	MFc	MFc	MFc	MFb	MFb
Date			11-28-2014	11-28-2014	11-28-2014	11-28-2014	11-28-2014	11-28-2014	11-28-2014	11-28-2014	11-28-2014	11-28-2014
Sample Type			Sandstone	Sandstone	Sandstone	Sandstone	Sandstone	Sandstone	Sandstone	Sandstone	Sandstone	Sandstone
C	%	LECO	0.05	0.04	0.05	0.05	0.06	0.06	0.06	0.05	0.04	0.04
S	%	LECO	0.01	0.01	0.01	0.01	0.01	0.01	0.01	0.01	0.01	0.01
B	ppm	fusion	423	37	30	31	23	27	19	12	9	3
LOI	%	1000°C	0.6	0.4	0.5	0.7	0.8	1.3	0.7	0.8	1.1	0.8
Al_2O_3	%	ICP-OES	1.84	1.38	2.4	2.72	2.7	4.42	1.94	2.08	2.89	1.79
CaO	%	ICP-OES	0.01	0.01	0.01	0.02	0.01	0.01	0.01	0.01	0.01	<0.01
Fe_2O_3	%	ICP-OES	0.19	0.1	0.22	0.12	0.12	0.12	0.1	0.18	0.13	0.12
K_2O	%	ICP-OES	0.226	0.373	0.671	0.642	0.339	0.454	0.218	0.122	0.097	0.061
MgO	%	ICP-OES	0.243	0.038	0.066	0.176	0.03	0.04	0.02	0.015	0.014	0.01
MnO	%	ICP-OES	<0.001	<0.001	<0.001	0.004	<0.001	<0.001	0.003	<0.001	<0.001	<0.001
Na_2O	%	ICP-OES	0.02	<0.01	<0.01	<0.01	<0.01	<0.01	<0.01	<0.01	<0.01	<0.01
P_2O_5	%	ICP-OES	0.03	0.031	0.043	0.078	0.054	0.039	0.023	0.021	0.017	0.02
SiO_2	%	ICP-OES	96.6	97.6	96	95.4	96	93.8	96.7	96.7	95.1	96.8
TiO_2	%	ICP-OES	0.085	0.11	0.149	0.224	0.068	0.235	0.075	0.148	0.056	0.11
Ag	ppm	ICP-MS	0.04	0.05	0.06	0.08	0.04	0.08	0.04	0.05	0.03	0.03
Ba	ppm	ICP-OES	15	12	13	31	9	14	17	19	19	20
Be	ppm	ICP-MS	0.3	0.2	0.2	0.2	0.1	0.2	0.2	0.2	0.2	0.1
Bi	ppm	ICP-MS	<0.1	<0.1	<0.1	<0.1	<0.1	<0.1	<0.1	<0.1	<0.1	<0.1
Cd	ppm	ICP-MS	<0.1	<0.1	0.1	0.2	<0.1	0.2	<0.1	0.2	<0.1	0.1
Ce	ppm	ICP-OES	41	32	33	38	31	41	24	35	28	33
Co	ppm	ICP-MS	0.25	0.06	0.12	0.16	0.1	0.1	0.15	0.12	0.1	0.14
Cr	ppm	ICP-OES	7	7	6	8	9	4	11	12	9	13
Cs	ppm	ICP-MS	<0.1	<0.1	<0.1	<0.1	<0.1	<0.1	<0.1	<0.1	<0.1	<0.1
Cu	ppm	ICP-MS	3.5	1.9	3	2.6	1.2	1.8	0.9	0.7	0.6	0.7
Dy	ppm	ICP-MS	0.6	0.66	0.73	1.26	0.92	1.12	0.67	0.58	0.39	0.6
Er	ppm	ICP-MS	0.36	0.35	0.45	0.68	0.46	0.74	0.44	0.45	0.23	0.46
Eu	ppm	ICP-MS	0.28	0.23	0.25	0.42	0.29	0.4	0.25	0.24	0.22	0.21
Ga	ppm	ICP-MS	2.4	1.9	3.4	4.4	2.9	4.4	2.5	2.8	3.4	2.2
Gd	ppm	ICP-MS	2	1.8	1.8	3.1	2.2	2.6	1.8	1.6	1.3	1.5
Hf	ppm	ICP-MS	3.5	3.8	4.9	7.8	2.5	8.6	3.8	7.6	2.8	6.6
Ho	ppm	ICP-MS	0.13	0.13	0.16	0.27	0.18	0.26	0.15	0.14	0.08	0.14
La	ppm	ICP-OES	17	14	15	17	14	20	11	17	13	17
Li	ppm	ICP-OES	4	2	5	14	5	12	5	8	12	7
Mo	ppm	ICP-MS	0.29	0.11	0.27	0.18	0.15	0.11	0.15	0.14	0.1	0.13
Nb	ppm	ICP-MS	2	3	3.7	5.5	1.8	5.8	2	3.5	1.5	2.8
Nd	ppm	ICP-MS	14.1	11.1	12	15.5	11.9	16.3	10.1	12.4	10.4	11.3
Ni	ppm	ICP-MS	3.5	0.7	1.7	3.9	0.7	0.6	0.5	0.4	0.5	0.5
^{204}Pb	ppm	ICP-MS	0.047	0.03	0.102	0.027	0.05	0.078	0.033	0.041	0.047	0.034
^{206}Pb	ppm	ICP-MS	1.09	1.43	2.55	0.803	0.907	1.88	0.694	0.879	0.85	0.762
^{207}Pb	ppm	ICP-MS	0.718	0.569	1.64	0.446	0.773	1.25	0.505	0.631	0.698	0.54
^{208}Pb	ppm	ICP-MS	2.29	1.45	5.77	1.52	2.14	4.51	1.55	2.05	1.86	1.85
Pb	ppm	ICP-MS	4.15	3.47	10.1	2.8	3.86	7.72	2.78	3.6	3.46	3.18
$^{206}Pb/^{204}Pb$	--	ICP-MS	23.19	47.67	25.00	29.74	18.14	24.10	21.03	21.44	18.09	22.41
$^{207}Pb/^{206}Pb$	--	ICP-MS	0.66	0.40	0.64	0.56	0.85	0.66	0.73	0.72	0.82	0.71
$^{207}Pb/^{204}Pb$	--	ICP-MS	15.28	18.97	16.08	16.52	15.46	16.03	15.30	15.39	14.85	15.88
$^{208}Pb/^{206}Pb$	--	ICP-MS	2.10	1.01	2.26	1.89	2.36	2.40	2.23	2.33	2.19	2.43
$^{208}Pb/^{204}Pb$	--	ICP-MS	48.72	48.33	56.57	56.30	42.80	57.82	46.97	50.00	39.57	54.41
Pr	ppm	ICP-MS	4.2	3.4	3.6	4.4	3.6	4.8	3	4	3.2	3.8
Rb	ppm	ICP-MS	2.8	3.7	6.5	6.9	3.1	4.1	2.1	1.4	1.2	0.8
Sc	ppm	ICP-MS	0.8	0.5	0.8	1	0.6	1	1.3	0.8	0.6	0.7
Sm	ppm	ICP-MS	2.6	2	2.2	3.1	2.3	3.1	2.1	1.9	1.6	1.7
Sn	ppm	ICP-MS	0.48	0.44	0.64	0.68	1.78	0.61	0.38	0.36	0.22	0.52
Sr	ppm	ICP-OES	80	123	199	392	303	141	96	48	44	55
Ta	ppm	ICP-MS	0.2	0.26	0.34	0.44	0.19	0.52	0.2	0.32	0.15	0.32
Tb	ppm	ICP-MS	0.13	0.16	0.16	0.27	0.2	0.23	0.15	0.12	0.08	0.11
Th	ppm	ICP-MS	7.34	8.96	13.1	12.8	5.7	15.2	7.48	13.4	6.62	14.2
U	ppm	ICP-MS	4.93	3.17	3.63	6.3	2.13	3.91	2.64	2.85	2.65	2.83
V	ppm	ICP-MS	12.8	4.3	6.5	7.4	3.5	6.2	4.6	3.6	4.2	3.2
W	ppm	ICP-MS	0.5	0.3	0.3	0.5	0.2	0.5	0.3	0.3	0.2	0.3
Y	ppm	ICP-MS	3.2	3	4	6.4	4.5	6.6	3.9	3.7	1.8	3.6
Yb	ppm	ICP-MS	0.37	0.35	0.52	0.78	0.42	0.82	0.47	0.52	0.25	0.58
Zn	ppm	ICP-MS	6	5	6	5	4	4	4	6	4	3
Zr	ppm	ICP-OES	114	119	162	261	76	291	117	244	82	218

Carbon and Sulfur: a 0.2 g pulp is analyzed in a Leco SC144DR C/S analyzer for Carbon and Sulfur.

SiO_2 Analysis: A 0.1 gram pulp is fused at 1000 C with lithium metaborate then dissolved in dilute HNO_3.

LOI: A 1.00 gram pulp is heated at 1000 C overnight and the weight loss determined.

Boron: A 0.1 gram pulp is fused at 650 C in a mixture of Na_2O_2/Na_2CO_3.

Total Digestion: A 0.250 g pulp is gently heated in a mixture of ultrapure $HF/HNO_3/HClO_4$ until dry and the residue dissolved in dilute ultrapure HNO_3.

Group #			G-2014-2155	G-2014-2155	G-2014-2155	G-2014-2155	G-2014-2155	G-2014-2155	G-2014-2155	G-2014-2155	G-2014-2155	G-2014-2155
Description			SG156	SG157	SG158	SG159	SG160	SG161	SG162	SG163	SG164	SG165
Fence			Zone 4	Zone 4	Zone 4	Zone 4	Zone 4	Zone 4	Zone 4	Zone 4	Zone 4	Zone 4
HoleID			MAC-255	MAC-255	MAC-255	MAC-255	MAC-255	MAC-255	MAC-255	MAC-255	MAC-255	MAC-255
From			426.30	429.50	451.78	462.07	469.36	479.27	483.68	501.32	503.26	559.00
To			426.60	429.63	451.96	462.24	469.63	479.31	483.93	501.50	503.49	559.10
Lithofacies			MFb	MFa	MFa	MFa	MFa	MFa	MFa	MFa	MFa	MFa
Date			11-28-2014	11-28-2014	11-28-2014	11-28-2014	11-28-2014	11-28-2014	11-28-2014	11-28-2014	11-28-2014	11-28-2014
Sample Type			Sandstone	Sandstone	Sandstone	Sandstone	Sandstone	Sandstone	Sandstone	Sandstone	Sandstone	Sandstone
C	%	LECO	0.05	0.03	0.04	0.04	0.03	0.04	0.06	0.06	0.07	0.08
S	%	LECO	0.02	0.01	0.01	0.01	0.01	0.01	0.01	0.11	0.01	0.06
B	ppm	fusion	7	3	45	5	3	2	8	31	10	34
LOI	%	1000°C	1.2	1.2	1.4	0.8	0.3	0.5	0.5	1	0.6	0.9
Al_2O_3	%	ICP-OES	2.92	2.95	4.14	1.99	0.39	1.12	0.94	2.2	1.34	1.46
CaO	%	ICP-OES	0.01	0.01	0.02	0.02	0.02	<0.01	0.02	0.03	0.01	0.03
Fe_2O_3	%	ICP-OES	0.09	0.11	0.32	0.58	0.16	0.11	0.13	0.38	0.16	0.51
K_2O	%	ICP-OES	0.079	0.043	0.266	0.042	0.029	0.094	0.079	0.504	0.038	0.03
MgO	%	ICP-OES	0.01	0.012	0.032	0.013	0.013	0.014	0.028	0.039	0.255	0.67
MnO	%	ICP-OES	<0.001	<0.001	<0.001	<0.001	<0.001	<0.001	<0.001	<0.001	<0.001	0.002
Na_2O	%	ICP-OES	<0.01	<0.01	<0.01	<0.01	<0.01	<0.01	0.01	0.01	<0.01	0.01
P_2O_5	%	ICP-OES	0.022	0.02	0.03	0.033	0.012	0.013	0.011	0.021	0.014	0.024
SiO_2	%	ICP-OES	95.2	95.3	93.6	96.2	98.5	97.3	97.5	95.4	97	96.2
TiO_2	%	ICP-OES	0.096	0.052	0.097	0.167	0.041	0.033	0.03	0.112	0.084	0.102
Ag	ppm	ICP-MS	0.06	0.03	0.04	0.05	<0.02	0.04	0.03	0.08	0.04	0.06
Ba	ppm	ICP-OES	34	26	37	33	20	40	19	48	25	10
Be	ppm	ICP-MS	0.2	0.1	0.2	0.2	0.1	0.2	0.1	0.3	0.3	1.4
Bi	ppm	ICP-MS	<0.1	<0.1	<0.1	<0.1	<0.1	<0.1	<0.1	<0.1	<0.1	0.2
Cd	ppm	ICP-MS	0.1	<0.1	0.1	0.3	0.1	<0.1	<0.1	<0.1	<0.1	<0.1
Ce	ppm	ICP-OES	33	30	33	29	12	17	14	41	21	47
Co	ppm	ICP-MS	0.09	0.2	0.19	0.17	0.09	0.15	0.13	0.71	1.28	4.03
Cr	ppm	ICP-OES	11	19	12	11	14	8	15	11	17	13
Cs	ppm	ICP-MS	<0.1	<0.1	<0.1	<0.1	<0.1	<0.1	<0.1	0.1	<0.1	<0.1
Cu	ppm	ICP-MS	0.9	0.7	1.1	0.8	0.6	1.3	1.3	5.3	5.5	17.2
Dy	ppm	ICP-MS	0.6	0.4	0.78	0.78	0.43	0.59	0.37	0.79	0.49	1.32
Er	ppm	ICP-MS	0.41	0.24	0.47	0.56	0.31	0.42	0.22	0.5	0.3	0.92
Eu	ppm	ICP-MS	0.25	0.22	0.38	0.3	0.12	0.19	0.15	0.29	0.17	0.19
Ga	ppm	ICP-MS	3	2.9	3.6	2.1	0.6	1.3	1.1	1.9	2.3	3.3
Gd	ppm	ICP-MS	1.6	1.3	2	1.9	0.8	1	0.8	2.1	1.2	2.1
Hf	ppm	ICP-MS	5.2	2.2	5.4	12.9	4.8	4.2	2	2.2	1.6	2.5
Ho	ppm	ICP-MS	0.14	0.09	0.17	0.18	0.11	0.15	0.08	0.19	0.11	0.32
La	ppm	ICP-OES	17	15	17	15	5	8	7	22	11	36
Li	ppm	ICP-OES	11	11	18	9	4	11	8	22	15	50
Mo	ppm	ICP-MS	0.09	0.15	0.12	0.18	0.15	0.21	0.7	1.42	2	0.38
Nb	ppm	ICP-MS	2.6	1.5	2	3.7	1	1	0.9	2.1	1.4	2.3
Nd	ppm	ICP-MS	12.6	10.7	13.6	12	4.5	6.1	5.6	16.1	8.8	14.4
Ni	ppm	ICP-MS	0.5	0.6	0.8	0.5	0.4	0.5	0.6	2.5	10	14.1
^{204}Pb	ppm	ICP-MS	0.038	0.04	0.068	0.078	0.028	0.043	0.037	0.11	0.018	0.009
^{206}Pb	ppm	ICP-MS	0.843	0.766	1.33	1.58	0.724	1.04	0.798	4.32	1.64	7.89
^{207}Pb	ppm	ICP-MS	0.64	0.587	1.05	1.16	0.467	0.67	0.532	1.73	0.299	0.222
^{208}Pb	ppm	ICP-MS	1.99	1.65	2.59	3.1	1.17	1.62	1.34	6.19	0.986	1.08
Pb	ppm	ICP-MS	3.51	3.04	5.04	5.92	2.39	3.38	2.71	12.3	2.94	9.2
$^{206}Pb/^{204}Pb$	--	ICP-MS	22.18	19.15	19.56	20.26	25.86	24.19	21.57	39.27	91.11	876.67
$^{207}Pb/^{206}Pb$	--	ICP-MS	0.76	0.77	0.79	0.73	0.65	0.64	0.67	0.40	0.18	0.03
$^{207}Pb/^{204}Pb$	--	ICP-MS	16.84	14.68	15.44	14.87	16.68	15.58	14.38	15.73	16.61	24.67
$^{208}Pb/^{206}Pb$	--	ICP-MS	2.36	2.15	1.95	1.96	1.62	1.56	1.68	1.43	0.60	0.14
$^{208}Pb/^{204}Pb$	--	ICP-MS	52.37	41.25	38.09	39.74	41.79	37.67	36.22	56.27	54.78	120.00
Pr	ppm	ICP-MS	4	3.5	4.1	3.6	1.4	1.8	1.7	4.9	2.7	5.1
Rb	ppm	ICP-MS	1	0.6	2.2	0.6	0.4	1.1	1	6.7	0.8	0.6
Sc	ppm	ICP-MS	1.1	0.6	0.8	0.9	0.6	1	0.3	1.2	0.9	1.3
Sm	ppm	ICP-MS	1.9	1.6	2.5	2	0.9	1.1	0.9	2.8	1.6	2
Sn	ppm	ICP-MS	0.35	0.22	0.42	0.41	0.12	0.28	0.18	1.02	0.45	0.65
Sr	ppm	ICP-OES	69	67	84	107	32	32	31	46	28	44
Ta	ppm	ICP-MS	0.27	0.14	0.17	0.38	0.09	0.11	0.08	0.18	0.12	0.33
Tb	ppm	ICP-MS	0.12	0.09	0.16	0.16	0.08	0.1	0.07	0.16	0.1	0.22
Th	ppm	ICP-MS	11.7	6.29	5.43	9.59	3.23	3.04	2.58	11.4	4.5	24
U	ppm	ICP-MS	3.09	3.47	6.01	9.6	6.58	8.43	4.57	10.1	3.08	5.12
V	ppm	ICP-MS	3.6	2.4	3.4	3.2	1.5	2.6	1.9	12.9	20.3	18.9
W	ppm	ICP-MS	0.3	0.2	0.4	0.4	0.2	0.2	0.2	0.8	0.4	1.1
Y	ppm	ICP-MS	3.2	2	4.4	4.9	2.9	4.1	2.2	5.9	3	8.6
Yb	ppm	ICP-MS	0.48	0.24	0.51	0.75	0.39	0.48	0.25	0.42	0.3	0.97
Zn	ppm	ICP-MS	4	6	4	5	3	3	3	6	6	6
Zr	ppm	ICP-OES	171	70	193	458	159	140	59	71	52	74

Carbon and Sulfur: a 0.2 g pulp is analyzed in a Leco SC144DR C/S analyzer for Carbon and Sulfur.

SiO_2 Analysis: A 0.1 gram pulp is fused at 1000 C with lithium metaborate then dissolved in dilute HNO_3.

LOI: A 1.00 gram pulp is heated at 1000 C overnight and the weight loss determined.

Boron: A 0.1 gram pulp is fused at 650 C in a mixture of Na_2O_2/Na_2CO_3.

Total Digestion: A 0.250 g pulp is gently heated in a mixture of ultrapure $HF/HNO_3/HClO_4$ until dry and the residue dissolved in dilute ultrapure HNO_3.

Group #			G-2014-2155	G-2014-2155	G-2014-2155	G-2014-2155	G-2014-2155	G-2014-2155	G-2014-2155	G-2014-2155	G-2014-2155	G-2014-2155
Description			SG166	SG167	SG168	SG169	SG170	SG171	SG172	SG173	SG174	SG175
Fence			Zone 4	Zone C	Zone C	Zone C	Zone C	Zone C	Zone C	Zone C	Zone C	Zone C
HoleID			MAC-255	MC-413	MC-413	MC-413	MC-413	MC-413	MC-413	MC-413	MC-413	MC-413
From			564.36	71.64	130.00	183.26	224.00	258.26	282.17	299.00	303.50	317.96
To			564.50	71.80	130.22	183.43	224.32	258.50	282.40	299.16	303.80	318.16
Lithofacies			MFa	MFd	MFc	MFc	MFc	MFc	MFc	MFb	MFb	MFb
Date			11-28-2014	11-28-2014	11-28-2014	11-28-2014	11-28-2014	11-28-2014	11-28-2014	11-28-2014	11-28-2014	11-28-2014
Sample Type			Sandstone	Sandstone	Sandstone	Sandstone	Sandstone	Sandstone	Sandstone	Sandstone	Sandstone	Sandstone
C	%	LECO	0.1	0.05	0.04	0.05	0.04	0.05	0.05	0.08	0.05	0.05
S	%	LECO	0.07	0.01	0.01	0.01	0.01	0.01	0.01	0.01	0.01	0.01
B	ppm	fusion	265	141	38	168	81	371	617	169	104	1150
LOI	%	1000°C	1.4	0.3	0.3	1	0.3	0.4	0.4	0.6	0.3	0.3
Al_2O_3	%	ICP-OES	2.7	0.75	0.52	2.6	0.65	1.18	1.34	2.45	1.48	1.48
CaO	%	ICP-OES	0.19	0.01	<0.01	0.02	<0.01	0.01	0.01	0.02	0.02	0.01
Fe_2O_3	%	ICP-OES	0.86	0.03	0.03	0.14	0.17	0.06	0.08	0.57	0.1	0.08
K_2O	%	ICP-OES	0.083	0.033	0.023	0.1	0.027	0.062	0.083	0.58	0.352	0.012
MgO	%	ICP-OES	1.01	0.132	0.089	0.543	0.111	0.187	0.224	0.148	0.069	0.276
MnO	%	ICP-OES	0.008	<0.001	<0.001	<0.001	<0.001	<0.001	<0.001	<0.001	<0.001	<0.001
Na_2O	%	ICP-OES	0.02	<0.01	<0.01	<0.01	<0.01	0.01	0.02	<0.01	<0.01	0.02
P_2O_5	%	ICP-OES	0.177	0.018	0.013	0.024	0.016	0.026	0.027	0.066	0.078	0.045
SiO_2	%	ICP-OES	92.8	98.2	98.4	95.2	98.3	97.2	97.1	95.3	97.7	97.6
TiO_2	%	ICP-OES	0.145	0.037	0.038	0.13	0.047	0.106	0.045	0.207	0.187	0.134
Ag	ppm	ICP-MS	0.14	0.03	<0.02	0.05	<0.02	0.05	0.03	0.08	0.06	0.06
Ba	ppm	ICP-OES	18	10	10	24	9	14	12	25	24	13
Be	ppm	ICP-MS	1.7	0.2	0.1	0.4	0.2	0.3	0.4	0.4	0.3	0.4
Bi	ppm	ICP-MS	0.1	<0.1	<0.1	<0.1	<0.1	<0.1	<0.1	<0.1	<0.1	<0.1
Cd	ppm	ICP-MS	<0.1	<0.1	<0.1	0.2	<0.1	0.1	<0.1	0.1	0.2	0.1
Ce	ppm	ICP-OES	111	19	23	31	16	37	27	43	44	34
Co	ppm	ICP-MS	4.57	0.24	0.08	0.24	0.11	0.1	0.1	0.12	0.07	0.1
Cr	ppm	ICP-OES	23	4	5	8	5	4	6	9	8	14
Cs	ppm	ICP-MS	<0.1	<0.1	<0.1	0.1	<0.1	<0.1	<0.1	<0.1	<0.1	<0.1
Cu	ppm	ICP-MS	5.2	1.6	0.9	2.4	3	1.8	1.6	5.3	1	1.3
Dy	ppm	ICP-MS	2.13	0.79	0.61	1.2	0.7	1.06	0.56	1.02	1.08	0.82
Er	ppm	ICP-MS	1.2	0.43	0.36	0.75	0.44	0.65	0.3	0.62	0.62	0.5
Eu	ppm	ICP-MS	0.49	0.17	0.19	0.34	0.17	0.29	0.22	0.37	0.35	0.24
Ga	ppm	ICP-MS	4.9	1.8	1.3	5.1	1.5	2.1	1.7	2.8	1.6	1.7
Gd	ppm	ICP-MS	4.4	1.3	1.1	2.1	1.1	2	1.5	2.5	2.8	1.9
Hf	ppm	ICP-MS	2.9	3	2.2	8.3	3.4	4.9	2.4	7	7.3	4.6
Ho	ppm	ICP-MS	0.46	0.18	0.13	0.28	0.16	0.24	0.11	0.23	0.23	0.18
La	ppm	ICP-OES	74	9	10	13	7	15	11	19	21	16
Li	ppm	ICP-OES	45	2	2	8	2	2	2	5	3	<1
Mo	ppm	ICP-MS	0.57	0.06	0.04	0.09	0.29	0.08	0.06	0.22	0.1	0.14
Nb	ppm	ICP-MS	3.2	1	0.8	3.3	0.9	2.5	1.3	5	4.5	3.7
Nd	ppm	ICP-MS	33.6	7.6	8	11.6	6.1	12.8	9.7	16	15.2	12.6
Ni	ppm	ICP-MS	54.1	2.3	1.3	5.8	2.2	1.8	1.7	1.8	0.8	2.1
^{204}Pb	ppm	ICP-MS	0.031	0.027	0.036	0.077	0.025	0.05	0.02	0.042	0.029	0.024
^{206}Pb	ppm	ICP-MS	5.44	0.696	0.636	1.28	0.506	0.918	0.52	0.968	0.743	0.692
^{207}Pb	ppm	ICP-MS	0.636	0.428	0.551	1.13	0.384	0.769	0.335	0.629	0.477	0.399
^{208}Pb	ppm	ICP-MS	2.14	1.13	1.37	3.05	1.02	2.18	1.08	2	1.84	1.72
Pb	ppm	ICP-MS	8.24	2.28	2.59	5.54	1.94	3.92	1.95	3.64	3.09	2.84
$^{206}Pb/^{204}Pb$	--	ICP-MS	175.48	25.78	17.67	16.62	20.24	18.36	26.00	23.05	25.62	28.83
$^{207}Pb/^{206}Pb$	--	ICP-MS	0.12	0.61	0.87	0.88	0.76	0.84	0.64	0.65	0.64	0.58
$^{207}Pb/^{204}Pb$	--	ICP-MS	20.52	15.85	15.31	14.68	15.36	15.38	16.75	14.98	16.45	16.63
$^{208}Pb/^{206}Pb$	--	ICP-MS	0.39	1.62	2.15	2.38	2.02	2.37	2.08	2.07	2.48	2.49
$^{208}Pb/^{204}Pb$	--	ICP-MS	69.03	41.85	38.06	39.61	40.80	43.60	54.00	47.62	63.45	71.67
Pr	ppm	ICP-MS	11.6	2.4	2.5	3.4	1.9	3.8	3	4.8	4.7	3.9
Rb	ppm	ICP-MS	2.4	0.7	0.5	1.8	0.6	1.1	1.1	5.7	3.6	0.4
Sc	ppm	ICP-MS	2.7	0.5	0.4	0.7	0.8	0.5	0.4	1.5	0.7	0.9
Sm	ppm	ICP-MS	4.6	1.3	1.4	2.2	1.2	2.3	1.8	3	2.9	2.1
Sn	ppm	ICP-MS	1.61	0.24	0.17	0.53	0.35	0.34	0.24	1.13	0.49	0.44
Sr	ppm	ICP-OES	165	80	34	63	33	74	84	198	341	194
Ta	ppm	ICP-MS	0.35	0.09	0.07	0.31	0.09	0.22	0.12	0.45	0.41	0.38
Tb	ppm	ICP-MS	0.38	0.15	0.11	0.21	0.12	0.19	0.13	0.21	0.23	0.17
Th	ppm	ICP-MS	28.3	4.05	4.43	12.9	4.88	11.5	11.4	15.7	22	23
U	ppm	ICP-MS	17.3	1.82	0.98	2.35	2.88	2.18	1.9	6.92	3.3	2.08
V	ppm	ICP-MS	37.4	3.9	2	4.1	6.8	2.9	2.4	9.2	3.5	3.6
W	ppm	ICP-MS	2.5	0.2	0.1	0.4	0.4	0.3	0.1	0.5	0.4	0.4
Y	ppm	ICP-MS	12.6	4.5	3.3	7.5	4.4	6.4	2.8	5.6	5.7	4.4
Yb	ppm	ICP-MS	1.12	0.44	0.34	0.83	0.44	0.56	0.31	0.68	0.66	0.54
Zn	ppm	ICP-MS	6	4	4	4	3	3	3	5	3	3
Zr	ppm	ICP-OES	96	98	74	276	108	159	69	239	247	144

Carbon and Sulfur: a 0.2 g pulp is analyzed in a Leco SC144DR C/S analyzer for Carbon and Sulfur.

SiO_2 Analysis: A 0.1 gram pulp is fused at 1000 C with lithium metaborate then dissolved in dilute HNO_3.

LOI: A 1.00 gram pulp is heated at 1000 C overnight and the weight loss determined.

Boron: A 0.1 gram pulp is fused at 650 C in a mixture of Na_2O_2/Na_2CO_3.

Total Digestion: A 0.250 g pulp is gently heated in a mixture of ultrapure $HF/HNO_3/HClO_4$ until dry and the residue dissolved in dilute ultrapure HNO_3.

Group #			G-2014-2155	G-2014-2155	G-2014-2155	G-2014-2155	G-2014-2155	G-2014-2155	G-2014-2155	G-2014-2155	G-2014-2155	G-2014-2155
Description			SG176	SG177	SG178	SG179	SG175 R	SG180	SG181	SG182	SG183	SG184
Fence			Zone C	Zone C	Zone C	Zone C	Zone C	Zone C	Zone C	Zone C	Zone C	Zone C
HoleID			MC-413	MC-413	MC-413	MC-413	MC-413	MC-413	MC-413	MC-413	MC-413	MC-413
From			328.54	354.67	388.82	404.00	317.96	430.57	456.68	482.25	501.66	527.67
To			328.57	354.90	389.00	404.25	318.16	430.79	456.95	482.43	501.85	527.92
Lithofacies			MFb	MFb	MFb	MFb	MFb	MFa	MFa	MFa	MFa	MFa
Date			11-28-2014	11-28-2014	11-28-2014	11-28-2014	11-28-2014	11-28-2014	11-28-2014	11-28-2014	11-28-2014	11-28-2014
Sample Type			Sandstone	Sandstone	Sandstone	Sandstone	Repeat	Sandstone	Sandstone	Sandstone	Sandstone	Sandstone
C	%	LECO	0.07	0.06	0.07	0.04	0.05	0.06	0.08	0.04	0.04	0.06
S	%	LECO	0.02	0.01	0.08	0.01	0.01	0.01	0.01	0.01	0.01	0.01
B	ppm	fusion	30	32	118	806	1120	48	130	40	9	6
LOI	%	1000°C	0.6	0.6	1.4	0.5	0.3	0.8	0.5	0.6	0.5	0.7
Al_2O_3	%	ICP-OES	1.93	1.96	3.31	1.9	1.46	1.96	1.14	1.56	1.18	1.6
CaO	%	ICP-OES	0.02	0.01	0.05	0.01	0.01	0.01	0.01	0.01	0.01	0.01
Fe_2O_3	%	ICP-OES	0.06	0.05	0.09	0.17	0.08	0.12	0.06	0.33	0.14	0.11
K_2O	%	ICP-OES	0.351	0.291	0.07	0.111	0.01	0.068	0.034	0.081	0.042	0.061
MgO	%	ICP-OES	0.029	0.024	0.037	0.23	0.272	0.021	0.049	0.014	0.013	0.013
MnO	%	ICP-OES	<0.001	<0.001	<0.001	<0.001	<0.001	<0.001	<0.001	<0.001	<0.001	<0.001
Na_2O	%	ICP-OES	<0.01	<0.01	<0.01	0.03	0.02	<0.01	<0.01	<0.01	<0.01	<0.01
P_2O_5	%	ICP-OES	0.134	0.045	0.355	0.035	0.045	0.028	0.016	0.041	0.015	0.013
SiO_2	%	ICP-OES	96.7	96.8	93.7	96.4	97.6	96.3	98	97.2	98.1	97.1
TiO_2	%	ICP-OES	0.051	0.095	0.509	0.251	0.141	0.212	0.043	0.475	0.037	0.049
Ag	ppm	ICP-MS	0.02	0.04	0.31	0.08	0.06	0.07	0.02	0.13	<0.02	<0.02
Ba	ppm	ICP-OES	27	11	118	41	14	23	20	28	24	19
Be	ppm	ICP-MS	0.2	0.1	0.6	0.6	0.5	0.2	0.1	0.2	0.1	<0.1
Bi	ppm	ICP-MS	<0.1	<0.1	<0.1	<0.1	<0.1	<0.1	<0.1	<0.1	<0.1	<0.1
Cd	ppm	ICP-MS	<0.1	<0.1	0.5	0.4	<0.1	0.2	<0.1	0.4	<0.1	<0.1
Ce	ppm	ICP-OES	32	35	265	42	36	45	25	56	18	18
Co	ppm	ICP-MS	0.05	0.06	0.11	0.2	0.14	0.1	0.1	0.08	0.12	0.1
Cr	ppm	ICP-OES	6	9	9	17	16	15	15	12	16	9
Cs	ppm	ICP-MS	<0.1	<0.1	<0.1	<0.1	<0.1	<0.1	<0.1	<0.1	<0.1	<0.1
Cu	ppm	ICP-MS	0.9	0.7	3.5	2	1.5	1	1.1	1.1	0.8	0.5
Dy	ppm	ICP-MS	1.02	0.8	4.27	1.19	0.87	0.57	0.32	1.12	0.39	0.4
Er	ppm	ICP-MS	0.37	0.44	2.22	0.88	0.5	0.38	0.21	0.86	0.25	0.25
Eu	ppm	ICP-MS	0.37	0.27	1.9	0.36	0.25	0.25	0.2	0.39	0.18	0.18
Ga	ppm	ICP-MS	1.7	1.9	2.6	2	1.7	1.8	1.2	1.7	1.3	1.6
Gd	ppm	ICP-MS	2.7	2.1	19.2	2.7	2	1.8	1.2	2.9	1.1	1
Hf	ppm	ICP-MS	2.4	3.3	25.2	16.8	5	6.6	2.2	19.8	3.9	3.1
Ho	ppm	ICP-MS	0.16	0.17	0.75	0.28	0.19	0.13	0.07	0.28	0.09	0.09
La	ppm	ICP-OES	13	16	115	21	16	21	12	29	8	9
Li	ppm	ICP-OES	3	3	6	3	<1	6	3	6	6	9
Mo	ppm	ICP-MS	0.13	0.1	0.19	0.14	0.15	0.24	0.08	0.17	0.1	0.09
Nb	ppm	ICP-MS	1.3	2.4	12.2	6.2	4	5.1	1.2	11.7	1	1.1
Nd	ppm	ICP-MS	12.2	13.3	152	17.7	13.3	15.4	10.7	21.2	8.2	6.9
Ni	ppm	ICP-MS	0.4	0.4	0.8	1.5	1.8	0.7	0.7	0.5	0.6	0.4
^{204}Pb	ppm	ICP-MS	0.031	0.03	0.036	0.023	0.024	0.045	0.028	0.047	0.037	0.046
^{206}Pb	ppm	ICP-MS	0.803	0.626	1.21	0.765	0.675	1.11	0.583	1.2	0.708	0.763
^{207}Pb	ppm	ICP-MS	0.501	0.455	0.62	0.401	0.394	0.744	0.394	0.755	0.544	0.676
^{208}Pb	ppm	ICP-MS	1.48	1.47	5.09	2.18	1.73	2.96	1.29	3.49	1.45	1.68
Pb	ppm	ICP-MS	2.81	2.58	6.96	3.37	2.82	4.86	2.3	5.49	2.74	3.17
$^{206}Pb/^{204}Pb$	--	ICP-MS	25.90	20.87	33.61	33.26	28.13	24.67	20.82	25.53	19.14	16.59
$^{207}Pb/^{206}Pb$	--	ICP-MS	0.62	0.73	0.51	0.52	0.58	0.67	0.68	0.63	0.77	0.89
$^{207}Pb/^{204}Pb$	--	ICP-MS	16.16	15.17	17.22	17.43	16.42	16.53	14.07	16.06	14.70	14.70
$^{208}Pb/^{206}Pb$	--	ICP-MS	1.84	2.35	4.21	2.85	2.56	2.67	2.21	2.91	2.05	2.20
$^{208}Pb/^{204}Pb$	--	ICP-MS	47.74	49.00	141.39	94.78	72.08	65.78	46.07	74.26	39.19	36.52
Pr	ppm	ICP-MS	3.5	4	36.9	5.5	4.1	5	3.1	6.7	2.3	2.1
Rb	ppm	ICP-MS	3.2	2.7	1	1.5	0.3	1	0.5	1	0.5	0.7
Sc	ppm	ICP-MS	0.5	0.6	4	2.5	0.9	0.6	0.4	1.3	0.4	0.3
Sm	ppm	ICP-MS	2.5	2.4	35.4	3.4	2.3	2.2	1.7	3.5	1.5	1.1
Sn	ppm	ICP-MS	0.23	0.46	1.11	0.68	0.53	0.64	0.27	0.93	0.21	0.13
Sr	ppm	ICP-OES	767	228	2130	99	196	89	56	126	49	32
Ta	ppm	ICP-MS	0.14	0.22	1.18	0.66	0.38	0.5	0.13	1.29	0.11	0.1
Tb	ppm	ICP-MS	0.25	0.17	1.17	0.23	0.18	0.12	0.07	0.22	0.08	0.08
Th	ppm	ICP-MS	6.46	7.18	83.1	34.1	24.2	21.3	5.14	43.9	5.73	3.02
U	ppm	ICP-MS	3.27	1.77	11.4	5.89	2.18	4.01	1.59	4.97	2.04	1.11
V	ppm	ICP-MS	2.5	3	6.4	4.7	3.6	3.4	3.2	6.4	2.4	1.1
W	ppm	ICP-MS	0.2	0.2	2.8	0.6	0.4	0.5	0.3	0.8	0.2	0.1
Y	ppm	ICP-MS	3.2	4	16.9	7.6	4.6	3.3	1.7	7.6	2.2	2.3
Yb	ppm	ICP-MS	0.34	0.45	2.26	1.12	0.55	0.42	0.22	1.05	0.28	0.25
Zn	ppm	ICP-MS	3	3	4	4	4	3	3	4	3	3
Zr	ppm	ICP-OES	72	104	909	555	145	217	66	713	124	106

Carbon and Sulfur: a 0.2 g pulp is analyzed in a Leco SC144DR C/S analyzer for Carbon and Sulfur.

SiO_2 Analysis: A 0.1 gram pulp is fused at 1000 C with lithium metaborate then dissolved in dilute HNO_3.

LOI: A 1.00 gram pulp is heated at 1000 C overnight and the weight loss determined.

Boron: A 0.1 gram pulp is fused at 650 C in a mixture of Na_2O_2/Na_2CO_3.

Total Digestion: A 0.250 g pulp is gently heated in a mixture of ultrapure $HF/HNO_3/HClO_4$ until dry and the residue dissolved in dilute ultrapure HNO_3.

Group #			G-2014-2155	G-2014-2155	G-2014-2155	G-2014-2155	G-2014-2155	G-2014-2155	G-2014-2155	G-2014-2155	G-2014-2155	G-2014-2155
Description			SG185	SG186	SG187	SG188	SG189	SG190	SG191	SG192	SG193	SG194
Fence			Zone C	Zone C	Zone C	Zone C	Zone C	Zone C	Zone C	Zone C	Zone C	Zone C
HoleID			MC-413	MC-413	MC-413	MC-413	MC-413	MC-413	MC-413	MC-413	MC-413	MC-415
From			547.30	557.44	559.73	566.28	603.83	614.83	623.78	638.86	649.00	76.73
To			547.51	557.57	559.91	566.52	604.11	615.05	624.09	639.19	649.20	76.92
Lithofacies			MFa	MFa	MFa	MFa	MFa	MFa	MFa	MFa	MFa	MFd
Date			11-28-2014	11-28-2014	11-28-2014	11-28-2014	11-28-2014	11-28-2014	11-28-2014	11-28-2014	11-28-2014	11-28-2014
Sample Type			Sandstone	Sandstone	Sandstone	Sandstone	Sandstone	Sandstone	Sandstone	Sandstone	Sandstone	Sandstone
C	%	LECO	0.05	0.05	0.06	0.05	0.05	0.07	0.05	0.07	0.07	0.05
S	%	LECO	0.01	0.01	0.01	0.01	0.02	0.02	0.01	0.01	0.01	0.01
B	ppm	fusion	8	27	6	87	225	1480	136	244	747	58
LOI	%	1000°C	0.9	0.4	0.8	1.4	1.1	0.7	0.2	0.5	0.6	0.3
Al_2O_3	%	ICP-OES	2.3	1.12	1.74	6.94	3.92	2.45	0.32	2.29	2.67	0.57
CaO	%	ICP-OES	<0.01	0.01	0.01	0.02	0.04	0.04	0.02	0.02	0.02	<0.01
Fe_2O_3	%	ICP-OES	0.08	0.15	0.59	0.51	0.29	0.22	1.99	2.48	1.52	0.04
K_2O	%	ICP-OES	0.045	0.255	0.018	1.62	0.703	0.034	0.015	0.558	0.414	0.032
MgO	%	ICP-OES	0.007	0.03	0.016	0.136	0.541	0.53	0.056	0.113	0.231	0.114
MnO	%	ICP-OES	<0.001	<0.001	<0.001	<0.001	<0.001	<0.001	<0.001	0.002	0.001	<0.001
Na_2O	%	ICP-OES	<0.01	<0.01	<0.01	0.01	0.02	0.05	0.01	0.02	0.04	<0.01
P_2O_5	%	ICP-OES	0.018	0.031	0.019	0.048	0.088	0.09	0.011	0.029	0.05	0.011
SiO_2	%	ICP-OES	96.2	97	96.5	89.2	92.8	95.6	97.3	93.7	94.2	98.4
TiO_2	%	ICP-OES	0.062	0.078	0.143	0.249	0.738	0.334	0.078	0.18	0.31	0.034
Ag	ppm	ICP-MS	0.04	0.04	0.05	0.16	0.19	0.1	0.04	0.02	0.06	0.04
Ba	ppm	ICP-OES	62	41	17	40	35	28	10	20	31	10
Be	ppm	ICP-MS	0.1	0.2	0.6	0.5	1.4	2.2	0.2	0.2	0.6	0.2
Bi	ppm	ICP-MS	<0.1	<0.1	<0.1	<0.1	<0.1	0.5	<0.1	<0.1	<0.1	<0.1
Cd	ppm	ICP-MS	<0.1	<0.1	<0.1	0.2	0.4	0.3	0.2	<0.1	0.3	<0.1
Ce	ppm	ICP-OES	24	54	48	78	167	115	19	59	141	19
Co	ppm	ICP-MS	0.1	0.22	0.56	0.4	11.9	6.92	0.6	1.12	0.46	0.16
Cr	ppm	ICP-OES	12	19	17	23	59	43	19	26	30	12
Cs	ppm	ICP-MS	<0.1	<0.1	<0.1	0.2	0.1	<0.1	<0.1	<0.1	<0.1	<0.1
Cu	ppm	ICP-MS	1.1	1.5	7.8	4.4	5.6	18.2	0.7	0.8	0.5	0.8
Dy	ppm	ICP-MS	0.87	1.06	1.33	1.77	1.79	1.59	0.36	2.86	1.51	0.55
Er	ppm	ICP-MS	0.56	0.74	0.67	1.09	1.16	1.07	0.27	2.96	1	0.3
Eu	ppm	ICP-MS	0.28	0.45	0.22	0.6	0.73	0.51	0.13	0.49	0.44	0.16
Ga	ppm	ICP-MS	2.3	1.7	3.3	9	4.4	4.4	0.6	3.4	3.2	1.4
Gd	ppm	ICP-MS	1.6	4.1	2.9	3.9	5.5	4.7	0.9	3.6	4.2	1
Hf	ppm	ICP-MS	4.6	3.2	2.4	8.6	19.4	14.1	7.1	3.7	12.4	2.1
Ho	ppm	ICP-MS	0.21	0.24	0.27	0.41	0.4	0.36	0.09	0.84	0.37	0.12
La	ppm	ICP-OES	12	26	23	43	102	62	10	28	77	9
Li	ppm	ICP-OES	8	9	12	20	44	7	4	9	18	2
Mo	ppm	ICP-MS	0.12	0.19	0.54	0.29	2.2	0.64	0.5	0.69	0.75	0.1
Nb	ppm	ICP-MS	1.7	1.6	2.9	5.6	13.6	6.8	1.6	1.8	5.3	1
Nd	ppm	ICP-MS	10	30	19.7	29.3	52.1	41.9	7.8	28	45.1	7.3
Ni	ppm	ICP-MS	0.5	0.9	10.2	1.6	27.2	12	2.3	3.6	1.6	1.6
^{204}Pb	ppm	ICP-MS	0.057	0.031	0.013	0.149	0.041	0.056	0.02	0.016	0.053	0.026
^{206}Pb	ppm	ICP-MS	1.18	0.92	1.77	3.49	4.25	7.78	1.48	0.519	1.25	0.549
^{207}Pb	ppm	ICP-MS	0.869	0.492	0.287	2.32	0.803	1.2	0.35	0.251	0.871	0.427
^{208}Pb	ppm	ICP-MS	2.23	1.79	1.52	6.83	5.39	4.38	1.11	1.07	3.67	1.08
Pb	ppm	ICP-MS	4.34	3.23	3.6	12.8	10.5	13.4	2.97	1.85	5.84	2.08
$^{206}Pb/^{204}Pb$	--	ICP-MS	20.70	29.68	136.15	23.42	103.66	138.93	74.00	32.44	23.58	21.12
$^{207}Pb/^{206}Pb$	--	ICP-MS	0.74	0.53	0.16	0.66	0.19	0.15	0.24	0.48	0.70	0.78
$^{207}Pb/^{204}Pb$	--	ICP-MS	15.25	15.87	22.08	15.57	19.59	21.43	17.50	15.69	16.43	16.42
$^{208}Pb/^{206}Pb$	--	ICP-MS	1.89	1.95	0.86	1.96	1.27	0.56	0.75	2.06	2.94	1.97
$^{208}Pb/^{204}Pb$	--	ICP-MS	39.12	57.74	116.92	45.84	131.46	78.21	55.50	66.88	69.25	41.54
Pr	ppm	ICP-MS	3	7.6	6	9.6	18.5	13.7	2.5	7.9	16	2.3
Rb	ppm	ICP-MS	0.8	3.6	0.4	24	8.2	1.4	0.4	6.5	4.2	0.7
Sc	ppm	ICP-MS	1	1.4	1.8	3.4	4.2	2	0.4	1.4	2.6	0.3
Sm	ppm	ICP-MS	1.8	7.1	3.6	4.5	6.6	6.4	1.2	5	5.1	1.2
Sn	ppm	ICP-MS	0.28	0.7	1.08	1.96	3.67	1.68	0.4	0.53	1.45	0.18
Sr	ppm	ICP-OES	46	89	21	100	246	293	44	61	110	30
Ta	ppm	ICP-MS	0.18	0.18	0.34	0.56	1.84	0.82	0.17	0.2	0.6	0.09
Tb	ppm	ICP-MS	0.15	0.22	0.26	0.32	0.32	0.31	0.07	0.4	0.24	0.11
Th	ppm	ICP-MS	5.83	14.1	18.6	19.4	138	49.2	9.29	11.8	49.3	3.72
U	ppm	ICP-MS	7.46	6.56	19.7	13	31.2	34.4	4.72	1.54	1.98	1.07
V	ppm	ICP-MS	3	7.1	31	19.5	38.7	88.5	4.4	40.9	28.6	1.6
W	ppm	ICP-MS	0.2	0.4	0.7	0.8	1.9	3.3	0.6	0.5	0.8	0.2
Y	ppm	ICP-MS	4.6	6.3	7.1	9.9	10.2	9.2	2.3	23.3	7.6	3
Yb	ppm	ICP-MS	0.64	0.8	0.62	1.13	1.26	1.16	0.35	3.62	1.19	0.3
Zn	ppm	ICP-MS	3	3	4	4	8	25	4	3	3	3
Zr	ppm	ICP-OES	147	105	77	280	689	475	254	124	415	63

Carbon and Sulfur: a 0.2 g pulp is analyzed in a Leco SC144DR C/S analyzer for Carbon and Sulfur.

SiO_2 Analysis: A 0.1 gram pulp is fused at 1000 C with lithium metaborate then dissolved in dilute HNO_3.

LOI: A 1.00 gram pulp is heated at 1000 C overnight and the weight loss determined.

Boron: A 0.1 gram pulp is fused at 650 C in a mixture of Na_2O_2/Na_2CO_3.

Total Digestion: A 0.250 g pulp is gently heated in a mixture of ultrapure $HF/HNO_3/HClO_4$ until dry and the residue dissolved in dilute ultrapure HNO_3.

Group #			G-2014-2155	G-2014-2155	G-2014-2155	G-2014-2155	G-2014-2155	G-2014-2155	G-2014-2155	G-2014-2155	G-2014-2155	G-2014-2155
Description			SG195	SG196	SG197	SG198	SG199	SG200	SG201	SG202	SG203	SG204
Fence			Zone C	Zone C	Zone C	Zone C	Zone C	Zone C	Zone C	Zone C	Zone C	Zone C
HoleID			MC-415	MC-415	MC-415	MC-415	MC-415	MC-415	MC-415	MC-415	MC-415	MC-415
From			127.56	173.74	197.00	222.34	232.50	295.67	341.40	345.80	350.35	359.10
To			127.73	173.90	197.22	222.44	232.70	295.86	341.50	345.90	350.52	360.20
Lithofacies			MFc	MFc	MFc	MFc	MFc	MFc	MFb	MFb	MFb	MFb
Date			11-28-2014	11-28-2014	11-28-2014	11-28-2014	11-28-2014	11-28-2014	11-28-2014	11-28-2014	11-28-2014	11-28-2014
Sample Type			Sandstone	Sandstone	Sandstone	Sandstone	Sandstone	Sandstone	Sandstone	Sandstone	Sandstone	Sandstone
C	%	LECO	0.15	0.05	0.06	0.05	0.05	0.05	0.05	0.03	0.04	0.05
S	%	LECO	0.01	0.01	0.01	0.01	0.01	0.01	0.02	0.01	0.01	0.01
B	ppm	fusion	27	247	31	72	66	177	257	1410	1410	2270
LOI	%	1000°C	0.3	0.7	0.3	0.3	0.4	0.4	0.5	1	0.4	0.5
Al_2O_3	%	ICP-OES	0.5	2.05	0.59	0.59	0.74	1.59	2.06	4.75	1.93	2.93
CaO	%	ICP-OES	<0.01	0.01	<0.01	<0.01	0.01	0.01	0.02	0.02	0.02	0.01
Fe_2O_3	%	ICP-OES	0.03	0.08	0.03	0.03	0.05	0.05	0.07	0.15	0.1	0.1
K_2O	%	ICP-OES	0.027	0.078	0.031	0.03	0.033	0.333	0.455	0.538	0.008	0.039
MgO	%	ICP-OES	0.098	0.443	0.132	0.121	0.133	0.112	0.097	0.395	0.359	0.549
MnO	%	ICP-OES	<0.001	<0.001	0.003	0.003	<0.001	<0.001	<0.001	<0.001	<0.001	<0.001
Na_2O	%	ICP-OES	<0.01	<0.01	<0.01	<0.01	<0.01	<0.01	0.01	0.05	0.04	0.06
P_2O_5	%	ICP-OES	0.013	0.018	0.01	0.01	0.022	0.032	0.131	0.092	0.082	0.036
SiO_2	%	ICP-OES	98.8	96.3	98.7	98.7	98.2	97.2	96.6	92.7	96.9	95.1
TiO_2	%	ICP-OES	0.06	0.071	0.028	0.034	0.093	0.127	0.231	0.152	0.28	0.116
Ag	ppm	ICP-MS	0.04	0.03	<0.02	<0.02	0.05	0.06	0.08	0.06	0.09	0.05
Ba	ppm	ICP-OES	11	18	9	8	15	18	23	20	19	10
Be	ppm	ICP-MS	0.1	0.3	0.1	0.1	0.2	0.3	0.3	0.7	1.1	1.1
Bi	ppm	ICP-MS	<0.1	<0.1	<0.1	<0.1	<0.1	<0.1	<0.1	<0.1	<0.1	<0.1
Cd	ppm	ICP-MS	<0.1	<0.1	<0.1	<0.1	0.1	<0.1	0.2	0.1	0.2	<0.1
Ce	ppm	ICP-OES	22	26	21	16	32	28	41	57	62	31
Co	ppm	ICP-MS	0.11	0.18	0.26	0.22	0.1	0.06	0.09	0.22	0.27	0.16
Cr	ppm	ICP-OES	4	8	7	5	8	4	11	7	19	11
Cs	ppm	ICP-MS	<0.1	<0.1	<0.1	<0.1	<0.1	<0.1	<0.1	<0.1	<0.1	<0.1
Cu	ppm	ICP-MS	0.9	3.5	2.4	1.4	1.5	0.9	1.1	2.1	1.7	1.7
Dy	ppm	ICP-MS	0.63	0.66	0.44	0.5	0.78	0.73	1.8	1.18	0.74	0.56
Er	ppm	ICP-MS	0.34	0.39	0.25	0.29	0.47	0.42	0.86	0.48	0.4	0.32
Eu	ppm	ICP-MS	0.19	0.25	0.18	0.14	0.27	0.2	0.46	0.45	0.58	0.3
Ga	ppm	ICP-MS	1.6	3.6	1.6	1.5	1.7	1.8	2.4	5.3	2.1	3.2
Gd	ppm	ICP-MS	1.2	1.5	1	0.9	1.8	1.6	3.9	3.7	3.8	2
Hf	ppm	ICP-MS	2.7	3.3	1.3	1.6	5	3.8	8	6	7.9	4.5
Ho	ppm	ICP-MS	0.14	0.14	0.09	0.11	0.17	0.16	0.34	0.18	0.13	0.11
La	ppm	ICP-OES	10	12	10	7	13	13	19	28	28	14
Li	ppm	ICP-OES	2	6	2	2	2	3	3	5	1	1
Mo	ppm	ICP-MS	0.05	0.12	0.16	0.06	0.17	0.06	0.13	0.12	0.12	0.12
Nb	ppm	ICP-MS	1.4	1.7	0.6	0.6	2.3	3.2	5.7	4.1	6.7	2.9
Nd	ppm	ICP-MS	7.7	10	7.5	6	11	10.1	16.2	22.1	25.7	11.7
Ni	ppm	ICP-MS	1.7	4.7	2.1	1.8	2	1.3	0.7	1.8	2.1	2.8
^{204}Pb	ppm	ICP-MS	0.033	0.063	0.027	0.021	0.041	0.03	0.035	0.04	0.034	0.034
^{206}Pb	ppm	ICP-MS	0.63	1.05	0.515	0.454	0.728	0.64	0.946	0.945	0.776	0.702
^{207}Pb	ppm	ICP-MS	0.511	0.948	0.416	0.341	0.609	0.47	0.582	0.614	0.55	0.52
^{208}Pb	ppm	ICP-MS	1.3	2.37	1.05	0.861	1.74	1.37	1.98	2.32	2.6	2.92
Pb	ppm	ICP-MS	2.48	4.43	2.01	1.68	3.12	2.51	3.54	3.92	3.96	2.92
$^{206}Pb/^{204}Pb$	--	ICP-MS	19.09	16.67	19.07	21.62	17.76	21.33	27.03	23.63	22.82	20.65
$^{207}Pb/^{206}Pb$	--	ICP-MS	0.81	0.90	0.81	0.75	0.84	0.73	0.62	0.65	0.71	0.74
$^{207}Pb/^{204}Pb$	--	ICP-MS	15.48	15.05	15.41	16.24	14.85	15.67	16.63	15.35	16.18	15.29
$^{208}Pb/^{206}Pb$	--	ICP-MS	2.06	2.26	2.04	1.90	2.39	2.14	2.09	2.46	3.35	4.16
$^{208}Pb/^{204}Pb$	--	ICP-MS	39.39	37.62	38.89	41.00	42.44	45.67	56.57	58.00	76.47	85.88
Pr	ppm	ICP-MS	2.4	3	2.4	1.8	3.3	3.1	4.6	6.7	7.3	3.4
Rb	ppm	ICP-MS	0.6	1.2	0.6	0.6	0.7	3.3	3.9	4.9	0.3	0.5
Sc	ppm	ICP-MS	0.4	0.5	0.3	0.2	0.4	0.4	1.2	1.4	0.8	0.7
Sm	ppm	ICP-MS	1.3	1.7	1.3	1	2	1.7	3.4	4.2	5.4	2.3
Sn	ppm	ICP-MS	0.17	0.57	0.38	0.22	0.46	0.35	0.44	0.54	0.55	0.39
Sr	ppm	ICP-OES	34	45	31	27	75	90	733	354	473	135
Ta	ppm	ICP-MS	0.13	0.14	0.06	0.06	0.2	0.32	0.49	0.38	0.6	0.27
Tb	ppm	ICP-MS	0.11	0.13	0.08	0.09	0.15	0.14	0.41	0.29	0.22	0.14
Th	ppm	ICP-MS	3.75	4.71	3.21	3.1	14	8.76	16.9	14.8	32.8	10.3
U	ppm	ICP-MS	1.44	1.44	1.38	1.1	2.03	1.47	3.31	2.84	2.32	1.45
V	ppm	ICP-MS	4.2	5	1.6	3	6.4	2.8	5.4	7.9	4.4	2.4
W	ppm	ICP-MS	0.2	0.3	<0.1	0.1	0.3	0.4	0.4	0.3	0.9	0.4
Y	ppm	ICP-MS	3.4	4	2.4	2.9	4.6	4.1	9.1	4.5	3.3	2.9
Yb	ppm	ICP-MS	0.36	0.38	0.26	0.28	0.48	0.46	0.84	0.47	0.45	0.35
Zn	ppm	ICP-MS	4	3	3	3	4	5	3	3	4	4
Zr	ppm	ICP-OES	90	111	40	51	164	121	268	196	263	148

Carbon and Sulfur: a 0.2 g pulp is analyzed in a Leco SC144DR C/S analyzer for Carbon and Sulfur.

SiO_2 Analysis: A 0.1 gram pulp is fused at 1000 C with lithium metaborate then dissolved in dilute HNO_3.

LOI: A 1.00 gram pulp is heated at 1000 C overnight and the weight loss determined.

Boron: A 0.1 gram pulp is fused at 650 C in a mixture of Na_2O_2/Na_2CO_3.

Total Digestion: A 0.250 g pulp is gently heated in a mixture of ultrapure $HF/HNO_3/HClO_4$ until dry and the residue dissolved in dilute ultrapure HNO_3.

Group #			G-2014-2155	G-2014-2155	G-2014-2155	G-2014-2155	G-2014-2155	G-2014-2155	G-2014-2155	G-2014-2155	G-2014-2155	G-2014-2155
Description			SG205	SG206	SG207	SG208	SG209	SG210	SG211	SG212	SG213	SG214
Fence			Zone C	Zone C	Zone C	Zone C	Zone C	Zone C	Zone C	Zone C	Zone C	Zone C
HoleID			MC-415	MC-415	MC-415	MC-415	MC-415	MC-415	MC-415	MC-415	MC-415	MC-415
From			389.00	416.08	432.38	455.72	477.00	490.78	497.62	503.32	508.60	513.34
To			389.24	416.28	432.61	455.92	477.20	490.91	497.86	503.54	508.75	513.45
Lithofacies			MFb	MFb	MFb	MFa	MFa	MFa	MFa	MFa	MFa	MFa
Date			11-28-2014	11-28-2014	11-28-2014	11-28-2014	11-28-2014	11-28-2014	11-28-2014	11-28-2014	11-28-2014	11-28-2014
Sample Type			Sandstone	Sandstone	Sandstone	Sandstone	Sandstone	Sandstone	Sandstone	Sandstone	Sandstone	Sandstone
C	%	LECO	0.05	0.05	0.06	0.06	0.04	0.03	0.04	0.04	0.04	0.04
S	%	LECO	0.01	0.01	0.01	0.01	0.01	0.01	0.01	0.01	0.01	0.01
B	ppm	fusion	2220	1160	1850	1940	2990	331	1480	506	668	580
LOI	%	1000°C	0.5	0.4	0.5	0.4	0.6	0.3	0.4	0.3	0.9	0.4
Al_2O_3	%	ICP-OES	2.83	2.13	2.64	2.38	3.55	0.54	2.13	0.63	3.38	1.43
CaO	%	ICP-OES	0.02	0.01	0.02	0.02	0.02	0.02	0.02	0.02	0.02	0.02
Fe_2O_3	%	ICP-OES	0.16	0.24	0.22	0.18	0.15	0.04	0.13	0.1	0.24	0.25
K_2O	%	ICP-OES	0.013	0.193	0.028	0.008	0.009	0.019	0.01	0.008	0.308	0.16
MgO	%	ICP-OES	0.544	0.293	0.499	0.463	0.67	0.1	0.408	0.117	0.206	0.166
MnO	%	ICP-OES	<0.001	<0.001	<0.001	<0.001	<0.001	<0.001	<0.001	<0.001	0.001	<0.001
Na_2O	%	ICP-OES	0.05	0.04	0.06	0.04	0.06	0.02	0.04	0.02	0.03	0.02
P_2O_5	%	ICP-OES	0.056	0.023	0.027	0.024	0.028	0.009	0.019	0.012	0.016	0.021
SiO_2	%	ICP-OES	95.6	96.5	95.5	95.9	95	98.8	97	98.7	95	97.5
TiO_2	%	ICP-OES	0.339	0.064	0.087	0.065	0.107	0.018	0.048	0.054	0.031	0.049
Ag	ppm	ICP-MS	0.08	0.03	0.04	0.03	0.04	<0.02	<0.02	<0.02	<0.02	0.02
Ba	ppm	ICP-OES	23	13	22	13	17	16	23	17	27	19
Be	ppm	ICP-MS	1.3	0.4	0.7	0.8	1.2	0.2	0.7	0.3	0.3	0.3
Bi	ppm	ICP-MS	<0.1	<0.1	<0.1	<0.1	<0.1	<0.1	<0.1	<0.1	<0.1	<0.1
Cd	ppm	ICP-MS	0.3	<0.1	<0.1	<0.1	0.2	<0.1	<0.1	0.1	<0.1	<0.1
Ce	ppm	ICP-OES	70	34	35	29	35	12	21	14	17	23
Co	ppm	ICP-MS	0.22	0.16	0.17	0.16	0.21	0.06	0.23	0.08	0.2	0.15
Cr	ppm	ICP-OES	15	14	14	18	18	8	18	14	18	14
Cs	ppm	ICP-MS	<0.1	<0.1	<0.1	<0.1	<0.1	<0.1	<0.1	<0.1	<0.1	<0.1
Cu	ppm	ICP-MS	2.7	1.8	1.9	1.3	1.7	0.5	1.7	0.7	2	8.9
Dy	ppm	ICP-MS	0.81	0.31	0.51	0.44	0.62	0.3	0.51	0.46	0.4	0.48
Er	ppm	ICP-MS	0.56	0.22	0.32	0.3	0.45	0.15	0.34	0.36	0.23	0.31
Eu	ppm	ICP-MS	0.44	0.16	0.27	0.26	0.28	0.13	0.21	0.15	0.18	0.2
Ga	ppm	ICP-MS	3.1	2.4	2.8	2.4	3.6	0.6	2.3	0.7	3.2	1.4
Gd	ppm	ICP-MS	3.2	1.2	1.7	1.8	1.6	0.7	1.2	0.9	1	1.1
Hf	ppm	ICP-MS	14.6	3.2	4.1	3.9	6.1	1.2	4.2	6.2	2	4.3
Ho	ppm	ICP-MS	0.18	0.07	0.11	0.1	0.14	0.06	0.12	0.12	0.08	0.11
La	ppm	ICP-OES	37	18	16	13	18	5	11	7	8	11
Li	ppm	ICP-OES	1	3	3	3	3	4	4	2	14	4
Mo	ppm	ICP-MS	0.2	0.13	0.12	0.1	0.11	0.07	0.09	0.08	0.15	0.24
Nb	ppm	ICP-MS	8.1	1.7	2.1	1.6	2.7	0.5	1	1.2	0.8	1.2
Nd	ppm	ICP-MS	22.8	11.5	15	15.5	13.4	5.5	8.3	5.5	6.9	8.7
Ni	ppm	ICP-MS	2.6	1.6	2.1	2.4	2.8	0.6	2.2	0.8	1.8	1.6
^{204}Pb	ppm	ICP-MS	0.028	0.019	0.032	0.024	0.032	0.029	0.038	0.027	0.045	0.036
^{206}Pb	ppm	ICP-MS	0.762	0.44	0.651	0.531	0.701	0.476	0.71	0.628	0.782	0.706
^{207}Pb	ppm	ICP-MS	0.446	0.291	0.489	0.369	0.474	0.406	0.573	0.415	0.655	0.541
^{208}Pb	ppm	ICP-MS	3.38	1.19	1.61	1.13	1.58	1.02	1.47	1.03	1.61	1.4
Pb	ppm	ICP-MS	10.4	1.94	2.78	2.05	2.78	1.93	2.79	2.1	3.1	2.69
$^{206}Pb/^{204}Pb$	--	ICP-MS	27.21	23.16	20.34	22.13	21.91	16.41	18.68	23.26	17.38	19.61
$^{207}Pb/^{206}Pb$	--	ICP-MS	0.59	0.66	0.75	0.69	0.68	0.85	0.81	0.66	0.84	0.77
$^{207}Pb/^{204}Pb$	--	ICP-MS	15.93	15.32	15.28	15.38	14.81	14.00	15.08	15.37	14.56	15.03
$^{208}Pb/^{206}Pb$	--	ICP-MS	4.44	2.70	2.47	2.13	2.25	2.14	2.07	1.64	2.06	1.98
$^{208}Pb/^{204}Pb$	--	ICP-MS	120.71	62.63	50.31	47.08	49.38	35.17	38.68	38.15	35.78	38.89
Pr	ppm	ICP-MS	7.4	4	4.3	4.1	4.2	1.5	2.5	1.7	2.1	2.7
Rb	ppm	ICP-MS	0.3	1.8	0.5	0.2	0.2	0.3	0.2	0.2	3.3	1.7
Sc	ppm	ICP-MS	1.2	0.7	0.8	0.7	1.6	0.3	1	0.6	0.6	0.5
Sm	ppm	ICP-MS	4	1.5	2.5	3.2	2	0.9	1.5	1	1.2	1.4
Sn	ppm	ICP-MS	1.44	0.27	0.37	0.36	0.5	0.11	0.4	0.17	0.23	1.6
Sr	ppm	ICP-OES	182	71	72	61	68	23	44	27	32	42
Ta	ppm	ICP-MS	0.92	0.18	0.21	0.19	0.27	0.05	0.1	0.14	0.07	0.12
Tb	ppm	ICP-MS	0.19	0.06	0.11	0.1	0.12	0.06	0.1	0.08	0.08	0.09
Th	ppm	ICP-MS	78	11.7	10.6	5.92	10.7	1.68	4.06	3.14	2.43	3.98
U	ppm	ICP-MS	4.65	1.7	2.18	2.23	3.41	0.92	3.36	3.42	2.61	4.18
V	ppm	ICP-MS	4.9	3.8	2.6	1.6	2.6	0.5	2.1	1.2	4	4.5
W	ppm	ICP-MS	1.4	0.2	0.4	0.4	0.6	<0.1	0.3	0.2	0.2	0.1
Y	ppm	ICP-MS	4.9	1.9	2.7	2.5	3.8	1.4	3	3.2	2.1	2.9
Yb	ppm	ICP-MS	0.69	0.23	0.36	0.36	0.54	0.16	0.41	0.46	0.22	0.37
Zn	ppm	ICP-MS	3	3	3	3	3	3	5	3	3	3
Zr	ppm	ICP-OES	515	94	132	128	196	35	145	210	64	147

Carbon and Sulfur: a 0.2 g pulp is analyzed in a Leco SC144DR C/S analyzer for Carbon and Sulfur.

SiO_2 Analysis: A 0.1 gram pulp is fused at 1000 C with lithium metaborate then dissolved in dilute HNO_3.

LOI: A 1.00 gram pulp is heated at 1000 C overnight and the weight loss determined.

Boron: A 0.1 gram pulp is fused at 650 C in a mixture of Na_2O_2/Na_2CO_3.

Total Digestion: A 0.250 g pulp is gently heated in a mixture of ultrapure $HF/HNO_3/HClO_4$ until dry and the residue dissolved in dilute ultrapure HNO_3.

Group #			G-2014-2155	G-2014-2155	G-2014-2155	G-2014-2155	G-2014-2155	G-2014-2155	G-2014-2155	G-2014-2155	G-2014-2155	G-2014-2155
Description			SG215	SG216	SG213 R	SG217	SG218	SG219	SG220	SG221	SG222	SG223
Fence			Zone C	Zone C	Zone C	Zone C	Background	Background	Background	Background	Background	Background
HoleID			MC-415	MC-415	MC-415	MC-415	MC-434	MC-434	MC-434	MC-434	MC-434	MC-434
From			520.15	537.00	508.60	539.69	11.10	31.63	54.07	93.9	119.66	168.25
To			520.35	537.15	508.75	539.84	11.22	31.78	54.12	94.10	119.88	168.38
Lithofacies			MFa	MFa	MFa	MFa	MFd	MFd	MFd	MFd	MFd	MFc
Date			11-28-2014	11-28-2014	11-28-2014	11-28-2014	11-28-2014	11-28-2014	11-28-2014	11-28-2014	11-28-2014	11-28-2014
Sample Type			Sandstone	Sandstone	Repeat	Sandstone	Sandstone	Sandstone	Sandstone	Sandstone	Sandstone	Sandstone
C	%	LECO	0.04	0.04	0.05	0.03	0.04	0.11	0.06	0.06	0.06	0.03
S	%	LECO	0.01	0.01	0.01	0.01	0.01	0.01	0.01	0.02	0.01	0.01
B	ppm	fusion	814	51	664	44	99	92	109	31	33	38
LOI	%	1000°C	0.5	0.5	0.9	0.7	0.3	0.3	0.3	0.2	1.8	0.3
Al_2O_3	%	ICP-OES	2.28	1.24	3.49	2.2	0.9	1.1	0.92	0.62	5.48	0.72
CaO	%	ICP-OES	0.02	0.02	0.02	0.02	<0.01	<0.01	<0.01	<0.01	<0.01	<0.01
Fe_2O_3	%	ICP-OES	0.48	0.12	0.25	0.21	0.06	0.09	0.03	0.03	0.12	0.03
K_2O	%	ICP-OES	0.303	0.186	0.319	0.246	0.224	0.238	0.133	0.088	0.369	0.142
MgO	%	ICP-OES	0.235	0.138	0.213	0.313	0.038	0.032	0.03	0.013	0.025	0.018
MnO	%	ICP-OES	0.001	<0.001	0.001	0.001	<0.001	<0.001	<0.001	<0.001	<0.001	<0.001
Na_2O	%	ICP-OES	0.03	<0.01	0.03	<0.01	<0.01	<0.01	<0.01	<0.01	<0.01	<0.01
P_2O_5	%	ICP-OES	0.028	0.069	0.016	0.124	0.012	0.013	0.009	0.009	0.028	0.009
SiO_2	%	ICP-OES	95.7	96.9	94.8	95.8	97.7	97.4	98.2	98	91.8	98
TiO_2	%	ICP-OES	0.06	0.336	0.033	0.072	0.083	0.11	0.066	0.022	0.173	0.057
Ag	ppm	ICP-MS	0.02	0.09	0.03	0.04	0.04	0.03	<0.02	<0.02	0.07	0.02
Ba	ppm	ICP-OES	23	38	27	19	10	10	7	6	19	6
Be	ppm	ICP-MS	0.4	0.4	0.3	0.4	0.2	0.1	0.1	<0.1	0.2	<0.1
Bi	ppm	ICP-MS	<0.1	<0.1	<0.1	<0.1	<0.1	<0.1	<0.1	<0.1	<0.1	<0.1
Cd	ppm	ICP-MS	<0.1	0.3	<0.1	<0.1	0.1	0.2	0.2	<0.1	0.2	<0.1
Ce	ppm	ICP-OES	29	85	17	308	20	21	16	18	33	15
Co	ppm	ICP-MS	0.22	0.17	0.19	0.28	0.11	0.08	0.06	0.05	0.08	0.06
Cr	ppm	ICP-OES	12	30	20	16	6	11	7	7	10	5
Cs	ppm	ICP-MS	<0.1	<0.1	<0.1	<0.1	<0.1	<0.1	<0.1	<0.1	<0.1	<0.1
Cu	ppm	ICP-MS	3.5	2.2	2	2.2	2.3	0.7	0.5	0.4	1.5	0.4
Dy	ppm	ICP-MS	0.45	1.85	0.42	1.23	0.57	0.56	0.39	0.24	0.78	0.3
Er	ppm	ICP-MS	0.32	1.12	0.24	0.79	0.4	0.43	0.32	0.14	0.49	0.24
Eu	ppm	ICP-MS	0.22	0.64	0.19	1.71	0.18	0.18	0.11	0.13	0.32	0.12
Ga	ppm	ICP-MS	2.4	2.1	3.4	4.6	1.2	1.2	0.9	0.6	4.1	1
Gd	ppm	ICP-MS	1.3	5.2	1	14.7	1.3	1.2	0.8	0.7	1.8	0.8
Hf	ppm	ICP-MS	5.4	13.9	2.1	2.2	5.8	8.6	7.4	1.2	7.3	4.1
Ho	ppm	ICP-MS	0.11	0.4	0.09	0.17	0.14	0.14	0.1	0.05	0.18	0.08
La	ppm	ICP-OES	15	45	9	123	11	10	8	8	15	7
Li	ppm	ICP-OES	5	9	14	12	2	3	3	2	19	3
Mo	ppm	ICP-MS	0.2	0.33	0.15	0.36	0.14	0.08	0.05	0.05	0.16	0.08
Nb	ppm	ICP-MS	1.4	7.8	1.1	2.2	1.9	2.2	1.6	0.5	4.2	1.3
Nd	ppm	ICP-MS	10	32.7	7.4	181	10.6	8.2	5.6	5.9	11.9	5.8
Ni	ppm	ICP-MS	1.5	1.6	1.9	2.5	0.7	0.6	0.4	0.3	0.6	0.4
^{204}Pb	ppm	ICP-MS	0.027	0.032	0.046	0.085	0.052	0.026	0.023	0.03	0.17	0.027
^{206}Pb	ppm	ICP-MS	0.867	1.04	0.811	1.67	1.2	0.57	0.465	0.525	3.51	0.497
^{207}Pb	ppm	ICP-MS	0.43	0.522	0.696	1.29	0.816	0.435	0.342	0.477	2.6	0.382
^{208}Pb	ppm	ICP-MS	1.22	3.9	1.69	3.54	2.55	1.26	0.989	1.16	7.7	1.19
Pb	ppm	ICP-MS	2.54	5.5	3.24	6.58	4.62	2.3	1.82	2.2	14	2.09
$^{206}Pb/^{204}Pb$	--	ICP-MS	32.11	32.50	17.63	19.65	23.08	21.92	20.22	17.50	20.65	18.41
$^{207}Pb/^{206}Pb$	--	ICP-MS	0.50	0.50	0.86	0.77	0.68	0.76	0.74	0.91	0.74	0.77
$^{207}Pb/^{204}Pb$	--	ICP-MS	15.93	16.31	15.13	15.18	15.69	16.73	14.87	15.90	15.29	14.15
$^{208}Pb/^{206}Pb$	--	ICP-MS	1.41	3.75	2.08	2.12	2.13	2.21	2.13	2.21	2.19	2.39
$^{208}Pb/^{204}Pb$	--	ICP-MS	45.19	121.88	36.74	41.65	49.04	48.46	43.00	38.67	45.29	44.07
Pr	ppm	ICP-MS	3.3	10.1	2.2	45.1	3.2	2.6	1.9	2	3.8	1.8
Rb	ppm	ICP-MS	3.2	2.6	3.5	4	2.2	2.4	1.4	0.8	3.2	1.3
Sc	ppm	ICP-MS	0.7	1.5	0.6	2.8	0.8	0.9	0.7	0.2	0.9	0.3
Sm	ppm	ICP-MS	1.5	6.3	1.2	29.4	1.8	1.4	0.9	0.9	2.1	0.9
Sn	ppm	ICP-MS	0.38	2.2	0.26	0.74	0.54	0.3	0.27	0.14	0.5	0.27
Sr	ppm	ICP-OES	57	241	33	335	37	40	31	30	72	35
Ta	ppm	ICP-MS	0.12	1.1	0.13	0.27	0.18	0.19	0.15	0.04	0.37	0.11
Tb	ppm	ICP-MS	0.09	0.4	0.08	0.36	0.1	0.1	0.07	0.05	0.14	0.06
Th	ppm	ICP-MS	5.7	113	2.47	10.2	8.39	7.72	7.48	2.43	9.41	7.29
U	ppm	ICP-MS	6.18	10.2	2.6	3.66	1.38	1.36	1.44	0.59	4.51	0.9
V	ppm	ICP-MS	7.9	15.3	4	12.3	2	2.2	1.5	1	7.1	2.9
W	ppm	ICP-MS	0.2	0.8	0.3	2.4	0.4	0.4	0.3	<0.1	0.8	0.2
Y	ppm	ICP-MS	2.7	10.3	2.2	3.3	3.4	3.3	2.5	1.1	4	1.8
Yb	ppm	ICP-MS	0.39	1.19	0.24	0.36	0.5	0.62	0.49	0.16	0.57	0.33
Zn	ppm	ICP-MS	4	4	4	4	4	4	3	3	4	3
Zr	ppm	ICP-OES	184	489	61	73	193	282	249	35	241	137

Carbon and Sulfur: a 0.2 g pulp is analyzed in a Leco SC144DR C/S analyzer for Carbon and Sulfur.

SiO_2 Analysis: A 0.1 gram pulp is fused at 1000 C with lithium metaborate then dissolved in dilute HNO_3.

LOI: A 1.00 gram pulp is heated at 1000 C overnight and the weight loss determined.

Boron: A 0.1 gram pulp is fused at 650 C in a mixture of Na_2O_2/Na_2CO_3.

Total Digestion: A 0.250 g pulp is gently heated in a mixture of ultrapure $HF/HNO_3/HClO_4$ until dry and the residue dissolved in dilute ultrapure HNO_3.

Group #			G-2014-2155	G-2014-2155	G-2014-2155	G-2014-2155	G-2014-2155	G-2014-2155	G-2014-2155	G-2014-2155	G-2014-2155	G-2014-2155
Description			SG224	SG225	SG226	SG227	SG228	SG229	SG230	SG231	SG232	SG233
Fence			Background	Background	Background	Background	Background	Background	Background	Background	Background	Background
HoleID			MC-434	MC-434	MC-434	MC-434	MC-434	MC-434	MC-434	MC-434	MC-434	MC-434
From			183.4	217.84	253.64	256.65	282.2	328.83	338.05	348.28	370.63	397.53
To			183.54	218.00	253.78	256.78	282.36	329.00	338.20	348.45	370.75	397.67
Lithofacies			MFc	MFc	MFc	MFc	MFc	MFb	MFb	MFb	MFb	MFa
Date			11-28-2014	11-28-2014	11-28-2014	11-28-2014	11-28-2014	11-28-2014	11-28-2014	11-28-2014	11-28-2014	11-28-2014
Sample Type			Sandstone	Sandstone	Sandstone	Sandstone	Sandstone	Sandstone	Sandstone	Sandstone	Sandstone	Sandstone
C	%	LECO	0.03	0.04	0.03	0.05	0.04	0.06	0.04	0.05	0.06	0.04
S	%	LECO	0.01	0.01	0.01	0.01	0.02	0.01	0.01	0.01	0.01	0.01
B	ppm	fusion	45	19	32	28	39	28	22	23	34	29
LOI	%	1000°C	0.3	0.3	0.6	0.4	0.5	0.9	1.2	0.9	0.9	0.9
Al_2O_3	%	ICP-OES	0.91	0.64	1.65	1.14	1.49	2.4	3.33	2.36	2.36	2.37
CaO	%	ICP-OES	<0.01	<0.01	<0.01	<0.01	0.01	0.02	<0.01	0.01	0.01	<0.01
Fe_2O_3	%	ICP-OES	0.04	0.15	0.04	0.11	0.1	0.19	0.41	0.18	0.38	0.08
K_2O	%	ICP-OES	0.139	0.106	0.187	0.153	0.173	0.153	0.202	0.201	0.224	0.054
MgO	%	ICP-OES	0.016	0.012	0.017	0.013	0.015	0.012	0.014	0.016	0.018	0.013
MnO	%	ICP-OES	<0.001	<0.001	<0.001	<0.001	<0.001	<0.001	<0.001	<0.001	<0.001	<0.001
Na_2O	%	ICP-OES	<0.01	<0.01	<0.01	<0.01	<0.01	<0.01	<0.01	<0.01	<0.01	<0.01
P_2O_5	%	ICP-OES	0.014	0.018	0.039	0.026	0.049	0.064	0.026	0.026	0.019	0.026
SiO_2	%	ICP-OES	97.4	97.8	97.2	97.8	96.8	96	94.2	95.7	95.4	96.2
TiO_2	%	ICP-OES	0.093	0.072	0.096	0.097	0.099	0.108	0.045	0.227	0.191	0.119
Ag	ppm	ICP-MS	0.04	0.03	0.05	0.04	0.03	0.04	0.03	0.06	0.07	0.04
Ba	ppm	ICP-OES	8	9	9	8	8	8	6	10	8	8
Be	ppm	ICP-MS	0.1	<0.1	0.1	0.1	0.1	0.1	0.1	0.2	0.2	0.2
Bi	ppm	ICP-MS	<0.1	<0.1	<0.1	<0.1	<0.1	<0.1	<0.1	<0.1	<0.1	<0.1
Cd	ppm	ICP-MS	<0.1	<0.1	<0.1	<0.1	<0.1	<0.1	<0.1	0.2	0.2	0.1
Ce	ppm	ICP-OES	25	27	33	24	28	33	26	38	29	43
Co	ppm	ICP-MS	0.07	0.08	0.05	0.09	0.05	0.06	0.08	0.06	0.1	0.11
Cr	ppm	ICP-OES	4	4	4	5	5	3	5	5	6	9
Cs	ppm	ICP-MS	<0.1	<0.1	<0.1	<0.1	<0.1	<0.1	<0.1	<0.1	<0.1	<0.1
Cu	ppm	ICP-MS	0.6	1	0.6	0.7	0.8	0.5	1.4	0.8	0.7	0.6
Dy	ppm	ICP-MS	0.37	0.39	0.55	0.44	0.52	0.57	0.36	0.5	0.44	0.47
Er	ppm	ICP-MS	0.23	0.26	0.28	0.29	0.31	0.3	0.2	0.36	0.33	0.32
Eu	ppm	ICP-MS	0.15	0.21	0.24	0.18	0.2	0.24	0.17	0.28	0.19	0.3
Ga	ppm	ICP-MS	1.1	0.8	1.6	1.2	1.5	2.2	2.9	2.3	2.3	1.9
Gd	ppm	ICP-MS	1	1.5	1.8	1.4	1.6	2	1.4	1.9	1.4	2.3
Hf	ppm	ICP-MS	4	3.6	2.8	4.8	4.6	4	1.8	9.6	7.9	5.4
Ho	ppm	ICP-MS	0.07	0.09	0.1	0.1	0.11	0.11	0.07	0.11	0.1	0.1
La	ppm	ICP-OES	11	11	14	11	13	16	12	18	15	19
Li	ppm	ICP-OES	4	2	6	4	5	6	9	7	7	7
Mo	ppm	ICP-MS	0.08	0.06	0.08	0.6	0.08	0.05	0.12	0.1	0.13	0.06
Nb	ppm	ICP-MS	2.1	2	2.7	2.4	2.5	2.9	1.3	5.3	4.7	2.8
Nd	ppm	ICP-MS	8	9.7	11.3	9	10.6	13.2	10	12.9	11	20.2
Ni	ppm	ICP-MS	0.4	0.3	0.4	0.3	0.4	0.2	0.9	0.4	0.4	0.4
^{204}Pb	ppm	ICP-MS	0.039	0.066	0.036	0.02	0.027	0.028	0.023	0.031	0.019	0.024
^{206}Pb	ppm	ICP-MS	0.665	1.46	0.592	0.452	0.624	0.575	0.475	0.668	0.494	0.456
^{207}Pb	ppm	ICP-MS	0.59	1.02	0.509	0.323	0.447	0.433	0.358	0.478	0.318	0.373
^{208}Pb	ppm	ICP-MS	1.59	3.48	1.43	1.23	1.32	1.46	1.04	1.89	1.53	1.24
Pb	ppm	ICP-MS	2.88	6.03	2.57	2.03	2.41	2.49	1.9	3.07	2.36	2.09
$^{206}Pb/^{204}Pb$	--	ICP-MS	17.05	22.12	16.44	22.60	23.11	20.54	20.65	21.55	26.00	19.00
$^{207}Pb/^{206}Pb$	--	ICP-MS	0.89	0.70	0.86	0.71	0.72	0.75	0.75	0.72	0.64	0.82
$^{207}Pb/^{204}Pb$	--	ICP-MS	15.13	15.45	14.14	16.15	16.56	15.46	15.57	15.42	16.74	15.54
$^{208}Pb/^{206}Pb$	--	ICP-MS	2.39	2.38	2.42	2.72	2.12	2.54	2.19	2.83	3.10	2.72
$^{208}Pb/^{204}Pb$	--	ICP-MS	40.77	52.73	39.72	61.50	48.89	52.14	45.22	60.97	80.53	51.67
Pr	ppm	ICP-MS	2.6	3	3.5	2.8	3.2	4	3	4.2	3.6	5.5
Rb	ppm	ICP-MS	1.4	1.2	1.8	1.5	1.6	1.5	1.8	1.9	2.1	0.7
Sc	ppm	ICP-MS	0.4	0.3	0.5	0.6	0.5	0.6	0.5	0.9	0.8	0.6
Sm	ppm	ICP-MS	1.2	1.7	1.9	1.6	1.7	2.3	1.7	2.2	1.7	3.7
Sn	ppm	ICP-MS	0.2	0.22	0.3	0.26	0.28	0.28	0.25	0.4	0.37	0.28
Sr	ppm	ICP-OES	52	64	206	132	252	319	94	105	68	78
Ta	ppm	ICP-MS	0.19	0.18	0.22	0.23	0.21	0.27	0.12	0.52	0.51	0.3
Tb	ppm	ICP-MS	0.07	0.1	0.15	0.11	0.13	0.15	0.1	0.12	0.09	0.11
Th	ppm	ICP-MS	6.41	7.37	5.59	11.6	7.2	8.21	3.7	20.2	21.9	9.85
U	ppm	ICP-MS	1.1	1.9	0.64	1.07	1.08	1.14	2.23	1.66	1.1	0.96
V	ppm	ICP-MS	4	2.6	4.1	3.5	2.9	2.9	2.9	3.5	3.7	2.2
W	ppm	ICP-MS	0.2	0.2	0.2	0.2	0.2	0.2	0.1	0.3	0.4	0.5
Y	ppm	ICP-MS	1.7	2	2.4	2.3	2.4	2.5	1.6	2.7	2.5	2.4
Yb	ppm	ICP-MS	0.3	0.31	0.34	0.36	0.4	0.35	0.22	0.48	0.43	0.37
Zn	ppm	ICP-MS	3	4	3	4	5	3	4	3	3	3
Zr	ppm	ICP-OES	127	106	84	158	144	124	54	314	249	171

Carbon and Sulfur: a 0.2 g pulp is analyzed in a Leco SC144DR C/S analyzer for Carbon and Sulfur.

SiO_2 Analysis: A 0.1 gram pulp is fused at 1000 C with lithium metaborate then dissolved in dilute HNO_3.

LOI: A 1.00 gram pulp is heated at 1000 C overnight and the weight loss determined.

Boron: A 0.1 gram pulp is fused at 650 C in a mixture of Na_2O_2/Na_2CO_3.

Total Digestion: A 0.250 g pulp is gently heated in a mixture of ultrapure $HF/HNO_3/HClO_4$ until dry and the residue dissolved in dilute ultrapure HNO_3.

Group #			G-2014-2155	G-2014-2155
Description			SG234	SG234 R
Fence			Background	Background
HoleID			MC-434	MC-434
From			421.67	421.67
To			421.83	421.83
Lithofacies			MFa	MFa
Date			11-28-2014	11-28-2014
Sample Type			Sandstone	Repeat
C	%	LECO	0.08	0.08
S	%	LECO	0.01	0.01
B	ppm	fusion	22	20
LOI	%	1000°C	0.7	0.7
Al_2O_3	%	ICP-OES	1.58	1.6
CaO	%	ICP-OES	0.02	0.02
Fe_2O_3	%	ICP-OES	0.39	0.4
K_2O	%	ICP-OES	0.062	0.065
MgO	%	ICP-OES	0.021	0.021
MnO	%	ICP-OES	<0.001	<0.001
Na_2O	%	ICP-OES	<0.01	<0.01
P_2O_5	%	ICP-OES	0.018	0.019
SiO_2	%	ICP-OES	96.8	96.7
TiO_2	%	ICP-OES	0.07	0.075
Ag	ppm	ICP-MS	0.04	0.04
Ba	ppm	ICP-OES	6	7
Be	ppm	ICP-MS	0.1	0.1
Bi	ppm	ICP-MS	<0.1	<0.1
Cd	ppm	ICP-MS	<0.1	<0.1
Ce	ppm	ICP-OES	26	27
Co	ppm	ICP-MS	0.06	0.09
Cr	ppm	ICP-OES	8	9
Cs	ppm	ICP-MS	<0.1	<0.1
Cu	ppm	ICP-MS	0.7	0.7
Dy	ppm	ICP-MS	0.32	0.34
Er	ppm	ICP-MS	0.21	0.21
Eu	ppm	ICP-MS	0.2	0.2
Ga	ppm	ICP-MS	1.4	1.4
Gd	ppm	ICP-MS	1.5	1.5
Hf	ppm	ICP-MS	3.8	3.6
Ho	ppm	ICP-MS	0.06	0.07
La	ppm	ICP-OES	12	13
Li	ppm	ICP-OES	5	5
Mo	ppm	ICP-MS	0.08	0.06
Nb	ppm	ICP-MS	1.9	2
Nd	ppm	ICP-MS	11	11
Ni	ppm	ICP-MS	0.3	0.4
^{204}Pb	ppm	ICP-MS	0.018	0.019
^{206}Pb	ppm	ICP-MS	0.436	0.449
^{207}Pb	ppm	ICP-MS	0.3	0.3
^{208}Pb	ppm	ICP-MS	1.1	1.12
Pb	ppm	ICP-MS	1.86	1.88
$^{206}Pb/^{204}Pb$	--	ICP-MS	24.22	23.63
$^{207}Pb/^{206}Pb$	--	ICP-MS	0.69	0.67
$^{207}Pb/^{204}Pb$	--	ICP-MS	16.67	15.79
$^{208}Pb/^{206}Pb$	--	ICP-MS	2.52	2.49
$^{208}Pb/^{204}Pb$	--	ICP-MS	61.11	58.95
Pr	ppm	ICP-MS	3.3	3.3
Rb	ppm	ICP-MS	0.8	0.8
Sc	ppm	ICP-MS	0.4	0.4
Sm	ppm	ICP-MS	1.9	1.9
Sn	ppm	ICP-MS	0.33	0.47
Sr	ppm	ICP-OES	63	66
Ta	ppm	ICP-MS	0.24	0.21
Tb	ppm	ICP-MS	0.09	0.08
Th	ppm	ICP-MS	9.56	9.61
U	ppm	ICP-MS	0.81	0.8
V	ppm	ICP-MS	1.5	1.4
W	ppm	ICP-MS	0.3	0.4
Y	ppm	ICP-MS	1.6	1.6
Yb	ppm	ICP-MS	0.26	0.24
Zn	ppm	ICP-MS	4	3
Zr	ppm	ICP-OES	121	118

Carbon and Sulfur: a 0.2 g pulp is analyzed in a Leco SC144DR C/S analyzer for Carbon and Sulfur.

SiO_2 Analysis: A 0.1 gram pulp is fused at 1000 C with lithium metaborate then dissolved in dilute HNO_3.

LOI: A 1.00 gram pulp is heated at 1000 C overnight and the weight loss determined.

Boron: A 0.1 gram pulp is fused at 650 C in a mixture of Na_2O_2/Na_2CO_3.

Total Digestion: A 0.250 g pulp is gently heated in a mixture of ultrapure $HF/HNO_3/HClO_4$ until dry and the residue dissolved in dilute ultrapure HNO_3.